Automatic Generation Control of the Petroleum Development Oman (PDO) and the Oman Electricity Transmission Company (OETC) Interconnected Power Systems

ADIL GHALIB AL-BUSAIDI

A thesis submitted in partial fulfilment of the
requirements of the University of Teesside
for the degree of Doctor of Philosophy

September 2012

Abstract

Petroleum Development Oman (PDO) and Oman Electricity Transmission Company (OETC) are running the main 132kV power transmission grids in the Sultanate of Oman. In the year 2001, PDO and OETC grids were interconnected with a 132kV Over head transmission line linking Nahada 132kV substation at PDO's side to Nizwa 132kV sub-station at OETC's side. Since then the power exchange between PDO and OETC is driven by the natural impedances of the system and the frequency and power exchange is controlled by manually re-dispatching the generators. In light of the daily load profile and the forecasted Gulf Cooperation Council (GCC) states electrical interconnection, it is a great challenge for PDO and OETC grids operators to maintain the existing operation philosophy. The objective of this research is to investigate Automatic Generation Control (AGC) technology as a candidate to control the grid frequency and the power exchange between PDO and OETC grid. For this purpose, a dynamic power system model has been developed to represent PDO-OETC interconnected power system. The model has been validated using recorded data from the field which has warranted the requirement of refining the model. Novel approaches have been followed during the course of the model refining process which have reduced the modelling error to an acceptable limit. The refined model has then been used to assess the performance of different AGC control topologies. The recommended control topologies have been further improved using sophisticated control techniques like Linear Quadratic Regulator (LQR) and Fuzzy Logic (FL). Hybrid Fuzzy Logic Proportional Integral Derivative (FLPID) AGC controller has produced outstanding results. The FLPID AGC controller parameters have then been optimised using Multidimensional Unconstrained Nonlinear Minimization function (fminsearch) and Particle Swarm Optimisation (PSO) method. The PSO has been proved to be much superior to fminsearch function. The robustness of the LQR, the fminsearch optimized FLPID and the PSO FLPID optimized AGC controllers has been assessed. The LQR robustness found to be slightly better than the FLPID technique. However the FLPID supercedes the LQR due to the limited number of field feedback signals in comparison to the LQR. Finally, a qualitative assessment of the benefits of the ongoing GCC interconnection project on PDO and OETC has been done through modelling approach. The results proved that the GCC interconnection will bring considerable benefits to PDO and OETC but the interconnection capacity between PDO and OETC needs to be enhanced. However, the application of AGC on PDO and OETC will alleviate the PDO-OETC interconnection capacity enhancement imposed by the GCC interconnection.

List of contents

List of tables

Preface

The field of Automatic Generation Control (AGC) has been extensively explored by researchers during the last few decades. Due to the developing control technologies and the power sector in general, the field of AGC has always been the interest of many researchers. However most of the researchers have considered small sized power systems in their analysis and most of them are focused on developing competitive controller performance. Therefore the modelling process for AGC studies remained virtually the same as it was originally developed in the early seventies of the last century.

PDO and OETC are running the main interconnected power system networks in Oman. In the other hand, there are ongoing projects to interconnect all electrical networks of all the six member states of the Gulf Cooperation Council (GCC). There are advantages and challenges associated with the future GCC electrical interconnection. One of the challenges is the control of system frequency and power exchange. AGC is one of the potential candidates which can be considered to address the control issue of system frequency and power exchange.

The aspiration of this research is to investigate the implementation of AGC to a practical size power system and to explore new horizons in the modelling process.

Therefore, this report details the findings of a comprehensive case study of applying Automatic Generation Control (AGC) to the PDO-OETC interconnected power system. The investigation covers the modelling process and the AGC controller design aspects. The report also demonstrates the results of a qualitative assessment of the implication of the Gulf Countries Council (GCC) electrical interconnection project on PDO-OETC interconnected power system.

Acknowledgement

I would like to thank first and foremost my project supervisor Dr. Ian. G. French for his patience, care and guidance given to me throughout the duration of my project.

Special thanks to my family for the support and encouragement given to me to strive for my goals.

I would also thank my colleagues at Petroleum Development Oman for their encouragement and motivation. Special thanks go to the UIE department team headed by Mr. Saif Al-Sumry for their continuous support.

I would also thank Dr. Amer Al-Hinai from Sultan Qaboos University and Dr. Sekhar Patibanda from Tebodin & Partner for the fruitful discussions and support.

I would also thank Oman Electricity Transmission Company Load Dispatch Centre team and the Planning department team for their support.

I would also thank my cousin Waleed for his support and friendship.

Last but not least a special thanks to whomever that I have missed out and had helped me in one way or another.

Definitions

AAAC: All Aluminum Alloy Conductor

ACE: Area Control Error

AET: Absolute Error multiplied by Time

AGC: Automatic Generation Control

DLN: Dry Low NOx combustor

FL: Fuzzy Logic

FLPID: Fuzzy Logic Proportional Integral Derivative controller

GCC: Gulf Cooperation Council

GRC: Generation Rate Constraint

GTG: Gas Turbine Generator

HVDC: High Voltage Direct Current

Hz: Hertz

IAET: Integral of Absolute Error multiplied by Time

IPS: Integrated Power Station

LDC: Load Dispatch Centre

LQR: Linear Quadratic Regulator

MF: Membership Function

MVA: Mega Volt Ampere

MVAr: Mega Volt Ampere reactive

MW: Mega Watt

NERC: North American Electric Reliability Corporation

OETC: Oman Electricity Transmission Company

PDO: Petroleum Development Oman

PI: Proportional Integral controller

PID: Proportional Integral Derivative controller

PSO: Particle Swarm Optimisation method

SCADA: Supervisory Control And Data Acquisition

UAE: United Arab Emirates

UIE: Utility Infrastructure-Electrical department within PDO

Chapter 1: Introduction

Petroleum Development Oman (PDO) company owns and operates the largest industrial power system in the Sultanate of Oman. PDO owns all the power stations, transmission grid and the distribution network comprising its power system. The PDO power system is about 40 years old and is supplying all PDO's oil and gas fields.

PDO's power system got interconnected with Oman Electricity Transmission Company grid (OETC) in the year 2001. OETC operates the government power system which consists of independent power producers and the transmission grid. The two power systems are interconnected with a 132kV transmission line between Nahada 132kV substation (PDO) and Nizwa 132kV substation (OETC). The power exchange is driven naturally by the system impedances. Therefore the scheduled power exchange is controlled through manual generation dispatch but there is no automatic control. With the continuously changing operating points, it has always been difficult to maintain the scheduled power exchange. From this perspective, the feasibility of Automatic Generation Control (AGC) becomes apparent. In this research, the Automatic Generation Control (AGC) of PDO-OETC interconnected power systems will be studied in detail. This work can be regarded as a case study which will touch most of the practical aspects of AGC modelling and application.

Furthermore, the Gulf Cooperation Council (GCC) states that the electrical interconnection project is ongoing and is being commissioned in stages. Once the project is substantially completed, all six member states (Kingdom of Saudi Arabia, Kuwait, Kingdom of Bahrain, Qatar, United Arab Emirates and the Sultanate of Oman) electrical networks will be fully integrated as one electrical grid. The GCC electrical interconnection will address its own challenges in operating the individual states power systems. This study will focus on the dynamic and steady state implications of the GCC interconnection on PDO and OETC power systems.

The layout of this report is divided into fifteen chapters. Chapter one comprises this introduction. Chapter two discusses the aims and objectives of this study. Chapter three reviews the literature published in the field under study including Automatic Generation Control and GCC interconnection. Chapter four illustrates the modelling approach of PDO and OETC interconnection power systems from its basic principles. Chapter five illustrates the different approaches followed in testing the developed PDO and OETC power systems model and discusses the main features of the model. Chapter six discusses two different approaches in validating the developed PDO and OETC power systems model, the

mathematical validation approach and the validation against real life scenarios logs. Chapter seven discusses the model refining approaches followed to minimise the model error considering different practical concepts. This chapter has also discussed the key model parameters fine tuning process using the commonly used "fminsearch" MATLAB function. Chapter eight illustrates the approach followed in developing the state space representation of the developed PDO and OETC power systems model. The design of PDO and OETC power systems Automatic Generation Control (AGC) has been discussed in depth in Chapter nine. Fifteen AGC control topologies have been designed and simulated and the best AGC control topologies have been recommended for both PDO and OETC power systems. Chapter ten goes one step further and illustrates the design of certain AGC control topologies using Linear Quadratic Regulator method and compares the results with the ones which have been obtained in chapter nine. Chapter eleven goes a further step forward and illustrates the design of PDO and OETC AGC control using the Fuzzy Logic theory. The results have been compared with the previously obtained results in chapter nine and ten. The PDO and OETC AGC control performance using the previously adopted Fuzzy Logic control theory has been further optimised in chapter twelve using different optimisation methods like fminsearch MATLAB function and the Particle Swarm Optimisation Method (PSO). Certain AGC performance guidelines have been adopted for the optimisation process and the performance of the optimised AGC controllers has been compared with the results obtained in chapter nine, ten and eleven. The robustness of the PDO and OETC AGC controllers to the modelling process uncertainties has been verified in chapter thirteen. Chapter fourteen of this report discusses the implications of the GCC interconnection on PDO and OETC power systems dynamic and steady state performance with and without the application of AGC control. Chapter fifteen acts as a summary of the findings of the whole study and has identified a scope of work which can be considered in future studies. In light of the data sourcing difficulties, every effort has been made to make reasonable practical assumptions where deemed necessary. The practical recommendations out of this study can be used by PDO and OETC power systems engineers.

Based on the results of this research, two conference papers have been published so far and are given in Appendix 1.

Chapter 2: Aims and Objectives

The research topic in hand is very wide and the focus of the study is to implement the very well established Automatic Generation Control theory to PDO-OETC electrical power system and to explore new horizons in the modelling approach.

The following summarises the objectives of this research:

- To model PDO and OETC power systems for Automatic Generation Control study
- To investigate the response of the model to step load changes.
- To investigate the effect of model uncertainties and non-linearity on the general model response characteristics.
- To investigate new horizons in modelling for Automatic Generation Control studies.
- To investigate the effect of practical generation constraints by incorporating these practical limitations into the model.
- To validate the developed PDO-OETC power system model against real life data
- To explore the suitable Automatic Generation Control topologies
- To design Automatic Generation Controller which can accommodate all model uncertainties and non-linearity.
- To optimise the controller performance to suite both PDO and OETC control standards considering the nature of each system.
- To assess the robustness of the developed controllers
- To study the impact of GCC interconnection on both PDO and OETC power systems.
- To assess the performance of PDO-OETC AGC in light of the GCC interconnection

Chapter 3: Literature review

Power supply frequency is considered as a key factor of power supply quality. Speed of induction and synchronous motors are dependant on the supply frequency. A deviation in the supply frequency will affect the speed of these motors and consequently, the performance of the process in which they are installed. Therefore it is extremely important to maintain the supply frequency at its nominal value. And in case of frequency deviation due to transient conditions, nominal frequency must be restored in an acceptable period of time. Power systems regulators usually specify performance indices which must be maintained by the power systems operators.

Frequency deviations are caused by an unbalance between the output power of the generators and the load demand. This power mismatch will be compensated by a change in the rotational kinetic energy of the generators ending up with a deviation in the generators speed and hence the frequency. The general idea of controlling the frequency is to maintain the balance between the generated power and the consumed power. Since the existence of alternating current power systems, different philosophies have been applied to maintain the supply frequency. The most common control modes are the Isochronous control, Droop control and Automatic Generation Control. In the Isochronous control mode, a big generator will be assigned the task of maintaining the frequency and the rest of generators will be running at constant power output. In the Droop control mode, all generators will respond to the frequency deviation. Automatic Generation Control (AGC) is achieved by adding a supervisory control loop to the Droop control loop in order to achieve better performance. The main aim of AGC is to maintain zero steady state frequency deviation and to track the load demands.

AGC has been around for the past few decades and it came into practical applications in many power systems around the world. AGC becomes particularly useful in interconnected power systems as it can control the power exchange between the neighbouring systems and enhances the overall system stability. The interest in AGC is growing up rapidly due to the interest in interconnected power systems.

Modelling of power systems will be associated with different types of uncertainties due to the continuously changing parameters and characteristics, load fluctuations and modelling errors (Shayeghi and Shayanfar, 2006; Ali and Abd-Elazim, 2011). Moreover, power system parameters are a function of the operating points (Karnavas and Papadopoulos, 2002) and these points do change continuously due to the daily load variation and generation scheduling.

Conventionally, Proportional Integral (PI) controllers have been adopted to solve the AGC problem (Oysal, 2005). The PI controller is successful in achieving a zero steady state frequency deviation. However, due to the non-linear power systems, PI controller has a poor dynamic response (Karnavas and Papadopoulos, 2002).

Many of the published literature have proposed a number of control strategies to improve the AGC performance. Some researchers focused on utilising better tuning methods to tune a PID based AGC like Maximum Peak Resonance Specification (MPRS) method (Khodabakhshian and Hooshmand, 2010) and Particle Swarm Optimisation method (Jadhav and Vadirajacharya, 2012). In some of the literature, optimal control techniques (Azzam, 1999; Elgerd and Fosha [(2)], 1970) and variable structure control (Bengiamin and Chan, 1982) were proposed to solve the AGC problem and have shown a robust control results. However they are based on state feedback which makes it very difficult to implement because information about the states are either not available or difficult to obtain (Shayeghi et al [(2)], 2006).

A significant number of the published papers attempted to apply the fuzzy logic controllers to AGC (Karnavas and Papadopoulos, 2002; Shayeghi et al [(2)], 2006; Shayeghi et al [(1)], 2007; Güzelkaya and Eksin, 2004; Çam, 2007; Çam and Kocaarslan [(1)], 2005; Demiroren and Yesil, 2004; Lee et al, 2006; El-Sherbiny et al, 2002; Feliachi and Rerkpreedapong, 2005; Kocaarslan and Çam [(3)], 2005; Çam and Kocaarslan [(2)], 2005; Chang and Fu, 1997; Ghoshal and Goswami, 2003; Ghoshal [(1)], 2004; Ghoshal [(2)], 2004). Since fuzzy logic controllers are good in dealing with complicated, non-linear, indefinite and time-variant systems (Çam and Kocaarslan [(2)], 2005), they seem to be feasible for the AGC. In the published literature, many fuzzy logic arrangements were proposed like the basic PI & PID fuzzy controllers (Demiroren and Yesil, 2004), self tuning & Fuzzy gain scheduling (Yesil et al, 2004; Çam, 2007; Çam and Kocaarslan [(1)], 2005; Feliachi and Rerkpreedapong, 2005; Kocaarslan and Çam [(3)], 2005; Çam and Kocaarslan [(2)], 2005; Chang and Fu, 1997) and multi-stage fuzzy controller (Shayeghi et al [(2)], 2006; Shayeghi et al [(1)], 2007; Sudha and Santhi, 2011).

Artificial Neural Networks (ANN) controllers were also used by some researchers to solve the AGC problem (Shayeghi and Shayanfar, 2006; Shayeghi et al [(3)], 2007; Hemeida, 2005). The merit of ANN is that it can deal with uncertain system models and parameters making it quite suitable for power systems applications. The merits of combining ANN and Fuzzy logic for AGC controllers has also been explored by researchers (Khuntia and Panda, 2012). However, ANN needs some recorded data from the field for the training purpose which again imposes some difficulties in its practical applications.

Genetic algorithm is also used by some researchers (Ghoshal and Goswami, 2003; Ghoshal, 2004) to calculate the initial controller gains in cooperation with fuzzy logic controllers.

It became obvious requirement that AGC controllers must be robust to cater for system non-linearity and uncertainties and decentralised to reduce the required signals from the field.

The effects of the generating units' limitations received a considerable attention by the researchers in the AGC filed. Generation rate constraint and governors dead band have been modelled by some researchers (Shayeghi et al [(2)], 2006; Yesil et al, 2004; Demiroren and Yesil, 2004; El-Sherbiny et al, 2002) in an effort to eliminate modelling errors.

The power market in some countries has been restructured from the vertical hierarchy to the bilateral contracts environment where distribution companies can make direct contracts with generation companies elsewhere in the grid (Shayeghi et al [(2)], 2006). This mode of operation puts more burdens on the grid operators. Some work has been done to use the traditional AGC with some modification to operate the new deregulated power system environment (Shayeghi et al [(2)], 2006; Shayeghi et al [(3)], 2007; Bevrani et al, 2004). The possible bilateral contracts are represented by introducing the concept of an augmented generation participation matrix which represents all possible contracts between generation and distribution companies (Shayeghi et al [(2)], 2006; Rakhshani and Sadeh, 2010). The effects of the possible contracts are then treated as a set of new input disturbances (Shayeghi et al [(3)], 2007).

Almost all the published papers have considered simple power system models with few control areas and generators for the analysis. The general idea can then be applied to any specific power system. However the scale of the problem can be better quantified by using practical size power systems models.

The Gulf Cooperation Council (GCC) states, Kingdom of Saudi Arabia, Sultanate of Oman, United Arab Emirates, State of Qatar, State of Kuwait and Kingdom of Bahrain, have established the GCC Electrical Interconnection Authority in July 2001 aiming for fully integrated electrical infrastructure within the GCC states. Most of researchers in the field of GCC electrical interconnection have studied the GCC interconnection from its economics and viability point of view (Konstantinos et al, 2007; Al-Asaad, 2009; Al-Alawi, 1999). Less attention was given by the researchers to the technical challenges like the power system dynamics and power exchange, a gap which will be filled by this study.

Chapter 4: Model Development

4.1. Introduction

This part of the report demonstrates the power system modelling approach followed to model PDO and OETC electrical power systems. The modelling process is kept fit for purpose to produce a reasonably sized model which can be used to study and analyse PDO and OETC power systems in order to achieve the objectives of this research project.

For example, modelling of generators prime movers can be a very complicated task due to the complexity of these units. In general, full thermodynamic or hydrodynamic models development leads to a computationally expensive solution (Smith and Chen, 1993, p. 83). Often the level of complicity can be alleviated by making the model fit for purpose and by accepting a certain amount of errors. For Automatic Generation Control (AGC) studies a simplified model of prime movers can be used which leads to an acceptable accuracy of the input power variation to the generator (Smith and Chen, 1993, p. 83).

Moreover, there are significant difficulties and challenges to get "name plate" data for all installed equipments to be modelled. Instead, realistic assumptions have been made throughout the modelling process based on information about similar installations or commonly used figures in international journals and text books.

4.2. Steam turbine modelling

There are different types of steam turbines installations. Steam turbine can be either tandem-compound or cross-compound depending on the number of shafts it has (KUNDUR, 1994, p. 418). Tandem-compound turbine has all turbines sections on a single shaft driving a single generator (KUNDUR, 1994, p. 418). Cross-compound turbine has two shafts each with its turbine's sections driving two generators each connected to a different shaft (KUNDUR, 1994, p. 418). The cross-compound steam turbines are of better efficiency but they are rarely used because they are expensive. Tandem-compound is commonly used and can be of reheating or non-reheating steam cycle (KUNDUR, 1994, pp. 418-421).

There are no steam turbines generators connected to PDO grid but there are steam turbines generators connected to OETC grid and are of non-reheating tandem-compound type. Therefore, in this study, the non-reheating tandem-compound steam turbines will only be modelled for steam turbines generators representation.

4.2.1. Principle of operation

In steam turbines installations, fuel is burned under a boiler, whereby steam is produced. The produced steam, at high pressure and speed, will hit the inclined blades of a turbine wheel and will drive it round. There will be a pressure drop across the first wheel blades, but enough is left to drive the second wheel and a third or fourth on the same shaft. Finally the steam is exhausted into a condenser, turned back into water and returned to the boiler to be heated and used again (Shell Global Solutions, 2007). Figure 4.1 shows the different stages of the operation cycle of a non reheat steam turbine. The available mechanical torque on the shaft can be used to drive the generator by coupling it to the main turbine shaft.

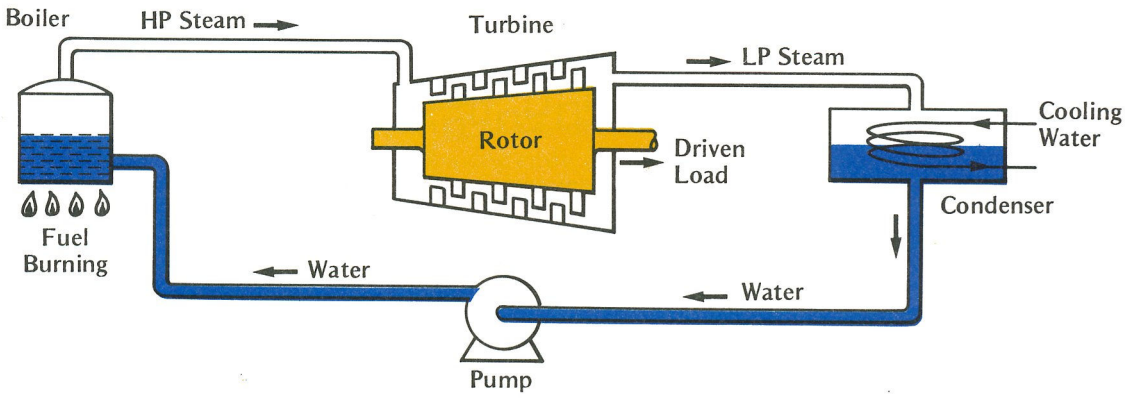

Figure 4.1: Non-reheating steam turbine system (Shell Global Solutions, 2007)

4.2.2. Modeling of steam turbines for dynamic studies

The real power generated by a steam turbine generator is controlled by means of the prime mover torque. This torque is affected by opening or closing the steam control valve of the steam turbine. The steam control valve is controlled by the governor which modulates the steam control valve opening in response to the turbine speed. A load change will affect the electrical torque and will cause a mismatch between the electrical torque and the machine mechanical torque. Hence the machine speed will change and the governor will respond accordingly.

Figure 4.2 depicts schematically the typical turbine control arrangement (Elgerd and Fosha [(1)], 1970; Elgerd and Fosha [(2)], 1970).

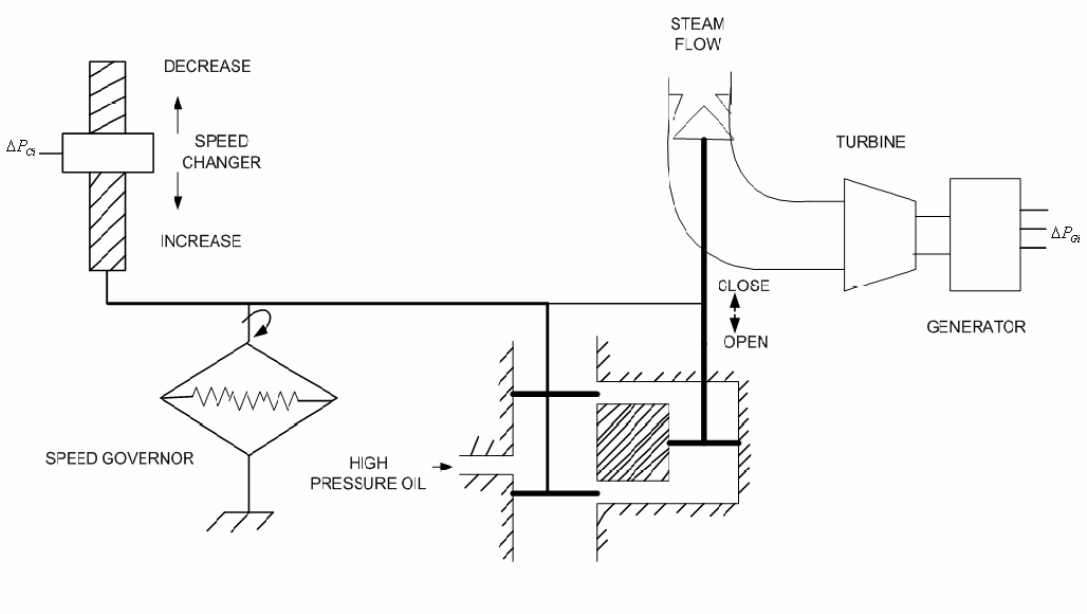

Figure 4.2: Typical turbine control arrangement.

The steam control valve housing is called the steam chest (KUNDUR, 1994, p. 425). A substantial amount of steam can be accommodated in the steam chest and the inlet piping to the high pressure section of the steam turbine (KUNDUR, 1994, p. 425). The response of the steam flow to a change in the control valve opening exhibits a time constant T_{CH} due to the charging time of the steam chest and the inlet piping (KUNDUR, 1994, p. 425). For AGC studies, a steam turbine can be represented by first order transfer function with a time constant T_{CH} (KUNDUR, 1994, p. 598).

The steam turbine governing system can be Mechanical-hydraulic, Electrohydraulic or Digital Electrohydraulic (KUNDUR, 1994, pp. 434-443). The governing system response exhibits a time constant T_G due to the response time of the overall governor. For dynamic studies, a steam turbine governing system can be represented by first order transfer function with a time constant T_G (KUNDUR, 1994, p. 589).

For AGC studies the non-reheating steam turbine and its governing system can be represented by two first order transfer functions as shown in Figure 4.3 (Elgerd and Fosha [(1)], 1970; Elgerd and Fosha [(2)], 1970; KUNDUR, 1994, pp. 589-598).

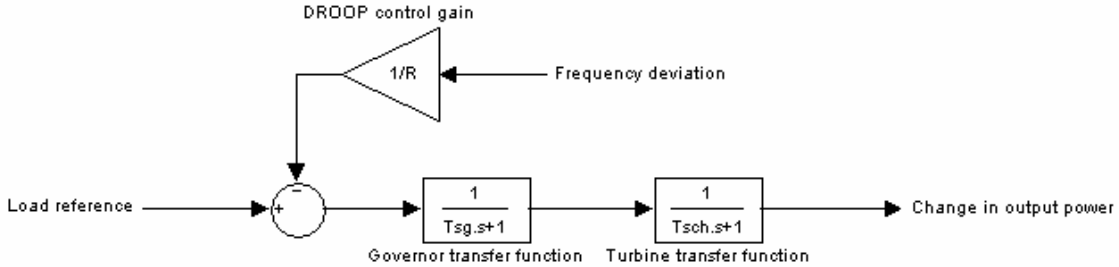

Figure 4.3: Steam turbine and governor model (Elgerd and Fosha [(1)], 1970; KUNDUR, 1994, pp. 593-598)

In Figure 4.3 Tg (in seconds) is the governor time constant, Tch (in seconds) is the charging time constant of the turbine and R (Hz/p.u MW) is the static speed droop of the turbine generator. To a very good approximation, the typical values of these constants are 0.3 s for Tgh and 0.2 s for Tg (KUNDUR, 1994, p. 598). In PDO and OETC, the droop control is set to 4% of the nominal frequency of 50Hz and hence:

$R = 0.04 \times 50Hz = 2Hz / puMW$

4.3. Gas turbine modelling

Gas turbines can be provided in one shaft or two shafts designs. In the two shaft design, the second shaft is used to drive a low pressure turbine that requires a low speed. However, in practice the single shaft is the most common one (Anderson and Fouda, 2003, p 514). All gas turbine generators sets at PDO and OETC are of the single shaft design.

4.3.1. Principle of operation

The principle of gas turbine is similar to that of the steam turbine except that there is no boiler or water. Instead, the fuel is burned in a combustion chamber where it produces a hot, high-pressure gas. The burned gas will expand causing a reaction on each row of blades on a rotor and will drive it round (Shell Global Solutions, 2007).

In order for the fuel to burn, oxygen is needed, and it must be at high pressure in order to enter the combustion chamber. Therefore an air compressor is fitted integrally with the turbine (Shell Global Solutions, 2007).The principle of the gas turbine is shown schematically in Figure 4.4.

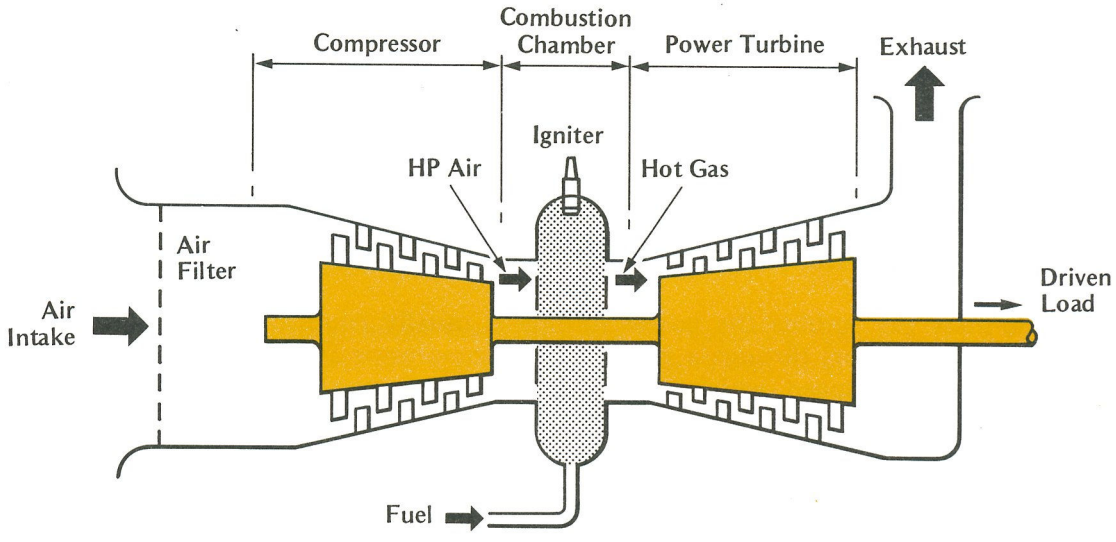

Figure 4.4: Single Shaft Gas Turbine Set

4.3.2. Modelling of gas turbine for dynamic studies

The amount of fuel flowing to the combustion chamber is controlled by the governor and hence controlling the output mechanical power on the shaft.

Modern electrohydraulic governors are used in all PDO and OETC power systems gas turbine generating units. The schematic of the electrohydraulic governor is shown in Figure 4.5. For gas turbine generators, the governor will sense the frequency deviation by comparing the turbine speed with the set speed and will actuate the Fuel Control Valve accordingly.

Studies of the system in Figure 4.5 revealed that the gas turbine and its governing system can be represented by three first order transfer functions (Smith and Chen, 1993, pp.121-122 & p. 221). One transfer function represents the governor lag time, the second transfer function represents the control valve lag time and the third transfer function represents the fuel charging characteristics. Figure 4.6 shows the dynamic model of gas turbine generators which will be used for this study. The same model is used by PDO for dynamic studies (Petroleum Development Oman [3], 2004). The governor time constant (Tg) is 0.05 s, the control valve time constant (Tc) is 0.05 s and the fuel system time constant (Tf) is 0.4s. The droop control is set to 4% of the nominal frequency of 50Hz and hence:

$R = 0.04 \times 50 = 2Hz / puMW$

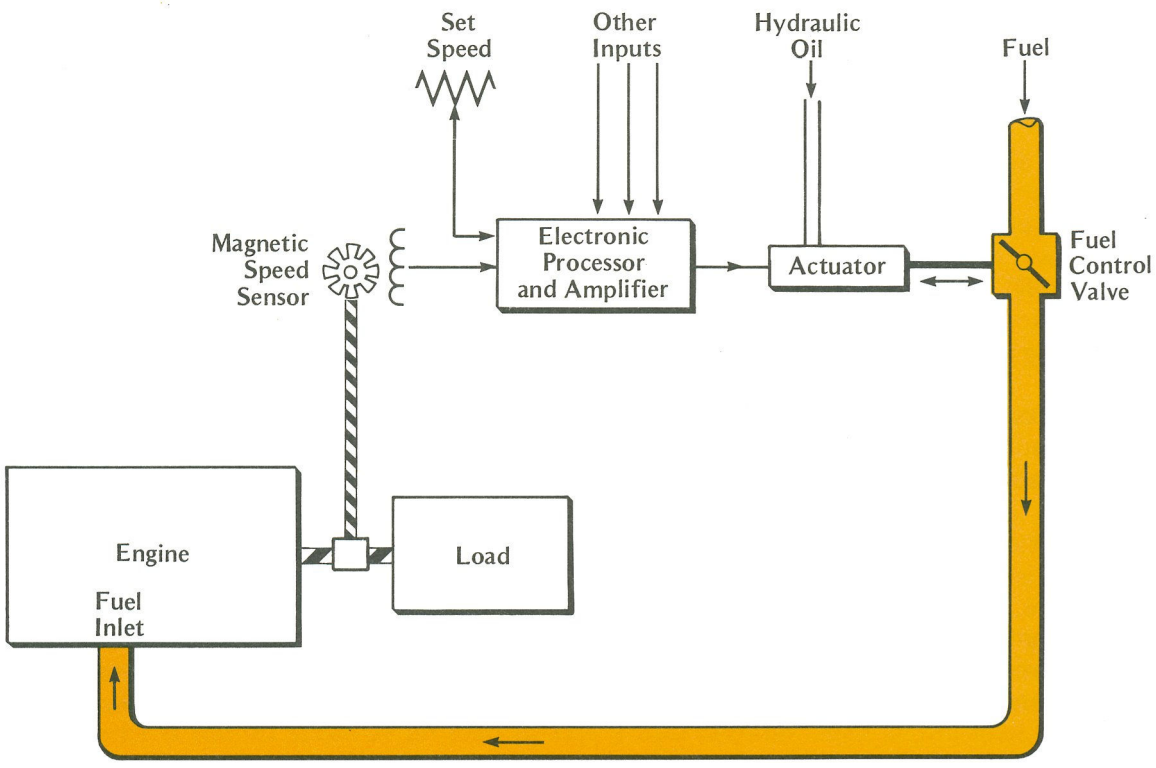

Figure 4.5: Electrohydraulic governor schematic (Shell Global Solutions, 2007)

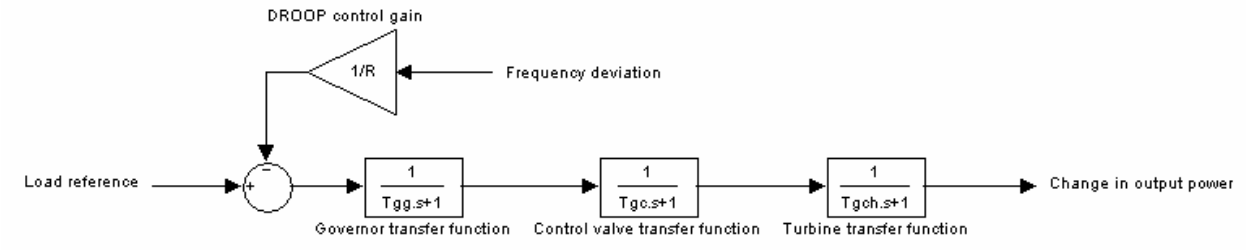

Figure 4.6: Governor/turbine model of gas turbine generator (Petroleum Development Oman [3], 2004)

4.4. Oman Power System Topology

Oman power systems consist of two major independently owned and operated power system grids, PDO grid and the government grid. The government grid is operated by Oman Electricity Transmission Company (OETC) with independent power producers connected to it. The main Load Dispatch Centre (LDC) of OETC is located in the capital of Oman "Muscat".

PDO owns and operates its own power system. The main control centre is Located in the interior of Oman "Yibal".

Both PDO and OETC grids operate at 132kV transmission level. OETC does also have overhead power transmission lines operating at 220kV level. PDO and OETC are interconnected through Nahada→Nizwa 132kV OHTL. The normal operation of the line is within ±10 MW and is providing extra security for both grids during emergencies and peak hours. PDO and OETC are not sharing the spinning reserve and each is maintaining N-1 security spinning reserve.

Both PDO and OETC grids are monitored and controlled via SCADA software. The exchange of power between PDO and OETC is controlled manually by the generation dispatch. Figure 4.7 shows the general topology of both PDO (in red) and OETC (in green) grids.

Figure 4.7: PDO and OETC grids

4.5. PDO power system model

PDO power system consists of thirteen power stations located near the load centres. These power stations are interconnected together with 132kV transmission network. It is a very practical feature of the system that generating units are distributed along the grid where supply security and voltage profile are enhanced.

PDO power system consists of different sizes of gas turbines driven generators which are Frame 5, Frame 6B, Frame 6A and Frame 9E. The MW rating of these turbines based on Oman normal summer ambient temperature is shown in Table 4.1.

Gas Turbine Generator	F5	F6B	F6A	F9E
Rating (MW)	15.2	28.2	51.6	96.2

Table 4.1: PDO Gas Turbine Generators rating

Table 4.2 shows the number of each type of Gas Turbine Generators installed in each power station of PDO.

Power station	F5	F6B	F6A	F9E
Lekhwair		2		
Yibal		2		
Fahud		1		
Saih Nihayda		1		
Qarn Alam			2	1
Saih Rawl IPS		2		
Suwaihat		1		
Mukhaiznah				2
Hubara		3		
Rima	2			
Nimr		2		
Marmul	3			
Haima West			1	

Table 4.2: PDO Gas Turbine generators locations and installed number.

Table 4.3 contains detailed information about PDO gas turbines generators. These information are extracted from the operation and maintenance manuals of the gas turbine generators. A 2000MVA base is assumed to be suitable base for the system and all subsequent calculations will be based on it. The per unit rating of each generator is calculated by dividing the rating of the generator by the base MVA. The constant of inertia is defined as the kinetic energy in watt-seconds at rated speed divided by the MVA base (KUNDUR, 1994, p. 128). The following Equation 4.1 is used to calculate the constant of inertia denoted by H in seconds (KUNDUR, 1994, p. 133):

$$H = 5.48\times10^{-9}\times\frac{J\times(RPM)^2}{MVA} \quad \text{---------- (4.1)}$$

Where J= moment of inertia in $kg.m^2$

RPM= rated speed

MVA= base MVA

Generator type	Per unit rating based on 2000MVA	Inertia ($kg.m^2$)	Speed (RPM)	Constant of inertia H (s)	Number installed	Total H (s)
F5	0.0076	1521	5121	0.109292	5	0.546461
F6B	0.0141	1892	5115	0.135632	14	1.898852
F6A	0.0258	8590	3000	0.211829	3	0.635488
F9E	0.0481	18521	3000	0.456728	3	1.370184
					Total accumulated H	4.450985

Table 4.3: Details of PDO Gas Turbine Generators

4.6. OETC power system model

OETC power system consists of seven major power stations interconnected by a 132kV transmission network. The load is distributed among the cities of Oman. However Muscat has the largest load demand since it is the capital of Oman. Minimal data are available about OETC power system to support this study; therefore some reasonable assumptions were made to accomplish this work.

OETC power system consists of different sizes of gas turbines driven generators and non-reheating tandem-compound steam turbines driven generators. The MW rating of these turbines based on Oman normal summer ambient temperature is shown in Table 4.4.

Turbine Generator	F5	F6B	F9E	ST1	ST2	ST3
Rating (MW)	15.2	28.2	96.2	10	40	220

Table 4.4: OETC generators rating

Table 4.5 shows the number of each type of generators installed in each power station connected to OETC grid.

Power station	F5	F6B	F9E	ST1	ST2	ST3
Ghubrah	9	2	2	3	3	
Rusail			6			
Wadi Jizzi	3	10				
Manah		3	2			
Al Kamil			3			
Barka			2			1
Sohar			3			1

Table 4.5: OETC generators locations and installed number

Due to non availability of data of steam turbines, ST1 steam turbine in Table 4.5 is assumed to be equivalent to F5 gas turbine in terms of inertia. However a steam turbine model will still be used to represent ST1. In the same manner, ST2 steam turbine is assumed to be equivalent to F6B gas turbine and ST3 steam turbine is equivalent to F9F gas turbine. Steam turbine models will be used to represent ST2 and ST3.

Table 4.6 contains detailed information about OETC generating units. A 2000MVA base is assumed to be suitable base for the system and all subsequent calculations will be based on it. The per unit rating of the each generator is calculated by dividing the rating of the generator by the base MVA .The constant of inertia H in Table 4.6 is calculated using Equation 4.1.

Generator type	Per units rating based on 2000MVA	Inertia	Speed	H (s)	Number installed	Total H (s)
F5	0.0076	1521	5121	0.109292	15	1.639384
F6B	0.0141	1892	5115	0.135632	18	2.441381
F9E	0.0481	18521	3000	0.456728	18	8.221101
F9F	0.11	35150	3000	0.866799	2	1.733598
Note ST1 is assumed to be equal to F5 ST2 is assumed to be equal to F6B ST3 is assumed to be equal to F9F					Total H of the system	14.03546

Table 4.6: Details of OETC Generators

4.7. PDO-OETC interconnected model for AGC studies

4.7.1. Modelling of control areas

The following analysis is based on the assumption that the electrical interconnection within each individual control area (PDO & OETC) (Figure 4.8) are so strong at least in relation to the ties between them, that the whole area can be characterized by a single frequency (Elgerd and Fosha [(1)], 1970).

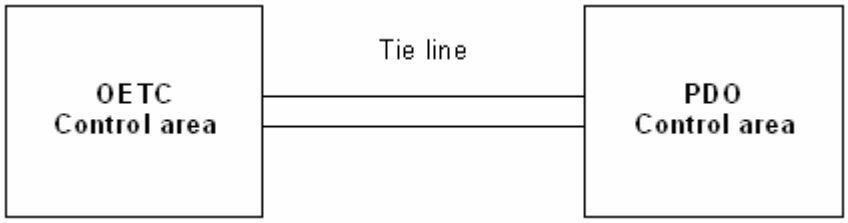

Figure 4.8: Interconnection of individual control areas.

Practically, when the system deviates from the constant nominal frequency, every bus voltage will experience its own angular velocity or frequency. Assuming electrical interconnection within a control area is so strong, this will result in all generators belonging to that area swing in unison. If this assumption is not permissible, then one must subdivide the area into sub-areas. Having said this assumption is valid for PDO and OETC grids, only two control areas will be considered, PDO and OETC. (Throughout this report,

Δ symbolises a perturbation of a first order magnitude. The superscript * indicates "nominal" value. Area i is a synonym of PDO and area v is a synonym of area OETC).

The net power surplus in the control area following a disturbance ΔP_D equals ΔP_G-ΔP_D MW, and this power will be absorbed by the system in three ways:

1) **By increasing the running generators' kinetic energy W_{kin} at the rate**;

$$\frac{d}{dt}W_{kin} = \frac{d}{dt}\left[W_{kin}^{*}\left(\frac{f}{f^*}\right)^2 \right]$$

$$\cong \frac{d}{dt}\left[W_{kin}^{*}\left(1+2\frac{\Delta f}{f^*}\right)\right]$$

$$= 2\frac{W_{kin}^{*}}{f^*}\frac{d}{dt}(\Delta f) \quad \text{---------- (4.2)}$$

2) By an increased load consumption: all typical loads (because of the dominance of motor load) experience an increase $D = \partial P_D / \partial f$ MW/Hz with speed or frequency. This D parameter can be found empirically (Elgerd and Fosha [(1)], 1970);

There are different types of loads supplied by PDO and OETC power systems. Static load characteristics are represented by the following equations (KUNDUR, 1994, p. 273):

$$P = P^o\left[p_1\overline{V}^2 + p_2\overline{V} + p_3\right](1 + D\Delta f) \text{----------(4.3)}$$

$$Q = Q^o\left[q_1\overline{V}^2 + q_2\overline{V} + q_3\right](1 + D\Delta f) \text{---------- (4.4)}$$

Where P is the new real power demand of load after the perturbation and Q is the reactive power. P^0 and Q^0 are respectively the nominal real and reactive power. V is the supply voltage and f is the supply frequency. The constants p_1 and q_1 account for constant impedance loads, p_2 and q_2 for constant current loads and p_3 and q_3 for constant power loads. The constant D is the damping factor and it counts for the percentage change in load power due to 1% change in supply frequency (Saadat, 2002, p. 530). D has different values in Equation 4.3 and Equation 4.4.

At this stage of this study we are only concerned about the real power P. Moreover, we assume that voltage remains unchanged when frequency changes. Equation 4.3 then reduces to:

$$P = P^o\left[p_1 + p_2 + p_3\right](1 + D\Delta f)$$
$$\because\ p_1 + p_2 + p_3 = 1$$
$$\therefore P = P^0(1 + D\Delta f) \qquad \text{----------(4.5)}$$

The typical value of D is 0 to 3 (KUNDUR, 1994, p. 273).

Kundur (1994, p. 311) suggested that residential load is having D=0.8 during summer and 1.0 during winter. On average we can assume that residential load is having D=0.9 through the year. Kundur (1994, p. 311) also suggested that industrial load is having D=2.6 through the year.

Considering PDO power system, 95% of the load is industrial and 5% is residential. This leads to the following calculation of D:

$$D = 5\% \times 0.9 + 95\% \times 2.6 = 2.515$$

Hence, the frequency damping factor for PDO power system under this study will be used as 2.515% change in load power for every 1% change in frequency. In this study, the nominal system frequency is 50Hz and a global 2000 MVA base is used, so the damping factor should be scaled to the 2000 MVA base and 50Hz nominal frequency. PDO power system load demand is about 540MW and using the base MVA, the frequency damping factor is calculated as below:

$$D = 2.515 \times \frac{540}{2000} \times \frac{1}{50} = 13.6 \times 10^{-3}\ puMW / Hz$$

Considering OETC power system, 20% of the load is industrial and 80% is residential. This leads to the following calculation of D:

$$D = 80\% \times 0.9 + 20\% \times 2.6 = 1.24$$

Hence, the frequency damping factor for OETC power system under this study will be used as 1.24% change in load power for every 1% change in frequency. OETC power system load demand is about 2400MW and using the system nominal frequency and the base MVA, the frequency damping factor is calculated as below:

$$D = 1.24 \times \frac{2400}{2000} \times \frac{1}{50} = 29.76 \times 10^{-3}\ puMW / Hz$$

Note that the per unit frequency damping factor (D) is dependant on the load type, size and time of the year, hence D changes as these parameters change. This adds uncertainty in the modelling process.

3) By increasing the export of power, via tie lines, with the total amount ΔP_{tie} MW defined positive out of the area.

In summary, the following power equilibrium equation applies to area i:

$$\Delta P_{Gi} - \Delta P_{Di} = 2\frac{W_{kini}^{*}}{f^{*}}\frac{d}{dt}(\Delta f_i) + D_i \Delta f_i + \Delta P_{tiei} \quad \text{----------(4.6)}$$

All terms have dimension MW. It is more practical to divide the equation by P_{ri}, the total rated area power expressed in MW. Since all area parameters are calculated in per unit base of 2000MVA, the term P_{ri} will equal to 2000MVA.

The equation then takes on to the form:

$$\Delta P_{Gi} - \Delta P_{Di} = \frac{2H_i}{f^{*}}\frac{d}{dt}(\Delta f_i) + D_i \Delta f_i + \Delta P_{tiei} \quad \text{----------(4.7)}$$

Where the inertia constant H_i is defined as:

$$H_i = \frac{W_{kini}^{*}}{P_{ri}} \text{ , MWs/MW or s.} \quad \text{----------(4.8)}$$

In equation (4.7) all powers are now in per unit of P_{ri} which equals the base MVA.

The differential equation (4.7) is linear with constant coefficients, and upon Laplace transformation it takes on the form:

$$[\Delta P_{Gi}(s) - \Delta P_{Di}(s) - \Delta P_{tiei}(s)]\frac{K_{pi}}{1 + sT_{pi}} = \Delta Fi(s) \quad \text{----------(4.9)}$$

Where for brevity, the following new parameters have been introduced:

$$T_{pi} = \frac{2H_i}{f^{*} \times D_i} \text{ , s} \quad \text{----------(4.10)}$$

$$K_{pi} = \frac{1}{D_i} \text{ , Hz/p.u.MW} \quad \text{----------(4.11)}$$

Upon defining the area transfer function:

$$G_{pi}(s) = \frac{K_{pi}}{1 + sT_{pi}} \quad \text{----------(4.12)}$$

The control area can be represented by the block diagram in Figure 4.9.

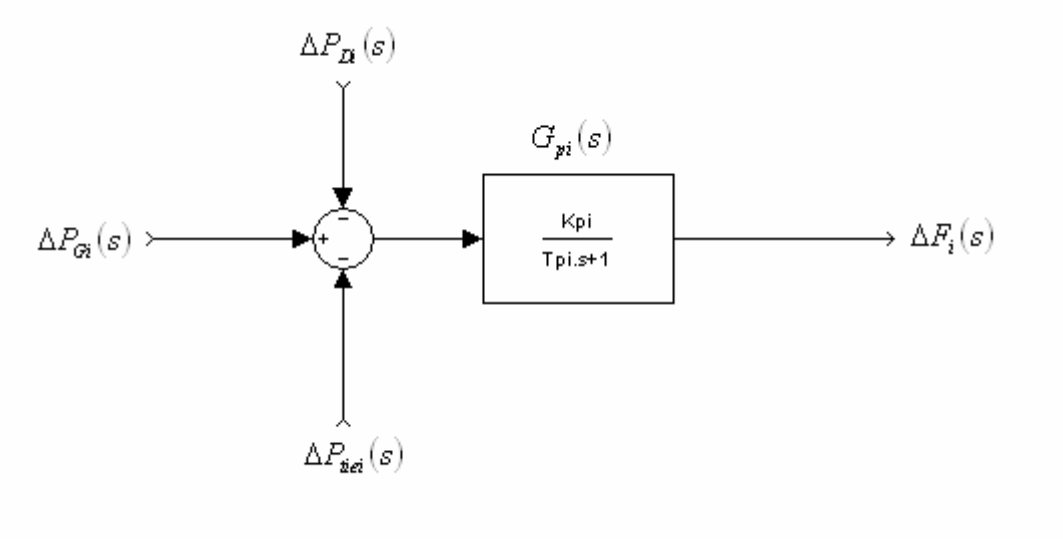

Figure 4.9: Control area block diagram.

Table 4.7 shows calculated parameters of PDO and OETC control areas:

Control area	Load MW	D (p.u.MW/Hz)	H (s)	Tp (s)	Kp (Hz/p.u.MW)
PDO	540	$13.6\text{x}10^{-3}$	4.450985	13.09113	73.53
OETC	2400	$29.76\text{x}10^{-3}$	14.03546	18.86487	33.6

Table 4.7: PDO and OETC control areas parameters.

Incremental Tie-Line Power ΔP_{tiei} : the total real power exported from area i, ΔP_{tiei}, equals the sum of all out flowing line powers, ΔP_{tieiv}, in the lines connecting area i with neighboring areas (Elgerd and Fosha [1], 1970), i.e.,

$$P_{tiei} = \sum_{v} P_{tieiv} \quad \text{----------(4.13)}$$

In our case, there is only one tie line between PDO and OETC which is Nahada-Nizwa 132kV interconnector.

If the line losses are neglected, the line power can be written in the form:

$$P_{tieiv} = \frac{|V_i||V_v|}{X_{iv}P_{ri}}\sin(\delta_i - \delta_v) \quad \text{----------(4.14)}$$

Where

$$V_i = |V_i|e^{j\delta i}$$

$$V_v = |V_v|e^{j\delta v}$$

are the terminal bus voltages of the line, and X_{iv} is its reactance. If the phase angles deviate from their nominal values δ_i^* and δ_v^* by the amounts $\Delta\delta_i$ and $\Delta\delta_v$, respectively, then we obtain:

$$\Delta P_{tieiv} = \frac{\partial P_{tieiv}}{\partial(\delta_i - \delta_v)}(\Delta\delta_i - \Delta\delta_v)$$ ----------(4.15)

Thus

$$\Delta P_{tieiv} = \frac{|V_i||V_v|}{X_{iv}P_{ri}}\cos(\delta_i^* - \delta_v^*)(\Delta\delta_i - \Delta\delta_v)$$ ----------(4.16)

the phase angle changes are related to the area frequency changes by

$$\Delta\delta_i = 2\pi\int \Delta f_i dt$$,

$$\Delta\delta_v = 2\pi\int \Delta f_v dt$$ ----------(4.17)

Upon combination of equations (4.16) and (4.17) one obtains:

$$\Delta P_{tieiv} = T_{iv}^*\left(\int \Delta f_i dt - \int \Delta f_v dt\right)$$ ----------(4.18)

Where:

$$T_{iv}^* = 2\pi\frac{|V_i||V_v|}{X_{iv}P_{ri}}\cos(\delta_i^* - \delta_v^*)$$, p.u.MW/Hz ----------(4.19)

is the synchronizing torque coefficient, or the electrical stiffness of the tie line. Note that it is expressed in per unit megawatts of the base MVA. Upon Laplace transformation one gets (Elgerd and Fosha [(1)], 1970):

$$\Delta P_{tieiv}(s) = \frac{T_{iv}^*}{s}[\Delta F_i(s) - \Delta F_v(s)]$$ ----------(4.20)

The total increment in exported power from area i (symbolised in block diagram in Figure 4.10) is finally obtained from equation (4.13):

$$\Delta P_{tiei}(s) = \frac{1}{s}\sum_v T_{iv}^*[\Delta F_i(s) - \Delta F_v(s)]$$ ----------(4.21)

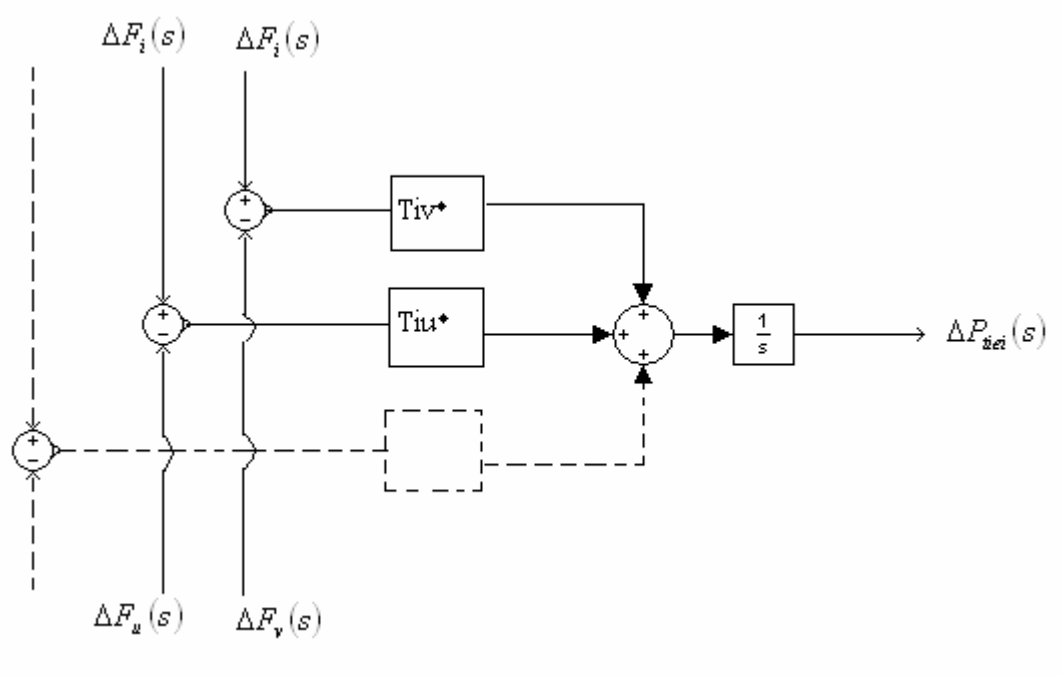

Figure 4.10: Incremental tie-line power out of area i.

In our study there are two areas involved, PDO and OETC, thus we have one synchronizing coefficient and Figure 4.10 reduces to Figure 4.11. Tiv is the sysnchronising torque coefficient between PDO and OETC power systems. ΔFi represents PDO frequency deviation and ΔFv represents OETC frequency deviation.

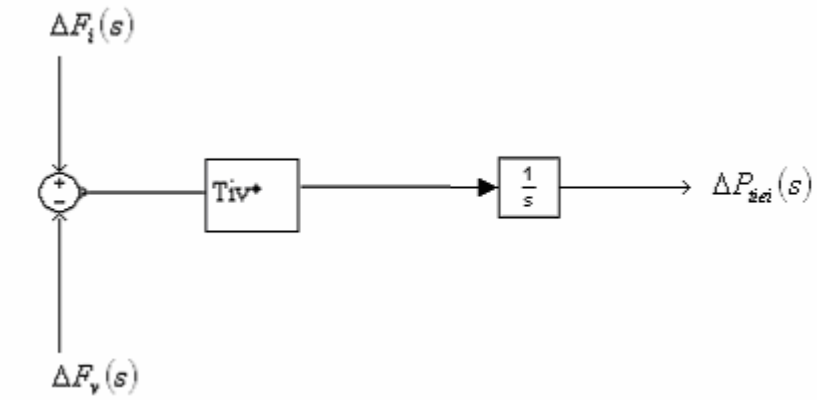

Figure 4.11: Tie line power between PDO and OETC

Referring to Equation 4.19, X_{iv} is calculated based on the impedances shown in Figure 4.12 where PDO and OETC systems are represented by a voltage source behind their respective network impedances and the tie line impedance. For typical power transmission lines, resistance is much smaller than reactance (KUNDUR, 1994, p. 204). Therefore lossless transmission line assumption yields acceptable results (Saadat, 2002, p.161). Hence, for AGC modelling the tie line between the control areas is represented by its reactance only (KUNDUR, 1994, p. 601; Saadat, 2002, p.545) and the resistance of the line is neglected (Bhatt et al, 2011). In Figure 4.12, X(OETC) is calculated from the short circuit level

impedance at Nizwa looking towards OETC grid. Similarly, X(PDO) is calculated from the short circuit level impedance at Nahada looking towards PDO grid. The mentioned short circuit level impedance covers the transmission network, generator transformer and the generator impedances.

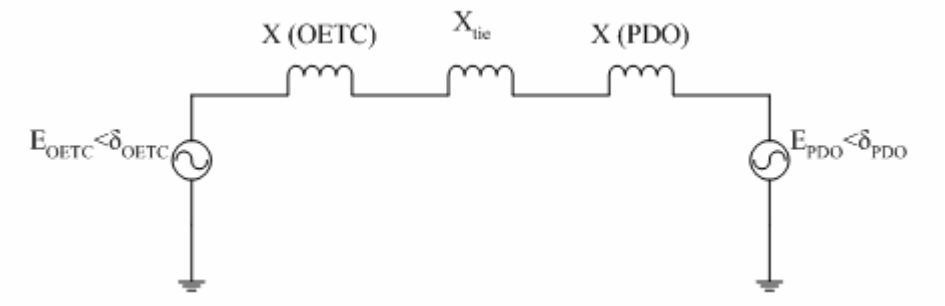

Figure 4.12: Impedance for calculating the synchronising coefficient

$E_{PDO}<\delta_{PDO}$: is the equivalent internal voltage source of PDO system

$E_{OETC}<\delta_{OETC}$: is the equivalent internal voltage source of OETC system

X_{tie}: is the tie line impedance

X(OETC): is the short circuit level impedance of OETC grid (without PDO) at Nizwa substation bus.

X(PDO): is the short circuit level impedance of PDO grid (without OETC) at Nahada substation bus.

Nizwa-Nahada 132kV line (the tie line) is constructed using AAAC (All Aluminum Alloy Conductor) with reactance of 0.2985Ω/km and the line is about 67km in length. The tie line impedance is then calculated as below:

$$Xtie = 0.2985 \times 67 \cong 20\Omega$$

The base impedance of the system is calculated as below:

$$Zbase = \frac{(132kV)^2}{2000MVA} = 8.712\Omega$$

The per unit tie line impedance is then calculated as below:

$$Xtie(pu) = \frac{Xtie(\Omega)}{Zbase(\Omega)} = \frac{20}{8.712} \cong 2.3 p.u.$$

From PDO document (Petroleum Development Oman LLC [(1)], 2006), the maximum short circuit level at Nizwa 132kV substation bus without PDO grid is 2286MVA. Using the 2000MVA base, the per unit impedance X(OETC) is calculated as below:

$$X(OETC) = \frac{2000MVA}{2286MVA} = 0.875 p.u.$$

From PDO document (Petroleum Development Oman LLC [1], 2006), the maximum short circuit level at Nahada 132kV substation bus without OETC grid is 571MVA. Using the 2000MVA base, the per unit impedance X(PDO) is calculated as below:

$$X(PDO) = \frac{2000MVA}{571MVA} = 3.503 p.u.$$

Back to Equation 4.19, the value of Xiv is the summation of Xtie, X(OETC) and X(PDO) and is calculated as below:

$$Xiv = Xtie + X(OETC) + X(PDO) = 2.3 + 0.875 + 3.503 = 6.678 p.u.$$

At a transmission level the real power (MW) flows from the leading voltage bus to the lagging voltage bus (Saadat, 2002, p. 546). For zero power exchange between two busses, their voltages angles should be equivalent. Considering Equation 4.19 and assuming zero power exchange between PDO and OETC power systems as the nominal condition and using per unit values of T_{iv} (KUNDUR, 1994, p. 602), the equation reduces to:

$$T_{iv}^{*} = 2\pi \frac{|V_i||V_v|}{X_{iv}} p.u.$$

Assuming internal voltages sources of the two systems are equivalent and equal to 1p.u, the synchronising torque coefficient between PDO and OETC systems is finally calculated as below:

$$T_{iv}^{*} = 2\pi \times \frac{1 \times 1}{6.678} \cong 0.94 p.uMW / Hz.$$

It is worth mentioning that synchronising coefficient is one source of non-linearity of the whole model because it depends on the system operating points like voltage values and angles which are continuously changing.

4.7.2. Overall PDO system model

Since PDO power system consists of thirteen power stations, each of them will be represented as subsystem in PDO model. Since there are no steam turbines installed at PDO, each subsystem in the model will contain its gas turbines model which was developed earlier as shown in Figure 4.6. For example, Lekhwair Power Station consists of two F6B gas turbine generators running in parallel as shown in Figure 4.13. The output of each turbine is multiplied by a factor (calculated earlier in Table 4.3) to counter for its rating in per unit.

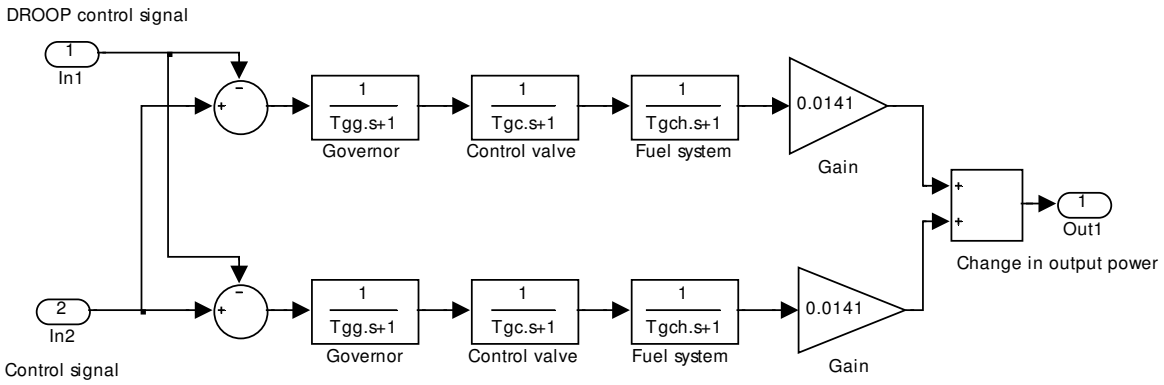

Figure 4.13: Lekhwair power station model

Upon combining the block diagrams of the Power Stations Subsystems and Figure 4.9, we obtain the overall PDO perturbation model shown in Figure 4.14.

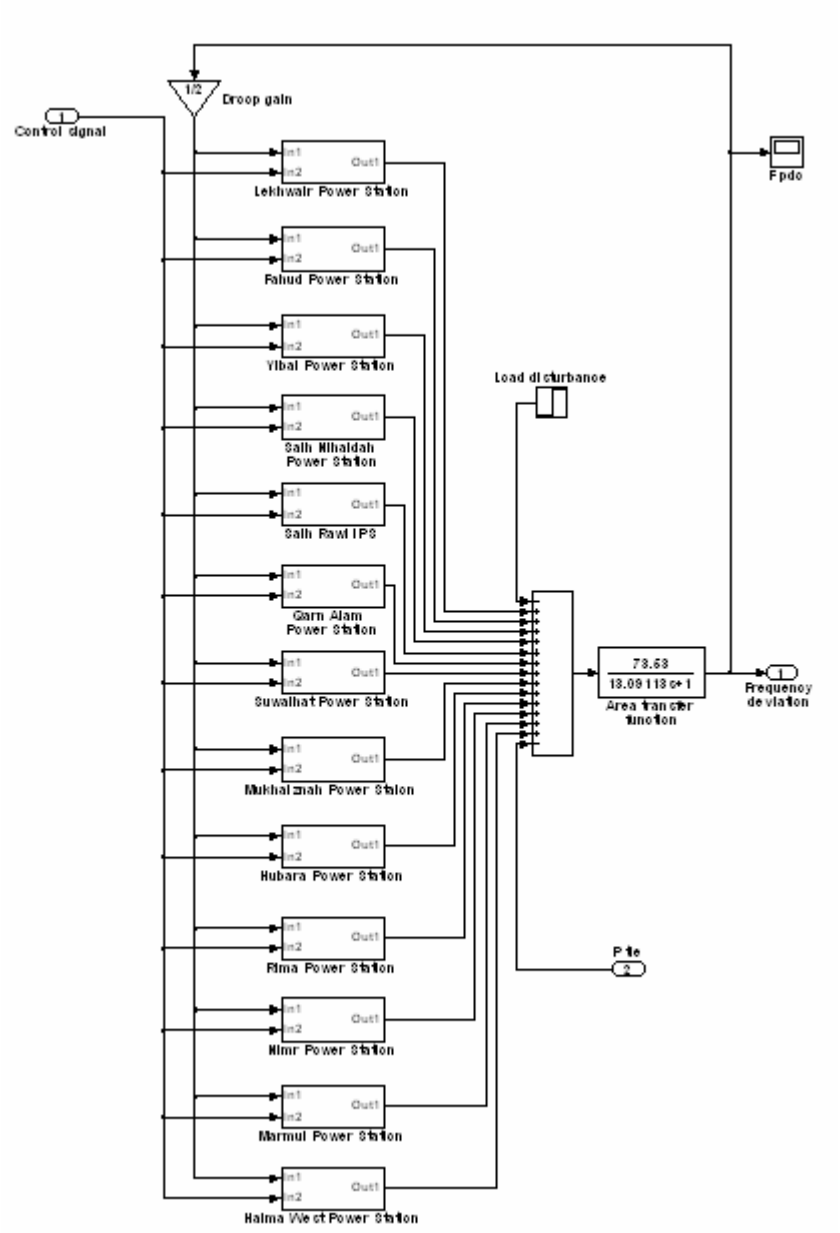

Figure 4.14: PDO power system perturbation model.

4.7.3. Overall OETC system model

OETC power system consists of seven power stations, so each of them will be represented as subsystem in OETC model. Since there are steam and gas turbines installed at OETC, each subsystem in the model will contain its steam and gas turbines models which were developed earlier in Figure 4.3 and Figure 4.6. For example, Barka Power Station consists of two F9E gas turbine generators and one steam turbine running in parallel as shown in Figure 4.15. The output of each turbine is multiplied by a factor (calculated earlier in Table 4.6) to counter for its rating in per unit.

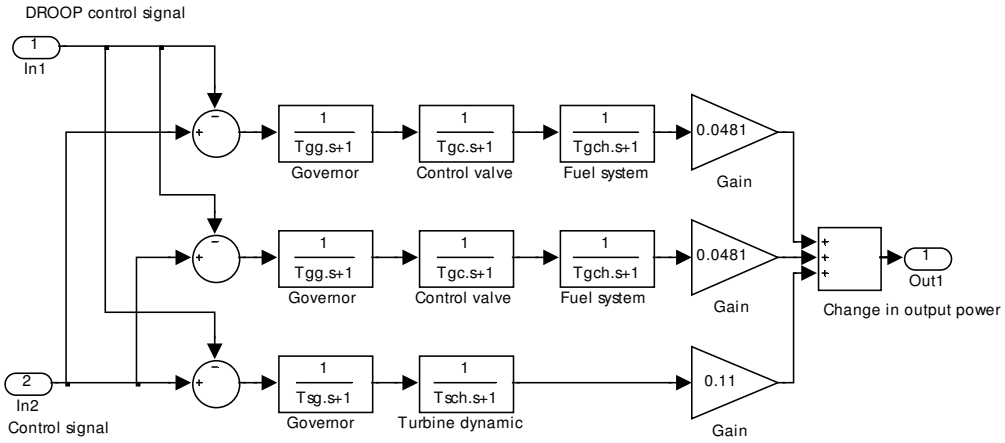

Figure 4.15: Barka power station model

Upon combining the block diagrams of the Power Stations Subsystems and Figure 4.9, we obtain the overall OETC perturbation model shown in Figure 4.16.

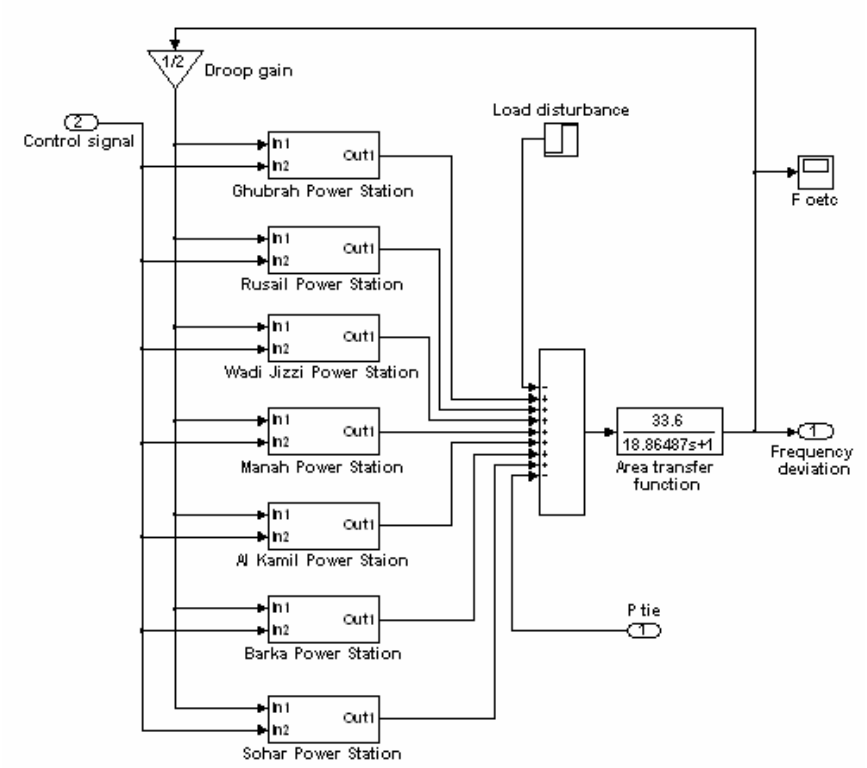

Figure 4.16: OETC power system perturbation model.

4.7.4. Overall perturbation model of PDO and OETC systems:

By masking Figure 4.14 and Figure 4.16 into subsystems and combining those with Figure 4.11, the overall perturbation model of PDO-OETC systems is achieved and is shown in Figure 4.17. This model will serve as the basis for further analysis.

Before proceeding we must explain the presence of the block constant a_{12}. This constant equals to the following:

$$a_{12} = -\frac{P_{rPDO}}{P_{rOETC}} \quad \text{----------(4.22)}$$

i.e. the negative ratio between the rated megawatts of PDO and OETC respectively.

In Figure 4.17, if the areas have different ratings, we clearly have the following relation between ΔP_{tiePDO} and $\Delta P_{tieOETC}$:

$$\Delta P_{tieOETC} = -\frac{P_{rPDO}}{P_{rOETC}} \Delta P_{tiePDO} = a_{12} \Delta P_{tiePDO} \quad \text{----------(4.23)}$$

In our case, both PDO and OETC control areas parameters has been calculated based on a common base MVA, hence a_{12} equals to -1.

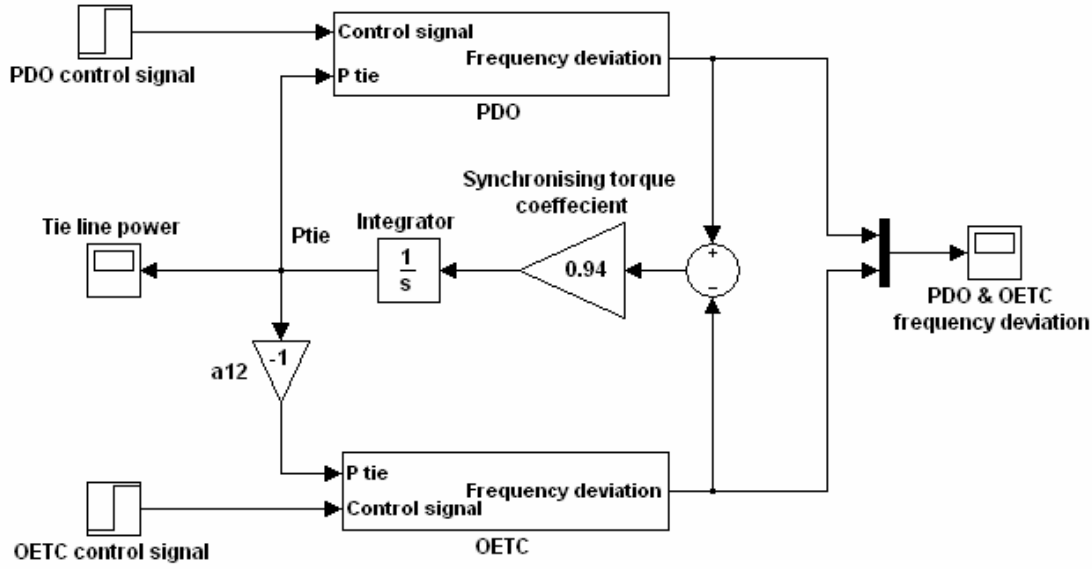

Figure 4.17: Block diagram of PDO-OETC perturbation model.

Table 4.8 summarisses the parameters values of the complete perturbation model of PDO and OETC system.

	Control area		Overall perturbation model	
	Tp	Kp	Tiv	a_{12}
PDO	13.09113	73.53	0.94	-1
OETC	18.86487	33.6		

Table 4.8: Overall perturbation model parameters.

Chapter 5: Model Testing

5.1. Testing Methodology

The complete PDO-OETC model went through step response test and parameters sensitivity test. Both tests are discussed in details in the following sections of the report.

The settling time of the responses is traditionally measured as the time taken to reach certain percentage of the final settling value, typically ±1% or ±2%. However since the power system frequency deviation is a very important indicator of the system healthiness, the typical percentage values could be erroneous as they could mean a very big value or too small value. Hence, for power system frequency deviation a certain value should be considered which will serve for either small or large load disturbances. From experience with PDO-OETC power system operation, a ±0.001Hz frequency deviation is an acceptable band. Therefore the settling time is always calculated as the time taken from the time frequency starts to deviate until it reaches ±0.001Hz of the steady state deviation value. Since, there are two transient frequencies, and one of them shall be selected for the settling time calculation, PDO frequency has been considered for settling time calculation. This approach of settling time calculation has been considered throughout the following chapters of the report.

5.1.1. Step response test

The step response test is aiming to investigate the overall model behaviour when subjected to step load disturbances. Step load disturbances are usually experienced when the load is peaking up instantaneously during summer due to the air conditioning requirement, when radial feeders trips due to protection operation and when process trip is initiated causing whole plant to stop. Another way of step disturbance is when generators trip which will have the same effect on the frequency as increasing loads. In this study three load disturbances values are used:

- 30MW: which is also approximately equivalent to F6B generator trip.
- 60MW: which is also approximately equivalent to F6A generator trip.
- 100MW: which is also approximately equivalent to F9E generator trip.

All these disturbances are applied one at a time at both PDO and OETC grids. The system frequency and the tie line power following the load disturbance are recorded.

5.1.2. Parameters sensitivity test

The parameters sensitivity test is aiming to investigate the sensitivity of the model to modelling uncertainties and errors associated with each parameter. Errors with the following model parameters are considered practically acceptable:

- Steam and Gas turbines parameters: ±10% error was used.
- PDO and OETC Load damping factor D: ±10% error was used.
- PDO and OETC systems inertia H: ±10% error was used.
- Synchronising Torque coefficient T_{iv}: ±20% error was used.

Error values were selected based on the extent of uncertainty and possible errors envisaged during the modelling process. A 30MW load disturbance at PDO was used to simulate the model. The plus error percentage and the minus error percentage were simulated separately each at a time.

5.2. Step response tests results

Following step load disturbance, each system (PDO and OETC) will have its own transient frequency. These two frequencies will then unify to one steady state frequency with the effect of the synchronising torque. For all step load disturbances tests, these two transient frequencies are shown together in one graph and the tie line power deviation is shown in a separate graph. In total, six step response tests have been carried out and the results are shown in Figures 5.1 to 5.12. A summary table of the graphical results is also shown in Table 5.1. In Table 5.1, the sign convention of the tie line power deviation is such that it is positive when the flow of power is from PDO towards OETC and negative when the flow of power is from OETC towards PDO. This sign convention is valid throughout the subsequent work.

The most important aspects of the simulation figures which might interest the reader are the steady state deviation, the settling time, the number of oscillations and the oscillations amplitudes.

1. 30MM step load disturbance at PDO grid:

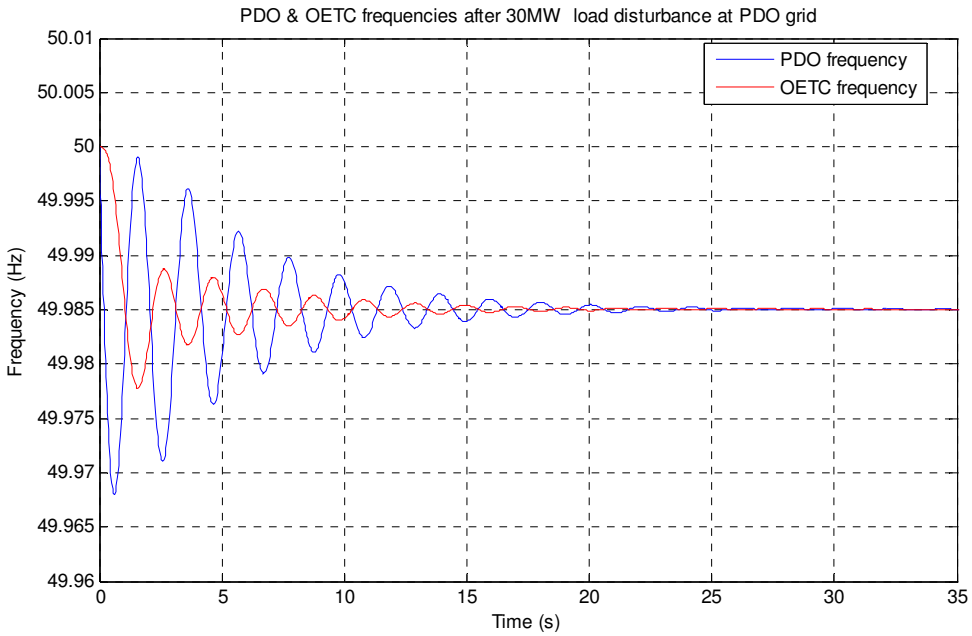

Figure 5.1: PDO and OETC frequencies following 30MW load disturbance at PDO grid

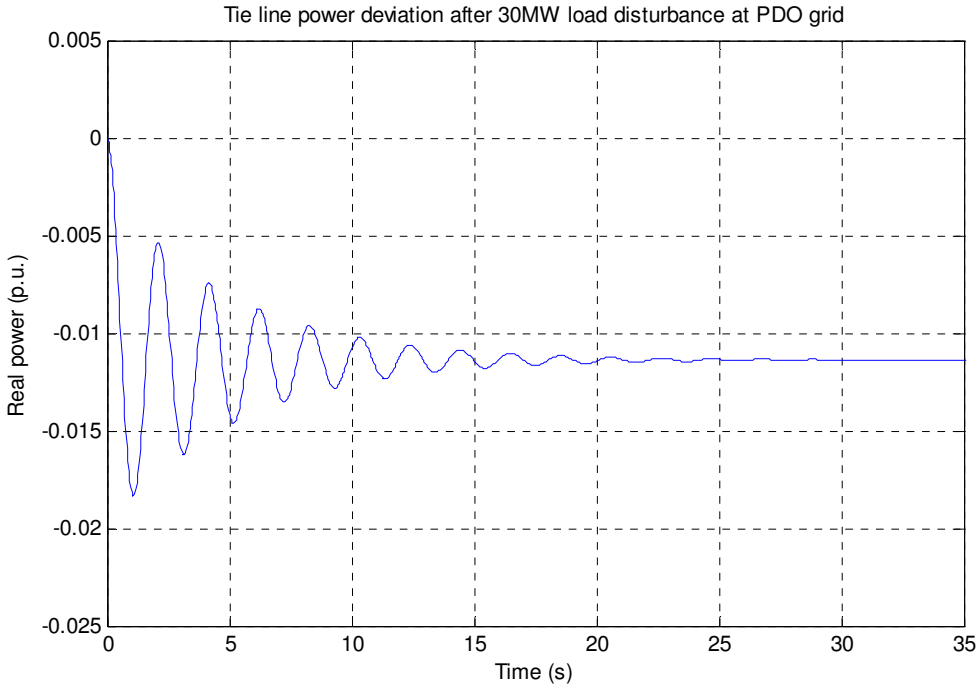

Figure 5.2: Tie line power following 30MW load disturbance at PDO grid

2. 30MW step load disturbance at OETC grid.

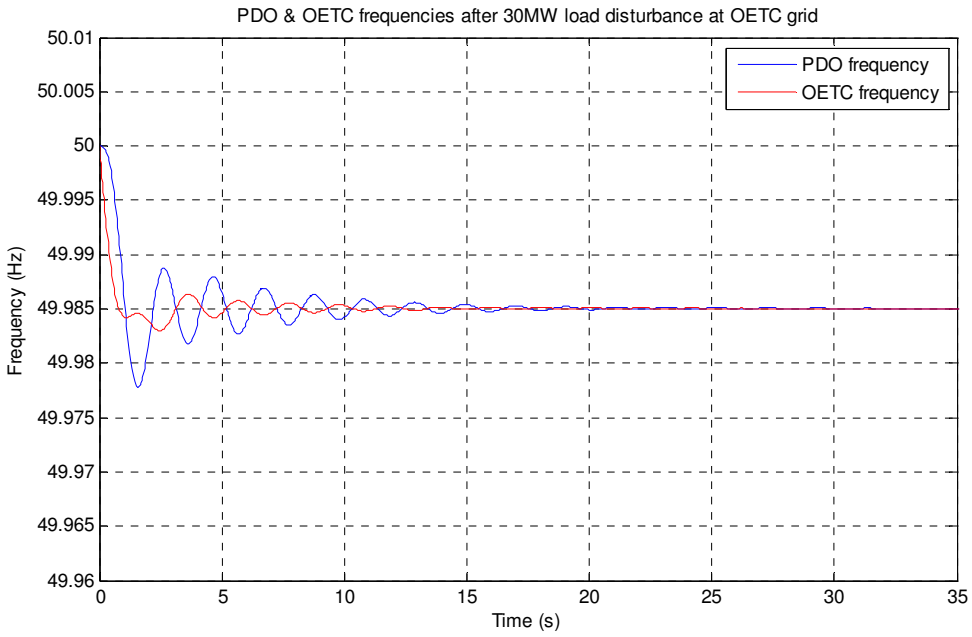

Figure 5.3: PDO and OETC frequencies following 30MW load disturbance at OETC grid

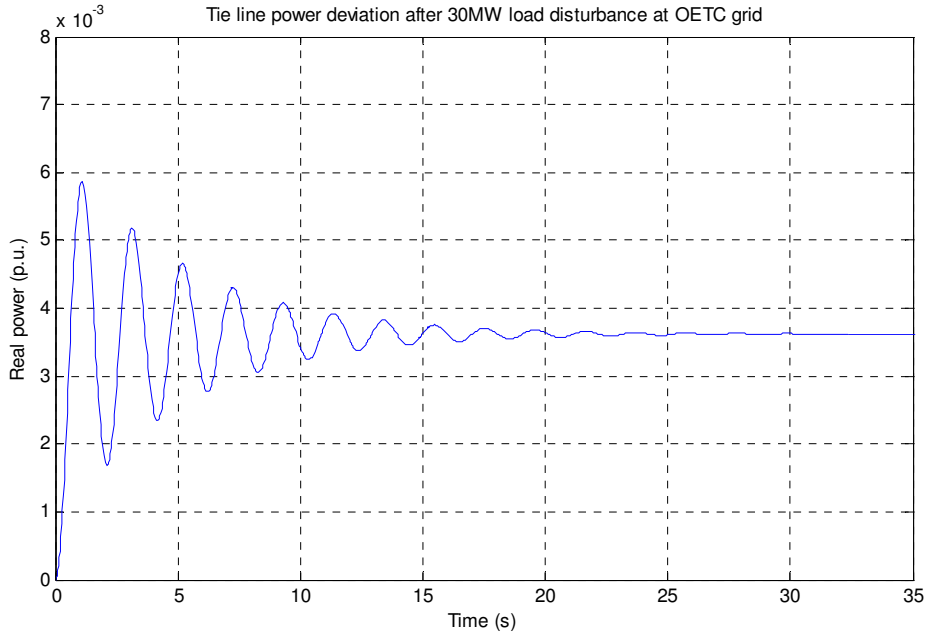

Figure 5.4: Tie line power following 30MW load disturbance at OETC grid

3. 60MW step load disturbance at PDO

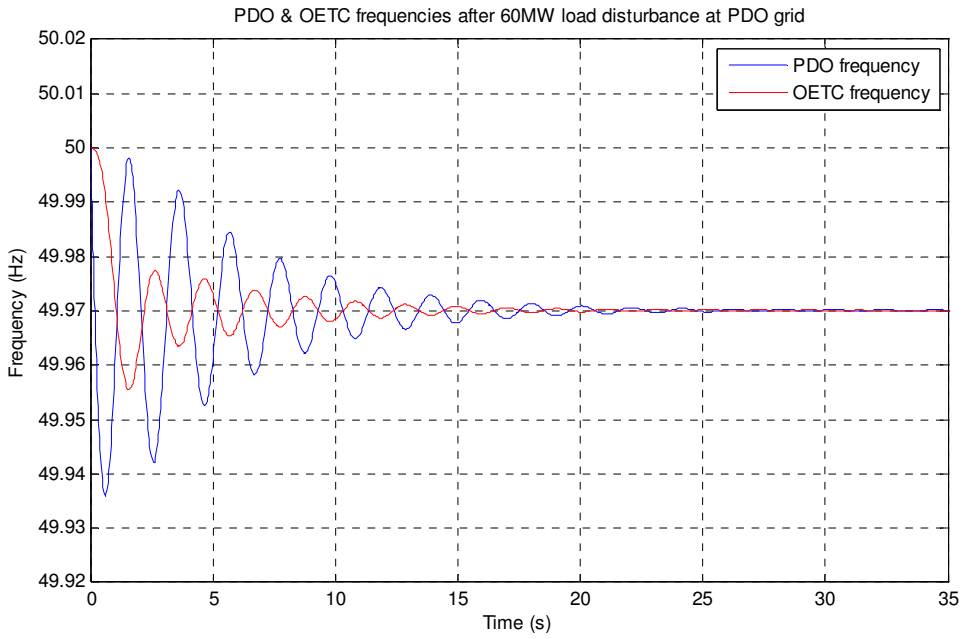

Figure 5.5: PDO and OETC frequencies following 60MW load disturbance at PDO grid

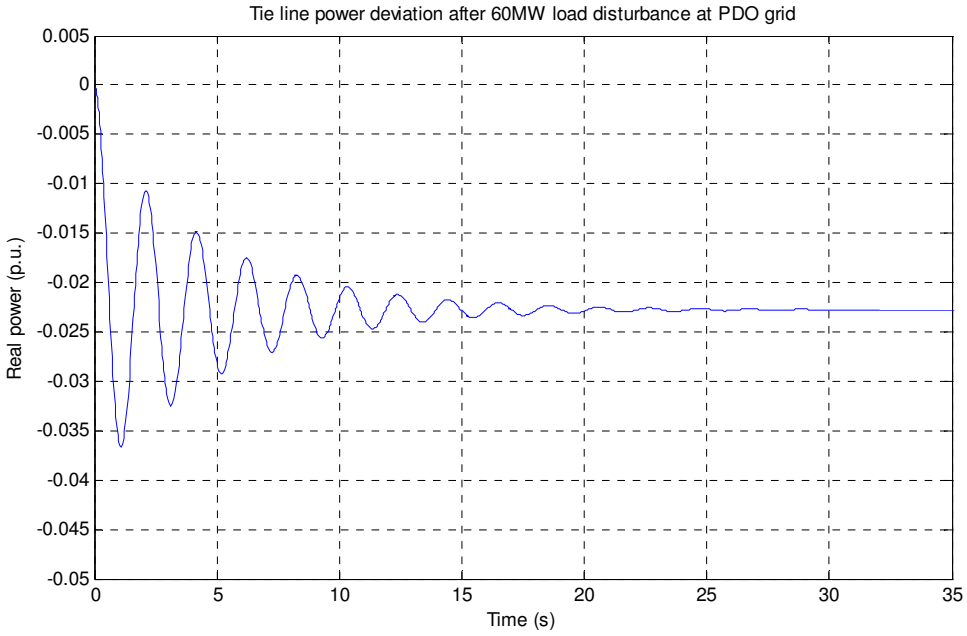

Figure 5.6: Tie line power following 60MW load disturbance at PDO grid

4. 60MW step load disturbance at OETC

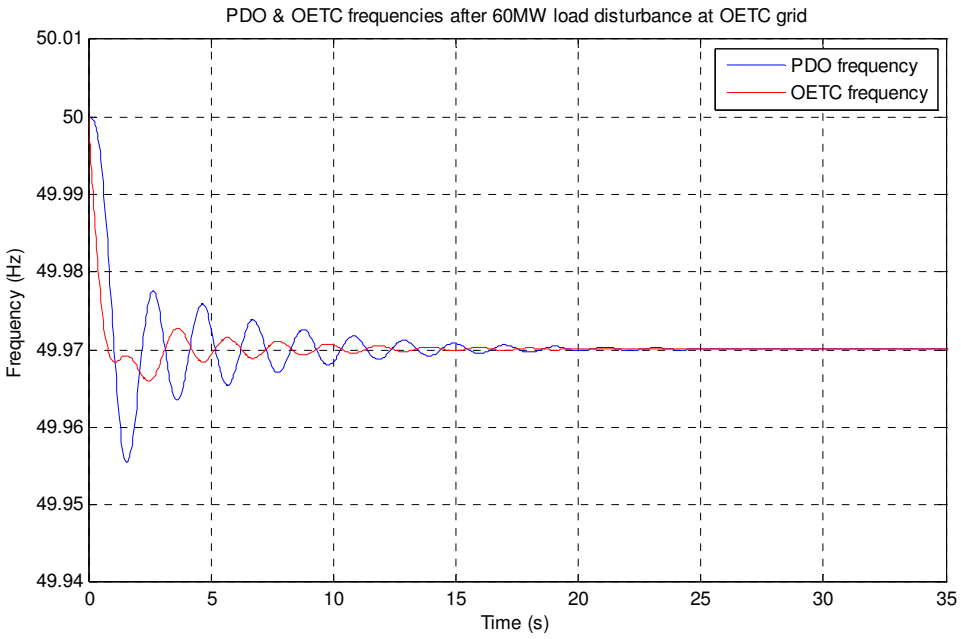

Figure 5.7: PDO and OETC frequencies following 60MW load disturbance at OETC grid

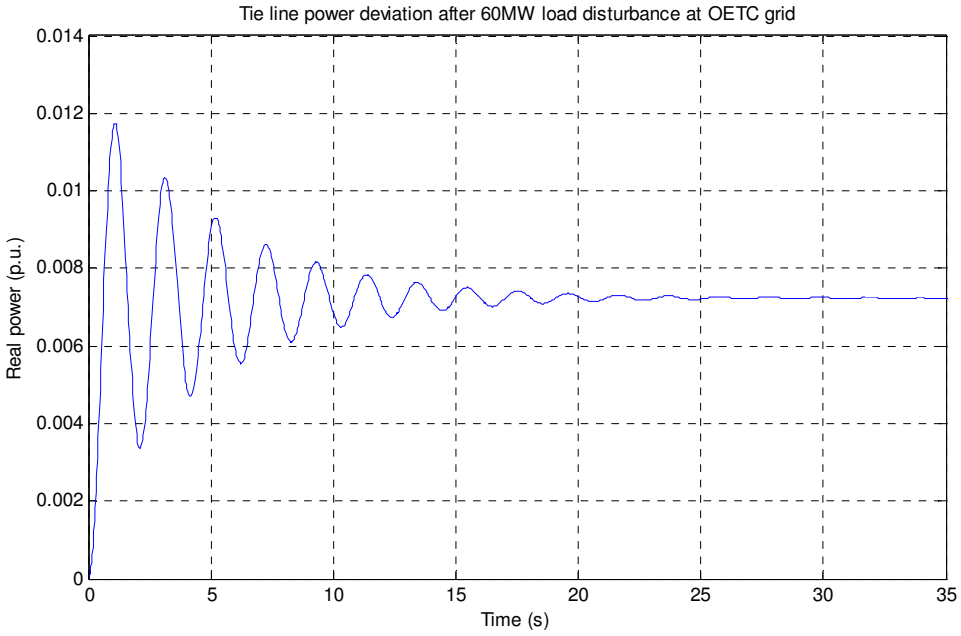

Figure 5.8: Tie line power following 60MW load disturbance at OETC grid

5. 100MW step load disturbance at PDO

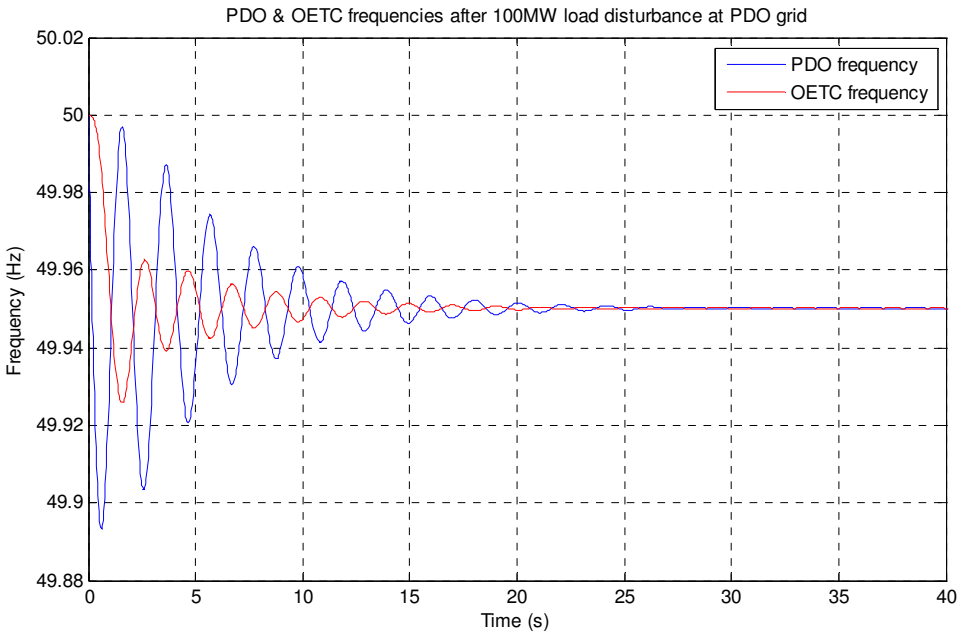

Figure 5.9: PDO and OETC frequencies following 100MW load disturbance at PDO grid

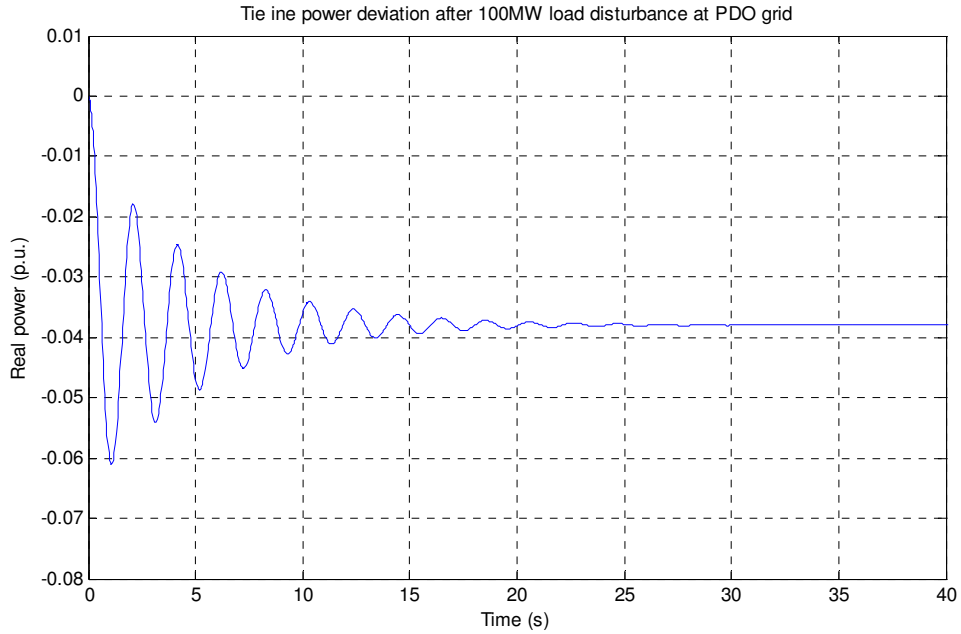

Figure 5.10: Tie line power following 100MW load disturbance at PDO grid

6. 100MW step load disturbance at OETC

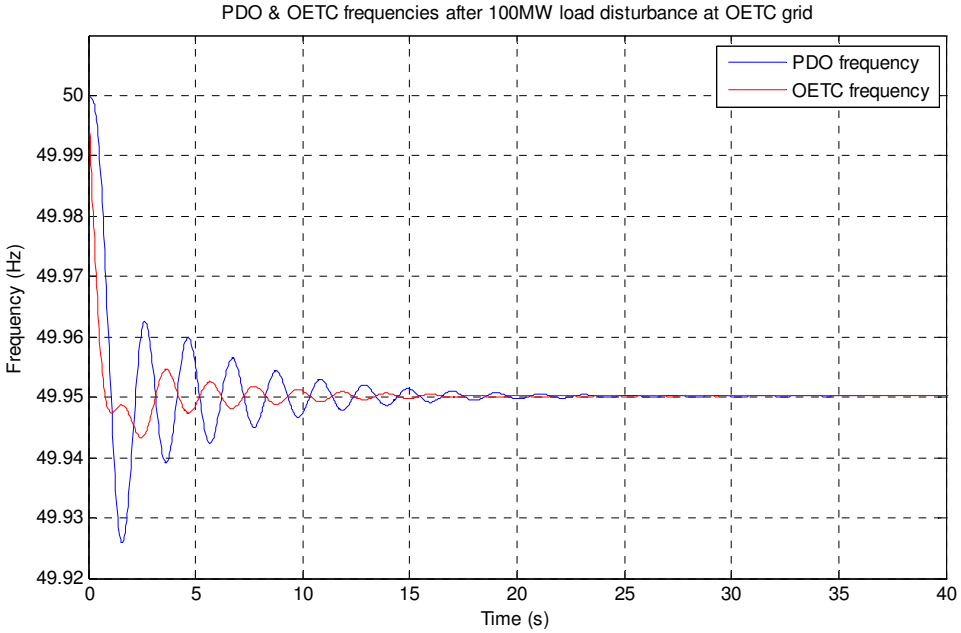

Figure 5.11: PDO and OETC frequencies following 100MW load disturbance at OETC grid

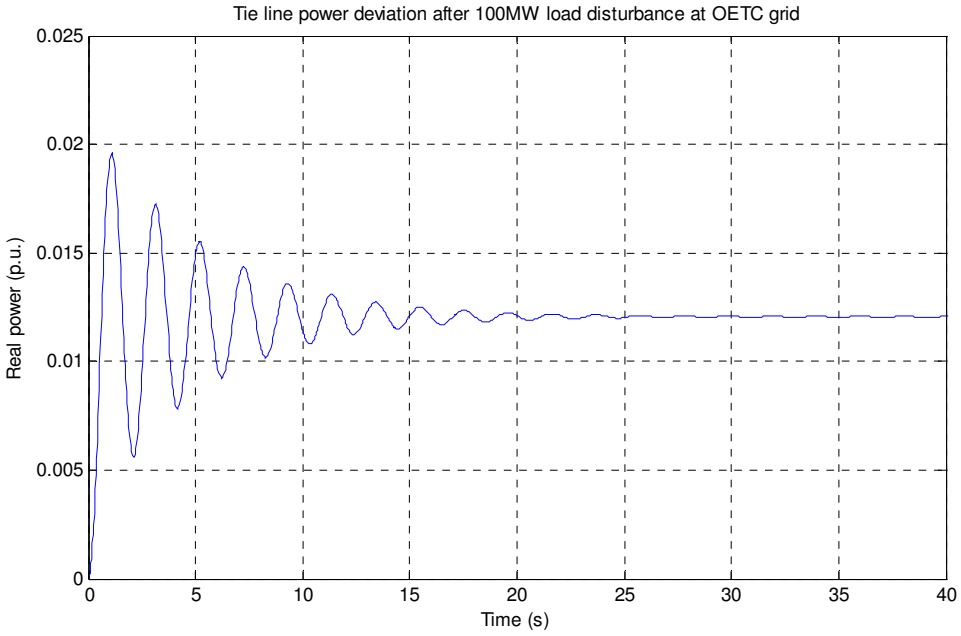

Figure 5.12: Tie line power following 100MW load disturbance at OETC grid

Location	Load disturbance (MW)	Load disturbance (p.u.)	Steady state frequency (Hz)	Steady state frequency deviation (Hz)	Settling time (s)	Steady state tie line power flow towards OETC (p.u.)	Steady state tie line power flow towards OETC (MW)
PDO	30	0.015	49.985	0.015	13.1	-0.0114	-22.8
PDO	60	0.03	49.97	0.03	16.2	-0.0228	-45.6
PDO	100	0.05	49.95	0.05	20.2	-0.0379	-75.8
OETC	30	0.015	49.985	0.015	6.97	0.0036	7.2
OETC	60	0.03	49.97	0.03	11.1	0.0072	14.4
OETC	100	0.05	49.95	0.05	13.2	0.0121	24.2

Table 5.1: Summary of step response results

5.3. Step response results discussion:

PDO and OETC power systems are interconnected by a relatively short overhead transmission line with low impedance. It has the effect of strong interconnection whereby a load disturbance in one system will noticeably affect the other system. Looking at Figures 5.1 to 5.12, it is clear that both PDO and OETC systems respond to load disturbances collaboratively. For example, in Figure 5.1 and Figure 5.2, a 30 MW load disturbance at PDO grid causes frequency oscillations in both PDO and OETC grids and both transient frequencies have settled to the same frequency with a steady state deviation from the nominal frequency.

In general, the simulated system response characteristics are similar for different load disturbances values. However settling time and steady state deviation values vary according to the size of the load disturbance. Looking at Table 5.1, one can see the settling time increases when the load disturbance size increases. Moreover, the steady state frequency deviation is directly proportional to the size of load disturbance.

Also from Table 5.1, one can see a load disturbance of the same size will cause exactly the same frequency deviation regardless whether it happens at PDO grid or at OETC grid. The reason behind it is all generators in both systems are synchronised together and they will

participate in recovering the system regardless of the load disturbance location. On the other hand, the tie line power deviation varies according to the load disturbance location because PDO and OETC grids have different generation capacities. For instance, OETC system has much larger generation capacity than PDO system and therefore during load disturbances at OETC grid most of the extra power will come from OETC generators. As a result, minimal power will flow from PDO to OETC. Whereas when load disturbance arise at PDO grid, some of the extra power will come from PDO generators but the bulk of it will flow from OETC to PDO.

5.4. Parameters sensitivity test results

A 30MW load disturbance at PDO grid was used for these tests. One frequency and the tie line power flow was enough to investigate the impact of modelling errors on the model response characteristics. PDO frequency is selected because it is the basis for settling time calculation. For each test, the model was simulated three different times, the first one with nominal parameters, the second one with the negative error in the parameters and the third one with the positive error in the parameters. All three cases results were shown together in one graph for both tie line power and PDO frequency. Therefore eight graphs were produced for four tests and are shown in Figure 5.13 to Figure 5.20. A summary of the graphical results is also shown in Table 5.2.

There are three important aspects of the simulation figures, the amplitude and frequency of oscillations and the change in steady state deviation.

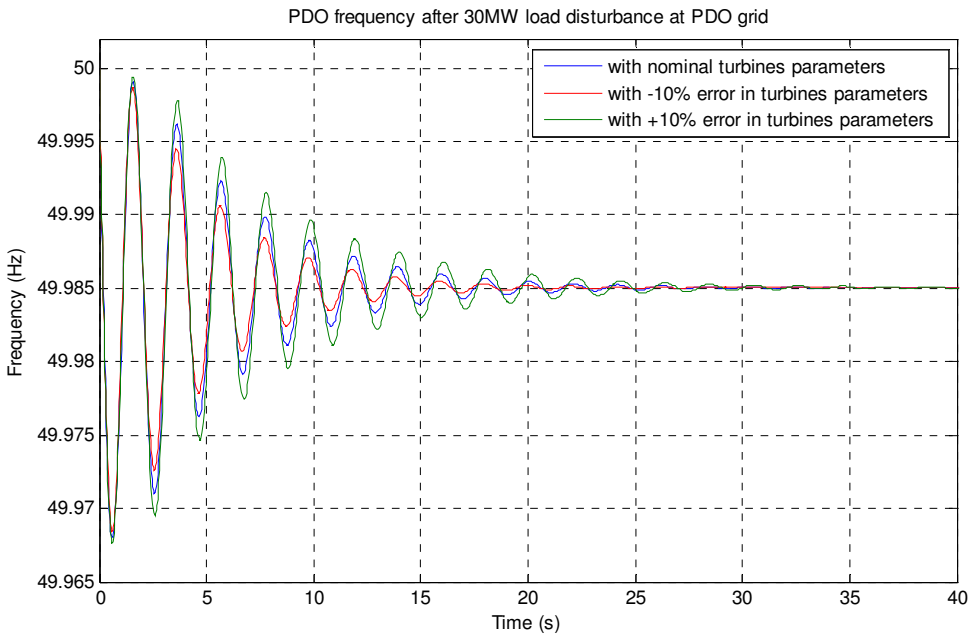

Figure 5.13: Turbines parameters uncertainty impact on the model step response characteristics (PDO frequency)

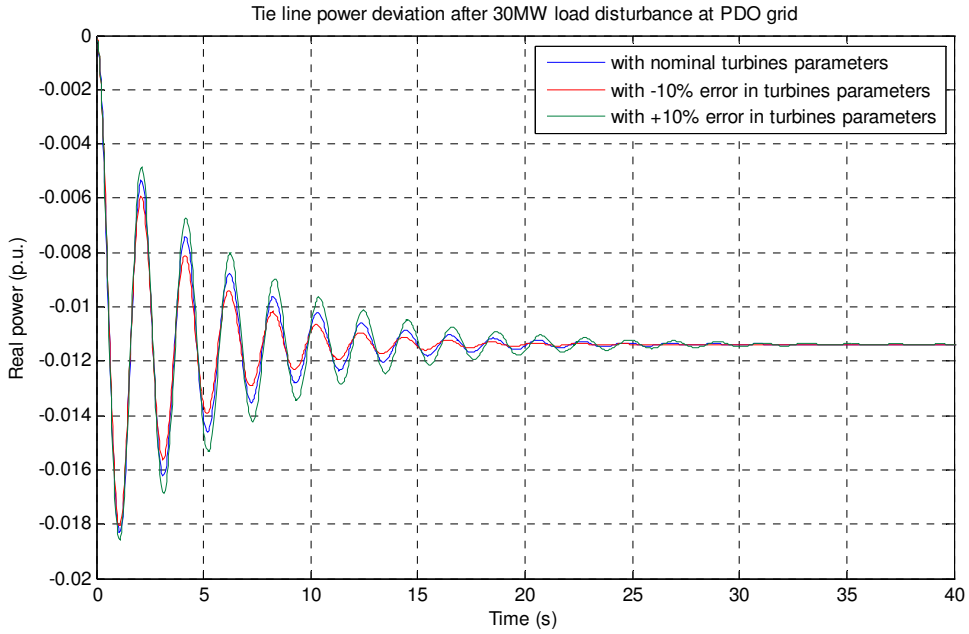

Figure 5.14: Turbines parameters uncertainty impact on the model step response characteristics (Tie line power)

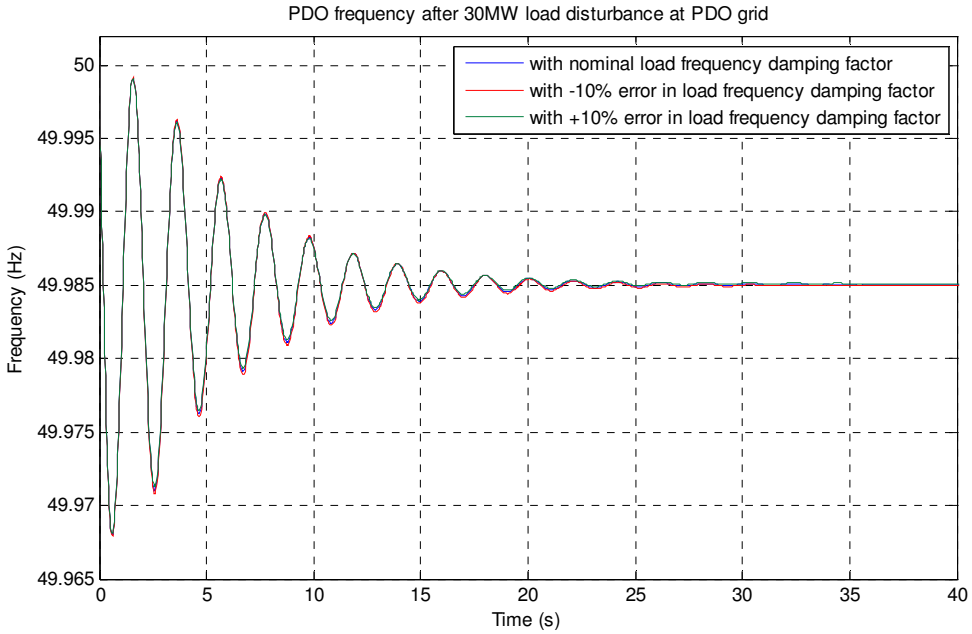

Figure 5.15: Load frequency damping factor uncertainty impact on the model step response characteristics (PDO frequency)

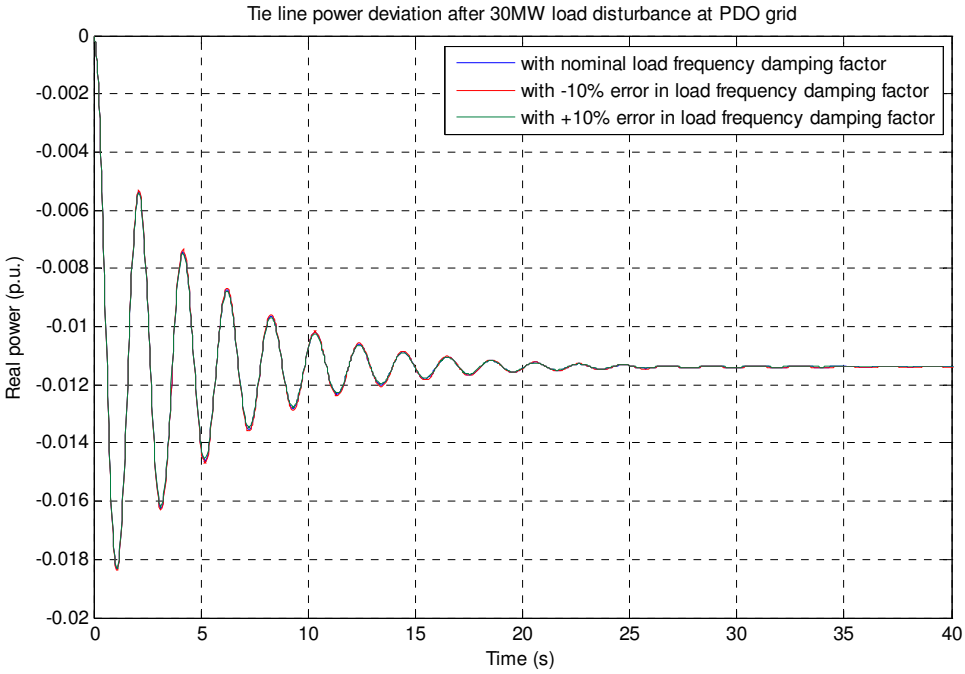

Figure 5.16: Load frequency damping factor uncertainty impact on the model step response characteristics (Tie line power)

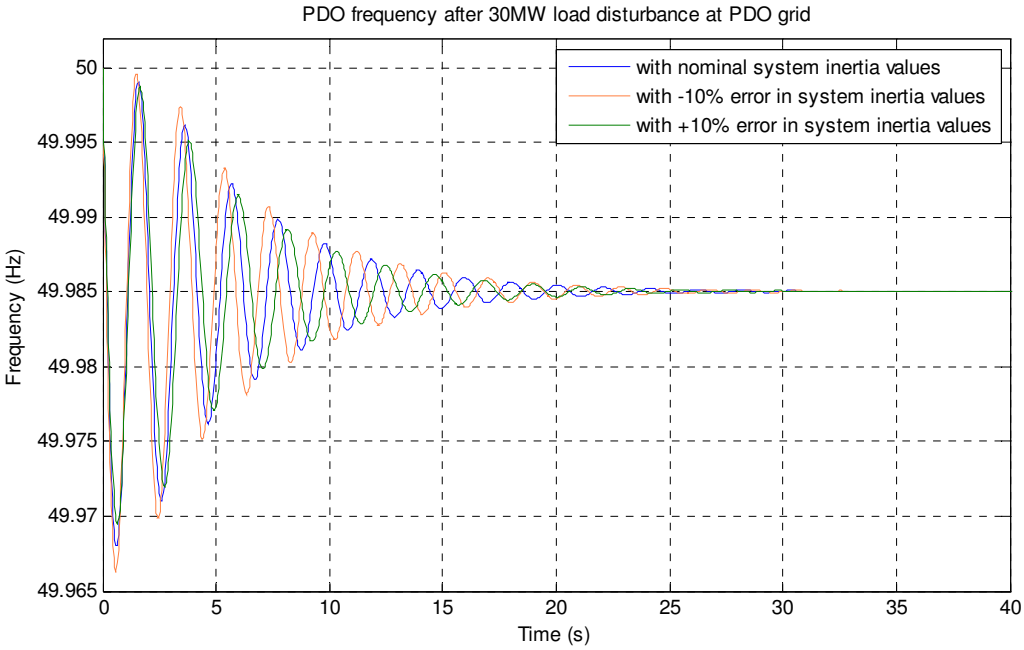

Figure 5.17: System inertia values uncertainty impact on the model step response characteristics (PDO frequency)

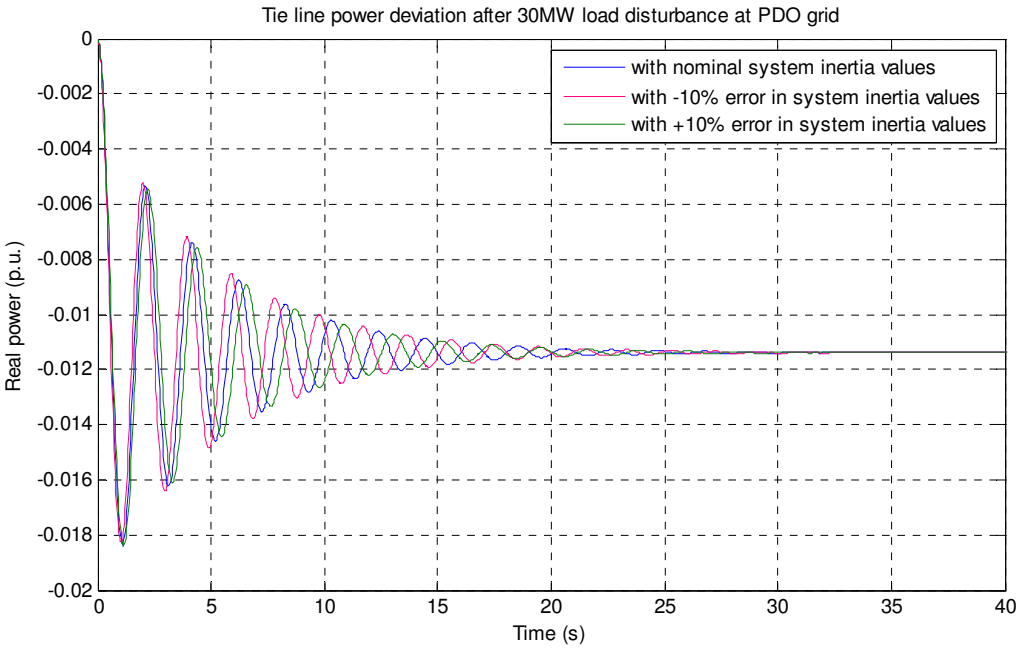

Figure 5.18: System inertia values uncertainty impact on the model step response characteristics (Tie line power)

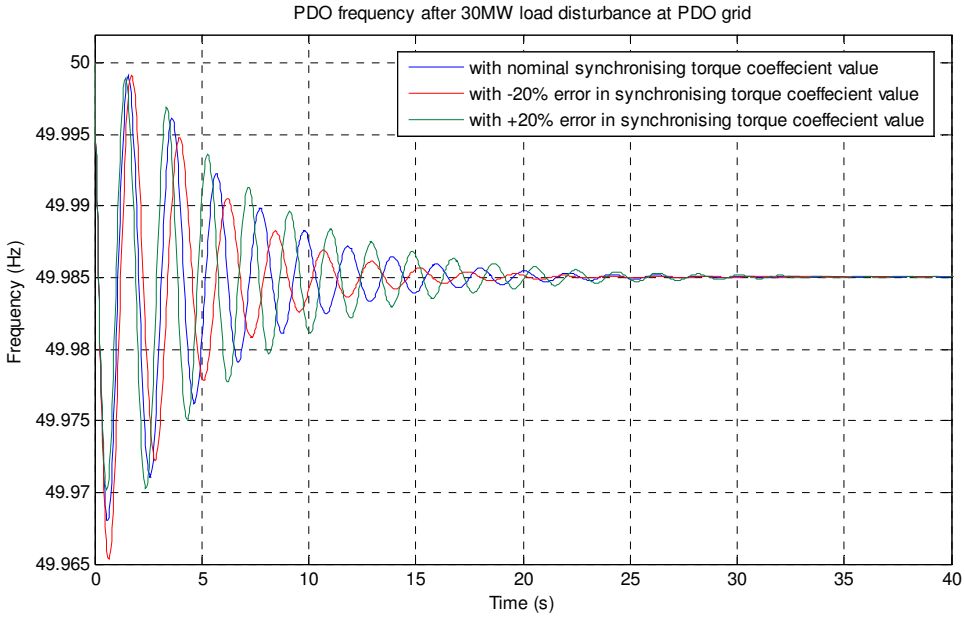

Figure 5.19: Synchronising torque coefficient value uncertainty impact on the model step response characteristics (PDO frequency)

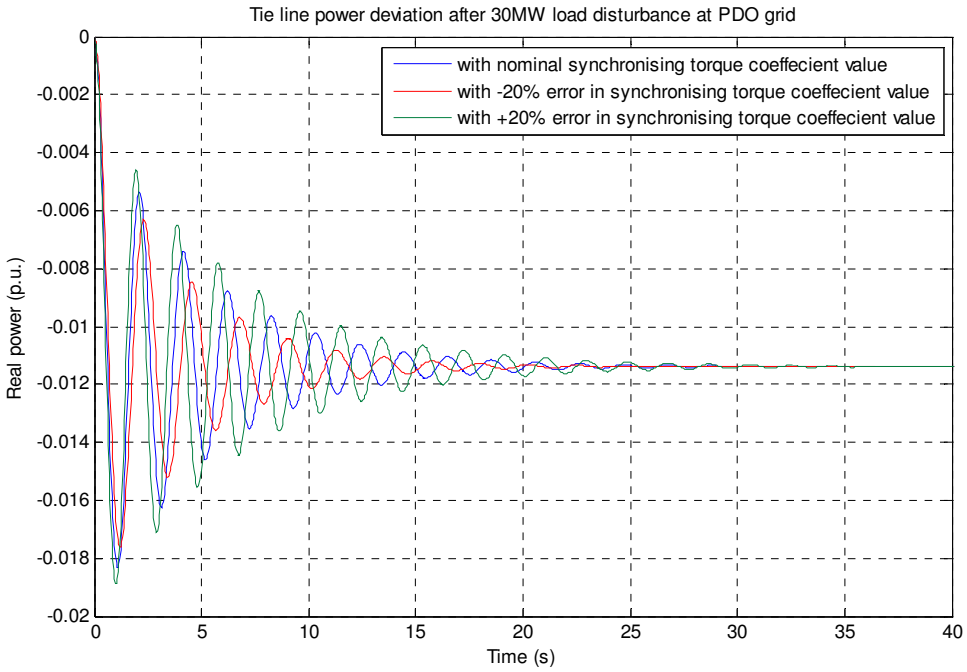

Figure 5.20: Synchronising torque coefficient value uncertainty impact on the model step response characteristics (Tie line power)

		Settling time (s)	Steady state PDO frequency (Hz)	Steady state Tie line power flow towards OETC (p.u.)
Turbines parameters	-10%	10.8	49.985	-0.0114
	Nominal	13.1	49.985	-0.0114
	10%	16.3	49.985	-0.0114
Load frequency damping factor	-10%	13.1	49.985	-0.0114
	Nominal	13.1	49.985	-0.0114
	10%	13	49.985	-0.0114
System inertia	-10%	13.4	49.985	-0.0114
	Nominal	13.1	49.985	-0.0114
	10%	12.7	49.985	-0.0114
Synchronising torque coefficient	-20%	11	49.985	-0.0114
	Nominal	13.1	49.985	-0.0114
	20%	15.1	49.985	-0.0114

Table 5.2: Summary table of parameters sensitivity tests results

5.5. Parameters sensitivity test results discussion

The model response characteristics depend on the model parameters values. However some parameters have bigger influence on the model response characteristics and hence their inherent errors have bigger impact on the model response characteristics. This can be clearly seen from Figure 5.13 to Figure 5.20 and Table 5.2.

A ±10% error in turbines parameters has a slight impact on the general shape of the system response characteristics; see Figure 5.13, Figure 5.14 and Table 5.2. There is no impact on the steady state frequency and tie line power value. The settling time is faster in the case of lower turbines time constants (-10% error) and slower in the case of higher turbines time constants (+10%). This is a logical result since with low time constants the turbines are faster in picking up the extra load and therefore they will settle quicker. The number of frequency oscillations is the same for all cases but amplitude is smaller in the case of slower turbines (+10% error) than in the case of faster turbines (-10% error). This is an expected result since with harsh acceleration and deceleration there will be more overshoot.

Although the errors in the turbine parameters has had an affect on the settling time it has had only a small impact on the amplitude and frequency of oscillations and no impact on the steady state deviation. Therefore, the model sensitivity to modelling errors in turbines parameters values is considered limited.

A ±10% error in the load frequency damping factor has negligible effect in the general shape of the model response characteristics; see Figure 5.15, Figure 5.16 and Table 5.2. The settling time is more or less the same in all three cases. The number of oscillations and amplitudes are also the same for all three cases. The final steady state values are approximately the same. All in all, the model is not sensitive to modelling uncertainty in the load frequency damping factor because an error in the load frequency damping factor will appear as a slight increase or decrease in the system load which usually has a negligible effect on the system.

A ±10% error in the system inertia values has a noticeable effect in the model response characteristics; see Figure 5.17, Figure 5.18 and Table 5.2. It is clear that the same number of oscillations exists but with a small difference in the oscillatory frequency. The amplitude of oscillations is also different for all three cases. The steady state values are the same for all three cases. With fixed mechanical driving torque, a lighter inertia (-10% error) will move quicker than a heavier inertia (+10% error) and that is exactly what is happening in Figure 5.17. Furthermore, a lighter inertia has less damping ability and so will have higher amplitude oscillations which have increased the settling time as it can be

seen from Table 5.2. In general, the model is sensitive to the system inertia values and modelling uncertainty in the system inertia will have a noticeable effect on the model response characteristics.

A ±20% error in synchronising torque coefficient has a significant effect on the general model response characteristics; see Figure 5.19, Figure 5.20 and Table 5.2. The bigger the synchronising torque coefficient is, the more oscillatory is the model response and the longer is the settling time. Synchronising torque coefficient is a measure of how strong is the link between the two power systems (PDO & OETC). Large synchronising torque coefficient results in more interaction between the two power systems and hence more oscillations are evident. A ±20% error is the expected modelling error due to the fact that synchronising torque coefficient value depends on the operating points of the system which are varying continuously. Generally speaking, the synchronising torque coefficient is the most important factor which influences the model response characteristics and therefore the model is quite sensitive to modelling uncertainty associated with it.

5.6. Summary

The developed PDO-OETC power system model went through two types of tests, step response test and parameters sensitivity test.

The step response tests proved that frequency deviation is directly proportional to the size of the load disturbance. The same load disturbance size will cause the same frequency deviation regardless of the location of the load disturbance being at PDO or at OETC side. However the tie line power deviation is dependant on the location of the load disturbance. The same size of load disturbance at PDO side will cause more tie line power deviation than when applied at OETC side.

The parameters sensitivity test proved that uncertainties and modelling errors in turbine parameters and load frequency damping factor has minimal impact on the model response characteristics. However uncertainties and modelling errors in the system inertia and the synchronising torque coefficient will have a measurable effect on the model response characteristics.

Chapter 6: Model validation

6.1. Introduction:

The AGC model has been around for the last three decades and often has been applied to two areas with one generating unit at each area. Few researchers have extended the model to three areas with more than one generating unit in each area. The majority of researchers have used the model published by Elgerd & Fosha (1970 [(1)]; 1970 [(2)]) in early seventies. In almost all published papers, researchers were rather concerned about designing controllers than the modelling process itself. In addition, most of the researchers in AGC field did not have the chance to use real life systems as basis for their studies. Therefore the model validity has received little attention.

In this study and as a novel approach, the AGC model was applied to two interconnected real life practical size power systems, PDO and OETC power systems. Furthermore, the model validity is of a concern which has led to exploring new horizons in the modelling process.

There are two types of errors inherited with almost any modelling process. The first type is the error associated with representing the system with mathematical equations. There might be a lack of understanding and imaginations of the system in hand which will result in optimistic assumptions and extreme simplifications. The second type of errors will be in the mathematical manipulations. Since no such model exists that can perfectly represent a real life system, we shall accept few percentages of error.

From the above argument, two steps of model validation become apparent; one is the mathematical validation process and the other one is the real life system comparison process.

The mathematical validation process will tell us how good we are in utilising the traditional AGC model principles. In the other hand, the real life system comparison process will tell us to what extent the traditional AGC model principles are representing the real system.

Both of those two model validation methods are followed. The outcome of both of those methods will be discussed and an overall summary will be provided at the end of this chapter.

6.2. Mathematical model validation:

The PDO-OETC AGC model was developed based on the principles introduced by Elgerd & Fosha (1970 [(1)]; 1970 [(2)]). The first process of model validation is the mathematical validation which involves comparing the calculated results with the model simulation results. The outcome of this process will give indication of any mathematical manipulation errors or errors associated with using the Simulink software. Kundur (1994, pp. 604-605) summarised equations to calculate the steady state frequency deviation at any area (Equation 6.1), the tie line power deviation following load disturbance at area 1 (Equation 6.2) and the tie line power deviation following load disturbance at area 2 (Equation 6.3) . These equations summarise the modelling process and they are straight forward as given below:

$$\Delta f = \frac{-\Delta P_L}{\left(\frac{1}{R_1}+\frac{1}{R_2}\right)+\left(D_1+D_2\right)} \quad \text{.....(6.1)}$$

$$\Delta P_{12} = -\Delta P_{21} = \frac{-\Delta P_{L1}\left(\frac{1}{R_2}+D_2\right)}{\left(\frac{1}{R_1}+\frac{1}{R_2}\right)+\left(D_1+D_2\right)} \quad \text{.....(6.2)}$$

$$\Delta P_{21} = -\Delta P_{12} = \frac{-\Delta P_{L2}\left(\frac{1}{R1}+D_1\right)}{\left(\frac{1}{R_1}+\frac{1}{R_2}\right)+\left(D_1+D_2\right)} \quad \text{.....(6.3)}$$

Where:

Δf : is the steady state frequency deviation in Hz

ΔP_{12} : is the tie line power flow from area 1 to area 2 in p.u. MW

ΔP_{21} : is the tie line power flow from area 2 to area 1 in p.u. MW

ΔP_L : is the total load disturbance in p.u. MW

ΔP_{L1} : is the load disturbance in area 1 in p.u. MW

ΔP_{L2} : is the load disturbance in area 2 in p.u. MW

R_1 : is the droop regulation setting in area 1 in Hz

R_2 : is the droop regulation setting in area 2 in Hz

D_1 : is the load damping factor in area 1 in p.u.MW/Hz

D_2 : is the load damping factor in area 2 in p.u.MW/Hz

For the mathematical model validation process, four scenarios have been assessed to examine the model validity. The scenarios are:

- 30MW step load disturbance at PDO grid
- 100MW step load disturbance at PDO grid
- 30MW step load disturbance at OETC grid
- 100MW step load disturbance at OETC grid

The PDO-OETC model parameters were used to calculate the steady state frequency deviation using Equation 6.1. The above four scenarios were also simulated using the developed PDO-OETC model.

6.2.1. Calculated results

For PDO-OETC model, the used parameters are as follows:

R_1 =2 Hz/p.u.MW

R_2 =2 Hz/p.u.MW

D_1 =13.6x10^{-3} p.u.MW/Hz

D_2 =29.76x10^{-3} p.u.MW/Hz

The terms $\frac{1}{R_1}$ and $\frac{1}{R_2}$ in equations 6.1 and 6.2 are in p.u.MW/Hz based on the size of generation capacity of each respective area. Therefore they have to be changed into the global 2000MVA based used in the modelling process. PDO has a total generation capacity of 914.2MW and OETC has a total generation capacity of 2927MW based on the summer ratings of their respective generation units.

A 30MW load disturbance equals to 0.015 p.u.MW and a 100MW load disturbance equals to 0.05 p.u.MW. The calculated results are as below:

- 30MW step load disturbance at PDO grid:

$$\Delta f = \frac{-0.015}{\left(\frac{914.2}{2000\times 2}+\frac{2927}{2000\times 2}\right)+\left(13.6\times 10^{-3}+29.76\times 10^{-3}\right)} = -0.014945 \approx -0.015 Hz$$

$$\Delta P_{12} = \frac{-0.015\left(\frac{2927}{2000\times 2}+29.76\times 10^{-3}\right)}{\left(\frac{914.2}{2000\times 2}+\frac{2927}{2000\times 2}\right)+\left(13.6\times 10^{-3}+29.76\times 10^{-3}\right)} = -0.0114\, p.u.MW$$

- 100MW step load disturbance at PDO grid:

$$\Delta f = \frac{-0.05}{\left(\frac{914.2}{2000\times 2}+\frac{2927}{2000\times 2}\right)+\left(13.6\times 10^{-3}+29.76\times 10^{-3}\right)} = -0.0498 \approx -0.05 Hz$$

$$\Delta P_{12} = \frac{-0.05\left(\frac{2927}{2000\times 2}+29.76\times 10^{-3}\right)}{\left(\frac{914.2}{2000\times 2}+\frac{2927}{2000\times 2}\right)+\left(13.6\times 10^{-3}+29.76\times 10^{-3}\right)} = -0.0379\, p.u.MW$$

- 30MW step load disturbance at OETC grid:

$$\Delta f = \frac{-0.015}{\left(\frac{914.2}{2000\times 2}+\frac{2927}{2000\times 2}\right)+\left(13.6\times 10^{-3}+29.76\times 10^{-3}\right)} = -0.014945 \approx -0.015 Hz$$

$$\Delta P_{21} = \frac{-0.015\left(\frac{914.2}{2000\times 2}+13.6\times 10^{-3}\right)}{\left(\frac{914.2}{2000\times 2}+\frac{2927}{2000\times 2}\right)+\left(13.6\times 10^{-3}+29.76\times 10^{-3}\right)} = -0.0036\, p.u.MW$$

- 100MW step load disturbance at OETC grid:

$$\Delta f = \frac{-0.05}{\left(\frac{914.2}{2000\times 2}+\frac{2927}{2000\times 2}\right)+\left(13.6\times 10^{-3}+29.76\times 10^{-3}\right)} = -0.0498 \approx -0.05 Hz$$

$$\Delta P_{21} = \frac{-0.05\left(\frac{914.2}{2000\times 2}+13.6\times 10^{-3}\right)}{\left(\frac{914.2}{2000\times 2}+\frac{2927}{2000\times 2}\right)+\left(13.6\times 10^{-3}+29.76\times 10^{-3}\right)} = -0.0121\, p.u.MW$$

6.2.2. Simulated results:

The simulation results were presented earlier during the step response tests and are shown in Table 5.1 in chapter 5.

Both the calculated results and simulated results are summarised in Table 6.1 below. The error percentage was calculated with reference to the calculated results.

	Steady state frequency deviation (Hz)			Tie line power deviation from PDO to OETC (p.u.MW)		
	Calculated results	Simulated results	Percentage error	Calculated results	Simulated results	Percentage error
30MW step load disturbance at PDO grid	-0.015	-0.015	0%	-0.0114	-0.0114	0%
100MW step load disturbance at PDO grid	-0.05	-0.05	0%	-0.0379	-0.0379	0%
30MW step load disturbance at OETC grid	-0.015	-0.015	0%	0.0036	0.0036	0%
100MW step load disturbance at OETC grid	-0.05	-0.05	0%	0.0121	0.0121	0%

Table 6.1: Summary of mathematical model validation results.

From above table 6.1 one can see that the simulated results are exactly the same as the mathematically calculated results. The error percentage was zero in all cases. Thus, it concludes that the modelling process is successful in implementing the traditional AGC modelling approach.

6.3. Real life system comparison

The simulation results of PDO-OETC model will be compared with real life system behaviour following load disturbances. The outcome of this process will give a clear indication whether the traditional AGC model mimics the real life system behaviour or not. This validation process is constrained by the availability of real life system disturbances scenarios.

Power system operators at PDO main control centre observe the frequency deviation following load disturbances though the SCADA system sampling time limitation doesn't permit precise recording of such oscillations. However, the disturbance recorder installed

at PDO grid in Yibal power station is able to record such oscillations. As discussed earlier in chapter 5, tripping of generators has almost equal effect on frequency profile as step load disturbances. Furthermore, tripping of generators scenarios happens frequently and so it will be used to validate the model.

Few scenarios of frequency deviation following tripping of generators have been recorded using the disturbance recorder installed at PDO Yibal power station. However the installed disturbance cannot produce the disturbance records in data format like spread sheet, therefore it has been necessary to manually interpret the graphs into data. It helps plotting the real graphs with the simulated graphs in one figure which will help in comparing the results. As per the operation practice, following any disturbance in the grid, the power systems operators will intervene as soon as possible to stabilise the system frequency by re-dispatching the generators. Assuming that fifteen seconds (15 s) is a reasonable time for the operator to react, the real graphs data are considered up to 15 seconds. After 15 seconds, the data are considered as unreliable because they may not be a natural dynamic response of the power system, but also contains operator intervention effort. Therefore, the real graphs are plotted up to 15 seconds. Furthermore, it is necessary to align the real graph with the simulated graph and both have to start from 50Hz nominal point for easy comparison. It has been achieved by subtracting or adding any starting deviation from 50Hz in the real graphs so that the starting point is sharp at 50Hz. The alignment has not affected the response characteristics but the starting and settling points.

6.3.1. Disturbance scenarios

The following six scenarios were captured during the year 2008 in which the real system configurations were the same as the model configuration. The scenarios were ordered based on the size of the disturbance:

1. 113MW loaded steam turbine generator tripped at OETC grid on 20/5/2008 @ 2159hrs.
2. 140MW loaded gas turbine generator load rejection test at OETC grid on 25/5/2008 @ 1047hrs.
3. 140MW loaded gas turbine generator load rejection test at OETC grid on 26/5/2008 @ 1128hrs.
4. 140MW loaded gas turbine generator load rejection test at OETC grid on 24/6/2008 @ 1754hrs.
5. 144MW loaded gas turbine generator load rejection test at OETC grid on 21/5/2008 @ 1029hrs.

6. 158MW loaded steam turbine generator tripped at OETC grid on 26/5/2008 @ 1510hrs.

The general operating conditions of PDO-OETC interconnected power system during the summer time can be summarised as follows:

- High load demand
- Low spinning reserve
- Some generating units are operating at base load (no spinning reserve)
- Combined cycles generating units are in preselect load (Droop control disabled)

6.3.1.1. Disturbance scenario 1:

On 20th of May 2008 @ 2159hrs, following the tripping of 113MW generator at OETC grid, the system frequency at PDO side behaved as shown in Figure 6.1. This scenario has been simulated using the developed PDO-OETC model and the system frequency at PDO side behaved as shown in Figure 6.2. which also shows the interpreted real graph aligned with the simulated graph.

The most important features of the figures to look at are the rate of the initial drop in the system frequency following the disturbance, the amplitude and frequency of oscillations and the steady state deviation.

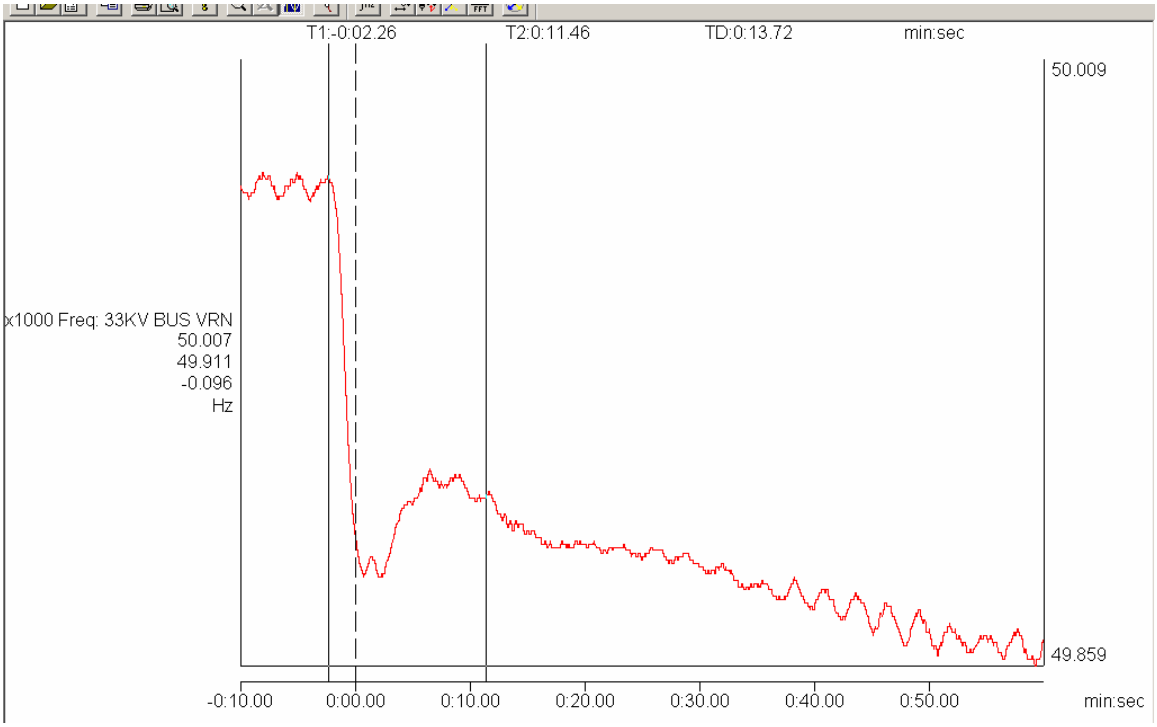

Figure 6.1: Scenario 1; Real behaviour of PDO frequency following 113MW generator trip at OETC grid

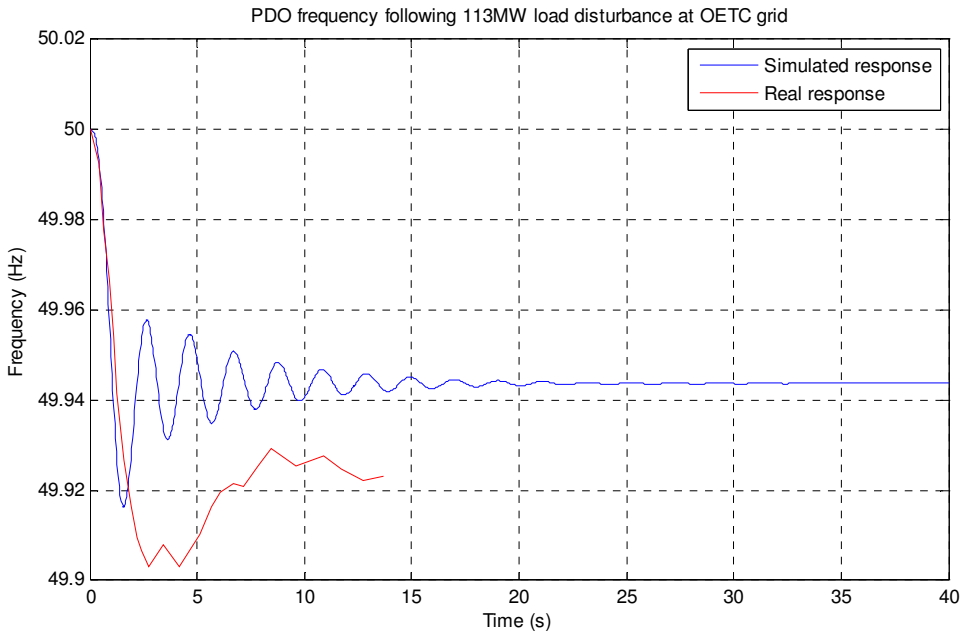

Figure 6.2.: Scenario 1; Real and Simulated behaviour of PDO frequency following 113MW generator trip at OETC grid

6.3.1.2. Disturbance scenario 2:

On 25th of May 2008 @ 1047hrs, following load rejection test of 140MW generator at OETC grid, the system frequency at PDO side behaved as shown in Figure 6.3. The scenario has been simulated using the developed PDO-OETC model and the system frequency at PDO side behaved as in Figure 6.4 which also shows the interpreted real graph aligned with the simulated graph. .

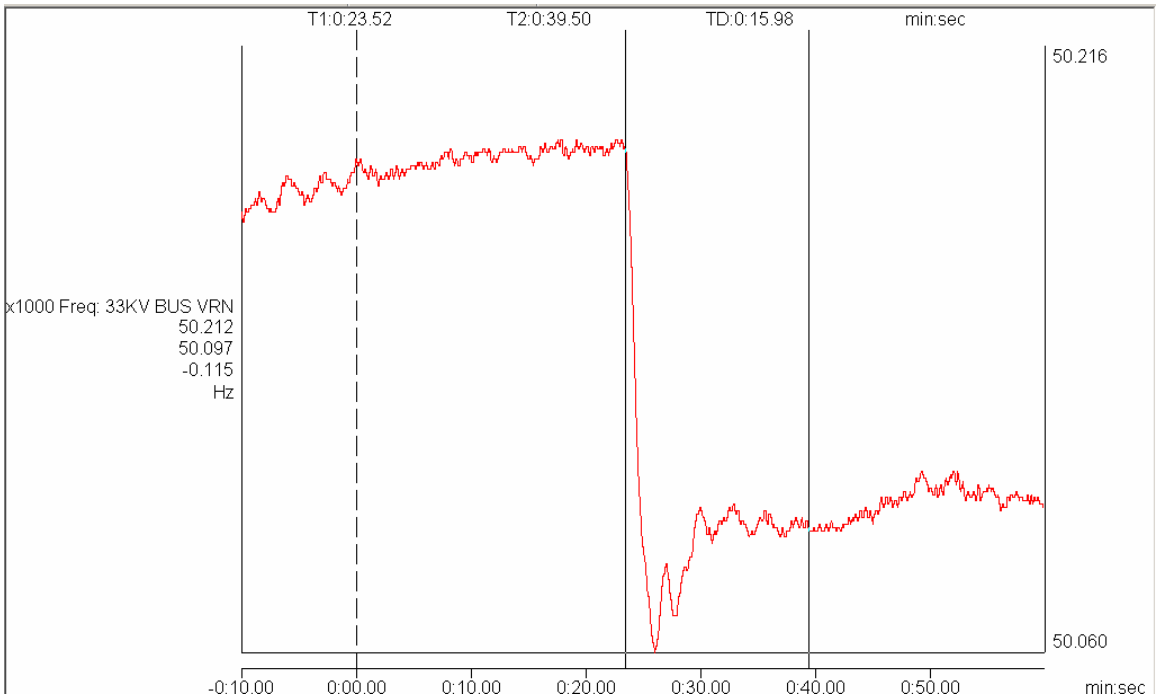

Figure 6.3: Scenario 2; Real behaviour of PDO frequency following 140MW generator load rejection test at OETC grid

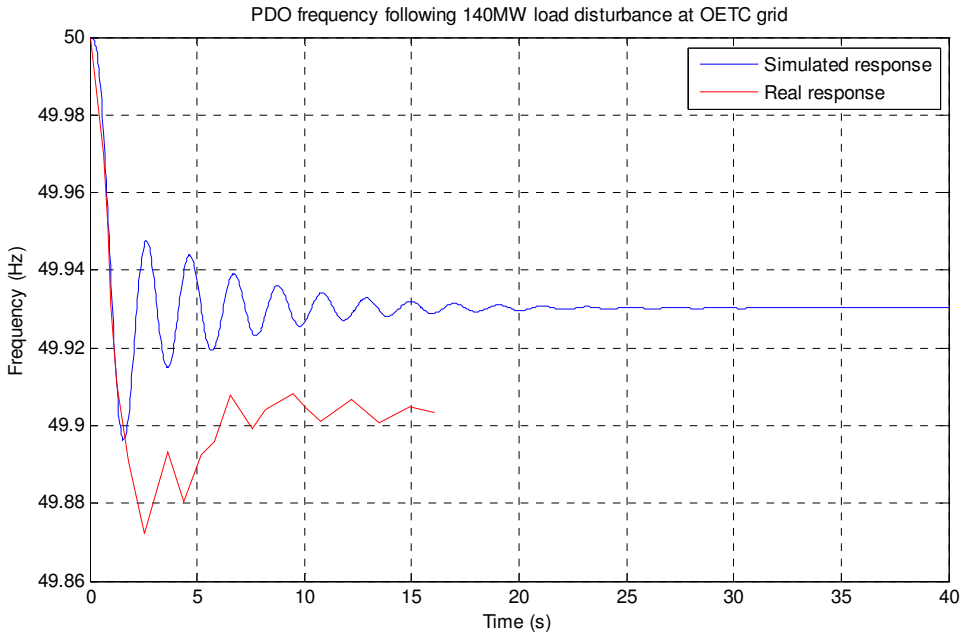

Figure 6.4: Scenario 2; Real and Simulated behaviour of PDO frequency following 140MW generator load rejection test at OETC grid

6.3.1.3. Disturbance scenario 3:

On 26th of May 2008 @ 1128hrs, following load rejection test of 140MW generator at OETC grid, the system frequency at PDO side behaved as shown in Figure 6.5. The scenario has been simulated using the developed PDO-OETC model and the system

frequency at PDO side behaved as in Figure 6.6 which also shows the interpreted real graph aligned with the simulated graph.

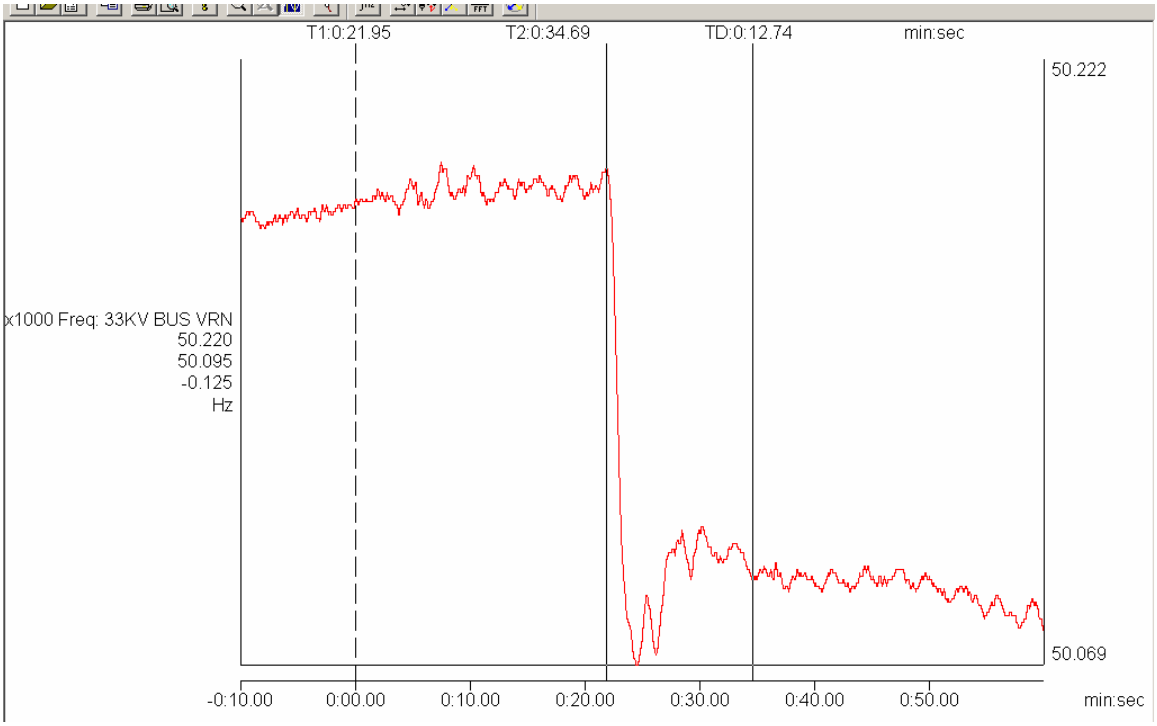

Figure 6.5: Scenario 3; Real behaviour of PDO frequency following 140MW generator load rejection test at OETC grid

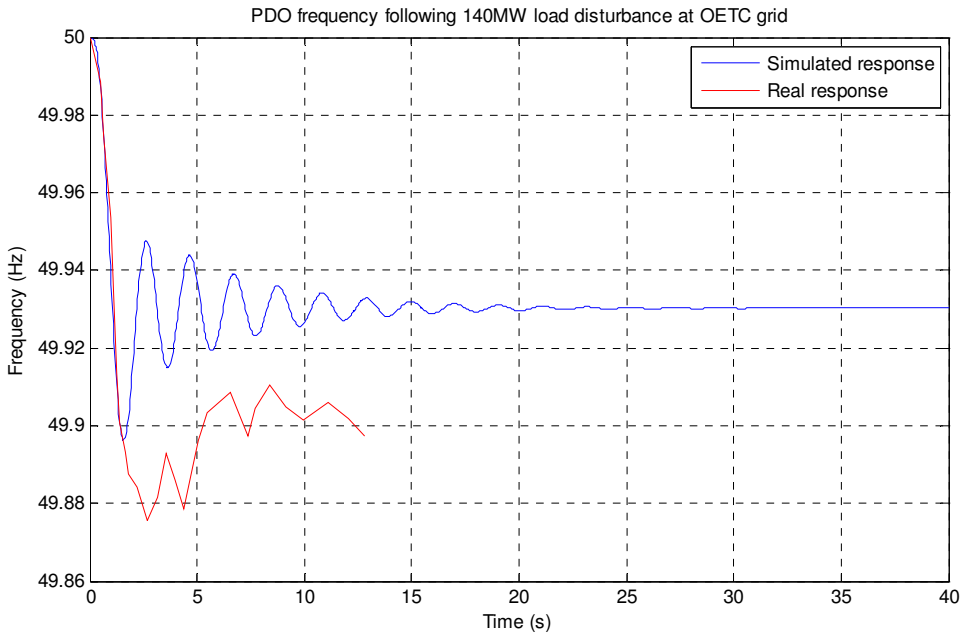

Figure 6.6: Scenario 3; Real and Simulated behaviour of PDO frequency following 140MW generator load rejection test at OETC grid

6.3.1.4. Disturbance scenario 4:

On 24th of June 2008 @ 1754hrs, following load rejection test of 140MW generator at OETC grid, the system frequency at PDO side behaved as shown in Figure 6.7. The scenario has been simulated using the developed PDO-OETC model and the system frequency at PDO side behaved as in Figure 6.8 which also shows the interpreted real graph aligned with the simulated graph.

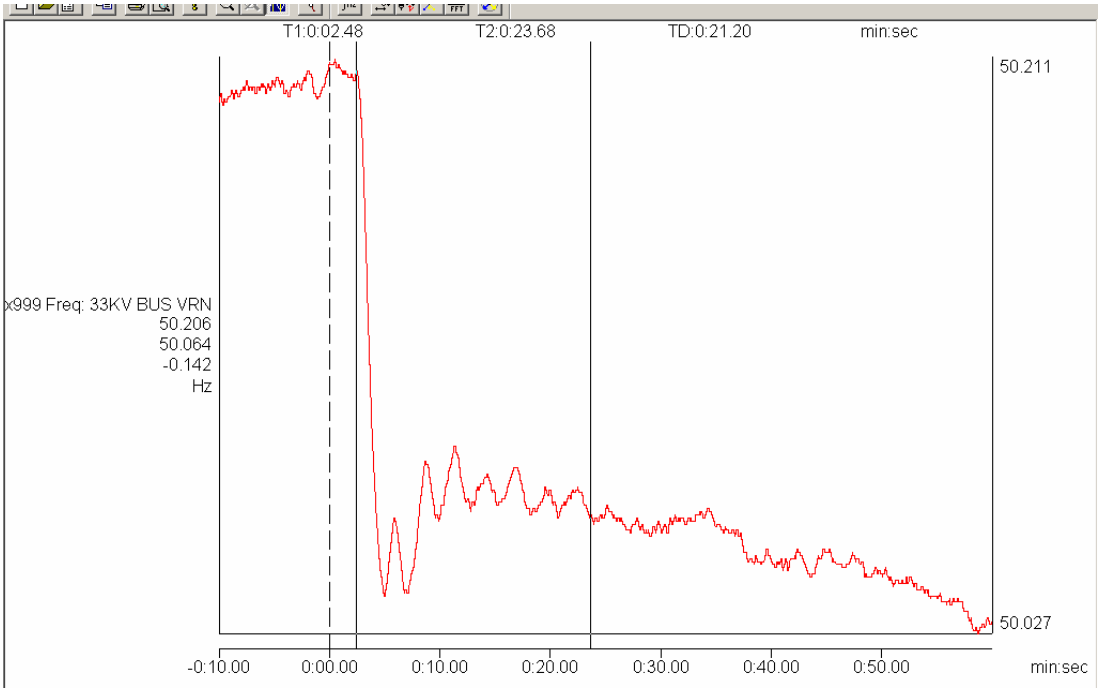

Figure 6.7: Scenario 4; Real behaviour of PDO frequency following 140MW generator load rejection test at OETC grid

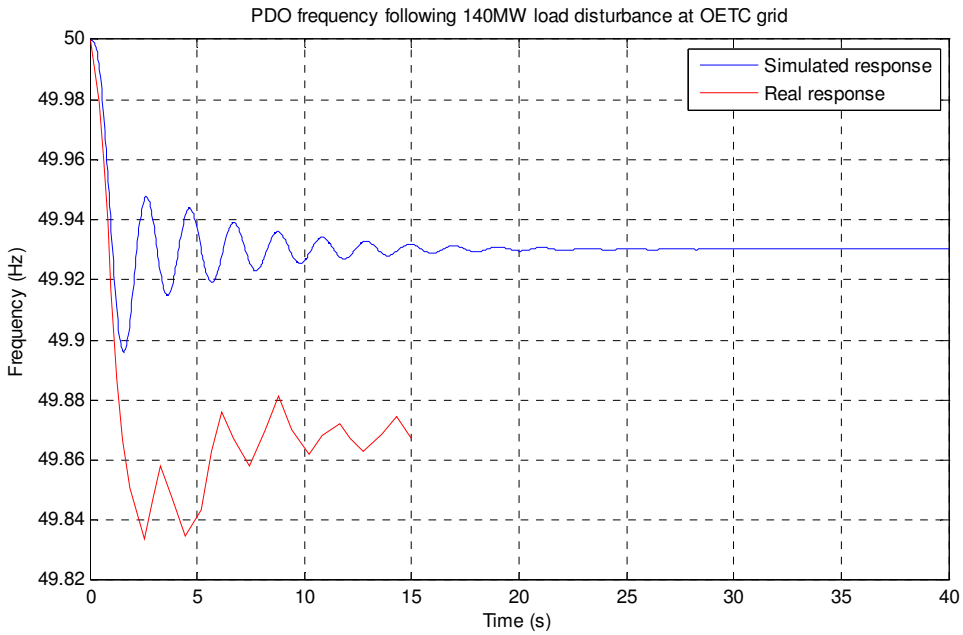

Figure 6.8: Scenario 4; Real and Simulated behaviour of PDO frequency following 140MW generator load rejection test at OETC grid

6.3.1.5. Disturbance scenario 5:

On 21st of May 2008 @ 1029hrs, following load rejection test of 144MW generator at OETC grid, the system frequency at PDO side behaved as shown in Figure 6.9. The scenario has been simulated using the developed PDO-OETC model and the system frequency at PDO side behaved as in Figure 6.10 which also shows the interpreted real graph aligned with the simulated graph.

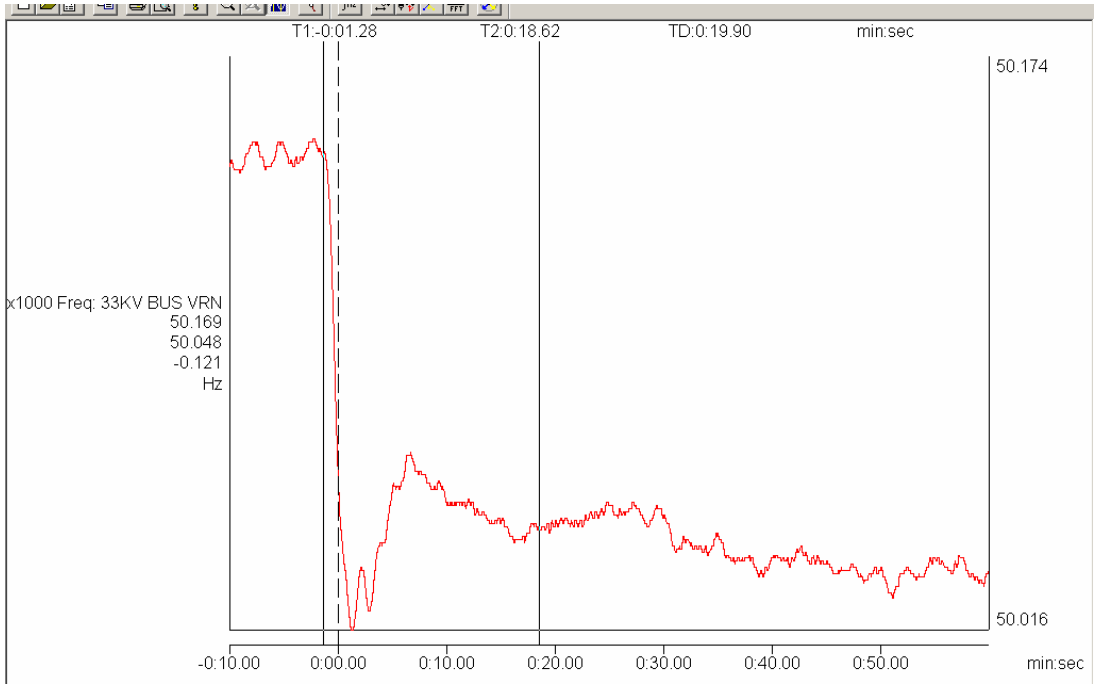

Figure 6.9: Scenario 5; Real behaviour of PDO frequency following 144MW generator load rejection test at OETC grid

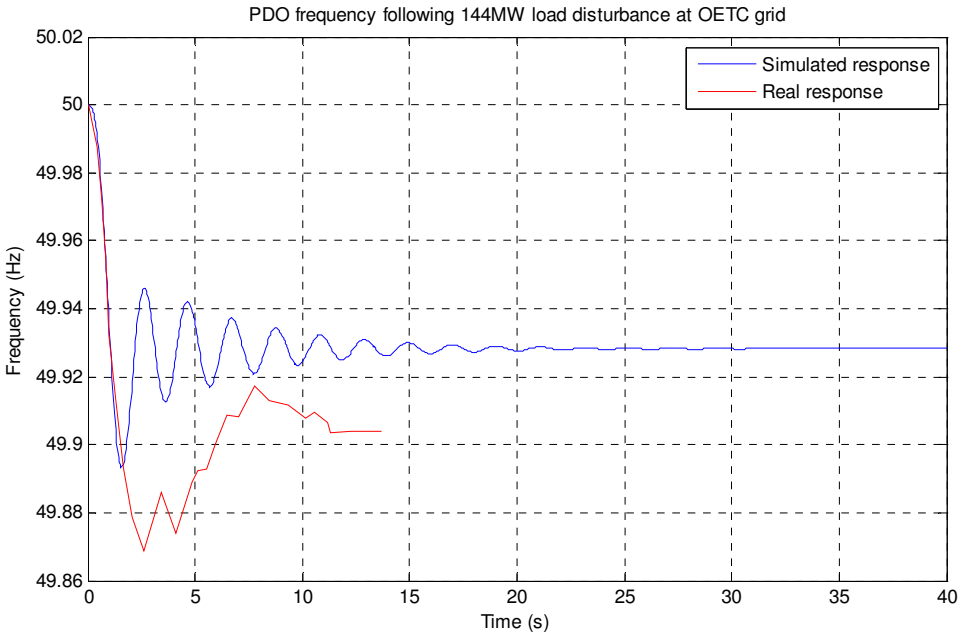

Figure 6.10: Scenario 5; Real and Simulated behaviour of PDO frequency following 144MW generator load rejection test at OETC grid

6.3.1.6. Disturbance scenario 6:

On 26th of May 2008 @ 1510hrs, following the tripping of 158MW generator at OETC grid, the system frequency at PDO side behaved as shown in Figure 6.11. The scenario has been simulated using the developed PDO-OETC model and the system frequency at PDO side behaved as in Figure 6.12 which also shows the interpreted real graph aligned with the simulated graph.

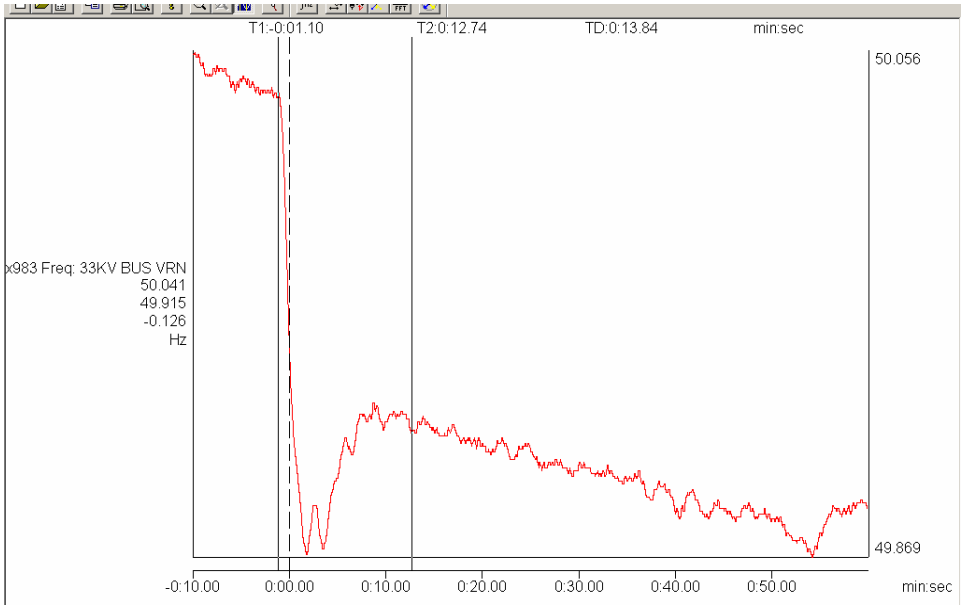

Figure 6.11: Scenario 6; Real behaviour of PDO frequency following 158MW generator trip at OETC grid

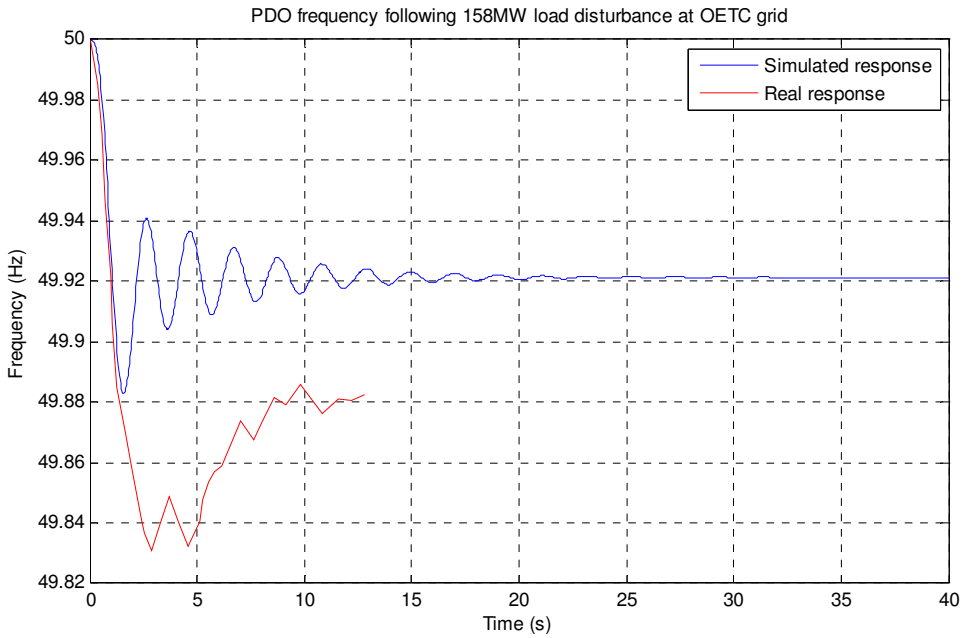

Figure 6.12: Scenario 6; Real and Simulated behaviour of PDO frequency following 158MW generator trip at OETC grid

6.3.2. Summary of real life comparison validation process:

From above scenarios, the following results shown in Table 6.2 can be summarised where the error percentage is calculated with reference to the real data. Note that the settling time is not considered in the comparison because we don't consider the real data beyond the 15s which is the estimated time for the operator intervention to start.

			Real system results	Simulated results	Percentage error
Scenario 1	113MW disturbance at OETC on 20/5/2008 @2159hrs	Frequency deviation (Hz)	-0.077	-0.056	-27.3%
Scenario 2	140MW disturbance at OETC on 25/5/2008 @1047hrs	Frequency deviation (Hz)	-0.097	-0.07	-27.8%
Scenario 3	140MW disturbance at OETC on 26/5/2008 @1128hrs	Frequency deviation (Hz)	-0.103	-0.07	-32%
Scenario 4	140MW disturbance at OETC on 24/6/2008 @1754hrs	Frequency deviation (Hz)	-0.133	-0.07	-47.4%
Scenario 5	144MW disturbance at OETC on 21/5/2008 @1029hrs	Frequency deviation (Hz)	-0.096	-0.072	-25%
Scenario 6	158MW disturbance at OETC on 26/5/2008 @1510hrs	Frequency deviation (Hz)	-0.117	-0.079	-32.5%

Table 6.2: Summary of model validation results.

6.3.3. Discussion of real life comparison validation process

Looking at the six scenarios in hand, one can see that all of them were captured during the summer time, May and June. Hence, the analysis of the scenarios should consider the operating conditions of the power system during that period of time. In hot countries like Oman, the summer time imposes high demand for electricity due to the excessive usage of air conditioning. Unfortunately, the power generation units have the lowest generation capability during summer due to the high ambient temperature. The summer peak load period starts at about 1200hrs and ends at about 1600hrs. The top of the load pyramid is

usually reached at about 1400hrs in the afternoon which is coinciding with the ambient temperature peak point. During the peak load hours the power system generators are usually at maximum output and minimal spinning reserve is available. Depending on the location, process and economics, some generating units will be loaded to their maximum load and they have zero spinning reserve; this is what we call the base load of the generating units. The system operators have to maintain enough spinning reserve to maintain the "N-1" security standard. In most occasions they are able to get most of the spinning reserve from particular units but not all. This will have an impact on the system frequency response following disturbance.

Let us assume that all synchronised generating units have spinning reserve of few MWs and they are in droop control mode. Following load disturbance, all generating units droop control loop will start and continue acting while there is a rate of change of the frequency. As a result, most of the accumulated system spinning reserve will be consumed and turned into extra MW generation. However there will be some spinning reserve still not consumed and is not turned into MW generation because the frequency has already settled with steady state error. This is because the droop control loop has stopped acting when the rate of change of the frequency is zero. Here it is worth mentioning that frequency would have settled down with steady state error even if there was no extra generation of MWs. The load disturbance would have been compensated from the kinetic energy of all generators and frequency would have settled with huge steady state error. However, since we have many generators with spinning reserve ready to be converted during the existence of the rate of change of frequency, we managed to settle the frequency with minimum steady state deviation. Moreover, since the spinning reserve has not been totally consumed, the system operator role now comes in picture where he will start changing the loading reference point of the generators which are still having some spinning reserve and will bring back the frequency to the acceptable range of 50Hz.

Now imagine that we have all the spinning reserve stipulated by the "N-1" supply security standard reserved in few generating units but not all. Following the load disturbance, those few generators will be the only ones which are able to produce extra MWs because they are the only ones which are having the spinning reserve. Although the total spinning reserve is enough to compensate the load disturbance, however there is a limited time frame for those few generators to convert as much as possible of the available spinning reserve into extra MW generation. The generators droop control loop will continue acting while there is a rate of change of frequency. When the later becomes zero, then the droop control loop will stop acting leaving most of the available spinning reserve unconverted to

MW generation. Therefore, the steady state frequency deviation will be much bigger than in the first case where we have had the spinning reserve distributed amongst all generators in the grid.

This is what really happens during the summer peak load period, even if enough spinning reserve is maintained; it will be distributed amongst small number of generators but not all. Therefore we expect, same size load disturbance will cause more steady state frequency deviation during the summer period than during the winter period especially if it happens during the peak load hours.

Looking at the real scenarios summary Table 6.2, one can see all scenarios happen during the summer period but at different times of the day. The settling time was not considered as a criterion for the comparison and validation due to many error sources involved with it. Therefore only visual comparison from the produced graphs is considered; this will help avoiding misleading conclusions.

Looking at Figures 6.2, 6.4, 6.6, 6.8, 6.10 and 6.12, it is crystal clear that there is significant error in the frequency steady state deviation between the real system behaviour and the simulated one. From Table 6.2, this error is -27.3% for scenario one, -27.8% for scenario two, -32% for scenario 3, -47.4% for scenario 4, -25% for scenario 5 and -32.5% for scenario six. Scenarios one, two, three, five and six all happened in May whereas scenario four happened in June. It is noticed that the steady state frequency deviation error for scenario happened in May are all in the range of -30% and the error of the scenario happened in June was -47.4%. All scenarios occurred in May have similar effect on the frequency because the power system operating conditions are almost the same due to a similar profile of the ambient temperature. However, June will be much hotter and therefore the power system would have different operating conditions. The generators spinning reserve is lower in June than in May. Moreover, the number of units operating at base load is more in June than in May. All this contributed to having more error between real life and simulated system behaviour in the June than in May.

From all the above arguments, there is an error between the simulations and the real data and the extent of the error depends on the system operating points. The error came from optimistic assumptions and modelling errors. The model is assuming that all installed units are synchronised to the grid, operating at droop control mode and all of them are having spinning reserve. This operating condition is very rare in real life power systems; therefore the simulation has resulted in some errors.

From the comparison Figures, we can conclude that we need to do more work to resolve the frequency steady state deviation error and to improve the damping effort of the

oscillations. The simulated response oscillations are mimicking the real response oscillation with some differences in the amplitude and frequency of oscillations.

From modelling perspective, we want to be as close as practically possible to the real system response. However it is not practically possible and is not feasible to get exactly the same simulation response as the real system response.

For instance, there is an error in the frequency steady state deviation; therefore we need to consider the practical system operating conditions to reduce this error. Moreover, the simulation response is more oscillatory than the real one; therefore we need to further improve the damping torque of the model. On the other hand, there is a huge work to be done on the prime movers modelling and synchronising torque, therefore it is not feasible to put all this efforts to eliminate the difference in the oscillatory frequency. However we can fine tune some of the model parameters to reduce the difference in the oscillatory frequency and get as close as possible to the real response.

Overall, the model response does not exactly match the real response of the system but it performs very well. Further refining the model will bring the two responses closer to each other and will minimise the overall error. Two approaches will be followed in the model refining process, one is to revisit the modelling assumption and process in order to model and incorporate the feasible practical aspects. The second one is to fine tune selected model parameters which were calculated at the early stage of the modelling process. As a novel approach in the field of AGC modelling, there are two identified fields where we can improve our model based on the feasibility:

- Considering the generation units which are at base load and which are at preselect load (fixed load)
- Considering the generators damping torque.

Adding to those two points, the commonly known Generation Rate Constraint will be considered and its impact on the model response will be determined.

After considering the above practical aspects, the fine tuning process of some selected parameters will be done using the common MATLAB "fminsearch" technique.

6.3.4. Summary of real life comparison validation process

The following points summarise this validation process:

- Simulated results are having a certain error in the steady state frequency deviation when compared with the real results. The error sources are understood.
- The real life system responses followed the same pattern in all scenarios.
- The simulated responses mimic the real responses in general.

- The simulated responses are more oscillatory than the real life responses. The reason behind this is understood.
- Feasible further work scope is identified to improve the model response.

6.4. Overall discussion of the model validation process

The mathematical validation process proved that the traditional AGC modelling principles were applied successfully to the PDO-OETC interconnected power system.

The real life comparison validation process proved that the developed model response is having almost the same pattern as the real life system with some explainable shortfalls.

In spite the difficulty in modelling such complex power system, the developed model proved to be acceptable and valid for further analysis.

However, the model needs to go through a refining process to bring it to the maximum possible accuracy. Some novel approaches will be followed during the refining process.

The following items are a summary of the key elements of the further work to be carried out in order to refine the traditional AGC modelling process:

- Consider generating units which are in base load and units which are in preselect control mode. This is a novel approach.
- Consider the generators damper windings effect. This is a novel approach.
- Consider the Generation Rate Constraint
- Fine tuning a selected number of the model parameters using the common MATLAB "fminsearch" technique.

The next chapter will address and discuss the suggested further work.

Chapter 7: Model refining

In this part of the report, a process to refine the developed model will be followed. Some of the real life practical aspects will be assessed to see their impact on the model response characteristics and to evaluate the benefits of considering those aspects in the modelling process. In the other hand there are some assumptions introduced during the model development stage which are suspect of being the reason behind the errors encountered during the model validation process. Some of these assumptions will be revisited and incorporated in the model in order to make it close enough to the reality.

A more classical method of model fine tuning will then be followed to fine tune a selected number of the model parameters. This method is about minimising the error between the real data and simulated response by varying the values of certain parameters. The ultimate aim of this process is to reduce the difference in the oscillatory frequency between the simulated response and the real response of the power system. A common MATLAB function called the "fminsearch" will be used for this task. A unique Mfile programme will be written to execute this task. The whole process will be carried out after incorporating the practical aspects discussed earlier.

Overall, the model refining process will be done in two steps. The first part of the refining process will look into the following practical aspects:

- Peak load or base load effect on the model dynamic response.
- Preselect load control mode effect on the model dynamic response
- Modelling the generators damper windings effect.
- Consideration of Generation Rate Constraint (GRC)

The second part will be fine tuning a selected number of the model parameters. Those parameters are selected based on the results of the parameter sensitivity test discussed earlier in section 5.4 which are identified to be:

- System inertia
- Synchronising torque.

7.1. Base load effect test

Oman's summer is very hot and therefore the peak load occurs during summer due to the air conditioning requirements and the lower efficiency of motors. In addition to the high demand of electricity during summer, the generation capability of generation units is reduced due to high ambient temperature. High ambient temperature increases the exhaust

temperature and therefore the gas turbines reach their thermal limits with lower power outputs than in the winter. Therefore, it is quite normal phenomenon to see few generation units running on base load during summer. Generation units which are running on base load have no more power to deliver following an increase in load demand and their power output will remain at maximum. Running some of the generation units on base load confines the system available spinning reserve in a less number of units and hence reduces the system ability to recover following load disturbances. The load disturbances will be treated by the generation units which are maintaining the system spinning reserve.

The aim of this test is to illustrate the effect of reaching base load on the transient stability of PDO-OETC power system. So often some generation units from PDO and OETC reach their base load as per Table 7.1. The scenario will be implemented by introducing zero gain in series of the droop control signal to the particular generation unit in PDO-OETC power systems model. A 30MW load disturbance will be applied at PDO grid to conduct the test. PDO frequency and tie line power deviation will be monitored following the load disturbance at PDO grid.

PDO		OETC	
Power station	Generation units	Power station	Generation units
Fahud	1x F6B	Rusail	1x F9E
Lekhwair	2x F6B	Wadi Al-Jizzi	3x F6B
Yibal	2x F6B	Manah	1x F6B & 1x F9E
Saih Nihaydah	1x F6B	Al-Kamil	1x F9E
Suwaihat	1x F6B		

Table 7.1: Units running on base load during summer

7.1.1. Test results

The above test was conducted and the results are shown in Figure 7.1, Figure 7.2 and Table 7.2.

Considering the figures below, the reader should focus on the differences from the nominal model response in terms of steady state deviation, the amplitude and frequency of oscillations.

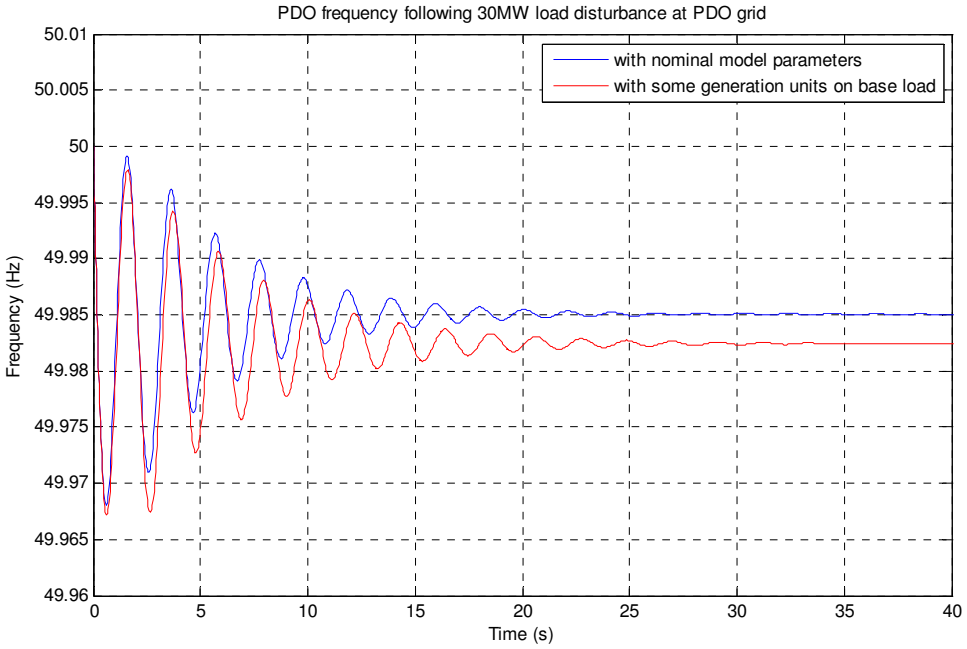

Figure 7.1: Comparison of PDO frequency following 30MW load disturbance at PDO grid using both the nominal model and model with generation units on base load.

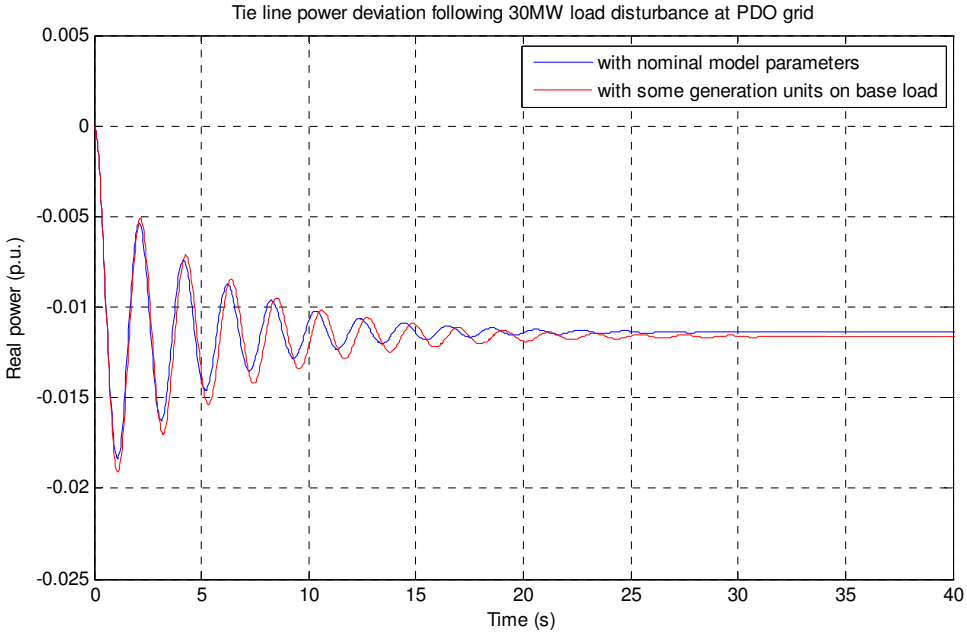

Figure 7.2: Comparison of Tie line power deviation following 30MW load disturbance at PDO grid using both the nominal model and model with generation units on base load.

	Steady state frequency (Hz)	Steady state power flow towards OETC (p.u.)	Settling time (s)
Nominal model	49.985	-0.0114	13.1
Nominal model with some units on peak load	49.982	-0.0116	16.6

Table 7.2: Summary of base load effect test

7.1.2. Discussion

From Figure 7.1, Figure 7.2 and Table 7.2, it is clear when some generation units reaches their maximum loading limit, the system has experienced more frequency and tie line power deviation than in the nominal model case. The system response was slower than in the nominal model case. The slower response can be seen from the slight difference in the oscillatory frequency between the oscillations of the nominal model response and the model with some generation units on base load.

The above results can be related to the fact that fewer machines are now available to turn the available system spinning reserve into extra load MW than in the nominal model case. Consequently, it has delayed the system response and caused more deviation.

In general, the above results lead to the fact that during summer the system transient stability is jeopardised to an extent depending on how many generation units has reached their loading saturation limits even when adequate system spinning reserve is maintained.

7.1.3. Summary

The base load phenomenon has considerable effect on the system response characteristics and therefore it is worth considering when refining the traditional approach of AGC modelling. It is a novel approach in the field of AGC studies.

7.2. Nominal model response with some generation units on preselect load

Practical operation philosophies sometimes tend to run big or complex generation units at fixed load by selecting base load or preselect load control mode in the unit control system. In this case the droop control will be disabled and the unit output power will not change even during load disturbances and frequency deviation. The unit will continue producing the same amount of power regardless of the frequency value.

Some gas turbines generators sets are equipped with complex mode of combustion in order to optimise the emission gases. The main exhaust gases are COx and NOx and the complex combustion mode is aimed to reduce the harm to the environment by optimising the combustion. Such mode of combustion is often referred to as the Dry Low NOx (DLN) mode. In the DLN mode of combustion, the fuel injection goes through two transitions as we increase the loading of the unit depending on the combustion temperature. During these transitions, combustion flame might be lost due to many factors ending up with tripping the unit. Once the unit passes the second transition it is then on the safe side and should run reliably. Unloading the unit is then risky as it goes back through the transition stages where it might loose flame and trip. For these types of gas turbine generators, it is always recommended to keep them loaded to the final stage of combustion. Therefore, gas turbines equipped with DLN combustion are often run at fixed load using the preselect load control mode in order to ensure stable operation. The preselect load control mode will ensure the unit is running on fixed loading regardless of the frequency value.

The preselect load control mode is quite popular control mode. It is also used for units running on combined power and heat cycle processes where a fixed exhaust temperature is needed. In this case the preselect load control will ensure the unit is running on fixed output and hence fixed exhaust temperature.

In PDO, there are eleven (11) units based on DLN mode of combustion and two (2) out of the eleven are on combined heat and power cycle. All these eleven units are often running on preselect load control mode for better system stability. The load variations and disturbances are catered by other units on the grid which are running on conventional combustion mode and are on droop control.

At OETC, The Grid Code (Oman Electricity Transmission Company, 2005) demands for all generating units to participate in frequency recovery following load disturbances as stated in clause CC.6.3.2.1 and SDC3.4.2. Therefore all generating units at OETC grid are assumed to be running on droop control.

The test will investigate the above discussed operation philosophy impact on the nominal system model response and the system ability to recover from load disturbances. The test was carried out under the following conditions:

- Eleven (11) units from PDO are running on preselect load control (2 F6B units at Saih Rawl IPS, 3 F6B units at Hubara PS, 2 F6A and 1 F9E at Qarn Alam PS, 2 F9E units at Mukhaiznah PS and 1 unit at Haima West PS)
- 30MW load disturbance is applied at PDO grid.

7.2.1. Test results

The above test was conducted by introducing zero gain in series with the droop control signal to the particular units running on preselect load control. Tie line power deviation and PDO frequency were considered for comparing the responses of the nominal model and model with preselect load units. The results are shown in Figure 7.3, Figure 7.4 and Table 7.3.

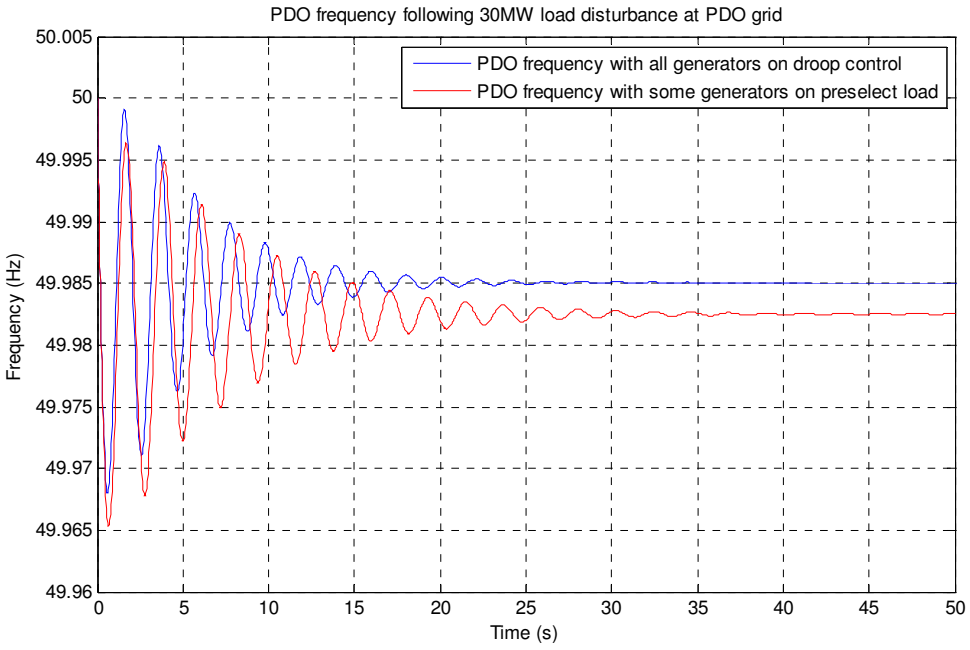

Figure 7.3: Comparison of PDO frequency following 30MW load disturbance at PDO grid using both the nominal model and model with preselect load units.

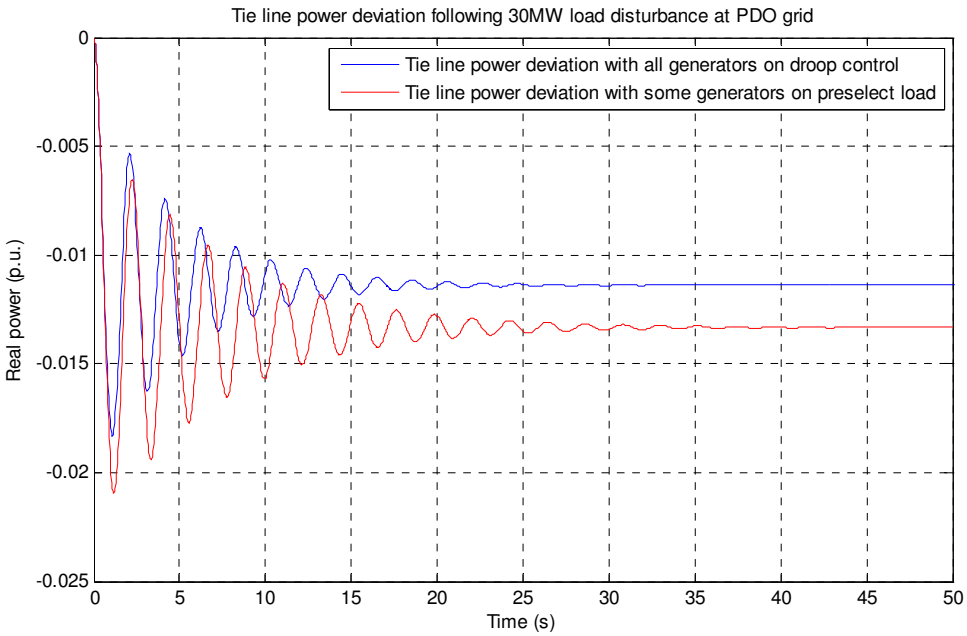

Figure 7.4: Comparison of Tie line power deviation following 30MW load disturbance at PDO grid using both the nominal model and model with preselect load units.

	Steady state frequency (Hz)	Steady state power flow towards OETC (p.u.)	Settling time (s)
Nominal model with all generation units on droop control	49.985	-0.0114	13.1
Nominal model with some units on preselect load	49.983	-0.0133	20.6

Table 7.3: Summary of Preselect load test

7.2.2. Discussion

From Figure 7.3, Figure 7.4 and Table 7.3, it is clear that the system is less stable with some generation units on preselect load control. This is obvious from the longer settling time and the bigger frequency deviation. When some generation units are in preselect load, they will not participate with real power during load disturbances. Even if adequate spinning reserve is maintained in the rest of the generation units, there is no enough time for droop control to convert the spinning reserve into MW generation. Hence, allowing

more deviation in the steady state frequency same as discussed earlier in section 7.1. The real power flow from OETC to PDO is also bigger in this case than the nominal system model. It can be understood as with limited generation units in PDO grid available for droop control, PDO grid will be less able to accommodate load disturbances and hence extra power will flow from OETC to PDO.

7.2.3. Summary

The Preselect load control mode has considerable effect on the system response characteristics and therefore it is worth considering when refining the traditional approach of AGC modelling. It is a novel approach in the field of AGC studies.

7.3. Modelling generators damper windings effect

During the nominal model development stage, it was assumed that following any load disturbances the net power will be absorbed by the system in three ways:

1. By increasing the running generators' kinetic energy W_{kin}
2. By increasing load consumption
3. By increasing the export of power

The above assumption has been accepted since the very early start of AGC modelling in the early seventies of the last century (Elgerd and Fosha [(1)], 1970; Elgerd and Fosha [(2)], 1970).

However, if we consider the power system dynamics in a global view, then we can trace other factors which influence the development of the perturbation model. For instant, there are many sources of damping power represented by (Saadat, 2002, p. 473):

- Load dynamics
- Damper windings
- Speed/torque characteristics of the prime movers

During the nominal model development process, the damping power resulting from the load dynamics was only considered. This power was represented by the load frequency damping factor D which was used in the perturbation model.

As a novel approach, the damping power resulting from generators damper windings will be modelled and incorporated to the well known AGC model. The generators damper windings are known to damp the power and frequency oscillations. The new model will be tested to study the effect of generators damper windings on the overall response of the perturbation model.

7.3.1. Modelling approach

Generators damper windings are usually in the form of copper or brass rods embedded in pole face of the generator rotor. Those rods are connected to end rings to form short-circuited windings similar to squirrel cage induction motors (KUNDUR, 1994, p. 47). As long as there is a slip between the system frequency and the generator rotor speed, induction motor action will take place between the rotating magnetic filed of the stator and the damper windings. Accordingly a damping torque will be established on the rotor trying to minimise the slip between the angular velocity of the rotor and the system frequency (Saadat, 2002, p. 473). The damping power is approximately proportional to the speed deviation and is represented as follows (Saadat, 2002, p. 473):

$$Pd = K_D \frac{d\delta}{dt} \quad \text{.....(7.1)}$$

Where K_D is the damping coefficient which can be determined either from the design data or by test. K_D is given in p.u. torque/p.u. speed (KUNDUR, 1994, p. 131). Since base torque is given as (KUNDUR, 1994, p. 130):

$$T_{base} = \frac{MVA_{base}}{\omega_0} \quad \text{.....(7.2)}$$

Where ω_0 is the rated angular speed in rad/s.

Therefore,

$$T_{p.u.} = \frac{T}{T_{base}} = \frac{MVA}{\omega_0} \times \frac{\omega_0}{MVA_{base}} = \frac{MVA}{MVA_{base}} = P_{p.u.} \quad \text{.....(7.3)}$$

Hence, K_D can be considered as in p.u. Power/p.u. speed.

The rate of change of torque angle represents a change in the angular frequency as follows:

$$\Delta\omega = \frac{d\delta}{dt} \quad \text{.....(7.4)}$$

The damping power is then given as:

$$Pd = K_D \Delta\omega \quad \text{.....(7.5)}$$

Where $\Delta\omega$ is in p.u.

In order to integrate the damping power to the overall model swing equation, speed deviation must be in Hz. Since,

$$\Delta\omega_{p.u.} = \Delta f_{p.u.} = \frac{\Delta\omega}{\omega_0} = \frac{\Delta f}{f_0} \quad \text{.....(7.6)}$$

Therefore,

$$Pd = \frac{K_D}{f_0} \Delta f \quad \text{.....(7.7)}$$

Introducing:

$$K = \frac{K_D}{f_0} \quad \text{……..(7.8)}$$

Where K is in p.u. Power/Hz

The damping power is then given by the simple expression:

$$Pd = K\Delta f \text{ …….(7.9)}$$

Where,

Pd = p.u. power

K= p.u. power/Hz

Δf = Hz

Back to the assumption during the model development stage, that all power stations in one area are strongly interconnected and therefore are assumed to be connected to one bus, the same assumption will be applied to the damper windings power. Based on this assumption, all generators will be swinging in unison and the damping power produced by all generators damper windings will be in phase and acting in the same direction. Hence all damper windings power of all generators in one area will be summated together and included in the swing equation as one element. Furthermore, during transients and for PDO generators, PDO frequency will be considered as the generators speed and OETC frequency will be considered as the grid speed. Therefore as long as there is a difference between PDO frequency and OETC frequency, PDO generators damper windings will try to minimise the transient slip between the two frequencies by producing a damping power. Similarly, for OETC generators, OETC frequency will be considered as OETC generators speed and PDO frequency will be considered as the grid speed. The term Δf will be the difference between the PDO and OETC frequencies deviation which effectively equals to the difference between the two frequencies. The Δf value will be used to calculate the PDO generators damper windings power and the same value but with a negative sign will be used to calculate the OETC generators damper windings.

From above discussion, the change in the generators damper windings power is given as:

$$\Delta Pd_i = K_i(\Delta f_i - \Delta f_v) \text{ …….(7.10)}$$

And by Laplace transform:

$$\Delta Pd_i(s) = K_i(\Delta F_i(s) - \Delta F_v(s)) \text{ ……..(7.11)}$$

The generators damper windings power can be integrated to the overall model swing equation as below (KUNDUR, 1994, p. 131; Saadat, 2002, p. 473):

$$\Delta P_{Gi} - \Delta P_{Di} = 2\frac{W^*_{kini}}{f^*}\frac{d}{dt}(\Delta f_i) + D_i \Delta f_i + \Delta P_{di} + \Delta P_{tiei} \quad \text{.....(7.12)}$$

And in the overall transfer function:

$$[\Delta P_{Gi}(s) - \Delta P_{Di}(s) - \Delta P_{tiei}(s) - \Delta P_{di}(s)]\frac{K_{pi}}{1 + sT_{pi}} = \Delta Fi(s) \quad \text{.....(7.13)}$$

7.3.2. Calculation of accumulated damping coefficient Ki

PDO (Petroleum Development Oman LLC [3], 2004, p. 6) has given a value of generators damping coefficient equal to 2 p.u. for F5, F6B, F6A and F9E gas turbine generators based on the rated MVA of each generator. The value is assumed to be applicable to all generators in PDO and OETC systems. Summary of generators, their ratings and installed number in each system is shown in Table 7.4.

	F5	F6B	F6A	F9E	ST1	ST2	ST3
MVA rating	22	35	77	121	12.5	50	275
Installed number in PDO	5	14	3	3	0	0	0
Installed number in OETC	12	15	0	18	3	3	2

Table 7.4: Summary of generators, ratings and installed number in PDO and OETC systems.

In order to calculate the accumulative generators damping coefficient, each generator coefficient has to be changed to the base MVA rather than the rated MVA.

Since individual generator damping factor is given as $K = \frac{K_D}{f_0}$, then the PDO accumulated generators damping coefficient is calculated as below:

$$K(PDO) = \frac{2}{2000 \times 50}(5 \times 22 + 14 \times 35 + 3 \times 77 + 3 \times 121) = 23.88 \times 10^{-3}\ p.u.MW / Hz$$

Similarly, OETC accumulated generators damping coefficient is calculated as below:

$$K(OETC) = \frac{2}{2000 \times 50}(12 \times 22 + 15 \times 35 + 18 \times 121 + 3 \times 12.5 + 3 \times 50 + 2 \times 275) = 74.09 \times 10^{-3}\ p.u.MW/Hz$$

The above two values can be directly used at the overall perturbation model.

The overall perturbation model will look as shown in Figure 7.5. PDO and OETC subsystems are shown in Figures 7.6 and 7.7 respectively where Kdwpdo is PDO generators damper windings torque coefficient and Kdwoetc is OETC generators damper windings torque coefficient.

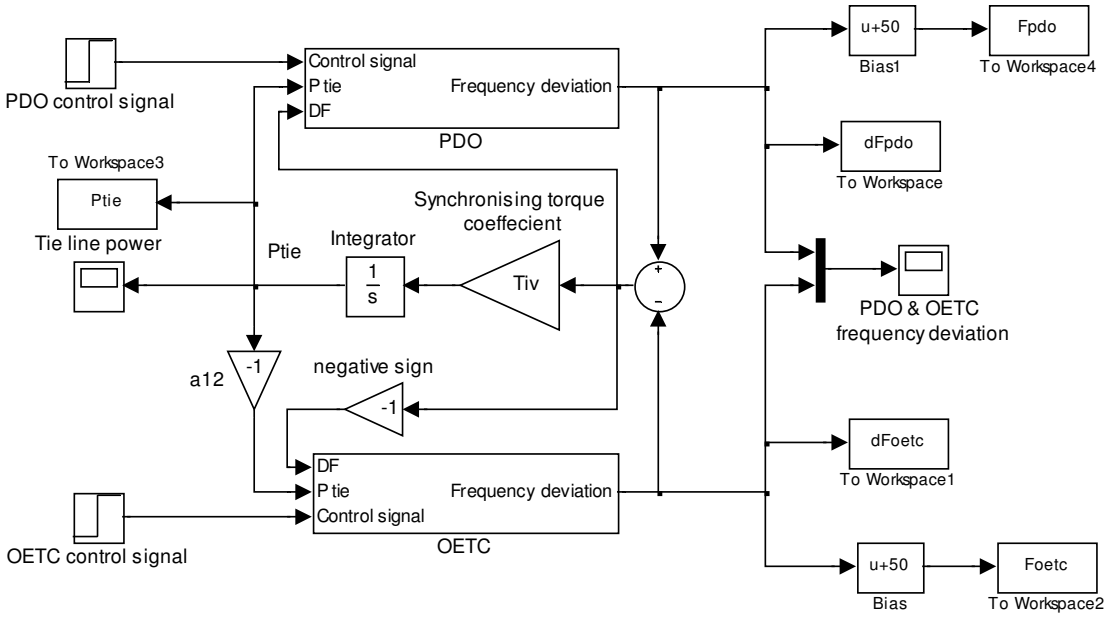

Figure 7.5: PDO-OETC perturbation model including generators damper windings torque

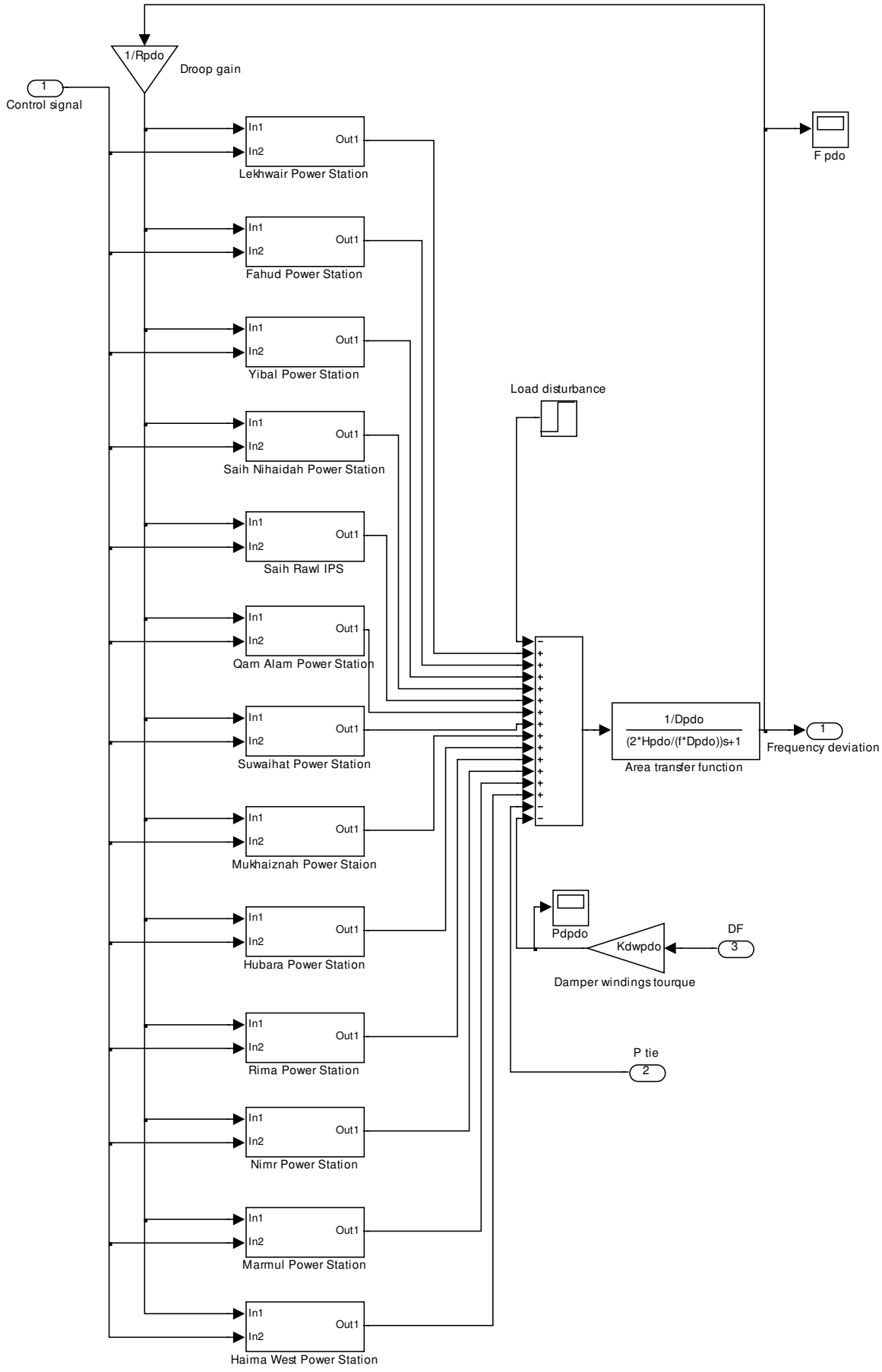

Figure 7.6: PDO perturbation model including generators damper windings torque

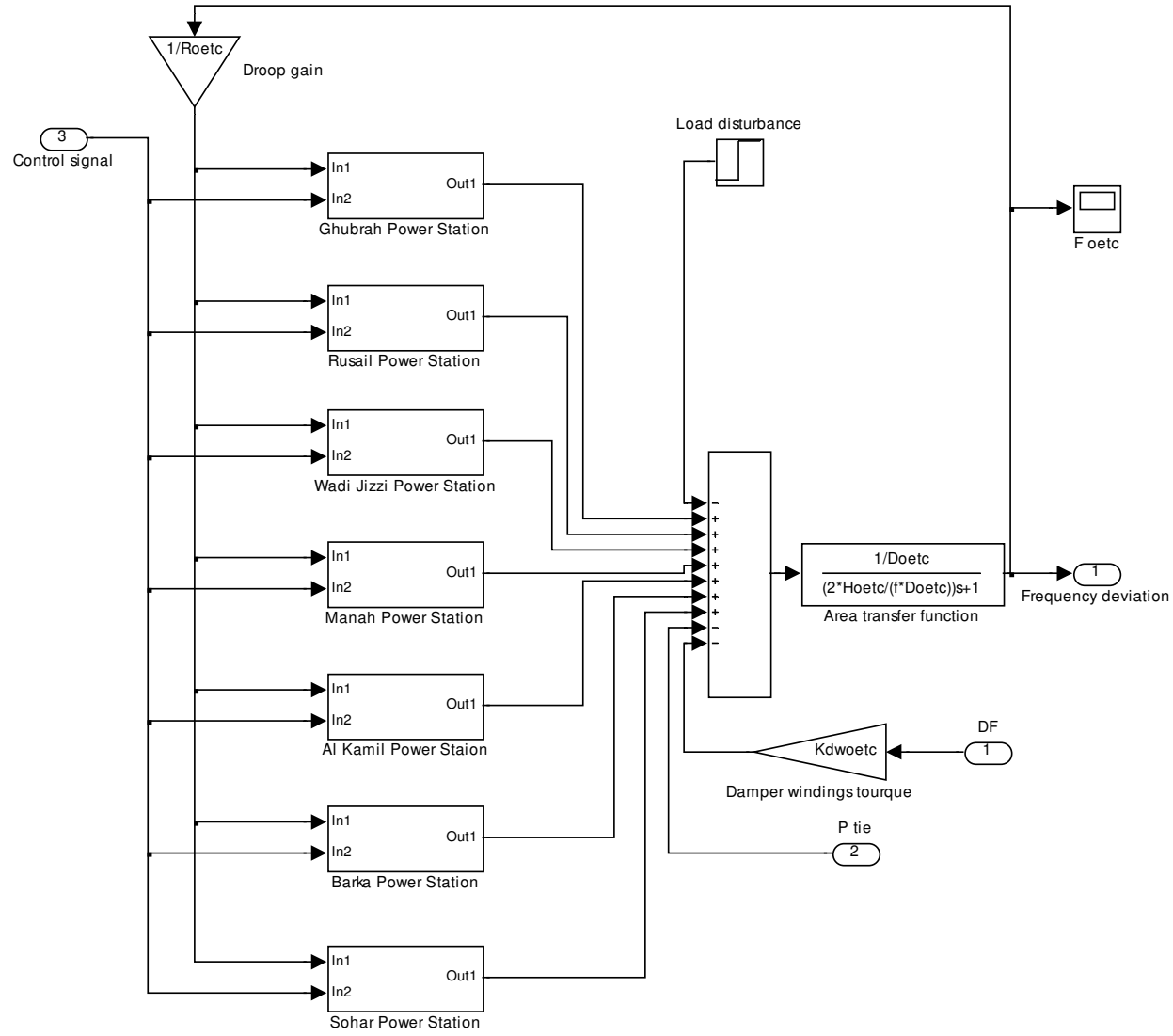

Figure 7.7: OETC perturbation model including generators damper windings torque

7.3.3. Testing the new model

The perturbation model with the generators damper windings torque coefficients was tested and the results are compared with the nominal perturbation model. The test was carried out under the following conditions:

- 30MW step load disturbance will be applied at PDO & OETC grids one at a time.
- Settling time will be considered as PDO frequency settling time to the nearest +- 0.001 Hz of the final steady state value.

The results are shown in Figures 7.8 to 7.13 and Table 7.5.

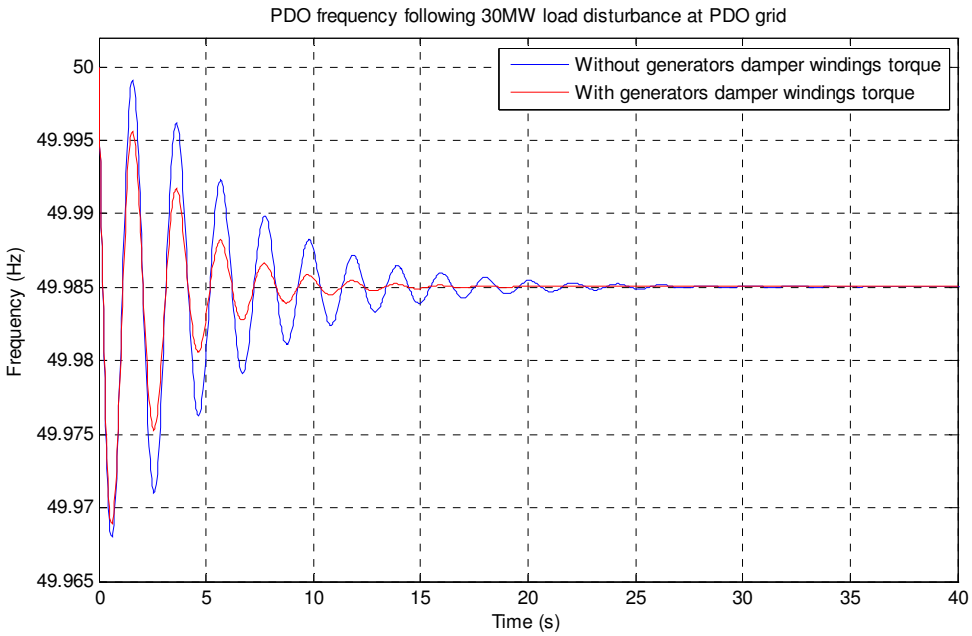

Figure 7.8: PDO frequency following 30MW load disturbance at PDO grid

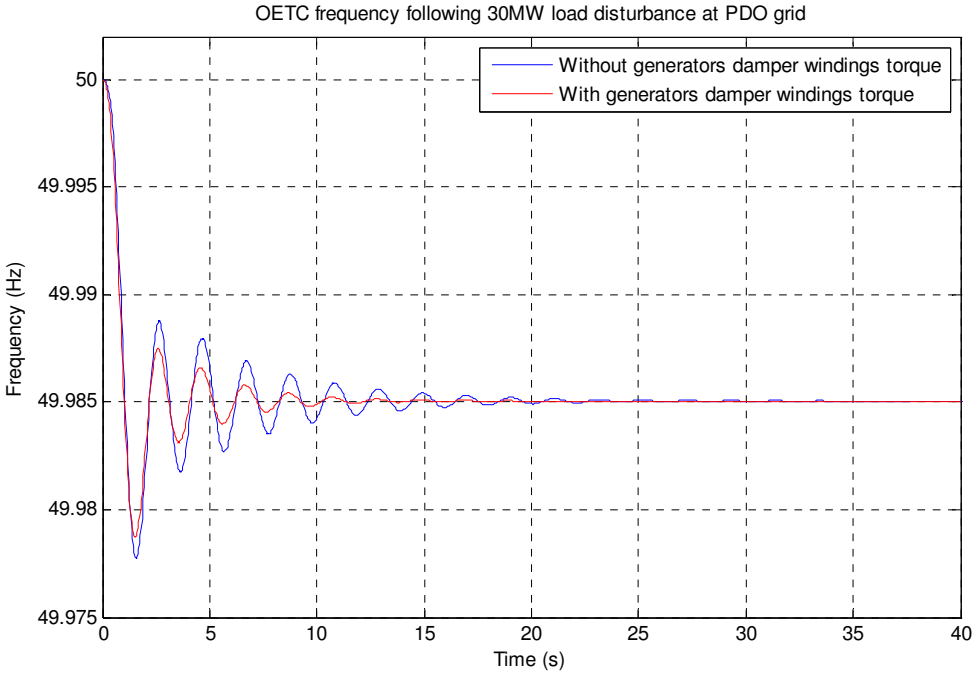

Figure 7.9: OETC frequency following 30MW load disturbance at PDO grid

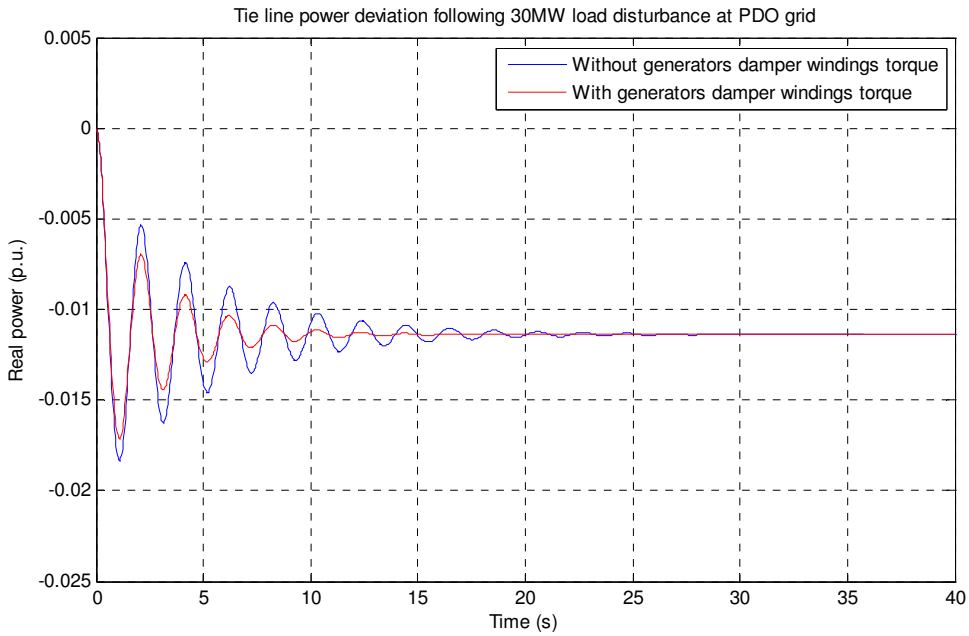

Figure 7.10: Tie line power deviation following 30MW load disturbance at PDO grid

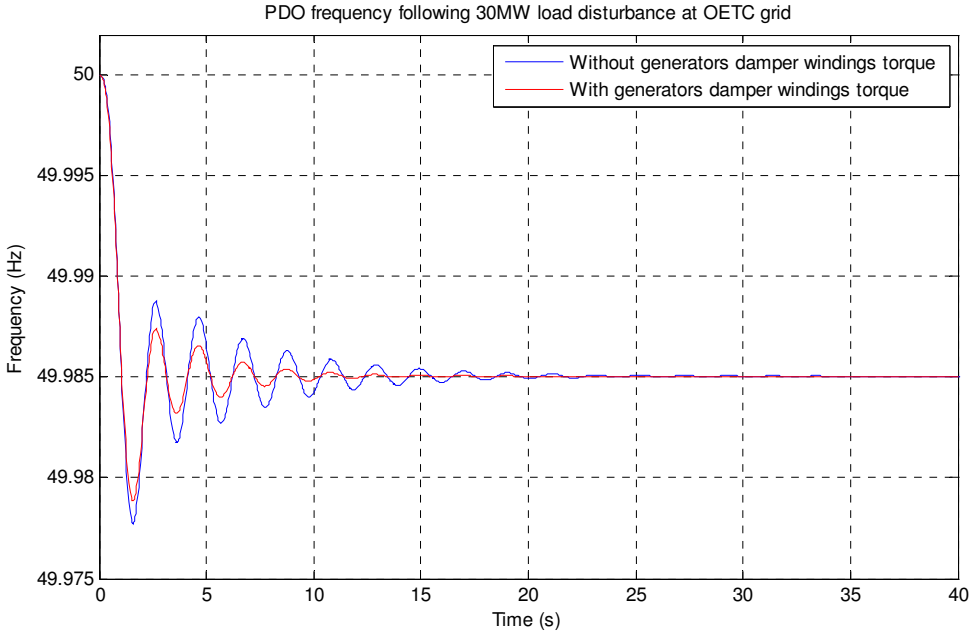

Figure 7.11: PDO frequency following 30MW load disturbance at OETC grid

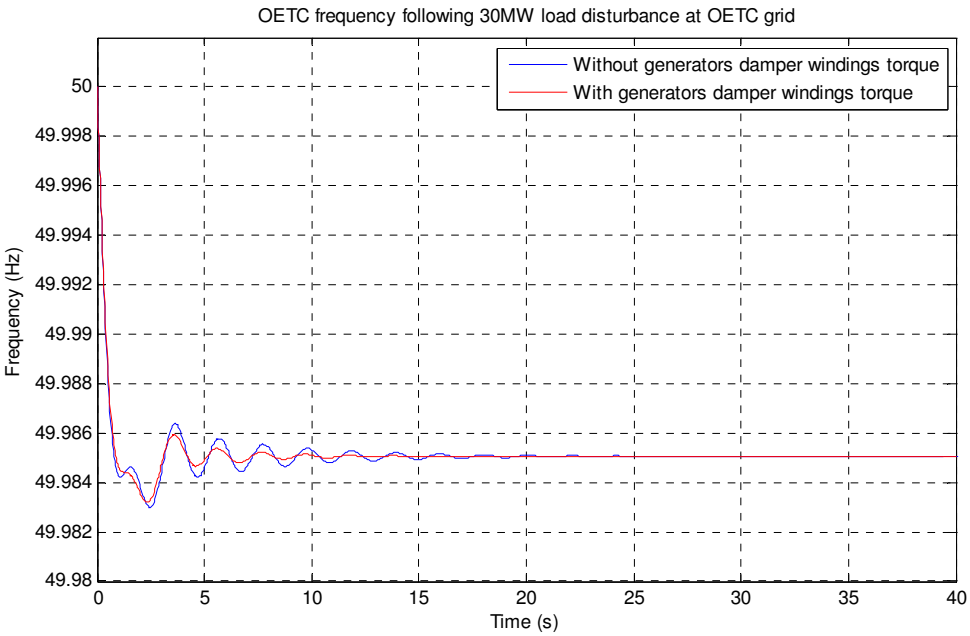

Figure 7.12: OETC frequency following 30MW load disturbance at OETC grid

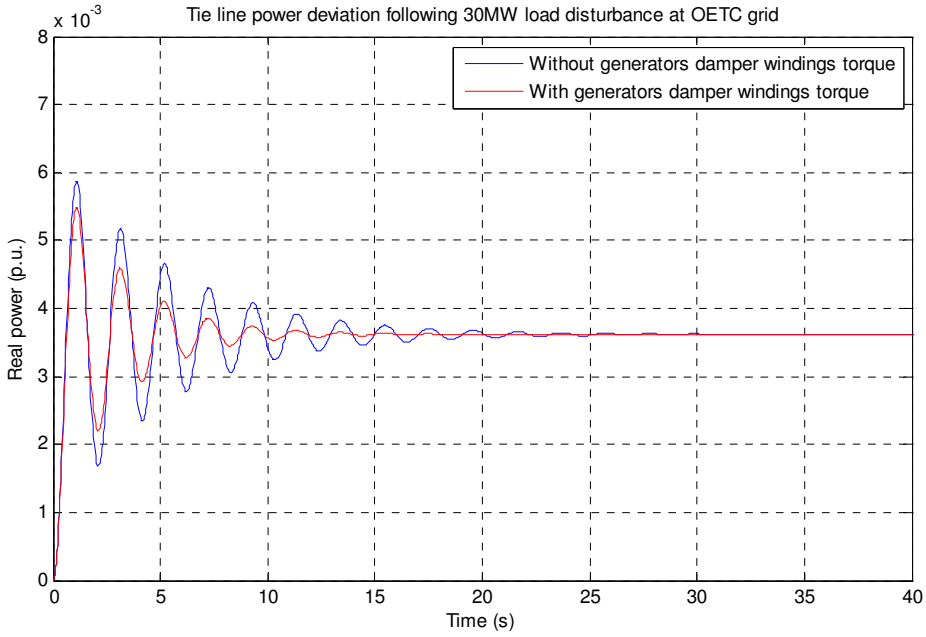

Figure 7.13: Tie line power deviation following 30MW load disturbance at OETC grid

Disturbance size and location	Model status	Steady state frequency (Hz)	Steady state power flow towards OETC (p.u.)	Settling time (s)
30MW load disturbance at PDO grid	Nominal model without generators damper windings torque	49.985	-0.0114	13.1
	Nominal model with generators damper windings torque	49.985	-0.0114	7.88
30MW load disturbance at OETC grid	Nominal model without generators damper windings torque	49.985	0.0036	6.97
	Nominal model with generators damper windings torque	49.985	0.0036	4.77

Table 7.5: Summary of generators damper windings effect test

7.3.4. Discussion

From Figure 7.8 to Figure 7.13 and Table 7.5, it is clear that incorporating the generators damper windings effect has improved the settling time of the overall system model response. The frequency oscillations are better damped with the consideration of the damper winding effect; therefore the oscillations amplitudes were reduced.

The incorporation of generators damper windings effect is a novel approach in the field of AGC modelling and it has proved some improvement in the model dynamic response.

7.3.5. Summary

The generators damper windings torque has noticeable effect on the system response characteristics. Therefore it is worth considering when refining the traditional approach of AGC modelling. This consideration is a novel approach in the field of AGC studies.

7.4. Generation Rate Constraint consideration

Different types of power generation plants exhibit different response to fast load pickup following load disturbances in the grid. The rate of change of the generation plant real power output is often limited depending on the type of the plant. For instant, rapid change in steam turbines power output will draw excessive steam from the boiler which will cause steam condensation due to adiabatic expansion (Moon et al, 2002). The steam condensation may produce water droplets which will abrade the turbine blades by hitting. Therefore it is a must to limit the generation rate of change to limit the excessive wear and tear on the turbine components. Hence steam turbines governing systems are provided with generation rate constraints. Likewise, gas turbines are limited on the maximum temperature which its combustion components can withstand without excessive wear and tear. Therefore gas turbines governing system is equipped with maximum fuel valves opening limit to limit the amount of fuel injected to the gas turbine combustion components.

Consideration of these generation rates limits or constraints will actually introduce non-linearity in gas turbines and steam turbines dynamic models.

Therefore, as part of the model refining process, it was decided to investigate the effect of Generation Rate Constraints (GRC) on the model response characteristics. A number of researchers have considered the GRC in their modelling process for AGC studies (Farhangi et al, 2012; Shayeghi and Shayanfar, 2006; Shayeghi, et al [(2)], 2006; Yesil et al, 2004; Demiroren and Yesil, 2004; El-Sherbiny et al, 2002; Chang and Fu, 1997; Konstantinos et al, 2007). However, most of the researchers whom considered the GRC have been dealing with small power systems consisting of a few number of generation units. In this section of the report, we are investigating the effect of GRC on the system frequency response characteristics of the practical size PDO-OETC model. The outcome of this work will determine the feasibility of considering the GRC when modelling large scale power systems for AGC studies.

7.4.1. Generation Rate Constraint

Generation Rate Constraint in gas turbines is achieved by limiting the fuel gas inlet to the gas turbine combustion chamber. It is achieved by introducing valve opening limits in the gas turbine governing system. PDO is following GE recommendations for modelling gas turbines GRC (Petroleum Development Oman LLC [(3)], 2004, p13]. The GRC limits the thermal stress of the gas turbines. As per PDO practice, the following limits shown in Table 7.6 are considered for gas turbines generators and therefore are used in this study:

Min limit of GRC (p.u.)	Max limit of GRC (p.u.)
-0.1	1.5

Table 7.6: Gas Turbines Generation Rate Constraint limits

The above values are assumed suitable for all installed gas turbines generators at PDO and OETC power systems. The values in Table 7.6 are in per unit of the Fuel Stroke Reference (FSR) value. A typical gas turbine model with a GRC incorporated will look like Figure 7.14.

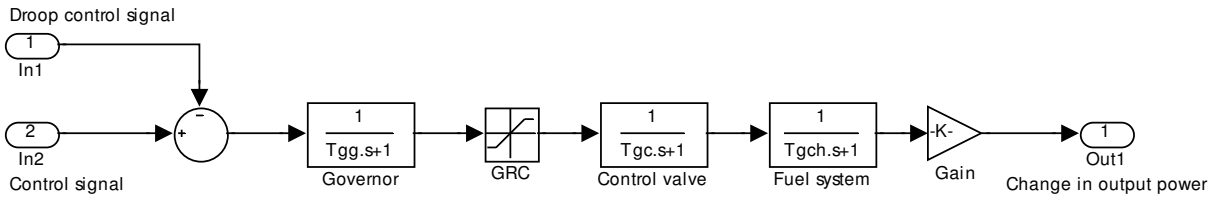

Figure 7.14: A power station model consisting of one gas turbine with GRC

Steam turbine generation rate constraint GRC is achieved by limiting the rate of the change of the steam flow through the steam turbine. All steam turbines installed at OETC grid are of the non-reheating type. This kind of steam turbines can demonstrate faster response than the reheating type due to the higher steam storing capacity of the boiler than the re-heater. This will allow the non-reheating steam turbine boiler giving up more steam without significant pressure drop. Yesil et al (2004) suggests the generation rate constraint GRC limits values shown in Table 7.7 for non-reheating type steam turbine generator which will be used in this study for all OETC side steam turbines.

Min limit of GRC (p.u./s)	Max limit of GRC (p.u./s)
-0.015	0.015

Table 7.7: Steam Turbine Generation Rate Constraint limits

A typical steam turbine model with a GRC incorporated will look like the one in Figure 7.15 (Farhangi et al, 2012; Shayeghi and Shayanfar, 2006; Shayeghi et al [(2)], 2006; Yesil, 2004).

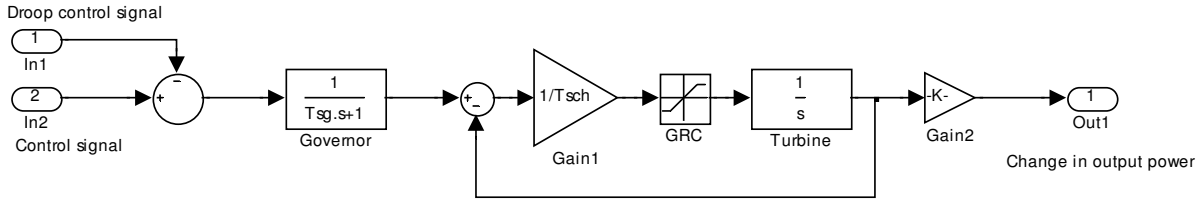

Figure 7.15: A power station model consisting of one steam turbine with GRC

7.4.2. Simulation results

The developed PDO-OETC model has been modified to include the GRC in all generating units' models in both PDO and OETC power systems. The modified PDO-OETC model has been simulated as per following conditions:

- -100MW load disturbance at OETC grid
- 100MW load disturbance at OETC grid
- -200MW load disturbance at OETC grid
- 200MW load disturbance at OETC grid

The selection of the above load disturbances sizes is based on the normal and maximum expected load disturbances that can arise within PDO. A 100 MW load disturbance can normally happen at PDO or OETC. A 200MW load disturbance is not usual at PDO but can happen at OETC side due to the larger size generating units installed at OETC. As far as the generators are concerned, the load disturbance can be at PDO or OETC grids. Therefore it was decided to consider a load disturbance at OETC grid for this test since OETC is vulnerable to both normal and maximum load disturbances scenarios. This wide range of load disturbances is essential to explore the effects of GRC. The above scenarios were simulated with the nominal model and with the modified model (with GRC) and the results are shown in figures 7.16 to 7.19 respectively.

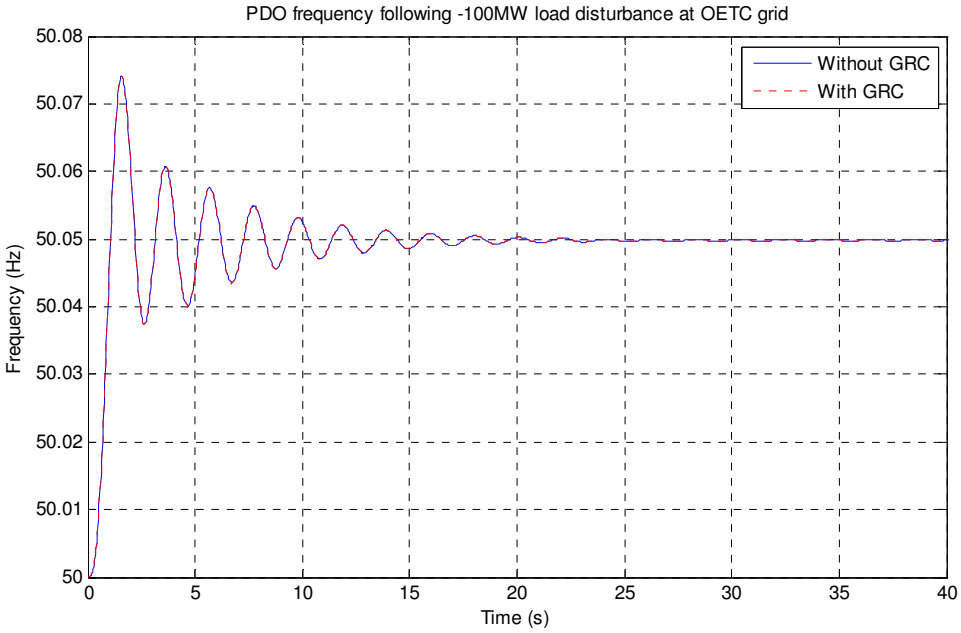

Figure 7.16: PDO frequency following -100MW load disturbance at OETC grid with and Without GRC

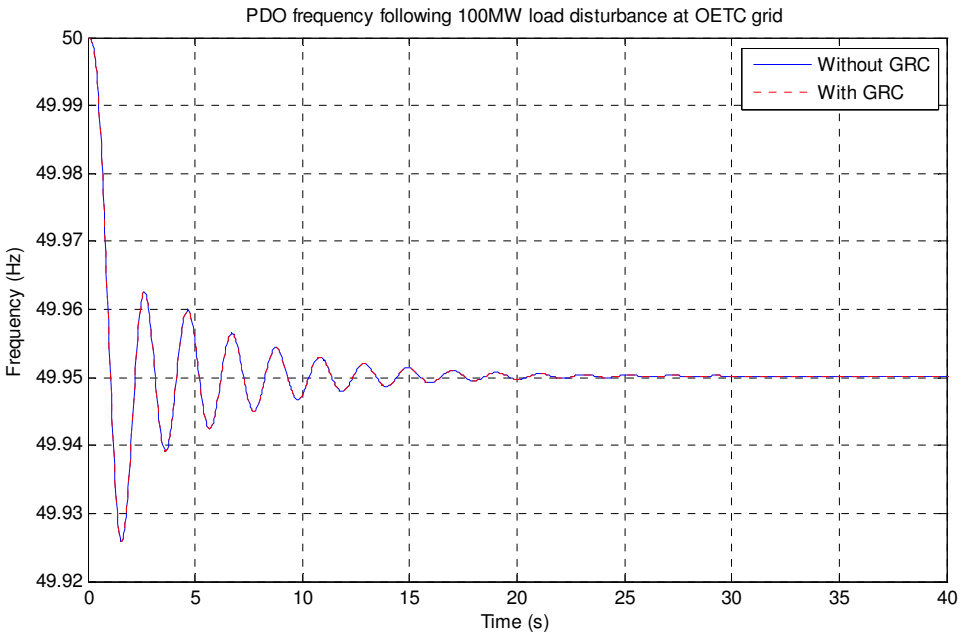

Figure 7.17: PDO frequency following +100MW load disturbance at OETC grid with and Without GRC

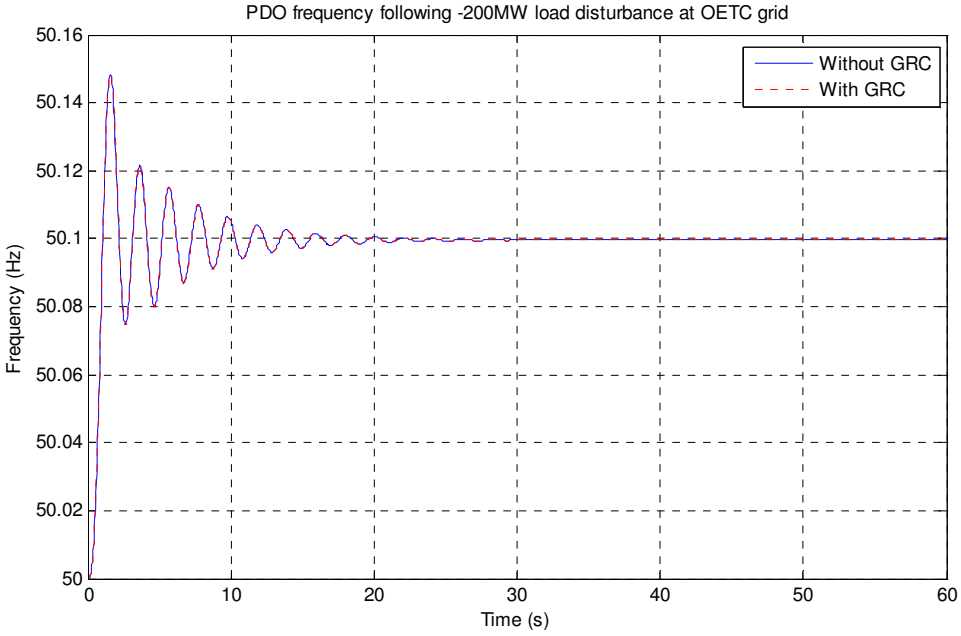

Figure 7.18: PDO frequency following -200MW load disturbance at OETC grid with and Without GRC

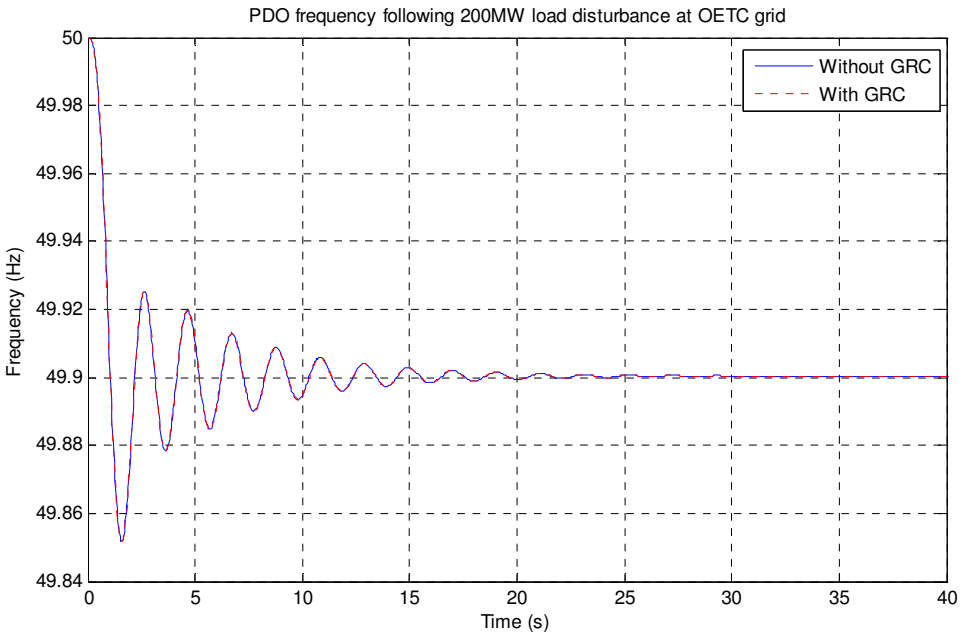

Figure 7.19: PDO frequency following +200MW load disturbance at OETC grid with and Without GRC

7.4.3. Results discussion

Figure 7.16 and Figure 7.17 show that the GRC has no effect on the system frequency response characteristics or the final steady state deviation when considering ±100MW load disturbance. The response is exactly the same with and without GRC. It means that the GRC limits do not come into picture for relatively small load disturbances because each generator in the grid is required to recover a small portion of the total load disturbance.

Similarly, Figure 7.18 and Figure 7.19 show that the response was exactly the same with and without the GRC limits. It implies that even a ±200MW load disturbance will not hit the GRC limits.

From the above analysis one can conclude that when modelling large scale interconnected power system for AGC studies, consideration of GRC will not add any practical value.

7.4.4. Summary

GRC is a limit which is introduced in the generation units control circuits to limit the thermal and mechanical stresses on the generation units. Modelling of GRC has been of interest to many researchers. The GRC modelling is feasible when we are considering small size power systems with small number of generators. Apparently, with small number of generation units, the GRC limits will be hit with small size load disturbance and hence introducing some nonlinearity into the system response. On the other hand, when considering large scale power system like the PDO-OETC power system, the GRC limits

will not be hit with practical size load disturbances. Furthermore, modelling of GRC will put extra burden on the modelling effort and the computation effort. Therefore it is concluded that as far as PDO-OETC power system is concerned, modelling of GRC is not feasible because it is not adding any practical value.

7.5. The refined PDO-OETC power systems model

This section summarises the efforts devoted in considering some of the practical aspects for the sake of refining PDO-OETC power systems model. From the analysis shown in the model refining process, it is apparent that some practical aspects are important and they directly impact the model response characteristics. The following are the practical aspects which are considered important to produce the refined model:

- Base load effect
- Preselect load control mode effect
- Generators damper windings effect.

The above three aspects are incorporated in the original PDO-OETC power system model to see their overall impact on the model response. The model is then simulated and compared with the real life scenarios.

7.5.1. Simulation results

The above three aspects have been modelled and incorporated in the refined model. The refined model has been used to simulate the six real scenarios discussed earlier in the model validation process. Accordingly six graphs have been produced one for each scenario and are shown in Figure 7.20 to Figure 7.25. The figures also compare the refined model response with the nominal model response and the real response. The focus is on the rate of change of the frequency following the disturbance, the steady state deviation and the amplitude and frequency of oscillations. A summary table has been also produced and is shown in Table 7.8. The table compares the simulation results of the nominal model and the refined model with the real system response.

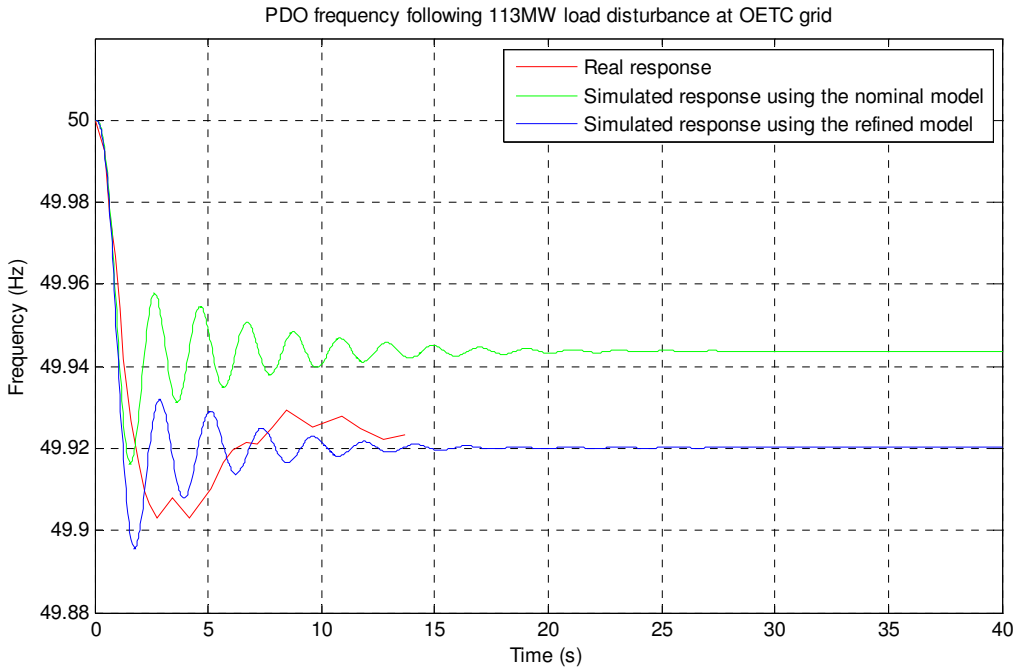

Figure 7.20: Scenario 1; Real and Simulated behaviour of PDO frequency following 113MW generator trip at OETC grid

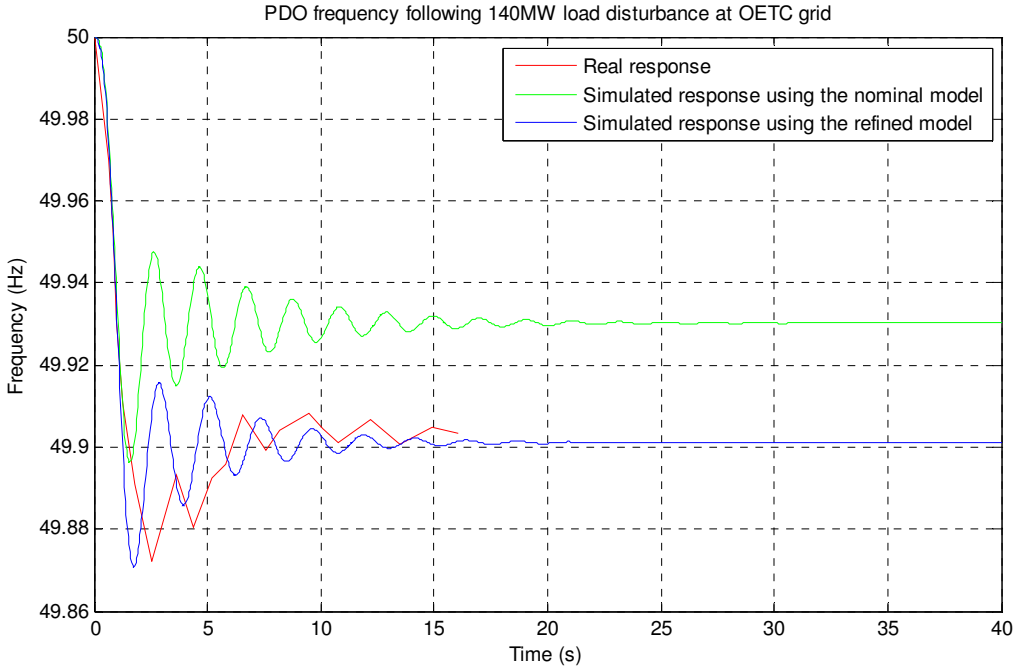

Figure 7.21.: Scenario 2; Real and Simulated behaviour of PDO frequency following 140MW generator trip at OETC grid

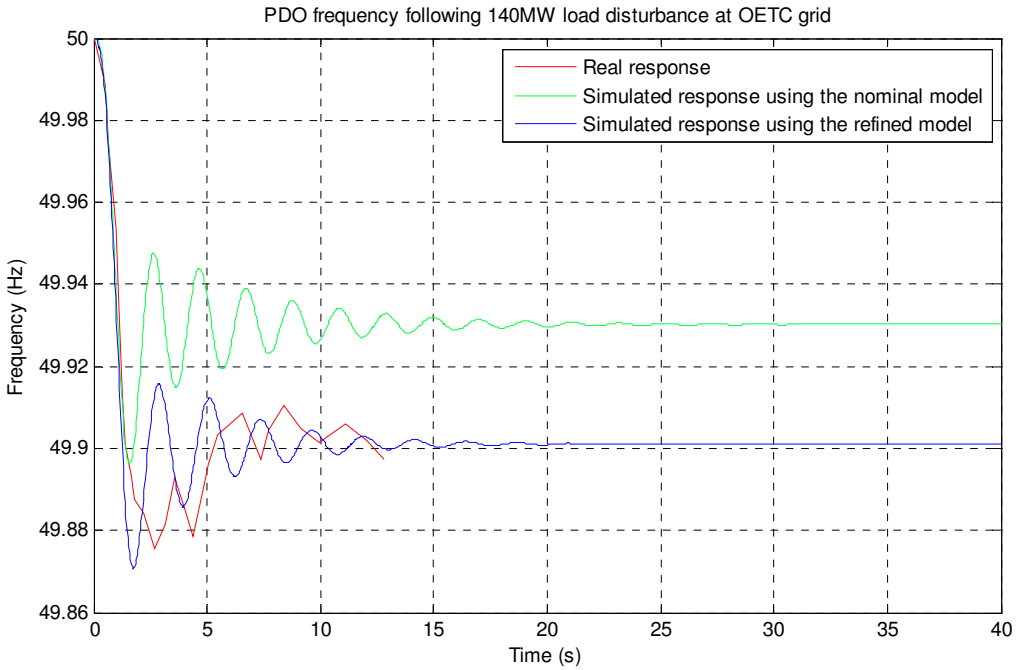

Figure 7.22: Scenario 3; Real and Simulated behaviour of PDO frequency following 140MW generator trip at OETC grid

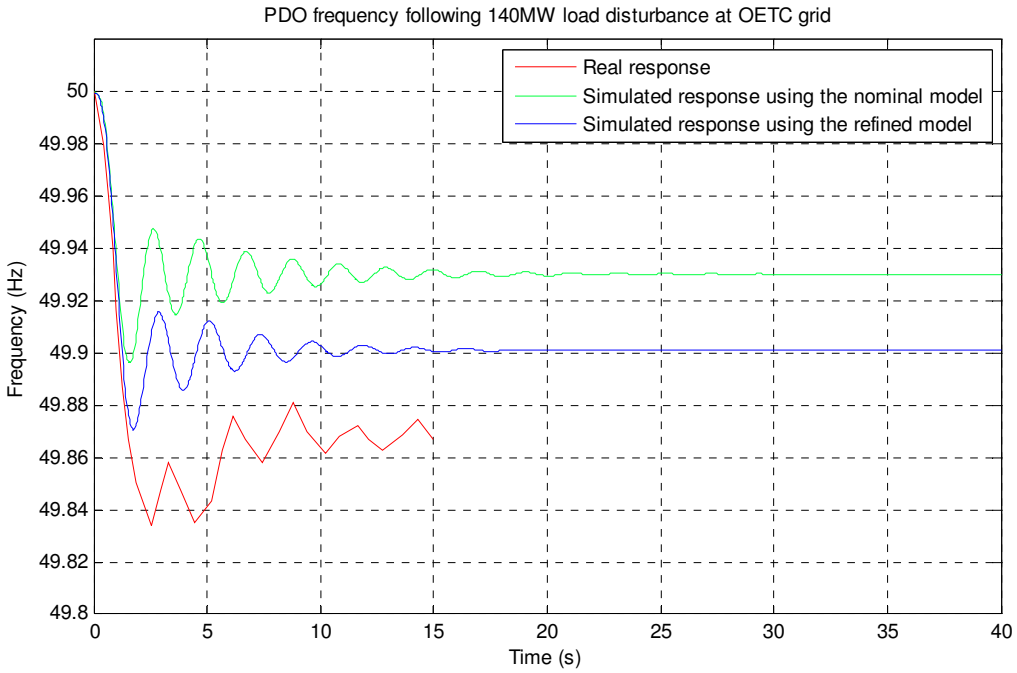

Figure 7.23: Scenario 4; Real and Simulated behaviour of PDO frequency following 140MW generator trip at OETC grid

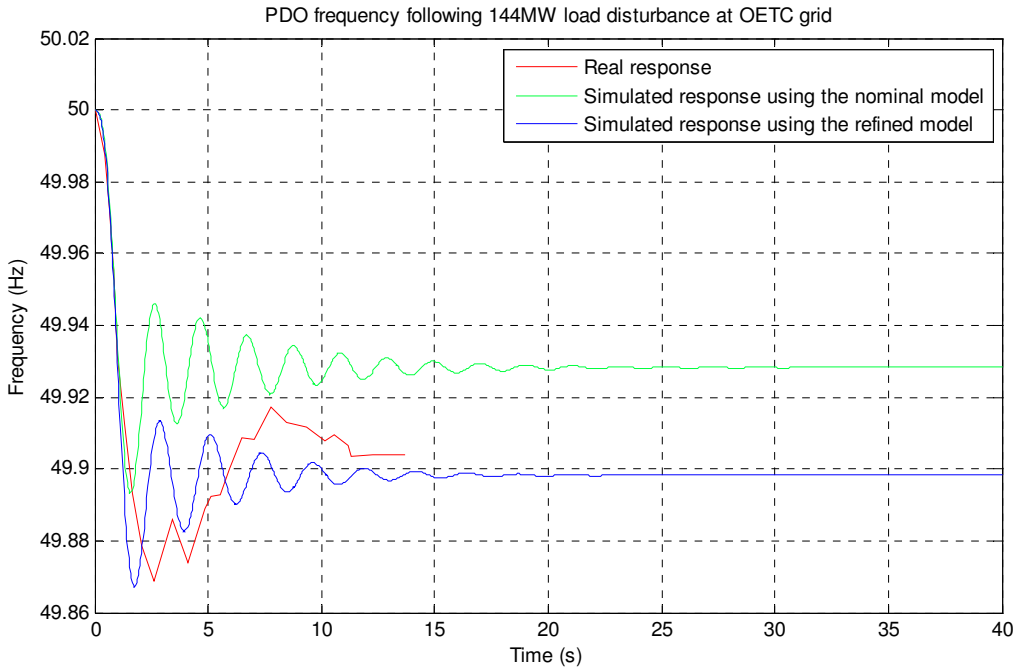

Figure 7.24: Scenario 5; Real and Simulated behaviour of PDO frequency following 144MW generator trip at OETC grid

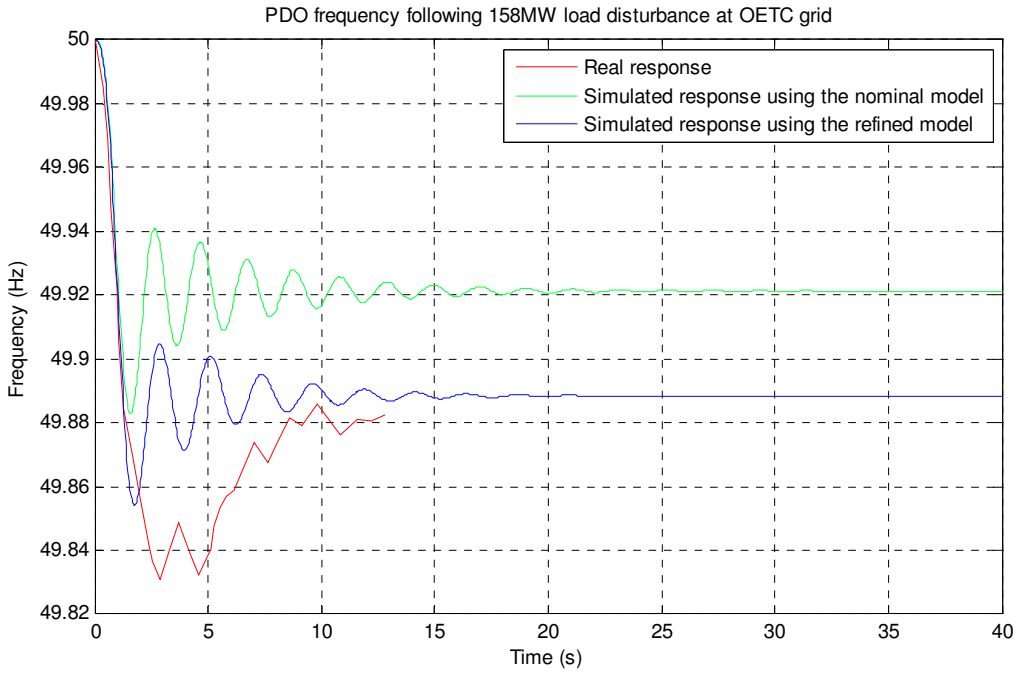

Figure 7.25: Scenario 6; Real and Simulated behaviour of PDO frequency following 158MW generator trip at OETC grid

			Model	Real system results	Simulated results	Percentage error
Scenario 1	113MW disturbance at OETC on 20/5/2008 @2159hrs	Frequency deviation (Hz)	Nominal Model	-0.077	-0.056	-27.3%
			Refined Model		-0.08	+3.9%
Scenario 2	140MW disturbance at OETC on 25/5/2008 @1047hrs	Frequency deviation (Hz)	Nominal Model	-0.097	-0.07	-27.8%
			Refined Model		-0.099	+2%
Scenario 3	140MW disturbance at OETC on 26/5/2008 @1128hrs	Frequency deviation (Hz)	Nominal Model	-0.103	-0.07	-32%
			Refined Model		-0.099	-3.9%
Scenario 4	140MW disturbance at OETC on 24/6/2008 @1754hrs	Frequency deviation (Hz)	Nominal Model	-0.133	-0.07	-47.4%
			Refined Model		-0.099	-25.6%
Scenario 5	144MW disturbance at OETC on 21/5/2008 @1029hrs	Frequency deviation (Hz)	Nominal Model	-0.096	-0.072	-25%
			Refined Model		-0.102	+6.25%
Scenario 6	158MW disturbance at OETC on 26/5/2008 @1510hrs	Frequency deviation (Hz)	Nominal Model	-0.117	-0.079	-32.5%
			Refined Model		-0.112	-4.3%

Table 7.8: Summary of nominal model and refined model results.

7.5.2. Discussion

From figures 7.20 to 7.25 and Table 7.8, it can be clearly seen that the consideration of the three practical aspects has greatly improved the model response accuracy with reference to the real system response. The percentage error is within ±10% limit for all scenarios which happened in the same month i.e. the same operating points. The only scenario which is still persisting around 20% error was scenario 4. This scenario happened at the end of June where the system has different operating points than other scenarios. It can be explained as there are more units operating at base load towards the hottest period of the summer, therefore we shall expect more deviation in the frequency.

However, the difference in the oscillatory frequency is still persisting between the simulated response and the real response. It will be dealt with in the next section of this report which is concerned about fine tuning some of the model parameters.

7.5.3. Summary

Utilising the practical understanding of the power system operation proved to be extremely useful in refining the modelling approach and the model response. The model response has been greatly improved to an acceptable error limits. The results proved that the refined model is of enough accuracy and is suitable for further analysis. However there is still some difference in the oscillatory frequency persisting between the simulated response and the real life system response which will be considered in the next section of this report.

7.6. Fine tuning of PDO-OETC power systems refined model

In this part, the refined model of PDO-OETC power systems will be further fine tuned using MATLAB "fminsearch" optimisation method. An Mfile has been written to do the task. Section 5.4 has summarised that the PDO-OETC power system model is quite sensitive to modelling errors in the following two parameters:

- Power system inertia
- Synchronising torque coefficient

Therefore the above two parameters will be fine tuned so that the simulated response closely matches the real response. An Mfile has been written to fine tune PDO inertia constant, OETC inertia constant and the synchronising torque coefficient.

7.6.1. MATLAB Mfile

Two Mfile programs have been written to execute the task. The first one is called the "PdoOetc_Opt" and the second one is the "Simulator". The second Mfile will call upon the first programme as part of the simulation process. The overall aim is to simulate the model while changing the three parameters PDO inertia constant (Hpdo), OETC inertia constant (Hoetc) and synchronising torque coefficient (Tiv). Each time, the integral of the squared error (difference between the simulated and real responses) will be calculated in order to be minimised. The simulation can be aborted anytime when the two responses (simulated and real) are closely matching with focus on the difference in the oscillatory frequency. The PDO-OETC refined model has been used and is shown in Figure 7.26. The two Mfiles are shown in Appendix 2.

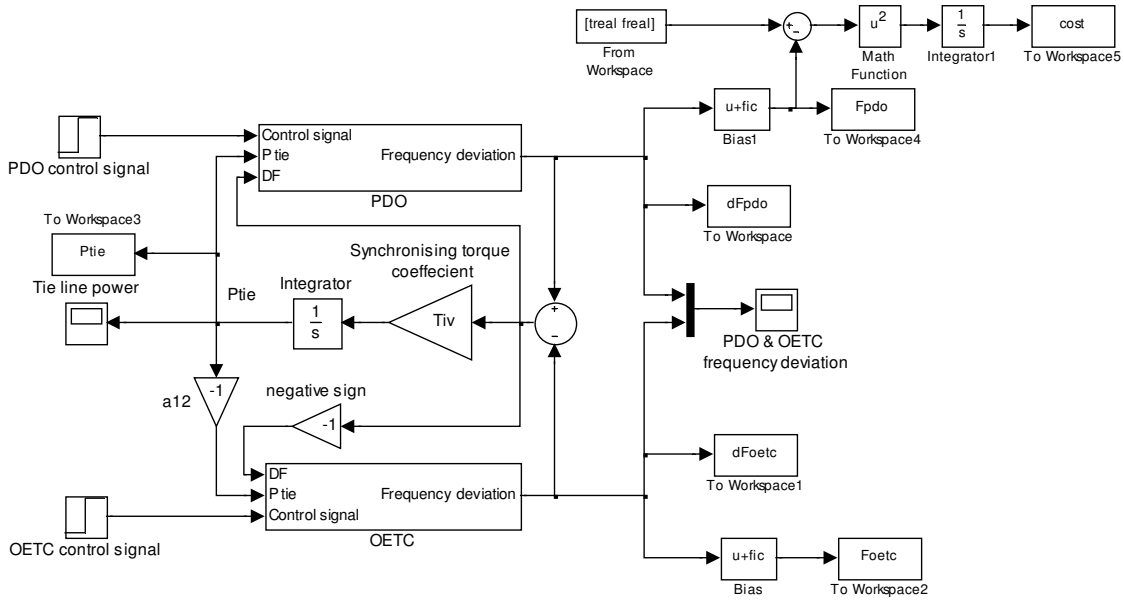

Figure 7.26: PDO-OETC refined model used for the parameters tuning process

7.6.2. Parameters tuning results

The two Mfiles developed earlier were used to simulate Real life scenario number 2. Scenario 2 is selected because it is proven earlier that it is the closest one to the simulated results. Therefore using scenario 2 for the tuning will avoid misleading results.

The tuning has been done and the result shown in Figure 7.27 is found to be the best in terms of reduction in the oscillatory frequency difference. The constants Hpdo, Hoetc and Tiv which produced Figure 7.27 are shown in Table 7.9.

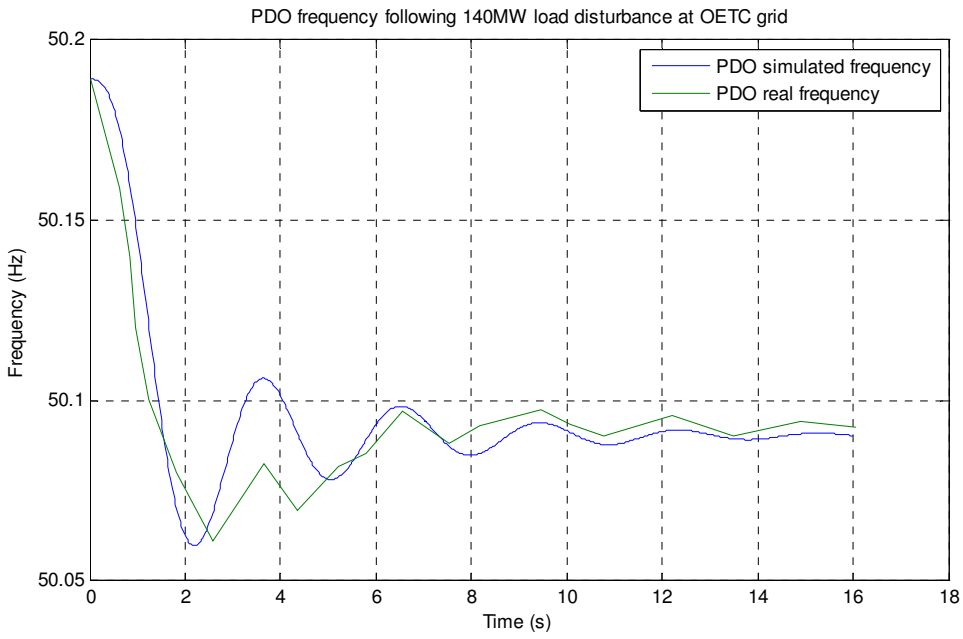

Figure 7.27: Scenario 2: PDO frequency following 140MW load disturbance at OETC side after model parameters tuning

	Hpdo	Hoetc	Tiv
Original values	4.45098	14.03546	0.94
Tuned values	4.8417	15.5023	0.7220
Percentage change	+ 8.8%	+ 10.5%	- 23.2%

Table 7.9: PDO-OETC refined model tuned parameters

From Table 7.9, one can see that the percentage changes in system inertia and synchronising torque coefficient are consistent with the error ranges used in the parameters sensitivity tests in section 5. The above tuned parameters will be used to simulate the remaining five scenarios discussed earlier in section 7.5.

7.6.3. Simulation results

The refined model with the tuned parameters has been used to simulate the other five real scenarios (1,3,4,5&6) discussed earlier in the model validation process. Scenario 2 is already shown in Figure 7.27 above. Accordingly five more graphs have been produced one for each scenario and are shown in Figure 7.28 to Figure 7.32. The figures also compare the refined model with the fine tuned parameters simulation response with the nominal model response, the refined model response and the real system response. Since this exercise is mainly to reduce the difference in the oscillatory frequency between the simulated and real responses, there is no necessity to calculate the steady state deviation error again as it was comprehensively discussed earlier in section 7.5.

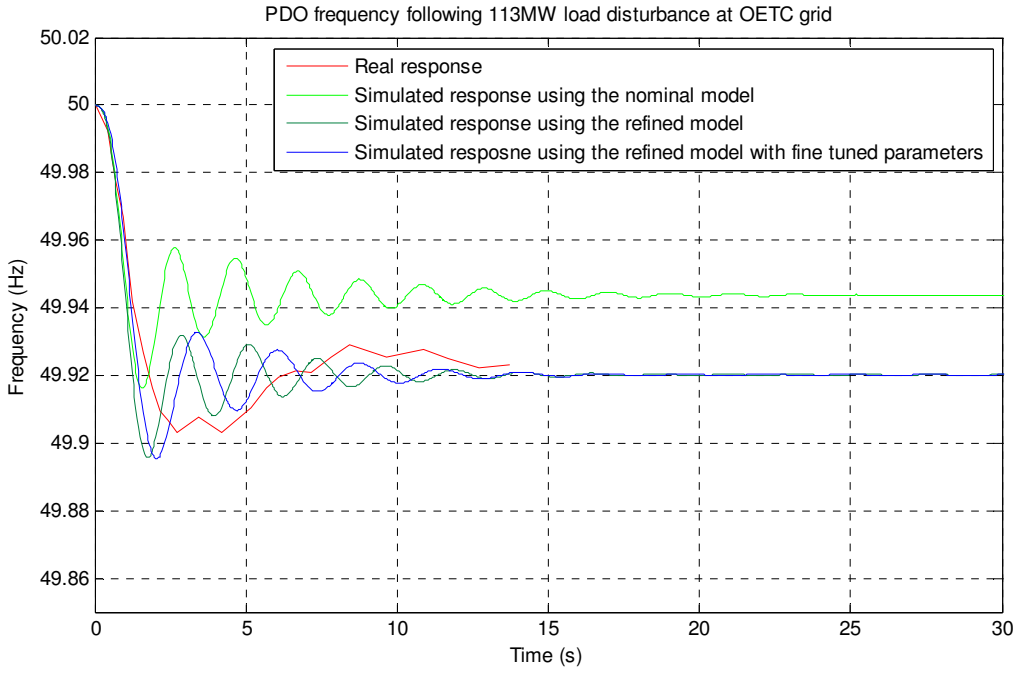

Figure 7.28: Scenario 1; Real and Simulated behaviour of PDO frequency following 113MW generator trip at OETC grid

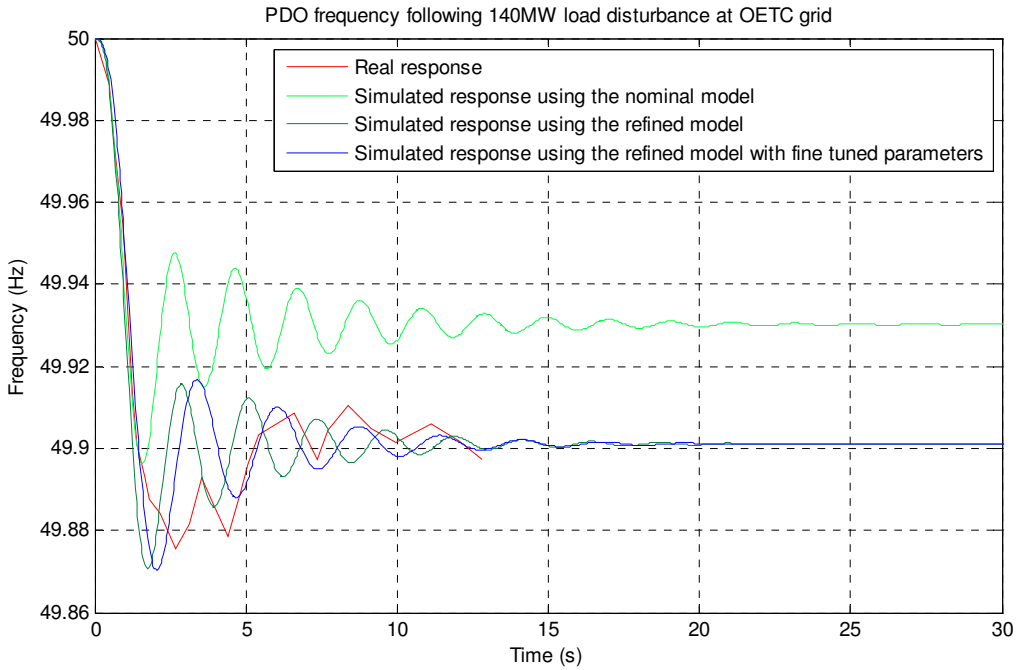

Figure 7.29: Scenario 3; Real and Simulated behaviour of PDO frequency following 140MW generator trip at OETC grid

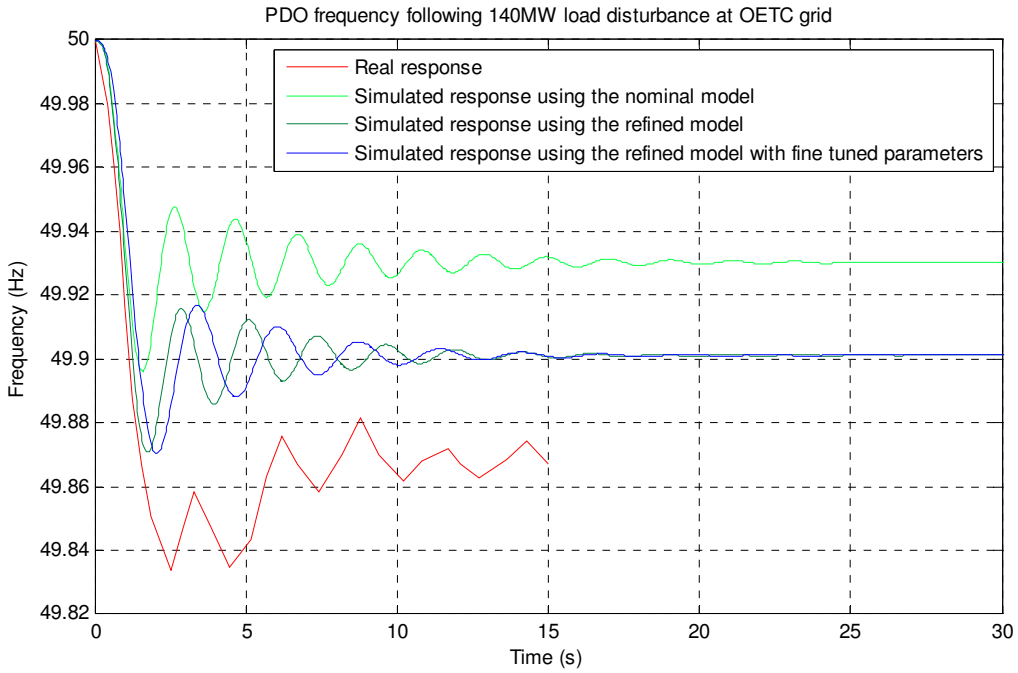

Figure 7.30: Scenario 4; Real and Simulated behaviour of PDO frequency following 140MW generator trip at OETC grid

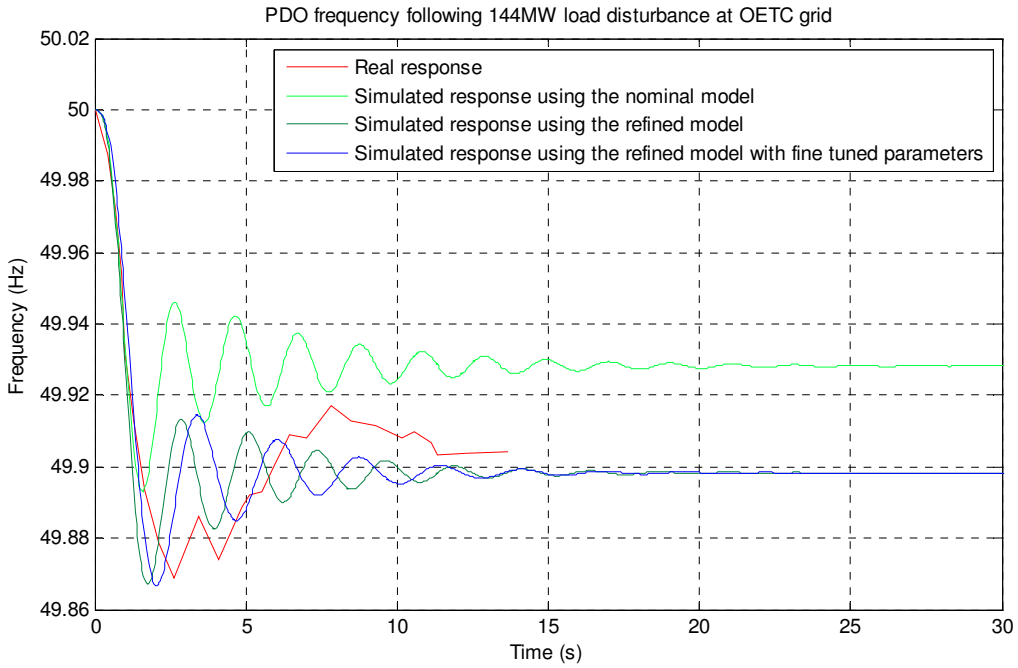

Figure 7.31: Scenario 5; Real and Simulated behaviour of PDO frequency following 144MW generator trip at OETC grid

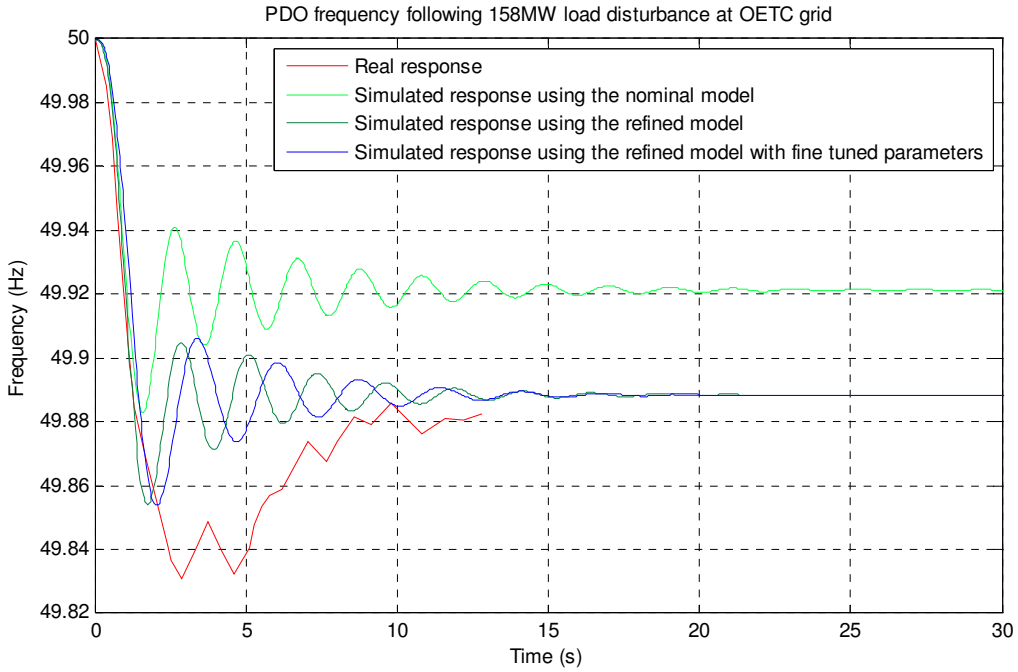

Figure 7.32: Scenario 6; Real and Simulated behaviour of PDO frequency following 158MW generator trip at OETC grid

7.6.4. Discussion

From Figures 7.27 to 7.32, it is qualitatively clear that the difference in the oscillatory frequency between the simulated response using the refined model with fine tuned parameters and real response has been remarkably reduced in all six scenarios if compared

with the nominal model and the refined model. It is apparent now that the simulated oscillations using the refined model with fine tuned parameters are more aligned with the real response oscillations although they are not perfectly aligned. Getting closer and closer to the real response proves that all the modelling effort devoted in this study is in the right direction. The percentage change in Hpdo, Hoetc and Tiv parameters is within an acceptable range as can be seen from Table 7.9. It is particularly acceptable if we consider the significant number of assumptions been placed during the modelling process and the large scale model in general.

The new deduced PDO-OETC model parameters which are shown in Table 7.9 completes the model refining process and the model will be considered for further analysis.

7.6.5. Summary

The parameters tuning method is considered as part of the model refining process and is targeted to reduce the difference in the oscillatory frequency between the simulated response and real response of PDO-OETC power system. A selected number of parameters have been considered based on the model sensitivity to those parameters. These parameters are PDO power system inertia constant, OETC power system inertia constant and the synchronising torque coefficient. The parameters tuning method has been successful in reducing the difference in the oscillatory frequency between the simulated response oscillations and the real life response oscillations. The newly tuned parameters will be used in the refined model for further analysis.

7.7. Summary of the model refining process

A systematic approach has been followed starting with the model development based on the traditional approach, then the model validation and finally the model refining process. The aim of the whole task is to get confidence on the model validity in representing the real system. Consequently all results and recommendations based on this model will be of sufficient accuracy. The final results proved that the modelling process is in the right direction and most of the assumptions made are realistic assumptions. On the other hand some assumptions have been revisited and verified in order to refine the model. The refined model proves to be of better accuracy than the nominal model. The refined model parameters have then been fine tuned for further accuracy. The refined model with the fine tuned parameters will be used to develop control philosophies and to design AGC controllers. All subsequent work will be based on the final fine tuned model of PDO-OETC power system.

Chapter 8: State space representation of PDO-OETC perturbation model

8.1. Introduction

In state space representation of dynamic systems, we are concerned with three types of variables, input variables, output variables and state variables. In order to represent a dynamic system in state space, the dynamic model must involve elements which can memorize the values of the inputs. Integrators are considered as memory devices therefore the output of such integrators can be considered as the variable that define the integral state of the dynamic system (OGATA, 2008, p. 71). For a given dynamic system, there are different state space representations but the number of states will remain the same in all of them. The number of states is a character of the dynamic model because it is based on the differential equations representing the system.

In this part, PDO-OETC model will be represented in state space form based on the differential equations of the model. Then the derived state space model step response will be compared with the earlier developed continuous model step response.

8.2. PDO-OETC model differential equations

For state space representation there are certain equations can be summated together and represented by one equation giving the same output as the whole set. For example PDO has 25 gas turbines running in parallel in different power stations and are represented by one gas turbine with a capacity equaling to the 25 gas turbines. OETC has two types of turbines, gas and steam turbines; therefore it will be represented by one steam turbine and one gas turbine. Their capacity will be equalling to the accumulated capacity of all turbines of the same type. The above assumption has resulted in great reduction in the number of the state variables of the states space representation. Hence, the following eleven equations are representing PDO-OETC perturbation model:

$$\frac{d}{dt}\Delta P_{tie} = T_{iv}\left(\Delta f_{pdo} - \Delta f_{oetc}\right) \quad \text{.....(8.1)}$$

$$\frac{d}{dt}\Delta f_{pdo} = \frac{f}{2H_{pdo}}\left(Kg_{pdo}\Delta Pgg_{pdo} - \Delta Pd_{pdo} - D_{pdo}\Delta f_{pdo} - \Delta P_{tie} - Kdw_{pdo}\left(\Delta f_{pdo} - \Delta f_{oetc}\right)\right) \quad \text{.....(8.2)}$$

$$\frac{d}{dt}\Delta Pgg_{pdo} = \frac{-1}{Tgch}\Delta Pgg_{pdo} + \frac{1}{Tgch}\Delta Xgc_{pdo} \quad \text{.....(8.3)}$$

$$\frac{d}{dt}\Delta Xgc_{pdo} = \frac{-1}{Tgc}\Delta Xgc_{pdo} + \frac{1}{Tgc}\Delta Xgg_{pdo} \text{ ……..(8.4)}$$

$$\frac{d}{dt}\Delta Xgg_{pdo} = \frac{-1}{Tgg}\Delta Xgg_{pdo} - \frac{1}{TggR_{pdo}}\Delta f_{pdo} + \frac{1}{Tgg}\Delta Pc_{pdo} \text{ ……..(8.5)}$$

$$\frac{d}{dt}\Delta f_{oetc} = \frac{f}{2H_{oetc}}\left(Kg_{oetc}\Delta Pgg_{oetc} + Ks_{oetc}\Delta Psg_{oetc} - \Delta Pd_{oetc} - D_{oetc}\Delta f_{oetc} - a_{12}\Delta P_{tie} - a_{12}Kdw_{oetc}\left(\Delta f_{pdo} - \Delta\right.\right.$$
……(8.6)

$$\frac{d}{dt}\Delta Pgg_{oetc} = \frac{-1}{Tgch}\Delta Pgg_{oetc} + \frac{1}{Tgch}\Delta Xgc_{oetc} \text{ ……..(8.7)}$$

$$\frac{d}{dt}\Delta Xgc_{oetc} = \frac{-1}{Tgc}\Delta Xgc_{oetc} + \frac{1}{Tgc}\Delta Xgg_{oetc} \text{ ……(8.8)}$$

$$\frac{d}{dt}\Delta Xgg_{oetc} = \frac{-1}{Tgg}\Delta Xgg_{oetc} - \frac{1}{TggR_{oetc}}\Delta f_{oetc} + \frac{1}{Tgg}\Delta Pc_{oetc} \text{ ……(8.9)}$$

$$\frac{d}{dt}\Delta Psg_{oetc} = \frac{-1}{Tsch}\Delta Psg_{oetc} + \frac{1}{Tsch}\Delta Xsg_{oetc} \text{ ……(8.10)}$$

$$\frac{d}{dt}\Delta Xsg_{oetc} = \frac{-1}{Tsg}\Delta Xsg_{oetc} - \frac{1}{TsgR_{oetc}}\Delta f_{oetc} + \frac{1}{Tsg}\Delta Pc_{oetc} \text{ ……(8.11)}$$

The above equations variables and constants are defined as below:

ΔP_{tie} : Tie line power deviation

Δf_{pdo} : PDO frequency deviation

ΔPgg_{pdo} : Change in the mechanical power output of PDO gas turbines generators

ΔXgc_{pdo} : Change in the control valve position of PDO gas turbines generators

ΔXgg_{pdo} : Change in the governor signal of PDO gas turbines generators

Δf_{oetc} : OETC frequency deviation

ΔPgg_{oetc} : Change in the mechanical power output of OETC gas turbines generators

ΔXgc_{oetc} : Change in the control valve position of OETC gas turbines generators

ΔXgg_{oetc} : Change in the governor signal of OETC gas turbines generators

ΔPsg_{oetc} : Change in the mechanical power output of OETC steam turbines generators

ΔXsg_{oetc} : Change in the governor signal of OETC steam turbines generators

ΔPc_{pdo} : Change in PDO generators loading reference point

ΔPc_{oetc} : Change in OETC generators loading reference point

ΔPd_{pdo} : Change in PDO load

ΔPd_{oetc} : Change in OETC load

f : Nominal frequency of 50Hz

a_{12} : Sign reversing constant (-1)

R_{pdo} : Droop control gain of PDO generators

R_{oetc} : Droop control gain of OETC generators

T_{iv} : Synchronizing torque coefficient

H_{pdo} : PDO generators accumulated inertia

Kg_{pdo} : PDO gas turbines generators p.u. capacity

D_{pdo} : PDO load damping coefficient

Kdw_{pdo} : Accumulated PDO generators damper windings torque coefficient

Kg_{oetc} : OETC gas turbines generators p.u. capacity

Ks_{oetc} : OETC steam turbines generators p.u. capacity

D_{oetc} : OETC load damping coefficient

Kdw_{oetc} : Accumulated PDO generators damper windings torque coefficient

$Tgch$: Gas turbine charging time constant

Tgc : Gas turbine control valve time constant

Tgg : Gas turbine governor time constant

$Tsch$: Steam turbine charging constant

Tsg : Steam turbine governor time constant

8.3. State space matrices formulation

In state space representation, the PDO-OETC perturbation model will be represented in the following form:

$$\begin{aligned} \dot{x}(t) &= Ax(t) + Bu(t) \\ y(t) &= Cx(t) + Du(t) \end{aligned} \quad \text{……(8.12)}$$

Where:

x : is the states vector

y : is the output vector

u : is the input vector

A : is the state matrix

B : is the input matrix

C : is the output matrix

D : is the direct transmission matrix

OGATA (2008, pp. 70-74) has very clear and constructive steps on how to formulate the state space matrices from the differential equations. Following the same steps the PDO-OETC model matrices are formulated as below:

1. The state matrix A:

There are eleven states, therefore the matrix A is 11x11.

$$A=\begin{bmatrix}
0 & T_{iv} & 0 & 0 & 0 & -T_{iv} & 0 & 0 & 0 & 0 & 0\\
-\frac{f}{2H_{pdo}} & -\frac{f}{2H_{pdo}}\left(D_{pdo}+Kdw_{pdo}\right) & \frac{f}{2H_{pdo}}Kgg_{pdo} & 0 & 0 & \frac{f}{2H_{pdo}}Kdw_{pdo} & 0 & 0 & 0 & 0 & 0\\
0 & 0 & \frac{-1}{Tgch} & \frac{1}{Tgch} & 0 & 0 & 0 & 0 & 0 & 0 & 0\\
0 & 0 & 0 & \frac{-1}{Tgc} & \frac{1}{Tgc} & 0 & 0 & 0 & 0 & 0 & 0\\
0 & \frac{-1}{TggR_{pdo}} & 0 & 0 & \frac{1}{Tgg} & 0 & 0 & 0 & 0 & 0 & 0\\
-\frac{fa_{12}}{2H_{oetc}} & -\frac{fa_{12}}{2H_{oetc}}Kdw_{oetc} & 0 & 0 & 0 & \frac{f}{2H_{oetc}}\left(a_{12}Kdw_{oetc}-D_{oetc}\right) & \frac{f}{2H_{oetc}}Kgg_{oetc} & 0 & 0 & \frac{f}{2H_{oetc}}Ksg_{oetc} & 0\\
0 & 0 & 0 & 0 & 0 & 0 & \frac{-1}{Tgch} & \frac{1}{Tgch} & 0 & 0 & 0\\
0 & 0 & 0 & 0 & 0 & 0 & 0 & \frac{-1}{Tgc} & \frac{1}{Tgc} & 0 & 0\\
0 & 0 & 0 & 0 & 0 & \frac{-1}{TggR_{oetc}} & 0 & 0 & \frac{-1}{Tgg} & 0 & 0\\
0 & 0 & 0 & 0 & 0 & 0 & 0 & 0 & 0 & \frac{-1}{Tsch} & \frac{1}{Tsch}\\
0 & 0 & 0 & 0 & 0 & \frac{-1}{TsgR_{oetc}} & 0 & 0 & 0 & 0 & \frac{-1}{Tsg}
\end{bmatrix}$$

2. The input matrix B:

There are two inputs in the model: PDO control input signal and OETC control input signal, therefore the B matrix is 11x2:

$$B=\begin{bmatrix}
0 & 0\\
0 & 0\\
0 & 0\\
0 & 0\\
\frac{1}{Tgg} & 0\\
0 & 0\\
0 & 0\\
0 & 0\\
0 & \frac{1}{Tgg}\\
0 & 0\\
0 & \frac{1}{Tsg}
\end{bmatrix}$$

3. The output matrix C:

In PDO-OETC model there are three outputs considered, PDO frequency, OETC frequency and the Tie line power. Therefore the C matrix is 3x11.

$$C = \begin{bmatrix} 0 & 1 & 0 & 0 & 0 & 0 & 0 & 0 & 0 & 0 & 0 \\ 0 & 0 & 0 & 0 & 0 & 1 & 0 & 0 & 0 & 0 & 0 \\ 1 & 0 & 0 & 0 & 0 & 0 & 0 & 0 & 0 & 0 & 0 \end{bmatrix}$$

4. The direct transmission matrix D:

In PDO-OETC model there are no direct links between the inputs and outputs i.e. no feed forward signal. Therefore the D matrix is a zero matrix of size 3x2.

$$D = \begin{bmatrix} 0 & 0 \\ 0 & 0 \\ 0 & 0 \end{bmatrix}$$

8.4. Testing of state space model

The derived state space form of PDO-OETC model has been tested by comparing its step response with the earlier developed PDO-OETC continuous-time model. The considered operating condition of the system is when all generators are online and all are on droop control. A MATLAB script has been written to calculate the state space matrices. The script is shown in Appendix 3.

Considering PDO control input signal, a step input signal of 1 p.u. size at PDO control input signal has produced the response shown in Figures 8.1 to 8.3 using both the state space model and the continuous model. The main focus of the simulation is to spot any difference between the state space model response and the continuous model response.

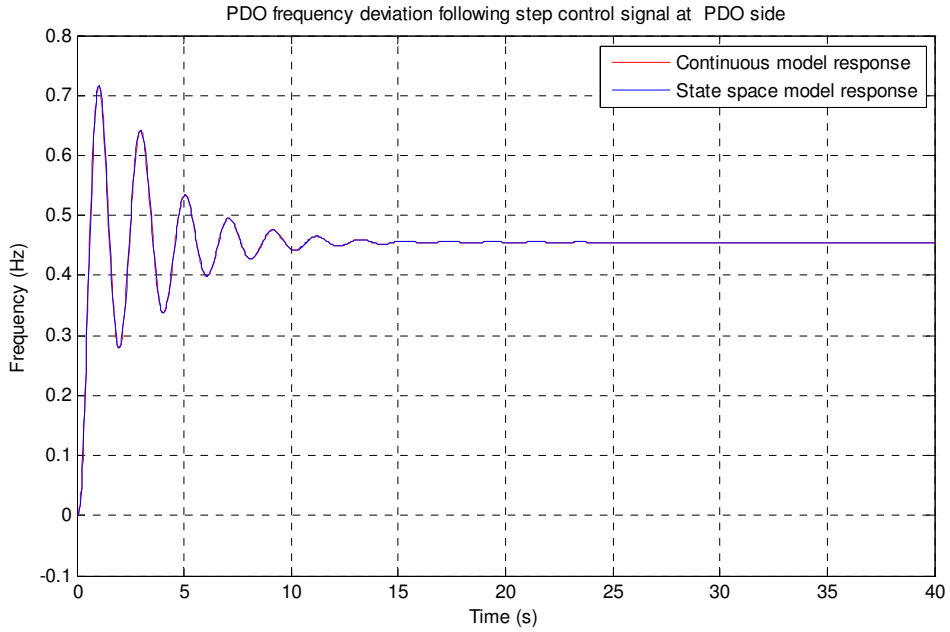

Figure 8.1: PDO frequency deviation following step control signal at PDO side using both the continuous model and state space model

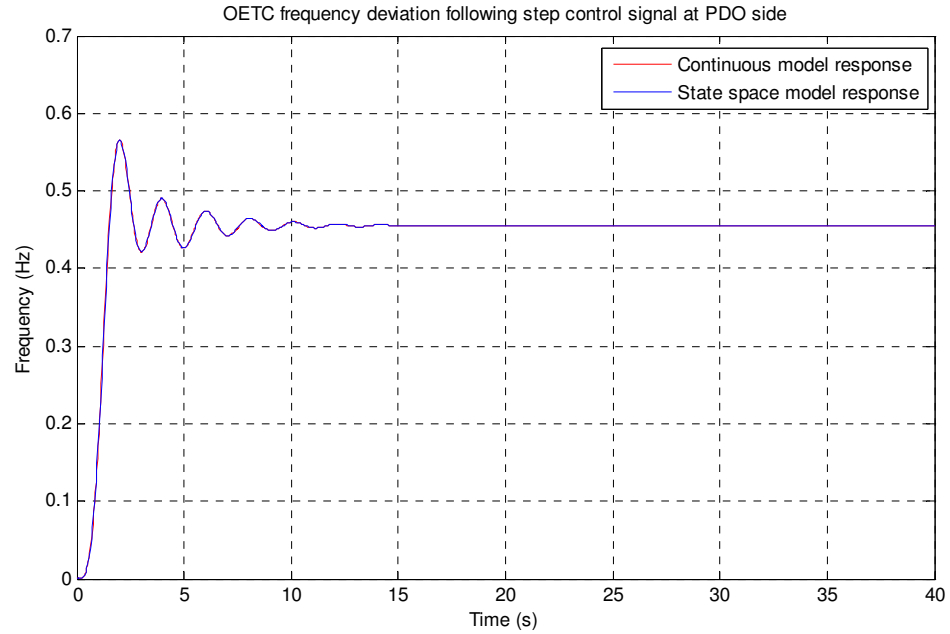

Figure 8.2: OETC frequency deviation following step control signal at PDO side using both the continuous model and state space model

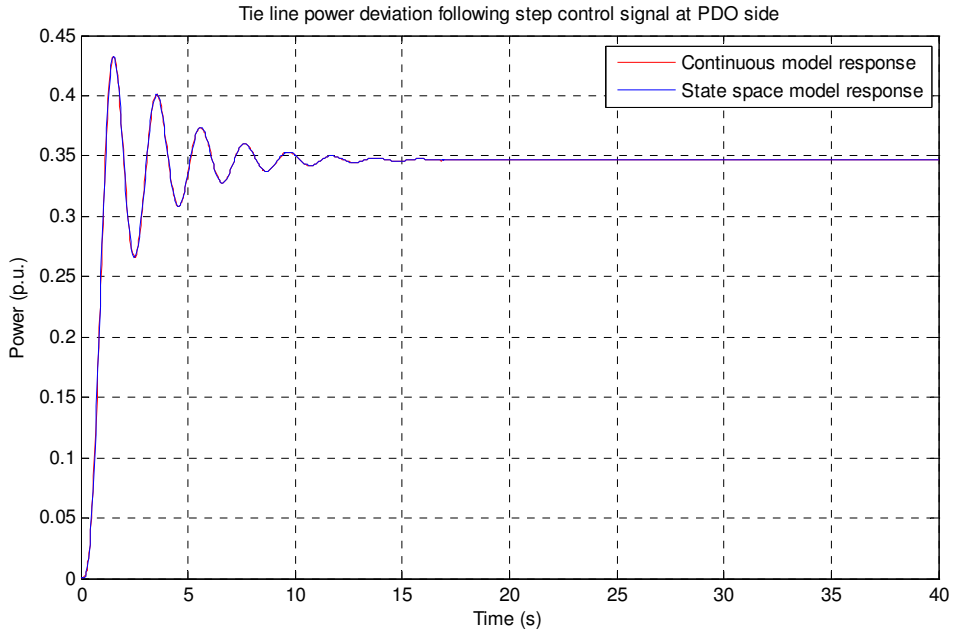

Figure 8.3: Tie line power deviation following step control signal at PDO side using both the continuous model and state space model

Considering OETC control input signal, a step input signal of 1 p.u. size at OETC control input signal has produced the response shown in Figures 8.4 to 8.6 using both the state space model and the continuous model.

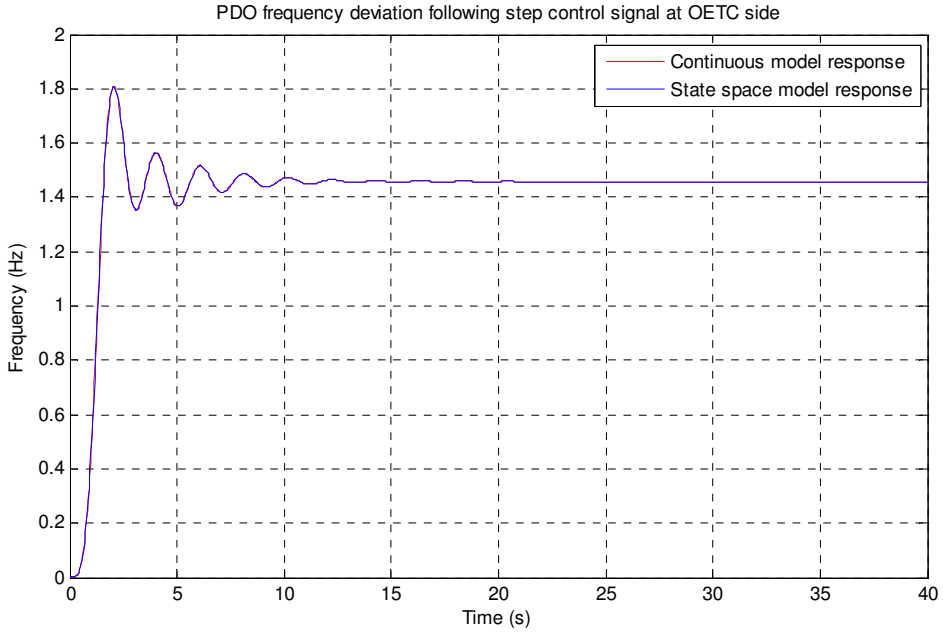

Figure 8.4: PDO frequency deviation following step control signal at OETC side using both the continuous model and state space model

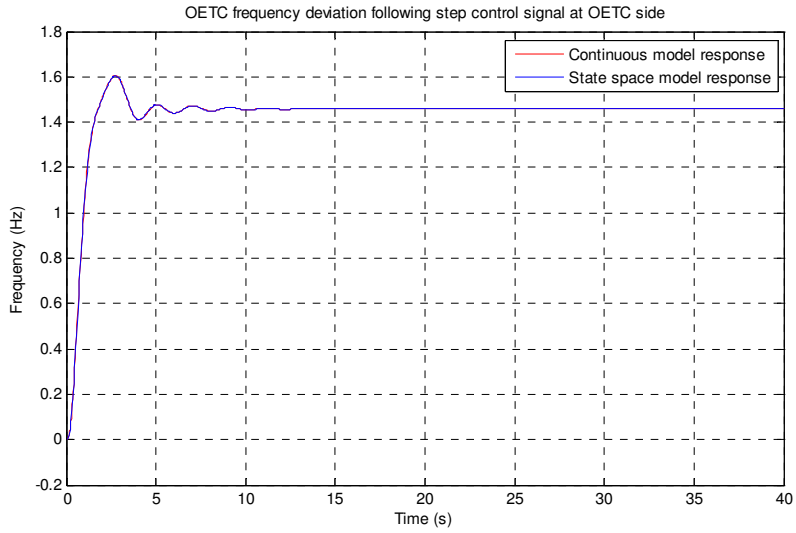

Figure 8.5: OETC frequency deviation following step control signal at OETC side using both the continuous model and state space model

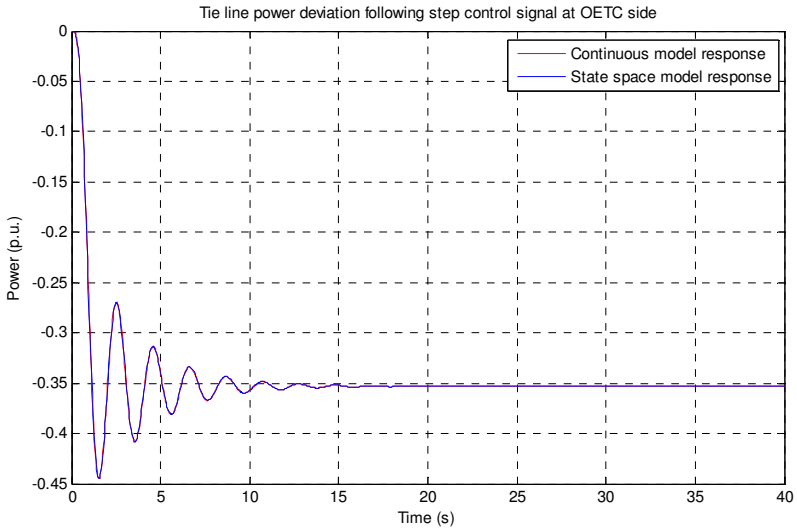

Figure 8.6: Tie line power deviation following step control signal at OETC side using both the continuous model and state space model

From Figures 8.1 to 8.6, it is crisp clear that the continuous-time model response is exactly the same as the state space model. It proves that the state space model formulation is successful and the derived state space form of PDO-OETC model can be used for further analysis.

8.5. Summary

State space form of PDO-OETC model has been derived and tested. The results prove that the derived state space model is accurate and has produced exactly the same response as the continuous-time model of PDO-OETC power systems. Therefore, the derived state space form of the model can be used for further analysis.

Chapter 9: Design of Automatic Generation Control of PDO-OETC interconnected power system

9.1. Introduction

PDO and OETC power systems are growing entities and their fast growth is driven by the wide scale development in the Sultanate of Oman. PDO power system has gone through many expansion projects to increase the generation capacity driven by the new load demand associated with the Enhanced Oil Recovery schemes. On the other side, OETC power system is growing in a faster pattern driven by the load demand of the large scale industrial projects and the increasing population. All this has resulted in a significant growth in both systems since they are first interconnected back in 2001. In the early days, the tie line power flow was controllable using the generation dispatch and there was no necessity for complicated control scheme to control the frequency and the power exchange. Nowadays, the large residential load demand profile at OETC side imposes a great challenge in the control and operation of the interconnected power system. The power flow through the tie line is dependant on the daily load profile and a huge effort is devoted by PDO and OETC power system operators to maintain it at the nominal limits of ±10MW. The traditional way of controlling the flow is now more exhaustive than the utilisation of AGC controller. During OETC peak load hours, PDO operators find themselves squeezed in holding their MW from flowing to OETC and the MW exchange often deviates from the agreed nominal limits. Therefore the idea of having AGC controller is gaining acceptance amongst both power systems operators.

The ultimate aim of AGC is to achieve the following fundamental requirements:

- Zero steady state frequency deviation following load disturbance
- Zero steady state tie line power deviation following load disturbance
- Load disturbance is compensated locally at the disturbed control area and restoration of the nominal generation dispatch of none disturbed control area in the steady state condition

Before commencing on the detailed technical design of an AGC controller and details of the controller types, it is of paramount importance to discuss the operational aspects of PDO and OETC power systems. Furthermore we need to draw a control philosophy that suits both PDO and OETC power systems considering the nature of both systems, the regulatory framework governing the operation of both systems and the endeavour of both systems to have an AGC controller.

9.2. Nature of PDO and OETC power systems

PDO power system is smaller than OETC power system in terms of generation capacity. This fact is reflected on the rotating inertias of both systems. OETC is having about three times the inertia than PDO is having and therefore PDO has about quarter of the overall power system inertia. This fact has an interesting impact on the frequency and tie line power flows. A disturbance at PDO side will greatly affect the power exchange than the same size disturbance at OETC side. Any power mismatch between the generation and the load will mainly be compensated by the rotating inertias resulting in frequency deviation. Since PDO is having about quarter of the system inertia, quarter of the mismatch will be compensated locally and three quarters will be compensated next door from OETC as a power flow through the tie lines. Vice versa, three quarters of the mismatch at OETC will be compensated locally and only one quarter will be compensated next door from PDO as a power flow through the tie lines. Therefore, a load disturbance at PDO will be obvious from the tie line flow and a load disturbance at OETC will be obvious from the frequency deviation.

On the other hand, PDO load is industrial in nature and is constant throughout the day. Whereas OETC load is mainly a residential load which peaks up for few hours during the day. Hence, there are less load disturbances within PDO when compared with OETC.

9.3. Regulations governing the control and operation of PDO and OETC power systems

PDO power system is a monopoly solely owned and operated by Petroleum Development Oman Ltd. PDO power system is designed and operated as per PDO specifications.

On the other hand, OETC power system is built according to the government standards. OETC power system is privatised where the transmission grid is solely run by OETC. The power generation is through independent power producers and the distribution is divided between other companies based on territorial basis. The Authority for Electricity Regulation is on top of all these companies as the regulator. The grid code (Oman Electricity Transmission Company SAOC, 2005) stipulates the operation interface requirements between the generation, transmission and distribution companies. In the grid code, PDO is annotated as an internally interconnected system with OETC. The grid code and the stand alone service level agreement between PDO and OETC forms the regulatory framework for the pool operation.

In general, PDO has better control on its power generation since all the power generation units and power transmission overhead lines are controlled by the same body. In the other

hand, OETC has less control on the power generation units due to the separate owner of the power generation units. Generation dispatch is done manually through paperwork and telephoning which imposes extraordinary challenge to the OETC grid operators to maintain the balance between load demand and generation.

The AGC controller is quite feasible especially for OETC which will make control and generation dispatch relatively easy to the present situation.

9.4. Control philosophies

AGC controller is a supervisory control loop which can be flexibly applied. Traditionally, the Area Control Error (ACE) is used as a feedback to the AGC controller which comprises both the frequency deviation and the tie line power deviation. The concept of ACE will be discussed in details in the subsequent sections. Usually one controller is installed at each control area and both of them cooperate together to maintain the nominal values of frequency and power exchange. Each controller is designed and tuned to compensate load disturbances arising within its control area in the steady state condition. During the load disturbance the neighbouring area controller will act during the transient period only and brings back its original generation dispatch in steady state condition. Consequently, each area is responsible for load disturbances arising within its territory and it will get help from the other area only during the transient period. Effectively, AGC will help both the frequency and tie line power to stabilise faster.

The study will consider three control philosophies and then in each control philosophy AGC will be designed and tested using different feedback signals. Eventually a short term and long term recommendations for PDO and OETC power systems will be attempted. The three control philosophies are:

1. AGC applied to PDO power system alone
    - Grid frequency as a feedback signal
    - Tie line power as a feedback signal
    - Area Control Error (ACE) as a feedback signal
2. AGC applied to OETC power system alone
    - Grid frequency as a feedback signal
    - Tie line power as a feedback signal
    - Area Control Error (ACE) as a feedback signal
3. AGC applied to both PDO and OETC power systems
    - PDO uses grid frequency as a feedback signal & OETC uses grid frequency as a feedback signal

- PDO uses grid frequency as a feedback signal & OETC uses tie line power as a feedback signal
- PDO uses grid frequency as a feedback signal & OETC uses Area Control Error (ACE) as a feedback signal
- PDO uses tie line power as a feedback signal & OETC uses grid frequency as a feedback signal
- PDO uses tie line power as a feedback signal & OETC uses tie line power as a feedback signal
- PDO uses tie line power as a feedback signal & OETC uses Area Control Error (ACE) as a feedback signal
- PDO uses Area Control Error (ACE) as a feedback signal & OETC uses grid frequency as a feedback signal
- PDO uses Area Control Error (ACE) as a feedback signal & OETC uses tie line power as a feedback signal
- PDO uses Area Control Error (ACE) as a feedback signal & OETC uses Area Control Error (ACE) as a feedback signal

Therefore a total number of 15 control topologies will be investigated. All above topologies will be initially investigated using Ziegler Nichols PID controller. The closed loop tuning method will be used for all control topologies.

Throughout the fifteen control topologies test, the following simulation conditions will be used:

- The controller performance is tested when subjected to internal load disturbance at PDO and external load disturbance at OETC.
- A step load disturbance of 100MW is used for all tests.
- PDO frequency is considered as the grid frequency for the settling time calculation.

9.5. Base case of PDO-OETC model

The refined PDO-OETC power system perturbation model developed in chapter 7 will be used. However the refined model has considered generation units which are normally in preselect load control and units which are reaching base load during the recorded real scenarios. Those considerations have been used only to validate the model using the prevailing operating conditions during the time the real scenarios were recorded. Since the refined model is proved valid, the AGC controller should be designed based on the ideal case whereby all generators are having enough spinning reserves and all of them are on droop control. The AGC controller robustness can be tested using different operating

conditions. Therefore the base case of the PDO-OETC model which will be used for the controller design and tuning is the same model as developed in chapter 7 except that there are no generation units running at base load or on preselect control mode.

As a reference point, the base case was simulated while subjected to 100MW load disturbance once at PDO side and once at OETC side. Since AGC will impact the common grid frequency, generators output and power exchange between PDO and OETC, the simulation results will focus on five main aspects:

1. PDO frequency,
2. OETC frequency,
3. Tie line power,
4. Mechanical power output of a sample gas turbine at PDO
5. Mechanical power output of a sample gas turbine at OETC.

The sample gas turbines size is selected to be F6B machines for both PDO and OETC. The simulation results are shown in Figures 9.1 to 9.6 which cover all mentioned five aspects. Table 9.1 shows a summary of settling times, power and frequency deviation. The settling time is always calculated based on PDO frequency when reaching the final steady state value ±0.001Hz.

Considering the frequency and tie line power figures, the steady state deviation, the settling time and the oscillatory nature of the response are the most important aspects to look at in those figures. On the other hand, the steady state deviation is the most important aspect when considering the mechanical power figures.

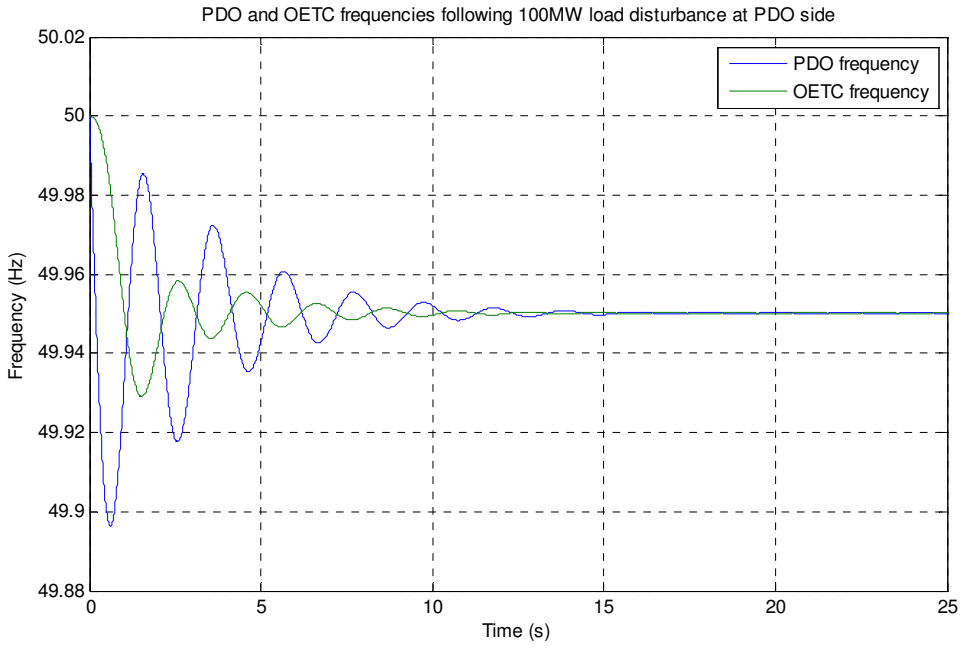

Figure 9.1: Grid frequency following 100MW load disturbance at PDO side

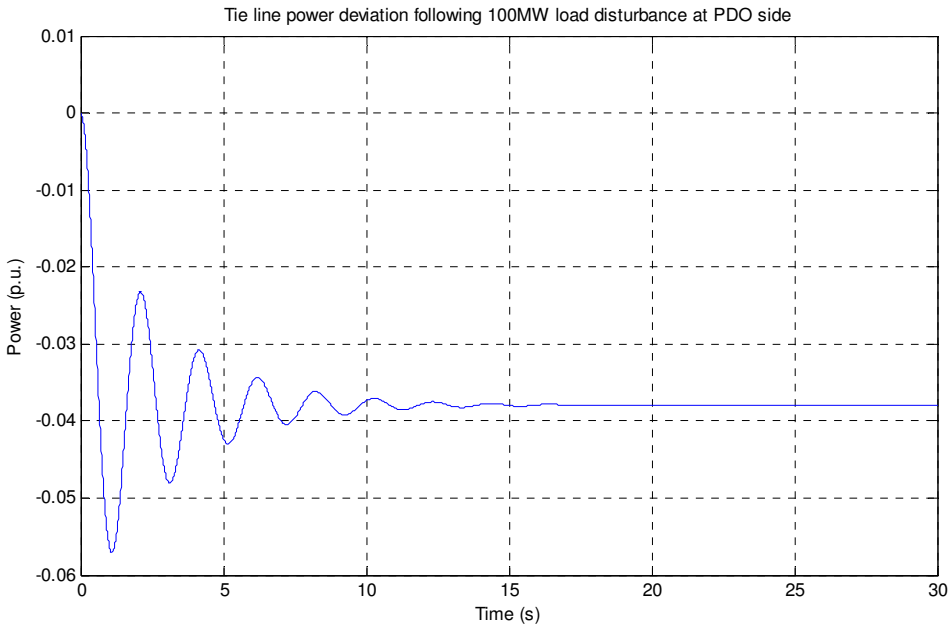

Figure 9.2: Tie line power deviation following 100MW load disturbance at PDO side

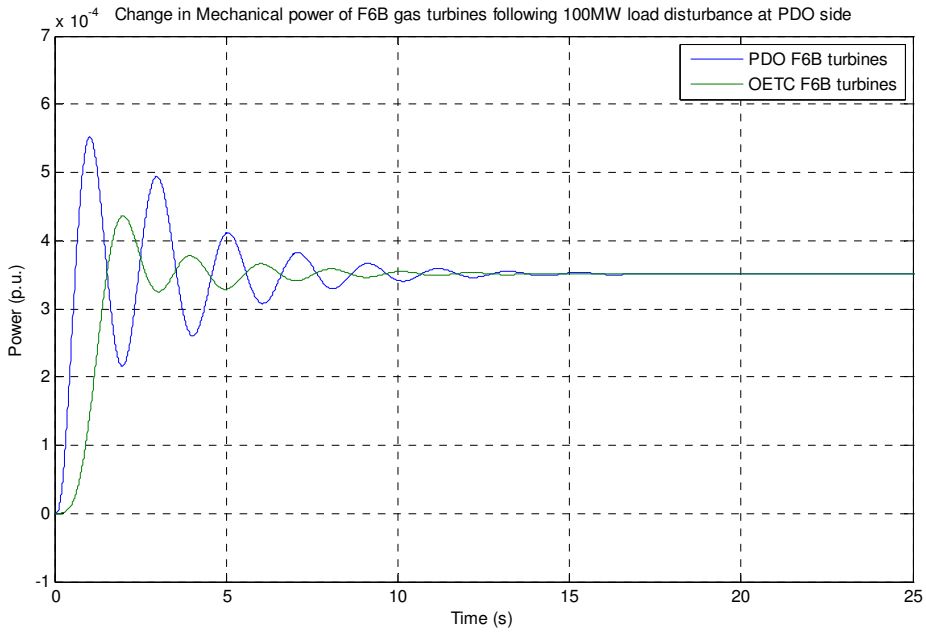

Figure 9.3: Change in Mechanical power of F6B gas turbines following 100MW load disturbance at PDO side

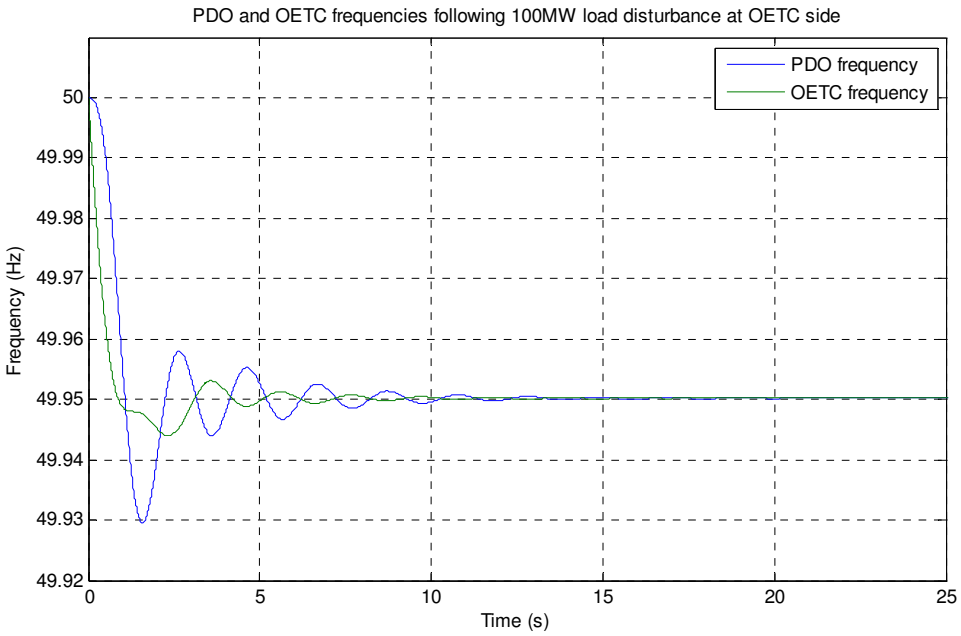

Figure 9.4: Grid frequency following 100MW load disturbance at OETC side

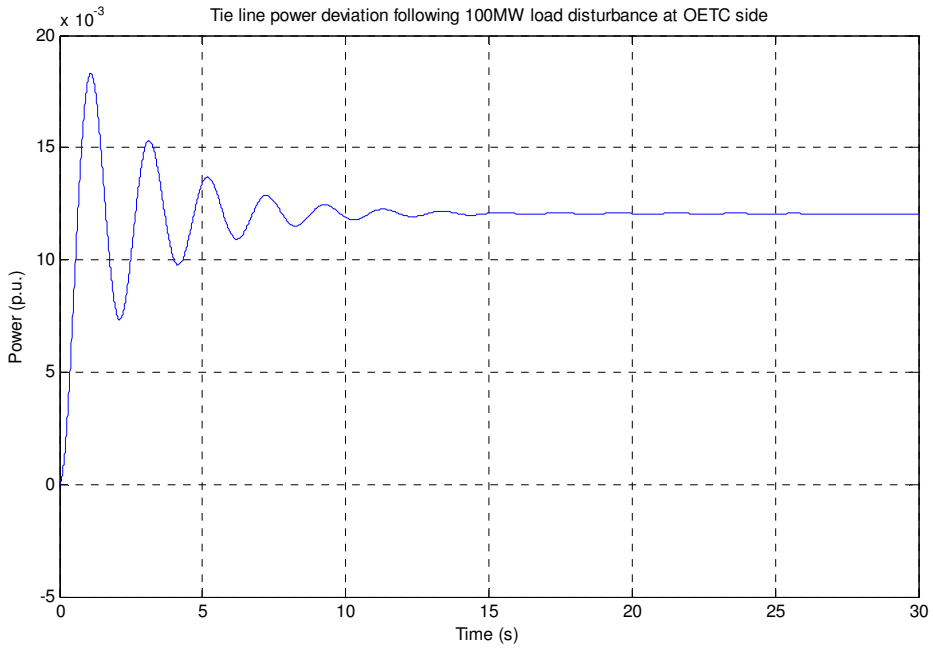

Figure 9.5: Tie line power deviation following 100MW load disturbance at OETC side

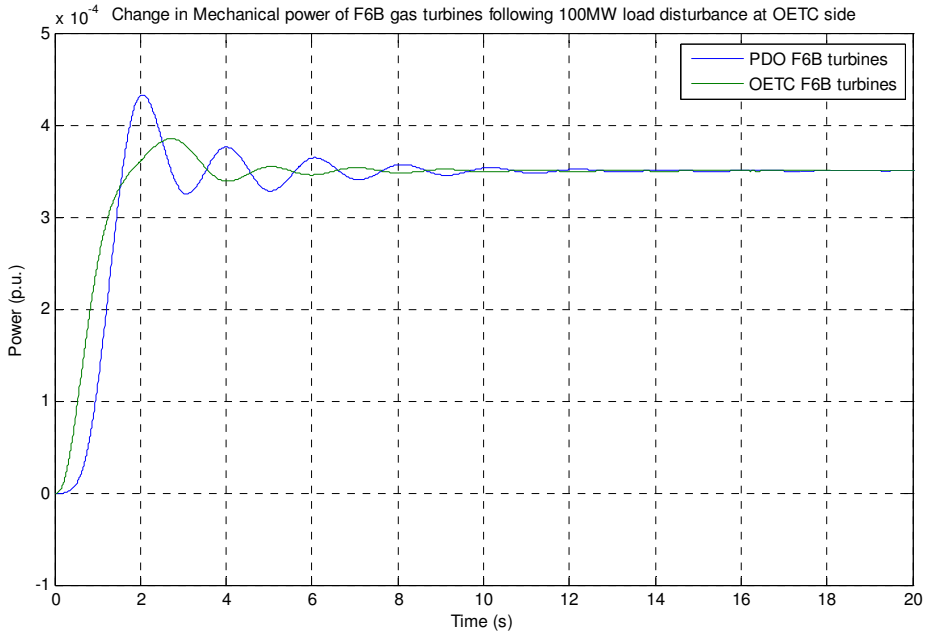

Figure 9.6: Change in Mechanical power of F6B gas turbines following 100MW load disturbance at OETC side

		Base case response
100MW load disturbance at PDO side	Frequency deviation (Hz)	-0.05
	Settling time (s)	10.9
	Tie line power deviation (p.u.)	-0.0379
100MW load disturbance at OETC side	Frequency deviation (Hz)	-0.05
	Settling time (s)	7.74
	Tie line power deviation (p.u.)	0.0121

Table 9.1: Base case response summary

From Figure 9.1 to Figure 9.6 and Table 9.1 one can summarise the base case model response characteristics following step load disturbance as:

- Frequency settles with a steady state offset
- Tie line power settles with a steady state offset
- The same size generators deliver the same amount of power regardless whether they are at PDO or at OETC side.
- Response is oscillatory but stable

9.6. AGC of PDO power system alone

In this part, three control topologies will be investigated using PID controller. The base case model will be used whereby PDO and OETC remain interconnected. The three control topologies are applying AGC to PDO power system only using different feedback signals to the controller:

1. PDO grid frequency as a feedback signal
2. Tie line power as a feedback signal
3. PDO Area Control Error as a feedback signal

The PID controller is not the best control technique however it is good to get the first impression about the control topology performance. The closed loop tuning method (Ultimate Sensitivity Method) will be used to tune the PID controller for all control topologies.

9.6.1. AGC of PDO using grid frequency as a feedback signal

The grid frequency recorded at PDO side is used as the feedback signal for the controller. The PDO-OETC model with the controller is shown in Figure 9.7 and the used PID controller is shown in Figure 9.8. The controller closed loop gain was increased gradually until the ultimate gain was reached which has produced the stable oscillatory response. The ultimate gain and oscillation period were recorded and are shown in Table 9.3.

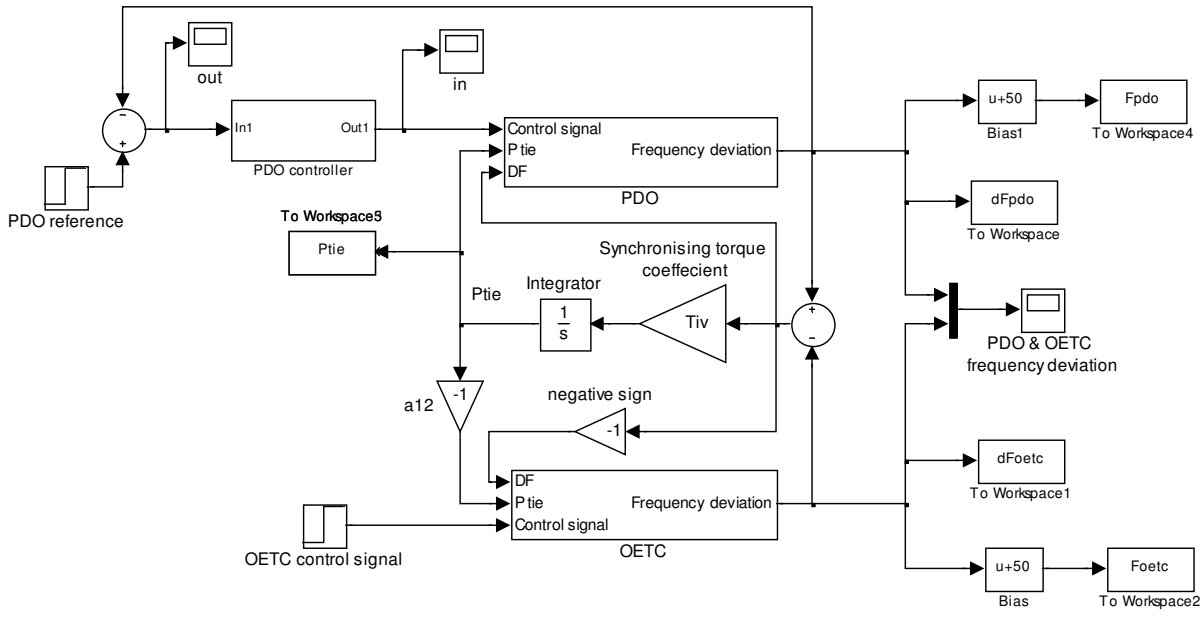

Figure 9.7: PDO-OETC model with PDO frequency PID AGC controller.

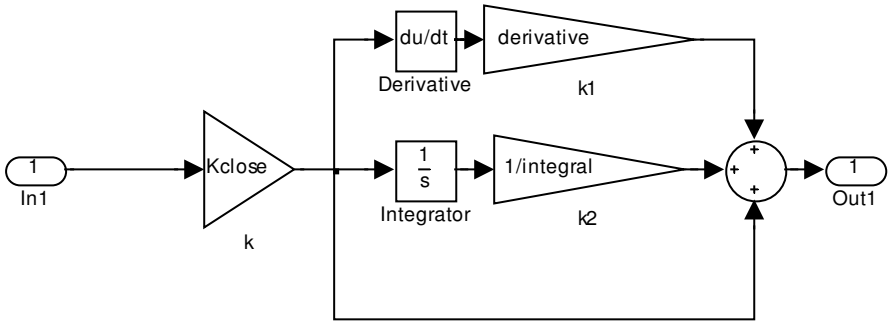

Figure 9.8: PID controller structure.

9.6.1.1 Calculation of the PID controller parameters

Once the ultimate gain (Ku) and period (Pu) are known, the PID controller parameters can be calculated using the look up table developed by Ziegler Nichols shown in Table 9.2 (OGATA, 2008, p. 685).

Type of controller	Kc	Ti	Td
P	0.5Ku	∞	0
PI	0.45Ku	(1/1.2)Pu	0
PID	0.6Ku	0.5Pu	0.125Pu

Table 9.2: Zeigler-Nichols tuning rule based on ultimate gain and ultimate period.

Table 9.3 summarises the PID controller parameters used in this part of the study:

Ku (ultimate gain)	Pu (ultimate period)	Kc (PID Controller gain)	Ti (Integral time constant)	Td (derivative time constant)
3.465	1.21	2.079	0.605	0.15125

Table 9.3: PDO AGC PID controller parameters based on grid frequency feedback

9.6.1.2. Simulation results

Totally six Figures have been produced to cover the five main aspects mentioned earlier in section 9.5 for each test. The results are shown in Figures 9.9 to 9.14 in Appendix 4. Table 9.4 shows a summary of the controller performance in terms of grid frequency and tie line power.

		Base case response	Controlled response
100MW load disturbance at PDO side	Frequency deviation (Hz)	-0.05	0
	Settling time (s)	10.9	5.6
	Tie line power deviation (p.u.)	-0.0379	0
100MW load disturbance at OETC side	Frequency deviation (Hz)	-0.05	0
	Settling time (s)	7.74	4.9
	Tie line power deviation (p.u.)	0.0121	0.05

Table 9.4: PDO alone frequency PID AGC controller performance summary

9.6.1.3. Results discussion

The simulation results with the PDO alone frequency PID AGC controller show clear improvements in comparison with the base case results. From Figure 9.9 to Figure 9.14 in Appendix 4 and Table 9.4, one can see the following:

- The frequency steady state offset is brought to zero when a step load disturbance is applied to PDO or OETC. It satisfies one of the fundamental requirements of AGC. The settling time is also superb in the range of 5 seconds. The frequency oscillations are better damped than in the base case.
- The tie line power steady state offset is brought to zero in the case when the load disturbance is applied at PDO side. It means the controller is able to accommodate any disturbance within PDO area and generate the required power locally at PDO without importing power from OETC. However when the disturbance is applied at OETC side, PDO contribution is much more with the controller than in the base case. From Table 9.4, one can see that PDO generators will be taking the whole burden due to the controller action when a disturbance is applied at OETC. The value of 0.05 p.u. equals to 100MW i.e. the whole load disturbance will be compensated by PDO generators. In fact, it will impose many challenges to PDO in terms of extra maintenance cost of turbines, extra fuel consumption and possible tripping of the tie line.
- PDO and OETC generators of the same size are no longer participating with the same amount of power following load disturbances. Figure 9.11 and Figure 9.14 show that PDO generators are taking the entire burden following load disturbance irrespective of the disturbance location. However, OETC droop control acts during the transients which helps damping the frequency oscillations.

- The load disturbance of 100MW is very common within PDO and OETC power systems and is considered as a realistic load disturbance which represents about 10.9% of PDO total generation capacity and 3.4% of OETC total generation capacity. Although not shown, inspection of the controller effort shows a maximum variation of approximately 20% of individual generation unit output which is about 5.6MW for a F6B unit. Hence, for the range of controller parameters considered here, the controller output is always well within the individual generation units capability and does not infringing any constraints or overstress the generation units.

9.6.1.4. Summary

The PDO alone frequency PID AGC controller was tuned using the closed loop method and its performance was good enough. However the control topology itself will impose great burden on PDO generators because the controller is using the grid frequency as the only feedback signal or reference point. It means the controller will act at any disturbance in the frequency regardless of its location. Furthermore, the developed control loop has also dominated the droop control loop of OETC generators therefore there steady state participation was always zero regardless of the disturbance location. Implementing this control topology at PDO will enquire more maintenance cost of its gas turbines due to the continuous manoeuvring of the governing systems. It will also increase fuel gas consumption, deviates from power exchange agreement and may cause tripping incidents of the tie line power.

Therefore this control topology is not recommended for implementation due to the adverse impact on PDO generation.

9.6.2. AGC of PDO using tie line power as feedback signal

The tie line power deviation is used as the feedback signal for the controller. The PDO-OETC model with controller is shown in Figure 9.15 and the used PID controller structure is the same as shown earlier in Figure 9.8. The controller closed loop gain was increased gradually until the ultimate gain has been reached which has produced the stable oscillatory response. The ultimate gain and oscillation period were recorded and are shown in Table 9.5.

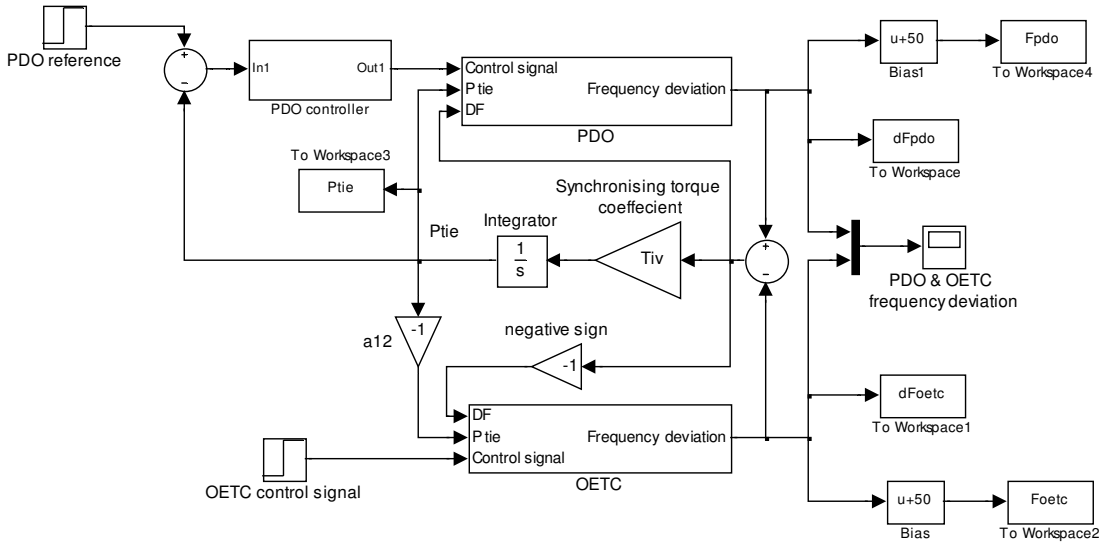

Figure 9.15: PDO-OETC model with PDO tie line power PID AGC controller.

9.6.2.1 Calculation of the PID controller parameters

Once the ultimate gain (Ku) and period (Pu) are known, the PID controller parameters can be calculated using the look up table developed by Ziegler Nichols shown earlier in Table 9.2.

Table 9.5 summarises the PID controller parameters used in this part of the study:

Ku (ultimate gain)	Pu (ultimate period)	Kc (PID Controller gain)	Ti (Integral time constant)	Td (derivative time constant)
1.402	1.989	0.8412	0.9945	0.248625

Table 9.5: PDO AGC PID controller parameters based on tie line power feedback

9.6.2.2. Simulation results

Totally six Figures have been produced to cover the five main aspects mentioned earlier in section 9.5 for each test. The results are shown in Figures 9.16 to 9.21 in Appendix 4. Table 9.6 shows a summary of the controller performance in terms of grid frequency and tie line power.

		Base case response	Controlled response
100MW load disturbance at PDO side	Frequency deviation (Hz)	-0.05	0
	Settling time (s)	10.9	38.61
	Tie line power deviation (p.u.)	-0.0379	0
100MW load disturbance at OETC side	Frequency deviation (Hz)	-0.05	-0.066
	Settling time (s)	7.74	29.8
	Tie line power deviation (p.u.)	0.0121	0

Table 9.6: PDO alone tie line power PID AGC controller performance summary

9.6.2.3. Results discussion

From Figure 9.16 to Figure 9.21 in Appendix 4 and from table 9.6, the following is noted:

- The model response with the PDO alone tie line power PID AGC controller is more oscillatory than in the base case. Therefore the settling time is longer than in the base case. The response is oscillatory because the tie line power suffers inter-area oscillations making it a bad feedback signal to the controller; hence the oscillatory response. The Zeigler Nichols closed loop tuning method gives first approximation of the PID controller parameters. Therefore the controller performance can be further improved by using more sophisticated tuning methods or by using different control techniques.
- The grid frequency steady state offset is brought back to zero when the disturbance is applied at PDO. This is because stopping tie line power flow from OETC to PDO requires PDO generators to generate the whole power mismatch. Therefore the generators kinetic energy is restored hence the frequency back to normal. The controller action is in favour of frequency because the disturbance is at PDO. However when the disturbance has been applied at OETC side, PDO controller was trying to hold the tie line power flow towards OETC by reducing PDO generation; hence jeopardising the frequency. Therefore the frequency deviation is more than in the base case. It is one of the drawbacks of this particular control topology.
- The tie line power was well controlled and brought back to zero following load disturbances at PDO and OETC. However the response was oscillatory, but it can be improved by using more sophisticated control methods.

- The change in mechanical power output of PDO and OETC gas turbines is fair in terms of the geographical location of the load disturbance. Load disturbance at PDO is mainly compensated by PDO generators and a load disturbance at OETC is mainly compensated by OETC generators. However, due to OETC has no AGC, when the load disturbance is applied at OETC the power mismatch has to be compensated by droop control only which will never bring the frequency deviation back to zero. In addition, PDO controller has reduced PDO generation to below nominal to stop the residual power resulting from kinetic energy reduction of PDO generators from flowing to OETC.

9.6.2.4. Summary

The Zeigler Nichols closed loop tuning method has been used to tune the PDO alone tie line power PID AGC controller. The controller has successfully maintained the power exchange at nominal values following load disturbances. The model response with controller was oscillatory and required more time to settle than in the base case. The PDO alone control topology using tie line power as feedback control has proved some drawbacks:

- It requires sophisticated tuning methods or modern control methods to improve the response
- It has jeopardised the frequency when the disturbance is at OETC and has reduced PDO generation to below nominal.

Therefore this particular control topology is not recommended for implementation due to the adverse consequences on the grid stability.

9.6.3. AGC of PDO using grid frequency and tie line power as feedback signal

The grid frequency and tie line power deviation are used to form the feedback signal for the controller. The concept of Area Control Error (ACE) will be introduced and discussed in details in the following section.

9.6.3.1. AGC controller structure using the Area Control Error (ACE)

The concept of ACE is introduced to satisfy the following two objectives of AGC following load disturbance at any control area (KUNDUR, 1994, p. 606):

- Maintain the grid frequency at the nominal value
- Maintain the power exchange between the control areas at scheduled value.

The ACE is a feedback signal to the AGC controller made up of the tie line power deviation added up to the frequency deviation weighted by a bias factor. The concept of ACE is proved to satisfy the above two objectives of AGC (KUNDUR, 1994, p. 606). The frequency-response characteristic factor β is used for calculating the ACE (KUNDUR, 1994, p. 606; Khodabakhshian et al, 2012). Thus the ACE for PDO is calculated as:

$$ACE_{pdo} = \Delta P_{tie} + \beta_{pdo}\Delta f_{pdo} \quad \ldots\ldots\ldots\ldots\ldots\ldots\ldots\ldots\ldots\ldots(9.1)$$

Where

$$\beta = \frac{1}{R} + D \quad \ldots\ldots\ldots\ldots\ldots\ldots\ldots\ldots\ldots\ldots\ldots\ldots\ldots\ldots\ldots\ldots(9.2)$$

R is the droop setting in Hz/p.u.MW and D is the load damping factor in p.u.MW/Hz. The term $\frac{1}{R}$ must be scaled to reflect the p.u. capacity of each area. This is achieved by multiplying the term $\frac{1}{R}$ by the area MW capacity and dividing by the base MVA which is 2000MVA. For PDO, the summer firm capacity is 914.2MW therefore β is calculated as below:

$$\beta_{pdo} = \frac{1}{R_{pdo}} + D_{pdo} = \frac{1}{2} \times \frac{914.2}{2000} + 13.6 \times 10^{-3} = 0.24215\, p.u.MW / Hz$$

The frequency-response characteristic factor β is one way of telling the AGC controller the weight of its area with respect to the rest of the system. By accurately calculating the frequency-response characteristic factor β, the AGC controller steady state contribution is diminished during outside load disturbances and the control area will respond to outside load disturbances as if there is no AGC controller applied. It means only droop control will be in action and will have a steady state contribution. Hence, the normal response to outside load disturbances is preserved. Higher values of the frequency-response characteristic factor β will incur positive AGC controller steady state contribution and lower values will incur negative AGC steady state contribution.

Considering the ACE of PDO power system, the PDO-OETC model with the controller is shown in Figure 9.22 and the used PID controller structure is the same as shown earlier in Figure 9.8. The controller closed loop gain has been increased gradually until the ultimate gain is reached which has produced the stable oscillatory response. The ultimate gain and oscillation period were recorded and are shown in Table 9.7.

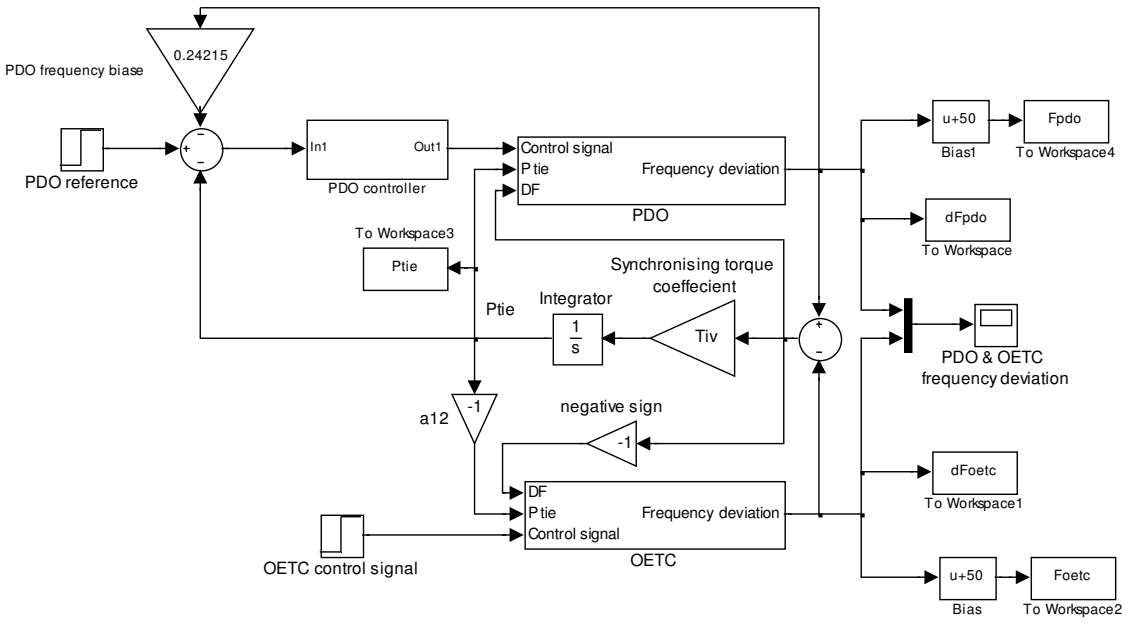

Figure 9.22: PDO-OETC model with PDO frequency and tie line power PID AGC controller.

9.6.3.1 Calculation of the PID controller parameters

Once the ultimate gain (Ku) and period (Pu) are known, the PID controller parameters can be calculated using the look up table developed by Ziegler Nichols shown earlier in Table 9.2. Table 9.5 summarises the PID controller parameters used in this part of the study:

Ku (ultimate gain)	Pu (ultimate period)	Kc (PID Controller gain)	Ti (Integral time constant)	Td (derivative time constant)
1.69	1.842	1.014	0.921	0.23025

Table 9.7: PDO AGC PID controller parameters based on tie line power feedback and grid frequency

9.6.3.2. Simulation results

Totally six Figures have been produced to cover the five main aspects mentioned earlier in section 9.5 for each test. The results are shown in Figures 9.23 to 9.28 in Appendix 4. Table 9.8 shows a summary of the controller performance in terms of grid frequency and tie line power.

		Base case response	Controlled response
100MW load disturbance at PDO side	Frequency deviation (Hz)	-0.05	0
	Settling time (s)	10.9	22.6
	Tie line power deviation (p.u.)	-0.0379	0
100MW load disturbance at OETC side	Frequency deviation (Hz)	-0.05	-0.05
	Settling time (s)	7.74	15.34
	Tie line power deviation (p.u.)	0.0121	0.0121

Table 9.8: PDO alone frequency and tie line power PID AGC controller performance summary

9.6.3.3. Results discussion

From Figure 9.23 to Figure 9.28 in Appendix 4 and from Table 9.8, the following is noted:

- The model response with the PDO alone frequency and tie line power PID AGC controller is more oscillatory than the base case. Therefore the settling time is longer. It is again due to the use of the tie line power signal for the PID controller feedback. The response can always be improved by fine tuning the controller parameters or by using different control technology.
- The frequency steady state offset is brought to zero following a load disturbance at PDO side. However following a load disturbance at OETC, the frequency settles with an offset equals the base case offset. It means that the controller did what it is ought to be done and limited its action to PDO side load disturbances.
- The tie line power deviation is brought back to zero following the load disturbance at PDO side. It means that the controller has satisfied its objective of controlling both PDO frequency and tie line power at nominal values. The AGC controller loop does not have a steady state contribution in response to load disturbance at OETC side. Although there is always a response during the transients, but there is no steady state impact. However the droop control loop of PDO generators contributes during the transient and steady state just as normal as there is no AGC control loop.
- The mechanical power change of F6B turbines shows that PDO turbines are the only ones responsible for balancing the power mismatch following load disturbances at PDO side. Furthermore they participate during load disturbances at OETC side with their droop control loop. Therefore they produce the same power as OETC turbines following load disturbances at OETC side. It proves that the PID controller has no steady state impact following load disturbances at OETC side.

Unlike previous control topologies of PDO alone AGC controller, this control topology proves to be more conservatives following load disturbances outside its control area. Hence it makes the controller more suitable for application.

9.6.3.4. Summary

The Zeigler Nichols closed loop tuning method was used to tune the PDO alone frequency and tie line power PID AGC controller. The controller has successfully maintained the grid frequency and power exchange at nominal values following load disturbances at PDO side. The controller did not respond to load disturbances at OETC side, therefore the results were exactly the same as in the base case. The model response with controller was oscillatory and required more time to settle than in the base case. The PDO alone control topology using frequency and tie line power as feedback control has proved the advantage of limiting its actions to PDO load disturbances only. Therefore OETC load disturbances will not be dumped on PDO generators.

Hence this control topology is recommended for implementation due to its conservative action.

9.7. AGC of OETC power system alone

In this part, three control topologies will be investigated using PID controller. The base case model will be used where PDO and OETC remain interconnected. The three control topologies are applying AGC to OETC power system only using different feedback signals to the controller:

1. Grid frequency as a feedback signal
2. Tie line power as a feedback signal
3. OETC Area Control Error as a feedback signal

The PID controller and the closed loop tuning method (Ultimate Sensitivity Method) will be used for all control topologies.

9.7.1. AGC of OETC using grid frequency as a feedback signal

The grid frequency measured at OETC side is used as the feedback signal for the controller. The PDO-OETC model with the controller is shown in Figure 9.29 and the used PID controller is the same as shown earlier in Figure 9.8. The controller closed loop gain has been increased gradually until the ultimate gain is reached which has produced the

stable oscillatory response. The ultimate gain and oscillation period were recorded and are shown in Table 9.9.

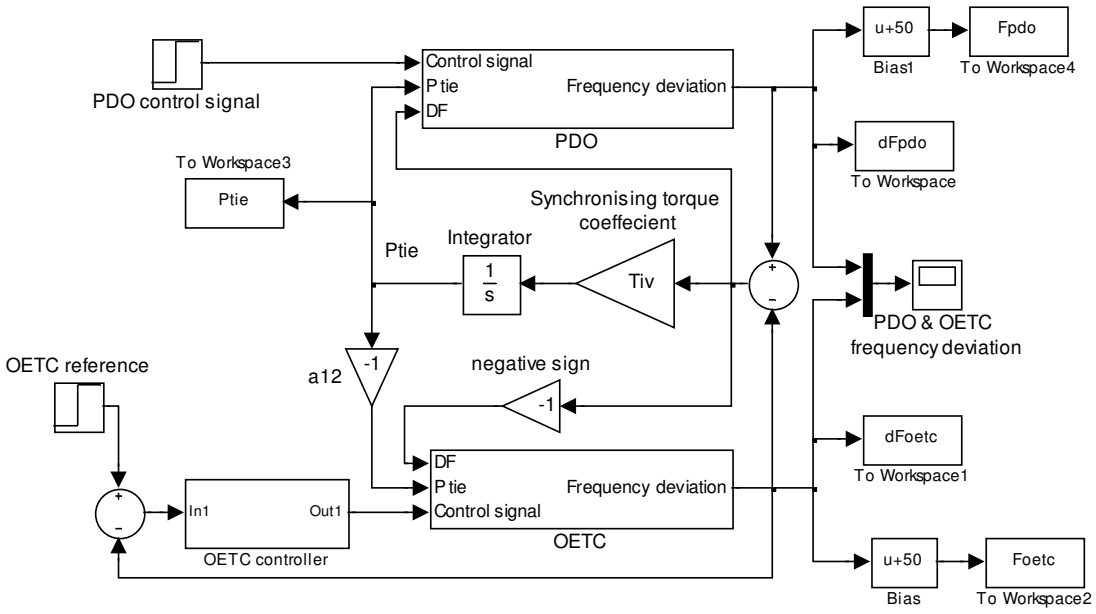

Figure 9.29: PDO-OETC model with OETC frequency PID AGC controller.

9.7.1.1 Calculation of the PID controller parameters

Once the ultimate gain (Ku) and period (Pu) are known, the PID controller parameters can be calculated using the look up table developed by Ziegler Nichols shown earlier in Table 9.2.

Table 9.9 summarises the PID controller parameters used in this part of the study:

Ku (ultimate gain)	Pu (ultimate period)	Kc (PID Controller gain)	Ti (Integral time constant)	Td (derivative time constant)
3.689	1.265	2.2134	0.6325	0.158125

Table 9.9: OETC AGC PID controller parameters based on grid frequency feedback

9.7.1.2. Simulation results

Totally six Figures have been produced to cover the five main aspects mentioned earlier in section 9.5 for each test. The results are shown in Figures 9.30 to 9.35 in Appendix 4. Table 9.10 shows a summary of the controller performance in terms of grid frequency and tie line power.

		Base case response	Controlled response
100MW load disturbance at PDO side	Frequency deviation (Hz)	-0.05	0
	Settling time (s)	10.9	10.5
	Tie line power deviation (p.u.)	-0.0379	-0.05
100MW load disturbance at OETC side	Frequency deviation (Hz)	-0.05	0
	Settling time (s)	7.74	5.84
	Tie line power deviation (p.u.)	0.0121	0

Table 9.10: OETC alone frequency PID AGC controller performance summary

9.7.1.3. Results discussion

The simulated results with the OETC alone frequency PID AGC controller show clear improvements in comparison with the base case results. From Figure 9.30 to Figure 9.35 in Appendix 4 and Table 9.10, one can see the following:

- The frequency steady state offset is brought to zero when a step load disturbance is applied at PDO or OETC. Thus, satisfying one of the fundamental requirements of AGC. The settling time is also good. The frequency oscillations are better damped than in the base case.
- The tie line power steady state offset is brought to zero in the case when the load disturbance is applied at OETC side. This means the controller is able to accommodate any disturbance within OETC area and generate the required power locally at OETC without importing power from PDO. However when the disturbance is applied at PDO side, OETC contribution is more with the controller than in the base case. From Table 9.10 and Figure 9.32, one can see that OETC generators will be taking the whole burden due to the controller action when a disturbance is applied at PDO side. The tie line power deviation value of 0.05 p.u. equals to 100MW i.e. the whole load disturbance will be compensated by OETC generators. It will impose many challenges to OETC in terms of extra maintenance cost of turbines, extra fuel consumption and possible tripping of the tie line (depends on the over current protection settings of the line).
- PDO and OETC generators of the same size are no longer participating with the same amount of power following disturbance. Figure 9.32 and Figure 9.35 show that OETC generators are taking the entire burden following load disturbance

irrespective of the disturbance location. However, PDO generators droop control acts during the transient which helps damping the frequency oscillations.

- In general, the results follow the same pattern as in the case when the frequency AGC controller was applied to PDO only. However in OETC case, the system response takes more time to settle; this is because the controller is manoeuvring the speed of the dominating inertia of the grid which will need more damping effort to settle.

9.7.1.4. Summary

The OETC alone frequency PID AGC controller was tuned using the closed loop method and its performance was good enough. However the control topology itself will impose great burden on OETC generators because the controller is using the grid frequency as the only feedback signal or reference point. It means the controller will act for any disturbance in the frequency regardless of its location. Furthermore, the developed control loop has also dominated the droop control loop of PDO generators therefore their steady state participation is always zero regardless of the disturbance location. If OETC is going to implement this control topology, they will enquire more maintenance cost of their gas turbines due to the continuous manoeuvring of the governing systems. It will also increase fuel gas consumption, deviates from power exchange agreement and may cause tripping incidents of the tie line.

Therefore this control topology is not recommended for implementation due to the adverse impact on OETC generation.

9.7.2. AGC of OETC using tie line power as a feedback signal

The tie line power deviation is used as the feedback signal for the controller. The PDO-OETC model with controller is shown in Figure 9.36 and the used PID controller structure is the same as shown earlier in Figure 9.8. The controller closed loop gain was increased gradually until the ultimate gain has been reached which has produced the stable oscillatory response. The ultimate gain and oscillation period were recorded and are shown in Table 9.11.

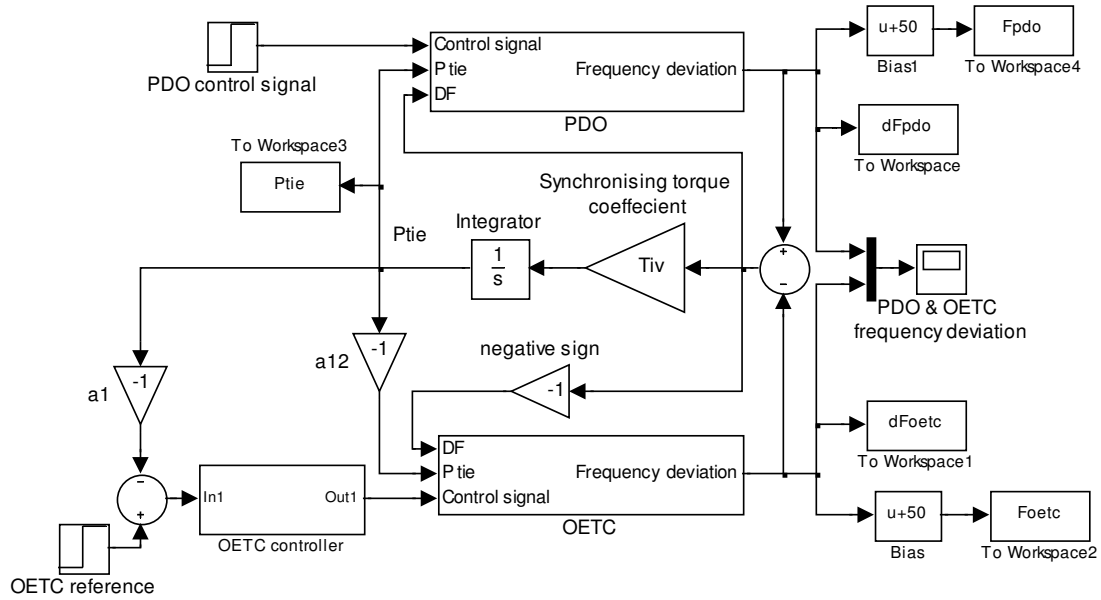

Figure 9.36: PDO-OETC model with OETC tie line power PID AGC controller.

9.7.2.1 Calculation of the PID controller parameters

Once the ultimate gain (Ku) and period (Pu) are known, the PID controller parameters can be calculated using the look up table developed by Ziegler Nichols shown earlier in Table 9.2.

Table 9.11 summarises the PID controller parameters used in this part of the study:

Ku (ultimate gain)	Pu (ultimate period)	Kc (PID Controller gain)	Ti (Integral time constant)	Td (derivative time constant)
1.348	1.996	0.8088	0.998	0.2495

Table 9.11: OETC AGC PID controller parameters based on tie line power feedback

9.7.2.2. Simulation results

Totally six Figures have been produced to cover the five main aspects mentioned earlier in section 9.5 for each test. The results are shown in Figures 9.37 to 9.42 in Appendix 4. Table 9.12 shows a summary of the controller performance in terms of grid frequency and tie line power.

		Base case response	Controlled response
100MW load disturbance at PDO side	Frequency deviation (Hz)	-0.05	-0.206
	Settling time (s)	10.9	41.6
	Tie line power deviation (p.u.)	-0.0379	0
100MW load disturbance at OETC side	Frequency deviation (Hz)	-0.05	0
	Settling time (s)	7.74	25.1
	Tie line power deviation (p.u.)	0.0121	0

Table 9.12: OETC alone tie line power PID AGC controller performance summary

9.7.2.3. Results discussion

From Figure 9.37 to Figure 9.42 in Appendix 4 and from table 9.12, the following is noted:

- The model response with the OETC alone tie line power PID AGC controller is more oscillatory than in the base case. Therefore the settling time is longer than in the base case. The tie line power suffers inter-area oscillations making it a bad feedback signal to the controller; hence the oscillatory response. The Zeigler Nichols closed loop tuning method gives first approximation of the PID controller parameters. Therefore the controller performance can be further improved by fine tuning its parameters. In general the controller performance can be improved by using more sophisticated tuning method or by using different control method.
- The grid frequency steady state offset is brought back to zero when the disturbance is applied at OETC. This is because stopping tie line power flow from PDO to OETC required OETC generators to generate the whole power mismatch therefore the generators kinetic energy is restored hence the frequency back to normal. The controller action was in favour of frequency because the disturbance was at OETC. However when the disturbance was applied at PDO side, OETC controller was trying to hold the tie line power flow towards PDO by reducing OETC generation; hence jeopardising the frequency. Therefore the frequency deviation was more than in the base case. This is one of the drawbacks of this control topology.
- The tie line power was well controlled and brought back to zero following load disturbances at PDO and OETC. However the response was oscillatory, but it can be treated by using more sophisticated control methods.
- The change in mechanical power output of PDO and OETC gas turbines is fair in terms of the geographical location of the load disturbance. Load disturbance at PDO is mainly compensated by PDO generators and a load disturbance at OETC is

mainly compensated by OETC generators. However, due to PDO has no AGC, when the load disturbance is applied at PDO the power mismatch has to be compensated by droop control only which will never bring the frequency deviation back to zero. Add to that, OETC controller has reduced OETC generation to below nominal to stop the residual power resulting from kinetic energy reduction of OETC generators from flowing to PDO.

9.7.2.4. Summary

The Zeigler Nichols closed loop tuning method is used to tune the OETC alone tie line power PID AGC controller. The controller has successfully maintained the power exchange at nominal values following load disturbances. The model response with controller is oscillatory and requires more time to settle than in the base case. The OETC alone control topology using tie line power as feedback control has proved some drawbacks:

- It requires sophisticated tuning methods or modern control methods to improve the response
- It has jeopardised the frequency when the load disturbance was at PDO and has reduced OETC generation to below nominal dispatch.

Therefore this control topology is not recommended for implementation due to the adverse consequences on the grid stability.

9.7.3. AGC of OETC using Area Control Error as a feedback signal

The grid frequency and tie line power deviation are used to form the feedback signal for the controller. The concept of Area Control Error (ACE) will be used. The frequency-response characteristic factor β of OETC is calculated following the same procedure shown earlier in section 9.7.3.1.

For OETC, the summer firm capacity is 2927MW therefore β is calculated as below:

$$\beta_{oetc} = \frac{1}{R_{oetc}} + D_{oetc} = \frac{1}{2} \times \frac{2927}{2000} + 29.76 \times 10^{-3} = 0.76151 p.u.MW / Hz$$

Considering the ACE of OETC power system, the PDO-OETC model with the controller is shown in Figure 9.43 and the used PID controller structure is the same as shown earlier in Figure 9.8. The controller closed loop gain was increased gradually until the ultimate gain has been reached which has produced the stable oscillatory response. The ultimate gain and oscillation period were recorded and are shown in Table 9.13.

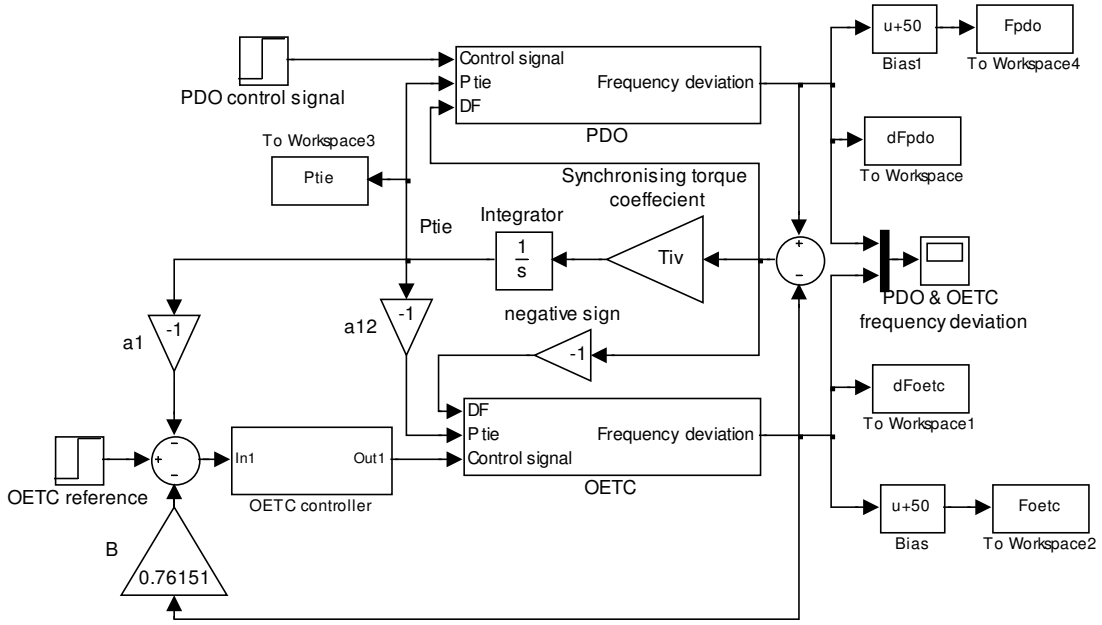

Figure 9.43: PDO-OETC model with OETC frequency and tie line power PID AGC controller.

9.7.3.1 Calculation of the PID controller parameters

Once the ultimate gain (Ku) and period (Pu) are known, the PID controller parameters can be calculated using the look up table developed by Ziegler Nichols shown earlier in Table 9.2.

Table 9.13 summarises the PID controller parameters used in this part of the study:

Ku (ultimate gain)	Pu (ultimate period)	Kc (PID Controller gain)	Ti (Integral time constant)	Td (derivative time constant)
1.468	1.755	0.8808	0.8775	0.219375

Table 9.13: OETC AGC PID controller parameters based on frequency and tie line power feedback

9.7.3.2. Simulation results

Totally six Figures have been produced to cover the five main aspects mentioned earlier in section 9.5 for each test. The results are shown in Figures 9.44 to 9.49 in Appendix 4. Table 9.14 shows a summary of the controller performance in terms of grid frequency and tie line power.

		Base case response	Controlled response
100MW load disturbance at PDO side	Frequency deviation (Hz)	-0.05	-0.05
	Settling time (s)	10.9	14
	Tie line power deviation (p.u.)	-0.0379	-0.0379
100MW load disturbance at OETC side	Frequency deviation (Hz)	-0.05	0
	Settling time (s)	7.74	10.4
	Tie line power deviation (p.u.)	0.0121	0

Table 9.14: OETC alone frequency and tie line power PID AGC controller performance summary

9.7.3.3. Results discussion

From Figure 9.44 to Figure 9.49 in Appendix 4 and from Table 9.14, the following is noted:

- The model response with the OETC alone frequency and tie line power PID AGC controller is more oscillatory than the base case. Therefore the settling time is longer. This is again due to the use of the tie line power signal for the PID controller feedback. The response can always be improved by fine tuning the controller parameters or by using different control technology.
- The frequency steady state offset was brought to zero following a load disturbance at OETC side. However following a load disturbance at PDO, the frequency settles with an offset equals the base case offset. It means the controller does what is ought to be done and limits its action to OETC side load disturbances.
- The tie line power deviation was brought back to zero following the load disturbance at OETC side. This means the controller has satisfied its objective of maintaining both OETC frequency and tie line power at nominal values. The AGC control loop did not respond to out-side zone disturbances at PDO side. Although there is always participation during the transients, but there is no steady state impact. However the OETC generators droop control loop has acted normally during load disturbance at PDO side as it can be seen from Figure 9.46
- The mechanical power change of F6B turbines shows that OETC turbines are the only ones responsible for balancing the power mismatch following load disturbances at OETC side. Whereas they participate during load disturbances at

PDO side with their droop control loop. Therefore they produced the same power as PDO turbines following load disturbances at PDO side.

Unlike previous control topologies of OETC alone AGC controller, this control topology proves to be more conservatives following load disturbances outside its control area. This makes the controller more suitable for practical application.

9.7.3.4. Summary

The Zeigler Nichols closed loop tuning method was used to tune the OETC alone frequency and tie line power PID AGC controller. The controller has successfully maintained the grid frequency and power exchange at nominal values following load disturbances at OETC side. The controller did not respond to load disturbances at PDO side. The model response with the controller was oscillatory and required more time to settle than in the base case. The OETC alone control topology using Area Control Error as a feedback signal has proved the advantage of limiting its actions to OETC load disturbances only. Therefore PDO load disturbances will not be dumped on OETC generators.

Hence this control topology is recommended for implementation due to its conservative action.

9.8. AGC of both PDO & OETC power systems

In this part, nine control topologies will be investigated using PID controller. The base case model will be used where PDO and OETC remain interconnected. The nine control topologies are applying AGC to both PDO and OETC power systems using different feedback signals to the controller:

1. PDO uses grid frequency as a feedback signal & OETC uses grid frequency as a feedback signal
2. PDO uses grid frequency as a feedback signal & OETC uses tie line power as a feedback signal
3. PDO uses grid frequency as a feedback signal & OETC uses Area Control Error (ACE) as a feedback signal
4. PDO uses tie line power as a feedback signal & OETC uses grid frequency as a feedback signal

5. PDO uses tie line power as a feedback signal & OETC uses tie line power as a feedback signal
6. PDO uses tie line power as a feedback signal & OETC uses Area Control Error (ACE) as a feedback signal
7. PDO uses Area Control Error (ACE) as a feedback signal & OETC uses grid frequency as a feedback signal
8. PDO uses Area Control Error (ACE) as a feedback signal & OETC uses tie line power as a feedback signal
9. PDO uses Area Control Error (ACE) as a feedback signal & OETC uses Area Control Error (ACE) as a feedback signal

The PID controller and the closed loop tuning method (Ultimate Sensitivity Method) are used for all control topologies. Since OETC is having most of the grid generation inertia connected to it, the PID controller of OETC will be tuned first. Then PDO PID controller will be tuned while the OETC PID is active. The ultimate aim of the investigation is to find out each control topology characteristics in terms of participation in disturbances recovery, frequency deviation and power exchange between the two control areas. The quality of the response is less important at this stage.

9.8.1. AGC of PDO (using grid frequency) and OETC (using grid frequency)

The grid frequency measured at PDO side is used as the feedback signal for PDO controller and the grid frequency measured at OETC side is used as a feedback signal for OETC controller. The PDO-OETC model with the controllers is shown in Figure 9.50 and the used PID controllers are the same as the one shown earlier in Figure 9.8. OETC controller is tuned first and therefore the PID parameters are the same as shown earlier in section 9.7.1.1. The OETC PID controller parameters were fed in the model and then PDO controller tuning started. The PDO controller closed loop gain was increased gradually until the ultimate gain has been reached which has produced the stable oscillatory response. The ultimate gain and oscillation period were recorded and are shown in Table 9.15 along with OETC controller parameters.

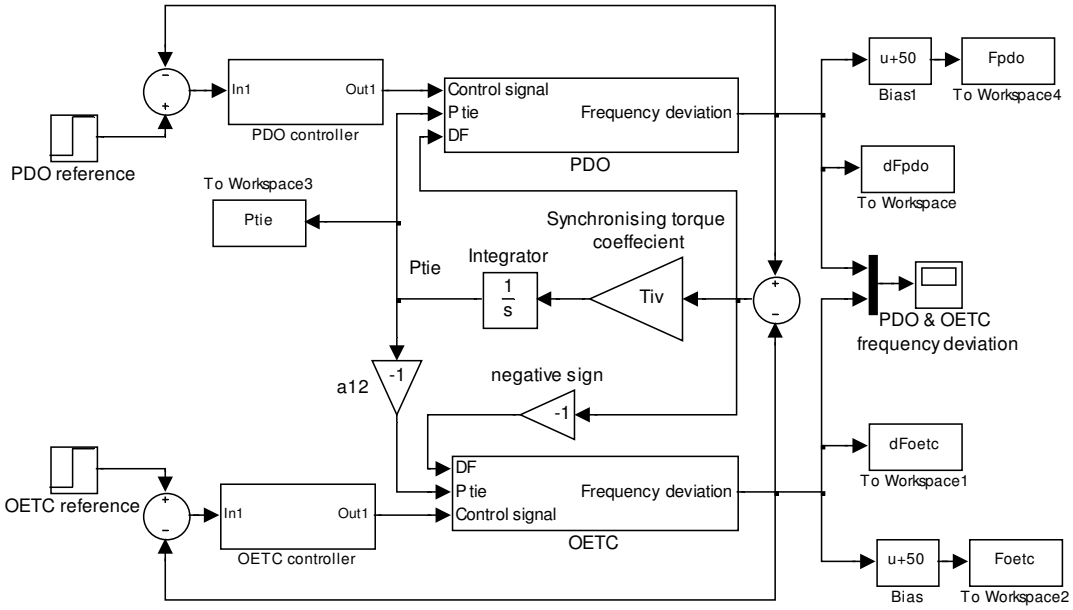

Figure 9.50: PDO-OETC model with PDO (using grid frequency) OETC (using grid frequency) PID AGC controller.

9.8.1.1 Calculation of the PID controller parameters

Once the ultimate gain (Ku) and period (Pu) are known, the PID controller parameters can be calculated using the look up table developed by Ziegler Nichols shown earlier in Table 9.2.

Table 9.15 summarises the PID controller parameters used in this part of the study:

	Ku (ultimate gain)	Pu (ultimate period)	Kc (PID Controller gain)	Ti (Integral time constant)	Td (derivative time constant)
PDO	3.767	1.171	2.2602	0.5855	0.146375
OETC	3.689	1.265	2.2134	0.6325	0.158125

Table 9.15: PDO & OETC AGC PID controller parameters based on grid frequency feedback

9.8.1.2. Simulation results

Totally six Figures have been produced to cover the five main aspects mentioned earlier (section 9.5) for each test. The results are shown in Figures 9.51 to 9.56 in Appendix 4. Table 9.16 shows a summary of the controller performance in terms of grid frequency and tie line power.

		Base case response	Controlled response
100MW load disturbance at PDO side	Frequency deviation (Hz)	-0.05	0
	Settling time (s)	10.9	4.65
	Tie line power deviation (p.u.)	-0.0379	-0.0155
100MW load disturbance at OETC side	Frequency deviation (Hz)	-0.05	0
	Settling time (s)	7.74	4.16
	Tie line power deviation (p.u.)	0.0121	0.0053

Table 9.16: PDO & OETC PID frequency based AGC controller performance summary

9.8.1.3. Results discussion

The simulation results with the PDO & OETC frequency PID AGC controller show clear improvements in comparison with the base case results. From Figure 9.51 to Figure 9.56 in Appendix 4 and Table 9.16, one can see the following:

- The frequency steady state offset is brought to zero when a step load disturbance is applied to PDO or OETC. It satisfies one of the fundamental requirements of AGC. The settling time is also good.
- The tie line power steady state offset is reduced by more than 50% than in the base case when the disturbance is applied at either side of the control areas. This will result in better stable operation of the tie line reducing the risk of tripping.
- The original generation dispatch is never restored even in the case of outside control area disturbance. Figure 9.53 and Figure 9.56 show that both PDO and OETC generators are participating in the disturbance compensation and their original dispatch has changed. However, it is noticed that when a disturbance arise within a certain control area, its own generators takes most of the compensation burden which is a fair phenomenon. This will maintain the cooperation spirit and fairness.
- In general, this control topology has good merits like removing the frequency offset and reducing the tie line exchange offset without jeopardising the system stability.

9.8.1.4. Summary

The PDO & OETC frequency based PID AGC controller was designed and tuned using the Ultimate Sensitivity Method. The control topology performance has satisfied one of the key aspects of AGC which is eliminating the frequency offset. However it failed to completely remove the power exchange offset but managed to reduce it significantly. The

controller performance was also good in terms of settling time and oscillations though the controller performance is not the focus of the analysis but the control topology.

This concludes that there is no envisaged risk of applying this topology though it will not satisfy all the AGC aims.

9.8.2. AGC of PDO (using grid frequency) and OETC (tie line power)

The grid frequency measured at PDO side is used as the feedback signal for PDO controller and the tie line power deviation is used as a feedback signal for OETC controller. The PDO-OETC model with the controllers is shown in Figure 9.57 and the used PID controllers are the same as the one shown earlier in Figure 9.8. OETC controller is tuned first and therefore the PID parameters are the same as shown earlier in section 9.7.2.1. The OETC PID controller parameters were fed in the model and then PDO controller tuning started. The PDO controller closed loop gain was increased gradually until the ultimate gain was reached which has produced the stable oscillatory response. The ultimate gain and oscillation period were recorded and are shown in Table 9.17 along with OETC controller parameters.

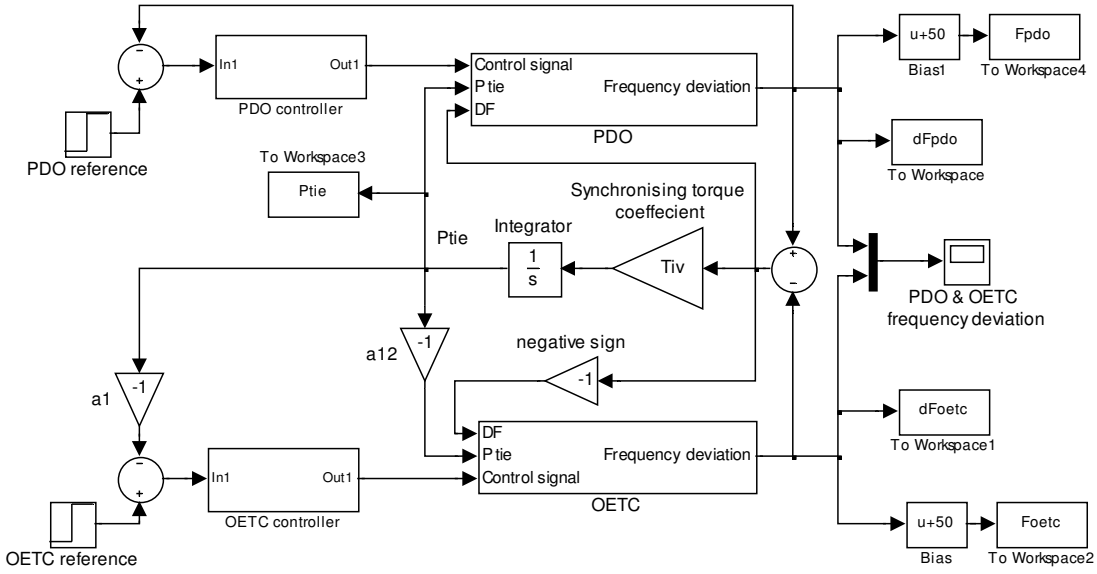

Figure 9.57: PDO-OETC model with PDO (using grid frequency) OETC (using tie line power) PID AGC controller.

9.8.2.1 Calculation of the PID controller parameters

Once the ultimate gain (Ku) and period (Pu) are known, the PID controller parameters can be calculated using the look up table developed by Ziegler Nichols shown earlier in Table 9.2.

Table 9.17 summarises the PID controller parameters used in this part of the study:

	Ku (ultimate gain)	Pu (ultimate period)	Kc (PID Controller gain)	Ti (Integral time constant)	Td (derivative time constant)
PDO	3.295	1.222	1.977	0.611	0.15275
OETC	1.348	1.996	0.8080	0.998	0.2495

Table 9.17: PDO (using grid frequency) & OETC (using tie line power) PID AGC controller parameters

9.8.2.2. Simulation results

Totally six Figures have been produced to cover the five main aspects mentioned earlier (section 9.5) for each test. The results are shown in Figures 9.58 to 9.63 in Appendix 4. Table 9.18 shows a summary of the controller performance in terms of grid frequency and tie line power.

		Base case response	Controlled response
100MW load disturbance at PDO side	Frequency deviation (Hz)	-0.05	0
	Settling time (s)	10.9	8.35
	Tie line power deviation (p.u.)	-0.0379	0
100MW load disturbance at OETC side	Frequency deviation (Hz)	-0.05	0
	Settling time (s)	7.74	8.175
	Tie line power deviation (p.u.)	0.0121	0

Table 9.18: PDO (using grid frequency) & OETC (using tie line power) PID AGC controller performance summary

9.8.2.3. Results discussion

The simulation results with the PDO (using grid frequency) & OETC (using tie line power) PID AGC controllers show clear improvements in comparison with the base case results. From Figure 9.58 to Figure 9.63 in Appendix 4 and Table 9.18, one can see the following:

- The frequency steady state offset is brought to zero when a step load disturbance is applied at PDO or OETC. It satisfies one of the fundamental requirements of AGC. The settling time is also good.
- The tie line power steady state offset is also brought to zero following load disturbances at PDO or OETC. It satisfies another requirement of AGC.

- The original generation dispatch is restored in the case of outside control area disturbance. Figure 9.60 shows that PDO generation takes the entire steady state load mismatch following load disturbance at PDO side whereas OETC generation participates only during the transients and then restores its original dispatch. The same scenario is reversed when the load disturbance is applied at OETC side as can be seen from Figure 9.63.
- In general, this control topology has satisfied all the fundamental requirements of AGC which makes it a good candidate for practical application. .

9.8.2.4. Summary

The PDO (using grid frequency) & OETC (using tie line power) PID AGC controller was designed and tuned using the Ultimate Sensitivity Method. The control topology performance has satisfied all the key aspects of AGC which are eliminating the frequency offset, eliminating the tie line offset and restoring the original generation dispatch following load disturbances. The controller performance is also good in terms of settling time and oscillations though the controller performance is not the focus of the analysis but the control topology.

This concludes that this control topology has a great potential and can be considered for practical application.

9.8.3. AGC of PDO (using grid frequency) and OETC (Area Control Error)

The grid frequency measured at PDO side is used as the feedback signal for PDO controller and OETC's Area Control Error (ACE) is used as the feedback signal for OETC controller. The PDO-OETC model with the controllers is shown in Figure 9.64 and the used PID controllers are the same as the one shown earlier in Figure 9.8. OETC controller is tuned first and therefore the PID parameters are the same as shown earlier in section 9.7.3.1. The OETC PID controller parameters were fed into the model and then PDO controller tuning started. The PDO controller closed loop gain was increased gradually until the ultimate gain has been reached which has produced the stable oscillatory response. The ultimate gain and oscillation period were recorded and are shown in Table 9.19 along with OETC controller parameters.

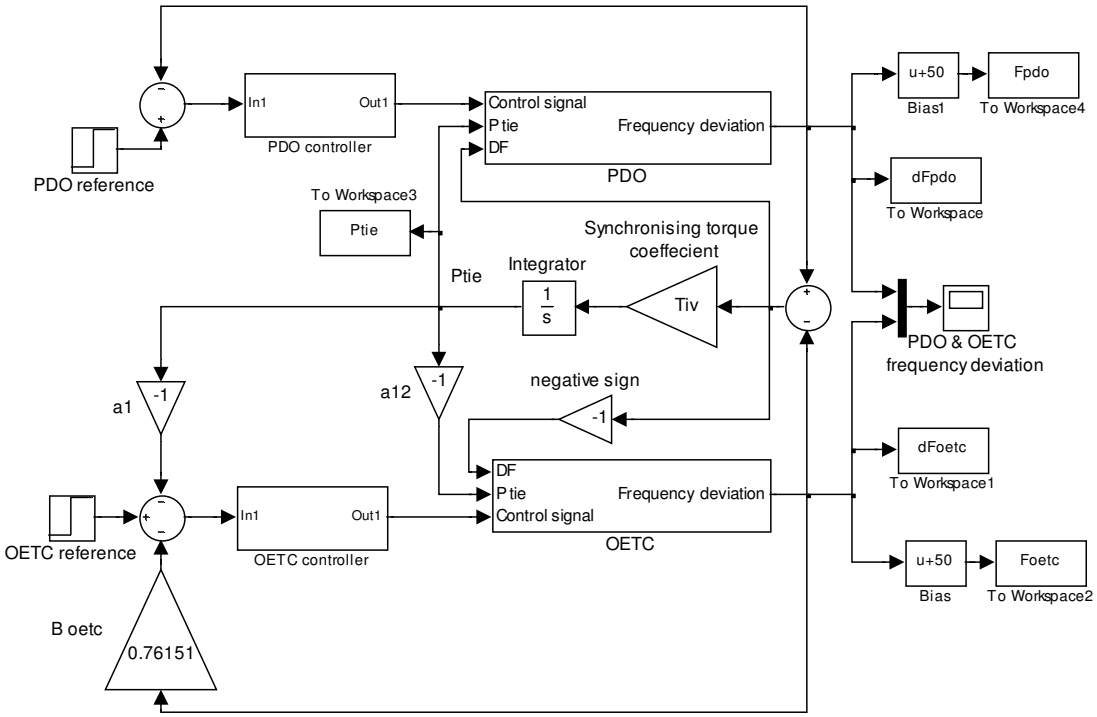

Figure 9.64: PDO-OETC model with PDO (using grid frequency) & OETC (using Area Control Error) PID AGC controller.

9.8.3.1 Calculation of the PID controller parameters

Once the ultimate gain (Ku) and period (Pu) are known, the PID controller parameters can be calculated using the look up table developed by Ziegler Nichols shown earlier in Table 9.2. Table 9.19 summarises the PID controller parameters used in this part of the study:

	Ku (ultimate gain)	Pu (ultimate period)	Kc (PID Controller gain)	Ti (Integral time constant)	Td (derivative time constant)
PDO	1.355	1.796	0.813	0.898	0.2245
OETC	1.468	1.755	0.8808	0.8775	0.219375

Table 9.19: PDO (using grid frequency) & OETC (using Area Control Error) PID AGC controller parameters

9.8.3.2. Simulation results

Totally six Figures have been produced to cover the five main aspects mentioned earlier (section 9.5) for each test. The results are shown in Figures 9.65 to 9.70 in Appendix 4. Table 9.20 shows a summary of the controller performance in terms of grid frequency and tie line power.

		Base case response	Controlled response
100MW load disturbance at PDO side	Frequency deviation (Hz)	-0.05	0
	Settling time (s)	10.9	5.76
	Tie line power deviation (p.u.)	-0.0379	0
100MW load disturbance at OETC side	Frequency deviation (Hz)	-0.05	0
	Settling time (s)	7.74	4.52
	Tie line power deviation (p.u.)	0.0121	0

Table 9.20: PDO (using grid frequency) & OETC (using Area Control Error) PID AGC controller performance summary

9.8.3.3. Results discussion

The simulation results with the PDO (using grid frequency) & OETC (using Area Control Error) PID AGC controller show clear improvements in comparison with the base case results. From Figure 9.65 to Figure 9.70 in Appendix 4 and Table 9.20, one can see the following:

- The frequency steady state offset is brought to zero when a step load disturbance is applied to PDO or OETC. It satisfies one of the fundamental requirements of AGC. The settling time is also good.
- The tie line power steady state offset is brought to zero following load disturbances at PDO or OETC. It satisfies another requirement of AGC.
- The original generation dispatch is restored in the case of outside control area load disturbances. Figure 9.67 shows that PDO generation takes the entire steady state load mismatch following load disturbance at PDO side whereas OETC generation participates only during the transients and then restores its original dispatch. The same scenario is reversed when the load disturbance is applied at OETC side as can be seen from Figure 9.70.
- In general, this control topology has satisfied all the fundamental requirements of AGC making it a good candidate for practical application. .

9.8.3.4. Summary

The PDO (using grid frequency) & OETC (using Area Control Error) PID AGC controller was designed and tuned using the Ultimate Sensitivity Method. The control topology performance has satisfied all the key aspects of AGC which are eliminating the frequency

offset, eliminating the tie line power offset and restoring the original generation dispatch for outside control area disturbances. The controller performance is also good in terms of settling time and oscillations though the controller performance is not the focus of the analysis at this stage but the control topology.

This concludes that this control topology has a great potential and can be considered for practical application.

9.8.4. AGC of PDO (using tie line power) and OETC (using grid frequency)

The tie line power deviation is used as the feedback signal for PDO controller and the grid frequency measured at OETC side is used as the feedback signal for OETC controller. The PDO-OETC model with the controllers is shown in Figure 9.71 and the used PID controllers are the same as the one shown earlier in Figure 9.8. OETC controller is tuned first and therefore the PID parameters are the same as shown earlier in section 9.7.1.1. The OETC PID controller parameters were fed into the model and then PDO controller tuning started. The PDO controller closed loop gain was increased gradually until the ultimate gain has been reached which has produced the stable oscillatory response. The ultimate gain and oscillation period were recorded and are shown in Table 9.21 along with OETC controller parameters.

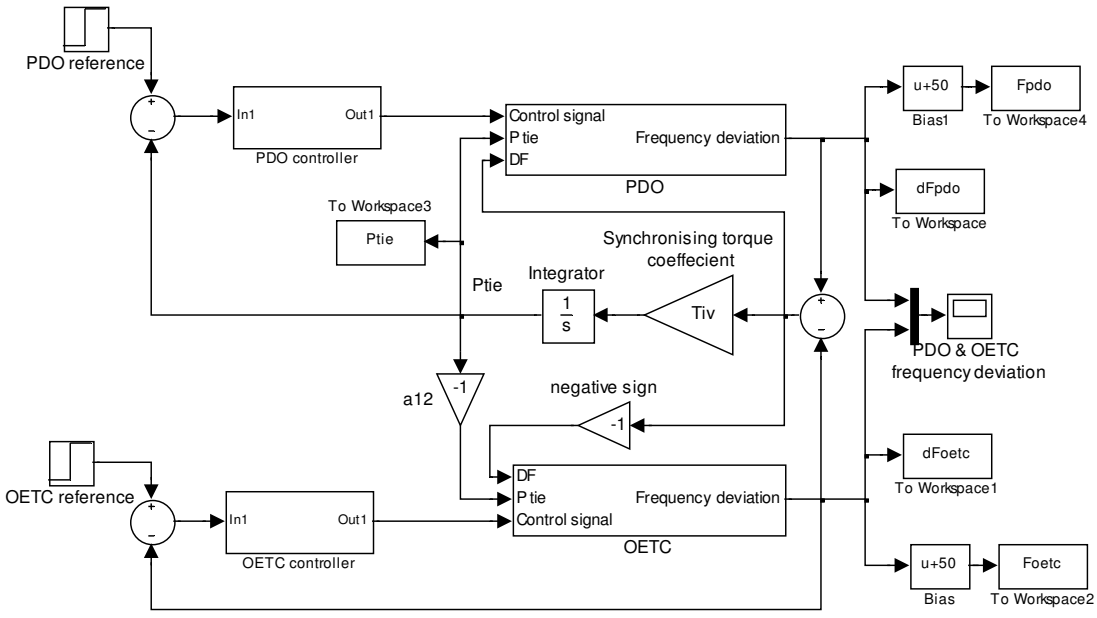

Figure 9.71: PDO-OETC model with PDO (using tie line power) & OETC (using grid frequency) PID AGC controller.

9.8.4.1 Calculation of the PID controller parameters

Once the ultimate gain (Ku) and period (Pu) are known, the PID controller parameters can be calculated using the look up table developed by Ziegler Nichols shown earlier in Table 9.2. Table 9.21 summarises the PID controller parameters used in this part of the study:

	Ku (ultimate gain)	Pu (ultimate period)	Kc (PID Controller gain)	Ti (Integral time constant)	Td (derivative time constant)
PDO	1.605	2.269	0.963	1.1345	0.283625
OETC	3.689	1.265	2.2134	0.6325	0.158125

Table 9.21: PDO (using tie line power) & OETC (using grid frequency) PID AGC controller parameters

9.8.4.2. Simulation results

Totally six Figures have been produced to cover the five main aspects mentioned earlier (section 9.5) for each test. The results are shown in Figures 9.72 to 9.77 in Appendix 4. Table 9.22 shows a summary of the controller performance in terms of grid frequency and tie line power.

		Base case response	Controlled response
100MW load disturbance at PDO side	Frequency deviation (Hz)	-0.05	0
	Settling time (s)	10.9	31.8
	Tie line power deviation (p.u.)	-0.0379	0
100MW load disturbance at OETC side	Frequency deviation (Hz)	-0.05	0
	Settling time (s)	7.74	18.8
	Tie line power deviation (p.u.)	0.0121	0

Table 9.22: PDO (using tie line power) & OETC (using grid frequency) PID AGC controller performance summary

9.8.4.3. Results discussion

The simulation results with the PDO (using tie line power) & OETC (using grid frequency) PID AGC controller show clear improvements in terms of offset in comparison with the base case results. However the response is more oscillatory and hence the settling time is longer. The settling time and oscillations can be improved by using advanced control

techniques. From Figure 9.72 to Figure 9.77 in Appendix 4 and Table 9.22, one can see the following:

- The frequency steady state offset is brought to zero when a step load disturbance is applied at PDO or OETC. It satisfies one of the fundamental requirements of AGC.
- The tie line power steady state offset is brought to zero following disturbances at PDO or OETC. It satisfies another requirement of AGC. The tie line signal suffers inter area oscillations and it is used for the lower inertia system (PDO) therefore it has made the system response more oscillatory.
- The original generation dispatch is restored in the case of outside control area disturbance. Figure 9.74 shows that PDO generation takes the entire steady state load mismatch following load disturbance at PDO side whereas OETC generation participates only during the transients and then restores its original dispatch. The same scenario is reversed when the load disturbance is applied at OETC side as can be seen from Figure 9.77.
- In general, this control topology has satisfied all the fundamental requirements of AGC making it a good candidate for practical application. A different control technique or tuning method will improve the settling time and oscillations.

9.8.4.4. Summary

The PDO (using tie line power) & OETC (using grid frequency) PID AGC controller was designed and tuned using the Ultimate Sensitivity Method. The control topology performance has satisfied all the key aspects of AGC which are eliminating the frequency offset, eliminating the tie line offset and restoring the original generation dispatch for outside control area disturbances. The controller performance is not good in terms of settling time and oscillations but can be improved by using a different control technique or a different tuning method.

This concludes that this control topology has a relatively good performance and can be considered for practical application.

9.8.5. AGC of PDO (using tie line power) and OETC (using tie line power)

The tie line power deviation is used as the feedback signal for both PDO and OETC controllers. The PDO-OETC model with the controllers is shown in Figure 9.78 and the used PID controllers are the same as the one shown earlier in Figure 9.8. OETC controller

is tuned first and therefore the PID parameters are the same as shown earlier in section 9.7.2.1. The OETC PID controller parameters were fed into the model and then PDO controller tuning started. The PDO controller closed loop gain was increased gradually until the ultimate gain has been reached which has produced the stable oscillatory response. The ultimate gain and oscillation period were recorded and are shown in Table 9.23 along with OETC controller parameters.

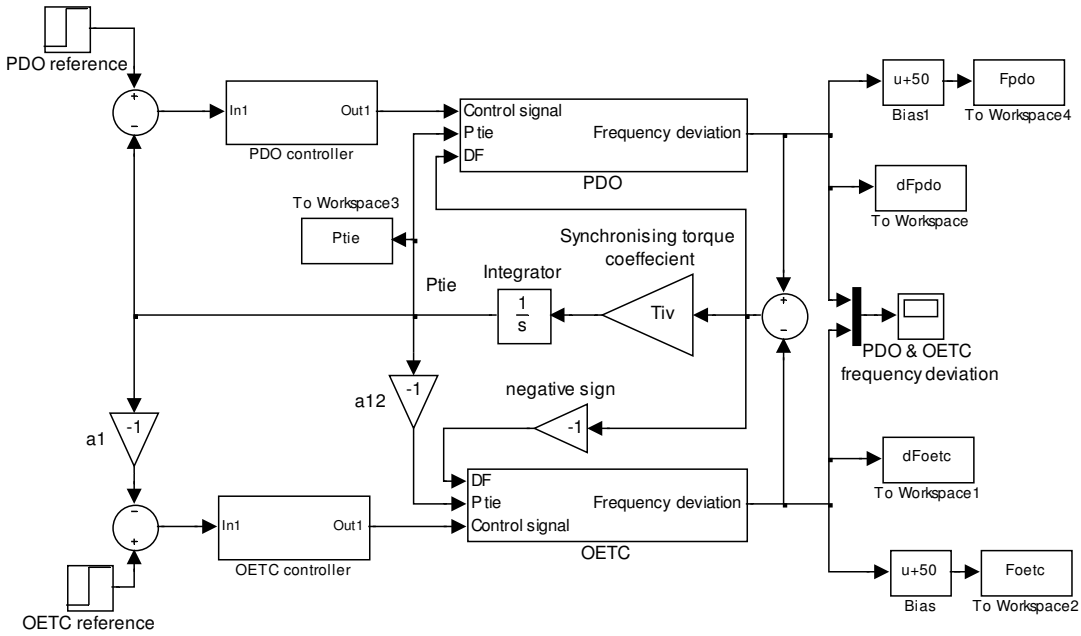

Figure 9.78: PDO-OETC model with PDO (using tie line power) & OETC (using tie line power) PID AGC controller.

9.8.5.1 Calculation of the PID controller parameters

Once the ultimate gain (Ku) and period (Pu) are known, the PID controller parameters can be calculated using the look up table developed by Ziegler Nichols shown earlier in Table 9.2.

Table 9.23 summarises the PID controller parameters used in this part of the study:

	Ku (ultimate gain)	Pu (ultimate period)	Kc (PID Controller gain)	Ti (Integral time constant)	Td (derivative time constant)
PDO	0.45	1.935	0.27	0.9675	0.241875
OETC	1.348	1.996	0.8088	0.998	0.2495

Table 9.23: PDO (using tie line power) & OETC (using tie line power) PID AGC controller parameters

9.8.5.2. Simulation results

Totally six Figures have been produced to cover the five main aspects mentioned earlier (section 9.5) for each test. The results are shown in Figures 9.79 to 9.84 in Appendix 4. Table 9.24 shows a summary of the controller performance in terms of grid frequency and tie line power.

		Base case response	Controlled response
100MW load disturbance at PDO side	Frequency deviation (Hz)	-0.05	-0.154
	Settling time (s)	10.9	133
	Tie line power deviation (p.u.)	-0.0379	0
100MW load disturbance at OETC side	Frequency deviation (Hz)	-0.05	-0.017
	Settling time (s)	7.74	102
	Tie line power deviation (p.u.)	0.0121	0

Table 9.24: PDO (using tie line power) & OETC (using tie line power) PID AGC controller performance summary

9.8.5.3. Results discussion

The simulation results with the PDO (using tie line power) & OETC (using tie line power) PID AGC controller show clear drawbacks in terms of offset and oscillations in comparison with the base case results. The response is highly oscillatory and the settling time is very long. The settling time and oscillations may not be improved dramatically even by using advanced control techniques. From Figure 9.79 to Figure 9.84 in Appendix 4 and Table 9.24, one can see the following:

- The frequency always settles with an offset whenever a step load disturbance is applied at PDO or OETC. In fact it settles with a higher steady state deviation than in the base case when the disturbance is applied at PDO side. The high frequency oscillations are not only due to the deficiency of the basic tuning method but also because both systems are pulling each other due to using the same signal but having different inertia values. The high inertia value makes the overall response slower than in the lower inertia case and hence the pulling scenario.
- The tie line power steady state offset is brought to zero following disturbances at PDO or OETC. It satisfies one requirement of AGC. The tie line signal suffers inter area oscillations and it is used for both the lower inertia system and the higher inertia system, hence causing the oscillatory response with the high settling time.

- The original generation dispatch is never restored whether the disturbance is within or outside the control area. Figure 9.81 shows that PDO generation takes most of the steady state load mismatch following load disturbance at PDO side but OETC generation original dispatch has also been affected. The same scenario is reversed when the load disturbance is applied at OETC side as can be seen from Figure 9.84.
- In general, this control topology has satisfied only one fundamental requirements of AGC and jeopardised the overall stability of the power system. A different control technique or tuning method may not be able to improve the settling time and oscillations. Consequently, this control topology is a bad one and there might be high risks associated with its practical applications.

9.8.5.4. Summary

The PDO (using tie line power) & OETC (using tie line power) PID AGC controller was designed and tuned using the Ultimate Sensitivity Method. The control topology performance has satisfied only one of the key aspects of AGC which is eliminating the tie line offset. The controller performance is very poor in terms of settling time and oscillations which may not be easily improved by using a different control technique or a different tuning method.

This concludes that this control topology has a bad performance and should not be considered for practical application.

9.8.6. AGC of PDO (using tie line power) and OETC (using Area Control Error)

The tie line power deviation is used as the feedback signal to PDO controller and OETC's Area Control Error (ACE) is used as the feedback signal to OETC controller. The PDO-OETC model with the controllers is shown in Figure 9.85 and the used PID controllers are the same as the one shown earlier in Figure 9.8. OETC controller is tuned first and therefore the PID parameters are the same as shown earlier in section 9.7.3.1. The OETC PID controller parameters were fed in the model and then PDO controller tuning started. The PDO controller closed loop gain was increased gradually until the ultimate gain has been reached which has produced the stable oscillatory response. The ultimate gain and oscillation period were recorded and are shown in Table 9.25 along with OETC controller parameters.

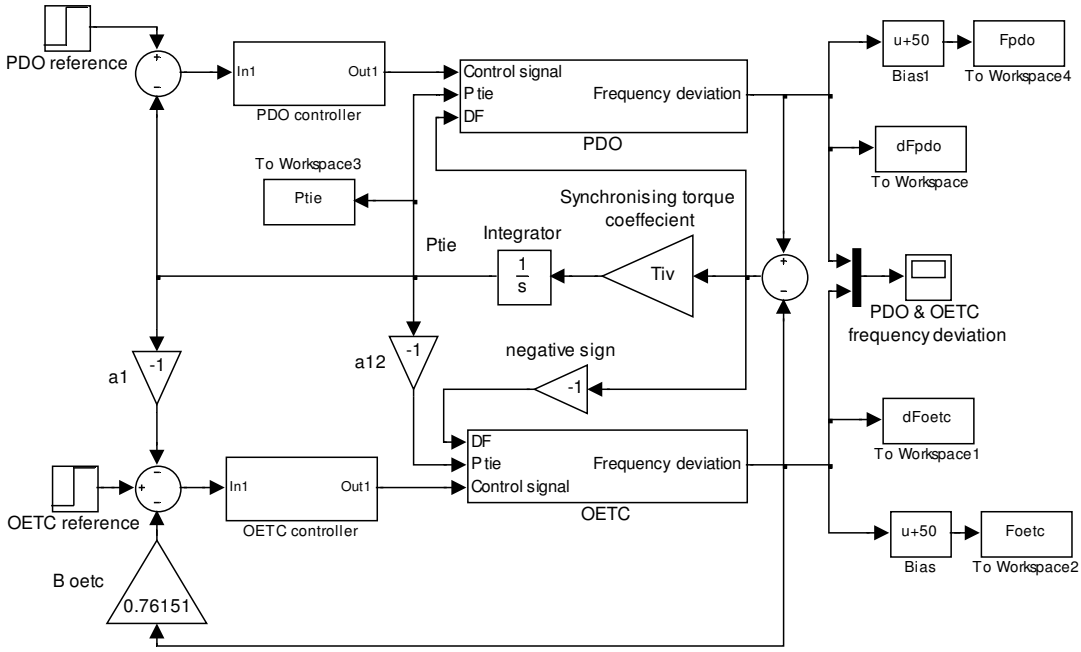

Figure 9.85: PDO-OETC model with PDO (using tie line power) & OETC (using Area Control Error) PID AGC controller.

9.8.6.1 Calculation of the PID controller parameters

Once the ultimate gain (Ku) and period (Pu) are known, the PID controller parameters can be calculated using the look up table developed by Ziegler Nichols shown earlier in Table 9.2.

Table 9.25 summarises the PID controller parameters used in this part of the study:

	Ku (ultimate gain)	Pu (ultimate period)	Kc (PID Controller gain)	Ti (Integral time constant)	Td (derivative time constant)
PDO	1.355	1.796	0.813	0.898	0.2245
OETC	1.468	1.755	0.8808	0.8775	0.219375

Table 9.25: PDO (using tie line power) & OETC (using Area Control Error) PID AGC controller parameters

9.8.6.2. Simulation results

Totally six Figures have been produced to cover the five main aspects mentioned earlier (section 9.5) for each test. The results are shown in Figures 9.86 to 9.91 in Appendix 4. Table 9.26 shows a summary of the controller performance in terms of grid frequency and tie line power.

		Base case response	Controlled response
100MW load disturbance at PDO side	Frequency deviation (Hz)	-0.05	0
	Settling time (s)	10.9	58.8
	Tie line power deviation (p.u.)	-0.0379	0
100MW load disturbance at OETC side	Frequency deviation (Hz)	-0.05	0
	Settling time (s)	7.74	44.6
	Tie line power deviation (p.u.)	0.0121	0

Table 9.26: PDO (using tie line power) & OETC (using Area Control Error) PID AGC controller performance summary

9.8.6.3. Results discussion

The simulation results with the PDO (using tie line power) & OETC (using Area Control Error) PID AGC controller show clear improvements in terms of offset in comparison with the base case results. The response is oscillatory and the settling time is longer than in the base case. The settling time and oscillations can be improved by using advanced control techniques. From Figure 9.86 to Figure 9.91 in Appendix 4 and Table 9.26, one can see the following:

- The frequency offset is eliminated whenever a step load disturbance is applied at PDO or OETC. It has satisfied a fundamental requirement of AGC. The response is oscillatory and the settling time is longer than in the base case.
- The tie line power steady state offset is brought to zero following load disturbances at PDO or OETC. It satisfies another requirement of AGC. The tie line signal suffers inter area oscillations and it is used in calculating the Area Control Error of OETC as well a direct feedback signal to PDO AGC controller hence causing the oscillatory response with the high settling time.
- The original generation dispatch is restored whenever the disturbance is outside the control area. Figure 9.88 shows that PDO generation takes the entire steady state load mismatch following load disturbance at PDO. Similarly, as can be seen from Figure 9.91, OETC generation takes the entire steady state load mismatch following load disturbance at OETC.
- In general, this control topology has satisfied all the fundamental requirements of AGC. A different control technique or tuning method will be able to improve the settling time and oscillations. There are visible advantages of practically applying

this control topology if the response oscillations can be improved using a better control technique

9.8.6.4. Summary

The PDO (using tie line power) & OETC (using Area Control Error) PID AGC controller was designed and tuned using the Ultimate Sensitivity Method. The control topology performance has satisfied all of the key aspects of AGC which are eliminating frequency offset, eliminating the tie line offset and restoring the original generation dispatch for outside control area load disturbances. The controller performance is poor in terms of settling time and oscillations which can be improved by using a different control technique or a different tuning method.

This concludes that this control topology has a reasonable performance and can be considered for practical application especially if the response oscillations are reduced by using advanced control techniques.

9.8.7. AGC of PDO (using Area Control Error) and OETC (using grid frequency)

PDO's Area Control Error (ACE) is used as the feedback signal to PDO controller and the grid frequency measured at OETC side is used as the feedback signal to OETC controller. The PDO-OETC model with the controllers is shown in Figure 9.92 and the used PID controllers are the same as the one shown earlier in Figure 9.8. OETC controller is tuned first and therefore the PID parameters are the same as shown earlier in section 9.7.1.1. The OETC PID controller parameters were fed into the model and then PDO controller tuning started. The PDO controller closed loop gain was increased gradually until the ultimate gain has been reached which has produced the stable oscillatory response. The ultimate gain and oscillation period were recorded and are shown in Table 9.27 along with OETC controller parameters.

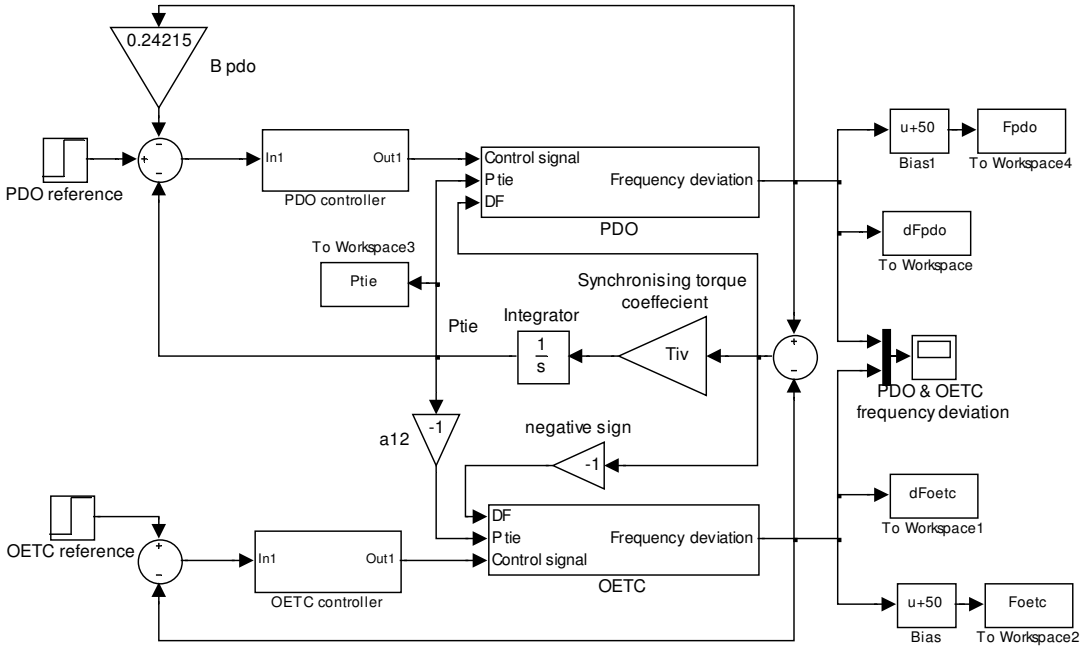

Figure 9.92: PDO-OETC model with PDO (using Area Control Error) & OETC (using grid frequency) PID AGC controller.

9.8.7.1 Calculation of the PID controller parameters

Once the ultimate gain (Ku) and period (Pu) are known, the PID controller parameters can be calculated using the look up table developed by Ziegler Nichols shown earlier in Table 9.2.

Table 9.27 summarises the PID controller parameters used in this part of the study:

	Ku (ultimate gain)	Pu (ultimate period)	Kc (PID Controller gain)	Ti (Integral time constant)	Td (derivative time constant)
PDO	2.688	1.887	1.6128	0.9435	0.235875
OETC	3.689	1.265	2.2134	0.6325	0.158125

Table 9.27: PDO (using Area Control Error) & OETC (using grid frequency) PID AGC controller parameters

9.8.7.2. Simulation results

Totally six Figures have been produced to cover the five main aspects mentioned earlier (section 9.5) for each test. The results are shown in Figures 9.93 to 9.98 in Appendix 4. Table 9.28 shows a summary of the controller performance in terms of grid frequency and tie line power.

		Base case response	Controlled response
100MW load disturbance at PDO side	Frequency deviation (Hz)	-0.05	0
	Settling time (s)	10.9	16.1
	Tie line power deviation (p.u.)	-0.0379	0
100MW load disturbance at OETC side	Frequency deviation (Hz)	-0.05	0
	Settling time (s)	7.74	10.6
	Tie line power deviation (p.u.)	0.0121	0

Table 9.28: PDO (using Area Control Error) & OETC (using grid frequency) PID AGC controller performance summary

9.8.7.3. Results discussion

The simulation results with the PDO (using Area Control Error) & OETC (using grid frequency) PID AGC controller show clear improvements in terms of offset in comparison with the base case results. The response is oscillatory and the settling time is slightly longer than in the base case. The settling time and oscillations can be improved by using advanced control techniques. From Figure 9.93 to Figure 9.98 in Appendix 4 and Table 9.28, one can see the following:

- The frequency offset is eliminated whenever a step load disturbance is applied to PDO or OETC. It has satisfied a fundamental requirement of AGC.
- The tie line power steady state offset is brought to zero following disturbances at PDO or OETC. It satisfies another requirement of AGC. The tie line signal suffers inter area oscillations and it has been used in calculating the Area Control Error of PDO, hence causing the oscillatory response with slightly longer settling time than in the base case.
- The original generation dispatch is restored whenever the disturbance is outside the control area, another requirement of AGC. Figure 9.5 shows that PDO generation takes the entire steady state load mismatch following load disturbance at PDO. On the other hand OETC generation takes the entire steady state load mismatch when the load disturbance is applied at OETC side as can be seen from Figure 9.98.
- In general, this control topology has satisfied all the fundamental requirements of AGC. Therefore this control topology is feasible for practical application.

9.8.7.4. Summary

The PDO (using Area Control Error) & OETC (using grid frequency) PID AGC controller was designed and tuned using the Ultimate Sensitivity Method. The control topology performance has satisfied all of the key aspects of AGC which are eliminating frequency offset, eliminating the tie line offset and restoring the original generation dispatch for outside control area load disturbances. The controller performance is good in terms of settling time and oscillations which can be further improved by using a different control technique or a different tuning method.

This concludes that this control topology has a good performance and can be considered for practical application.

9.8.8. AGC of PDO (using Area Control Error) and OETC (using tie line power)

PDO's Area Control Error (ACE) is used as the feedback signal to PDO controller and the tie line power deviation is used as the feedback signal to OETC controller. The PDO-OETC model with the controllers is shown in Figure 9.99 and the used PID controllers are the same as the one shown earlier in Figure 9.8. OETC controller is tuned first and therefore the PID parameters are the same as shown earlier in section 9.7.2.1. The OETC PID controller parameters were fed into the model and then PDO controller tuning started. The PDO controller closed loop gain was increased gradually until the ultimate gain has been reached which has produced the stable oscillatory response. The ultimate gain and oscillation period were recorded and are shown in Table 9.29 along with OETC controller parameters.

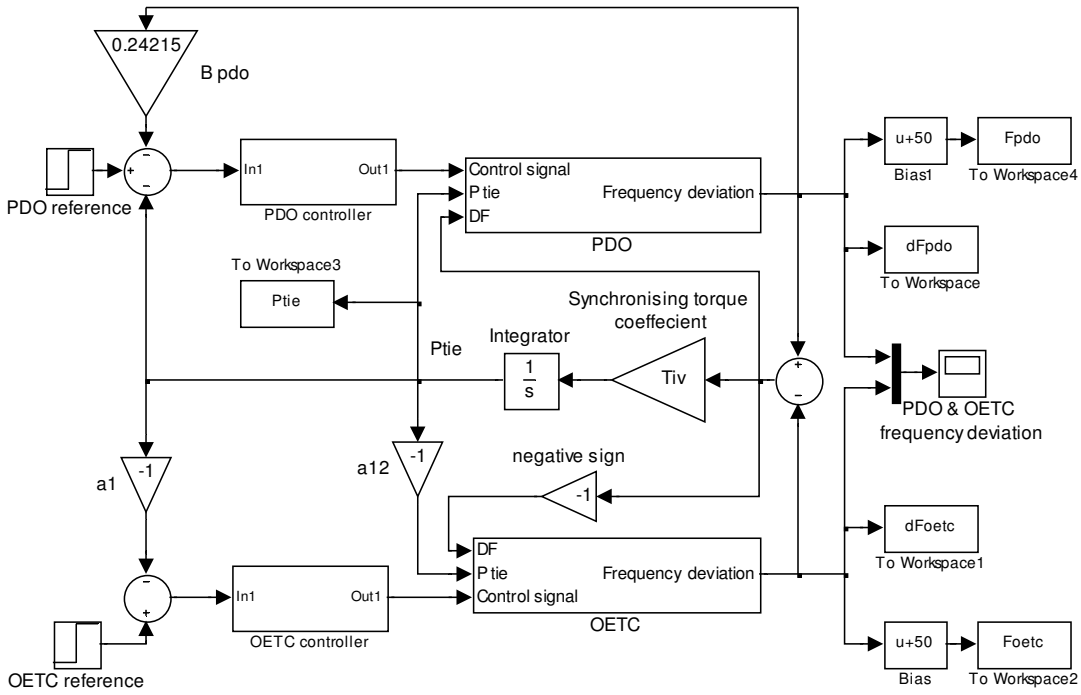

Figure 9.99: PDO-OETC model with PDO (using Area Control Error) & OETC (using tie line power) PID AGC controller.

9.8.8.1 Calculation of the PID controller parameters

Once the ultimate gain (Ku) and period (Pu) are known, the PID controller parameters can be calculated using the look up table developed by Ziegler Nichols shown earlier in Table 9.2.

Table 9.29 summarises the PID controller parameters used in this part of the study:

	Ku (ultimate gain)	Pu (ultimate period)	Kc (PID Controller gain)	Ti (Integral time constant)	Td (derivative time constant)
PDO	0.6	1.888	0.36	0.944	0.236
OETC	1.348	1.996	0.8088	0.998	0.2495

Table 9.29: PDO (using Area Control Error) & OETC (using tie line power) PID AGC controller parameters

9.8.8.2. Simulation results

Totally six Figures have been produced to cover the five main aspects mentioned earlier (section 9.5) for each test. The results are shown in Figures 9.100 to 9.105 in Appendix 4. Table 9.30 shows a summary of the controller performance in terms of grid frequency and tie line power.

		Base case response	Controlled response
100MW load disturbance at PDO side	Frequency deviation (Hz)	-0.05	0
	Settling time (s)	10.9	71.3
	Tie line power deviation (p.u.)	-0.0379	0
100MW load disturbance at OETC side	Frequency deviation (Hz)	-0.05	0
	Settling time (s)	7.74	49.6
	Tie line power deviation (p.u.)	0.0121	0

Table 9.30: PDO (using Area Control Error) & OETC (using tie line power) PID AGC controller performance summary

9.8.8.3. Results discussion

The simulation results with the PDO (using Area Control Error) & OETC (using tie line power) PID AGC controller show clear improvements in terms of offset in comparison with the base case results. The response is oscillatory and the settling time is longer than in the base case. The settling time and oscillations can be further improved by using advanced control techniques. From Figure 9.100 to Figure 9.105 in Appendix 4 and Table 9.30, one can see the following:

- The frequency offset is eliminated whenever a step load disturbance is applied at PDO or OETC. It has satisfied a fundamental requirement of AGC. The response is oscillatory and the settling time is longer than in the base case.
- The tie line power steady state offset is brought to zero following load disturbances at PDO or OETC. It satisfies another requirement of AGC. The tie line signal suffers inter area oscillations and It is used in calculating the Area Control Error of PDO and also is used as a feedback signal to OETC controller and therefore causes the oscillatory response with the high settling time.
- The original generation dispatch is restored whenever the load disturbance is outside the control area. Figure 9.102 shows that PDO generation takes the entire steady state load mismatch following load disturbance at PDO. The same scenario is applicable to OETC generators when the load disturbance is applied at OETC side as can be seen from Figure 9.105.
- In general, this control topology has satisfied all the fundamental requirements of AGC. A different control technique or tuning method will be able to improve the settling time and oscillations. There are visible advantages of practically applying

this control topology if the response oscillations can be improved by a better control technique

9.8.8.4. Summary

The PDO (using Area Control Error) & OETC (using tie line power) PID AGC controller was designed and tuned using the Ultimate Sensitivity Method. The control topology performance has satisfied all of the key aspects of AGC which are eliminating frequency offset, eliminating the tie line offset and restoring the original generation dispatch for outside control area load disturbances. The controller performance is poor in terms of settling time and oscillations which can be improved by using a different control technique or a different tuning method.

This concludes that this control topology has a reasonable performance and can be considered for practical application especially if the response oscillations are reduced by using advanced control techniques.

9.8.9. AGC of PDO (using Area Control Error) and OETC (using Area Control Error)

PDO's Area Control Error (ACE) is used as the feedback signal to PDO controller and OETC's Area Control Error is used as the feedback signal to OETC controller. This control topology is widely used and applied by researchers in designing AGC controllers.

The calculation of the frequency-response characteristic factor β of each area is less sensitive to errors for this particular control topology. This is because each control area has its own AGC controller dealing with internal load disturbances and there is no need for steady state support from neighbouring control areas. However, as the factor β value changes, the dynamic interaction between the two control areas will change affecting the overall system dynamic response.

The PDO-OETC model with the controllers is shown in Figure 9.106 and the used PID controllers are the same as the one shown earlier in Figure 9.8. OETC controller is tuned first and therefore the PID parameters are the same as shown earlier in section 9.7.3.1. The OETC PID controller parameters were fed into the model and then PDO controller tuning has started. The PDO controller closed loop gain was increased gradually until the ultimate gain has been reached which has produced the stable oscillatory response. The ultimate gain and oscillation period were recorded and are shown in Table 9.31 along with OETC controller parameters.

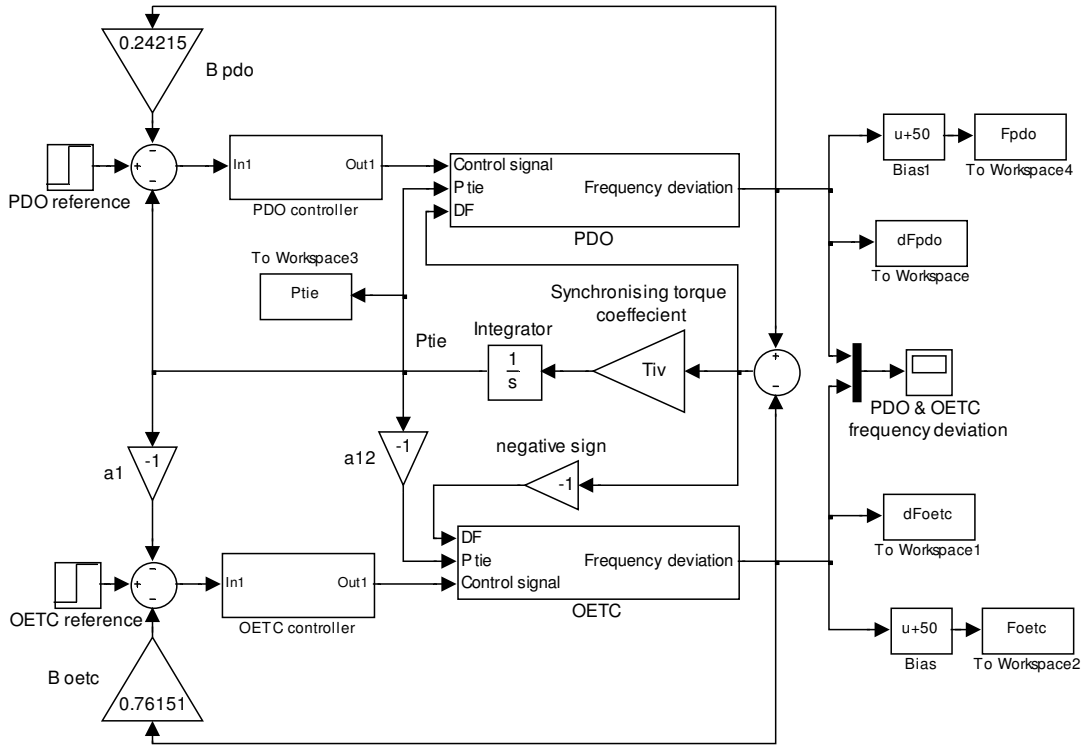

Figure 9.106: PDO-OETC model with PDO (using Area Control Error) & OETC (using Area Control Error) PID AGC controller.

9.8.9.1 Calculation of the PID controller parameters

Once the ultimate gain (Ku) and period (Pu) are known, the PID controller parameters can be calculated using the look up table developed by Ziegler Nichols shown earlier in Table 9.2. Table 9.31 summarises the PID controller parameters used in this part of the study:

	Ku (ultimate gain)	Pu (ultimate period)	Kc (PID Controller gain)	Ti (Integral time constant)	Td (derivative time constant)
PDO	1.375	1.73	0.825	0.865	0.21625
OETC	1.468	1.755	0.8808	0.8775	0.219375

Table 9.31: PDO (using Area Control Error) & OETC (using Area Control Error) PID AGC controller parameters

9.8.9.2. Simulation results

Totally six Figures have been produced to cover the five main aspects mentioned earlier (section 9.5) for each test. The results are shown in Figures 9.107 to 9.112 in Appendix 4. Table 9.32 shows a summary of the controller performance in terms of grid frequency and tie line power.

		Base case response	Controlled response
100MW load disturbance at PDO side	Frequency deviation (Hz)	-0.05	0
	Settling time (s)	10.9	34
	Tie line power deviation (p.u.)	-0.0379	0
100MW load disturbance at OETC side	Frequency deviation (Hz)	-0.05	0
	Settling time (s)	7.74	25.3
	Tie line power deviation (p.u.)	0.0121	0

Table 9.32: PDO (using Area Control Error) & OETC (using Area Control Error) PID AGC controller performance summary

9.8.9.3. Results discussion

The simulation results with the PDO (using Area Control Error) and OETC (using Area Control Error) PID AGC controller show clear improvements in terms of steady state offset in comparison with the base case results. The response is oscillatory and the settling time is longer than in the base case. The settling time and oscillations can be further improved by using advanced control techniques. From Figure 9.107 to Figure 9.112 in Appendix 4 and Table 9.32, one can see the following:

- The frequency steady state offset is eliminated whenever a step load disturbance is applied at PDO or OETC. It has satisfied a fundamental requirement of AGC. The response is oscillatory and the settling time is longer than in the base case.
- The tie line power steady state offset is brought to zero following load disturbances at PDO or OETC. It satisfies another requirement of AGC. The tie line signal suffers inter area oscillations and it is used in calculating the Area Control Error of both PDO and OETC, therefore causes the oscillatory response with the long settling time.
- The original generation dispatch is restored whenever the load disturbance is outside the control area. Figure 9.109 shows that PDO generation takes the entire steady state load mismatch following load disturbance at PDO. The same scenario is applicable to OETC generators when the load disturbance is applied at OETC side as can be seen from Figure 9.112.
- In general, this control topology has satisfied all the fundamental requirements of AGC. A different control technique or tuning method will be able to improve the settling time and oscillations. There are visible advantages of practically applying

this control topology. In fact this control topology is very famous and has been widely used by the researchers to design AGC controller.

9.8.9.4. Summary

The PDO (using Area Control Error) & OETC (using Area Control Error) PID AGC controller was designed and tuned using the Ultimate Sensitivity Method. The control topology performance has satisfied all of the key aspects of AGC which are eliminating frequency offset, eliminating the tie line offset and restoring the original generation dispatch for outside control area load disturbances. The controller performance is acceptable in terms of settling time and oscillations which can be further improved by using a different control technique or a different tuning method.

This concludes that this control topology has a good performance and can be considered for practical application.

9.9 AGC control topologies assessment summary

AGC can take different shapes depending on the type of feedback signals used. The term "control topology" refers to both PDO and OETC are interconnected together and are being controlled by independent AGC controllers using different feedback signals. The control topology can also be by applying the AGC to one control area only, PDO or OETC.

The control topologies assessment task has been completed using the ultimate sensitivity method in tuning the PID controller. A total number of fifteen control topologies have been assessed. The assessment criterion is based on satisfaction of the main requirements of AGC which are:

- Zero steady state frequency deviation following load disturbance
- Zero steady state tie line power deviation following load disturbance
- Load disturbance is compensated locally at the disturbed control area and restoration of the nominal generation dispatch of none disturbed control area in the steady state condition

Based on the above criterion and the control topology performance a recommendation is given for each control topology has been assessed. The performance settling time and oscillations are given less importance because they can be improved by using other sophisticated control technologies or tuning methods. However where applicable, it is indicated that some control topologies require sophisticated control techniques to improve oscillations and settling time.

Table 9.33 summarises all the control topologies performance in comparison to the base case performance. A traffic light table has been attempted to summarise and compare the recommendation for each control topology. It is shown in Table 9.34. In Table 9.34 the following different colours are used to indicate the goodness of the control topology performance:

	Indicates bad performance and has jeopardised the system stability or does not satisfy the AGC requirements. Cannot be applied.
	Indicates moderate performance and satisfied some of AGC requirements or requires sophisticated control technique to improve the oscillatory response. Can be applied with cautious.
	Indicates good performance and has satisfied all the AGC requirements. Recommended for application.

		100MW load disturbance at PDO			100MW load disturbance at OETC		
Case	Feedback signal	Frequency deviation	Settling time	Tie line power deviation	Frequency deviation	Settling time	Tie line power deviation
Base	None	-0.05	10.9	-0.0379	-0.05	7.74	0.0121
AGC applied to PDO alone	F	0	5.6	0	0	4.9	0.05
	P	0	38.61	0	-0.066	29.8	0
	ACE	0	22.6	0	-0.05	15.34	0.0121
AGC applied to OETC alone	F	0	10.5	-0.05	0	5.84	0
	P	-0.206	41.6	0	0	25.1	0
	ACE	-0.05	14	-0.0379	0	10.4	0
AGC applied to both PDO & OETC	PDO (F) & OETC (F)	0	4.65	-0.0155	0	4.16	0.0053
	PDO (F) & OETC (P)	0	8.35	0	0	8.175	0
	PDO (F) & OETC (ACE)	0	5.76	0	0	4.52	0
	PDO (P) & OETC (F)	0	31.8	0	0	18.8	0
	PDO (P) & OETC (P)	-0.154	133	0	-0.017	102	0
	PDO (P) & OETC (ACE)	0	58.8	0	0	44.6	0
	PDO (ACE) & OETC (F)	0	16.1	0	0	10.6	0
	PDO (ACE) & OETC (P)	0	71.3	0	0	49.6	0
	PDO (ACE) & OETC (ACE)	0	34	0	0	25.3	0

F= grid frequency deviation

P= tie line power deviation

ACE= Area Control Error

Table 9.33: Summary of all assessed control topologies performance in comparison to the base case performance

		OETC			
		None	Frequency	Power	ACE
PDO	None	Base case			
	Frequency				
	Power				
	ACE				

Table 9.34: Traffic lights application recommendation summary of all assessed control topologies

From table 9.34 one can see that only ACE signal can be used when applying AGC to PDO or OETC independently. Five control topologies are recommended when applying AGC to both PDO and OETC. A total number of five control topologies should be avoided and three can be applied with cautious.

AGC software has been around for long time and vendors are supplying a standard package to power system operators. The standard packages contain all three feedback signals for the operator to select from. However as indicated above, the operator should not freely select the feedback signal to the AGC controller when the power system is interconnected with a neighbouring one. Therefore PDO and OETC should apply an interlocking scheme which prevents operating in the prohibited control topologies. The interlocking scheme can be implemented either electrically through SCADA control telemetry or through normal paper work.

The following list summarises the recommended AGC control topologies for the interconnected operation of PDO and OETC:

When AGC is applied at PDO side only:

1. AGC is using ACE as a feedback signal

When AGC is applied at OETC side only:

1. AGC is using ACE as a feedback signal

When AGC is applied at both PDO & OETC sides:

1. PDO uses grid frequency as feedback signal & OETC uses tie line power as a feedback signal
2. PDO uses grid frequency as feedback signal & OETC uses Area Control Error (ACE) as a feedback signal

3. PDO uses tie line power as feedback signal & OETC uses grid frequency as a feedback signal
4. PDO uses Area Control Error (ACE) as feedback signal & OETC uses grid frequency as a feedback signal
5. PDO uses Area Control Error (ACE) as feedback signal & OETC uses Area Control Error (ACE) as a feedback signal

A selected number of the above recommended control topologies will be further analysed in the following parts of this study.

Chapter 10: Design of Automatic Generation Control using Linear Quadratic Regulator

10.1. Introduction

In the previous chapter, PDO-OETC AGC was designed and tuned using a basic control technique. In this part, a Linear Quadratic Regulator (LQR) technique will be considered to design an AGC controller of PDO-OETC power systems. The aim is to realise the difference in response the LQR technique can make in comparison to the classical approaches. Linear Quadratic Regulator (LQR) is known of its robustness to dynamic systems non-linearity and parameters variations.

The Linear Quadratic Regulator is an optimal controller which can have different parameters for the same control topology depending on the design requirements. LQR can take the very basic format whereby all the system parameters are equally important. On the other hand, the designer can be selective and modify the basic LQR design so that he cares mostly of a selected number of system parameters.

For the sake of completeness, both the basic design of LQR AGC and the modified design of LQR AGC will be considered.

10.2. Basic Design of LQR AGC

10.2.1. Introduction

In the previous chapter of this report a total number of fifteen control topologies were tested from which seven control topologies are recommended for practical applications. In order to minimise the unnecessary prolonged discussion, in this part we will consider only one control topology for PDO alone, one control topology for OETC alone and one control topology when AGC is applied for both PDO & OETC. When considering AGC is applied to PDO alone, the only recommended topology is using ACE as a feedback signal. The same is applicable when considering AGC for OETC alone. On the other hand there are five control topologies recommended when AGC is applied at both PDO and OETC power systems. However the most widely practically applied topology is using ACE feedback signal, therefore it is considered here.

From above discussion, three control topologies will only be considered in this part of the study. Therefore the LQR will be applied to the following three control topologies:

- AGC applied to PDO alone using ACE as a feedback signal

- AGC applied to OETC alone using ACE as a feedback signal
- AGC applied to both PDO and OETC using ACE as a feedback signal

At the end, the performance of the Linear Quadratic control technique will be compared with the classical PID controller performance.

10.2.2. Theoretical background

Linear Quadratic Regulators are considered as one branch of modern optimal control theory which has enabled control engineers to handle large multivariable control problems with ease. Here, LQR will be used to design an AGC controller for PDO-OETC power system. The PDO-OETC power system has to be in the state variable form and the desired performance has to be mathematically represented in terms of a cost function to be minimised. The PDO-OETC power system state variable form was already constructed in chapter 8. However, the developed state variable form will be revisited to include the AGC controllers' error states depending on the considered control topology.

Given PDO-OETC power system represented by the state variable differential equation (OGATA, 2008, p. 897):

$$\dot{x} = Ax + Bu \quad \text{.....(10.1)}$$

Where:

x : n x 1 state vector

u : m x 1 control vector

A : n x n state distribution matrix

B : n x m control distribution matrix

And the dot indicates the time derivative d/dt.

The main job of LQR is to find the matrix K of the optimal control vector (OGATA, 2008, p 897):

$$u(t) = -Kx(t) \quad \text{.....(10.2)}$$

which minimises the cost function (OGATA, 2008, p 897):

$$C = \int_0^\infty \left(x^T Qx + u^T Ru\right)dt \quad \text{.....(10.3)}$$

where:

Q : n x n positive semidefinite symmetric state cost weighting matrix.

R : m x m positive definite symmetric control cost weighting matrix.

T : transpose.

10.2.2.1. Controllability and Observability

Consider the system described in state variable form given by equation 10.1. The system is said to be controllable if it is possible to transfer the system from any initial state $x(t_0)$ to any other state in a finite interval of time (OGATA, 2008, p. 779).

On the other hand, the system is said to be observable if it is possible to reconstruct the initial state $x(t_0)$ from the observation of the output over a finite interval of time (OGATA, 2008, p. 779).

Controllability and Observability are primarily conditions for the system optimal controller existence (OGATA, 2008, p. 779).

10.2.2.2. Cost function

The performance of the system is specified in terms of a cost function to be minimised by the optimal controller. The cost function can be formulated from the set of control standards which PDO and OETC are following for the power system operations. It may include but not limited to the frequency values and power exchange values. The components of Q and R matrices are ours to choose to mathematically specify the way we wish the system to perform. For example, if we let R=0 but require Q to be non-zero, we are saying in effect that there is no charge for the control effort used; but we penalise the state for being non-zero. Hence the best control strategy would be in the form of infinite impulses. This control will drive the state to zero in the shortest possible time with the greatest effort.

If we let Q=0 for non-zero R, then we penalise for control effort but we don't charge for the trajectory the state x follows. In this case the best control strategy to be used is u=0; i.e. not to provide any control effort at all (Elgerd and Fosha [(2)], 1970).

In this part we are mainly concerned with the basic design of LQR AGC controller. The aim is to compare the LQR controller performance with the classical PID controller. Hence the Q and R matrices will be considered as a diagonal matrix Q=R=[1] of a suitable size. It will ensure that we are equally penalizing both the control effort and states values.

The Q and R matrices will be different in size depending on the considered control topology.

10.2.2.3. The feedback gain matrix

Upon defining the state space matrices A and B, and the cost function matrices Q and R, the feedback gain matrix can be calculated provided that the system is controllable and observable. OGATA (2008, pp. 897-899) demonstrates the mathematical equations approach of calculating the feedback gain matrix. There is no added value going through the mathematical manipulation again. MATLAB has a single command which will calculate the feedback gain matrix. The command "lqr(A,B,Q,R)" will return the matrix K for the described system. This command will be used in all subsequent analysis. As an example, for a system with "n" number of states and two control inputs, the feedback gain matrix K will be in the form:

$$K = \begin{bmatrix} k_{1,1} & k_{1,2} & k_{1,3} & k_{1,4} & k_{1,5} & k_{1,6} & k_{1,7} & k_{1,8} & k_{1,9} & .... & k_{1,n} \\ k_{2,1} & k_{2,2} & k_{2,3} & k_{2,4} & k_{2,5} & k_{2,6} & k_{2,7} & k_{2,8} & k_{2,9} & .... & k_{2,n} \end{bmatrix} \ldots(10.4)$$

Knowing the fact that:

$u = -Kx$ ……..(10.7)

Each controller is a function of states of the whole system:

$$\therefore u_1 = -\begin{bmatrix} k_{1,1} & k_{1,2} & k_{1,3} & k_{1,4} & k_{1,5} & k_{1,6} & k_{1,7} & k_{1,8} & k_{1,9} & .... & k_{1,n} \end{bmatrix} \cdot x \ldots\ldots(10.5)$$

$$\therefore u_2 = -\begin{bmatrix} k_{2,1} & k_{2,2} & k_{2,3} & k_{2,4} & k_{2,5} & k_{2,6} & k_{2,7} & k_{2,8} & k_{2,9} & .... & k_{2,n} \end{bmatrix} \cdot x \ldots\ldots(10.6)$$

Assume we have a system with a number of 11 states; we will end up with the following equations for controllers 1 and 2:

$$u_1 = -k_{1,1}x_1 - k_{1,2}x_2 - k_{1,3}x_3 - k_{1,4}x_4 - k_{1,5}x_5 - k_{1,6}x_6 - k_{1,7}x_7 - k_{1,8}x_8 - k_{1,9}x_9 - k_{1,10}x_{10} - k_{1,11}x_{11} \quad \ldots\ldots(10.7)$$

$$u_2 = -k_{2,1}x_1 - k_{2,2}x_2 - k_{2,3}x_3 - k_{2,4}x_4 - k_{2,5}x_5 - k_{2,6}x_6 - k_{2,7}x_7 - k_{2,8}x_8 - k_{2,9}x_9 - k_{2,10}x_{10} - k_{2,11}x_{11} \quad \ldots\ldots..(10.8)$$

For PDO-OETC power system, a MATLAB "Mfile" will be written for each subsequent test which will calculate the K matrix, assign the feedback gain for each state in the model and simulate the model with the controller. The "Mfile" will also plot the required graphs.

10.2.2.4. Reduced PDO-OETC model

The PDO-OETC model has been reduced to eleven states in the state variable form as detailed earlier in section 8.2. We can reconstruct the SIMULINK block diagram from the reduced variable state form which will result in a much simpler form of the complete

model. The SIMULINK model was rebuilt and is shown in Figure 10.1. It will be used to simulate the performance of the LQR AGC controllers. The reduced model has exactly the same response as the complete model as proved earlier in chapter 8.

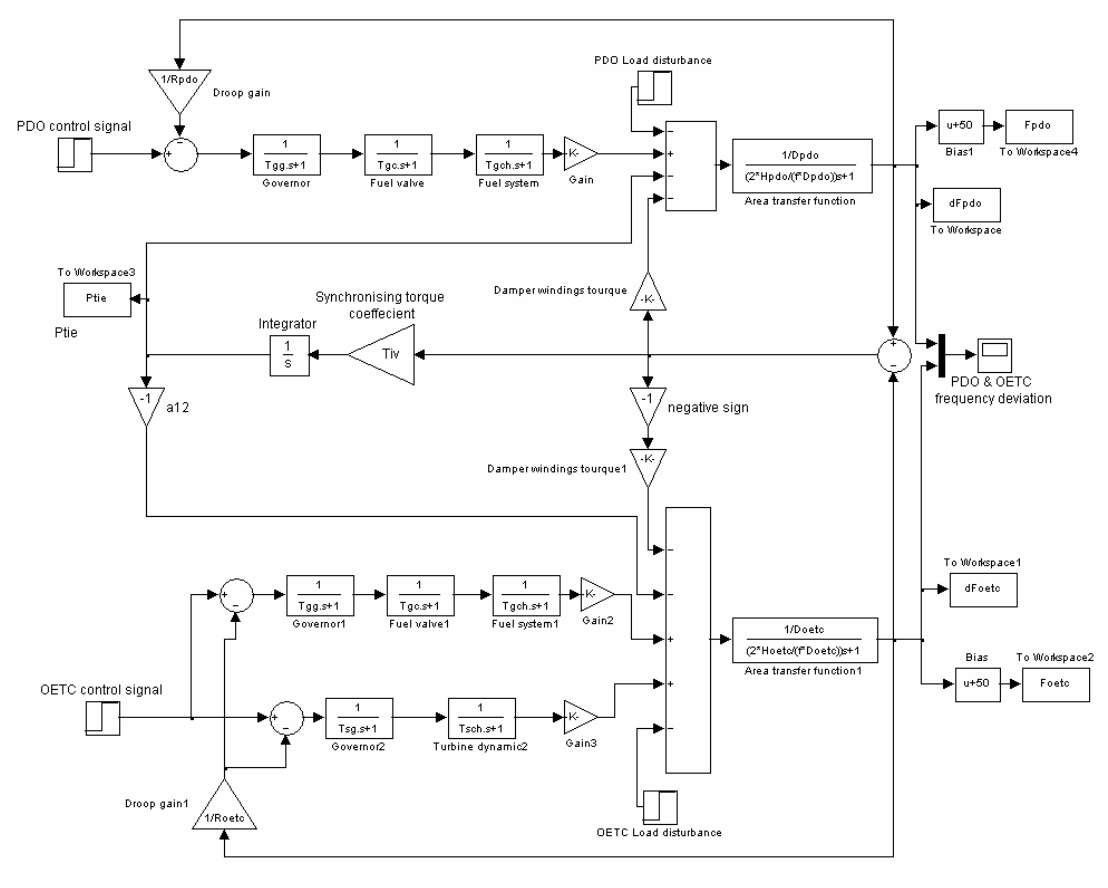

Figure 10.1: Reduced PDO-OETC model

10.2.3. LQR of PDO alone AGC using ACE as a feedback signal

The controller structure is such that the PDO ACE is fed to an integral and the integral output is summated with the feedbacks of the states. The gains of the integral output and the feedbacks of the states are calculated by the LQR technique. The overall controller layout is clear from Figure 10.2.

10.2.3.1. Calculation of the gain matrix

When the AGC is applied at PDO alone and the controller is using the ACE as the feedback signal, the new state variable form will include one more state, namely the Integral of PDO ACE. The new state is represented in the differential equation form as below:

$$\frac{d}{dt}\int ACE_{pdo}.dt = -\Delta P_{tie} - B_{Pdo}\Delta f_{pdo} \quad \ldots\ldots\ldots\ldots\ldots\ldots\ldots\ldots\ldots\ldots\ldots\ldots(10.9)$$

Where:

B_{pdo}: is PDO frequency bias factor

Adding up the above new state to the earlier developed state space model in chapter 8, the new A matrix will be 12x12 size as shown below:

$$A=\begin{bmatrix}
0 & T_{iv} & 0 & 0 & 0 & -T_{iv} & 0 & 0 & 0 & 0 & 0 & 0\\
-\frac{f}{2H_{pdo}} & -\frac{f}{2H_{pdo}}\left(D_{pdo}+Kdw_{pdo}\right) & \frac{f}{2H_{pdo}}Kgg_{pdo} & 0 & 0 & \frac{f}{2H_{pdo}}Kdw_{pdo} & 0 & 0 & 0 & 0 & 0 & 0\\
0 & 0 & \frac{-1}{Tgch} & \frac{1}{Tgch} & 0 & 0 & 0 & 0 & 0 & 0 & 0 & 0\\
0 & 0 & 0 & \frac{-1}{Tgc} & \frac{1}{Tgc} & 0 & 0 & 0 & 0 & 0 & 0 & 0\\
0 & \frac{-1}{TggR_{pdo}} & 0 & 0 & \frac{1}{Tgg} & 0 & 0 & 0 & 0 & 0 & 0 & 0\\
-\frac{fa_{12}}{2H_{oetc}} & -\frac{fa_{12}}{2H_{oetc}}Kdw_{oetc} & 0 & 0 & 0 & \frac{f}{2H_{oetc}}\left(a_{12}Kdw_{oetc}-D_{oetc}\right) & \frac{f}{2H_{oetc}}Kgg_{oetc} & 0 & 0 & \frac{f}{2H_{oetc}}Ksg_{oetc} & 0 & 0\\
0 & 0 & 0 & 0 & 0 & 0 & \frac{-1}{Tgch} & \frac{1}{Tgch} & 0 & 0 & 0 & 0\\
0 & 0 & 0 & 0 & 0 & 0 & 0 & \frac{-1}{Tgc} & \frac{1}{Tgc} & 0 & 0 & 0\\
0 & 0 & 0 & 0 & 0 & \frac{-1}{TggR_{oetc}} & 0 & 0 & \frac{-1}{Tgg} & 0 & 0 & 0\\
0 & 0 & 0 & 0 & 0 & 0 & 0 & 0 & 0 & \frac{-1}{Tsch} & \frac{1}{Tsch} & 0\\
0 & 0 & 0 & 0 & 0 & \frac{-1}{TsgR_{oetc}} & 0 & 0 & 0 & 0 & \frac{-1}{Tsg} & 0\\
-1 & -B_{pdo} & 0 & 0 & 0 & 0 & 0 & 0 & 0 & 0 & 0 & 0
\end{bmatrix}$$

…….(10.10)

Accordingly, the new B matrix will be changed to 12x1 size which will only include PDO control signal. The new B matrix is shown below:

$$B=\begin{bmatrix}0\\0\\0\\0\\\frac{1}{Tgg}\\0\\0\\0\\0\\0\\0\\0\end{bmatrix}$$ ……(10.11)

Similarly, the state cost weighting matrix Q is a diagonal matrix of the size 12x12 as shown below:

$$Q = \begin{bmatrix} 1 & 0 & 0 & 0 & 0 & 0 & 0 & 0 & 0 & 0 & 0 & 0 \\ 0 & 1 & 0 & 0 & 0 & 0 & 0 & 0 & 0 & 0 & 0 & 0 \\ 0 & 0 & 1 & 0 & 0 & 0 & 0 & 0 & 0 & 0 & 0 & 0 \\ 0 & 0 & 0 & 1 & 0 & 0 & 0 & 0 & 0 & 0 & 0 & 0 \\ 0 & 0 & 0 & 0 & 1 & 0 & 0 & 0 & 0 & 0 & 0 & 0 \\ 0 & 0 & 0 & 0 & 0 & 1 & 0 & 0 & 0 & 0 & 0 & 0 \\ 0 & 0 & 0 & 0 & 0 & 0 & 1 & 0 & 0 & 0 & 0 & 0 \\ 0 & 0 & 0 & 0 & 0 & 0 & 0 & 1 & 0 & 0 & 0 & 0 \\ 0 & 0 & 0 & 0 & 0 & 0 & 0 & 0 & 1 & 0 & 0 & 0 \\ 0 & 0 & 0 & 0 & 0 & 0 & 0 & 0 & 0 & 1 & 0 & 0 \\ 0 & 0 & 0 & 0 & 0 & 0 & 0 & 0 & 0 & 0 & 1 & 0 \\ 0 & 0 & 0 & 0 & 0 & 0 & 0 & 0 & 0 & 0 & 0 & 1 \end{bmatrix} \quad \text{……..(10.12)}$$

The control effort weighting matrix R is also formulated to represent PDO AGC controller only and is shown below:

$$R = [1] \text{……..(10.13)}$$

The resultant feedback gain matrix K will be of the size 1x12. The matrix is calculated using a MATLAB "Mfile" code written for this purpose and is shown in Appendix 5 code 1.

The calculated feedback gain matrix K is shown below:

$$K = [-1.1206 \;\; 0.4205 \;\; 0.7924 \;\; 0.2787 \;\; 0.5992 \;\; 0.1356 \;\; 0.0079 \;\; -0.0001 \;\; -0.0007 \;\; -0.0007 \;\; -0.0036 \;\; -1.000]$$

……..(10.14)

The reduced PDO-OETC power system model with the PDO LQR AGC controller is shown in Figure 10.2.

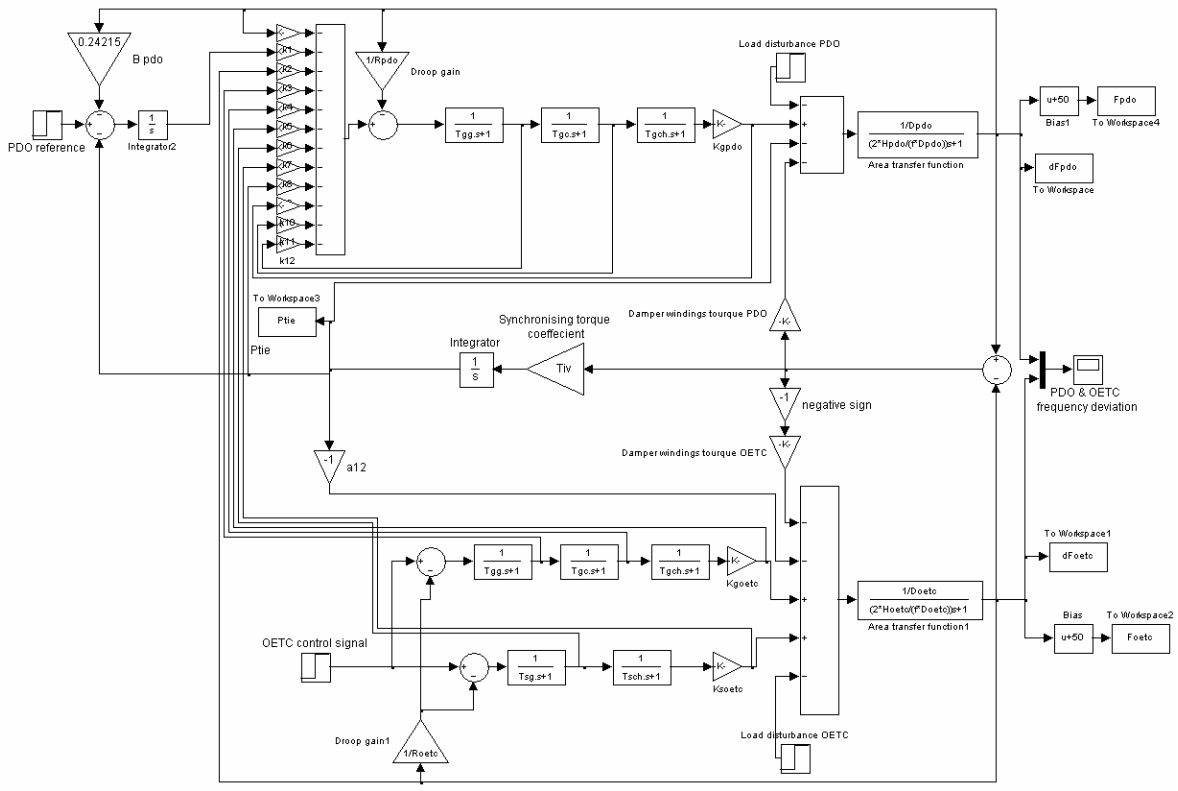

Figure 10.2: Reduced PDO-OETC power system with LQR AGC applied to PDO only

10.2.3.2. Simulation results

Using the "Mfile" and the PDO-OETC power system model developed for this part of the study, a load disturbance of 100MW is simulated once at PDO side and once at OETC side. PDO frequency, OETC frequency and tie line power are the key performance indices to be monitored. Figures 10.3-10.6 show PDO and OETC frequencies in one figure and the tie line power in a separate figure for both tests respectively. The important features to consider in the response figures are the settling time, the oscillatory nature of the response and the steady state deviation.

A summary of the performance values was attempted and is shown in Table 10.1. The summary also compares the results of the base case, classical PID AGC controller and the LQR AGC controller performance.

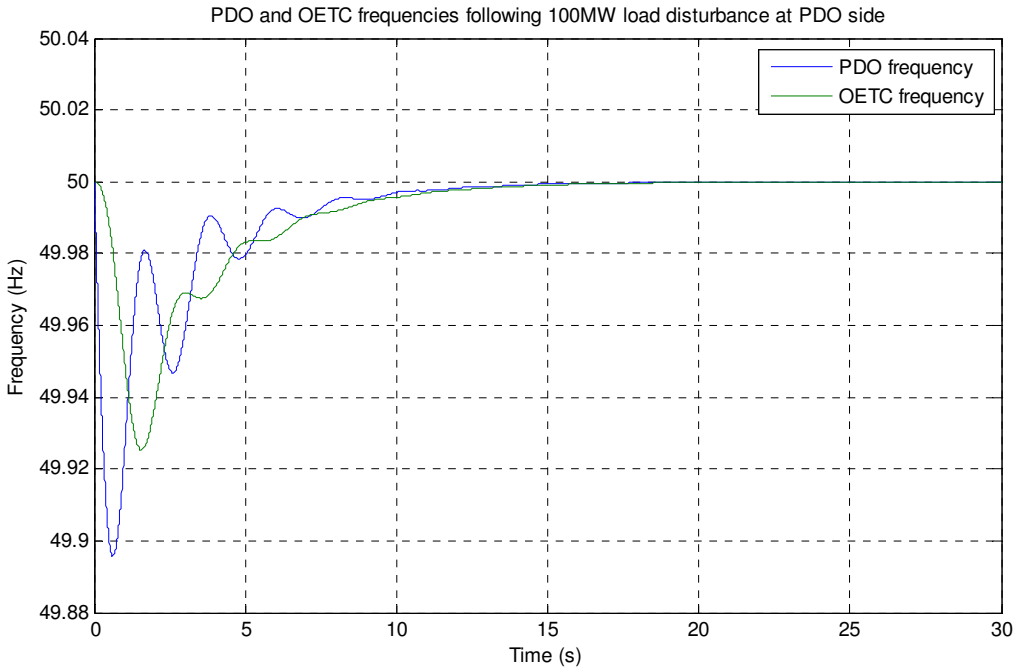

Figure 10.3: PDO and OETC frequencies following a 100MW load disturbance at PDO side with the LQR AGC applied at PDO only

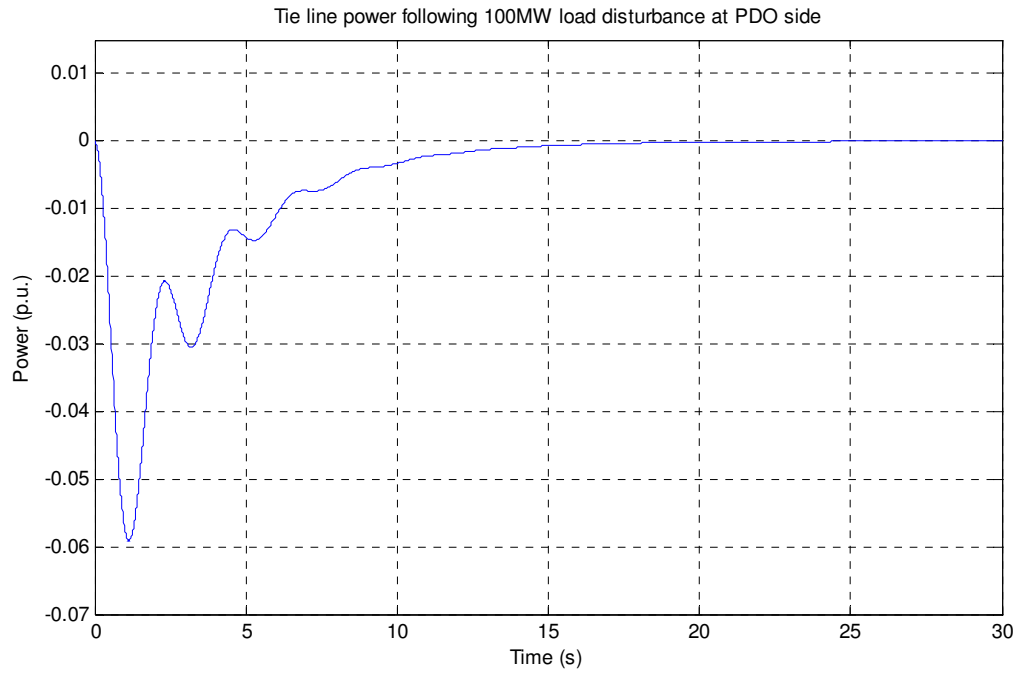

Figure 10.4: Tie line power deviation following a 100MW load disturbance at PDO side with the LQR AGC applied at PDO only.

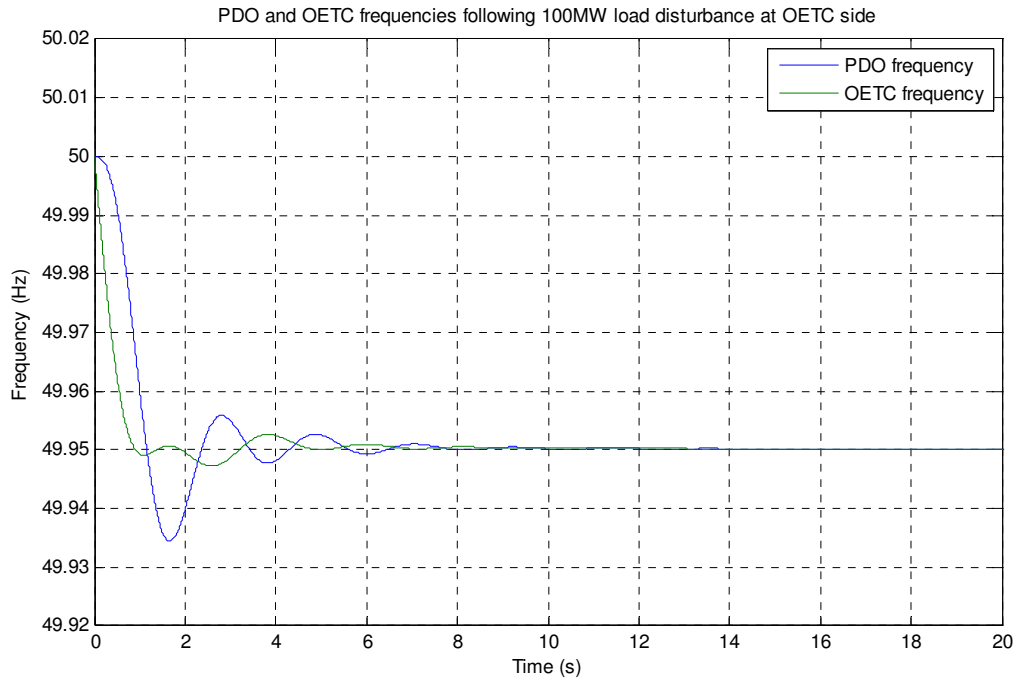

Figure 10.5: PDO and OETC frequencies following a 100MW load disturbance at OETC side with the LQR AGC applied at PDO only

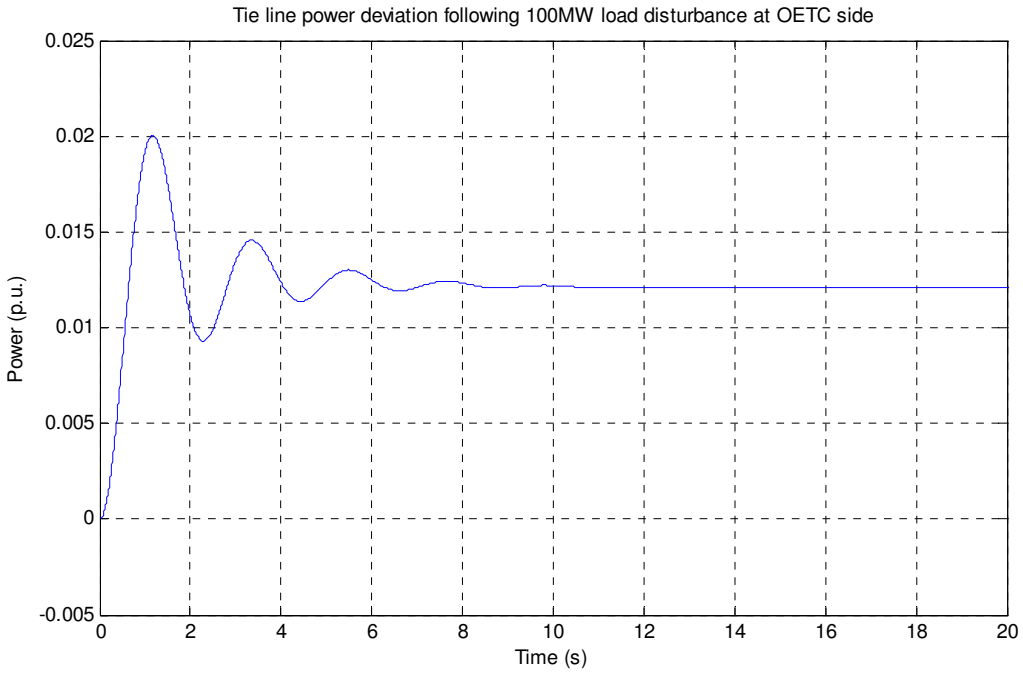

Figure 10.6: Tie line power deviation following a 100MW load disturbance at OETC side with the LQR AGC applied at PDO only.

		Base case response	PID controlled response	LQR controlled response
100MW load disturbance at PDO side	Frequency deviation (Hz)	-0.05	0	0
	Settling time (s)	10.9	22.6	12.3
	Tie line power deviation (p.u.)	-0.0379	0	0
100MW load disturbance at OETC side	Frequency deviation (Hz)	-0.05	-0.05	-0.05
	Settling time (s)	7.74	15.34	5.3
	Tie line power deviation (p.u.)	0.0121	0.0121	0.0121

Table 10.1: PDO alone LQR AGC controller performance in comparison to the base case and the classical PID controller.

10.2.3.3. Results discussion

From Figures 10.3-10.6 and Table 10.1, one can see that the LQR control technique has obvious merits over the classical PID control technique while it is maintaining the same control topology features. The following points summarise the impression about the results:

- The AGC controller has dealt with load disturbances within PDO control area only whereas load disturbances outside PDO are compensated by the droop control only. It has resulted in a zero steady state deviation in system frequency and tie line power when the load disturbance is applied at PDO and non zero values when the load disturbance is applied at OETC side.
- The response oscillations are very well damped if we compare the results obtained in Figures 10.3-10.6 with the same results obtained using the classical PID controller shown earlier in Figures 9.23-9.28. The settling time with the LQR controller is also much better than in the case of the classical PID controller.

10.2.3.4. Summary

The PDO alone LQR AGC controller has maintained the same control topology features observed when using the classical PID controller. However the system response oscillations and settling time have been remarkably improved.

10.2.4. LQR of OETC alone AGC using ACE as a feedback signal

The controller structure is such that the OETC ACE is fed to an integral and the integral output is summated with the negative feedbacks of the states. The gains of the integral

output and the feedbacks of the states are calculated by the LQR technique. The overall controller layout is clear from Figure 10.7.

10.2.4.1. Calculation of the gain matrix

When the AGC is applied at OETC alone and the controller is using the ACE as the feedback signal, the new state variable form will include one more state, namely the Integral of OETC ACE. The new state is represented in the differential equation form as below:

$$\frac{d}{dt}\int ACE_{oetc}.dt = -a_{12}\Delta P_{tie} - B_{oetc}\Delta f_{oetc} \quad \text{.....(10.15)}$$

Where:

B_{oetc} : is OETC frequency bias factor

a_{12} : is sign reversing constant (-1)

Adding up the above new state to the earlier developed state space model in chapter 8, the new A matrix will be 12x12 size as shown below:

$$A = \begin{bmatrix}
0 & T_{lv} & 0 & 0 & 0 & -T_{lv} & 0 & 0 & 0 & 0 & 0 & 0 \\
-\frac{f}{2H_{pdo}} & -\frac{f}{2H_{pdo}}\left(D_{pdo}+Kdw_{pdo}\right) & \frac{f}{2H_{pdo}}Kgg_{pdo} & 0 & 0 & \frac{f}{2H_{pdo}}Kdw_{pdo} & 0 & 0 & 0 & 0 & 0 & 0 \\
0 & 0 & \frac{-1}{Tgch} & \frac{1}{Tgch} & 0 & 0 & 0 & 0 & 0 & 0 & 0 & 0 \\
0 & 0 & 0 & \frac{-1}{Tgc} & \frac{1}{Tgc} & 0 & 0 & 0 & 0 & 0 & 0 & 0 \\
0 & \frac{-1}{TggR_{pdo}} & 0 & 0 & \frac{1}{Tgg} & 0 & 0 & 0 & 0 & 0 & 0 & 0 \\
-\frac{fa_{12}}{2H_{oetc}} & -\frac{fa_{12}}{2H_{oetc}}Kdw_{oetc} & 0 & 0 & 0 & \frac{f}{2H_{oetc}}\left(a_{12}Kdw_{oetc}-D_{oetc}\right) & \frac{f}{2H_{oetc}}Kgg_{oetc} & 0 & 0 & \frac{f}{2H_{oetc}}Ksg_{oetc} & 0 & 0 \\
0 & 0 & 0 & 0 & 0 & 0 & \frac{-1}{Tgch} & \frac{1}{Tgch} & 0 & 0 & 0 & 0 \\
0 & 0 & 0 & 0 & 0 & 0 & 0 & \frac{-1}{Tgc} & \frac{1}{Tgc} & 0 & 0 & 0 \\
0 & 0 & 0 & 0 & 0 & \frac{-1}{TggR_{oetc}} & 0 & 0 & \frac{-1}{Tgg} & 0 & 0 & 0 \\
0 & 0 & 0 & 0 & 0 & 0 & 0 & 0 & 0 & \frac{-1}{Tsch} & \frac{1}{Tsch} & 0 \\
0 & 0 & 0 & 0 & 0 & \frac{-1}{TsgR_{oetc}} & 0 & 0 & 0 & 0 & \frac{-1}{Tsg} & 0 \\
-a_{12} & 0 & 0 & 0 & 0 & -B_{oetc} & 0 & 0 & 0 & 0 & 0 & 0
\end{bmatrix}$$

…….(10.16)

Accordingly, the new B matrix will be changed to 12x1 size which will only include OETC control signal. The new B matrix is shown below:

$$B = \begin{bmatrix} 0 \\ 0 \\ 0 \\ 0 \\ 0 \\ 0 \\ 0 \\ 0 \\ \frac{1}{Tgg} \\ 0 \\ \frac{1}{Tsg} \\ 0 \end{bmatrix} \quad \text{……(10.17)}$$

Similarly, the state cost weighting matrix Q is a diagonal matrix of the size 12x12 as shown below:

$$Q = \begin{bmatrix} 1 & 0 & 0 & 0 & 0 & 0 & 0 & 0 & 0 & 0 & 0 & 0 \\ 0 & 1 & 0 & 0 & 0 & 0 & 0 & 0 & 0 & 0 & 0 & 0 \\ 0 & 0 & 1 & 0 & 0 & 0 & 0 & 0 & 0 & 0 & 0 & 0 \\ 0 & 0 & 0 & 1 & 0 & 0 & 0 & 0 & 0 & 0 & 0 & 0 \\ 0 & 0 & 0 & 0 & 1 & 0 & 0 & 0 & 0 & 0 & 0 & 0 \\ 0 & 0 & 0 & 0 & 0 & 1 & 0 & 0 & 0 & 0 & 0 & 0 \\ 0 & 0 & 0 & 0 & 0 & 0 & 1 & 0 & 0 & 0 & 0 & 0 \\ 0 & 0 & 0 & 0 & 0 & 0 & 0 & 1 & 0 & 0 & 0 & 0 \\ 0 & 0 & 0 & 0 & 0 & 0 & 0 & 0 & 1 & 0 & 0 & 0 \\ 0 & 0 & 0 & 0 & 0 & 0 & 0 & 0 & 0 & 1 & 0 & 0 \\ 0 & 0 & 0 & 0 & 0 & 0 & 0 & 0 & 0 & 0 & 1 & 0 \\ 0 & 0 & 0 & 0 & 0 & 0 & 0 & 0 & 0 & 0 & 0 & 1 \end{bmatrix} \quad \text{…….(10.18)}$$

The control effort weighting matrix R is also formulated to represent OETC AGC controller only and is shown below:

$R = [1]$……..(10.19)

The resultant feedback gain matrix K will be of the size 1x12. The matrix is calculated using a MATLAB "Mfile" code written for this purpose and is shown in Appendix 5 code 2.

The calculated feedback gain matrix K is shown below:

$K = [0.1742 \quad -0.1892 \quad -0.0678 \quad -0.0060 \quad -0.0030 \quad 1.6077 \quad 1.3144 \quad 0.3243 \quad 0.6028 \quad 0.3477 \quad 0.3803 \quad -1.0000]$

……..(10.20)

The reduced PDO-OETC power system model with the OETC LQR AGC controller is shown in Figure 10.7.

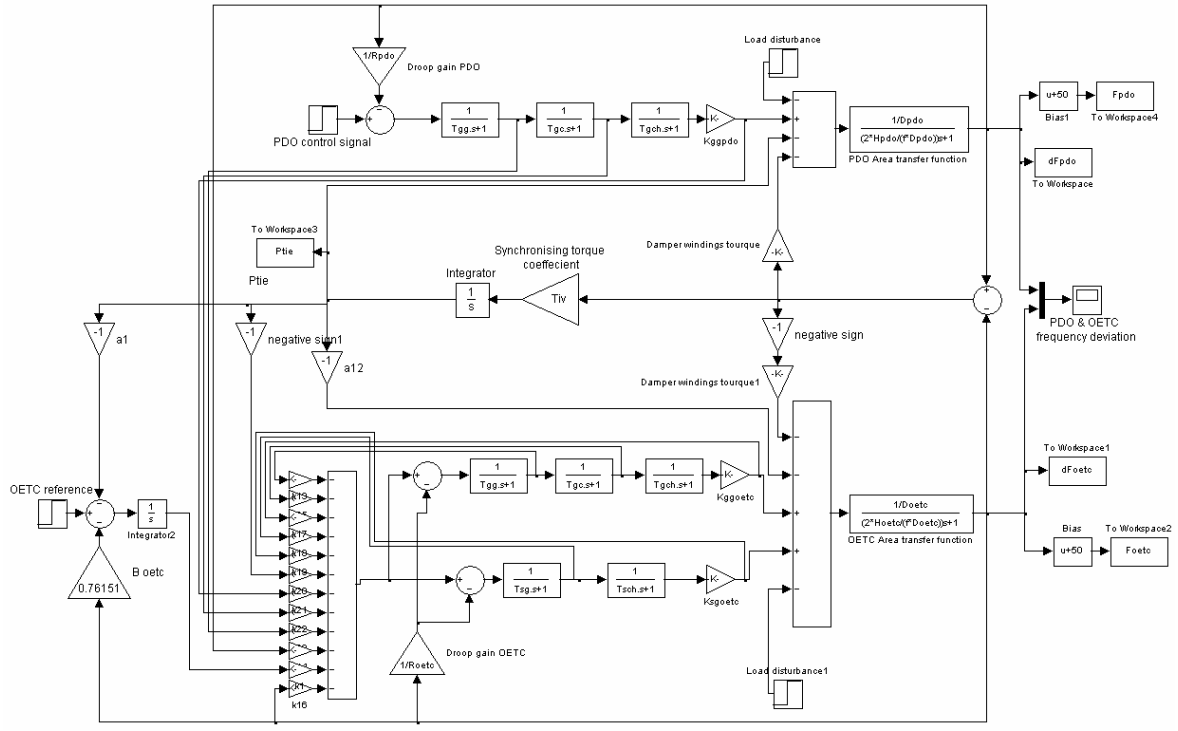

Figure 10.7: Reduced PDO-OETC power system with LQR AGC applied to OETC only

10.2.4.2. Simulation results

Using the "Mfile" and the PDO-OETC power system model developed for this part of the study, a load disturbance of 100MW was simulated once at PDO side and once at OETC side. PDO frequency, OETC frequency and tie line power are the key performance indices to be monitored. Figures 10.8-10.11 show PDO and OETC frequencies in one figure and the tie line power in a separate figure for both tests respectively.

A summary of the performance values was attempted and is shown in Table 10.2. The summary also compares the results of the base case, classical PID AGC controller and the LQR AGC controller performance.

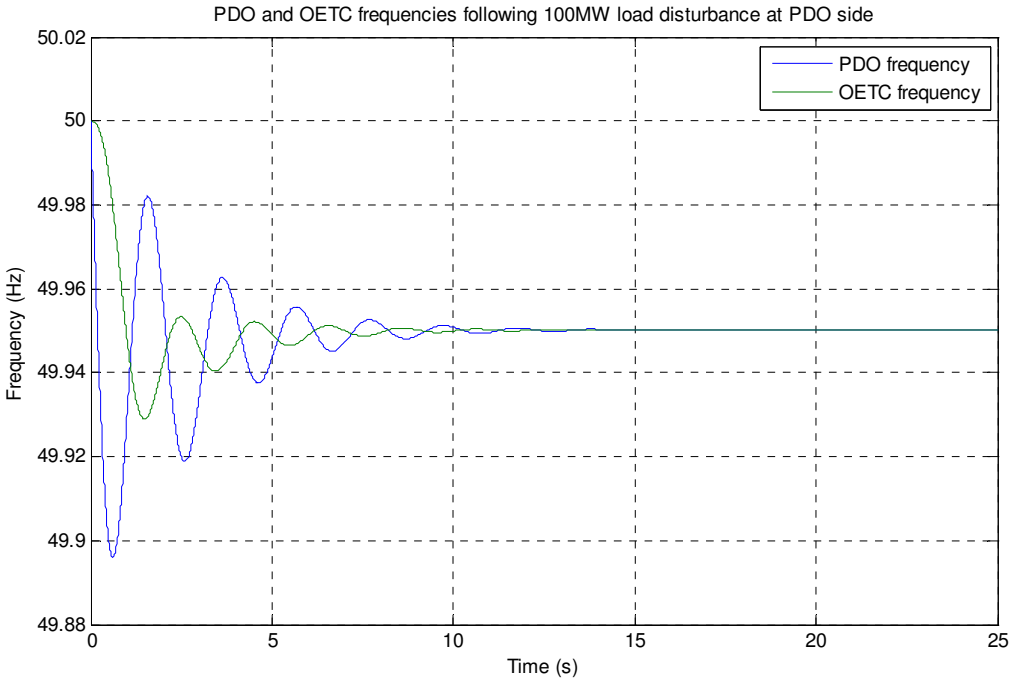

Figure 10.8: PDO and OETC frequencies following a 100MW load disturbance at PDO side with the LQR AGC applied at OETC only

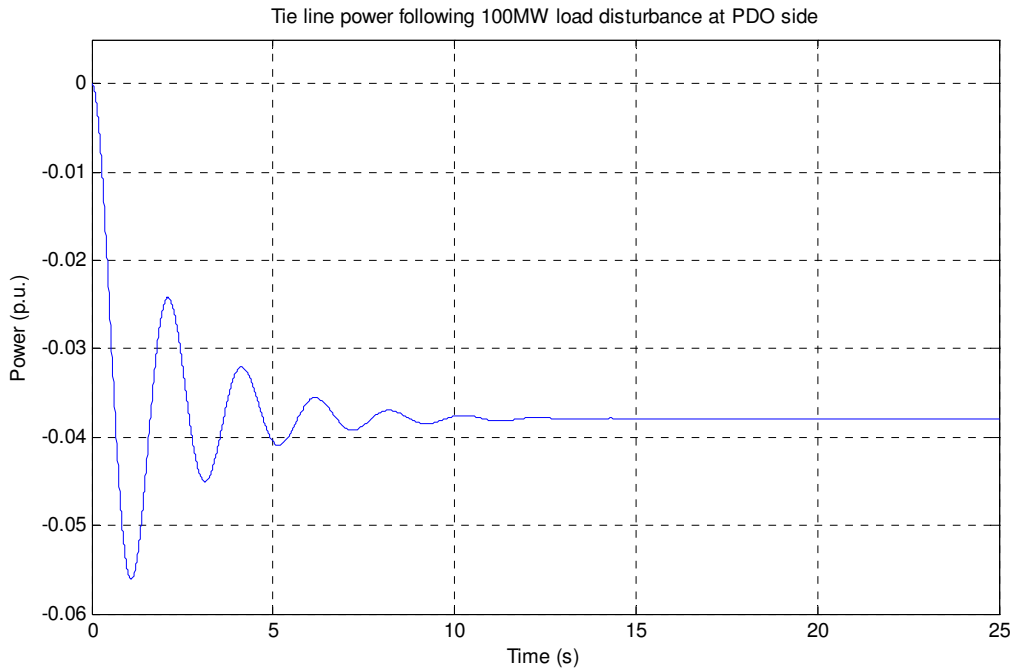

Figure 10.9: Tie line power deviation following a 100MW load disturbance at PDO side with the LQR AGC applied at OETC only.

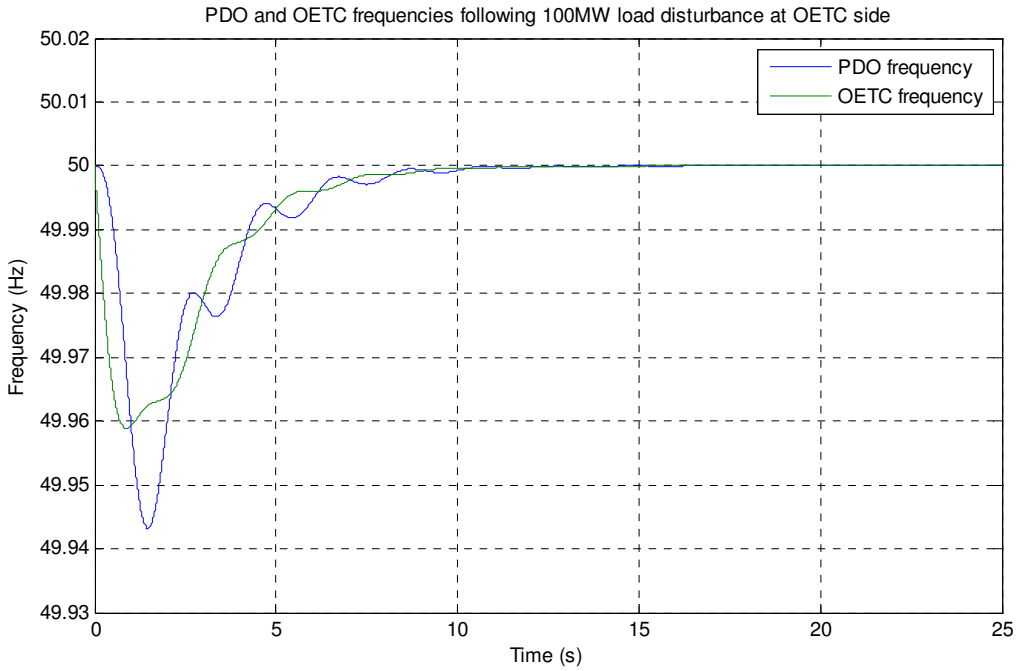

Figure 10.10: PDO and OETC frequencies following a 100MW load disturbance at OETC side with the LQR AGC applied at OETC only

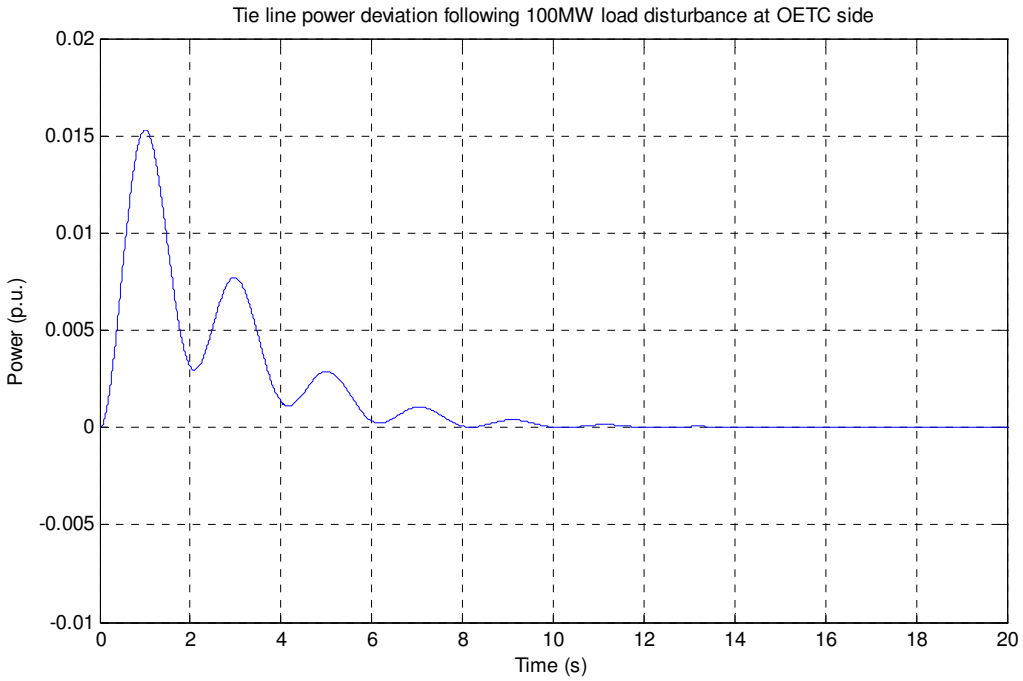

Figure 10.11: Tie line power deviation following a 100MW load disturbance at OETC side with the LQR AGC applied at OETC only.

		Base case response	PID controlled response	LQR controlled response
100MW load disturbance at PDO side	Frequency deviation (Hz)	-0.05	-0.05	-0.05
	Settling time (s)	10.9	14	8.92
	Tie line power deviation (p.u.)	-0.0379	-0.0379	-0.0379
100MW load disturbance at OETC side	Frequency deviation (Hz)	-0.05	0	0
	Settling time (s)	7.74	10.4	8.16
	Tie line power deviation (p.u.)	0.0121	0	0

Table 10.2: OETC alone LQR AGC controller performance in comparison to the base case and the classical PID controller.

10.2.4.3. Results discussion

From Figures 10.8-10.11 and Table 10.2, one can see that the LQR control technique has improved the system response when compared with the classical PID technique while it is maintaining the same control topology features. The following points summarise the overall performance:

- The AGC controller has dealt with load disturbances within OETC control area whereas load disturbances outside OETC are compensated by the droop control only. It has resulted in a zero steady state deviation in system frequency and tie line power when the load disturbance is applied at OETC and non zero values when the load disturbance is applied at PDO side.
- The response oscillations are slightly improved if we compare the results obtained in Figures 10.3-10.6 with the same results obtained using the classical PID controller shown earlier in Figures 9.44-9.49. The settling time with the LQR controller is also better than in the case of the classical PID controller.

10.2.4.4. Summary

The OETC alone LQR AGC controller has maintained the same control topology features observed when using the classical PID controller although the system response oscillations and settling time have been improved.

10.2.5. LQR of PDO-OETC AGC using ACE as a feedback signal

The controller structure is such that for PDO, the PDO ACE is fed to an integral and the integral output is summated with the negative feedbacks of the states. For OETC, the OETC ACE is also fed to an integral and the integral output is summated with the negative feedback of the states. The gains of the integral output and the negative feedback of the states are calculated by the LQR technique. The overall controller layout is shown in Figure 10.12.

10.2.6.1. Calculation of the gain matrix

Consider the control topology where AGC is applied at both PDO and OETC and the controllers are using the areas' ACE as the feedback signals. The new state variable form will include two more states, namely the Integral of PDO ACE and the Integral of OETC ACE. The two states are represented in the differential equation form as shown earlier in equations 10.9 and 10.15.

Adding up those two states to the earlier developed state space model in chapter 8, the new A matrix will of the size of 13x13 as shown below:

$$A=\begin{bmatrix}
0 & T_{iv} & 0 & 0 & 0 & -T_{iv} & 0 & 0 & 0 & 0 & 0 & 0 & 0\\
-\frac{f}{2H_{pdo}} & -\frac{f}{2H_{pdo}}\left(D_{pdo}+Kdw_{pdo}\right) & \frac{f}{2H_{pdo}}Kgg_{pdo} & 0 & 0 & \frac{f}{2H_{pdo}}Kdw_{pdo} & 0 & 0 & 0 & 0 & 0 & 0 & 0\\
0 & 0 & \frac{-1}{Tgch} & \frac{1}{Tgch} & 0 & 0 & 0 & 0 & 0 & 0 & 0 & 0 & 0\\
0 & 0 & 0 & \frac{-1}{Tgc} & \frac{1}{Tgc} & 0 & 0 & 0 & 0 & 0 & 0 & 0 & 0\\
0 & \frac{-1}{TggR_{pdo}} & 0 & 0 & \frac{1}{Tgg} & 0 & 0 & 0 & 0 & 0 & 0 & 0 & 0\\
-\frac{fa_{12}}{2H_{oetc}} & -\frac{fa_{12}}{2H_{oetc}}Kdw_{oetc} & 0 & 0 & 0 & \frac{f}{2H_{oetc}}\left(a_{12}Kdw_{oetc}-D_{oetc}\right) & \frac{f}{2H_{oetc}}Kgg_{oetc} & 0 & 0 & \frac{f}{2H_{oetc}}Ksg_{oetc} & 0 & 0 & 0\\
0 & 0 & 0 & 0 & 0 & 0 & \frac{-1}{Tgch} & \frac{1}{Tgch} & 0 & 0 & 0 & 0 & 0\\
0 & 0 & 0 & 0 & 0 & 0 & 0 & \frac{-1}{Tgc} & \frac{1}{Tgc} & 0 & 0 & 0 & 0\\
0 & 0 & 0 & 0 & 0 & \frac{-1}{TggR_{oetc}} & 0 & 0 & \frac{-1}{Tgg} & 0 & 0 & 0 & 0\\
0 & 0 & 0 & 0 & 0 & 0 & 0 & 0 & 0 & \frac{-1}{Tsch} & \frac{1}{Tsch} & 0 & 0\\
0 & 0 & 0 & 0 & 0 & \frac{-1}{TsgR_{oetc}} & 0 & 0 & 0 & 0 & \frac{-1}{Tsg} & 0 & 0\\
-1 & -B_{pdo} & 0 & 0 & 0 & 0 & 0 & 0 & 0 & 0 & 0 & 0 & 0\\
-a_{12} & 0 & 0 & 0 & 0 & -B_{oetc} & 0 & 0 & 0 & 0 & 0 & 0 & 0
\end{bmatrix}$$

…….(10.21)

Accordingly, the new B matrix will be changed to the size of 13x2 which will include both PDO and OETC control signal. The new B matrix is shown below:

$$B = \begin{bmatrix} 0 & 0 \\ 0 & 0 \\ 0 & 0 \\ 0 & 0 \\ \frac{1}{Tgg} & 0 \\ 0 & 0 \\ 0 & 0 \\ 0 & 0 \\ 0 & \frac{1}{Tgg} \\ 0 & 0 \\ 0 & \frac{1}{Tsg} \\ 0 & 0 \\ 0 & 0 \end{bmatrix} \quad \text{.....(10.22)}$$

Similarly, the state cost weighting matrix Q is a diagonal matrix of the size 13x13 as shown below:

$$Q = \begin{bmatrix} 1 & 0 & 0 & 0 & 0 & 0 & 0 & 0 & 0 & 0 & 0 & 0 & 0 \\ 0 & 1 & 0 & 0 & 0 & 0 & 0 & 0 & 0 & 0 & 0 & 0 & 0 \\ 0 & 0 & 1 & 0 & 0 & 0 & 0 & 0 & 0 & 0 & 0 & 0 & 0 \\ 0 & 0 & 0 & 1 & 0 & 0 & 0 & 0 & 0 & 0 & 0 & 0 & 0 \\ 0 & 0 & 0 & 0 & 1 & 0 & 0 & 0 & 0 & 0 & 0 & 0 & 0 \\ 0 & 0 & 0 & 0 & 0 & 1 & 0 & 0 & 0 & 0 & 0 & 0 & 0 \\ 0 & 0 & 0 & 0 & 0 & 0 & 1 & 0 & 0 & 0 & 0 & 0 & 0 \\ 0 & 0 & 0 & 0 & 0 & 0 & 0 & 1 & 0 & 0 & 0 & 0 & 0 \\ 0 & 0 & 0 & 0 & 0 & 0 & 0 & 0 & 1 & 0 & 0 & 0 & 0 \\ 0 & 0 & 0 & 0 & 0 & 0 & 0 & 0 & 0 & 1 & 0 & 0 & 0 \\ 0 & 0 & 0 & 0 & 0 & 0 & 0 & 0 & 0 & 0 & 1 & 0 & 0 \\ 0 & 0 & 0 & 0 & 0 & 0 & 0 & 0 & 0 & 0 & 0 & 1 & 0 \\ 0 & 0 & 0 & 0 & 0 & 0 & 0 & 0 & 0 & 0 & 0 & 0 & 1 \end{bmatrix} \quad \text{.....(10.23)}$$

The control effort weighting matrix R will be 2x2 matrix and is shown below:

$$R = \begin{bmatrix} 1 & 0 \\ 0 & 1 \end{bmatrix} \quad \text{.....(10.24)}$$

The resultant feedback gain matrix K will be of the size of 2x13. The matrix is calculated using a MATLAB "Mfile" code written for this purpose and is shown in Appendix 5 code 3.

The calculated feedback gain matrix K is shown below:

$$K = \begin{bmatrix} -1.0993 & 0.4092 & 0.7827 & 0.2776 & 0.5985 & 0.1557 & 0.0171 & 0.0010 & 0.0005 & 0.0018 & -0.0028 & -1.0000 & 0.0065 \\ 0.1256 & -0.0715 & -0.0169 & -0.0010 & -0.0002 & 1.5061 & 1.2598 & 0.3187 & 0.5995 & 0.3366 & 0.3781 & -0.0065 & -1.0000 \end{bmatrix}$$

……..(10.25)

The reduced PDO-OETC power system model with the PDO and OETC LQR AGC controller is shown in Figure 10.12.

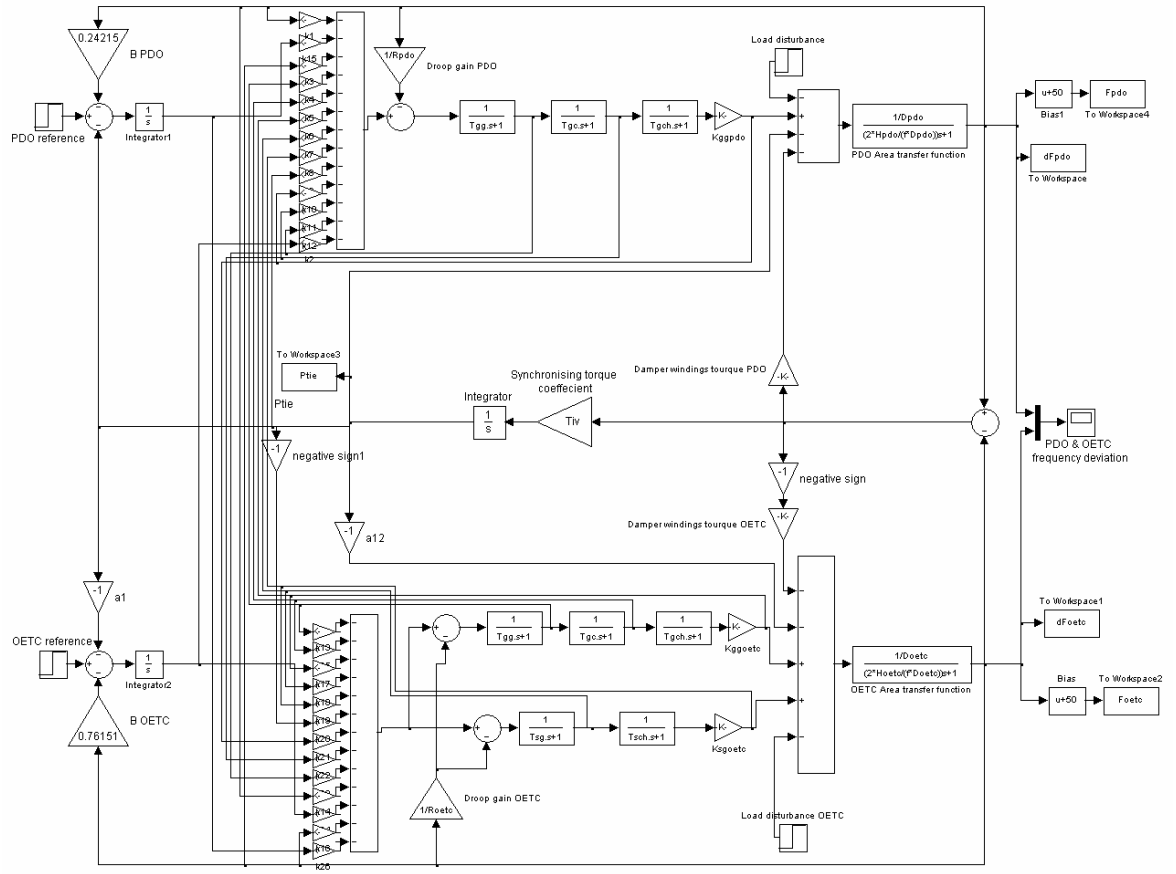

Figure 10.12: Reduced PDO-OETC power system with LQR AGC applied to both PDO and OETC

10.2.5.2. Simulation results

Using the "Mfile" and the PDO-OETC power system model developed for this part of the study, a load disturbance of 100MW was simulated once at PDO side and once at OETC side. PDO frequency, OETC frequency and tie line power are monitored. Figures 10.13-10.16 show PDO and OETC frequencies in one figure and the tie line power in a separate figure for both tests respectively.

A summary of the performance values was attempted and is shown in Table 10.3. The summary also compares the results of the base case, classical PID AGC controller and the LQR AGC controller performance.

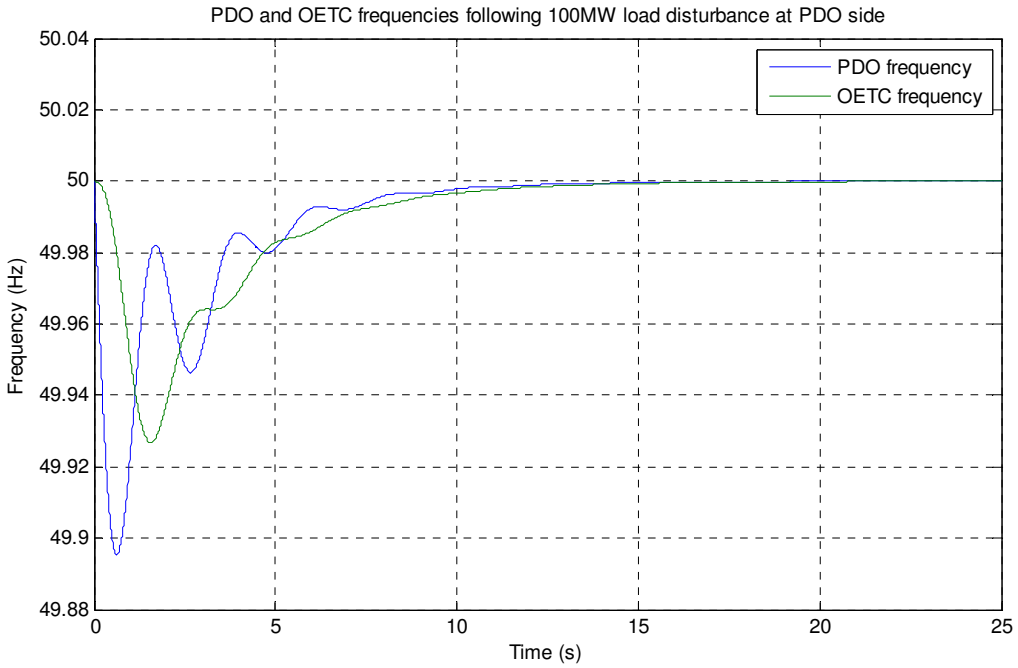

Figure 10.13: PDO and OETC frequencies following a 100MW load disturbance at PDO side with the LQR AGC applied at both PDO and OETC

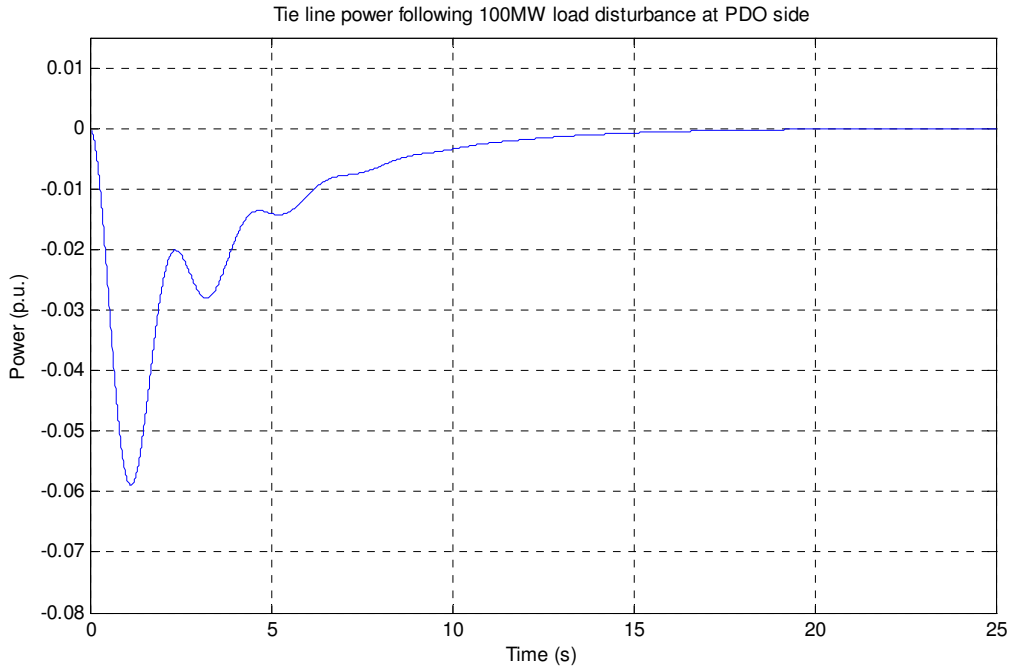

Figure 10.14: Tie line power deviation following a 100MW load disturbance at PDO side with the LQR AGC applied at both PDO and OETC

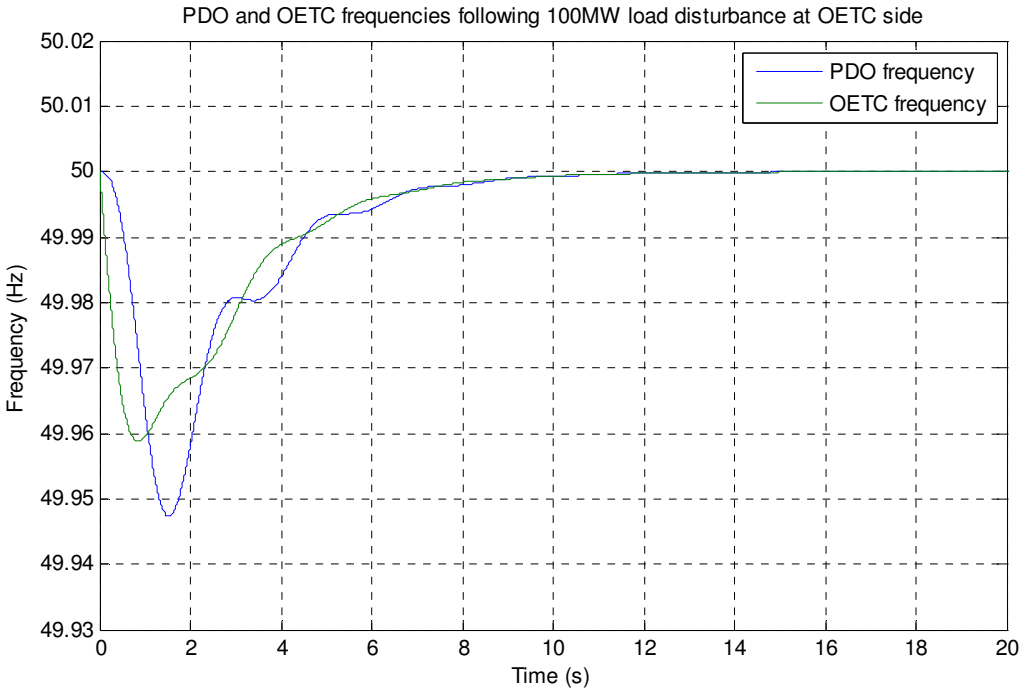

Figure 10.15: PDO and OETC frequencies following a 100MW load disturbance at OETC side with the LQR AGC applied at both PDO and OETC

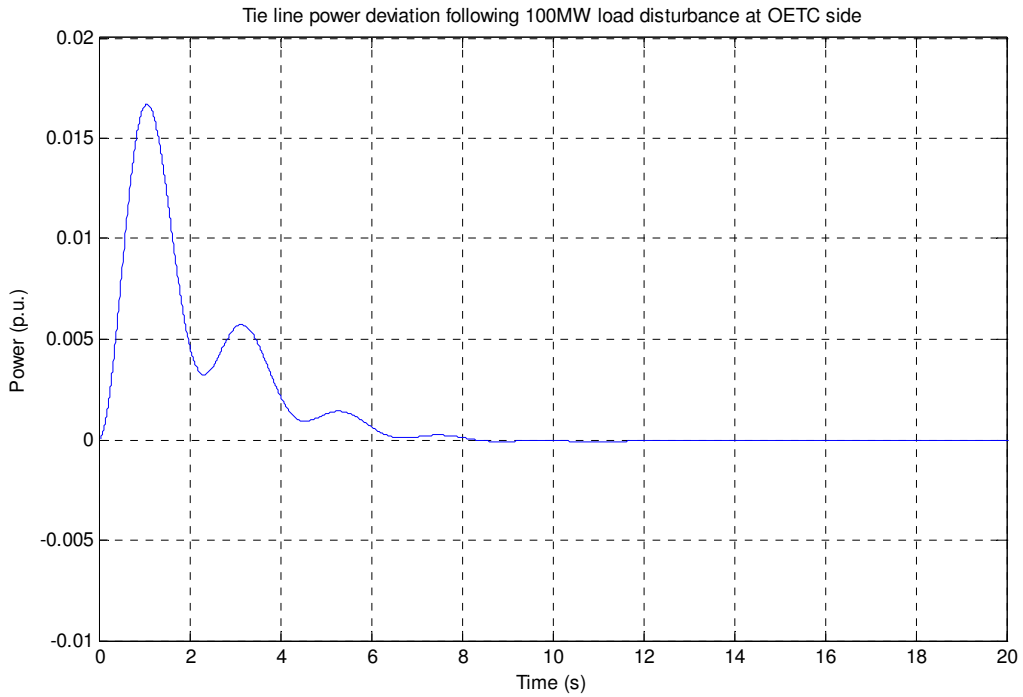

Figure 10.16: Tie line power deviation following a 100MW load disturbance at OETC side with the LQR AGC applied at both PDO and OETC

		Base case response	PID controlled response	LQR controlled response
100MW load disturbance at PDO side	Frequency deviation (Hz)	-0.05	0	0
	Settling time (s)	10.9	34	11.3
	Tie line power deviation (p.u.)	-0.0379	0	0
100MW load disturbance at OETC side	Frequency deviation (Hz)	-0.05	0	0
	Settling time (s)	7.74	25.3	8.59
	Tie line power deviation (p.u.)	0.0121	0	0

Table 10.3: PDO and OETC LQR AGC controllers' performance in comparison to the base case and the classical PID controllers.

10.2.5.3. Results discussion

From Figures 10.13-10.16 and Table 10.3, it is clear that the LQR control technique has improved the system response when compared with the classical PID technique. The following points summarise the overall performance:

- Applying AGC to both PDO and OETC leads to the AGC is dealing with all load disturbances in both control areas, PDO and OETC. This has resulted in a zero steady state deviation in the system frequency and tie line following any load disturbance at PDO or OETC. It concludes that the LQR has maintained the same control topology features concluded earlier in chapter 9.
- The response oscillations are dramatically improved if we compare the results obtained in Figures 10.13-10.16 with the same results obtained using the classical PID controller shown earlier in Figures 9.107-9.112. The settling time with the LQR controller is also much better than in the case of the classical PID controller.
- The LQR performance can be further improved by optimising the values of the Q and R matrices.

10.2.5.4. Summary

The PDO and OETC LQR AGC controller has maintained the same control topology features observed when using the classical PID controller although the system response oscillations and settling time have been significantly improved.

10.2.6. Summary

Overall, the LQR AGC controller has performed much better than the classical PID controller. The same control topologies features explored earlier in chapter 9 are maintained. There is always improvement in the response oscillations and settling time. The LQR performance can be further improved by fine tuning the state cost and control effort weighting matrices.

10.3. Modified Design of LQR AGC

10.3.1. Introduction

In this part, the LQR AGC controllers will be modified by changing the Q matrix according to specific control performance requirements. Then the modified LQR AGC controllers will be fine tuned. There are two ways to fine tune the LQR performance. The first one is to change the weighting of the Q matrix elements with respect to each other without changing the relative weight of Q matrix with respect to R matrix. This is achieved by multiplying the Q matrix elements with different weighting factors in order to penalise one state more or less than the others.

The second way is to change the weight of the Q matrix with respect to the R matrix. This is achieved by multiplying the Q matrix by a weighting factor. Multiplying the Q matrix by a factor of 10 means we are penalising the states ten times more than the control effort which will usually results in faster settling time, more fuel consumption and more maintenance requirements. Multiplying the R matrix by a factor of 10 means we are penalising the control effort ten times more than the states and therefore there will be a mild control action resulting in longer settling time, less fuel consumption and less maintenance requirements.

The above two methods are used to fine tune the modified LQR AGC performance. PDO-OETC LQR AGC topology based on ACE feedback signals is used here due to its good performance.

A set of AGC control guidelines has been developed in the subsequent section to be used for the modification of the AGC controller performance.

10.3.2. PDO-OETC AGC control guidelines

In this part, the PDO-OETC AGC controller's performance requirements are defined based on the operation philosophy of both power systems, PDO and OETC. At this point of the

time, there are no national AGC controller performance indices stipulated in the grid code (Oman Electricity Transmission Company SAOC, 2005). Instead, a general frequency control requirements are stipulated in the grid code (Oman Electricity Transmission Company SAOC, 2005) in clause CC.6 and below is an extract from the grid code (Oman Electricity Transmission Company SAOC, 2005):

"CC.6.1.1 Frequency deviations
During normal operating conditions, the nominal System Frequency of the Transmission System shall be 50.00 Hz and will be controlled normally between 49.95Hz and 50.05Hz. During exceptional steady state conditions, Frequency deviations will not exceed 49.90Hz to 50.1Hz unless Disturbed circumstances prevail.
Under Disturbed conditions, System Frequency could rise transiently to 51.50 Hz or fall to 48.00 Hz."

Moreover, the Service Level Agreement between PDO and OETC demanded for the tie line power exchange to be within ±10MW during normal operating conditions. Any excess power exchange has to be communicated and agreed in advance.

The above grid code and Service Level Agreement requirements can be summarised into three important control requirements:

1. Steady state frequency shall be within ±0.05Hz of nominal frequency 50Hz
2. Transient frequency shall not rise above 51.50Hz and shall not go below 48Hz
3. Steady state tie line power deviation shall not exceed ±10MW

The above three requirements are not meant to be as an AGC performance requirements and therefore they cannot be treated so.

The North American Electric Reliability Corporation (NERC) in its Reliability Standards for the Bulk Electric Systems of North America (North American Electric Reliability Corporation (NERC), 2009) demanded for some AGC control performance standards, CPS1 and CPS2. The CPS1 assesses the impact of ACE on frequency over a 12-month window (Feliachia and Rerkpreedapongb, 2005). The CPS2 limits the magnitude of short-term ACE values (Feliachia and Rerkpreedapongb, 2005). For any utility providing the AGC ancillary service to comply with NERC standards, it has to achieve CPS1 ≥100% and CPS2≥90%. The CPS1 and CPS2 are practical performance standards which are used to measure the performance of AGC over a calendar year. Therefore, it is not practical to estimate the compliance of a certain AGC controller to NERC CPS1 and CPS2 standards through simulation approach. A one year load disturbance profile would probably be required in order to estimate the AGC compliance through model simulation. On the other hand some researchers (Feliachia and Rerkpreedapongb, 2005; Hosseini and Etemadi,

2008) have presented AGC controller design which complies to NERC CPS1 and CPS2 performance standards but they didn't provide the calculation basis for that.

Alternatively, since CPS1 and CPS2 are dependant on ACE and frequency deviation, an AGC controller minimizing ACE and frequency deviation will implicitly comply with CPS1 and CPS2 performance standards.

For PDO and OETC, the following guidelines are suggested to be used for optimizing the AGC controller performance:

1. The static frequency deviation following a step-load change must be zero.
2. The static change in tie-line power following a step-load change must be zero.
3. Minimise time error represented by the integral of frequency deviation
4. Minimise the wear and tear on governor and turbine equipments
5. Minimise the CO2 emissions by reducing the amount of burnt fuel

10.3.3. Modified design of LQR AGC

10.3.3.1. The LQR cost function based on AGC requirements

Looking back at the above five AGC requirements, one can summarize the following:

- First requirement is achieved by minimizing the square of Δf_{pdo} and Δf_{oetc} which are represented by states X2 and X6 respectively in the state space model
- Second requirement can be achieved by minimizing the square of ΔP_{tie} which is represented by state X1 in the state space model
- Third requirement can be achieved by minimizing the square of $\int ACE_{pdo}$ and $\int ACE_{oetc}$ which are represented by states X12 and X13 respectively in the state space model.
- Fourth requirement can be achieved by minimizing the square of ΔXgg_{pdo}, ΔXgg_{oetc} and ΔXsg_{oetc} which are represented by states X5, X9 and X11 respectively in the state space model.
- Fifth requirement can be achieved by minimizing the square of ΔPgg_{pdo}, ΔPgg_{oetc} and ΔPsg_{oetc} which are represented by states X3, X7 and X10 respectively in the state space model.

Recall the LQR cost function presented earlier in equation 10.3:

$$C = \int_0^{\infty} (x'Qx + u'Ru)dt$$

For the optimum solution to be calculated considering the AGC requirements stated above, the term x'Qx in the above cost function must equal to the sum of the square of Δf_{pdo}, Δf_{oetc}, ΔP_{tie}, $\int ACE_{pdo}$, $\int ACE_{oetc}$, ΔXgg_{pdo}, ΔXgg_{oetc}, ΔXsg_{oetc}, ΔPgg_{pdo}, ΔPgg_{oetc} and ΔPsg_{oetc}.

Therefore:

$$x'Qx = (\Delta f_{pdo})^2 + (\Delta f_{oetc})^2 + (\Delta P_{tie})^2 + (\int ACE_{pdo})^2 + (\int ACE_{oetc})^2 + (\Delta Xgg_{pdo})^2 + (\Delta Xgg_{oetc})^2 + (\Delta Xsg_{oetc})^2 + (\Delta Pgg_{pdo})^2 + (\Delta Pgg_{oetc})^2 + (\Delta Psg_{oetc})^2 \quad \text{.....(10.26)}$$

For the equilibrium stated in equation 10.26 to be achieved, the Q matrix shall look as shown below:

$$Q = \begin{bmatrix} 1 & 0 & 0 & 0 & 0 & 0 & 0 & 0 & 0 & 0 & 0 & 0 & 0 \\ 0 & 1 & 0 & 0 & 0 & 0 & 0 & 0 & 0 & 0 & 0 & 0 & 0 \\ 0 & 0 & 1 & 0 & 0 & 0 & 0 & 0 & 0 & 0 & 0 & 0 & 0 \\ 0 & 0 & 0 & 0 & 0 & 0 & 0 & 0 & 0 & 0 & 0 & 0 & 0 \\ 0 & 0 & 0 & 0 & 1 & 0 & 0 & 0 & 0 & 0 & 0 & 0 & 0 \\ 0 & 0 & 0 & 0 & 0 & 1 & 0 & 0 & 0 & 0 & 0 & 0 & 0 \\ 0 & 0 & 0 & 0 & 0 & 0 & 1 & 0 & 0 & 0 & 0 & 0 & 0 \\ 0 & 0 & 0 & 0 & 0 & 0 & 0 & 0 & 0 & 0 & 0 & 0 & 0 \\ 0 & 0 & 0 & 0 & 0 & 0 & 0 & 0 & 1 & 0 & 0 & 0 & 0 \\ 0 & 0 & 0 & 0 & 0 & 0 & 0 & 0 & 0 & 1 & 0 & 0 & 0 \\ 0 & 0 & 0 & 0 & 0 & 0 & 0 & 0 & 0 & 0 & 1 & 0 & 0 \\ 0 & 0 & 0 & 0 & 0 & 0 & 0 & 0 & 0 & 0 & 0 & 1 & 0 \\ 0 & 0 & 0 & 0 & 0 & 0 & 0 & 0 & 0 & 0 & 0 & 0 & 1 \end{bmatrix} \quad \text{.....(10.27)}$$

The matrix R is similar to what has been presented in equation 10.24.

10.3.3.1. Simulation Results

In a similar way as shown earlier in section 10.2.6.1, the gain matrix K is calculated and produced to be:

$$K = \begin{bmatrix} -1.0703 & 0.4650 & 0.8029 & 0.1004 & 0.4835 & 0.1361 & 0.0066 & -0.0004 & -0.0004 & 0.0000 & -0.0029 & -0.9999 & -0.0115 \\ 0.0863 & -0.0872 & -0.0308 & -0.0026 & -0.0011 & 1.4496 & 1.2009 & 0.1454 & 0.4920 & 0.3323 & 0.3916 & 0.0115 & -0.9999 \end{bmatrix}$$

.....(10.28)

Using the "Mfile" and the PDO-OETC power system used in section 10.2.5, a load disturbance of 100MW was simulated once at PDO side and once at OETC side. PDO frequency, OETC frequency and tie line power are monitored. Figures 10.17-10.20 show PDO and OETC frequencies in one figure and the tie line power in a separate figure for

both tests respectively. The figures also compare the results with the results obtained earlier using the basic LQR.

A summary of the performance values was attempted and is shown in Table 10.4. The summary also compares the results of the base case, classical PID AGC controller, basic LQR AGC with the modified LQR AGC controller performance.

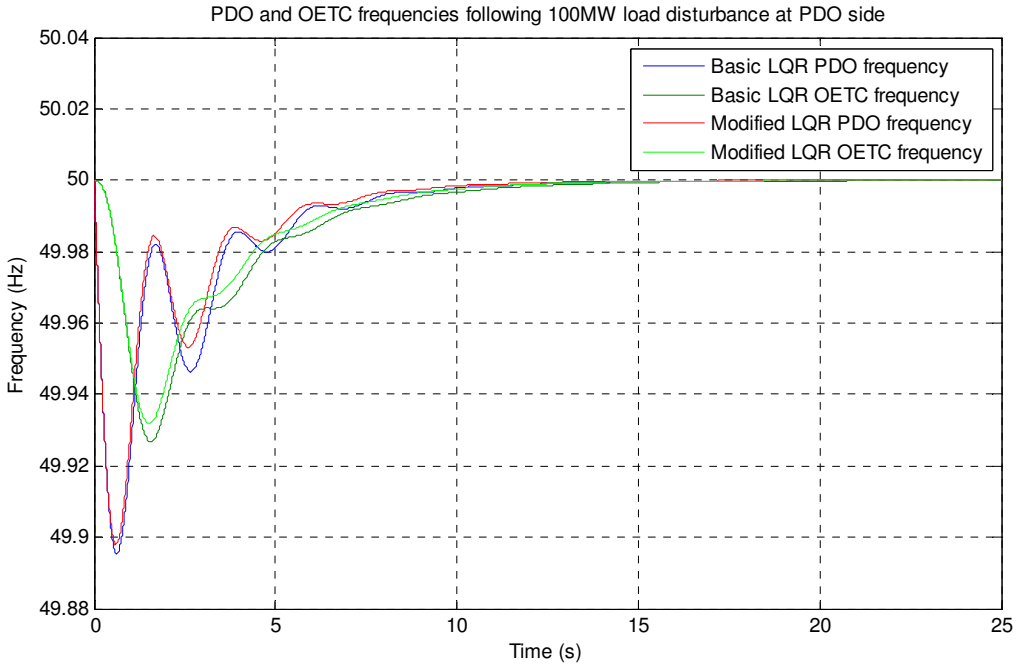

Figure 10.17: PDO and OETC frequencies following a 100MW load disturbance at PDO side with the modified LQR AGC applied at both PDO and OETC

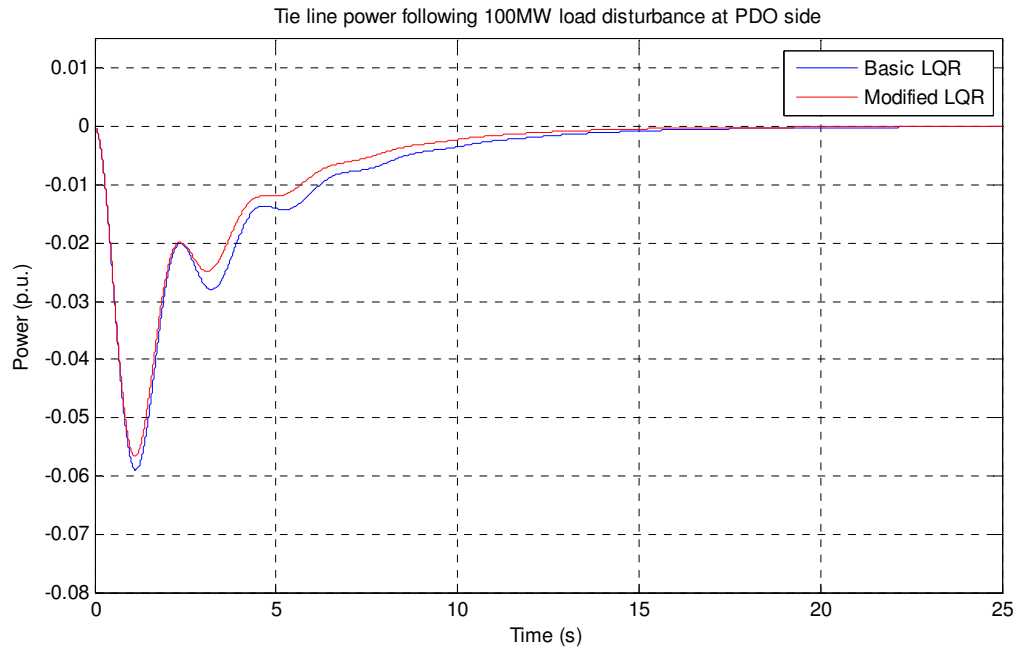

Figure 10.18: Tie line power deviation following a 100MW load disturbance at PDO side with the modified LQR AGC applied at both PDO and OETC

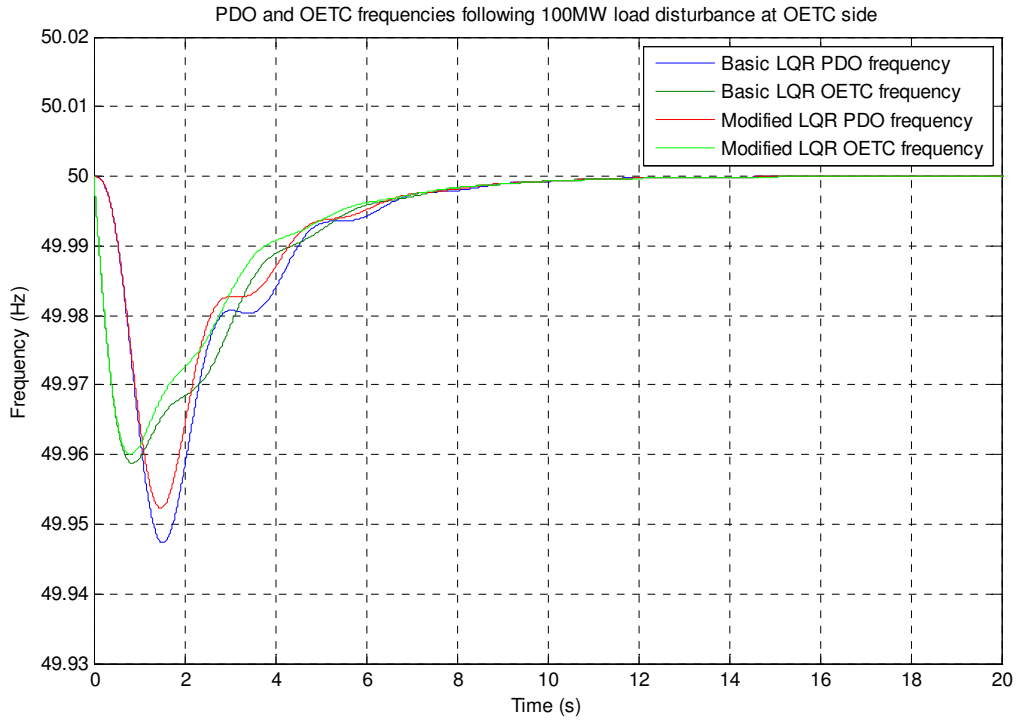

Figure 10.19: PDO and OETC frequencies following a 100MW load disturbance at OETC side with the modified LQR AGC applied at both PDO and OETC

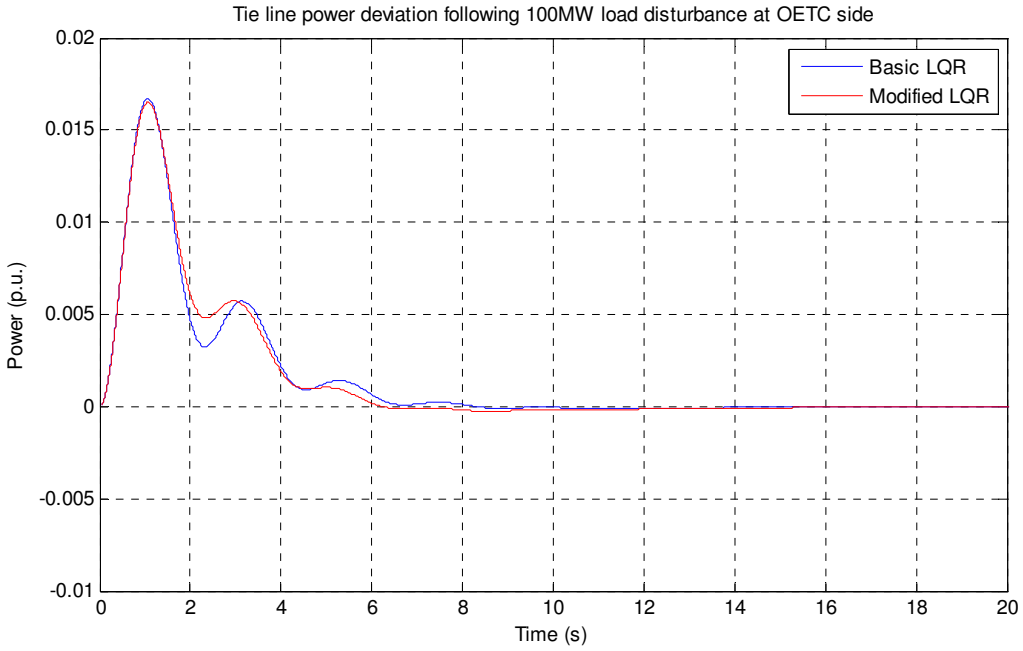

Figure 10.20: Tie line power deviation following a 100MW load disturbance at OETC side with the modified LQR AGC applied at both PDO and OETC

		Base case response	PID controlled response	LQR controlled response	Modified LQR controlled response
100MW load disturbance at PDO side	Frequency deviation (Hz)	-0.05	0	0	0
	Settling time (s)	10.9	34	11.3	10.1
	Tie line power deviation (p.u.)	-0.0379	0	0	0
100MW load disturbance at OETC side	Frequency deviation (Hz)	-0.05	0	0	0
	Settling time (s)	7.74	25.3	8.59	8.39
	Tie line power deviation (p.u.)	0.0121	0	0	0

Table 10.4: PDO and OETC Modified LQR AGC controllers' performance in comparison to the base case, the classical PID and the LQR controllers.

10.3.3.2. Discussion

From Figures 10.17-10.20 and table 10.4, it is clear that the modified LQR AGC has maintained the same control topology features as of the basic LQR AGC. The modified LQR AGC has slightly improved the system response to load disturbances in terms of oscillations and settling time if compared with the basic LQR AGC.

10.3.3.3. Summary

The LQR AGC design can be customized based on the control performance requirements. A change in the Q matrix elements can improve the LQR AGC controller performance. The modified LQR AGC has slightly improved the system response to load disturbances when compared with the basic LQR AGC.

10.3.4. Fine tuning the modified design of LQR AGC

10.3.4.1. Methodology

Four scenarios are investigated in this part:

Scenario 1: the first scenario is to multiply the Q matrix elements which affect the AGC requirements 1, 2 and 3 by a factor of 10.

Scenario 2: the second scenario is to multiply the Q matrix elements which affect the AGC requirements 4 and 5 by a factor of 10.

Scenario 3: the third scenario is to multiply the Q matrix by a factor of 10

Scenario 4: the fourth scenario is to multiply the R matrix by a factor of 10

For scenario one, the R matrix remains the same as in section 10.3.3 and the Q matrix is shown in equation 10.29 below:

$$Q = \begin{bmatrix} 10 & 0 & 0 & 0 & 0 & 0 & 0 & 0 & 0 & 0 & 0 & 0 & 0 \\ 0 & 10 & 0 & 0 & 0 & 0 & 0 & 0 & 0 & 0 & 0 & 0 & 0 \\ 0 & 0 & 1 & 0 & 0 & 0 & 0 & 0 & 0 & 0 & 0 & 0 & 0 \\ 0 & 0 & 0 & 0 & 0 & 0 & 0 & 0 & 0 & 0 & 0 & 0 & 0 \\ 0 & 0 & 0 & 0 & 1 & 0 & 0 & 0 & 0 & 0 & 0 & 0 & 0 \\ 0 & 0 & 0 & 0 & 0 & 10 & 0 & 0 & 0 & 0 & 0 & 0 & 0 \\ 0 & 0 & 0 & 0 & 0 & 0 & 1 & 0 & 0 & 0 & 0 & 0 & 0 \\ 0 & 0 & 0 & 0 & 0 & 0 & 0 & 0 & 0 & 0 & 0 & 0 & 0 \\ 0 & 0 & 0 & 0 & 0 & 0 & 0 & 0 & 1 & 0 & 0 & 0 & 0 \\ 0 & 0 & 0 & 0 & 0 & 0 & 0 & 0 & 0 & 1 & 0 & 0 & 0 \\ 0 & 0 & 0 & 0 & 0 & 0 & 0 & 0 & 0 & 0 & 1 & 0 & 0 \\ 0 & 0 & 0 & 0 & 0 & 0 & 0 & 0 & 0 & 0 & 0 & 10 & 0 \\ 0 & 0 & 0 & 0 & 0 & 0 & 0 & 0 & 0 & 0 & 0 & 0 & 10 \end{bmatrix} \quad \text{.....(10.29)}$$

For scenario two, the R matrix remains the same as in section 10.3.3 and the Q matrix is shown in equation 10.30 below:

$$Q = \begin{bmatrix} 1 & 0 & 0 & 0 & 0 & 0 & 0 & 0 & 0 & 0 & 0 & 0 & 0 \\ 0 & 1 & 0 & 0 & 0 & 0 & 0 & 0 & 0 & 0 & 0 & 0 & 0 \\ 0 & 0 & 10 & 0 & 0 & 0 & 0 & 0 & 0 & 0 & 0 & 0 & 0 \\ 0 & 0 & 0 & 0 & 0 & 0 & 0 & 0 & 0 & 0 & 0 & 0 & 0 \\ 0 & 0 & 0 & 0 & 10 & 0 & 0 & 0 & 0 & 0 & 0 & 0 & 0 \\ 0 & 0 & 0 & 0 & 0 & 1 & 0 & 0 & 0 & 0 & 0 & 0 & 0 \\ 0 & 0 & 0 & 0 & 0 & 0 & 10 & 0 & 0 & 0 & 0 & 0 & 0 \\ 0 & 0 & 0 & 0 & 0 & 0 & 0 & 0 & 0 & 0 & 0 & 0 & 0 \\ 0 & 0 & 0 & 0 & 0 & 0 & 0 & 0 & 10 & 0 & 0 & 0 & 0 \\ 0 & 0 & 0 & 0 & 0 & 0 & 0 & 0 & 0 & 10 & 0 & 0 & 0 \\ 0 & 0 & 0 & 0 & 0 & 0 & 0 & 0 & 0 & 0 & 10 & 0 & 0 \\ 0 & 0 & 0 & 0 & 0 & 0 & 0 & 0 & 0 & 0 & 0 & 1 & 0 \\ 0 & 0 & 0 & 0 & 0 & 0 & 0 & 0 & 0 & 0 & 0 & 0 & 1 \end{bmatrix} \quad \text{.....(10.30)}$$

For scenario three, the Q and R matrices remain the same as in section 10.3.3 but the Q matrix is multiplied by a factor of 10.

For scenario four, the Q and R matrices remain the same as in section 10.3.3 but the R matrix is multiplied by a factor of 10.

10.3.4.2. Simulation results

The K matrix has been calculated for all above four scenarios and the model has been simulated for each scenario with a 100MW load disturbance is applied once at PDO and

once at OETC. The results are shown in Figures 10.21-10.26. The Figures compare the results obtained for all four scenarios with the results obtained earlier using the modified LQR AGC.

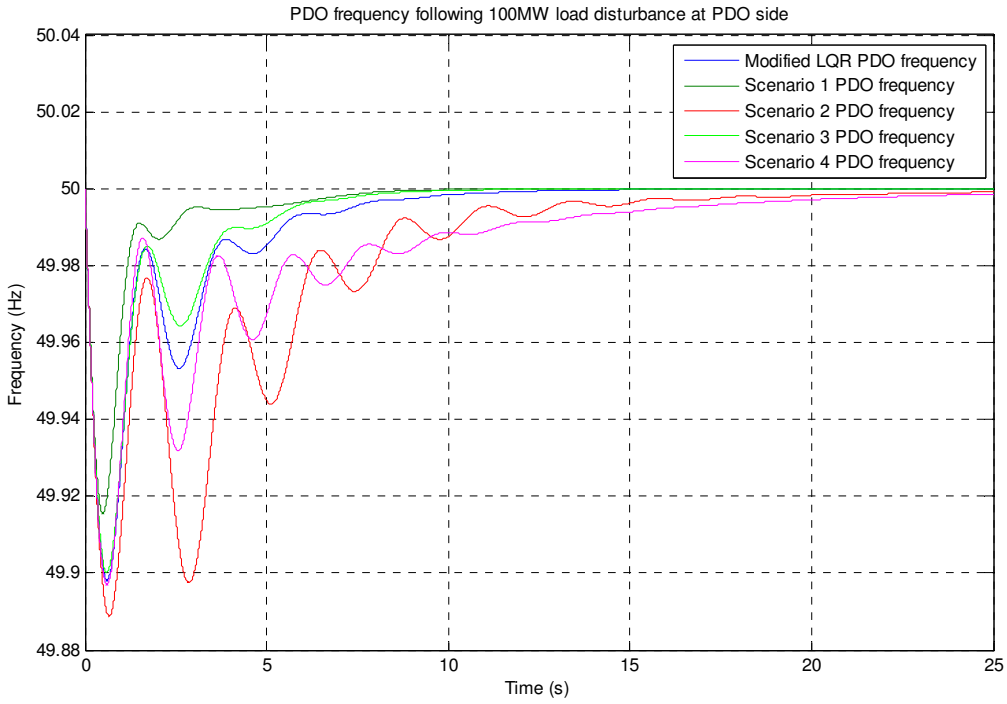

Figure 10.21: PDO frequency following a 100MW load disturbance at PDO side with the tuned LQR AGC applied at both PDO and OETC

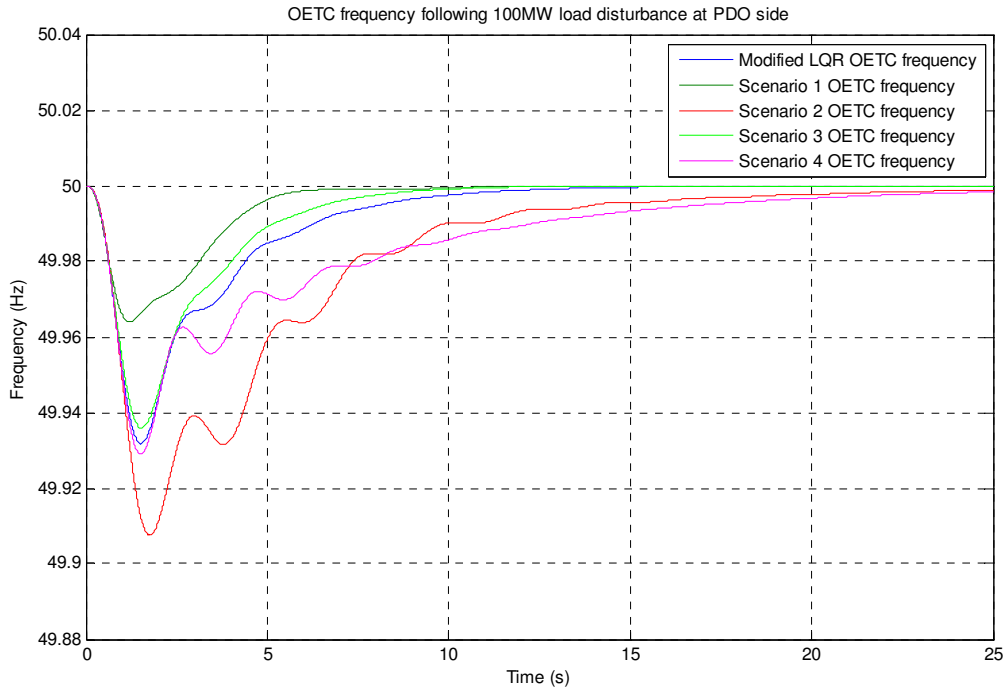

Figure 10.22: OETC frequency following a 100MW load disturbance at PDO side with the tuned LQR AGC applied at both PDO and OETC

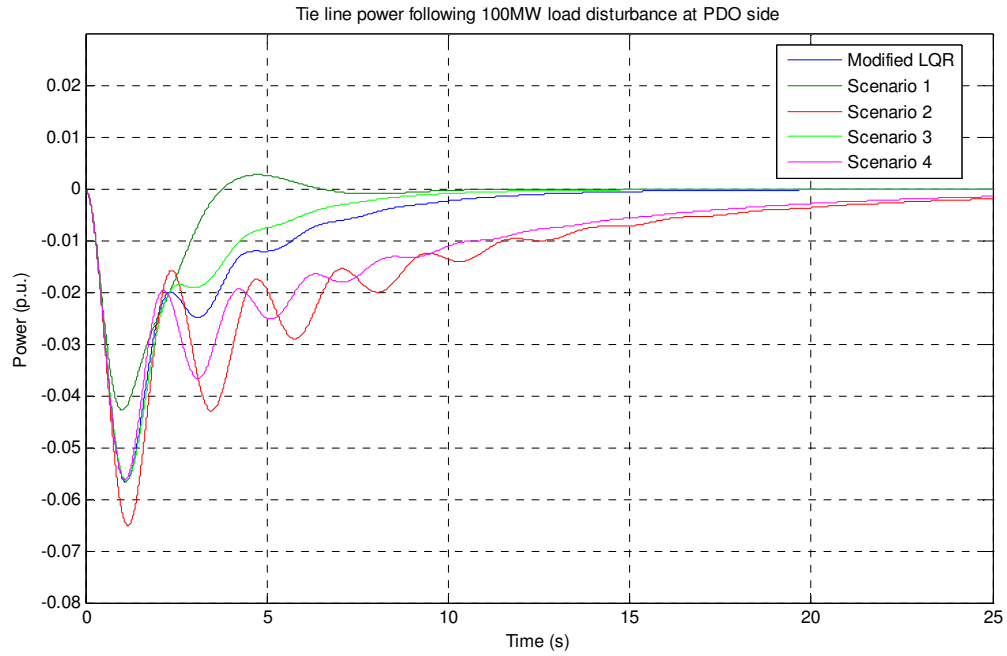

Figure 10.23: Tie line power deviation following a 100MW load disturbance at PDO side with the tuned LQR AGC applied at both PDO and OETC

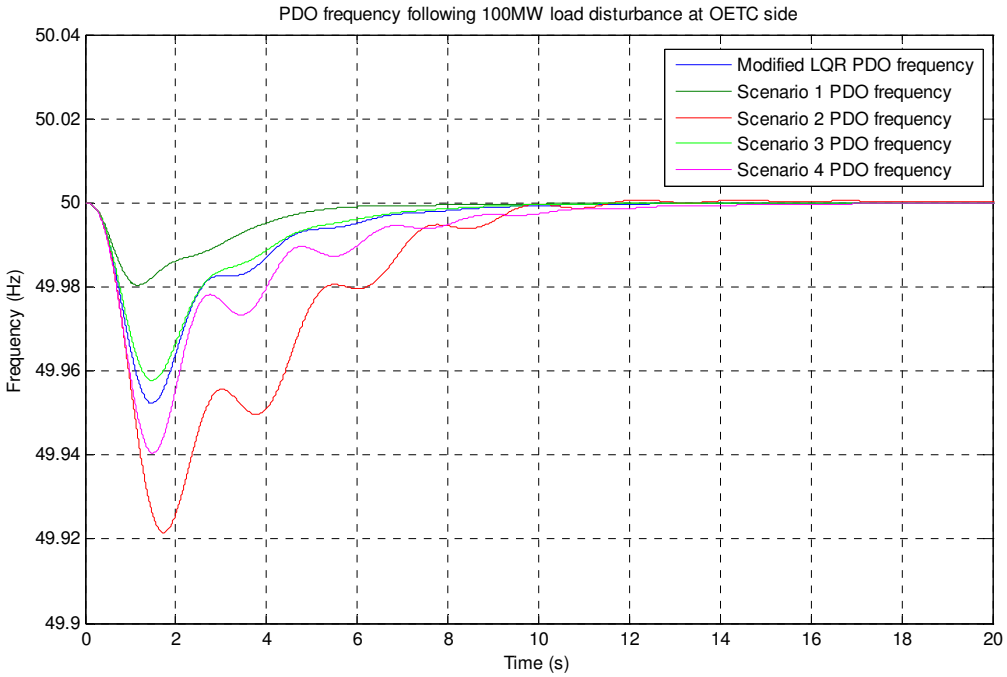

Figure 10.24: PDO frequency following a 100MW load disturbance at OETC side with the LQR AGC applied at both PDO and OETC

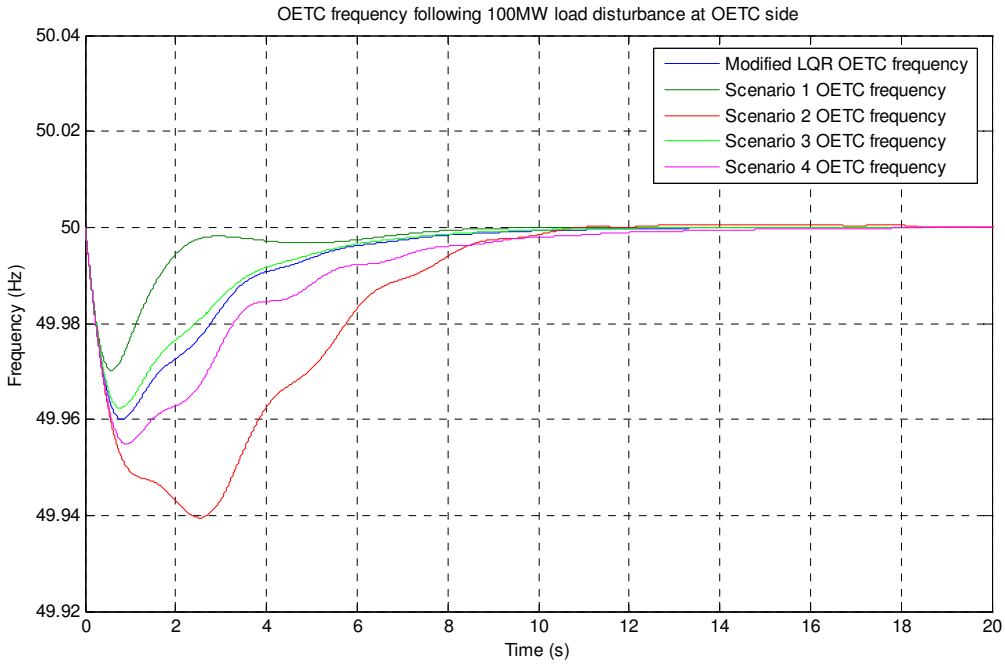

Figure 10.25: OETC frequency following a 100MW load disturbance at OETC side with the tuned LQR AGC applied at both PDO and OETC

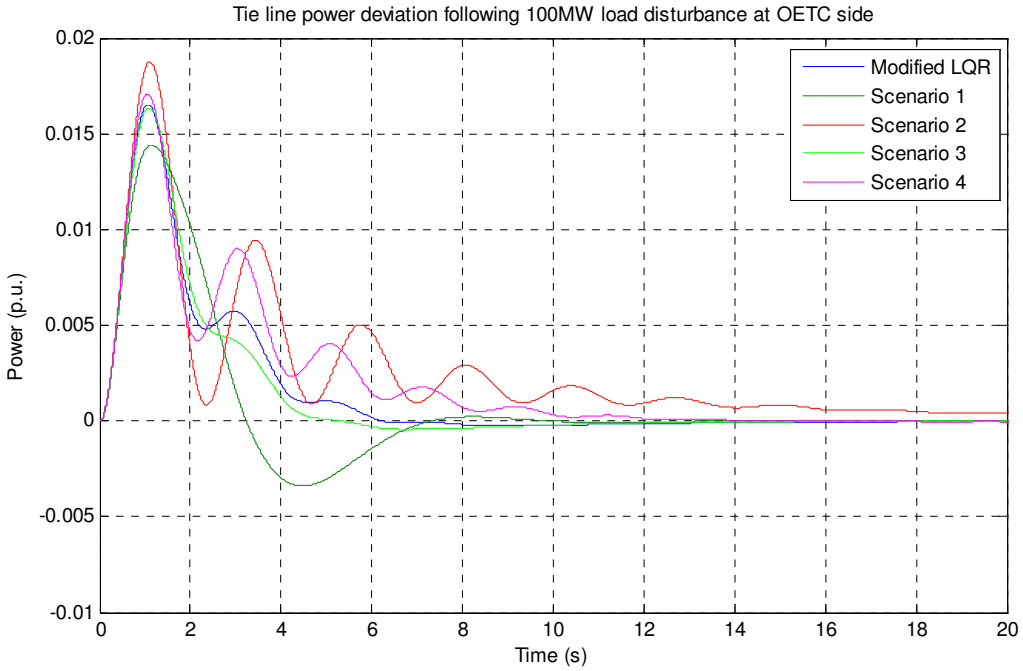

Figure 10.20: Tie line power deviation following a 100MW load disturbance at OETC side with the tuned LQR AGC applied at both PDO and OETC

10.3.4.3. Discussion

Looking at the results shown in Figures 10.21-10.26 with specific emphasis on the maximum deviation, settling time and the oscillations damping one can see that scenario 1

has the best response and scenario 2 has the worst response. From scenario 1 and 2, it is clear that changing the weighting of the individual elements within the Q matrix can cause dramatic change in the LQR AGC performance. In scenario one, the elements which are directly linked to frequency and tie line power deviation have been given extra weight when compared with the turbines states which are directly linked with fuel and maintenance requirements. This has resulted in stiff controller action which will incur extra maintenance and fuel costs. On the other hand, scenario 2 gives more priority to saving fuel and maintenance costs by giving extra weight to the elements which are directly linked to the fuel and maintenance requirements. It has resulted in mild control action allowing more dynamic deviation, oscillatory response and longer settling time.

Scenario 3 has slightly better controller performance than the modified LQR performance. This is due to giving the Q matrix more weight than the control effort matrix R. It will result in more fuel consumption in comparison to the slight improvement in the overall controller response.

Scenario 4 has more oscillatory response than the modified LQR. In scenario 4 the controller effort has been given more weight so that fuel and maintenance cost can be saved regardless of the trajectory the individual states will follow. Consequently it has resulted in more oscillatory response with longer settling time.

All in all, it is clear form Figures 10.21-10.26 that the modified LQR has an average performance in comparison of the other scenarios and therefore is considered as the best performance taking care of all the AGC control requirements.

10.3.4.4. Summary

Four scenarios of fine tuning the modified LQR AGC controller performance have been investigated. The four scenarios have produced different responses to load disturbances some of which are better than the modified LQR response. However, the modified LQR AGC performance is still considered to be the best LQR controller because it balances between all the AGC controller performance requirements whilst having an average controller performance when compared with the other four scenarios.

10.4. Overall Summary

Linear Quadratic Regulator is an optimal controller which can easily be customized to suit certain controller design requirements. The LQR has been used to design AGC controller for PDO-OETC interconnected power system. The results proved that LQR can produce much better performance than the classical PID controller. The PDO-OETC LQR AGC

controller has been modified to suit certain AGC control guidelines. The modified LQR AGC controller has produced better performance. The modified LQR AGC went through a fine tuning exercise which proved that the modified LQR AGC has a reasonable performance catering for all AGC control requirements.

Although the LQR AGC controller is very flexible to design and optimize, it is practically difficult and costly to implement. This is because LQR requires states feedback of all the states in the field which will demand a huge telecommunication infrastructure. Alternatively, the states feedback can be received from an observer model which is also difficult to maintain due to the growing nature of electrical power systems.

Therefore the next chapter will investigate the utilization of non linear controllers which can accommodate field changes and uncertainties with minimal feedback signals from the field.

Chapter 11: Design of Automatic Generation Control using Fuzzy Logic

11.1. Introduction

In this part of the study the Fuzzy Logic (FL) technique is considered to design an AGC controller of PDO-OETC power systems. The study aims to realise the difference in response the Fuzzy Logic technique can make in comparison to the classical approaches. Fuzzy Logic theory is known of its flexibility and ability to deal with non linear systems.
Same as the previous chapter, three control topologies will only be considered. Therefore the Fuzzy Logic will be applied to the following three control topologies:

- AGC applied to PDO alone using ACE as a feedback signal
- AGC applied to OETC alone using ACE as a feedback signal
- AGC applied to both PDO and OETC using ACE as a feedback signal

All in all, the performance of the Fuzzy Logic control technique will be compared with the previously adopted techniques performance, the classical PID and the LQR.

11.2. Theoretical background

Nowadays, fuzzy logic has been used in almost all sectors of industries including power systems control. Shayeghi et al [4] (2009) surveyed the most recent applications of FL to the AGC problem. The fuzzy logic fundamental structure for all controller design is summarised in Figure 11.1 (Demiroren and Yesil, 2004).

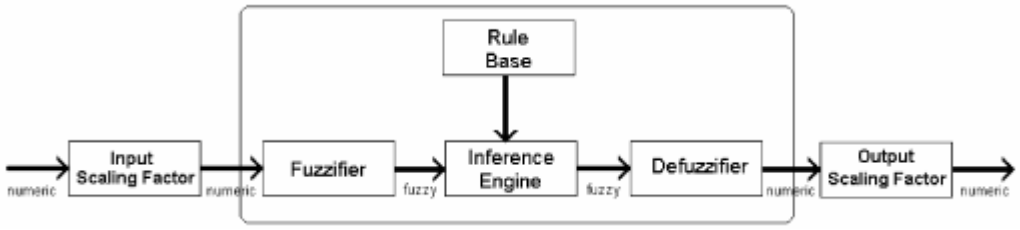

Figure 11.1: components of a fuzzy system

The fuzzy logic theory is very well established and is available for readers in almost all recent control engineering text books (Nagrath and Gopal, 2008, pp.783-800; Ghosh, 2007, pp. 585-591; Ross, 2007). There are four main parts in a Fuzzy Logic system (Demiroren and Yesil, 2004):

1. The Fuzzifier: this structure is meant to transform the numeric values into fuzzy sets. It measures the values of input variables then performs a scale transformation

which maps the physical values of the process state variables into a normalised universe of discourse (Nagrath and Gopal, 2008, p. 790). The measured crisp value will eventually be converted to a fuzzy set. The so called Membership Functions (MF) are spread over the universe of discourse where any input crisp value will have a membership in one or more of MFs. There are many shapes for the MFs but the most popular one is the triangular one. The MFs can overlap in the universe of discourse depending on the design requirements.

2. The Inference Engine: it is the engine that performs all logic manipulations in a fuzzy system. The result of the inference process is an output represented by a fuzzy set.
3. The Rule Base: the Rule Base basic function is representing the control policy of an experienced process operator and/or control engineer in a structured way as a set of production rules e.g. If (process state)-Then (control output).
4. The Defuzzifier: transforms the output fuzzy set into a numeric value suitable to be fed to the process.

In addition, input and out scaling factors are used to tune the fuzzy controller to obtain the desired dynamic properties of the process controller closed loop (Demiroren and Yesil, 2004).

11.3. Proposed controllers topologies

In general, conventional Fuzzy Logic controllers are not suitable for controlling dynamic systems because they do not produce reliable transient response and are unable to eliminate steady state error (Kocaarslan and Çam, 2005). However combining Fuzzy logic technique with other techniques underwent an extensive research and has produced wonderful results (Shayeghi, et al [(2)], 2006; Shayeghi, et al [(1)], 2007; Yesil et al, 2004; Çam, 2007; Çam and Kocaarslan [(1)], 2005; Demiroren and Yesil, 2004; Feliachi and Rerkpreedapong, 2005; Kocaarslan and Çam [(3)], 2005; Çam and Kocaarslan [(2)], 2005; Chang and Fu, 1997).

In this part, the Fuzzy Logic PID control technique will be implemented to design an AGC of PDO-OETC interconnected power system. In the literature, two models of fuzzy PID AGC controller have been considered. Few researchers (Yesil et al, 2004; Demiroren and Yesil, 2004) have introduced the Fuzzy PID AGC controller shown in Figure 11.2. Shayeghi et al [(2)] (2006) has mentioned another topology of Fuzzy PID AGC controller and

is shown in Figure 11.3. Both Fuzzy PID AGC topologies shown in Figure 11.2 and Figure 11.3 will be implemented to PDO-OETC interconnected power system.

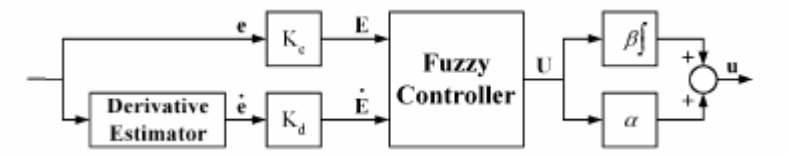

Figure 11.2: Fuzzy PID controller architecture 1 (Yesil et al, 2004)

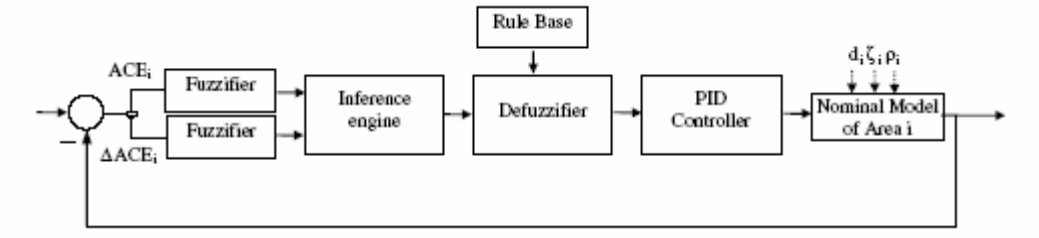

Figure 11.3: Fuzzy PID controller architecture 2 (Shayeghi et al [(2)], 2006)

From Figure 11.2 and Figure 11.3, it is clear that there are two distinctive parts in the controller architecture, the fuzzy and the PI or PID parts. Also one can see that there are two inputs to the fuzzy controller, the ACE and the derivative of the ACE. This is because human being can actually monitor and feel the errors and the rate of change of errors. This fact is important for the design of a fuzzy controller since it is intended to translate the human being experience into a control system. The error integrator cannot be part of the inputs to the fuzzy controller, simply because the operator or the control engineer cannot realise it. From Figure 11.2, adding a PI controller after the fuzzy controller actually has implicitly satisfied all the conditions required to form a PID controller. The error and the derivative of the error go into a traditional PI and the total output will contain the proportional, integral and derivative components. Therefore, the architecture shown in Figure 11.2 is named as Fuzzy PID controller (FPID).

On the other hand the controller shown in Figure 11.3 has explicit traditional PID controller after the fuzzy logic part. This topology ensures the derivative action is explicitly available after the fuzzy inference.

In the following sections, both FLPID controller architecture shown in Figure 11.2 (FLPID topology 1) and Figure 11.3 (FLPID topology 2) will be implemented to design an AGC controller for PDO-OETC interconnected power system and a detailed design and tuning

approach will be attempted for each control topology. Since it is common for both topologies, the fuzzy logic part will be designed only once as in the next section.

11.4. Fuzzy logic part design of PDO-OETC AGC controller

There are many options and alternatives which can compose a fuzzy logic control system. It must be noted that only one set of options compose the optimum fuzzy logic architecture for a given system. Also, it must be known that even if we managed to setup the optimum fuzzy logic architecture, we may not be successful to optimally tune the parameters to produce the optimum response for a set of control indices. Hence, from its name there is always fuzziness in the design process of a fuzzy logic control system which calls for a wide range of trials and errors to achieve an acceptable performance.

There are many Fuzzy logic design options which are briefly mentioned below but it may not be limited to:

- Mamdani method
- Sugeno method
- Shape of membership functions (MF)
- Number of inputs
- Number of membership functions
- Range of universe of discourse
- Values of input scaling factors
- Value of output scaling factor

There is no rule of thump which tells us which of the above options are most suitable for our case but trial and error method helps deciding some of the options. In our case, many trials and errors proved the below are the most suitable options:

- Mamdani method
- Triangular MF
- Seven MF for each input and output

As in Figures 11.2 and 11.3, two inputs to the fuzzy logic system have been used, the ACE and the rate of change of ACE. The input and output scaling factors are assumed to be unity.

The range of the universe of discourse was calculated empirically using the developed model. The model was subjected to the largest normal load disturbance (200MW) the AGC controller is intended to deal with and then the maximum ACE and rate of change of ACE

was recorded. The disturbance was applied once at PDO and another at OETC. From this test, the universe of discourse of both input MFs was decided as in Table 11.1. Moreover, the output MFs universe of discourse was assumed to be the same as the ACE input MFs because traditionally the control signal is biased by the error; it is also shown in Table 11.1.

	MFs universe of discourse		
	ACE input	ΔACE input	Output
PDO	-0.21 to +0.21	-0.36 to +0.36	-0.21 to +0.21
OETC	-0.12 to +0.12	-0.15 to +0.15	-0.12 to +0.12

Table 11.1: universe of discourse ranges of inputs and output membership functions

There are seven MFs evenly distributed in the universe of discourse of the two inputs and the output and are namely summarised as below:

LN: large negative

MN: medium negative

SN: small negative

Z: zero

SP: small positive

MP: medium positive

LP: large positive

The seven MFs ranges for the ACE, ΔACE and the output of PDO are shown in Figure 11.4, Figure 11.5 and Figure 11.6 respectively.

The seven MFs ranges for the ACE, ΔACE and the output of OETC are shown in Figure 11.7, Figure 11.8 and Figure 11.9 respectively.

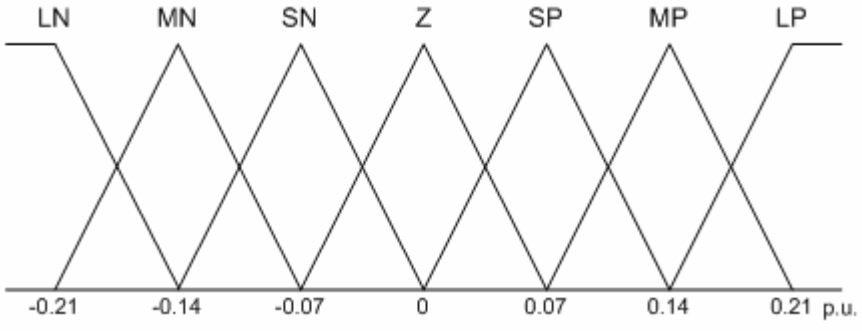

Figure 11.4: PDO fuzzy logic controller ACE input MFs

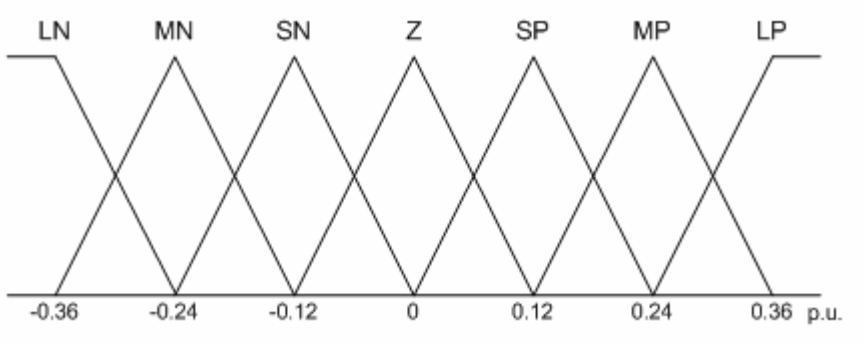

Figure 11.5: PDO fuzzy logic controller ΔACE input MFs

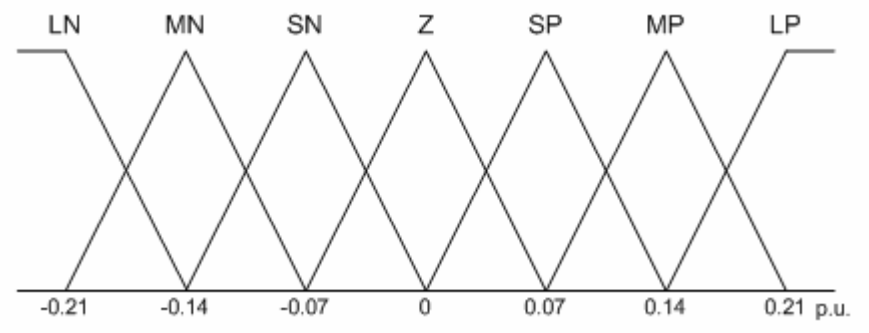

Figure 11.6: PDO fuzzy logic controller output MFs

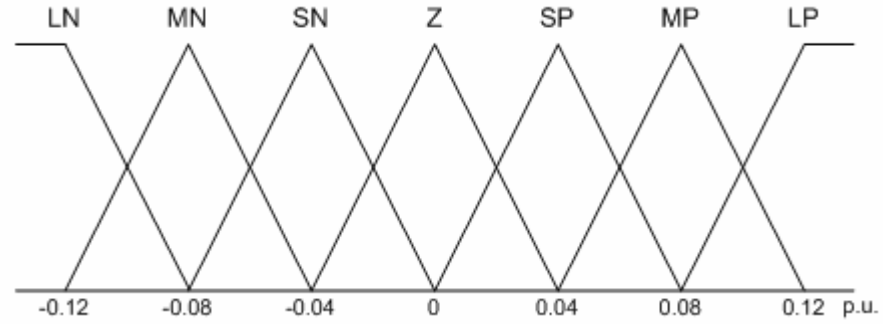

Figure 11.7: OETC fuzzy logic controller ACE input MFs

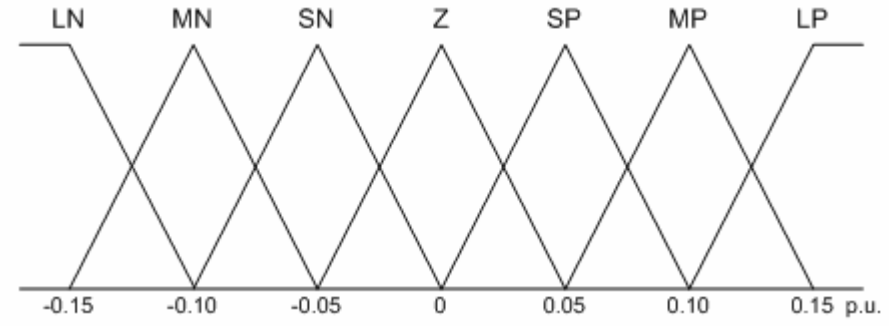

Figure 11.8: OETC fuzzy logic controller ΔACE input MFs

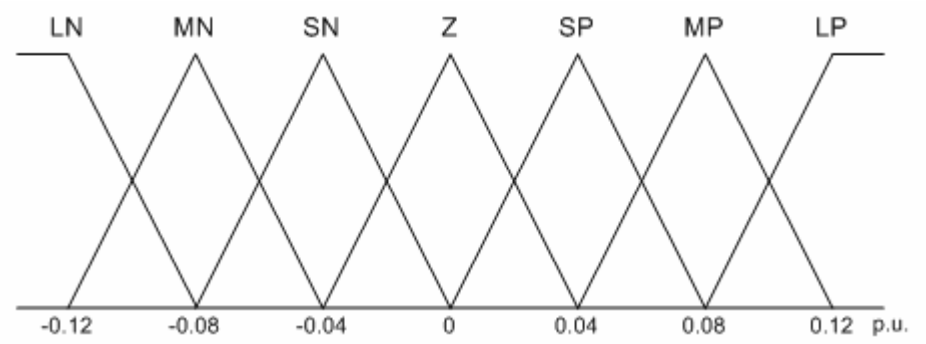

Figure 11.9: OETC fuzzy logic controller output MFs

The fuzzy inference rules are set in the form:

If ACE is A_i and ΔACE is B_i THEN u is $C_{i,}$, where:

i: 1,2,3,…,n

A, B, C: are fuzzy sets

u: is the output

A total number of 49 inference rules are used in both PDO and OETC fuzzy logic controllers which are based on the power system operator experience. They are summarised in Table 11.2.

Imagine a power system operator monitoring the system frequency and the tie line power. Two main factors will influence his reaction to sudden changes in the system frequency and tie line power, how much deviation is there and the rate of change of deviation. For example following large sudden load increase at PDO side, the operator will notice the frequency is dropping quickly and the tie line power import is increasing quickly. The operator will then realise that he has to act harshly to balance the generation with the new load, therefore he will harshly increase generators output. In other words, if the ACE is large negative and the rate of change of ACE is large negative, the natural response of the operator is large positive increase of power generation. Another example is when the ACE is large positive and there is a large negative rate of change of ACE, eventually things will be balanced out and the operator doesn't need to do any action i.e. zero action. So on and so forth, from the operator common sense and experience, Table 11.2 is constructed. The out put states, LP, MP, SP, Z, SN, MN and LN are solely decided by the operator experience and can be always further optimised.

		ACE						
		LN	**MN**	**SN**	**Z**	**SP**	**MP**	**LP**
ΔACE	**LN**	LP	LP	LP	LP	MP	SP	Z
	MN	LP	LP	LP	MP	SP	Z	SN
	SN	LP	LP	MP	SP	Z	SN	MN
	Z	LP	MP	SP	Z	SN	MN	LN
	SP	MP	SP	Z	SN	MN	LN	LN
	MP	SP	Z	SN	MN	LN	LN	LN
	LP	Z	SN	MN	LN	LN	LN	LN

Table 11.2: Fuzzy inference rules of PDO and OETC fuzzy logic controller

Using MATLAB fuzzy logic toolbox, the PDO and OETC fuzzy logic control systems were designed based on the above details. The generated rules surfaces for both PDO and OETC are shown in Figure 11.10 and 11.11 respectively.

Consider the rules surface in Figures 11.10 and 11.11 and knowing that the Fuzzy logic part will be followed by the integral action of PID part, it is clear that the overall Fuzzy Logic PID controller will have a mild action around the nominal operating points. It will also have a stiff action for large load disturbances since the rules surface saturates at large positive or large negative depending on the sign of the load disturbance.

This is in line with the control engineer requirements. During small disturbances where the frequency and tie line power deviations are within the normal operating envelop, there will be a mild control action from the control engineer. However, during heavy load disturbances, the control engineer will put maximum control effort to restore the frequency and tie line power exchange nominal values in order to stop the system from drifting to unstable condition.

Overall, the controller action is mild around the nominal operating points and stiff off the nominal operating points so that the system will not drift to the uncontrollable conditions.

The developed Fuzzy logic control system of both PDO and OETC will be used in the proposed control topologies suggested in section 11.3.

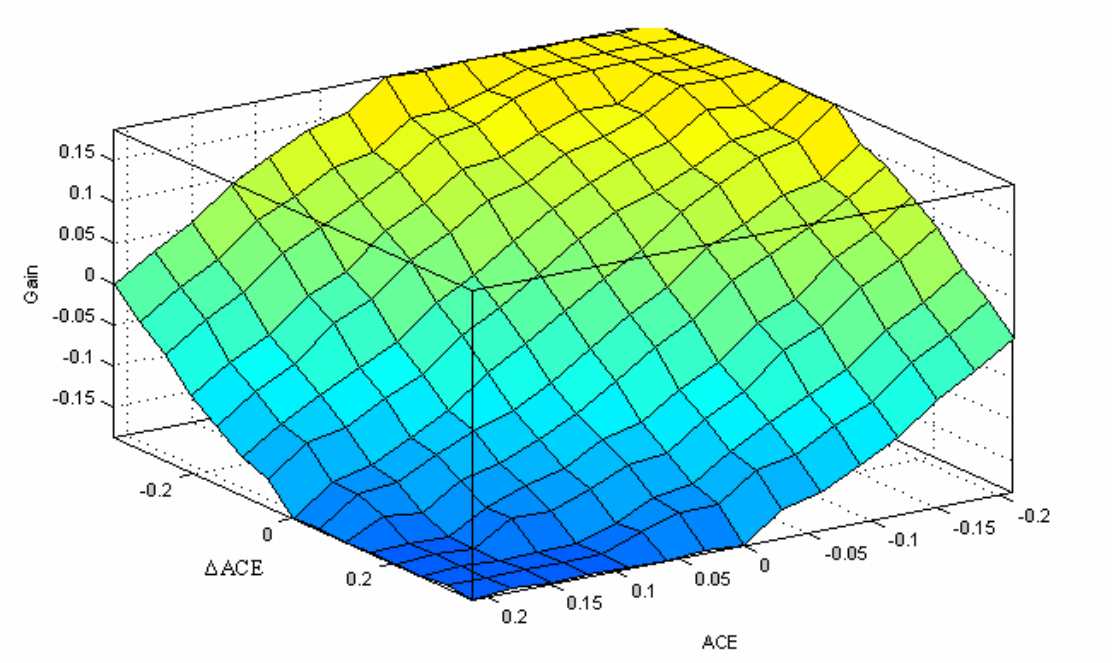

Figure 11.10: PDO fuzzy logic controller inference rules surface

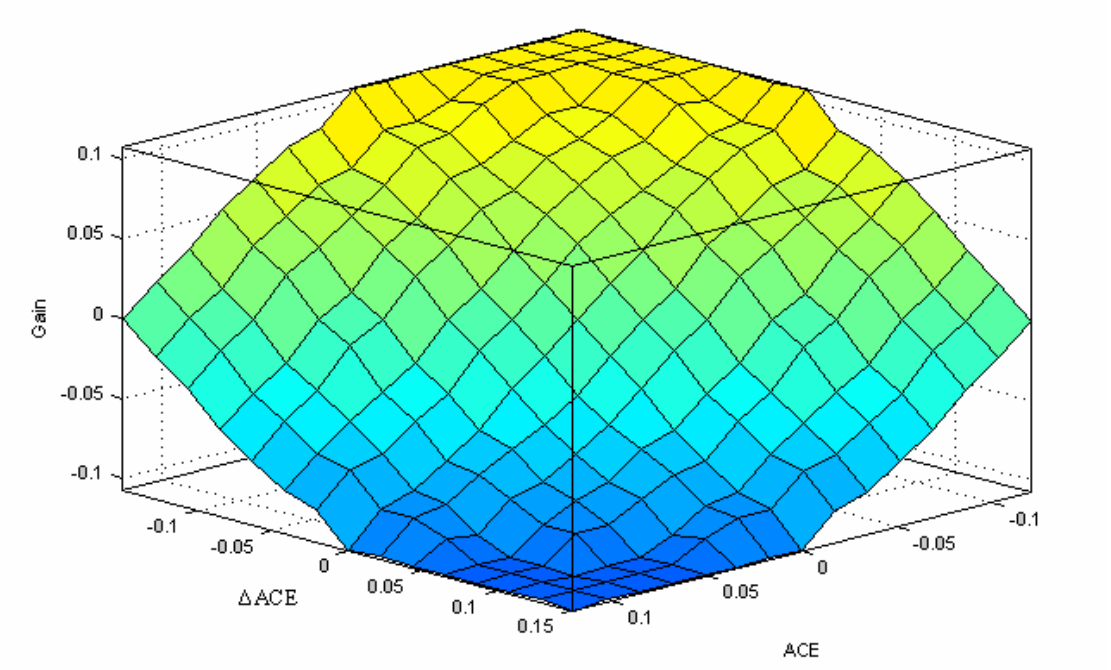

Figure 11.11: OETC fuzzy logic controller inference rules surface

11.5. Fuzzy Logic PID topology 1

11.5.1. Fuzzy Logic PID topology 1 applied to PDO alone AGC controller

11.5.1.1. Design approach

This part of the study demonstrates the performance of the controller structure shown in Figure 11.2. The design of the PDO AGC controller using this controller structure is completed in stages. The following approach is followed:

1. Design the Fuzzy logic control system part as shown earlier in section 11.4
2. Design a PI AGC controller for PDO power systems using the closed loop Ultimate Sensitivity Method. During the design and tuning of the PI controller, the uncontrolled complete PDO-OETC model is used without consideration of the fuzzy logic part.
3. Merge the developed Fuzzy logic parts with the respective tuned PI controller so that the controller structure shown in Figure 11.2 is formed.

Using MATLAB Simulink, the Fuzzy Logic PID 1 controller is designed as shown in Figure 11.12.

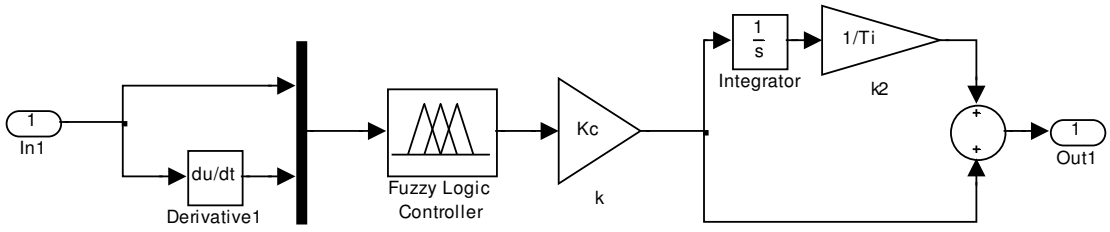

Figure 11.12: Fuzzy Logic PID 1 controller design

The complete PDO-OETC power system model with PDO alone Fuzzy PID 1 AGC is the same as shown earlier in Figure 9.22.

11.5.1.2. Controller tuning

The fuzzy logic part parameters will remain the same as developed earlier in section 11.4. The PI part was tuned using Ziegler Nichols (Ultimate sensitivity) method. The look up table shown earlier in Table 9.2 was used to calculate the PI controller parameters. The PI parameters for PDO are shown in Table 11.3.

Ku (ultimate gain)	Pu (ultimate period)	Kc (PI Controller gain)	Ti (Integral time constant)
1.69	1.842	0.7605	1.535

Table11.3: PDO alone PI controller parameters

11.5.1.3. Simulation results

The complete developed model of PDO-OETC interconnected power system was simulated with the Fuzzy Logic PID 1 applied to PDO input control signal only. A load disturbance of 100MW was simulated once at PDO side and once at OETC side. PDO frequency, OETC frequency and tie line power are the key performance indices to be monitored. Figures 11.13-11.16 show PDO and OETC frequencies in one figure and the tie line power in a separate figure for both tests respectively.

A summary of the performance values was attempted and is shown in Table 11.4. The summary also compares the results of the base case, classical PID AGC controller, the LQR AGC controller and the Fuzzy PID1 controller performance.

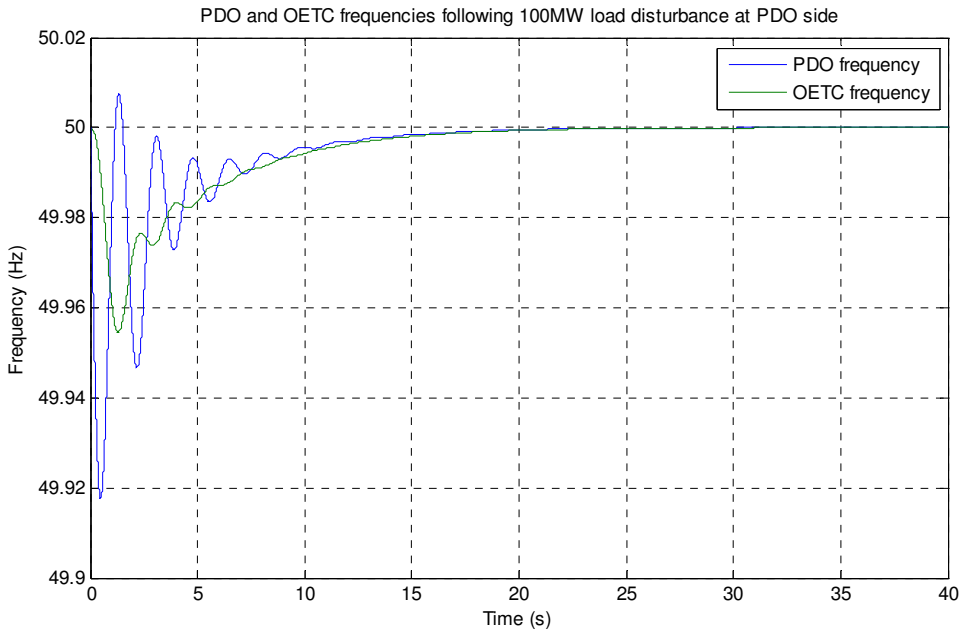

Figure 11.13: PDO and OETC frequencies following a 100MW load disturbance at PDO side with the Fuzzy PID 1 AGC applied at PDO only

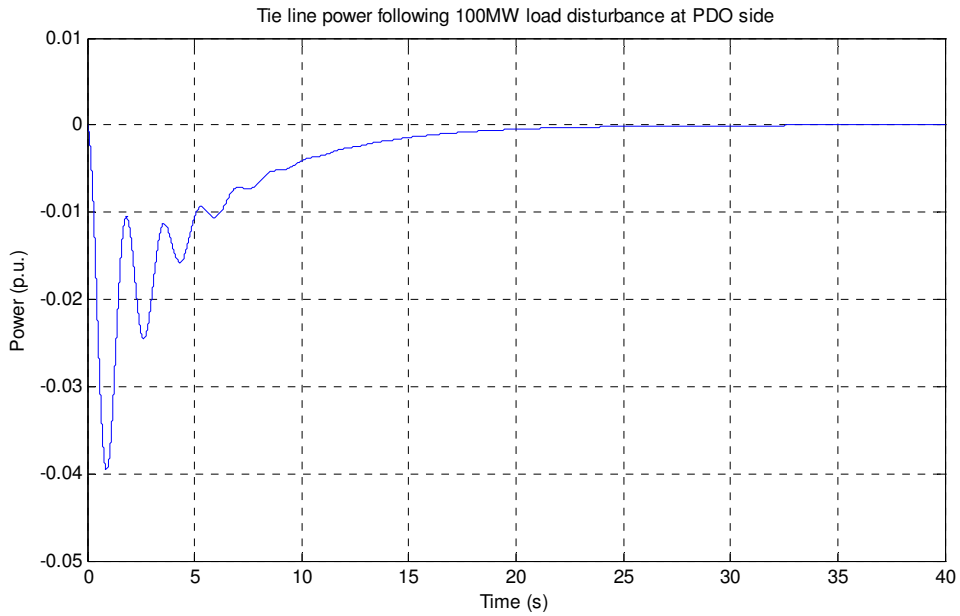

Figure 11.14: Tie line power deviation following a 100MW load disturbance at PDO side with the Fuzzy PID 1 AGC applied at PDO only.

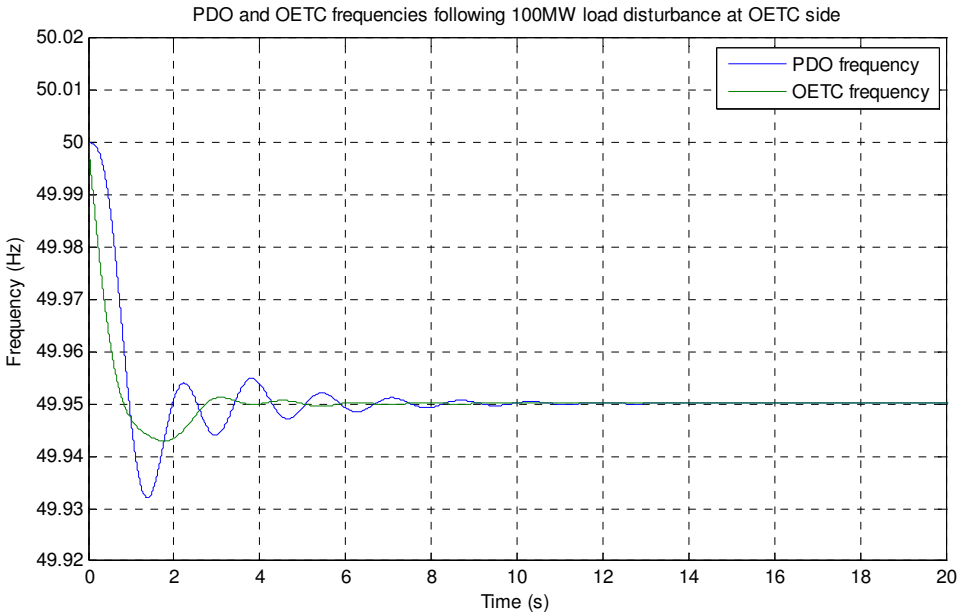

Figure 11.15: PDO and OETC frequencies following a 100MW load disturbance at OETC side with the Fuzzy PID 1 AGC applied at PDO only

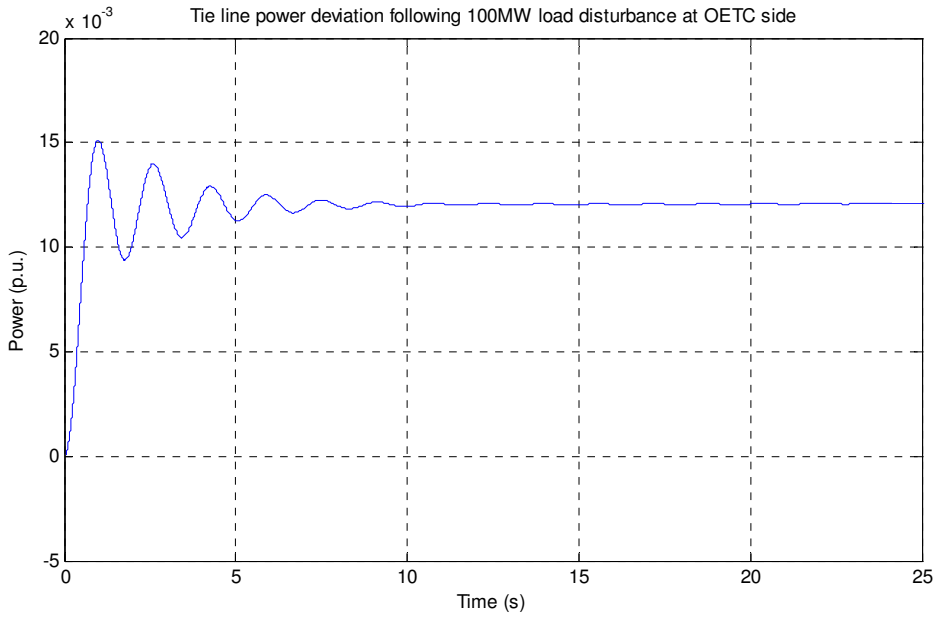

Figure 11.16: Tie line power deviation following a 100MW load disturbance at OETC side with the Fuzzy PID 1 AGC applied at PDO only.

		Base case response	PID controlled response	LQR controlled response	Fuzzy PID 1 controller response
100MW load disturbance at PDO side	Frequency deviation (Hz)	-0.05	0	0	0
	Settling time (s)	10.9	22.6	12.3	15.4
	Tie line power deviation (p.u.)	-0.0379	0	0	0
100MW load disturbance at OETC side	Frequency deviation (Hz)	-0.05	-0.05	-0.05	-0.05
	Settling time (s)	7.74	15.34	5.3	5.68
	Tie line power deviation (p.u.)	0.0121	0.0121	0.0121	0.0121

Table 11.4: PDO alone Fuzzy PID 1 AGC controller performance in comparison to the base case, the classical PID controller and LQR controller.

11.5.1.4. Results discussion

From Figures 11.13-11.16 and Table 11.4, one can see that the Fuzzy PID 1 control technique has obvious merits when compared with the classical PID control technique. However when compared with the LQR, they are almost having the same performance. The following points summarises the impression about the results:

- The Fuzzy PID 1 AGC controller maintained the same control topology characteristics as when using the PID and the LQR controllers. It has dealt with load disturbances within PDO control area only whereas load disturbances outside PDO were compensated by the droop control only. This has resulted in a zero

steady state deviation in system frequency and tie line power when the load disturbance was applied at PDO and non zero values when the load disturbance was applied at OETC side.

- The response oscillations were very well damped if we compare the results obtained in Figures 11.13-11.16 with the same results obtained using the classical PID controller shown earlier in Figures 9.23-9.28. The settling time with the Fuzzy PID 1 AGC controller was also much better than in the case of the classical PID controller. When comparing the Fuzzy Logic PID1 controller performance with the LQR controller performance shown in Figures 10.3-10.6, they almost have the same performance in terms of oscillations and settling time.

11.5.1.5. Summary

The PDO alone Fuzzy PID 1 AGC controller has maintained the same control topology features observed when using the classical PID and LQR controllers. The system response oscillations and settling time were remarkably improved when compared with the PID controller, and are more or less the same when compared with the LQR.

11.5.2. Fuzzy Logic PID 1 applied to OETC alone AGC controller

11.5.2.1. Design approach

The design of the OETC AGC controller using the FLPID1 controller structure is completed in stages. The following approach is followed:

1. Design the Fuzzy logic control system part as shown earlier in section 11.4
2. Design a PI AGC controller for OETC power systems using the closed loop Ultimate Sensitivity Method. During the design and tuning of the PI controller, the uncontrolled complete PDO-OETC model is used without consideration of the fuzzy logic part.
3. Merge the developed Fuzzy logic parts with the respective tuned PI controller so that the controller structure shown in Figure 11.2 is formed.

Using MATLAB Simulink, the Fuzzy Logic PID 1 controller is designed as shown in Figure 11.12.

The complete PDO-OETC power system model with OETC alone Fuzzy PID 1 AGC is the same as shown earlier in Figure 9.43.

11.5.2.2. Controller tuning

The fuzzy logic part parameters will remain the same as developed earlier in section 11.4. The PI part was tuned using Ziegler Nichols (Ultimate sensitivity) method. The look up table shown earlier in Table 9.2 was used to calculate the PI controller parameters. The PI parameters for OETC are shown in Table 11.5.

Ku (ultimate gain)	Pu (ultimate period)	Kc (PI Controller gain)	Ti (Integral time constant)
1.468	1.755	0.6606	1.4625

Table11.5: OETC alone PI controller parameters

11.5.2.3. Simulation results

The complete developed model of PDO-OETC interconnected power system was simulated with the Fuzzy Logic PID 1 applied to OETC input control signal only. A load disturbance of 100MW was simulated once at PDO side and once at OETC side. PDO frequency, OETC frequency and tie line power are the key performance indices to be monitored. Figures 11.17-11.20 show PDO and OETC frequencies in one figure and the tie line power in a separate figure for both tests respectively.

A summary of the performance values was attempted and is shown in Table 11.6. The summary also compares the results of the base case, classical PID AGC controller, the LQR AGC controller and the Fuzzy PID1 controller performance.

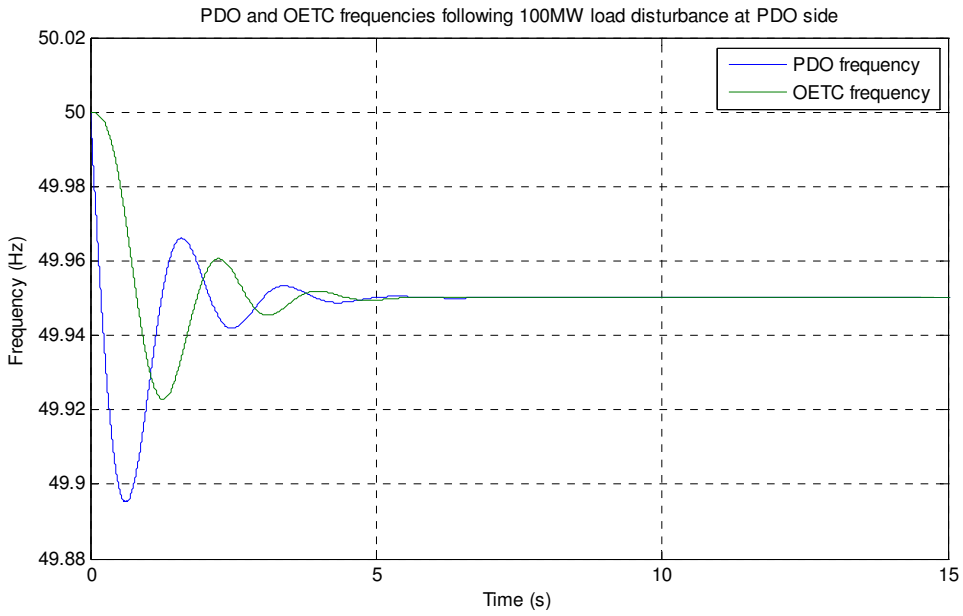

Figure 11.17: PDO and OETC frequencies following a 100MW load disturbance at PDO side with the Fuzzy PID 1 AGC applied at OETC only

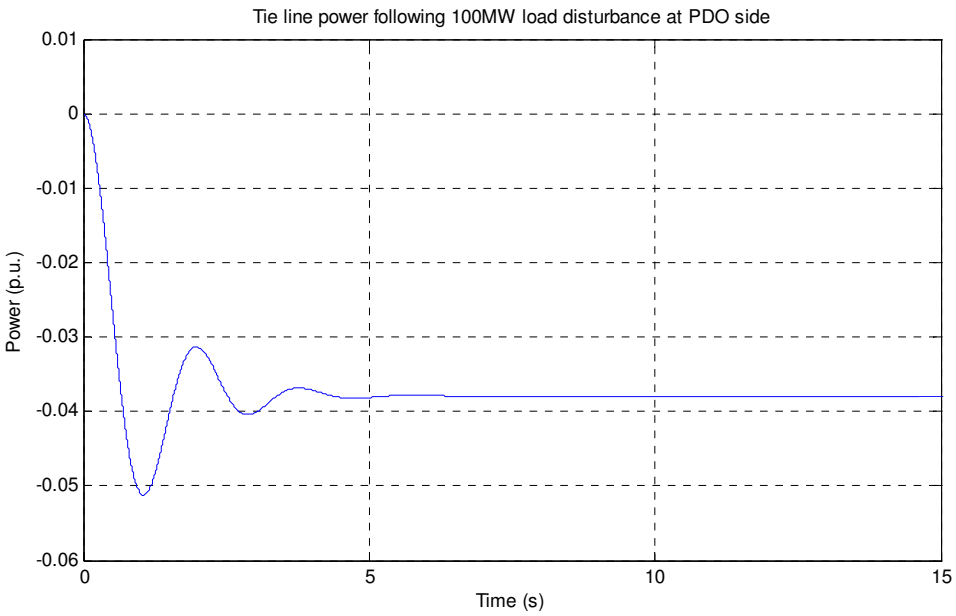

Figure 11.18: Tie line power deviation following a 100MW load disturbance at PDO side with the Fuzzy PID 1 AGC applied at OETC only.

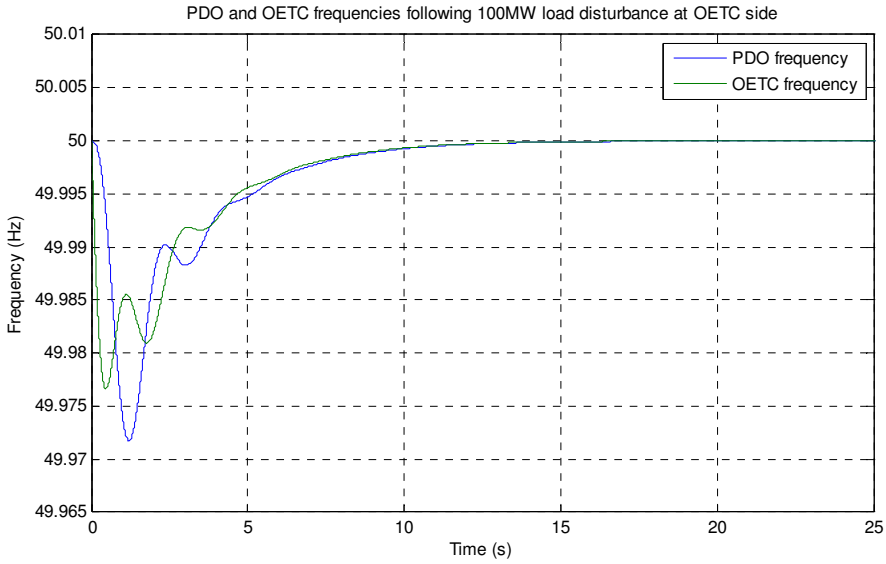

Figure 11.19: PDO and OETC frequencies following a 100MW load disturbance at OETC side with the Fuzzy PID 1 AGC applied at OETC only

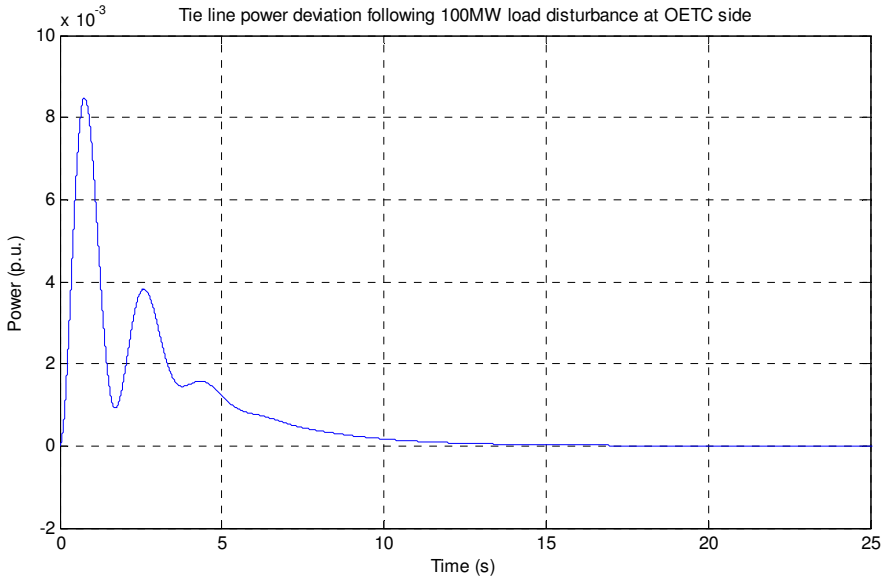

Figure 11.20: Tie line power deviation following a 100MW load disturbance at OETC side with the Fuzzy PID 1 AGC applied at OETC only.

		Base case response	PID controlled response	LQR controlled response	Fuzzy PID 1 controller response
100MW load disturbance at PDO side	Frequency deviation (Hz)	-0.05	-0.05	-0.05	-0.05
	Settling time (s)	10.9	14	8.92	3.75
	Tie line power deviation (p.u.)	-0.0379	-0.0379	-0.0379	-0.0379
100MW load disturbance at OETC side	Frequency deviation (Hz)	-0.05	0	0	0
	Settling time (s)	7.74	10.4	8.16	8.2
	Tie line power deviation (p.u.)	0.0121	0	0	0

Table 11.6: OETC alone Fuzzy PID 1 AGC controller performance in comparison to the base case, the classical PID controller and LQR controller.

11.5.2.4. Results discussion

From Figures 11.17-11.20 and Table 11.6, one can see that the Fuzzy PID 1 control technique has better performance when it is compared with the classical PID control technique and the LQR. The following points summarise the impression about the results:

- The Fuzzy PID 1 AGC controller has maintained the same control topology characteristics as when using the PID and the LQR controllers. It has dealt with load disturbances within OETC control area only whereas load disturbances outside OETC are compensated by the droop control only. It has resulted in a zero steady state deviation in system frequency and tie line power when the load disturbance is applied at OETC and non zero values when the load disturbance is applied at PDO side.

- The response oscillations are very well damped if we compare the results obtained in Figures 11.17-11.20 with the same results obtained using the classical PID controller shown earlier in Figures 9.44-9.49. The settling time with the Fuzzy PID 1 AGC controller is also better than in the case of the classical PID controller. Moreover when it is compared with the LQR controller response shown in Figures 10.8-10.11, the Fuzzy PID 1 has slightly better performance in terms of oscillations and settling time.

11.5.2.5. Summary

The OETC alone Fuzzy PID 1 AGC controller has maintained the same control topology features observed when using the classical PID and LQR controllers. The system response oscillations and settling time are remarkably improved when compared with the PID controller, and are slightly better when compared with the LQR.

11.5.3. Fuzzy Logic topology 1 applied to both PDO and OETC AGC controllers

11.5.3.1. Design approach

The design of the PDO-OETC AGC controller using the FLPID1 controller structure is completed in stages. The following approach is followed:

1. Design the Fuzzy logic control system part as shown earlier in section 11.4
2. Design a PI AGC controller for both PDO and OETC power systems using the closed loop Ultimate Sensitivity Method. OETC PI controller is tuned firstly and then PDO PI is tuned while OETC PI is active. During the design and tuning of the PI controller, the uncontrolled complete PDO-OETC model is used without consideration of the fuzzy logic part.
3. Merge the developed Fuzzy logic parts with the respective tuned PI controller so that the controller structure shown in Figure 11.2 is formed.

Using MATLAB Simulink, the Fuzzy Logic PID 1 controller is designed as shown in Figure 11.12.

The complete PDO-OETC power system model with PDO and OETC Fuzzy PID 1 AGC is the same as shown earlier in Figure 9.106.

11.5.3.2. Controller tuning

The fuzzy logic part parameters remain the same as developed earlier in section 11.4. The PI part was tuned using Ziegler Nichols (Ultimate sensitivity) method. The look up table shown earlier in Table 9.2 was used to calculate the PI controller parameters. The PI parameters for both PDO and OETC are shown in Table 11.7.

	Ku (ultimate gain)	Pu (ultimate period)	Kc (PI Controller gain)	Ti (Integral time constant)
PDO	0.861	1.874	0.38745	1.5617
OETC	1.468	1.755	0.6606	1.4625

Table11.7: PDO and OETC PI controller parameters

11.5.3.3. Simulation results

The complete developed model of PDO-OETC interconnected power system was simulated with the Fuzzy Logic PID 1 applied to both PDO and OETC input control signals. A load disturbance of 100MW was simulated once at PDO side and once at OETC side. PDO frequency, OETC frequency and tie line power are the key performance indices to be monitored. Figures 11.21-11.24 show PDO and OETC frequencies in one figure and the tie line power in a separate figure for both tests respectively.

A summary of the performance values was attempted and is shown in Table 11.8. The summary also compares the results of the base case, classical PID AGC controller, the LQR AGC controller and the Fuzzy PID1 controller performance.

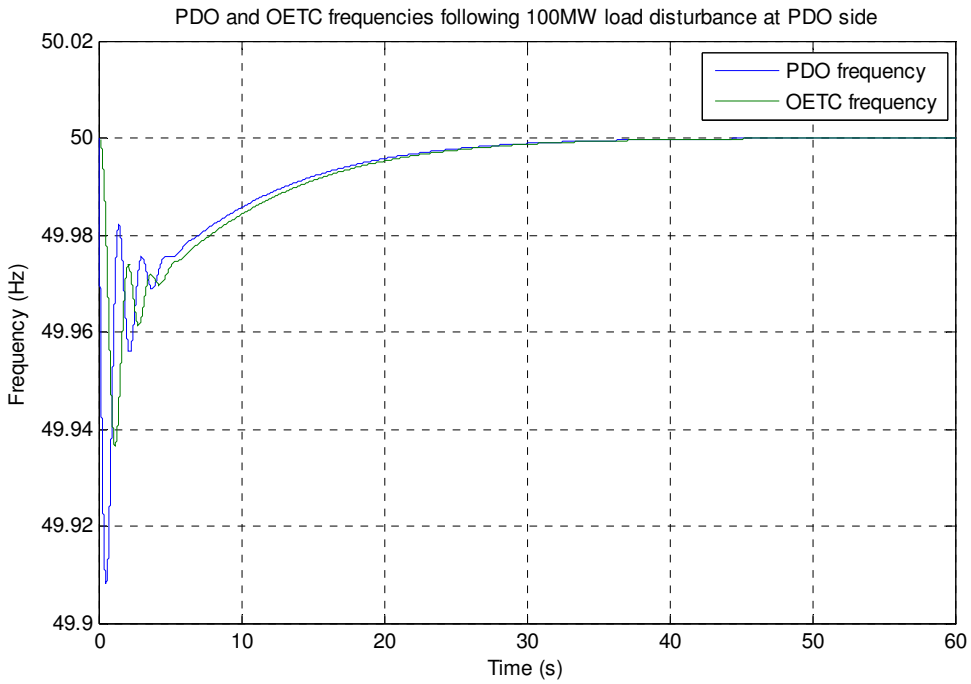

Figure 11.21: PDO and OETC frequencies following a 100MW load disturbance at PDO side with the Fuzzy PID 1 AGC applied at both PDO and OETC

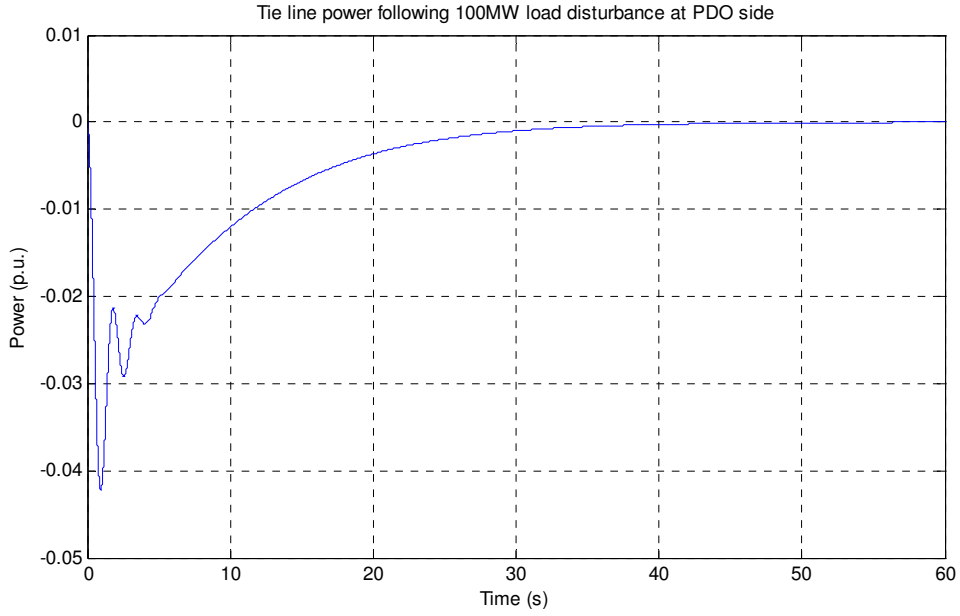

Figure 11.22: Tie line power deviation following a 100MW load disturbance at PDO side with the Fuzzy PID 1 AGC applied at both PDO and OETC.

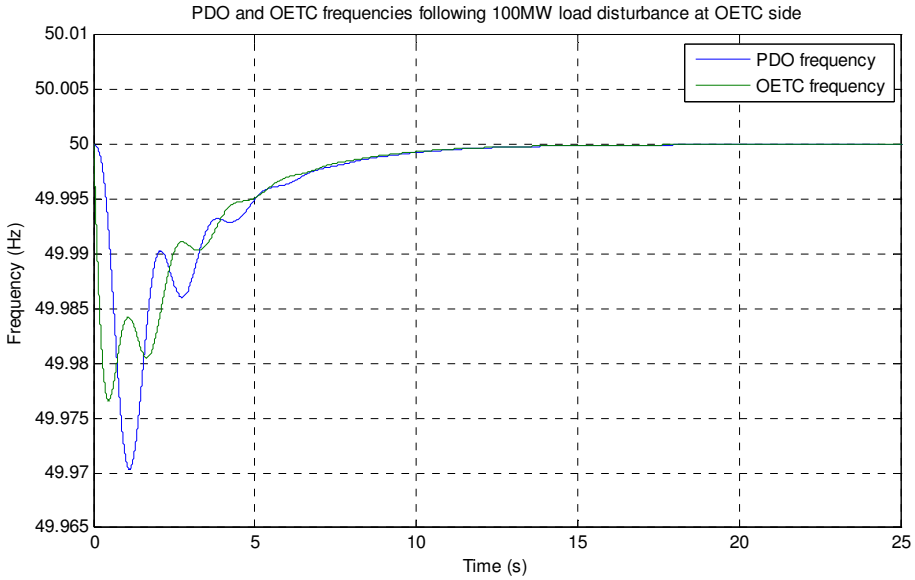

Figure 11.23: PDO and OETC frequencies following a 100MW load disturbance at OETC side with the Fuzzy PID 1 AGC applied at both PDO and OETC.

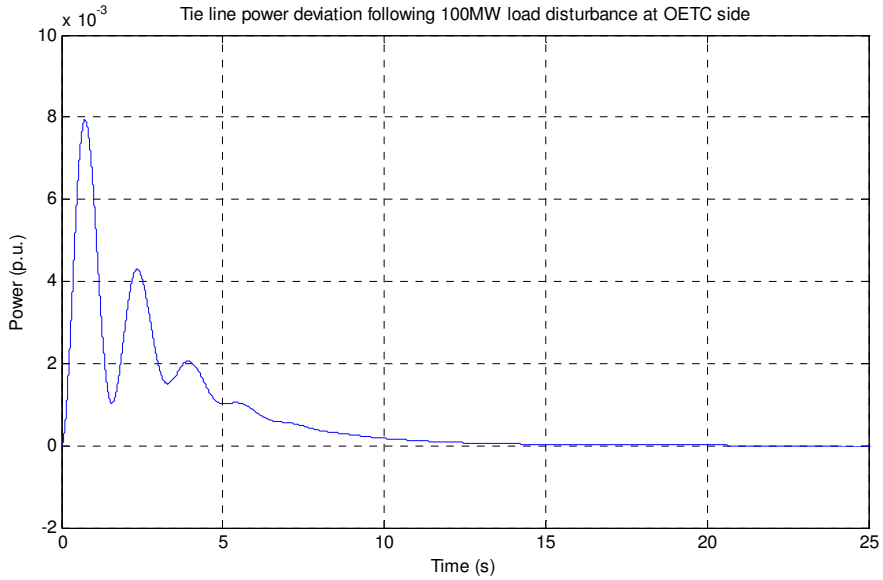

Figure 11.24: Tie line power deviation following a 100MW load disturbance at OETC side with the Fuzzy PID 1 AGC applied at both PDO and OETC.

		Base case response	PID controlled response	LQR controlled response	Fuzzy PID 1 controller response
100MW load disturbance at PDO side	Frequency deviation (Hz)	-0.05	0	0	0
	Settling time (s)	10.9	34	11.3	28.1
	Tie line power deviation (p.u.)	-0.0379	0	0	0
100MW load disturbance at OETC side	Frequency deviation (Hz)	-0.05	0	0	0
	Settling time (s)	7.74	25.3	8.59	8.18
	Tie line power deviation (p.u.)	0.0121	0	0	0

Table 11.8: PDO and OETC Fuzzy PID 1 AGC controllers' performance in comparison to the base case, the classical PID controller and LQR controller.

11.5.3.4. Results discussion

From Figures 11.21-11.24 and Table 11.8, one can see that the Fuzzy PID 1 control technique is better able to damp the system response oscillations than the classical PID control technique. In this case the LQR controller response is better than the Fuzzy PID1. The following points summarise the impression about the results:

- The Fuzzy PID 1 AGC controller has maintained the same control topology characteristics as when using the PID and the LQR controllers. It has dealt with the disturbances within both PDO and OETC control areas. It has resulted in a zero steady state deviation in the system frequency and the tie line power no matter whether the load disturbance is applied at PDO or at OETC.
- The response oscillations are better damped if we compare the results obtained in Figures 11.21-11.24 with the same results obtained using the classical PID controller shown earlier in Figures 9.107-9.112. Therefore the settling time with the Fuzzy PID 1 AGC controller is shorter than in the case of the classical PID controller. However, when it is compared with the LQR controller response shown in Figures 10.13-10.16, the LQR has a better performance in terms of oscillations and settling time.

11.5.3.5. Summary

The PDO and OETC Fuzzy PID 1 AGC controllers has maintained the same control topology features observed when using the classical PID and LQR controllers. The LQR system response oscillations and settling time are seen to be better when compared with the Fuzzy PID 1 controller.

11.6. Fuzzy logic PID 2

11.6.1. Fuzzy Logic PID topology 2 applied to PDO alone AGC controller

11.6.1.1. Design approach

This part demonstrates the performance of the controller structure shown in Figure 11.3. The design of the PDO AGC controller using this controller structure is completed in stages. The following approach is followed:

1. Design the Fuzzy logic control system part as shown earlier in section 11.4
2. Design a PID AGC controller for PDO power systems using the closed loop Ultimate Sensitivity Method. During the design and tuning of the PID controller, the uncontrolled complete PDO-OETC model is used without consideration of the fuzzy logic part.
3. Merge the developed Fuzzy logic parts with the respective tuned PID controller so that the controller structure shown in Figure 11.3 is formed.

Using MATLAB Simulink, the Fuzzy Logic PID 2 controller is designed as shown in Figure 11.25.

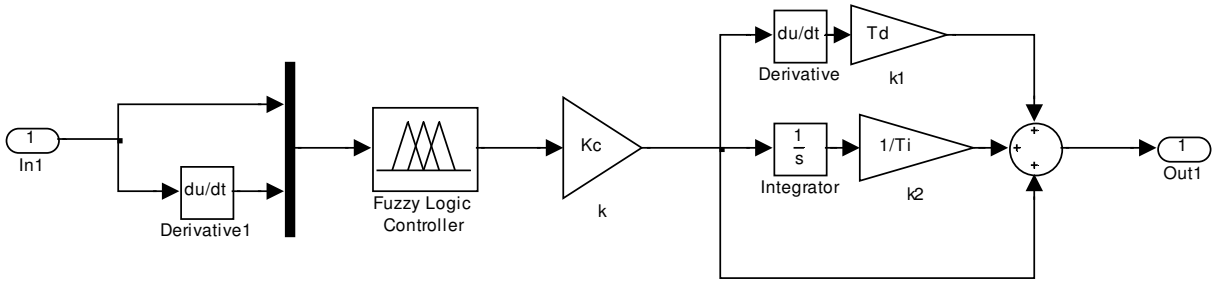

Figure 11.25: Fuzzy Logic PID 2 controller design

The complete PDO-OETC power system model with PDO alone Fuzzy PID 2 AGC will look the same as shown earlier in Figure 9.22.

11.6.1.2. Controller tuning

The fuzzy logic part parameters remain the same as developed earlier in section 11.4. The PID part was tuned using Ziegler Nichols (Ultimate sensitivity) method. The look up table shown earlier in Table 9.2 was used to calculate the PID controller parameters. The PID parameters for PDO are shown in Table 11.9.

Ku (ultimate gain)	Pu (ultimate period)	Kc (PID Controller gain)	Ti (Integral time constant)	Td (derivative time constant)
1.69	1.842	1.014	0.921	0.23025

Table11.9: PDO alone PID controller parameters

11.6.1.3. Simulation results

The complete developed model of PDO-OETC interconnected power system was simulated with the Fuzzy Logic PID 2 applied to PDO input control signal only. A load disturbance of 100MW was simulated once at PDO side and once at OETC side. PDO frequency, OETC frequency and tie line power are the key performance indices to be monitored. Figures 11.26-11.29 show PDO and OETC frequencies in one figure and the tie line power in a separate figure for both tests respectively.

A summary of the performance values was attempted and is shown in Table 11.10. The summary also compares the results of the base case, classical PID AGC controller, the LQR AGC controller, Fuzzy PID 1 controller with the Fuzzy PID 2 controller performance.

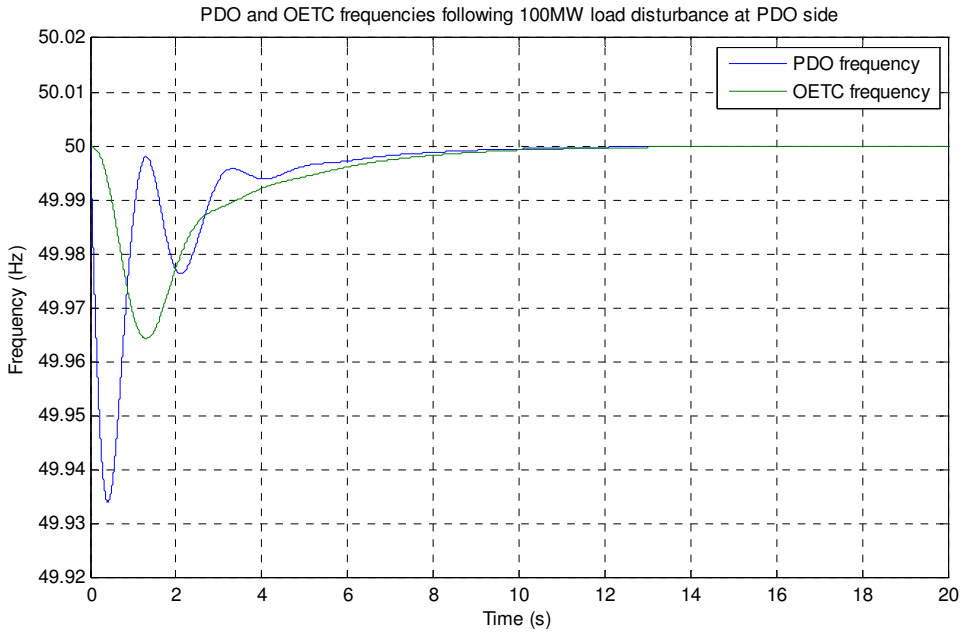

Figure 11.26: PDO and OETC frequencies following a 100MW load disturbance at PDO side with the Fuzzy PID 2 AGC applied at PDO only

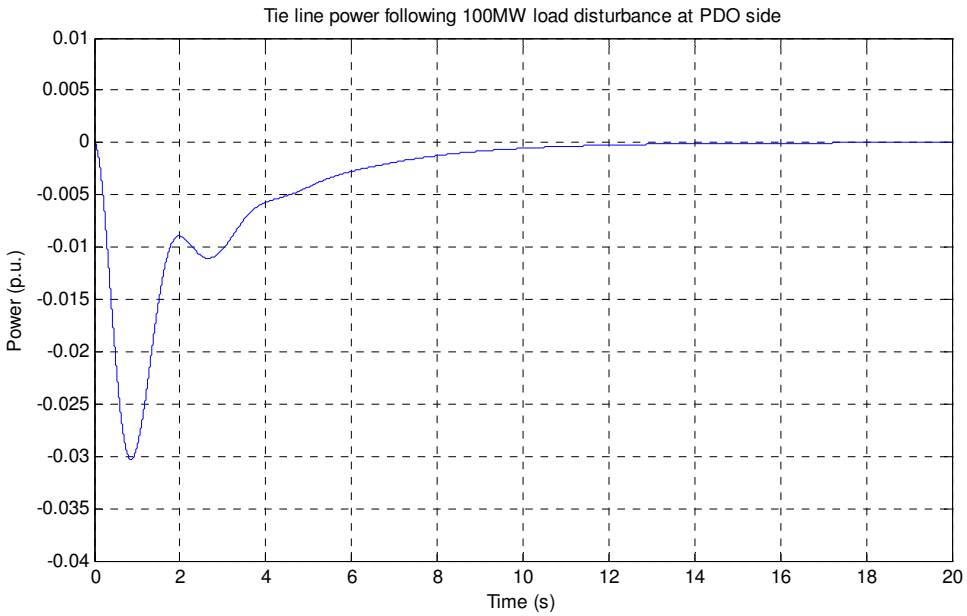

Figure 11.27: Tie line power deviation following a 100MW load disturbance at PDO side with the Fuzzy PID 2 AGC applied at PDO only.

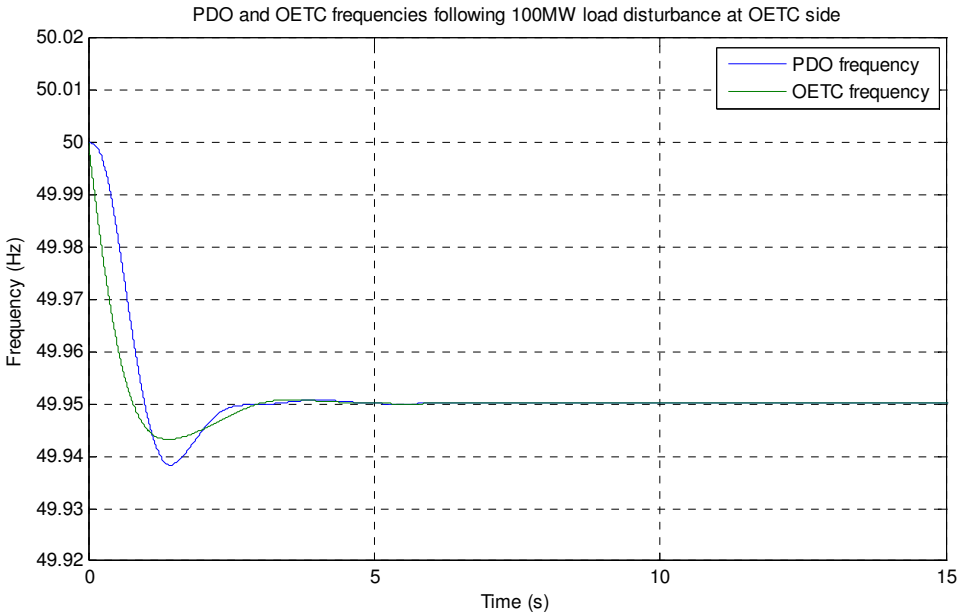

Figure 11.28: PDO and OETC frequencies following a 100MW load disturbance at OETC side with the Fuzzy PID 2 AGC applied at PDO only

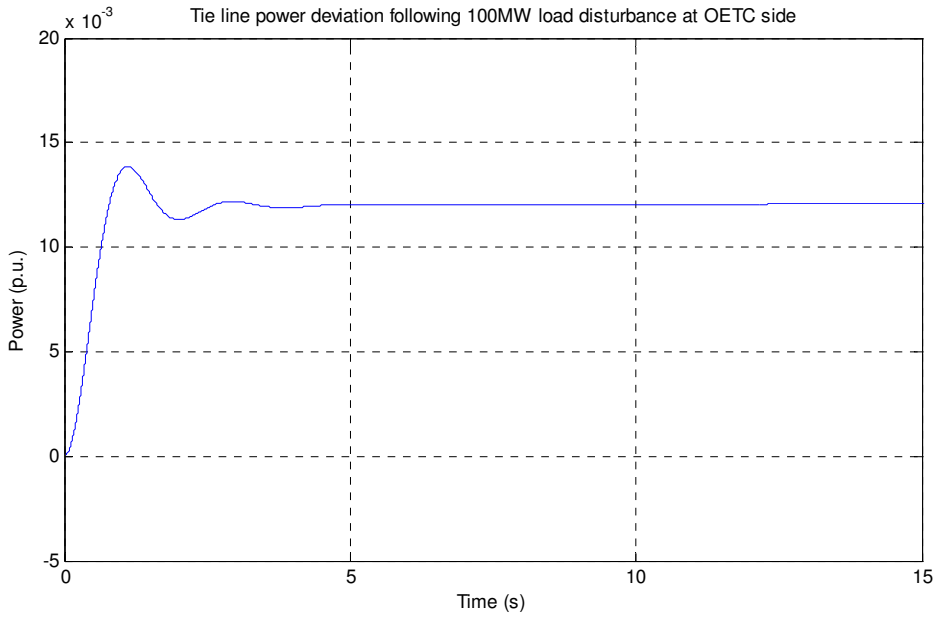

Figure 11.29: Tie line power deviation following a 100MW load disturbance at OETC side with the Fuzzy PID 2 AGC applied at PDO only.

		Base case response	PID controlled response	LQR controlled response	Fuzzy PID 1 controlled response	Fuzzy PID 2 controlled response
100MW load disturbance at PDO side	Frequency deviation (Hz)	-0.05	0	0	0	0
	Settling time (s)	10.9	22.6	12.3	15.4	7.36
	Tie line power deviation (p.u.)	-0.0379	0	0	0	0
100MW load disturbance at OETC side	Frequency deviation (Hz)	-0.05	-0.05	-0.05	-0.05	-0.05
	Settling time (s)	7.74	15.34	5.3	5.68	2.33
	Tie line power deviation (p.u.)	0.0121	0.0121	0.0121	0.0121	0.0121

Table 11.10: PDO alone Fuzzy PID 2 AGC controller performance in comparison to the base case, the classical PID controller, LQR controller and Fuzzy PID 1 controller.

11.6.1.4. Results discussion

From Figures 11.26-11.29 and Table 11.10, one can see that the Fuzzy PID 2 control technique has remarkably improved the system response to load disturbances when compared with the base case, PID controller case, LQR controller case and Fuzzy PID 1 controller case. The following points summarises the impression about the results:

- The Fuzzy PID 2 AGC controller has maintained the same control topology characteristics as when using the PID, the LQR and the Fuzzy PID 1 controllers. It has dealt with load disturbances within PDO control area whereas load disturbances outside PDO are compensated by the droop control only. It has resulted in a zero steady state deviation in system frequency and tie line power when the load disturbance is applied at PDO and non zero values when the load disturbance is applied at OETC side.

- The response oscillations are very well damped if we compare the results obtained in Figures 11.26-11.29 with the same results obtained using the classical PID controller (Figures 9.23-9.28), the LQR controller (Figures 10.3-10.6) and the Fuzzy PID 1 (Figures 11.13-11.16). As a result the settling time and maximum transient errors are reduced.

11.6.1.5. Summary

The PDO alone Fuzzy PID 2 AGC controller has maintained the same control topology features observed when using the classical PID, LQR and Fuzzy PID 1 controllers. However the Fuzzy PID 2 has remarkably improved the system response to load disturbances in terms of oscillations, settling time and maximum transient errors. Considering the design flexibility and the quality of performance, the Fuzzy PID 2 is a promising option for AGC application.

11.6.2. Fuzzy Logic PID 2 applied to OETC alone AGC controller

11.6.2.1. Design approach

The design of the OETC AGC controller using this controller structure is completed in stages. The following approach is followed:

1. Design the Fuzzy logic control system part as shown earlier in section 11.4
2. Design a PID AGC controller for OETC power system using the closed loop Ultimate Sensitivity Method. During the design and tuning of the PID controller, the uncontrolled complete PDO-OETC model is used without consideration of the fuzzy logic part.
3. Merge the developed Fuzzy logic parts with the respective tuned PID controller so that the controller structure shown in Figure 11.3 is formed.

Using MATLAB Simulink, the Fuzzy Logic PID 2 controller is designed as shown in Figure 11.25.

The complete PDO-OETC power system model with OETC alone Fuzzy PID 2 AGC will look the same as shown earlier in Figure 9.43.

11.6.2.2. Controller tuning

The fuzzy logic part parameters remain the same as developed earlier in section 11.4. The PI part was tuned using Ziegler Nichols (Ultimate sensitivity) method. The look up table

shown earlier in Table 9.2 was used to calculate the PID controller parameters. The PID parameters for OETC are shown in Table 11.11.

Ku (ultimate gain)	Pu (ultimate period)	Kc (PID Controller gain)	Ti (Integral time constant)	Td (derivative time constant)
1.468	1.755	0.8808	0.8775	0.219375

Table11.11: OETC alone PID controller parameters

11.6.2.3. Simulation results

The complete developed model of PDO-OETC interconnected power system was simulated with the Fuzzy Logic PID 2 applied to OETC input control signal only. A load disturbance of 100MW was simulated once at PDO side and once at OETC side. PDO frequency, OETC frequency and tie line power are the key performance indices to be monitored. Figures 11.30-11.33 show PDO and OETC frequencies in one figure and the tie line power in a separate figure for both tests respectively.

A summary of the performance values was attempted and is shown in Table 11.12. The summary also compares the results of the base case, classical PID AGC controller, the LQR AGC controller, the Fuzzy PID 1 AGC controller with the Fuzzy PID2 controller performance.

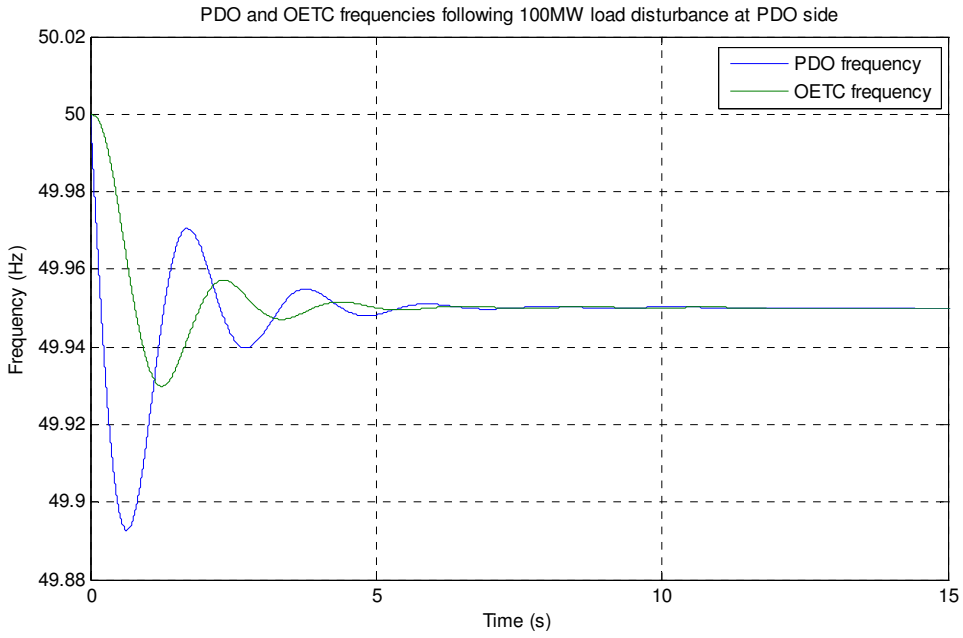

Figure 11.30: PDO and OETC frequencies following a 100MW load disturbance at PDO side with the Fuzzy PID 2 AGC applied at OETC only

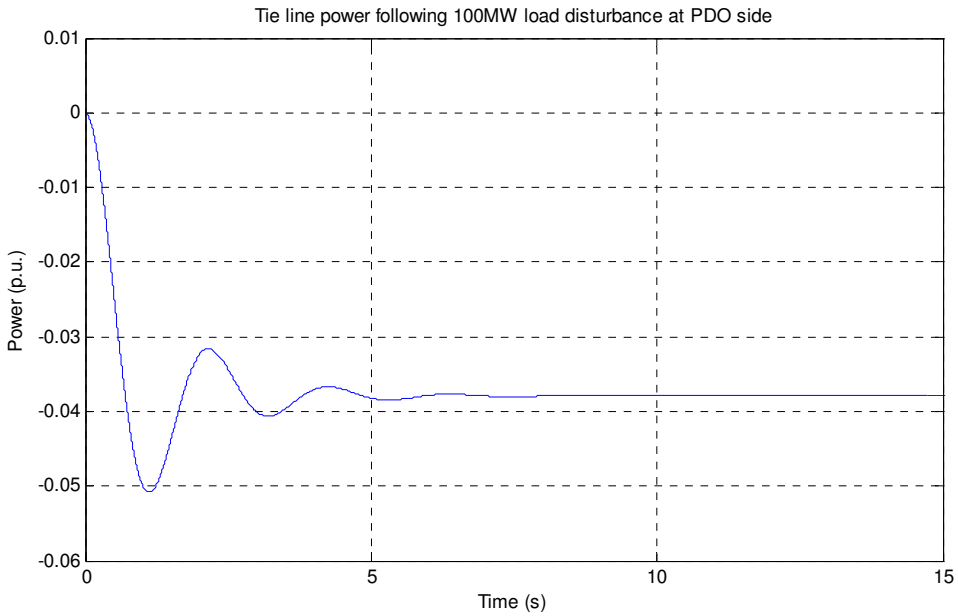

Figure 11.31: Tie line power deviation following a 100MW load disturbance at PDO side with the Fuzzy PID 2 AGC applied at OETC only.

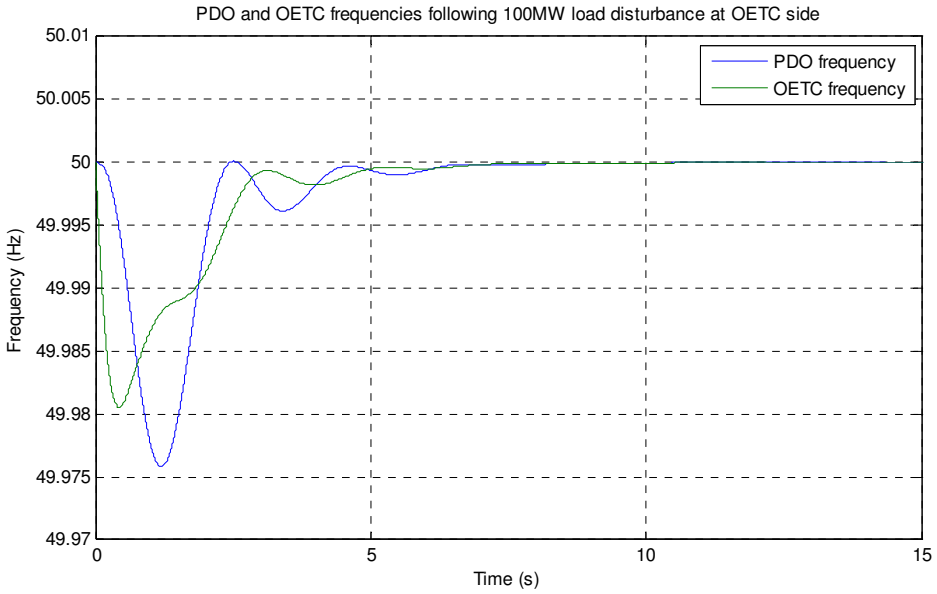

Figure 11.32: PDO and OETC frequencies following a 100MW load disturbance at OETC side with the Fuzzy PID 2 AGC applied at OETC only

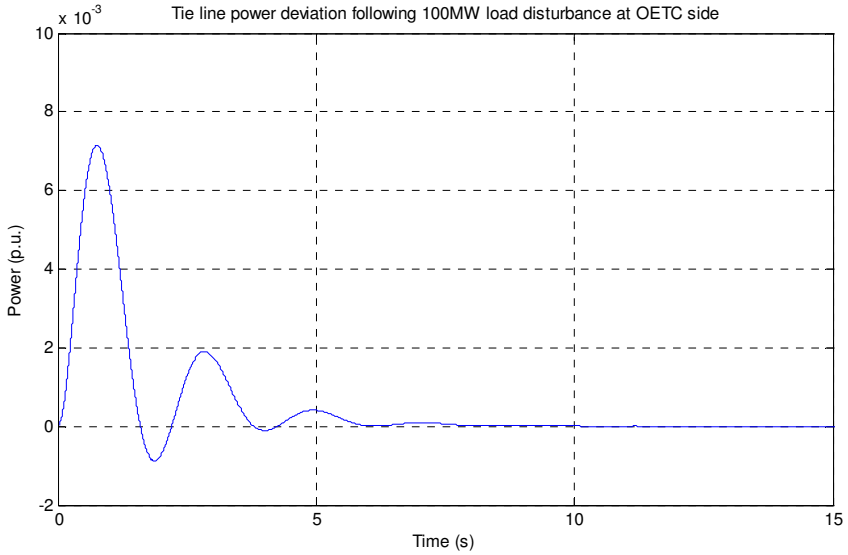

Figure 11.33: Tie line power deviation following a 100MW load disturbance at OETC side with the Fuzzy PID 2 AGC applied at OETC only.

		Base case response	PID controlled response	LQR controlled response	Fuzzy PID 1 controlled response	Fuzzy PID 2 controlled response
100MW load disturbance at PDO side	Frequency deviation (Hz)	-0.05	-0.05	-0.05	-0.05	-0.05
	Settling time (s)	10.9	14	8.92	3.75	5.07
	Tie line power deviation (p.u.)	-0.0379	-0.0379	-0.0379	-0.0379	-0.0379
100MW load disturbance at OETC side	Frequency deviation (Hz)	-0.05	0	0	0	0
	Settling time (s)	7.74	10.4	8.16	8.2	4.08
	Tie line power deviation (p.u.)	0.0121	0	0	0	0

Table 11.12: OETC alone Fuzzy PID 1 AGC controller performance in comparison to the base case, the classical PID controller and LQR controller.

11.6.2.4. Results discussion

From Figures 11.30-11.33 and Table 11.12, one can see that the Fuzzy PID 2 control technique has generally improved the system response to load disturbances when it is compared with the base case, PID controller case, LQR controller case and Fuzzy PID 1 controller case. The following points summarise the impression about the results:

- The Fuzzy PID 2 AGC controller has maintained the same control topology characteristics as when using the PID, the LQR and the Fuzzy PID 1 controllers. It has dealt with load disturbances within OETC control area whereas load disturbances outside OETC are compensated by the droop control only. It has resulted in a zero steady state deviation in system frequency and tie line power when the load disturbance is applied at OETC and non zero values when the load disturbance is applied at PDO side.
- The response oscillations are very well damped if we compare the results obtained in Figures 11.30-11.33 with the same results obtained using the classical PID

controller (Figures 9.44-9.49) and the LQR controller (Figures 10.8-10.11). As a result the settling time and maximum transient errors are also reduced. However, when comparing the results with the ones obtained using Fuzzy PID 1 (Figures 11.17-11.20), the response of Fuzzy PID 2 is generally better except in the case when the load disturbances is applied at PDO where longer settling time is noticed. Overall, the performance of the Fuzzy PID 2 controller can still be considered better than the performance of the Fuzzy PID1 controller.

11.6.2.5. Summary

The OETC alone Fuzzy PID 2 AGC controller has maintained the same control topology features observed when using the classical PID, LQR and Fuzzy PID 1 controllers. The Fuzzy PID 2 has generally improved the system response to load disturbances.

11.6.3. Fuzzy Logic topology 2 applied to both PDO and OETC AGC controllers

11.6.3.1. Design approach

The design of the PDO-OETC AGC controller using this controller structure is completed in stages. The following approach is followed:

1. Design the Fuzzy logic control system part as shown earlier in section 11.4
2. Design a PID AGC controller for both PDO and OETC power systems using the closed loop Ultimate Sensitivity Method. OETC PID controller is tuned firstly and then PDO PID is tuned while OETC PID is active. During the design and tuning of the PID controller, the uncontrolled complete PDO-OETC model is used without consideration of the fuzzy logic part.
3. Merge the developed Fuzzy logic parts with the respective tuned PID controller so that the controller structure shown in Figure 11.3 is formed.

Using MATLAB Simulink, the Fuzzy Logic PID 2 controller is designed as shown in Figure 11.25.

The complete PDO-OETC power system model with OETC alone Fuzzy PID 1 AGC will look like the one shown earlier in Figure 9.106.

11.6.3.2. Controller tuning

The fuzzy logic part parameters will remain the same as developed earlier in section 11.4. The PID part was tuned using Ziegler Nichols (Ultimate sensitivity) method. The look up

table shown earlier in Table 9.2 was used to calculate the PID controller parameters. The PID parameters for both PDO and OETC are shown in Table 11.13.

	Ku (ultimate gain)	Pu (ultimate period)	Kc (PID Controller gain)	Ti (Integral time constant)	Td (derivative time constant)
PDO	1.375	1.73	0.825	0.865	0.21625
OETC	1.468	1.755	0.8808	0.8775	0.219375

Table11.13: PDO and OETC PID controller parameters

11.6.3.3. Simulation results

The complete developed model of PDO-OETC interconnected power system was simulated with this Fuzzy Logic PID 2 applied to both PDO and OETC input control signals. A load disturbance of 100MW was simulated once at PDO side and once at OETC side. PDO frequency, OETC frequency and tie line power are the key performance indices to be monitored. Figures 11.34-11.37 show PDO and OETC frequencies in one figure and the tie line power in a separate figure for both tests respectively.

A summary of the performance values was attempted and is shown in Table 11.14. The summary also compares the results of the base case, classical PID AGC controller, the LQR AGC controller, the Fuzzy PID1 AGC controller with the Fuzzy PID 2 AGC controller performance.

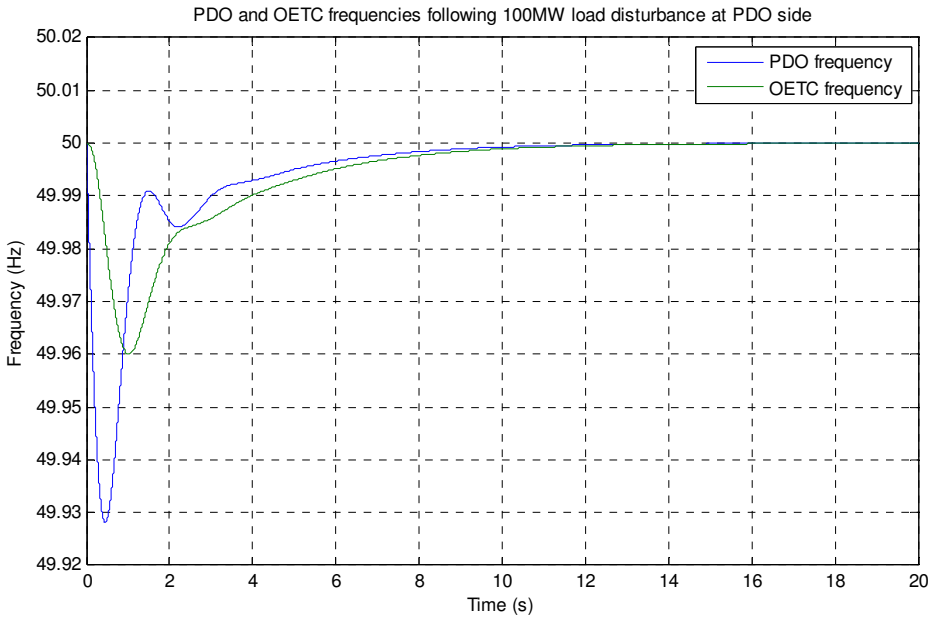

Figure 11.34: PDO and OETC frequencies following a 100MW load disturbance at PDO side with the Fuzzy PID 2 AGC applied at both PDO and OETC

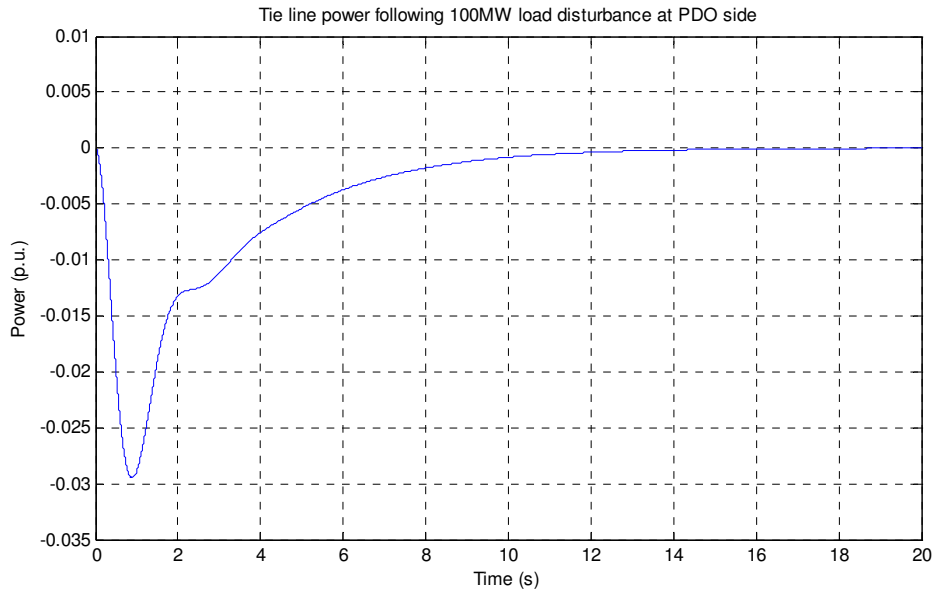

Figure 11.35: Tie line power deviation following a 100MW load disturbance at PDO side with the Fuzzy PID 2 AGC applied at both PDO and OETC.

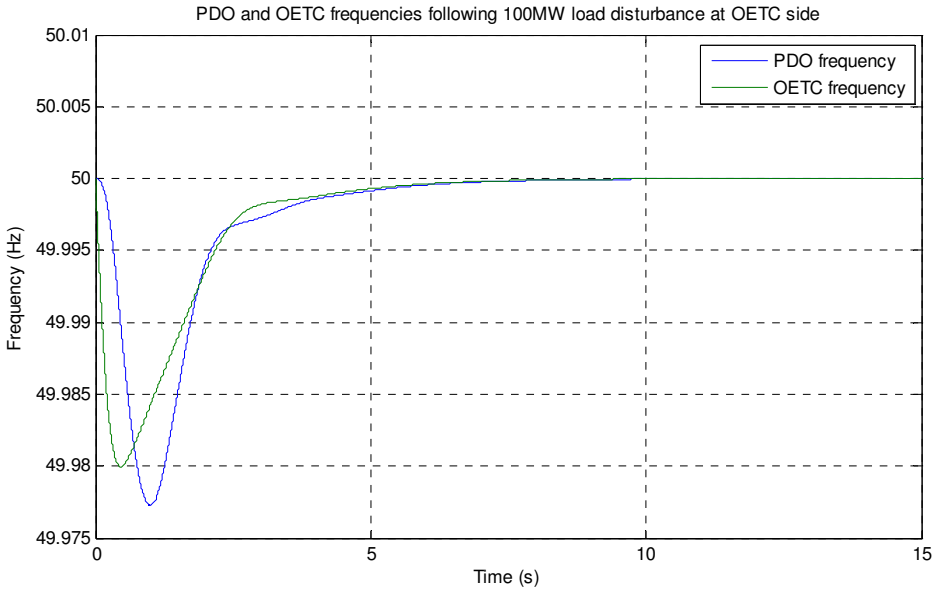

Figure 11.36: PDO and OETC frequencies following a 100MW load disturbance at OETC side with the Fuzzy PID 2 AGC applied at both PDO and OETC.

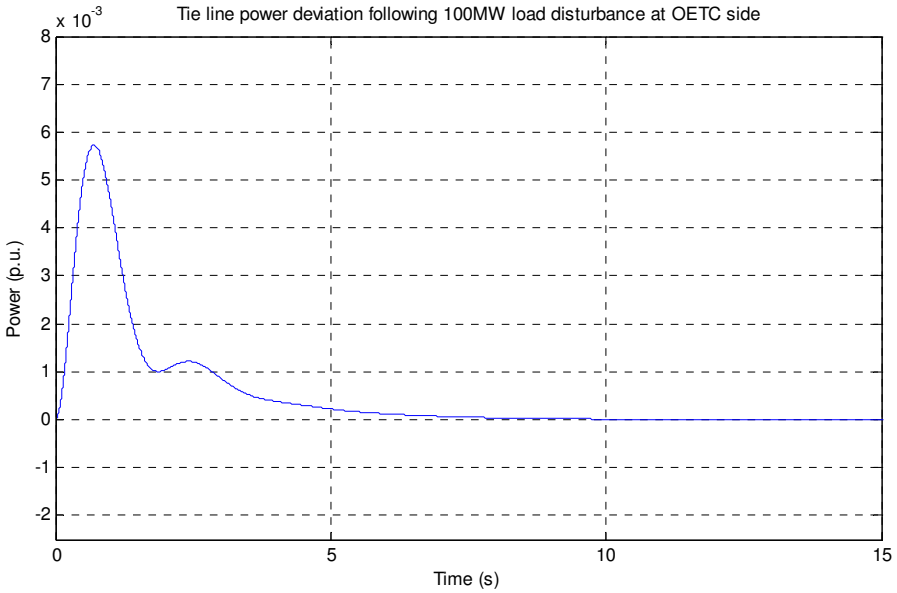

Figure 11.37: Tie line power deviation following a 100MW load disturbance at OETC side with the Fuzzy PID 2 AGC applied at both PDO and OETC.

		Base case response	PID controlled response	LQR controlled response	Fuzzy PID 1 controlled response	Fuzzy PID 2 controlled response
100MW load disturbance at PDO side	Frequency deviation (Hz)	-0.05	0	0	0	0
	Settling time (s)	10.9	34	11.3	28.1	8.17
	Tie line power deviation (p.u.)	-0.0379	0	0	0	0
100MW load disturbance at OETC side	Frequency deviation (Hz)	-0.05	0	0	0	0
	Settling time (s)	7.74	25.3	8.59	8.18	3.92
	Tie line power deviation (p.u.)	0.0121	0	0	0	0

Table 11.14: PDO and OETC Fuzzy PID 2 AGC controllers' performance in comparison to the base case, the classical PID controller, LQR controller and the Fuzzy PID1 controller.

11.6.3.4. Results discussion

From Figures 11.34-11.37 and Table 11.14, one can see that the Fuzzy PID 2 controller technique is better able to damp the system response oscillations than the classical PID controller, the LQR controller and the Fuzzy PID 1 controller. The settling time and the maximum transient error are remarkably reduced. The following points summarise the impression about the results:

- The Fuzzy PID 2 AGC controller has maintained the same control topology characteristics as when using the PID, the LQR and the Fuzzy PID 1 controllers. It has dealt with load disturbances within both PDO and OETC control areas. It has

resulted in a zero steady state deviation in system frequency and tie line power no matter whether the load disturbance is applied at PDO or OETC areas.

- The response oscillations are better damped if we compare the results obtained in Figures 11.34-11.37 with the same results obtained using the classical PID controller (Figures 9.107-9.112), the LQR controller (Figures 10.13-10.16) and the Fuzzy PID 1 (Figures 11.21-11.24). As a result, the settling time and maximum transient error are reduced.

11.6.3.5. Summary

The PDO and OETC Fuzzy PID 2 AGC controllers has maintained the same control topology features observed when using the classical PID, LQR and the Fuzzy PID1 controllers. Considering the good performance of this controller, it can be considered as a potential candidate for practical AGC application.

11.7. Overall discussion

Fuzzy logic controllers alone or hybrid with other control techniques have emerged in almost all kinds of industrial applications. In this part of the study, the Fuzzy PID controllers were applied for the AGC of PDO-OETC interconnected power systems. A basic unique design approach was followed to accomplish the Fuzzy PID controller structure. Without further tuning, the Fuzzy PID controllers are able to perform very well in comparison with the classical PID and the LQR controllers. Further tuning can be attempted to obtain the optimum goals of the individual costumer.

11.8. Summary

Two Fuzzy PID AGC controllers were tried for the PDO-OETC AGC application. The second proposed Fuzzy PID (section 11.5) proves to be more effective than the first proposed Fuzzy PID (section 11.4). However both controllers have produced competing results in comparison with classical PID and Basic LQR controllers. This concludes that the Fuzzy PID controllers are one of the potential options for the AGC applications.

Chapter 12: PDO-OETC AGC controller optimisation

12.1. Introduction

PDO-OETC AGC controller optimisation is about getting the best performance of the controller without changing the controller structure. It is achieved by optimising the controller parameters to achieve certain control performance requirements stipulated by the customer.

In chapter 10, Linear Quadratic Regulator AGC has been proved to be costly for practical application due to the significant number of states feedback requirement. Alternatively, a hybrid Fuzzy Logic PID AGC has been proposed in chapter 11 and proved to be very efficient. The hybrid FLPID2 has performed better than the hybrid FLPID1 therefore the FLPID2 is selected for further optimisation in this chapter.

The FLPID2 AGC controllers parameters will be optimised based the set of AGC control requirements stipulated in section 10.3.2. Recalling those AGC control requirements, they are as follows:

1. The static frequency deviation following a step-load change must be zero.
2. The static change in tie-line power following a step-load change must be zero.
3. Minimise time error represented by the integral of frequency deviation
4. Minimise the wear and tear on governor and turbine equipments
5. Minimise the CO2 emissions by reducing the amount of burnt fuel

A range of optimisation techniques has been evaluated for optimizing PDO-OETC FLPID2 AGC controller. Multidimensional unconstrained nonlinear minimization (fminsearch) function, Genetic Algorithm and Particle Swarm optimisation techniques have been evaluated. The selection criterion is to consider a basic optimisation technique and an advanced optimisation technique. Therefore Multidimensional unconstrained nonlinear minimization (fminsearch) function is selected as the basic optimisation technique. Shayeghi et al [4] (2009) reported that Particle Swarm Optimisation is much faster than Genetic Algorithm. Therefore Particle Swarm Optimisation has been considered as the advanced technique.

The Multidimensional unconstrained nonlinear minimization (fminsearch) function and the Particle Swarm optimisation techniques will be used to optimize the FLPID2 parameters based on the set of the AGC control requirements mentioned earlier. For simplicity, only

one control topology will be studied which is when both PDO and OETC are using Area Control Error (ACE) as AGC feedback signal.

The system response with the optimized controllers will be compared and discussed at the end of this chapter. The comparison will focus on the performance of the controllers in light of the above five AGC control requirements. It will include the steady state deviation, settling time and the integral of controller effort. The integral of controller effort is new in the comparison if it is compared with the previous chapters of this report. The integral of controller effort measures the relative energy used over a finite period of time and is a trade off between faster settling time and higher fuel consumption and maintenance cost. The integral of controller effort is calculated by integrating the AGC controller output over certain period of time. For fair comparison between the different optimized Integral of controllers' efforts, the time taken by the frequency to settle is used for calculating the Integral of controller effort.

A common cost function is developed and used for both fminsearch and Particle Swarm Optimisation techniques.

12.2. Optimization of PDO-OETC AGC controller using Multidimensional unconstrained nonlinear minimization (fminsearch) function

12.2.1. Introduction

In a very similar way as in section 7.6 of this report, the MATLAB built in fminsearch minimization technique will be used to optimize the Fuzzy logic PID 2 controller parameters. The fminsearch will be tasked to minimise a certain cost function which comprise selected model outputs by changing a pre-defined controller parameters. The fminsearch will start with initial parameters values and will return the final parameters values which have produced the minimum cost function value. Three different scenarios of initial parameters have been used in order to test the effectiveness of fminsearch technique and to see if it can be trapped in a local minimal. The best result out of three scenarios will be compared with the Particle swarm optimized controller

Revisiting the assumption made in section 11.4 which states that the input scaling factors to the fuzzy logic part are assumed to be unity. In this part, the Fuzzy logic input scaling factors will be optimized as well as the PID part parameters.

Two of the initial parameters scenarios are selected randomly and the third scenario is based on the FLPID2 parameters developed earlier in the last chapter. All three scenarios are listed below:

1. All FLPID2 input scaling factors and PID parameters for both PDO and OETC AGC controllers equal to 0.5
2. All FLPID2 input scaling factors and PID parameters for both PDO and OETC AGC controllers equal to 1
3. The initial parameters values will be the same as developed earlier in section 11.6.3 which are as shown below:

   PDO AGC controller:

   ACE input scaling factor (k1) = 1

   Rate of Change of ACE input scaling factor (k2) = 1

   PID gain (Kcpdo) = 0.825

   PID integral time constant (Tipdo) = 0.865

   PID differential time constant (Tdpdo) =0.21625

   OETC AGC controller:

   ACE input scaling factor (k3) = 1

   Rate of Change of ACE input scaling factor (k4) = 1

   PID gain (Kcoetc) =0.8808

   PID integral time constant (Tioetc) = 0.8775

   PID differential time constant (Tdoetc) = 0.219375

In this controller performance optimisation process, the five AGC guidelines mentioned earlier will be followed. Minimising the following values will ensure the optimum controller performance:

- Minimise the Integral of the Absolute Error multiplied by Time (IAET) and the Absolute Error multiplied by Time (AET) of PDO frequency. It will satisfy guideline 1 & 3.
- Minimise the Integral of the Absolute Error multiplied by Time (IAET) and the Absolute Error multiplied by Time (AET) of OETC frequency. It will satisfy guideline 1 & 3.
- Minimise the Integral of the Absolute Error multiplied by Time (IAET) and the Absolute Error multiplied by Time (AET) of the tie line power. It will satisfy guideline 2.

- Minimise the Integral of the Absolute Error multiplied by Time (IAET) and the Absolute Error multiplied by Time (AET) of PDO AGC controller output. It will satisfy guideline 4 & 5.
- Minimise the Integral of the Absolute Error multiplied by Time (IAET) and the Absolute Error multiplied by Time (AET) of OETC AGC controller output. It will satisfy guideline 4 & 5.

Accordingly the cost function will comprise the above listed elements and is shown in Equation 12.1.

$$\cos t = \sum \left[\int_0^\infty t\left|\Delta f_{pdo}\right|.dt + t\left|\Delta f_{pdo}\right| + \int_0^\infty t\left|\Delta f_{oetc}\right|.dt + t\left|\Delta f_{oetc}\right| + \int_0^\infty t\left|\Delta P_{tie}\right|.dt + t\left|\Delta P_{otie}\right| + \int_0^\infty t\left|\Delta AGC_{pdo}\right|.dt + t\left|\Delta AGC_{pdo}\right| + \int_0^\infty t\left|\Delta AGC_{oetc}\right|.dt + t\left|\Delta AGC_{oetc}\right| \right]$$

…….(12.1)

Figure 12.1 shows PDO-OETC power system model with the AGC controllers and the inputs to the cost function.

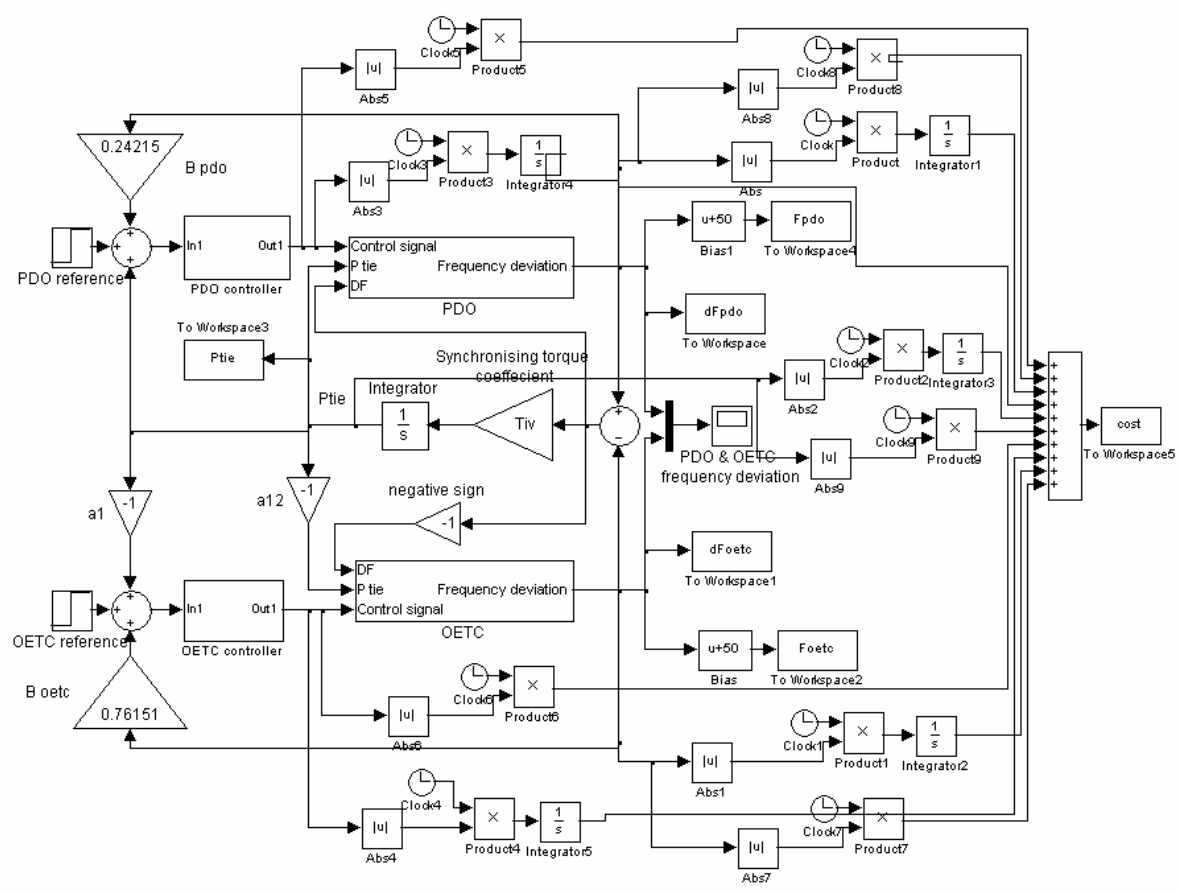

Figure 12.1: PDO-OETC model with the AGC controllers and the inputs to the controllers' optimisation cost functions.

The PDO and OETC FLPID2 AGC controllers are shown in Figures 12.2 and 12.3 respectively.

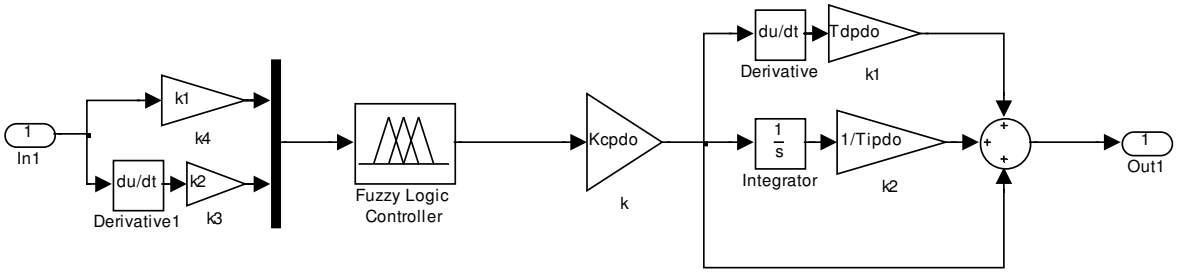

Figure 12.2: PDO FLPID2 AGC controller

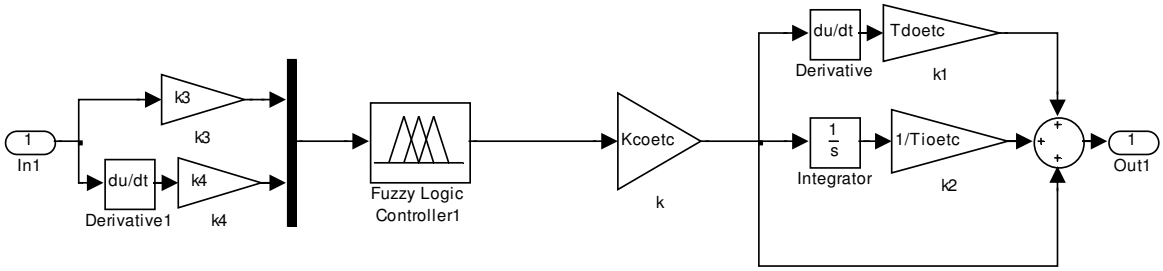

Figure 12.3: OETC FLPID2 AGC controller

12.2.2. MATLAB Mfile

In a similar fashion as in section 7.6.1, two Mfile programs were written to execute the task. The first one is called the "PdoOetcAGC_Opt" and the second one is the "Simulator". The second Mfile will call upon the first programme as part of the simulation process. The overall aim is simulating the model while changing the AGC controllers' parameters in order to minimise the cost function. Trial and error experience proves that best results are achieved when both PDO and OETC controllers' parameters are optimised simultaneously. Therefore, a 100MW load disturbance is applied at both PDO and OETC power systems while the simulation is running. It will ensure both PDO and OETC AGC controllers are optimised simultaneously while considering load disturbance within its own control area. The simulation will be aborted automatically when the cost functions settled at the least possible minimum value. Both Mfile programmes are shown in Appendix 6.

12.2.3. Optimisation results

The optimisation has been carried out using the above two Mfile programs and the PDO-OETC power system refined model for all three scenarios. The simulation has returned the optimum AGC controllers parameters when the least minimum cost function value has been reached. Table 12.1 shows the optimum AGC controllers' parameters.

Scenario	Controller	ACE input gain	Rate of Change of ACE input gain	PID controller gain	PID controller Integral time constant	PID controller derivative time constant
Scenario 1	PDO	0.3594	0.5213	0.6091	0.6124	0.4303
	OETC	0.6248	0.6324	0.7163	0.0601	0.5108
Scenario 2	PDO	1.0035	0.9909	1.0142	1.0128	1.0397
	OETC	1.0075	1.0001	0.9955	0.9943	0.9870
Scenario 3	PDO	1.001	1.0017	0.8261	0.8664	0.2155
	OETC	0.9987	1.0013	0.8854	0.9002	0.2226

Table 12.1: Optimum FLPID2 AGC controllers' parameters using fminsearch function

From the above table it is clear that fminsearch has produced different optimum results using the same cost function depending on the initial parameters values. It is clear that fminsearch can be trapped by local minimal.

Scenario 1 controllers have produced highly oscillatory response whether the load disturbance has been applied at PDO or OETC. Scenario 2 controllers have produced oscillatory response when the load disturbance is applied at OETC. Scenario 3 controllers have produced the best response among the three scenarios whether the load has been applied at PDO or OETC. Scenario 3 controllers optimized parameters are selected for further analysis and the detailed simulation results are shown in the following section.

12.2.4. Simulation results

The PDO-OETC power system refined model with the FLPID 2 AGC controllers using the optimum controllers' parameters of scenario 3 shown in Table 12.1 was simulated while 100MW load disturbance is applied once at PDO side and once at OETC side. PDO frequency, OETC frequency, tie line power, PDO Integral of controller effort and OETC Integral of controller effort were monitored. Figures 12.4 -12.9 show PDO and OETC frequencies in one figure, the tie line power in a separate figure and PDO and OETC Integral of controllers efforts in one figure for both tests respectively.

Table 12.2 shows a summary of the performance values. The summary also compares the results of the base case, classical PID AGC controller, the LQR AGC controller, the Fuzzy PID 1 AGC controller, the fuzzy PID 2 AGC controller, the modified LQR AGC controller with the fminsearch optimised FLPID 2 AGC controller performance.

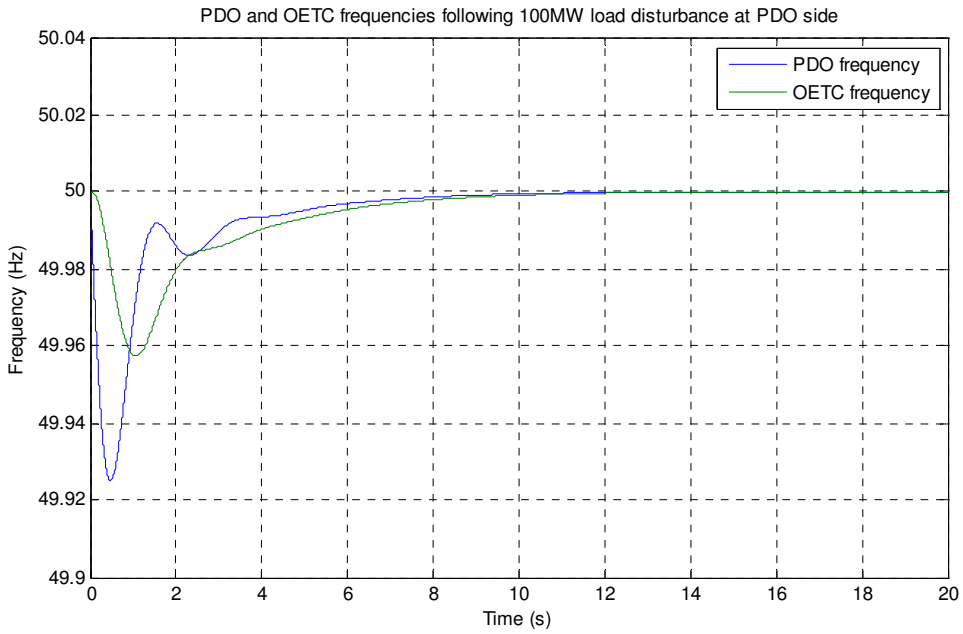

Figure 12.4: PDO and OETC frequencies following a 100MW load disturbance at PDO side with the fminsearch optimised FLPID 2 AGC controller

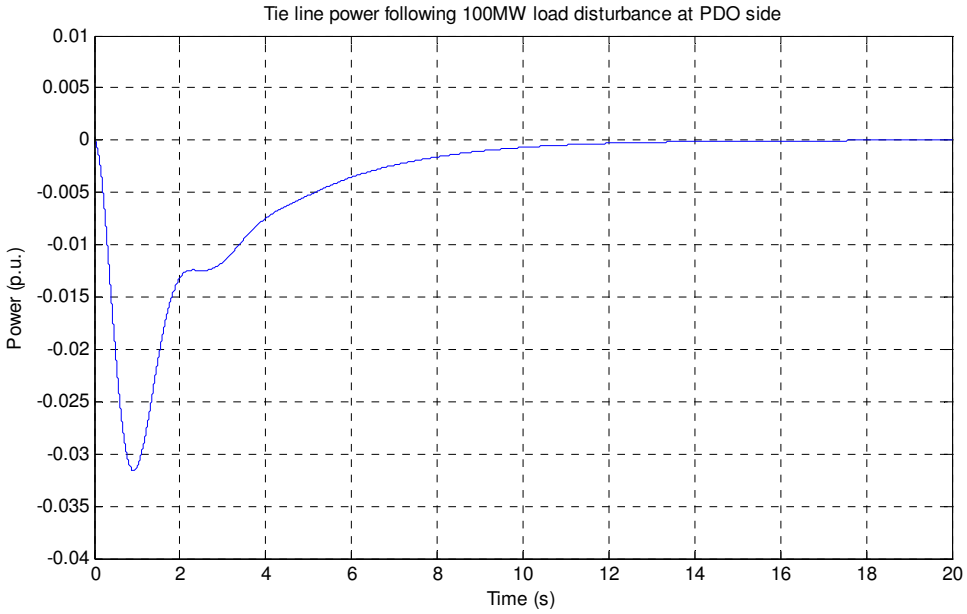

Figure 12.5: Tie line power deviation following a 100MW load disturbance at PDO side with the fminsearch optimised FLPID 2 AGC controller

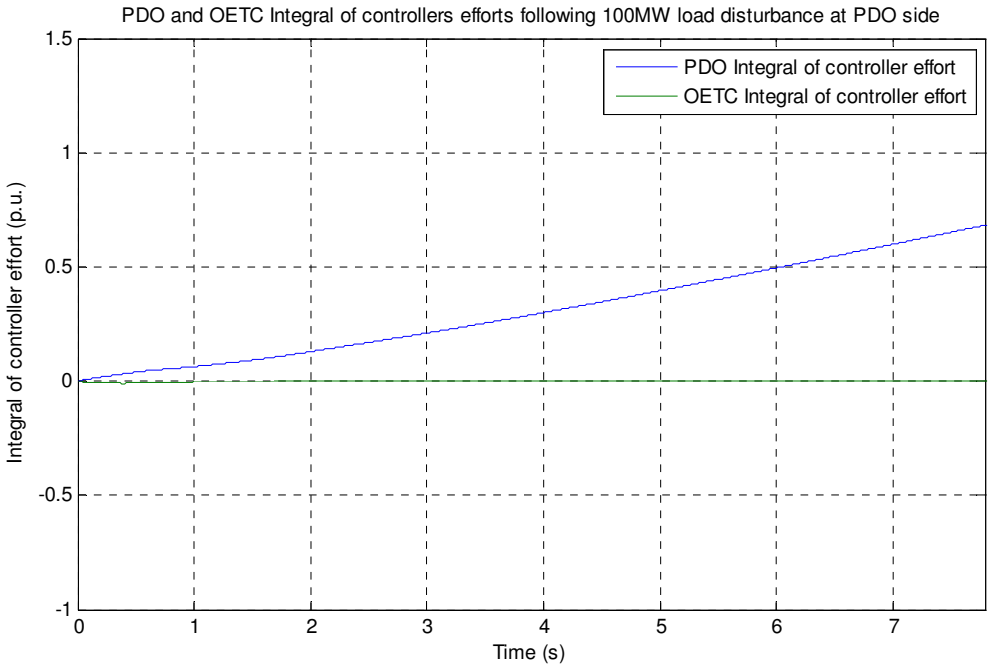

Figure 12.6: PDO and OETC fminsearch optimised FLPID 2 AGC Integral of controllers' efforts following a 100MW load disturbance at PDO side

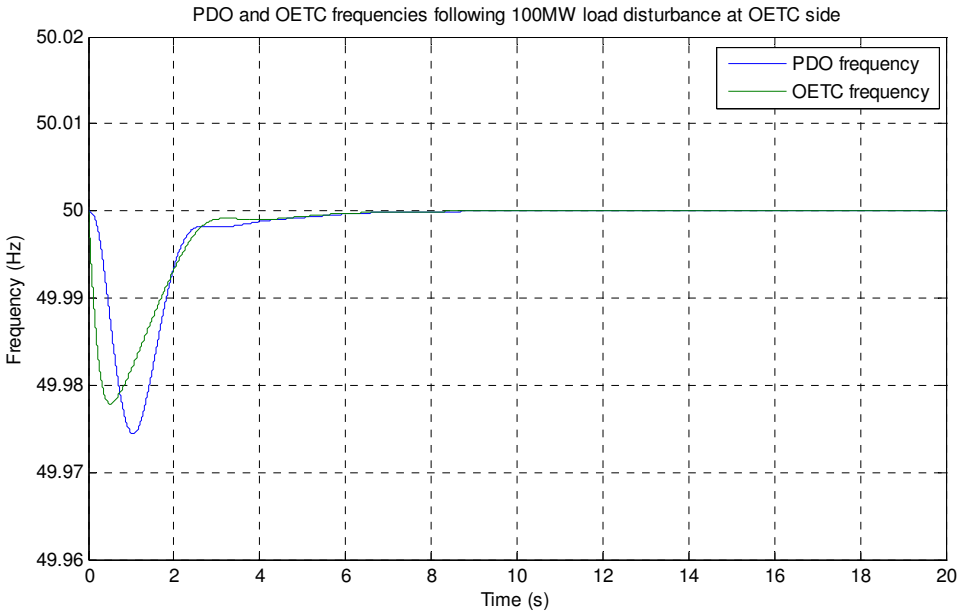

Figure 12.7: PDO and OETC frequencies following a 100MW load disturbance at OETC side with the fminsearch optimised FLPID2 AGC controller

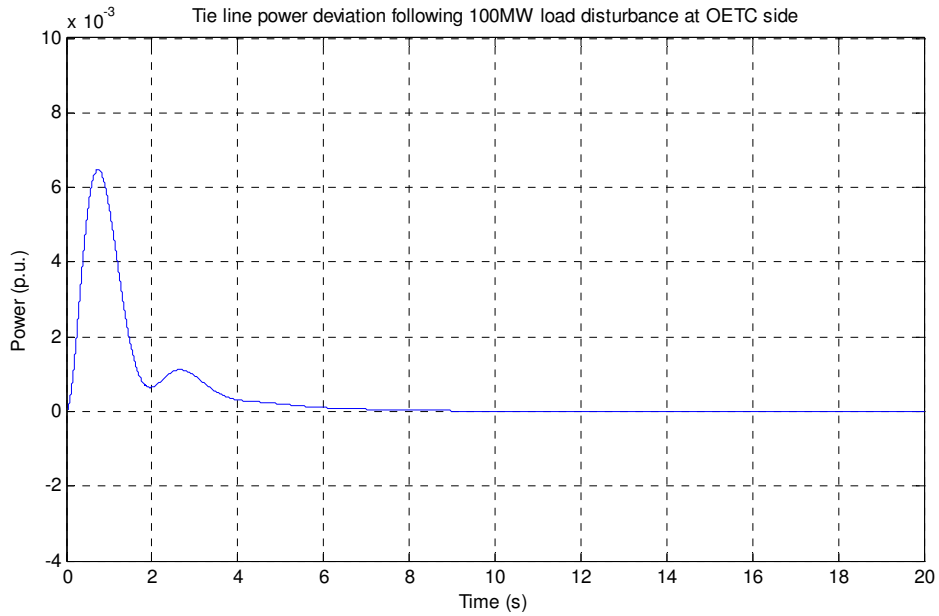

Figure 12.8: Tie line power deviation following a 100MW load disturbance at OETC side with the fminsearch optimised FLPID 2 AGC controller

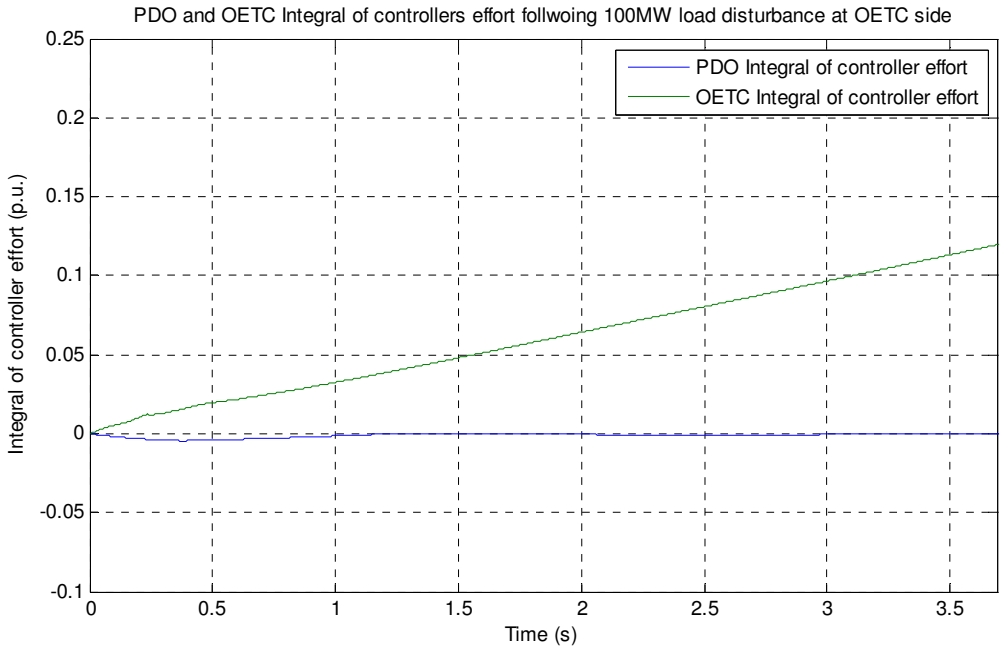

Figure 12.10: PDO and OETC fminsearch optimised FLPID 2 AGC Integral of controllers' efforts following a 100MW load disturbance at OETC side

		Base case response	PID controlled response	LQR controlled response	Fuzzy PID 1 controlled response	Fuzzy PID 2 controlled response	Modified LQR controlled response	Fminsearch optimised FLPID 2 controlled response
100MW load disturbance at PDO side	Frequency deviation (Hz)	-0.05	0	0	0	0	0	0
	Settling time (s)	10.9	34	11.3	28.1	8.17	10.1	7.79
	Tie line power deviation (p.u.)	-0.0379	0	0	0	0	0	0
100MW load disturbance at OETC side	Frequency deviation (Hz)	-0.05	0	0	0	0	0	0
	Settling time (s)	7.74	25.3	8.59	8.18	3.92	8.39	3.69
	Tie line power deviation (p.u.)	0.0121	0	0	0	0	0	0

Table 12.2: PDO and OETC optimised FLPID 2 AGC controllers' performance in comparison to the base case, the classical PID controller, the LQR controller, the Fuzzy PID1 controller, the Fuzzy PID2 controller and the modified LQR controller.

12.2.5. Results discussion

From Figure 12.4 to 12.09 one can see that the fminsearch optimized FLPID 2 AGC controller has satisfied the basic AGC requirements and the dynamic response is very good. Table 12.2 also shows that the fminsearch optimized FLPID2 is superior to all previously adopted control techniques in terms of settling time. The steady state frequency and tie line power deviations have settled at zero, similar to other control techniques.

The fminsearch optimized FLPID 2 AGC has performed better than the basic FLPID 2 AGC controller. It proves that optimisation can improve the controller response while satisfying other economic and environmental requirements.

From figures 12.06 and 12.09, one can see that PDO AGC controller takes the whole control burden when the load disturbance is applied at PDO side and OETC AGC controller takes the whole control burden when the load disturbance is applied at OETC side. When the load disturbance is applied at PDO side, over a 7.79 seconds period of time (the time taken for the frequency to settle), PDO and OETC Integral of controllers' efforts are 0.68p.u. and 0 p.u. respectively. On the other hand, when the load disturbance is applied at OETC side, over a time period of 3.69 s (the time taken for the frequency to settle), PDO and OETC Integral of controllers' efforts are 0 p.u. and 0.12 p.u. respectively. From these results, minimal support is given by PDO and OETC AGC controllers when the load disturbance is applied outside its own control area.

Overall the fminsearch optimisation technique can produce good results depending on the initial controller parameters values. It is noticed that fminsearch has produced different

solutions depending on the initial controller parameters values. It means that the fminsearch can easily be trapped by local minimum making it non attractive optimisation method.

12.2.6. Summary

The fminsearch optimized FLPID 2 AGC controller has improved the system response to load disturbances and has satisfied the AGC requirements. The fminsearch optimized FLPID 2 AGC has performed better than the basic FLPID 2 AGC controller. The fminsearch optimisation method can produce sub-optimum solutions depending on the initial controller parameters.

12.3. Optimization of PDO-OETC AGC controller using Particle Swarm Optimisation method

12.3.1. Introduction

The particle swarm is an optimisation algorithm for finding the optimum regions in a complex search spaces through the interaction of individuals in a population of particles (Al-Omairi, 2007, p. 31). Particle Swarm Optimisation (PSO) is based on swarm of birds in the free space and is developed through simulation of a bird flocking in multi-dimensional space (Al-Omairi, 2007, p. 31). Each particle or agent is represented by position vector X(t) and associated with velocity V(t). The agent is modified based on position and velocity information. The Particle swarm Optimisation (PSO) is iterative and in each iteration the agent is evaluated via objective function so that it knows its best value (pbest) as well as its position (Al-Omairi, 2007, p. 31). Moreover, each agent knows the best value so far in the group (gbest) among pbest of all agents (Al-Omairi, 2007, p. 31). Figure 12.10 summarises the basic concept of Particle swarm Optimisation. The concept is that each particle tries to modify its current position and velocity according to the distance between its current position and pbest, and the distance between its current position and gbest (Al-Omairi, 2007, p. 32).

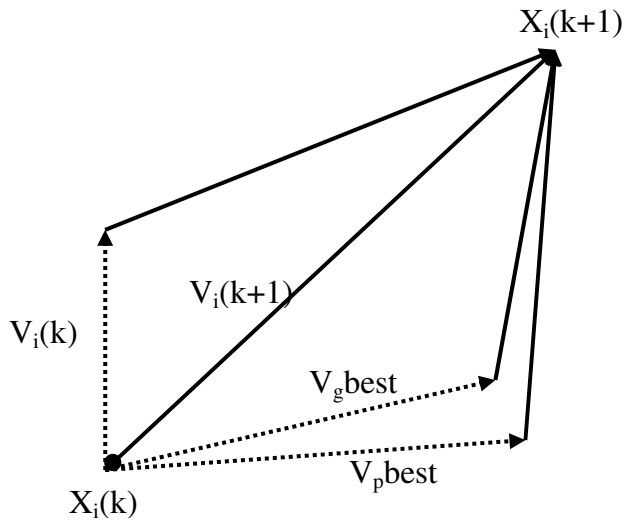

Figure 12.10: Concept of updating individual position in Particle Swarm Optimisation (Al-Omairi, 2007, p. 32)

The particle Swarm Optimisation (PSO) can be summarised by the following seven steps:

1. **Initialisation step**: starts by generating initial population randomly within the specified rang. Then, for each generated position an associated velocity is generated randomly within a calculated range based on position rang.

   $X_j(0) = \lfloor x_{j,1}(0) \quad ... \quad x_{j,m}(0) \rfloor$ within the range $\lfloor x_k^{\min} \quad , \quad x_k^{\max} \rfloor$.....(12.2)

   $V_j(0) = \lfloor v_{j,1}(0) \quad ... \quad v_{j,m}(0) \rfloor$ within the range $\lfloor -v_k^{\max} \quad , \quad v_k^{\max} \rfloor$.....(12.3)

   $$v_k^{\max} = \frac{x_k^{\max} - x_k^{\min}}{N} \quad \text{.....(12.4)}$$

   Where:

   n: the number of randomly generated position and velocity.

   m: number of variables.

   N: is a chosen number of intervals in the k^{th} dimension.

2. **Evaluation step**: the initial searching point is set to pbest for each agent. Then, each agent is evaluated via objective function. The best-evaluated value of pbest is set to gbest. The evaluation step follows the following sequence:

   1. Population is evaluated using objective function, J
   2. Set $X_j^*(0) = X_j(0)$ and $J_j^* = J_j$

3. Find the best value of objective function and set it to J_{best}

4. Set the particle associated with J_{best} as the global $X^{**}(0)$

3. **Velocity updating step**: the velocity of each agent is modified by the following equation:

$$v_{j,k}(t) = K\left[v_{j,k}(t-1) + c_1 r_1\left(x^{*}_{j,k}(t-1) - x_{j,k}(t-1)\right) + c_2 r_2\left(x^{**}_{j,k}(t-1) - x_{j,k}(t-1)\right)\right]$$

$$K = \frac{2}{2 - \varphi - \sqrt{\varphi^2 - 4\varphi}}$$

$$where: \varphi = c_1 + c_2, \varphi > 4$$

……..(12.5)

Where:

c_1 & c_2 are specific weighting factors

r_1 & r_2 are randomly generated numbers

The random weighting of the control parameters in the algorithm results in a kind of explosion as particles' velocities and positional coordinates go towards infinity. The explosion has traditionally been contained through implementation of a parameter V_{max}, which limits step size or velocity (Al-Omairi, 2007, p. 34). In other words, this parameter acts towards convergence of PSO.

4. **Position updating step**: based on the updated velocities each particle changes its position according to the following equation:

$$x_{j,k}(t) = v_{j,k} + x_{j,k}(t-1) \quad \text{…….(12.6)}$$

From physics perspective, it can be noted from this equation that the velocity is added with displacement because the time increment is always one unit (Al-Omairi, 2007, p. 34).

5. **Individual best updating step**: each particle is evaluated according to the updated position. If $J_j < J^{*}_j$ then the updated individual best as $X^{*}_j(t) = X_j(t)$ and $J^{*}_j = J_j$.

6. **Global best updating step**: searches for the minimum value J_{min} among J^{*}_j. If $J_{min} < J^{**}$ then the updated individual best is $X^{**} = X_{min}(t)$ and $J^{**} = J_{min}$.

7. **Stopping criteria step:** In this project, the search will stop if one of the following criteria is satisfied:

1. The number of iterations reaches the maximum allowable number.

2. The number of iterations since the last change of the best solution is greater than or equal to a pre-specified number.

Figure 12.11 shows a flow chart summarizing all above seven steps.

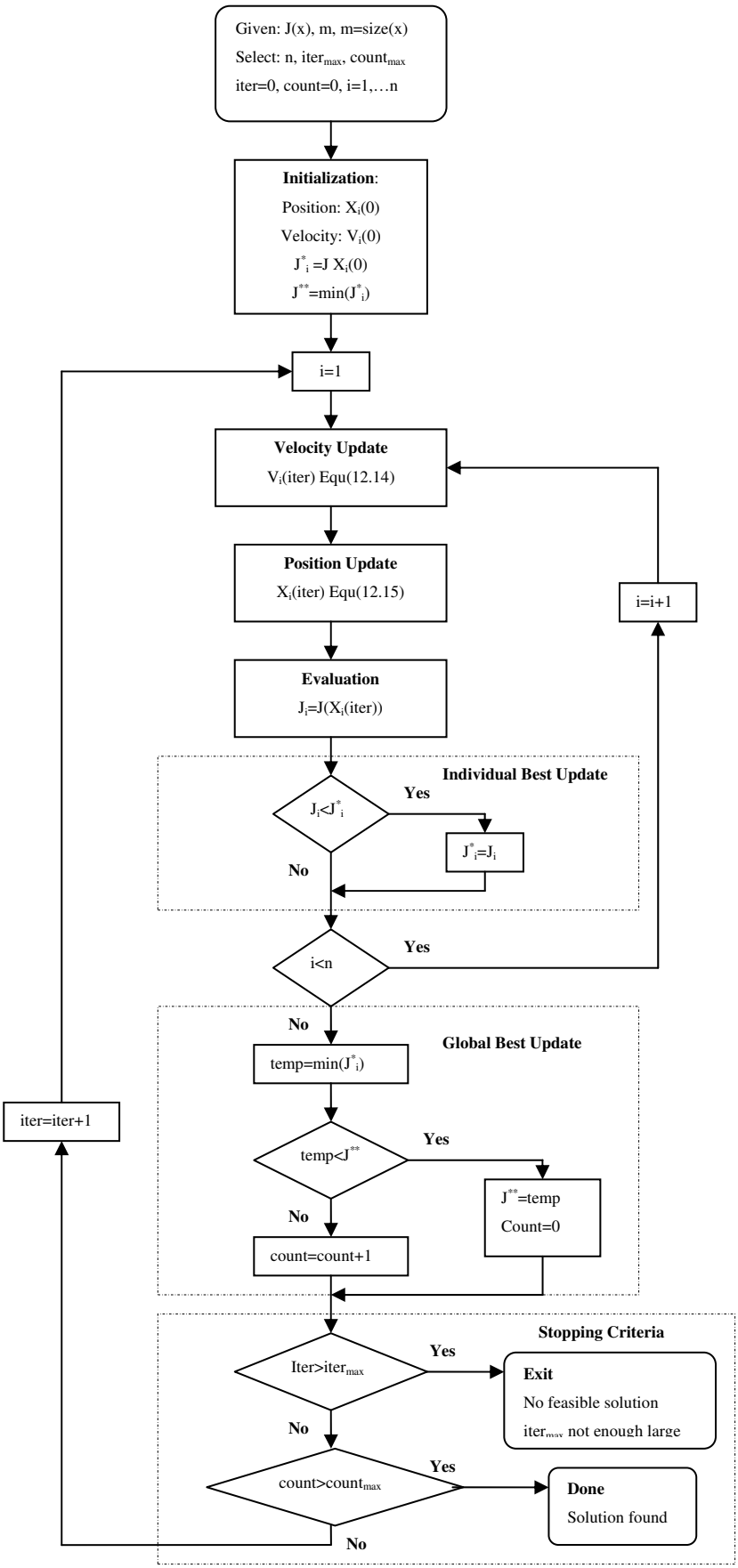

Figure 12.11: Particle Swarm Optimisation Algorithms (Al-Omairi, 2007, p. 35)

12.3.2. Optimisation of FLPID 2 AGC controller parameters using Particle Swarm Optimisation

The Particle Swarm Optimisation (PSO) algorithm is used in this part of the study to optimize the performance of the earlier developed Fuzzy Logic PID 2 AGC controllers of both PDO and OETC. In this controller performance optimisation process, the five AGC guidelines mentioned earlier will be followed. The same cost function shown earlier in section 12.2.1 presented in Equation 12.1 will be used in this optimisation process. Therefore the overall PDO-OETC power system model will remain the same as shown earlier in Figure 12.1.

In this optimisation process, the PSO will optimize both PDO and OETC FLPID2 AGC controllers' parameters simultaneously. There are ten parameters to be optimized, five of them are PDO AGC Fuzzy logic input scaling factors and the PID parameters. The other five are OETC AGC Fuzzy logic input scaling factors and the PID parameters. Unlike the fminsearch optimisation technique, the PSO does not require to start with initial values but it randomly generates the initial values. However, a specific range of parameters is required to limit the PSO search space. Limiting the search space will require less population number and hence less computation time. However limiting the search space might lead the PSO falling into local minima. To ensure the optimum solution is achieved, a careful guess of the parameters must be made. The personal experience and the trial and error are the only ways of determining the parameters range. Using trial and error approach, the following parameters ranges were found appropriate and are used for this optimisation process:

<u>PDO AGC controller:</u>

ACE input scaling factor (k1) = 0.5→1.5

Rate of Change of ACE input scaling factor (k2) = 0.5→1.5

PID gain (Kcpdo) = 0.5→1.5

PID integral time constant (Tipdo)= 0.5→1

PID differential time constant (Tdpdo) =0.25→0.75

<u>OETC AGC controller:</u>

ACE input scaling factor (k3) = 0.5→1.5

Rate of Change of ACE input scaling factor (k4) = 0.5→1.5

PID gain (Kcoetc) =0.5→1.5

PID integral time constant (Tioetc) = 0.5→1

PID differential time constant (Tdoetc) = 0.25→0.75

The population number is chosen to be 75 and the maximum number of iterations is chosen as 100. The number of iterations of unchanged solution is chosen to be 5.

The PSO algorithm shown in Figure 12.11 was interpreted into MATLAB Mfile code and is named "PSOmin". Another Mfile was written to coordinate the optimisation exercise and is called "corPSO". The coordination Mfile "corPSO" will specify the parameters ranges, the population number, the maximum iteration number and the number of the unchanged solution iteration number. It will then call upon another Mfile which is called "simulator" which will load the rest of the model parameters values to the MATLAB workspace. Then the coordinator "corPSO" will specify another Mfile called "objective" which will be used to simulate the model and evaluate the cost function. The coordinator Mfile "corPSO" will then run PSO optimisation based on the given information. The "PSOmin" Mfile will run all the iterations and will return the answer as a set of optimised parameters. The process takes long time and sometime as long as 12 hrs depending on the computation speed, the parameters ranges, the population number and the maximum iteration number. All the used four Mfile codes are shown in Appendix 7.

The optimisation process was run and returned the optimal FLPID2 AGC controllers parameters as shown in Table 12.3.

	ACE input gain	Rate of Change of ACE input gain	PID controller gain	PID controller Integral time constant	PID controller derivative time constant
PDO	1.1497	0.9267	0.9574	0.5274	0.3814
OETC	1.3478	0.7249	1.4312	0.8123	0.2889

Table 12.3: Optimum FLPID2 AGC controllers' parameters using Particle Swarm Optimisation method

12.3.3. Simulation results

The PDO-OETC power system refined model with the FLPID 2 AGC controllers using the optimum controllers' parameters shown in Table 12.3 was simulated when 100MW load disturbance is applied once at PDO side and once at OETC side. PDO frequency, OETC frequency, tie line power, PDO Integral of controller effort and OETC Integral of controller effort were monitored. Figures 12.12 -12.17 show PDO and OETC frequencies in one figure, the tie line power in a separate figure and PDO and OETC Integral of controllers efforts in one figure for both tests respectively.

Table 12.4 shows a summary of the performance values. The summary also compares the results of the base case, classical PID AGC controller, the LQR AGC controller, the Fuzzy PID 1 AGC controller, the fuzzy PID 2 AGC controller, the modified LQR AGC controller and the fminsearch optimised FLPID 2 AGC controller with the PSO optimised FLPID 2 AGC controller performance.

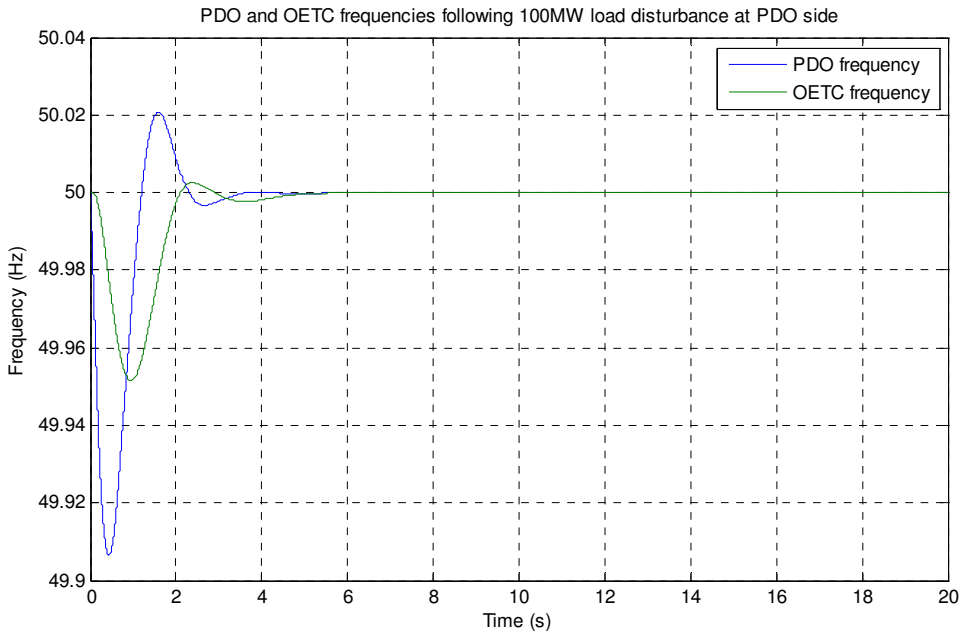

Figure 12.12: PDO and OETC frequencies following a 100MW load disturbance at PDO side with the PSO optimised FLPID 2 AGC controller

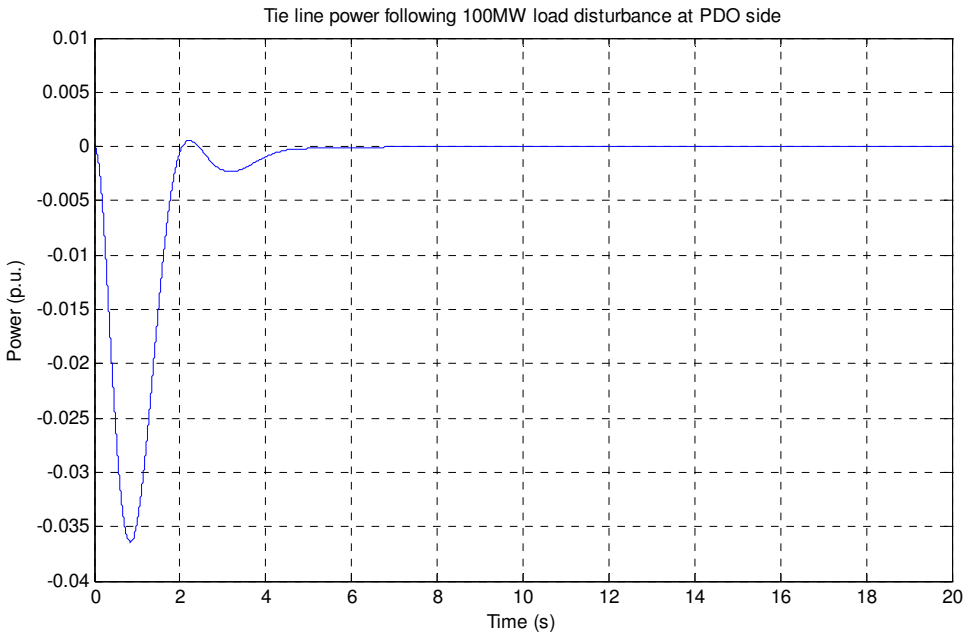

Figure 12.13: Tie line power deviation following a 100MW load disturbance at PDO side with the PSO optimised FLPID 2 AGC controller

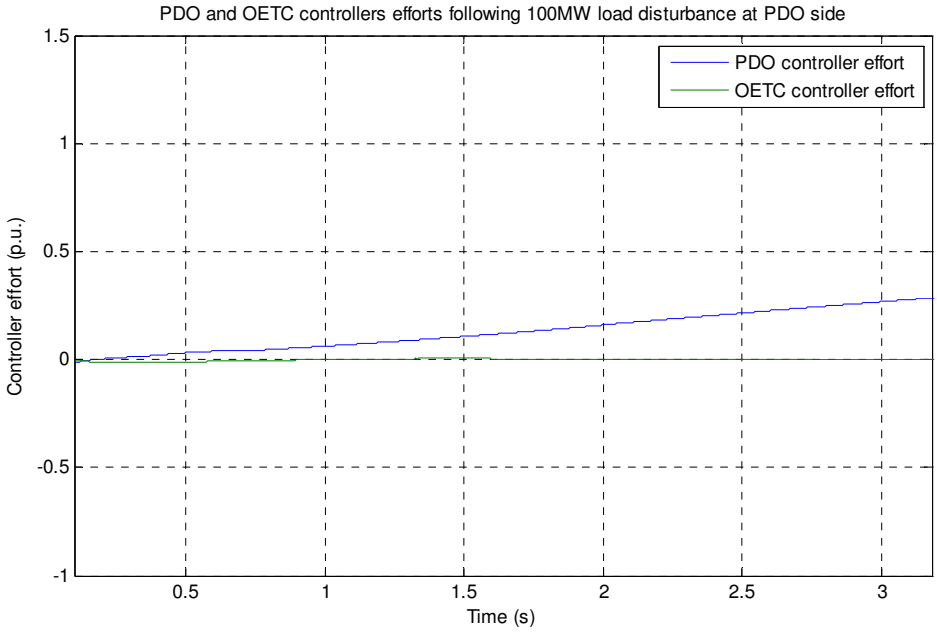

Figure 12.14: PDO and OETC PSO optimised FLPID 2 AGC Integral of controllers' efforts following a 100MW load disturbance at PDO side

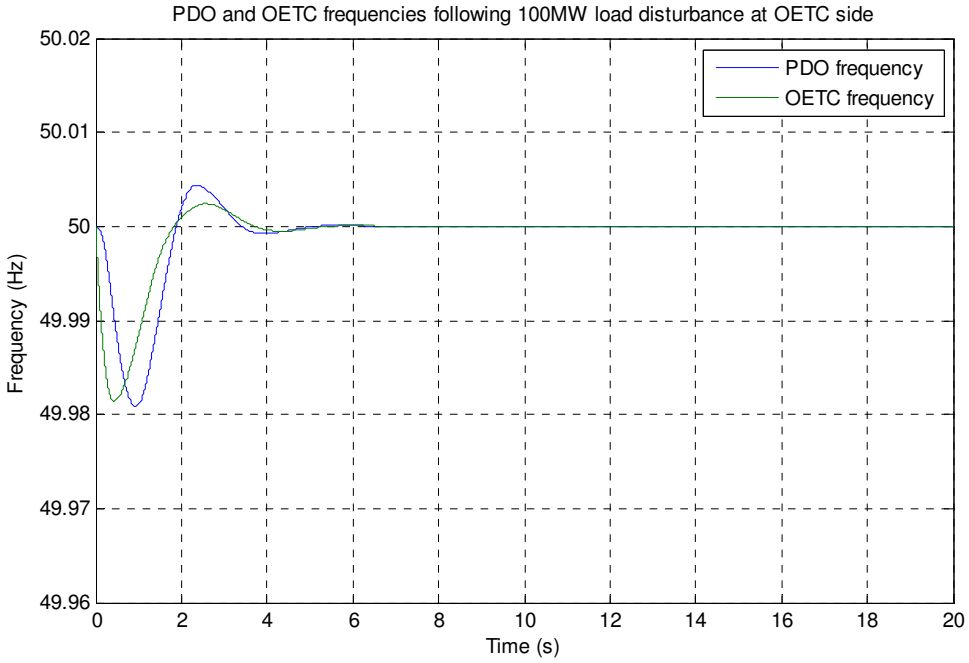

Figure 12.15: PDO and OETC frequencies following a 100MW load disturbance at OETC side with the PSO optimised FLPID2 AGC controller

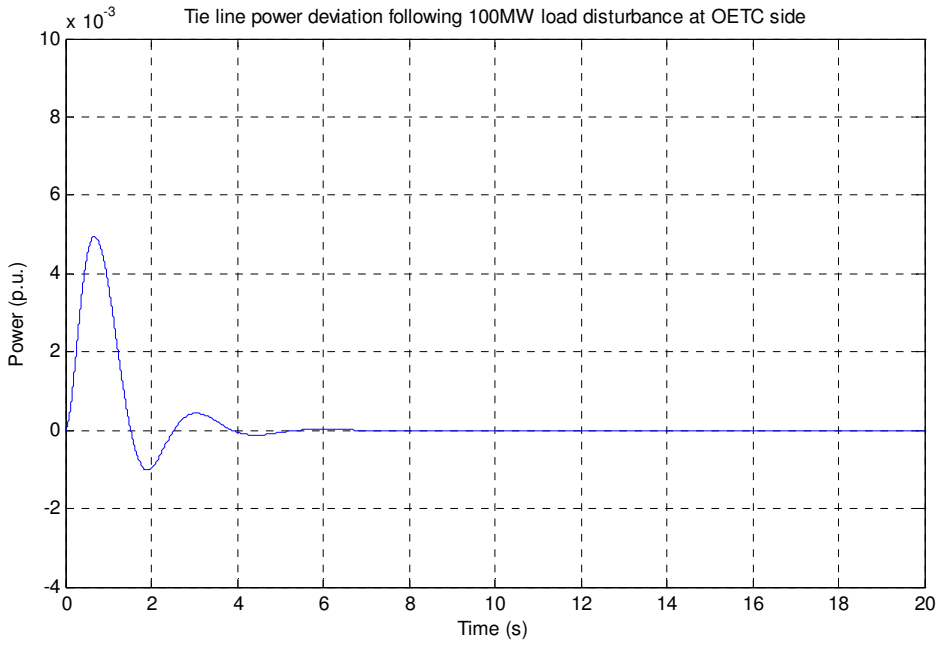

Figure 12.16: Tie line power deviation following a 100MW load disturbance at OETC side with the PSO optimised FLPID 2 AGC controller

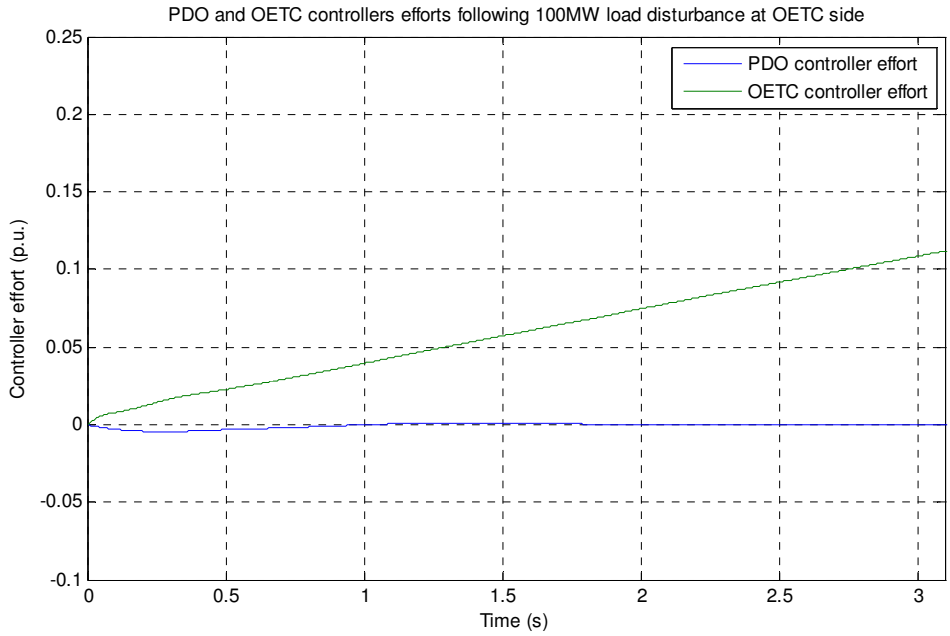

Figure 12.17: PDO and OETC PSO optimised FLPID 2 AGC Integral of controllers' efforts following a 100MW load disturbance at OETC side

		Base case response	PID controlled response	LQR controlled response	Fuzzy PID 1 controlled response	Fuzzy PID 2 controlled response	Modified LQR controlled response	Fminsearch optimised FLPID 2 controlled response	PSO optimised FLPID 2 controlled response
100MW load disturbance at PDO side	Frequency deviation (Hz)	-0.05	0	0	0	0	0	0	0
	Settling time (s)	10.9	34	11.3	28.1	8.17	10.1	7.79	3.18
	Tie line power deviation (p.u.)	-0.0379	0	0	0	0	0	0	0
100MW load disturbance at OETC side	Frequency deviation (Hz)	-0.05	0	0	0	0	0	0	0
	Settling time (s)	7.74	25.3	8.59	8.18	3.92	8.39	3.69	3.1
	Tie line power deviation (p.u.)	0.0121	0	0	0	0	0	0	0

Table 12.4: PDO and OETC PSO optimised FLPID 2 AGC controllers' performance in comparison to the base case, the classical PID controller, the LQR controller, the Fuzzy PID1 controller, the Fuzzy PID2 controller, the modified LQR controller and the fminsearch optimised FLPID 2 controller.

12.3.4. Results Discussion

From Figure 12.12 to 12.17 one can see that the Particle Swarm optimized FLPID 2 AGC controller has satisfied the basic AGC requirements and the dynamic response is very good. Table 12.4 also shows that the Particle Swarm optimized FLPID2 is superior to all previously adopted control techniques in terms of settling time. The steady state frequency and tie line power deviations settled at zero, similar to other control techniques.

Generally, the Particle Swarm optimized FLPID 2 AGC has performed better than the fminsearch optimized FLPID 2 AGC controller if we compare the settling time and dynamic oscillations. It suggests that the PSO will not be trapped in a local minimum and can search for the optimum solution in a wider space than fminsearch.

Similar to other control techniques and from figures 12.14 and 12.17, one can see that PDO AGC controller takes the whole control burden when the load disturbance is applied at PDO side and OETC AGC controller takes the whole control burden when the load disturbance is applied at OETC side. When the load disturbance is applied at PDO side, over a 3.18 seconds period of time (the time taken for the frequency to settle), PDO and OETC Integral of controllers' efforts are 0.2866p.u. and 0 p.u. respectively. On the other hand, when the load disturbance is applied at OETC side, over a time period of 3.1 s (the time taken for the frequency to settle), PDO and OETC Integral of controllers' efforts are 0 p.u. and 0.1119 p.u. respectively. From these results, minimal support has been given by PDO and OETC AGC controllers when the load disturbance is applied outside its own control area. Comparing the integral of control effort of the PSO optimized FLPID2 AGC

controller with the previously reported result using the fminsearch optimized FLPID 2 AGC controller, the Particle Swarm optimized FLPID 2 AGC controller has devoted less control effort and energy to get better dynamic response than the fminsearch optimized FLPID2 AGC controller.

12.3.5. Summary

The Particle Swarm optimized FLPID 2 AGC controller performance has been proved to be more superior in comparison to all previously adopted control techniques in this study. The Particle Swarm optimized FLPID 2 AGC controller has even devoted less Integral of control effort and produced better response in comparison to the fminsearch optimized FLPID 2 AGC controller. It suggests that PSO is better able to find the optimum solution than fminsearch.

12.4. Overall discussion

Two different optimisation techniques have been adopted to optimize PDO-OETC AGC controllers' performance using a set of AGC performance guidelines. The fminsearch technique has been adopted to optimize the FLPID 2 AGC controllers using a cost function which was built to satisfy all the AGC controller guidelines. Then the Particle Swarm Optimisation method is used to optimize the FLPID 2 AGC controllers using the same cost function which has been used in the fminsearch optimisation technique. The performance of both optimisation techniques is demonstrated through the performance of the associated AGC controllers and is summarised in Table 12.5.

		Fminsearch optimised FLPID 2 controlled response	PSO optimised FLPID 2 controlled response
100MW load disturbance at PDO side	Steady state Frequency deviation (Hz)	0	0
	Dynamic maximum frequency deviation	-0.075	-0.094
	Settling time (s)	7.79	3.18
	Steady state Tie line power deviation (p.u.)	0	0
	PDO AGC Integral of controller effort (p.u.)	0.68	0.2866
	OETC AGC Integral of controller effort (p.u.)	0	0
100MW load disturbance at OETC side	Steady state Frequency deviation (Hz)	0	0
	Dynamic maximum frequency deviation	-0.026	-0.019
	Settling time (s)	3.69	3.1
	Steady state Tie line power deviation (p.u.)	0	0
	PDO AGC Integral of controller effort (p.u.)	0	0
	OETC AGC Integral of controller effort (p.u.)	0.12	0.1119

Table 12.5: Summary of the optimized AGC controllers' performance

Furthermore the dynamic responses of both controllers are compared with each other through responses shown in Figures 12.18 to 12.23. The figures show PDO frequency

deviation, OETC frequency deviation and Tie line power deviation following a 100MW load disturbance at PDO and at OETC respectively.

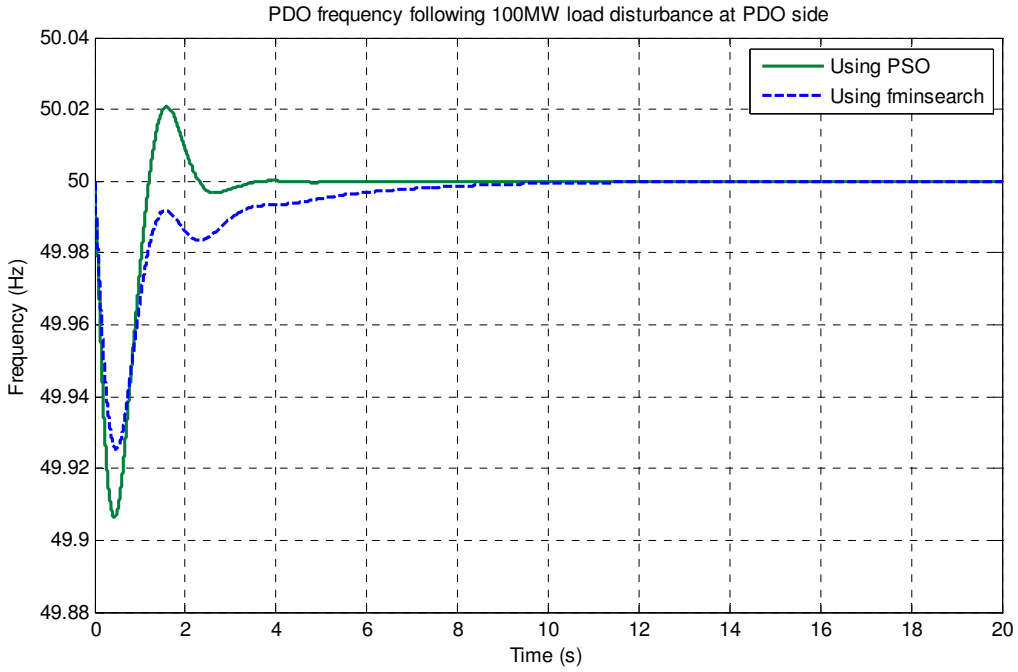

Figure 12.18: PDO frequency following 100MW load disturbance at PDO side using fminsearch and PSO optimized PDO-OETC AGC controllers

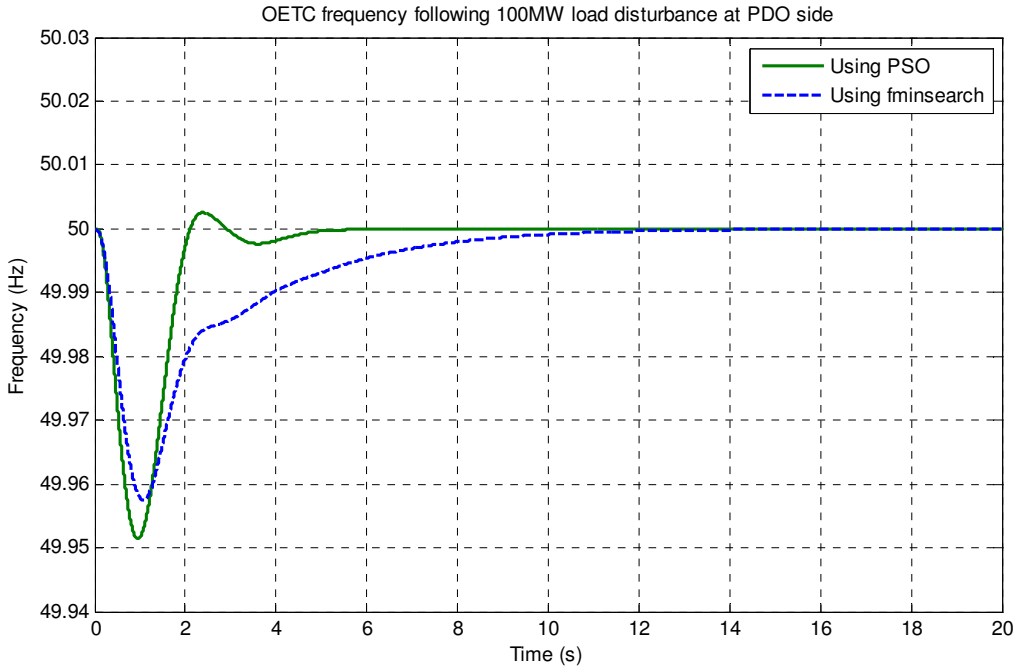

Figure 12.19: OETC frequency following 100MW load disturbance at PDO side using fminsearch and PSO optimized PDO-OETC AGC controllers

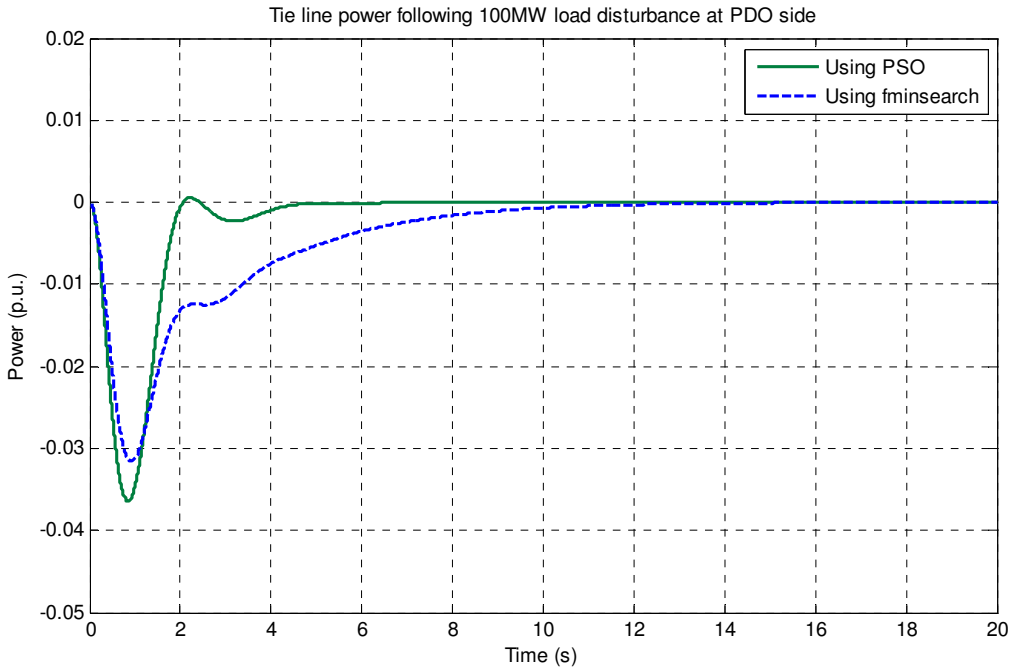

Figure 12.20: Tie line power deviation following 100MW load disturbance at PDO side fminsearch and PSO optimized PDO-OETC AGC controllers

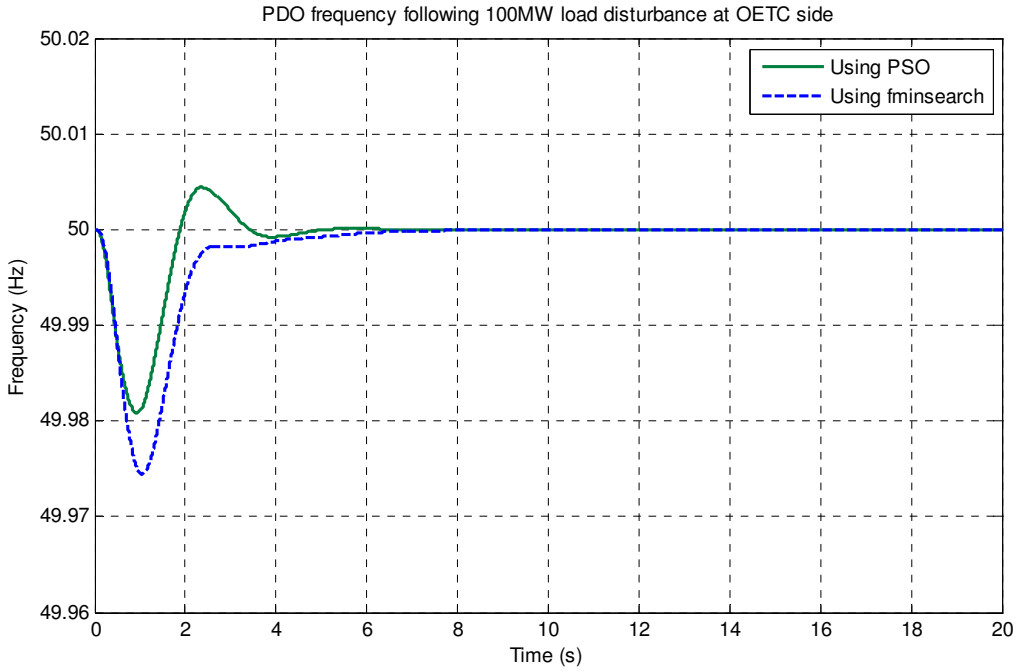

Figure 12.21: PDO frequency following 100MW load disturbance at OETC side using fminsearch and PSO optimized PDO-OETC AGC controllers

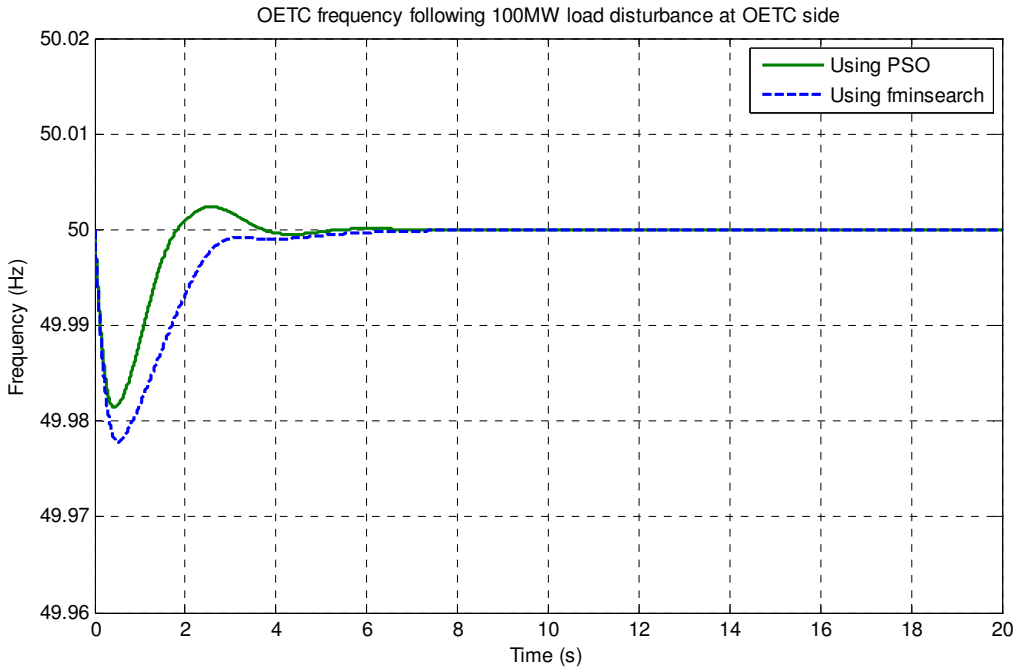

Figure 12.22: OETC frequency following 100MW load disturbance at OETC side using fminsearch and PSO optimized PDO-OETC AGC controllers

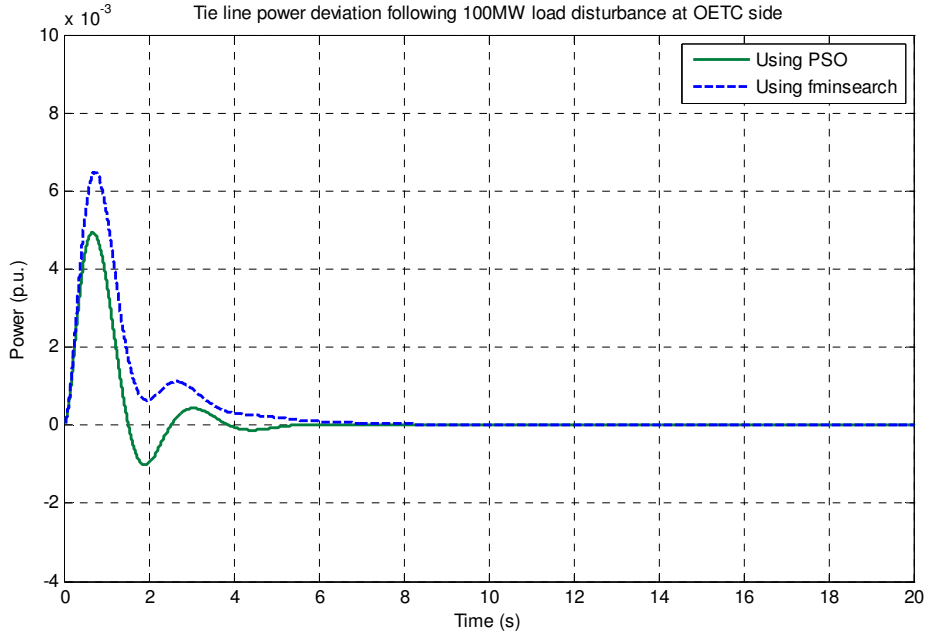

Figure 12.23: Tie line power deviation following 100MW load disturbance at OETC side using fminsearch and PSO optimized PDO-OETC AGC controllers

From Table 12.5, it can be noted that both controllers have satisfied the zero steady state condition of frequency deviation and tie line power deviation. When the disturbance is applied at PDO side and considering the maximum dynamic deviation, the fminsearch has

performed better than the PSO. The PSO settling time is superb and far better than the fminsearch. The PSO Integral of controller effort is also much better than the fminsearch.
When the disturbance is applied at OETC side, the PSO controller has performed better in terms of maximum dynamic deviation and settling time though the Integral of controllers' efforts are in the same range.
From Figures 12.18 to 12.23, one can see that the PSO optimized AGC controllers dynamic response is generally better than the fminsearch AGC controllers.
Moreover, the fminsearch optimum results depend very much on the initial values of the controller parameters. It means that fminsearch is more vulnerable to be trapped in local minimum.

12.5. Summary

Using general guidelines for the optimum AGC controller performance, two different optimisation techniques were used to optimize the PDO-OETC FLPID2 AGC controllers' performance. The Particle Swarm optimized AGC controller has produced better dynamic response than the fminsearch optimized AGC controller. It was also evident that fminsearch optimisation method can easily be trapped in local minimum and therefore producing sub-optimum solution.

Chapter 13: PDO-OETC AGC controllers robustness test

13.1. Introduction

In this part, the robustness of the optimised PDO-OETC AGC controllers will be assessed. The robustness assessment approach exposes the optimised AGC controllers to uncertain model whereby the model parameters are changed in a certain range. The robustness assessment is intended to show how robust is the optimised AGC controllers performance to model uncertainties and changing operating points.

In real life, the power system configuration and operating points change continuously resulting in key model parameters changes. For example, the number of synchronised generating units will affect the total inertia value and hence the system response to load disturbances. Moreover, modelling errors are inherited with any modelling process due to many factors like incomplete knowledge of the system and optimistic assumptions. Furthermore, the seasonal variation in the ambient temperature affects the droop control capability of the power system as identified earlier in the model validation chapter.

Certain model parameters have been identified contributing significantly to the overall PDO-OETC model response. Those particular parameters are used to accomplish this task.

13.2. Methodology

From the parameters sensitivity tests conducted earlier in section 5.4, the system inertia and synchronising torque coefficient were seen to have the most significant influence on the system response. In real life, the system inertia does change in line with the number of synchronised units to the grid. It also changes due to the natural growth of the power system and the addition of new generating units. The synchronising torque coefficient is a function of the torque angles and the system voltages; therefore it changes on daily basis due to the changing operating points. Add to that, increasing the interconnection capacity will have significant impact on the sysnchronising torque coefficient.

It is very well known that different droop control settings will significantly change the power system response to load disturbances. When some generating units loading is fixed due to preselect load control mode or some generating units reached their base load during the hot summer, the overall system droop capability is jeopardised and is seen as a change in the droop setting. Moreover, it could be the preference of some operators to operate the generating units on 3% or 5% droop setting rather than the nominal 4% droop setting.

As discussed in sections 9.6.3.1 and 9.8.9, the frequency-response characteristic factor β used for calculating Area Control Error (ACE) will have an impact on the system response to load disturbances. When the AGC is applied to both PDO and OETC control areas, errors in calculating the factor β will impact the dynamic system response to load disturbances.

Based on above discussion, the following four parameters are used to carry out the optimised AGC controllers' robustness test:

- System inertia (PDO and OETC)
- Synchronising torque coefficient
- Droop control setting (PDO and OETC)
- Frequency-response characteristic factor β

The following parameters ranges are assumed to be adequate for this task:

- PDO area inertia Hpdo (tuned value is 4.8417 s): 4 seconds to 5 seconds in steps of 0.25 seconds (allowing for a positive error equivalent to adding a new F6B generating unit and a negative error equivalent to taking one F9E, one F6A and F6B on standby mode or for maintenance during winter)
- OETC area inertia Hoetc (tuned value is 15.5023 s): 14 seconds to 16 seconds in steps of 0.5 seconds (allowing for a positive error equivalent to adding a new F9E generating unit and a negative error equivalent to taking three F9E, and F6B on standby mode or for maintenance during winter)
- Synchronising torque coefficient Tiv (tuned value is 0.7220 p.u.MW/Hz) :0.7 p.u.MW/Hz to 1 p.u.MW/Hz in steps of 0.1 p.u.MW/Hz (allowing for wide positive error equivalent to doubling the interconnection capacity in future and a narrower negative error for changing operating points)
- PDO droop control setting Rpdo (nominal value is 4%): 3% to 5% in steps of 1% (allowing for da change in droop settings, preselect load on some units or seasonal variations in ambient temperatures)
- OETC droop control setting Roetc (nominal value is 4%): 3% to 5% in steps of 1% (allowing for da change in droop settings, preselect load on some units or seasonal variations in ambient temperatures)
- PDO frequency-response characteristic factor Bpdo (nominal value is 0.24215 p.u.MW/Hz): 0.21794 to 0.26636 in steps of 0.02421 (to allow for ±10% calculation error)

- OETC frequency-response characteristic factor Boetc (nominal value is 0.76151 p.u.MW/Hz): 0.68536 to 0.83766 in steps of 0.07615 (to allow for ±10% calculation error)

A MATLAB Mfile code has been written to simulate the PDO-OETC refined model while changing the above parameters within the specified ranges. The code will eventually produce the model response envelop with all the simulated conditions. Four cases has been simulated which are,

1. The PDO-OETC power system refined model without AGC controllers
2. The PDO-OETC power system refined model with the modified LQR controller
3. The PDO-OETC power system refined model with the fminsearch optimised FLPID2 controller
4. The PDO-OETC power system refined model with the PSO optimised FLPID2 controller.

For simplicity, 100MW load disturbance is applied at PDO only and PDO frequency is the only monitored response. The MATLAB Mfile code is shown in Appendix 8.

13.3. Simulation results

The PDO-OETC power system model has been simulated as specified above in section 13.2 and the results are shown in shown in Figures 13.1 to 13.4. The controller robustness indicators which can be deduced from the envelop figures are the steady state values envelop, the dominant settling time and whether all response lines are following the same dynamic pattern or not.

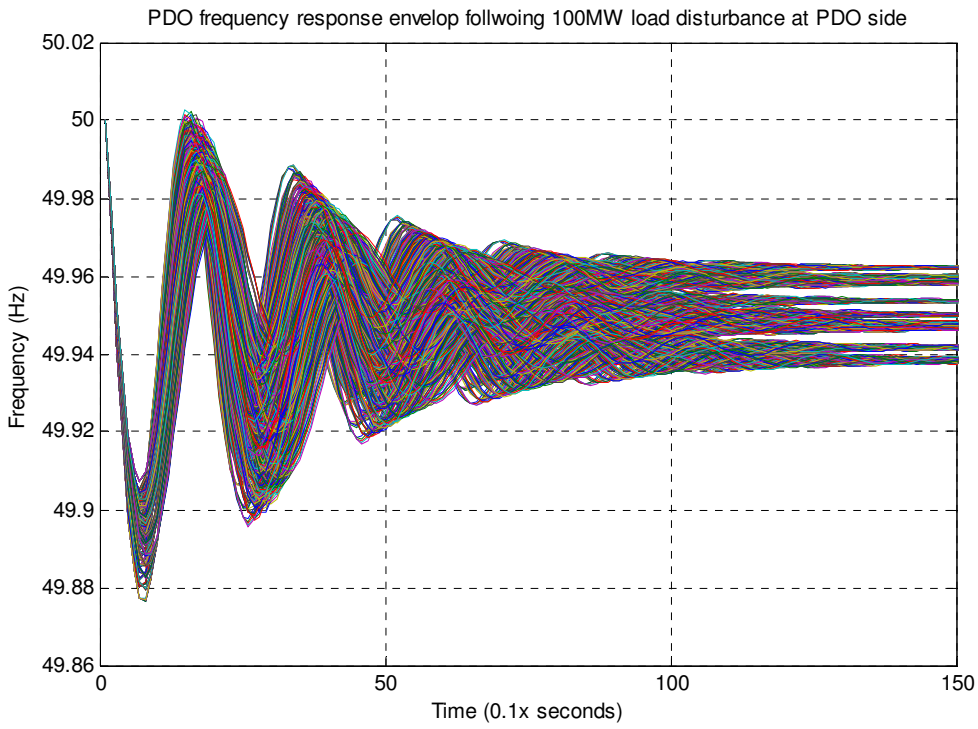

Figure 13.1: PDO frequency response envelop following 100MW load disturbance at PDO side without AGC controller

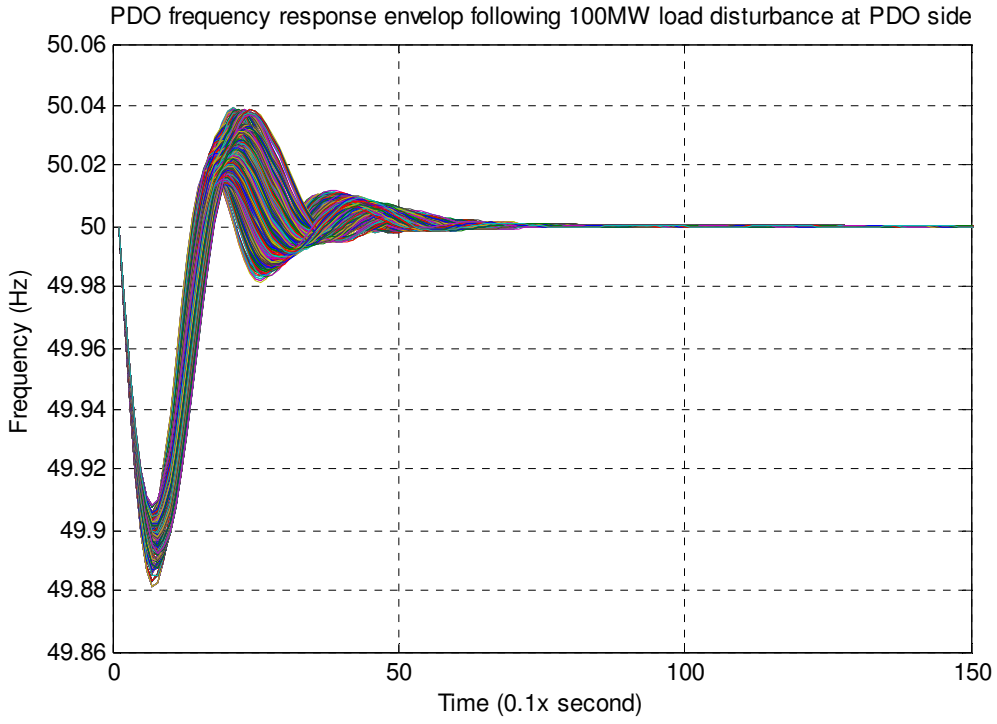

Figure 13.2: PDO frequency response envelop following 100MW load disturbance at PDO side with the modified LQR AGC controller

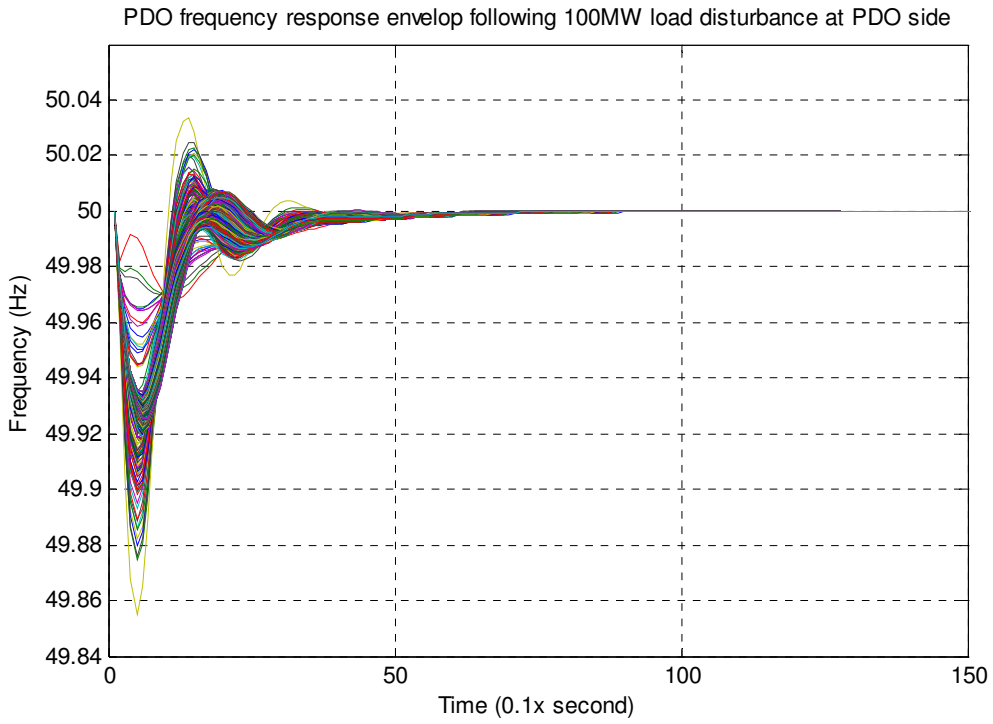

Figure 13.3: PDO frequency response envelop following 100MW load disturbance at PDO side with the fminsearch optimised FLPID2 AGC controller

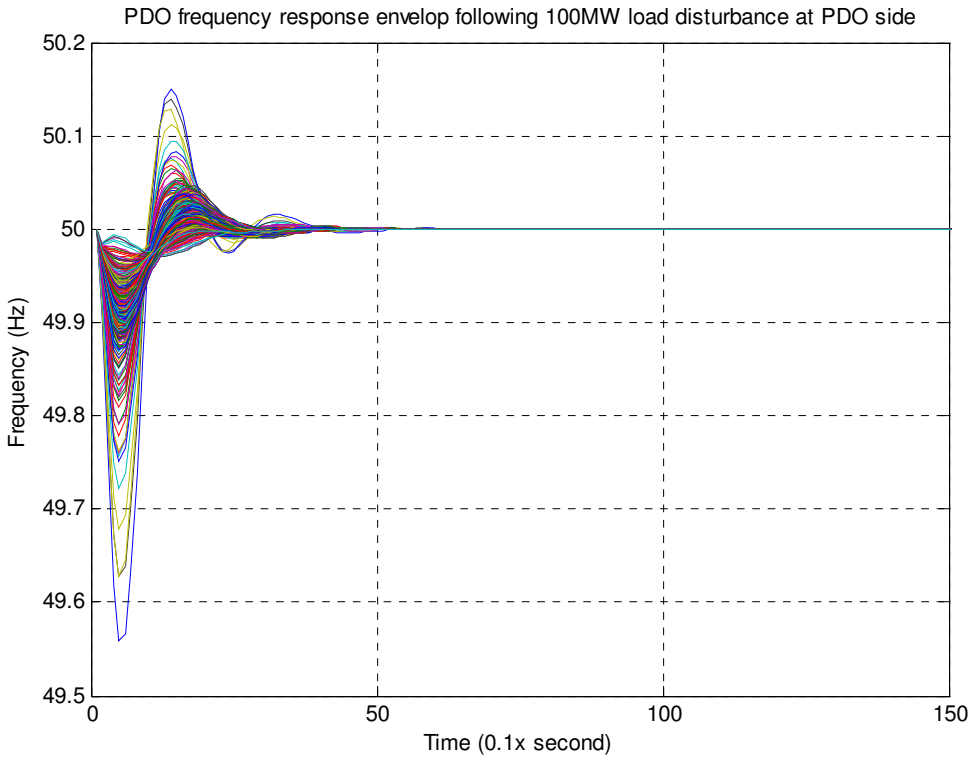

Figure 13.4: PDO frequency response envelop following 100MW load disturbance at PDO side with the PSO optimised FLPID2 AGC controller

13.4. Results discussion

From Figure 13.1, it can be seen that the PDO-OETC power system dynamic behaviour can change over time when the system operating points change. It is also evident that overall model dynamic response is sensitive to modelling errors and uncertainties. When considering the uncontrolled model, the response envelop is very wide especially towards the steady state value. The steady state deviation value is predominantly affected by the droop control settings. The frequency-response characteristic factor values, inertia values and the synchronising torque coefficient mainly affect the oscillations and settling time.

From Figures 13.2 to 13.4 one can see that the modified LQR AGC controlled response lines follow the same pattern whereas the fminsearch optimised FLPID2 AGC and the PSO optimised FLPID2 AGC controlled responses lines do not strictly follow the same pattern. The result suggests that the modified LQR AGC controller is more robust to power system operating points changes and modelling errors than the fminsearch optimised FLPID2 AGC and the PSO optimised FLPID2 AGC controllers. However the PSO optimised FLPID2 AGC and the fminsearch optimised FLPID2 AGC controllers have maintained the good performance in terms of settling time while the modified LQR AGC controllers has extended the settling time for different operating points.

In general, all the above three controllers show acceptable robustness to the model parameters changes which suggests that any of those three controllers will be suitable for practical application. It is also evident that there is a trade off between the controller performance in terms of settling time and the controller robustness.

13.5. Summary

The robustness of modified LQR, fminsearch optimised FLPID2 and the PSO optimised FLPID2 AGC controllers was tested. The modified LQR AGC controller shows better robustness to model parameters changes when it is compared with the fminsearch optimised FLPID2 and the PSO optimised FLPID2 AGC controllers. However, the fminsearch optimised FLPID2 and the PSO optimised FLPID2 AGC controllers have preserved the good settling time although their dynamic response does not strictly follow the same pattern for different model parameters. Overall all three controllers have shown acceptable robustness towards modelling errors and changes in the operating points of the PDO-OETC power system. Therefore, from robustness point of view, all three controllers can be recommended for practical application.

Chapter 14: Assessment of GCC interconnection impact on PDO-OETC power system AGC controllers performance

14.1. Introduction

The Gulf Cooperation Council (GCC) is a regional organization established in May 1981 by Sultanate of Oman, Bahrain, Kuwait, Qatar, Saudi Arabia and United Arab Emirates (Konstantinos et al, 2007). The main objective of the GCC is developing and solidifying the political, economical, and social ties among the member states (Al-Asaad, 2009). Together with the high population growth rate and the economic growth of about 6% annually, the GCC has been encountering exponential growth in electricity demand approaching 10 percent annually in many of member states (Al-Asaad, 2009). As one of the cooperation initiatives amongst the GCC states, and following extensive feasibility studies, the GCC Electrical Interconnection Authority was established in July 2001 by Royal Decree with its headquarter located in Dammam, and control center in Ghunan, Saudi Arabia. Since then the individual states has been investing in their respective transmission network looking forward towards fully integrated GCC network. The GCC electrical interconnection capacity was firmed as in Table 14.1 and the capital cost sharing was allocated accordingly. All the GCC states operate with a power supply of 50Hz frequency except Saudi Arabia operating at a power supply of 60Hz frequency which necessitates the introduction of HVDC link as shown in Figure 14.1. The overall GCC electrical interconnection route is shown in Figure 14.2.

System	Size (MW)
Kuwait	1200
Saudi Arabia	1200
Bahrain	600
Qatar	750
UAE	900
Oman	400

Table 14.1: Size of interconnection to each GCC state

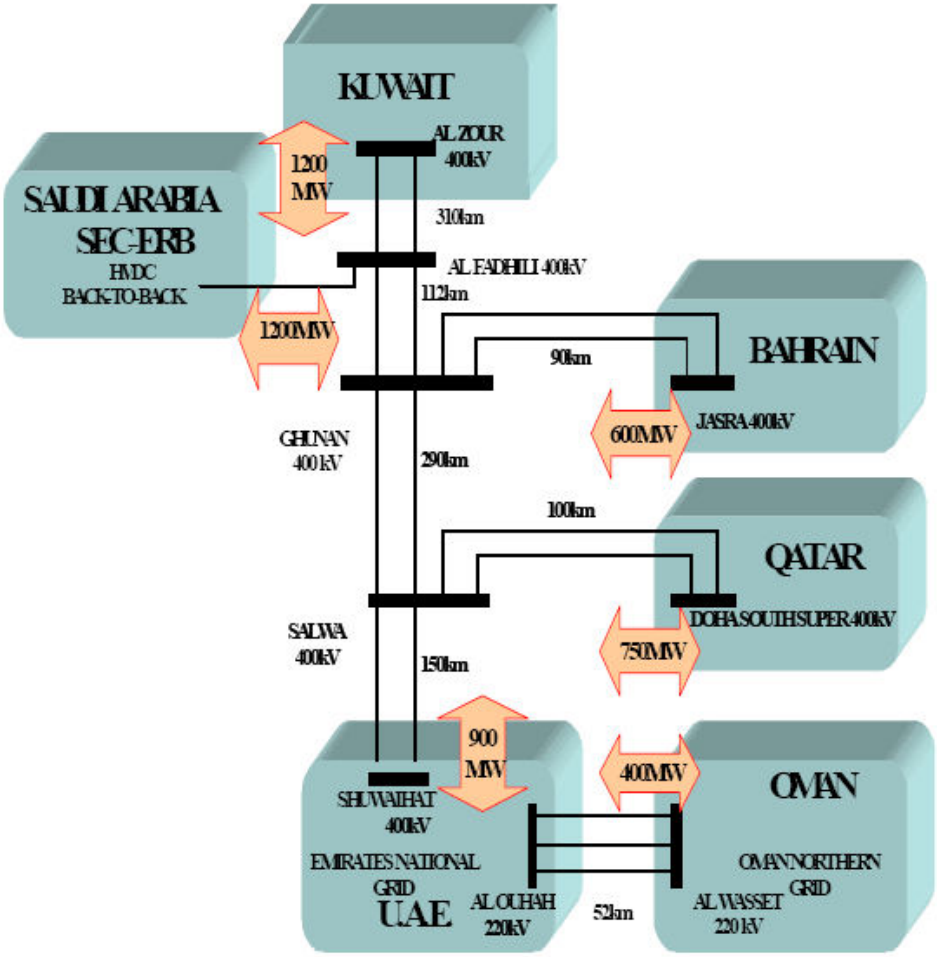

Figure 14.1: Conceptual diagram of the GCC interconnection system

Figure 14.2: Approximate route and layout of GCC interconnection

The GCC interconnection has an immediate benefit in terms of sharing spinning reserve. Sharing spinning reserve can be translated into less installed generation capacity requirement, lower fuel consumption and enhanced security of supply.

The GCC interconnection was planned to be completed in phases. Phase I is to interconnect Kuwait, Saudi Arabia, Bahrain and Qatar and the project was formally inaugurated on 14th of December 2009 and is called the GCC North grid. Phase II of the project is the interconnection of the independent systems in the UAE as well as Sultanate of Oman which is ongoing and is called the GCC South grid. Phase III of the project is to interconnect the GCC North grid with GCC South grid which is still pending. Upon completion of Phase II and Phase III of the project, all the six GCC states will be electrically interconnected.

14.2. Methodology

The main objectives of this part of the study are to study the impact of GCC interconnection on both PDO and OETC power systems and to assess the performance of PDO-OETC AGC in light of the GCC interconnection. The GCC interconnection Phase I is already in operation comprising the four states: Saudi Arabia, Kuwait, Bahrain and Qatar. Since Saudi Arabia is connected to the GCC grid through HVDC link, there will be minimal dynamic interaction between the GCC 50Hz frequency and the Saudi Arabia 60Hz frequency. Essentially, the power exchange between Saudi Arabia and the rest of GCC grid will act as a load disturbance at GCC grid. Hence Saudi Arabia power system will not be considered as a stand alone control area. Since Kuwait, Bahrain and Qatar are interconnected with a 400kV lines, they are electrically close to each other. Therefore they can be considered as one control area. Phase II of the GCC interconnection project is to interconnect Sultanate of Oman grid (OETC) to UAE grid, hence UAE power system can be assumed as a stand alone control area. Based on those two assumptions, there will be a total of 4 control areas upon completion of phase III of the GCC interconnection project:

1. PDO
2. OETC
3. UAE
4. GCC North (Kuwait, Bahrain and Qatar)

The above statement is good enough for qualitative frequency dynamics assessment but may not be true for sophisticated dynamic analysis. Since the focus of this part of the study is to assess the high level impact of GCC interconnection, the above assumptions are acceptable. The UAE control area and Kuwait, Qatar and Bahrain control area will be

modelled based on correlation with OETC control area in terms of inertia values, load damping torque and generators damper windings torque. The correlation will be based on the total installed capacity in each of UAE, Kuwait, Bahrain and Qatar. The turbines parameters will be assumed common for all control areas. All these assumptions are necessary to avoid the non-feasible amount of work required to accurately model each and every state power system based on the as built data.

In summary there are four cases during which the frequency dynamic and steady state response following load disturbances will be assessed:

1. PDO, OETC and UAE control areas interconnected and no AGC applied at PDO or OETC
2. PDO, OETC and UAE control areas interconnected with AGC applied at PDO and OETC
3. PDO, OETC, UAE and GCC North control areas interconnected and no AGC applied at PDO or OETC
4. PDO, OETC, UAE and GCC North control areas interconnected with AGC applied at PDO and OETC

14.3. Modelling

14.3.1. Overall GCC power system model

PDO and OETC control areas remain the same as per the base case used earlier in section 9.5. During cases 2 and 4 above, the PSO optimised FLPID2 PDO-OETC AGC controller will be used. However, the reference grid frequency of the generators damper windings torque will change. The following discussion demonstrates the reference grid frequency for the generators in each control area:

- Since PDO is interconnected with OETC only, the obvious reference grid frequency is OETC frequency.
- OETC is interconnected with both PDO and UAE. However OETC is interconnected with UAE using 220kV lines versus 132kv lines with PDO making it electrically closer to UAE. Therefore the reference grid frequency for OETC is UAE frequency.
- UAE is interconnected to both OETC and GCC North. Since UAE is interconnected with GCC North using 400kV lines versus 220kv lines with OETC, hence it is electrically closer to GCC North. Therefore the reference grid frequency

for UAE is GCC North frequency. However for the case when UAE is not yet interconnected with GCC North as of Phase II of the project, the obvious reference grid frequency is OETC frequency.

- Since GCC North is interconnected with UAE only, the obvious reference grid frequency is UAE frequency.

Based on the above discussion and the requirement of simulating the four cases mentioned in section 14.2 the overall GCC power system models adopted for this study comprises three control areas model and four control areas model which are shown in Figures 14.3 and 14.4 respectively. .

The third control area (UAE power system) and the fourth control area (GCC North grid) will be modelled in the following sections.

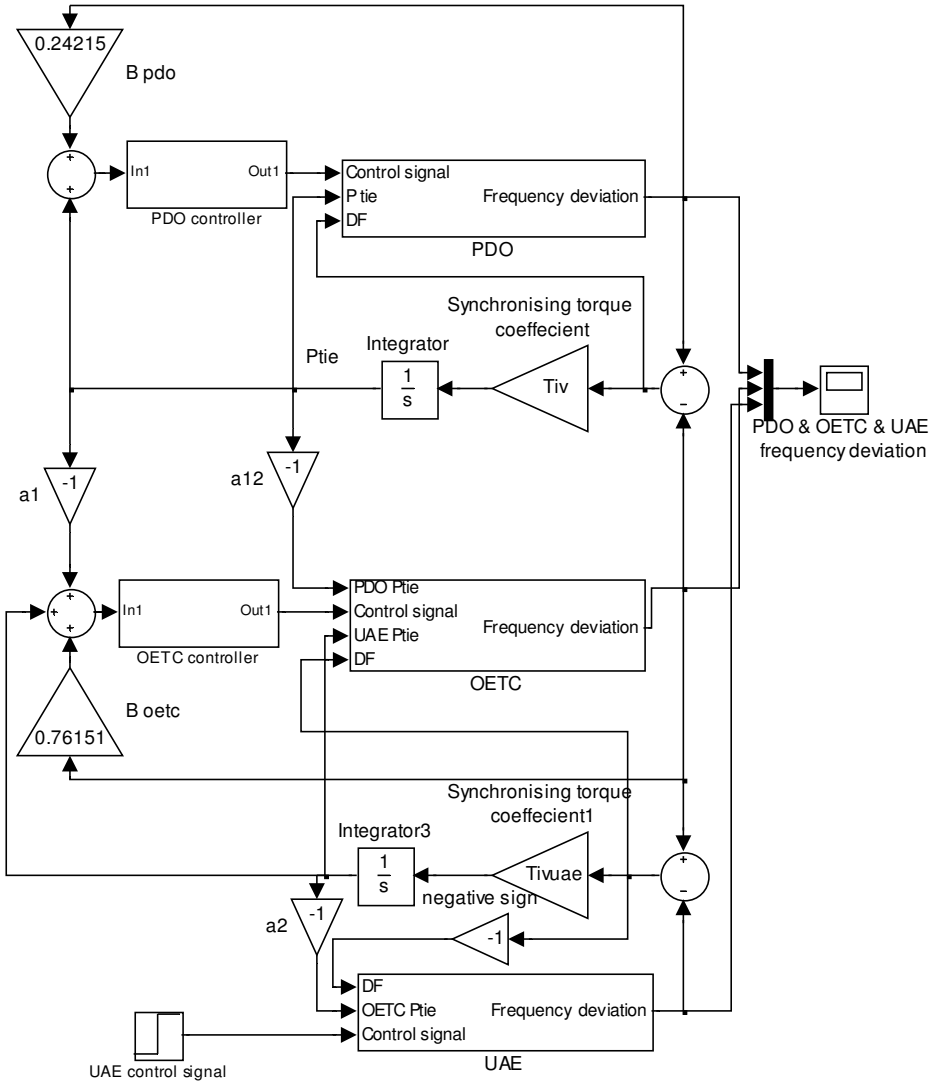

Figure 14.3: three control areas GCC interconnected power system model used for AGC study

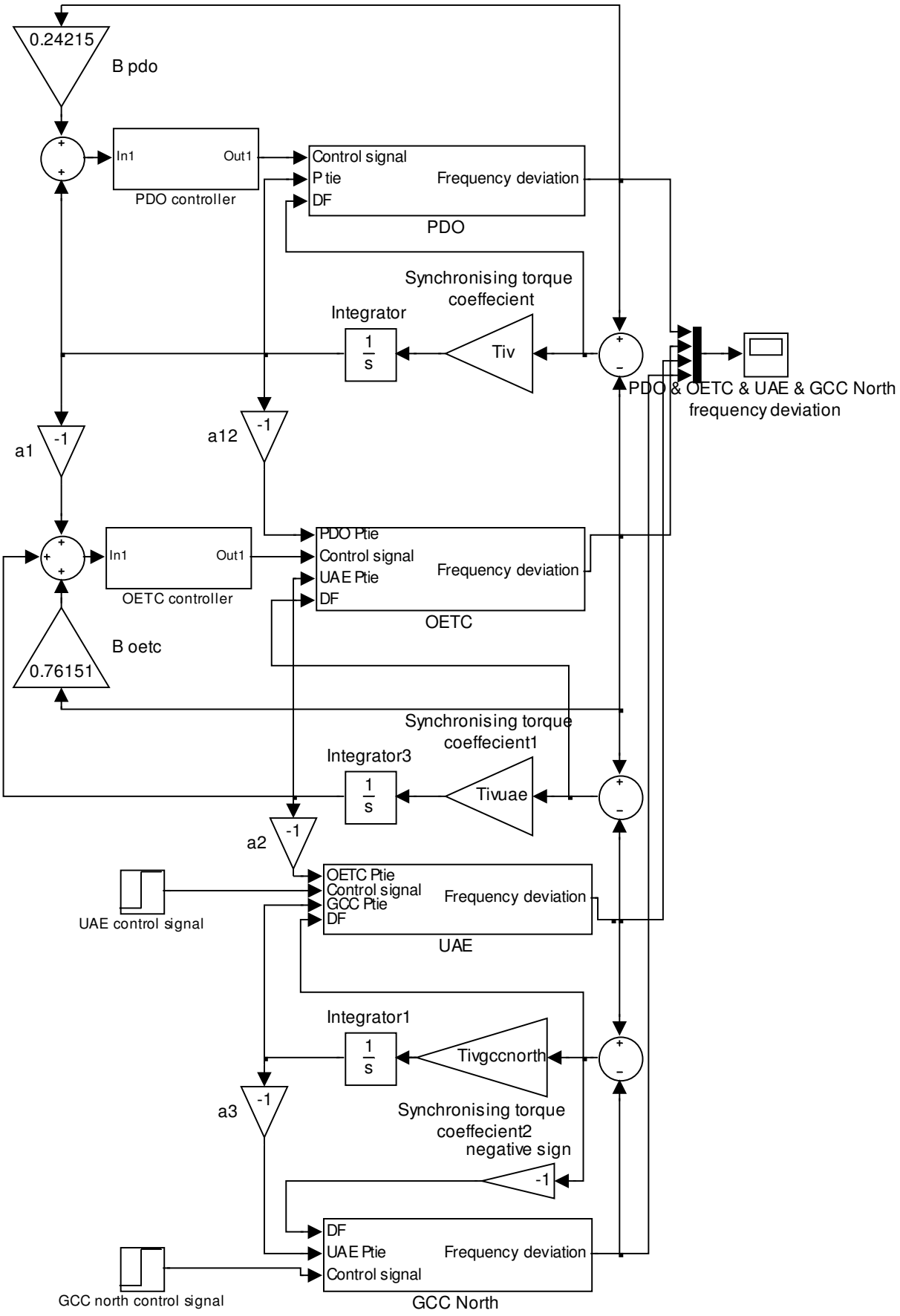

Figure 14.4: four control areas GCC interconnected power system model used for AGC study

14.3.2. Third GCC control area (UAE power system) model

14.3.2.1. Prime movers model

In this part, the gas turbines and the steam turbines parameters are assumed to be the same as in OETC and PDO. The droop control setting is assumed to be similar to PDO and OETC of 4% and therefore the UAE droop control constant (Ruae) is 2Hz.

14.3.2.2. Tie line model

Similar to the PDO-OETC synchronising torque calculation carried in section 4.7.1, the OETC-UAE synchronising torque coefficient can be calculated given the following information:

- Short circuit level at OETC AlWasit substation is 3239MVA (based on consultation with experts)
- Short circuit level at UAE AlOuhah substation is 3811MVA (based on consultation with experts)
- Typical 220kV overhead transmission line impedance is 0.3213 ohm per km (based on consultation with experts)
- There are three 52km of 220kV OHTL circuits between OETC and UAE

Following the same approach given in section 4.7.1, the synchronising torque coefficient of the interconnection between OETC and UAE is calculated to be 4.586 p.u. MW/Hz.

14.3.2.3. Control area model

Since there are no published actual data about generation and load of other GCC countries, forecasted figures have to be used. Al-Alawi (1999) has forecasted OETC load and Generation to be 2468MW and 3077MW respectively for the year 2010. Comparing these figures with the actual ones adopted for the base case in section 4.7.1 which are 2400MW for the load and 2927MW for the generation, we can see they are closely matching. Knowing that the base case figures in section 4.7.1 are based on 2007 actual data, we can assume that the annual growth assumed by Al-Alawi (1999) is less than the actual growth and therefore all the figures he forecasted for 2010 are actually suitable for the 2007 base case. Since Al-Alawi (1999) has forecasted that UAE generation capacity by the year 2010 is 7275MW and the load is 5971MW, these figures will be used for the 2007 base case. For modelling the UAE control area, a direct correlation with OETC control area is assumed reasonable. Since OETC generation is 2927MW and the calculated OETC inertia in section 4.7.1 is 14.03546 (s), the UAE system inertia is calculated as below:

UAE control area inertia constant H= (UAE generation/OETC generation) x OETC inertia= (7275/2927) x 14.03546 = 34.8849 s

Same calculation as in section 4.7.1 is followed to calculate the load frequency damping factor. Given that UAE load is 5971MW and assuming 30% of the load is industrial and 70% residential, the load frequency damping factor is calculated to be $84.2X10^{-3}$ p.u.MW/Hz.

The UAE generation damper winding coefficient can be calculated in a similar fashion as in section 7.3.2:

$$K(UAE) = \frac{2}{2000 \times 50} \times 7275 = 145.5 \times 10^{-3}\ p.u.MW / Hz$$

Since almost all the GCC states have the same requirements for water desalination and therefore the existence of steam turbines, it is fair to assume that they have the same percentage contribution from steam turbines in opposition to gas turbines as in OETC. Therefore UAE steam turbines and gas turbines contribution to the overall generation is calculated in correlation with OETC steam turbines and gas turbines contribution. The overall UAE p.u. generation based on 2000MVA base is 3.6375 p.u. MW. The steam turbines and gas turbines contribution is then calculated in correlation with OETC control area and is found to be:

- Steam turbines contribution = 0.73322p.u.MW
- Gas turbine contribution = 2.90428 p.u. MW

14.3.2.4. Overall UAE control area reduced model

The overall UAE control area reduced model is shown in Figure 14.5 and the model parameters are summarised in Table 14.2.

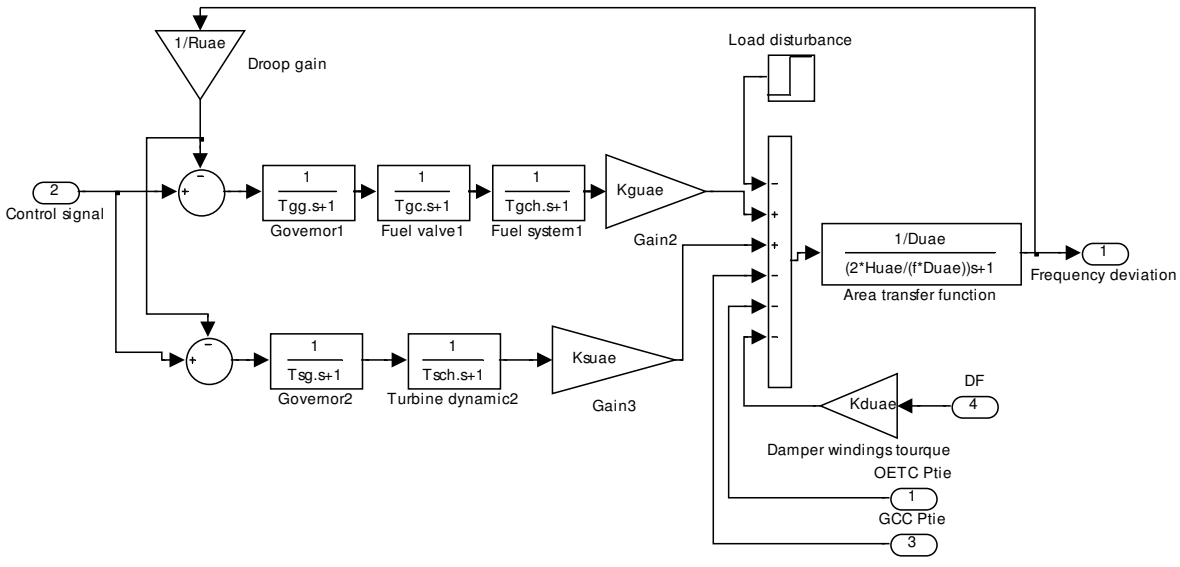

Figure 14.5: UAE control area reduced model

Tgg (s)	Tgc (s)	Tgch (s)	Tsg (s)	Tsch (s)	Kguae (p.u.MW)	Ksuae (p.u.MW)	Ruae (Hz)	Huae (s)	Kduae (p.u.MW/Hz)	Duae (p.u.MW/Hz)
0.05	0.05	0.4	0.2	0.3	2.90428	0.73322	2	34.8849	$145.5X10^{-3}$	$84.2X10^{-3}$

Table14.2: UAE control area reduced model parameters.

14.3.3. Fourth GCC control area (Kuwait, Bahrain, Qatar) model

14.3.3.1. Prime movers model

Same as in section 13.4.2.1, steam turbines and gas turbines models parameters are assumed to be the same as in OETC and PDO power system model. The droop control settings will also be assumed to be 4% as it is very common in the power system utilities. Therefore the GCC North grid control area droop control constant (Rgcc) will be 2Hz.

14.3.3.2. Tie line model

Similar to the PDO-OETC synchronising torque calculation carried in section 4.7.1, the UAE-North GCC system synchronising torque coefficient can be calculated given the following information:

- Short circuit level at UAE Shuwaihat substation is assumed to be 5000MVA (based on consultation with experts)
- Short circuit level at Qatar Salwa substation is assumed to be 5000MVA (based on consultation with experts)
- Typical 400kV overhead transmission line impedance is 0.310 ohm per km (based on consultation with experts)
- There are two 150km of 400kV OHTL circuits between UAE and GCC North grid

Following the same approach given in section 4.7.1, the synchronising torque coefficient of the interconnection between OETC and UAE is calculated to be 5.761 p.u. MW/Hz.

14.3.3.3. Control area model

Al-Alawi (1999) has forecasted that the total generation capacity of Kuwait, Bahrain and Qatar by the year 2010 is 20663MW and the total load is 16294MW. The same discussion as in section 14.3.2.3 is applicable here and therefore all the figures forecasted for 2010 are actually suitable for the 2007 base case. For modelling the GCC North grid control area, a direct correlation with OETC control area is assumed reasonable. Therefore since OETC generation is 2927MW and the calculated OETC inertia in section 4.7.1 is 14.03546 (s), the GCC North grid system inertia is calculated as below:

GCC North grid control area inertia constant H= (GCC North grid generation/OETC generation) x OETC inertia= (20663/2927) x 14.03546 = 99.0826 s

Same calculation as in section 4.7.1 is followed to calculate the load frequency damping factor. Given GCC North grid total load is 16294MW (Al-Alawi, 1999) and assuming 30% of the load is industrial and 70% residential, the load frequency damping factor is calculated to be 187.381X10^{-3} p.u.MW/Hz.

The GCC North generation damper winding coefficient can be calculated in a similar fashion as in section 7.3.2:

$$K(GCCnorth) = \frac{2}{2000 \times 50} \times 20663 = 413.26 \times 10^{-3}\ p.u.MW / Hz$$

Same as in section 14.3.2.3, the GCC North grid system steam turbines and gas turbines contribution to the overall generation is calculated in correlation with OETC steam turbines and gas turbines contribution. The overall GCC North grid p.u. generation based on 2000MVA base is 10.3315 p.u. MW. The steam turbines and gas turbines contribution is then calculated in correlation with OETC control area and it is found to be:

- Steam turbines contribution = 2.0825p.u.MW
- Gas turbine contribution = 8.249 p.u. MW

14.3.3.4. Overall GCC North grid control area reduced model

The overall GCC North grid control area reduced model is shown in Figure 14.6 and the model parameters are summarised in Table 14.3.

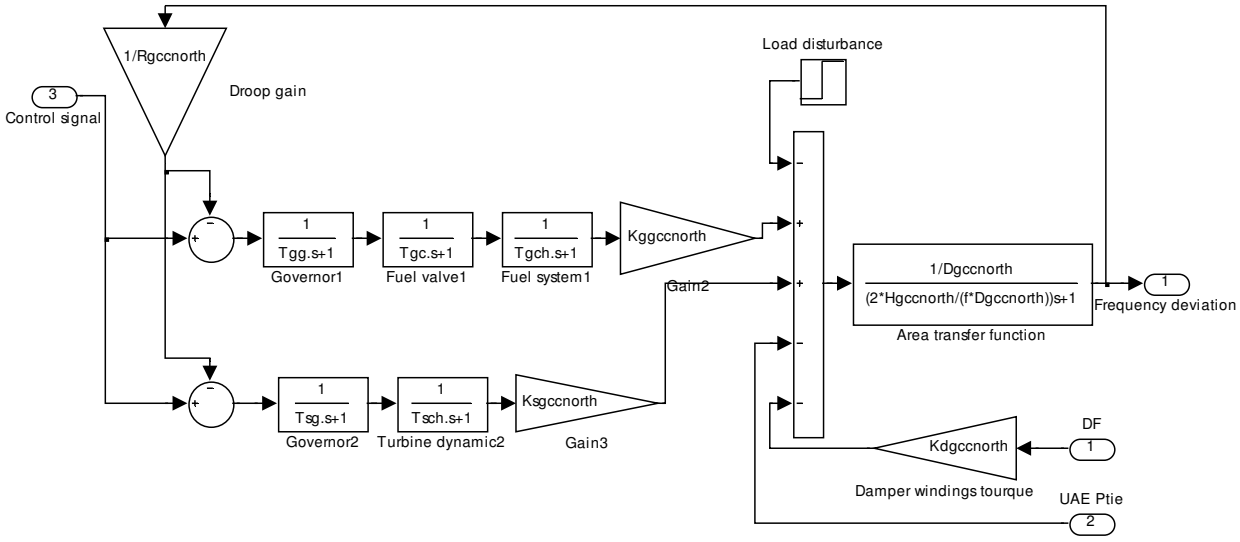

Figure 14.6: GCC North grid control area reduced model

Tgg (s)	Tgc (s)	Tgch (s)	Tsg (s)	Tsch (s)	Kggccnorth (p.u.MW)	Ksgccnorth (p.u.MW)	Rgccnorth (Hz)	Hgccnorth (s)	Kdgccnorth (p.u.MW/Hz)	Dgccnorth (p.u.MW/Hz)
0.05	0.05	0.4	0.2	0.3	8.249	2.0825	2	99.0826	413.26x10^{-3}	187.381X10^{-3}

Table14.3: GCC North grid control area reduced model parameters.

14.4. Simulation results

The three control areas model (PDO, OETC and UAE) shown in figure 14.3 has been used to simulate the following six scenarios:

1. 100MW load disturbance applied at PDO with NO AGC on PDO or OETC
2. 100MW load disturbance applied at OETC with NO AGC on PDO or OETC
3. 100MW load disturbance applied at UAE with NO AGC on PDO or OETC
4. 100MW load disturbance applied at PDO with AGC on PDO and OETC
5. 100MW load disturbance applied at OETC with AGC on PDO and OETC
6. 100MW load disturbance applied at UAE with AGC on PDO and OETC

The four control areas model shown in Figure 14.4 has been used to simulate the following eight scenarios:

1. 100MW load disturbance applied at PDO with NO AGC on PDO or OETC
2. 100MW load disturbance applied at OETC with NO AGC on PDO or OETC
3. 100MW load disturbance applied at UAE with NO AGC on PDO or OETC
4. 100MW load disturbance applied at GCC North grid with NO AGC on PDO or OETC
5. 100MW load disturbance applied at PDO with AGC on PDO and OETC
6. 100MW load disturbance applied at OETC with AGC on PDO and OETC
7. 100MW load disturbance applied at UAE with AGC on PDO and OETC
8. 100MW load disturbance applied at GCC North grid with AGC on PDO and OETC

The PSO optimised FLPID2 controller has been used whenever AGC is applied to PDO and OETC control areas in all above scenarios.

The size of load disturbance has been maintained as 100MW through all tests although it looks small for such a big interconnected power system. The reasons behind it are a) the system response characteristics are similar for different load disturbances values as discussed in section 5.3 and b) for ease of comparison with the previously obtained results.

For each scenario, two figures have been produced to show all control areas frequency in one figure and all tie line power exchanges in another figure. Accordingly for a total of fourteen scenarios, twenty eight graphs have been produced and are shown in Figures 14.7 to 14.34 in Appendix 9.

A summary table of all the frequency deviation, tie line power exchange and settling time of all control areas for all scenarios was produced and is shown in Table 14.4. The table also includes the frequency deviation, tie line deviation and settling times of the base case of PDO and OETC interconnected power system without AGC and with PSO optimised

FLPID 2 AGC controller for comparison purpose. All the settling times are taken as the time taken for PDO frequency to settle down to the nearest ±0.001Hz.

	Load disturbance	Steady state frequency deviation (Hz)	Settling time (s)	PDO-OETC tie line power deviation (p.u.)	OETC-UAE tie line power deviation (p.u.)	UAE-GCC North tie line power deviation (p.u.)
PDO & OETC only with No AGC	100MW load disturbance at PDO	-0.05	10.9	-0.0379	NA	NA
	100MW load disturbance at OETC	-0.05	7.74	0.0121	NA	NA
PDO & OETC only with AGC	100MW load disturbance at PDO	0	3.18	0	NA	NA
	100MW load disturbance at OETC	0	3.1	0	NA	NA
PDO, OETC and UAE with No AGC	100MW load disturbance at PDO	-0.017	12.7	-0.0458	-0.0327	NA
	100MW load disturbance at OETC	-0.017	10.6	0.0042	-0.0327	NA
	100MW load disturbance at UAE	-0.017	6.9	0.0042	0.0173	NA
PDO, OETC and UAE with AGC applied at PDO and OETC only	100MW load disturbance at PDO	0	5.52	0	0	NA
	100MW load disturbance at OETC	0	1.37	0	0	NA
	100MW load disturbance at UAE	-0.017	2.29	0.0042	0.0173	NA
PDO, OETC, UAE and GCC North with No AGC	100MW load disturbance at PDO	-0.006	11.3	-0.0485	-0.044	-0.0324
	100MW load disturbance at OETC	-0.006	11	0.0015	-0.044	-0.0324
	100MW load disturbance at UAE	-0.006	8.15	0.0015	0.0061	-0.0324
	100MW load disturbance at GCC North	-0.006	5.14	0.0015	0.0061	0.0176
PDO, OETC, UAE and GCC North with AGC applied at PDO and OETC only	100MW load disturbance at PDO	0	6.39	0	0	0
	100MW load disturbance at OETC	0	3.73	0	0	0
	100MW load disturbance at UAE	-0.006	3.66	0.0015	0.0061	-0.0324
	100MW load disturbance at GCC North	-0.006	2.55	0.0015	0.0061	0.0176

Table 14.4: Summary of GCC interconnection impact assessment results

14.5. Results discussion

From Figures 14.7 to 14.34 in Appendix 9, it is clear that the system frequency is stabilised following 100MW load disturbance at any particular control area considering all fourteen scenarios. In fact, the more interconnected generators are, the heavier is the system inertia and therefore the stiffer is the system frequency and the lesser is the steady state frequency deviation for a given load disturbance size. This is clearly demonstrated and can be seen from Table 14.4 by comparing the steady state frequency deviation following same load disturbances when PDO and OETC power systems are alone (-0.05Hz), when they are interconnected with UAE only (-0.017 Hz) and when they are interconnected with both UAE and GCC North control areas (-0.006Hz).

Consider the scenarios where PDO and OETC are interconnected with UAE with no AGC; it is clear from Figures 14.7 to 14.12 in Appendix 9 that the system frequency is highly oscillatory when the load disturbance is applied at the middle control area which is OETC in this particular case. This is caused by inter-area oscillations. The inter area oscillations exist because of the power flow in the tie lines between control areas is not in the same direction and will result on either ends control areas oscillating against each other. The system frequency oscillation has been significantly improved when the AGC is applied at PDO and OETC for the three control areas system which can be clearly seen from Figures 14.13-14.18 in Appendix 9.

Similarly for the four control areas interconnected system, from Figures 14.19 to 14.26 in Appendix 9, there is clear indication of serious inter area oscillations when the load disturbance is applied at the middle control areas OETC or UAE while AGC is not applied at PDO and OETC. This is again due to the cross flow of power in the tie lines between the control areas resulting in either ends control areas oscillating against each other. When the AGC is applied at PDO and OETC, the scenario has improved and the oscillations have been remarkably damped as can be seen from Figures 14.27 to 14.34 in Appendix 9.

From Table 14.4, considering the tie lines power exchange when AGC is not applied, one can deduce that individual control areas contributes with the same amount of power following load disturbance regardless of the disturbance location. For example, PDO contribution to outside 100MW load disturbances considering the three control areas system is 0.0042p.u. MW regardless of the disturbance location whether it has been at OETC or at UAE. Similarly for the four control areas system, when a 100MW load disturbance is applied at either OETC or UAE or GCC North, PDO contribution is 0.0015p.u. MW through the tie line power. From Table 14.4, it is also clear that control areas with AGC do not need steady state power support following internal load

disturbance. It is an important advantage of using AGC especially in a complicated interconnected power system.

Consider when all the four control areas PDO, OETC, UAE and GCC North are interconnected and AGC is not applied to any of those four control areas. When the disturbance of 100MW is applied at PDO, most of the power mismatch will be compensated by the other control areas as can be clearly seen from Figure 14.20 in Appendix 9 and Table 14.4. The power flow in the PDO-OETC tie line is 0.0485 p.u. MW towards PDO which equals to 97MW. There are two issues associated with the enormous support from the neighbouring control areas to PDO. The first one is that even if PDO is maintaining its own spinning reserve, it will not need it and PDO generators will not have the chance to convert the spinning reserve to MW. This is due to the very high accumulated generators inertia in the neighbouring control areas. Hence, it may not be economical for PDO to maintain its own spinning reserve. Therefore it is worth considering sharing spinning reserve with neighbouring control areas through formal agreement.

The second issue is the limitation in PDO-OETC tie line capacity. Knowing that the existing PDO-OETC tie line over-current protection is set to 100MVA for 1.5 seconds, there will be a great chance that the tie line over-current protection will capture the power swing shown in Figure 14.20 in Appendix 9 or even the steady state flow and trip the line creating a very difficult scenario at PDO. Therefore PDO and OETC will have to revise their interconnector over-current protection settings to avoid the unnecessary outage of the tie line during a 100MW load disturbance at PDO side. Increasing the setting is permissible since the thermal capacity of the line is 180MVA. However when AGC is applied at PDO, the PDO-OETC tie line power flow will not trigger the existing over-current protection as can be seen from Figure 14.28 in Appendix 9 and Table 14.4. Therefore AGC is advantageous in stabilising the power system and alleviating the need for upgrading the interconnector capacity or raising the protection settings.

14.6. Summary

PDO and OETC control areas will enjoy the stiff system frequency when interconnected with other GCC control areas. There will be an enormous power support following load disturbances when AGC is not considered to the extent that PDO and OETC need to revise the over-current protection settings of their tie line or increase the interconnection capacity before the GCC interconnection project is fully commissioned. However, the AGC will improve the dynamics and will help damping the inter-area oscillations if implemented.

Therefore the AGC will alleviate the need of revising the PDO-OETC interconnector protection settings or upgrading the interconnector capacity. PDO will not require maintaining its own spinning reserve hence it is recommended to share spinning reserve with the neighbouring control areas. Overall, the GCC interconnection project will have direct benefits to PDO and OETC.

Chapter 15: Conclusion

This research has presented a coherent case study of applying Automatic Generation Control to PDO-OETC interconnected power system. The study has started with traditional power system modelling for Automatic Generation Control analysis. The developed model has then been through extensive testing to explore its basic characteristics. The developed model has then been validated against real data recorded from the field during major occurrences at PDO-OETC interconnected power system. The validation process has proved that the developed model still needs further improvement.

Traditional and novel approaches have then been followed to refine the developed model aiming to match the developed model response with the real life recorded data. The refining process has achieved its milestone and the refined model response is very close to the reality. Accordingly the refined model has been declared suitable for further analysis. The refined model has also been suitably converted to state space representation ready for further use.

The refined PDO-OETC model has then been used as basis to study the performance characteristics of fifteen different AGC topologies. Traditional Zeigler Nichols PID controller has been used for this purpose. Although the traditional Zeigler Nichols PID controller is a very basic controller but it is very easy to design and fit for the purpose of investigating the general characteristics of each AGC control topology.

A total number of five control topologies out of the fifteen are found not suitable for AGC control practical application. A total number of seven control topologies are recommended for AGC practical application and another three control topologies can be applied but with cautious.

The AGC control topologies assessment has been followed by detailed design of AGC controller using different control techniques namely Linear Quadratic Regulator (LQR) and Fuzzy Logic theory. Both control techniques have been applied to PDO-OETC AGC control. A combination of Fuzzy logic and traditional PID AGC controller proved to be very efficient and has produced fantastic results. The LQR AGC controller has also produced comparable results as with the Fuzzy PID AGC controller.

The Fuzzy Logic PID AGC controllers' performance has then been further optimised using some control guidelines in order to produce better dynamic and steady state response, reduce wear and tear in the power system generation units and reduce the environmental impact by reducing fuel consumption. A set of control guidelines are stipulated for the optimisation process extracted from the Grid code and PDO-OETC service level

agreement. Different optimisation methods have been utilised like multidimensional unconstrained nonlinear minimization (fminsearch) function and Particle Swarm Optimisation (PSO) method. The optimized Fuzzy Logic PID AGC controllers have produced better results than the unconstrained Fuzzy Logic PID controllers.

The robustness of the developed AGC controllers using different techniques has then been tested. The LQR AGC controller has been proved to be more robust than the Fuzzy Logic PID AGC controllers. On the other hand, the Fuzzy Logic PID controller robustness is not bad considering its design flexibility and the less number of states feedback when it is compared with the LQR AGC controller.

Finally, a qualitative study of the impact of GCC electrical interconnection on the dynamic and steady state frequency of PDO-OETC power system is considered. The modelling of the neighboring GCC states control areas was very crude but rather useful to get the high level impression. Some reasonable assumptions have been made to formulate the overall GCC electrical interconnection model. The results of the assessment have proved that PDO and OETC will enjoy a very stiff system frequency. An enormous support from the neighboring states will be naturally available following load disturbances at PDO or OETC. PDO will not need to maintain its own spinning reserve and therefore it is recommended to share spinning reserve with its neighboring control areas.

However serious inter area oscillations have been noticed from the frequency response following load disturbances. These oscillations can actually trip the interconnection tie lines. The application of AGC at PDO and OETC control areas will help in damping out these oscillations and stabilizing the grid frequency. Furthermore, the existing interconnection capacity between PDO and OETC has been identified as a bottleneck and therefore needs to be reinforced before commissioning the final phase of GCC interconnection project. The application of AGC at PDO and OETC control areas will help alleviating such requirement.

As a continuation of this research effort, the following elements can be considered for further work:

- Design Automatic Generation Control for all GCC interconnection control areas using as build data of all GCC states power systems. The AGC design need to adopt a single performance index/cost function based upon the criteria used in this report or different criteria that suits all involved parties.
- Look into multivariable control structures as a potential control technique

Appendices

Appendix 1: Published papers

This research so far has been presented with two papers at two international conferences. Each paper is given with its abstract and reference:

1. Modelling of Petroleum Development Oman (PDO) and Oman Electricity Transmission Company (OETC) power systems for Automatic Generation Control studies

Abstract: Petroleum Development Oman (PDO) and Oman Electricity Transmission Company (OETC) are running the main 132kV power transmission grids in the Sultanate of Oman. In the year 2001, PDO and OETC grids got interconnected with a 132kV Over head transmission line linking Nahada 132kV substation at PDO's side to Nizwa 132kV sub-station at OETC's side. Since then the power exchange between PDO and OETC is driven by the natural impedances of the system. The only frequency and power exchange control mean available for the operators of the interconnected grids is re-dispatching their generators. It is a great challenge for PDO and OETC grids operators to maintain the existing philosophy of controlling the frequency and power exchange in light of the daily load profile and the forecasted Gulf Council Countries (GCC) interconnection. The objective of this research is to adopt the Automatic Generation Control technology to control the grid frequency as well as the power exchange between PDO and OETC grid. The first part of the research was to model and validate the model of the interconnected grids of PDO and OETC. This paper shows how the model has been developed and validated against the real data obtained from the field. For such a large scale power system a certain margin of modelling errors and uncertainties is anticipated and considered acceptable.

Reference: Adil Al-Busaidi & Ian. French “Modelling of Petroleum Development Oman (PDO) and Oman Electricity Transmission Company (OETC) power systems for Automatic Generation Control studies”, International Conference on Communication, Computer and Power (ICCCP'09), Muscat, February 15-18, 2009

2. Automatic Generation Control of PDO-OETC interconnected power system using LQR and FLPID with the novel approach of considering generators damper windings torque.

Abstract: Petroleum Development Oman (PDO) and Oman Electricity Transmission Company (OETC) are running the main 132kV power transmission grids in the Sultanate

of Oman. In the year 2001, PDO and OETC grids got interconnected with a 132kV over head transmission line. Since then, the power exchange between PDO and OETC is driven by the natural impedances of the system. The only frequency and power exchange control mean available for the operators of the interconnected grids is re-dispatching their generators. It is a great challenge for PDO and OETC grids operators to maintain the existing philosophy of controlling the frequency and power exchange in light of the daily load profile and the Gulf Cooperation Council (GCC) electrical interconnection. This paper presents the modelling process of PDO-OETC interconnected power system using traditional and novel approaches. It then shows the design of PDO-OETC Automatic Generation Control using different techniques namely Linear Quadratic Regulator (LQR) and Fuzzy Logic PID. The paper will also compare the performance of the different control techniques

Reference: Adil. Al-Busaidi & Ian. French "Automatic Generation Control of PDO-OETC interconnected power system using LQR and FLPID with the novel approach of considering generators damper windings torque", International Conference on Power Systems Engineering (ICPSE 2011), Bangkok, December 25-26, 2011

Both of the mentioned papers are attached herein:

Modelling of Petroleum Development Oman (PDO) and Oman Electricity Transmission Company (OETC) power systems for Automatic Generation Control studies

Mr Adil Al-Busaidi [1], Dr Ian French [2]

***Abstract*— Petroleum Development Oman (PDO) and Oman Electricity Transmission Company (OETC) are running the main 132kV power transmission grids in the Sultanate of Oman. In the year 2001, PDO and OETC grids got interconnected with a 132kV Over head transmission line linking Nahada 132kV substation at PDO's side to Nizwa 132kV sub-station at OETC's side. Since then the power exchange between PDO and OETC is driven by the natural impedances of the system. The only frequency and power exchange control mean available for the operators of the interconnected grids is re-dispatching their generators. It is a great challenge for PDO and OETC grids operators to maintain the existing philosophy of controlling the frequency and power exchange in light of the daily load profile and the forecasted Gulf Council Countries (GCC) interconnection. The objective of this research is to adopt the Automatic Generation Control technology to control the grid frequency as well as the power exchange between PDO and OETC grid. The first part of the research was to model and validate the model of the interconnected grids of PDO and OETC. This paper shows how the model has been developed and validated against the real data obtained from the field. For such a large scale power system a certain margin of modelling errors and uncertainties is anticipated and considered acceptable.**

***Index Terms*— Power systems modelling, Automatic Generation Control (AGC).**

I. INTRODUCTION

Power supply frequency is considered as a key factor of power supply quality. Speed of induction and synchronous motors are dependant on the supply frequency. A deviation in the supply frequency will affect the speed of these motors and consequently, the performance of the process in which they are installed. Therefore it is extremely important to maintain the supply frequency at its nominal value. And in case of frequency deviation due to transient conditions, nominal frequency must be restored in an acceptable amount of time. Power systems regulators usually specify performance indices which must be maintained by the power systems operators.

Frequency deviations are caused by an unbalance between the output power of the generators and the load demand. This power mismatch will be compensated by a change in the rotational kinetic energy of the generators ending up with a deviation in the generators speed and hence the frequency. The general idea of controlling the frequency is to maintain the balance between the generated power and the consumed power. Since the existence of alternating current power systems, different philosophies have been applied to maintain the supply frequency. The most common control modes are the Isochronous control, Droop control and Automatic Generation Control. In the Isochronous control mode, a big generator will be assigned the task of maintaining the frequency and the rest of generators will be running at constant power output. In the Droop control mode, all generators will respond to the frequency deviation. Automatic Generation Control (AGC) is achieved by adding a secondary control loop to the Droop control loop in order to achieve better performance. The main aim of AGC is to maintain zero steady state frequency deviation and to track the load demands.

AGC has been around for the past few decades and it came into practical applications in many power systems around the world. AGC becomes particularly useful in interconnected power systems as it can control the power exchange between the neighbouring systems and enhances the overall system stability. The interest in AGC is growing up rapidly due to the interest in interconnected power systems.

Modelling of power systems will be inherent with different types of uncertainties due to the continuously changing parameters and characteristics, load fluctuations and modelling errors [1]. Moreover, power system parameters are a function of the operating points [2] and these points do change continuously due to the daily load variation and generation scheduling.

Conventionally, Proportional Integral (PI) controllers have been adopted to solve the AGC problem [3]. The PI controller is successful in achieving a zero steady state frequency deviation. However, due to the non-linear power

[1] Petroleum Development Oman (Sultanate of Oman), University of Teesside, School of Science and Technology (UK) (phone: 968-92881980; fax: 968-243813571; e-mail: Adil.Al-Busaidi@pdo.co.om)
[2] University of Teesside, School of Science and Technology (UK) (phone: 44-1642342548; e-mail: I.french@tees.ac.uk)

 ISSN: 1813-419X

systems, PI controller has a poor dynamic response [2].

Many of the published literature have proposed a number of control strategies to improve the AGC performance. In some of the literature, optimal control techniques [4, 5] and variable structure control [6] were proposed to solve the AGC problem and have shown a robust control results. However they are based on states feedback which makes it very difficult to implement because information about the states are either not available or difficult to obtain [7].

A significant number of the published papers attempted to apply the fuzzy logic controllers to AGC [8-9]. Since fuzzy logic controllers are good in dealing with complicated, non-linear, indefinite and time-variant systems [10], they seem to be feasible for the AGC. In the published literature, many fuzzy logic arrangements were proposed like the basic PI & PID fuzzy controllers [11], self tuning & Fuzzy gain scheduling [12, 13, 14, 15, 16,10,17] and multi-stage fuzzy controller [8, 7].

Artificial Neural Networks (ANN) controllers were also used by some researchers to solve the AGC problem [18, 1, 19]. The merit of ANN is they can deal with uncertain system model and parameters making it quiet suitable for power systems applications. However, ANN needs some recorded data from the field for the training purpose which again imposes some difficulties in its practical application.

Genetic algorithm is also used by some researchers [20, 9] to calculate the initial controller gains in cooperation with fuzzy logic controllers.

It became obvious requirement that AGC controllers must be robust to cater for system non-linearities and uncertainties and decentralised to reduce the required signals from the field.

The effects of the generating units' limitations received a considerable attention by the investigators in the AGC filed. Generation rate constraint and governors dead band have been modelled by some researchers [12, 11, 21, 7] in an effort to eliminate modelling errors.

The power market in some countries has been restructured from the vertical hierarchy to the bilateral contracts environment where distribution companies can make direct contracts with generation companies elsewhere in the grid [7]. This mode of operation puts more burdens on the grid operators. Some work has been done to use the traditional AGC with some modification to operate the new deregulated power system environment [18, 22, 7]. The possible bilateral contracts are represented by introducing the concept of an augmented generation participation matrix which represents all possible contracts between generation and distribution companies [7]. The effects of the possible contracts are then treated as a set of new input disturbances [18].

Almost all the published papers used a simple power system models with few control areas and generators for the analysis. The general idea can then be applied to any specific power system. However the scale of the problem can be better explored by using practical size power systems models.

II. MODEL DEVELOPMENT

A. *Modelling of prime movers*

Modelling of generators prime movers can be a very complicated task due to the complexity of these units. In general, full thermodynamic or hydrodynamic models development leads to a computationally expensive solution [23 p 83]. Often the level of complicity can be alleviated by making the model fit for purpose and by accepting a certain amount of error. For Automatic Generation Control (AGC) studies a simplified model of prime movers can be used which leads to an acceptable accuracy of the input power variation to the generator [23 p 83]. The modelling process of prime movers is out of the scope of this paper. Instead, standard published models will be used for steam turbines and gas turbines.

1) *Modelling of steam turbines*

The real power generated by a steam turbine generator is controlled by means of the prime mover torque. This torque is affected by opening or closing the steam control valve of the steam turbine. The steam control valve is controlled by the governor which modulates the steam control valve opening in response to the turbine speed. A load change will affect the electrical torque and will cause a mismatch between the electrical torque and the machine mechanical torque. Hence the machine speed will change and the governor will respond accordingly.

The steam control valve housing is called the steam chest [24 p 425]. A substantial amount of steam can be accommodated in the steam chest and the inlet piping to the high pressure section of the steam turbine [24 p 425]. The response of the steam flow to a change in the control valve opening exhibits a time constant T_{CH} due to the charging time of the steam chest and the inlet piping [24 p 425]. For AGC studies, a steam turbine can be represented by first order transfer function with a time constant T_{CH} [24 p 598]

The steam turbine governing system can be Mechanical-hydraulic, Electrohydraulic or Digital Electro-hydraulic [24 pp 434-443]. The governing system response exhibits a time constant T_G due to the response time of the overall governor. For dynamic studies, a steam turbine governing system can be represented by first order transfer function with a time constant T_G [24 p 589].

For AGC studies the steam turbine and it governing system can be represented by two first order transfer functions as shown in Figure 1 [25, 5, 24 pp 589-598].

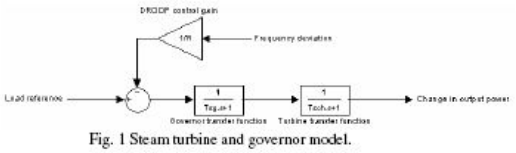

Fig. 1 Steam turbine and governor model.

In Figure 1 Tg (in seconds) is the governor time constant, Tch (in seconds) is the charging time constant of the turbine and R (Hz/pu MW) is the static speed droop of the turbine generator. To a very good approximation, the typical values of these constants are 0.3 s for Tch and 0.2 s for Tg [24 p 598]. In PDO and OETC, the droop control is set to 4% of the nominal frequency of 50Hz and hence:

$$R = 0.04 \times 50Hz = 2Hz / puMW$$

2) Modelling of gas turbines

Studies of gas turbines system revealed that the gas turbine and its governing system can be represented by three first order transfer functions [23 p121-122, p221]. One transfer function is to represent the governor lag time, the second transfer to represent the control valve lag time and the third transfer function is to represent the fuel charging characteristics. Figure 2 shows the dynamic model of gas turbine generators which will be used for this study. The same model is used by PDO for dynamic studies [26]. The governor time constant (Tg) is 0.05 s, the control valve time constant (Tc) is 0.05 s and the fuel system time constant (Tf) is 0.4s. The droop control is set to 4% of the nominal frequency of 50Hz and hence:

$$R = 0.04 \times 50 = 2Hz / puMW$$

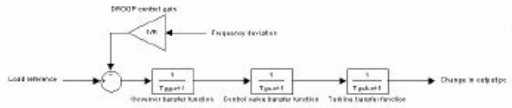

Fig. 2 Governor/turbine model of gas turbine generator [26].

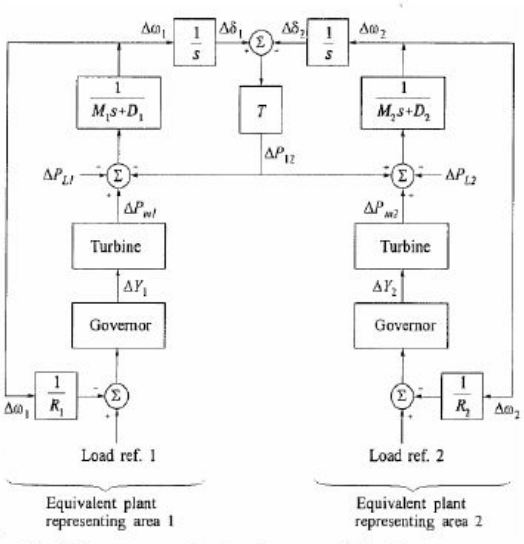

Fig. 4 Two-area system with only primary control [24 p603].

B. PDO-OETC interconnected model for AGC studies

1) Modelling of control areas

The following analysis is based on the assumption that the electrical interconnection within each individual control area (PDO & OETC) (Figure 3) is so strong, at least in relation to the ties between them, so that the whole area can be characterized by a single frequency only [25].

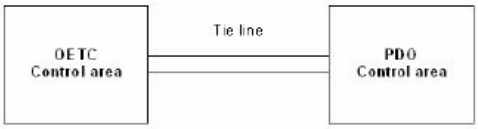

Fig. 3 Interconnection of individual control areas.

Practically, when the system deviates from the constant nominal frequency, every bus voltage will experience its own angular velocity or frequency. Assuming electrical interconnection within a control area is so strong, this will result in all generators belonging to that area swing in unison. Should this assumption not be permissible, then one must subdivide the area into sub-areas. Having said this assumption is valid for PDO and OETC grids, only two control areas will be considered; PDO and OETC.

To start with, exactly the same standard modelling process for AGC studies was followed as shown in reference 24 page 601. A general two areas with one turbine each AGC model is shown in the below Figure 4 [24 p 603]. There is no necessity to go through the whole modelling process in this paper. The paper will address how the standard model is customised to PDO and OETC systems.

2) Overall PDO system model

Since PDO power system consists of thirteen power stations, each of them will be represented as subsystem in PDO model where each subsystem will contain its turbines models in parallel. For example, a Power Station consisting of two gas turbine generators running in parallel is shown in Figure 5. The output of each turbine is multiplied by a factor to counter for its rating in per unit.

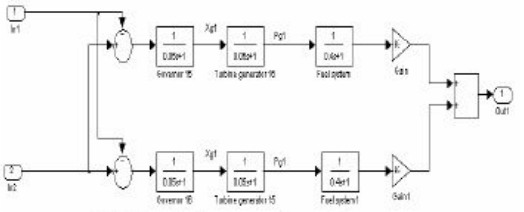

Fig. 5 Example of a power station model.

Upon combining the block diagrams of all Power Stations Subsystems as one equivalent area, we obtain the overall PDO perturbation model shown in Figure 6.

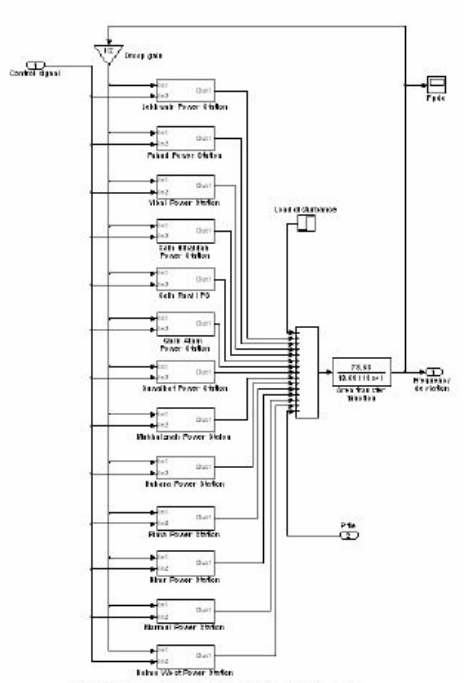

Fig. 6 PDO power system perturbation model.

3) Overall OETC system model

OETC power system was modeled in the same manner as PDO power system. Since there are steam and gas turbines installed in OETC, each subsystem in the model will contain its steam and gas turbines models accordingly. For example, a Power Station consisting of two gas turbine generators and one steam turbine generator running in parallel is shown in Figure 7. The output of each turbine is multiplied by a factor to counter for its rating in per unit.

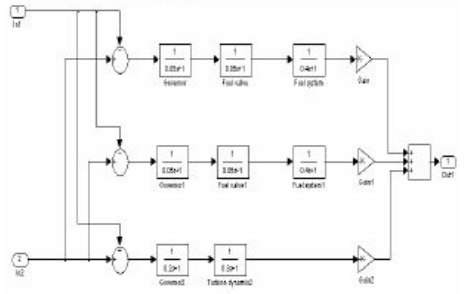

Fig. 7 Example of a power station model consisting of two gas turbines and one steam turbine generators.

C. *Overall perturbation model of PDO and OETC systems*

By masking PDO power system model and OETC power system model into subsystems and combining those as traditionally done as in Figure 4, the overall perturbation model of PDO-OETC systems is achieved and is shown in Figure 8. This model will serve as the basis for further analysis.

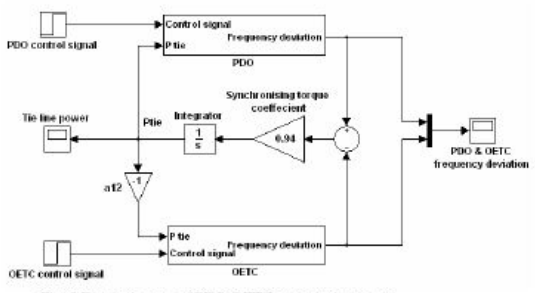

Fig. 8 Block diagram of PDO-OETC perturbation model.

Table 1 summarizes the parameters values of the complete perturbation model of PDO and OETC system.

	Control area		Overall perturbation model	
	Tp	Kp	Tiv	a_{12}
PDO	13.09113	73.53	0.94	-1
OETC	18.86487	33.6		

Table 1 Overall perturbation model parameters.

III. NOVEL APPROACHES

In order to make the developed model to behave as close as possible to the real system, some novel approaches were followed in this research. The following two phenomenons have been modelled as a novel approach in the modelling process of AGC:

A. *Base load and Pre-select load effect*

This is the effect of generators being at maximum load or fixed load. When the generator is at base load, it won't be able to supply any more power because it is already at its thermal limits. Moreover, when the generator is at fixed load, then it is not participating during load disturbances. All this will have an impact on the frequency response characteristics and need to be modelled.

Both of the above phenomenons have been modelled by introducing zero gain in series of the droop control signal to the particular generation unit. This worked fine during loss of generation scenarios.

B. *Generators damper windings effect*

Generators damper windings have twice the impact as the load damping effect during frequency transients. None of the literature attempt to incorporate this effect in the AGC modelling process. As a novel approach in this research, the generators damper windings effect was incorporated in the AGC modelling process. This was achieved by calculating the damping torque coefficient of all generators and incorporating it in the overall area model. This process showed great improvement in the frequency response characteristics.

IV. SIMULATION RESULTS & MODEL VALIDATION

Extensive work has been done in testing and validating the model. It was the field data that constrained the validation of the model. The model was validated based on the available field data. Figure 9 shows a real system response graph and simulated ones. The real scenario graph was captured at PDO side when a 140MW generator tripped at OETC grid. The real scenario then has been simulated twice using the developed models, one time using the traditional AGC model and the other time using the refined AGC model with the novel approaches. From Figure 9, it is clear that the novel approaches have improved the accuracy of the model. To a practical extent, the model response is close enough to the real system response. Considering the complexity of the real system a certain error is expected and should be acceptable. In fact the developed model is going to be used to develop a robust controller which will cater for some of the nonlinearities and uncertainties. From these results, the model is considered valid for further analysis.

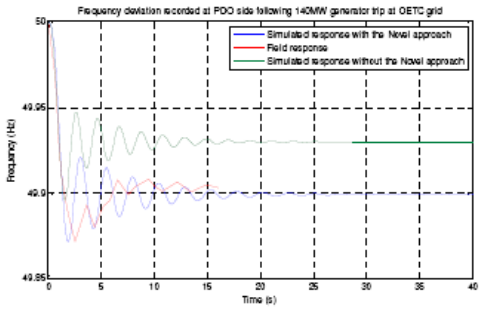

Fig. 9 Real and simulated frequency response to 140MW generator trip at OETC grid measured at PDO side.

V. CONCLUSION

The traditional modelling process for AGC studies were followed in modelling PDO-OETC interconnected power systems. As a novel approach, the traditional method has been refined and new ideas have been implemented. The new ideas contributed a lot to the model accuracy and validity.

The model will serve as basis for designing automatic generation controller which should be able to deal with nonlinearities and uncertainties of the model.

VI. FURTHER WORK

The work shown in this paper will serve as the basis for further work which is summarised as below:

- Design AGC controller representing a secondary control loop for all generators in the grid. The controller should be robust enough to cater for nonlinearities and modelling uncertainties. The controller should also consider market status and legal issues of both PDO and OETC power systems.
- Study PDO power system technical issues resulting from future GCC (Gulf Council Countries) interconnection.

ACKNOWLEDGMENT

The authors wish to thank Mr. Saif Al-Sumry (PDO Power System Manager) and Mr. Mohammed Al-Aghbari (PDO Head of Power System Operation and Maintenance) for their endless support.

REFERENCES

[1] H. Shayeghi and H.A. Shayanfar, Application of ANN technique based on μ-synthesis to load frequency control of interconnected power system, *International Journal of Electrical Power & Energy Systems*, Volume 28, Issue 7, September 2006, Pages 503-511.

[2] Y. L. Karnavas and D. P. Papadopoulos, AGC for autonomous power system using combined intelligent techniques, *Electric Power Systems Research*, Volume 62, Issue 3, 28 July 2002, Pages 225-239.

[3] Yusuf Oysal, A comparative study of adaptive load frequency controller designs in a power system with dynamic neural network models, *Energy Conversion and Management*, Volume 46, Issues 15-16, September 2005, Pages 2656-2668.

[4] M. Azzam, Robust automatic generation control, *Energy Conversion and Management*, Volume 40, Issue 13, September 1999, Pages 1413-1421.

[5] Fosha C.E. Jr. and Elgerd O.I., The megawatt-frequency control problem: a new approach via optimal control theory, IEEE Transactions on *Power* Apparatus and *Systems*, vol.Pas-89, no.4, April 1970. p. 563-77.

[6] N. N. Bengiamin and W. C. Chan, Variable Structure Control of Electric Power Generation., IEEE Transactions on *Power Apparatus and Systems*, Vol. PAS-101, No. 2 February 1982.

[7] H. Shayeghi, H.A. Shayanfar and A. Jalili, Multi-stage fuzzy PID power system automatic generation controller in deregulated environments, *Energy Conversion and Management*, Volume 47, Issues 18-19, November 2006, Pages 2829-2845.

[8] H. Shayeghi, A. Jalili and H.A. Shayanfar, Robust modified GA based multi-stage fuzzy LFC, *Energy Conversion and Management*, Volume 48, Issue 5, May 2007, Pages 1656-1670.

[9] S. P. Ghoshal, Application of GA/GA-SA based fuzzy automatic generation control of a multi-area thermal generating system, *Electric Power Systems Research*, *Volume* 70, Issue 2, July 2004, Pages 115-127.

[10] Ertuğrul Çam and İlhan Kocaarslan, A fuzzy gain scheduling PI controller application for an interconnected electrical power system, *Electric Power Systems Research*, Volume 73, Issue 3, March 2005, Pages 267-274.

[11] A. Demiroren and E. Yesil, Automatic generation control with fuzzy logic controllers in the power system including SMES units, *International Journal of Electrical Power & Energy Systems*, Volume 26, Issue 4, May 2004, Pages 291-305.

[12] E. Yeil, M. Güzelkaya and İ. Eksin, Self tuning fuzzy PID type load and frequency controller, *Energy Conversion and Management*, Volume 45, Issue 3, February 2004, Pages 377-390.

[13] Ertuğrul Çam, Application of fuzzy logic for load frequency control of hydroelectrical power plants, *Energy Conversion and Management*, Volume 48, Issue 4, April 2007, Pages 1281-1288.

[14] Ertuğrul Çam and İlhan Kocaarslan, Load frequency control in two area power systems using fuzzy logic controller, *Energy Conversion and Management*, Volume 46, Issue 2, January 2005, Pages 233-243.

[15] Ali Feliachi and Dulpichet Rerkpreedapong, NERC compliant load frequency control design using fuzzy rules, *Electric Power Systems Research*, Volume 73, Issue 2, February 2005, Pages 101-106.

[16] İlhan Kocaarslan and Ertuğrul Çam, Fuzzy logic controller in interconnected electrical power systems for load-frequency control, *International Journal of Electrical Power & Energy Systems*, Volume 27, Issue 8, October 2005, Pages 542-549.

[17] C.S. Chang and Weihui Fu, Area load frequency control using fuzzy gain scheduling of PI controllers, *Electric Power Systems Research*, Volume 42, Issue 2, August 1997, Pages 145-152.

[18] H. Shayeghi, H.A. Shayanfar and O.P. Malik, Robust decentralized neural networks based LFC in a deregulated power system, *Electric*

Power Systems Research, Volume 77, Issues 3-4, March 2007, Pages 241-251.

[19] Ashraf Mohamed Hemeida, Wavelet neural network load frequency controller, *Energy Conversion and Management*, Volume 46, Issues 9-10, June 2005, Pages 1613-1630.

[20] S. P. Ghoshal and S. K. Goswami, Application of GA based optimal integral gains in fuzzy based active power-frequency control of non-reheat and reheat thermal generating systems, *Electric Power Systems Research*, Volume 67, Issue 2, November 2003, Pages 79-88.

[21] M. K. El-Sherbiny, G. El-Saady and Ali M. Yousef, Efficient fuzzy logic load–frequency controller, *Energy Conversion and Management*, Volume 43, Issue 14, September 2002, Pages 1853-1863.

[22] H. Bevrani, Y. Mitani and K. Tsuji, Robust decentralized AGC in a restructured power system, *Energy Conversion and Management*, Volume 45, Issues 15-16, September 2004, Pages 2297-2312.

[23] John R.Smith & Meng-Jen Chen, *Three-Phase Electrical Machines Systems computer simulation*, Research Studies Press LTD, 1993, UK.

[24] PRABHA KUNDUR , *Power system stability and control*, 1st edition, McHill, 1994, USA

[25] Elgerd O.I and Fosha C.E. Jr., Optimum megawatt-frequency control of multiarea electric energy systems, IEEE Transactions on Power *Apparatus and* Systems, vol.Pas-89, no.4, April 1970. p. 556-63.

[26] Petroleum Development Oman LLC, Fault stability studies, April 2004, Oman.

Automatic Generation Control of PDO-OETC interconnected power system using LQR and FLPID with the novel approach of considering generators damper windings torque

Mr Adil Al-Busaidi and Dr Ian French

***Abstract*—** Petroleum Development Oman (PDO) and Oman Electricity Transmission Company (OETC) are running the main 132kV power transmission grids in the Sultanate of Oman. In the year 2001, PDO and OETC grids got interconnected with a 132kV over head transmission line. Since then, the power exchange between PDO and OETC is driven by the natural impedances of the system. The only frequency and power exchange control mean available for the operators of the interconnected grids is re-dispatching their generators. It is a great challenge for PDO and OETC grids operators to maintain the existing philosophy of controlling the frequency and power exchange in light of the daily load profile and the Gulf Cooperation Council (GCC) electrical interconnection. This paper presents the modelling process of PDO-OETC interconnected power system using traditional and novel approaches. It then shows the design of PDO-OETC Automatic Generation Control using different techniques namely Linear Quadratic Regulator (LQR) and Fuzzy Logic PID. The paper will also compare the performance of the different control techniques.

***Keywords*—**Automatic Generation Control (AGC), Linear Quadratic Regulator (LQR), Fuzzy Logic PID (FLPID)

I. Introduction

Power supply frequency is considered as a key factor of power supply quality. Speed of induction and synchronous motors are dependant on the supply frequency. A deviation in the supply frequency will affect the speed of these motors and consequently, the performance of the process in which they are installed. Therefore it is extremely important to maintain the supply frequency at its nominal value. And in case of frequency deviation due to transient conditions, nominal frequency must be restored in an acceptable amount of time. Power systems regulators usually specify performance indices which must be maintained by the power systems operators.

Frequency deviations are caused by an unbalance between the output power of the generators and the load demand. This power mismatch will be compensated by a change in the rotational kinetic energy of the generators ending up with a deviation in the generators speed and hence the frequency. The general idea of controlling the frequency is to maintain the balance between the generated power and the consumed power. Since the existence of alternating current power systems, different philosophies have been applied to maintain the supply frequency. The most common control modes are the Isochronous control, Droop control and Automatic Generation Control. In the Isochronous control mode, a big generator will be assigned the task of maintaining the frequency and the rest of generators will be running at constant power output. In the Droop control mode, all generators will respond to the frequency deviation. Automatic Generation Control (AGC) is achieved by adding a supervisory control loop to the Droop control loop in order to achieve better performance. The main aim of AGC is to maintain zero steady state frequency deviation and to track the load demands.

AGC has been around for the past few decades and it came into practical applications in many power systems around the world. AGC becomes particularly useful in interconnected power systems as it can control the power exchange between the neighbouring systems and enhances the overall system stability. The interest in AGC is growing up rapidly due to the interest in interconnected power systems.

Modelling of power systems will be inherent with different types of uncertainties due to the continuously changing parameters and characteristics, load fluctuations and modelling errors [1]. Moreover, power system parameters are a function of the operating points [2] and these points do change continuously due to the daily load variation and generation scheduling.

Conventionally, Proportional Integral (PI) controllers have been adopted to solve the AGC problem [3]. The PI controller is successful in achieving a zero steady state frequency deviation. However, due to the non-linear power systems, PI controller has a poor dynamic response [2].

Many of the published literature have proposed a number of control strategies to improve the AGC performance. In some of the literature, optimal control techniques [4, 5] and variable structure control [6] were proposed to solve the AGC problem and have shown a robust control results. However they are based on states feedback which makes it very difficult to implement because information about the states are either not available or difficult to obtain [7].

A significant number of the published papers attempted to apply the fuzzy logic controllers to AGC [8, 9]. Since fuzzy logic controllers are good in dealing with complicated, non-linear, indefinite and time-variant systems [10], they seem to be feasible for the AGC. In the published literature, many fuzzy logic arrangements were proposed like the basic PI &

Mr Adil Al-Busaidi is with Petroleum Development Oman (Sultanate of Oman), University of Teesside, School of Science and Technology (UK) (phone: 968-92881980; fax: 968-243813571; e-mail: Adil.Al-Busaidi@pdo.co.om)

Dr Ian French is with University of Teesside, School of Science and Technology (UK) (phone: 44-1642342548; e-mail: I.french@tees.ac.uk)

PID fuzzy controllers [11], self tuning & Fuzzy gain scheduling [10, 12, 13, 14, 15, 16, 17] and multi-stage fuzzy controller [7, 8].

Artificial Neural Networks (ANN) controllers were also used by some researchers to solve the AGC problem [1, 18, 19]. The merit of ANN is they can deal with uncertain system model and parameters making it suitable for power systems applications. However, ANN needs some recorded data from the field for the training purpose which again imposes some difficulties in its practical application.

Genetic algorithm is also used by some researchers [9, 20] to calculate the initial controller gains in cooperation with fuzzy logic controllers.

It became obvious requirement that AGC controllers must be robust to cater for system non-linearities and uncertainties and decentralised to reduce the required signals from the field.

The effects of the generating units' limitations received a considerable attention by the investigators in the AGC filed. Generation rate constraint and governors dead band have been modelled by some researchers [7, 11, 12, 21] in an effort to eliminate modelling errors.

The power market in some countries has been restructured from the vertical hierarchy to the bilateral contracts environment where distribution companies can make direct contracts with generation companies elsewhere in the grid [7]. This mode of operation puts more burdens on the grid operators. Some work has been done to use the traditional AGC with some modification to operate the new deregulated power system environment [7, 18, 22]. The possible bilateral contracts are represented by introducing the concept of an augmented generation participation matrix which represents all possible contracts between generation and distribution companies [7]. The effects of the possible contracts are then treated as a set of new input disturbances [18].

Almost all the published papers used a simple power system models with few control areas and generators for the analysis. The general idea can then be applied to any specific power system. However the scale of the problem can be better explored by using practical size power systems models.

The work in hand presents a case study of designing an AGC for PDO-OETC interconnected power system. The system has been modelled from first principles and the model has been validated against real life scenarios. Some novel approaches have been adopted for refining the model. Different control techniques are used to design the PDO-OETC AGC, namely LQR and FLPID.

II. PDO-OETC POWER SYSTEM MODEL

A. *Modelling of prime movers*

Modelling of generators prime movers can be a very complicated task due to the complexity of these units. In general, full thermodynamic or hydrodynamic models development leads to a computationally expensive solution [23 p 83]. Often the level of complicity can be alleviated by making the model fit for purpose and by accepting a certain amount of error. For Automatic Generation Control (AGC) studies a simplified model of prime movers can be used which leads to an acceptable accuracy of the input power variation to the generator [23 p 83]. The modelling process of prime movers is out of the scope of this paper. Instead, standard published models will be used for steam turbines and gas turbines.

1) *Modelling of steam turbines*

The real power generated by a steam turbine generator is controlled by means of the prime mover torque. This torque is affected by opening or closing the steam control valve of the steam turbine. The steam control valve is controlled by the governor which modulates the steam control valve opening in response to the turbine speed. A load change will affect the electrical torque and will cause a mismatch between the electrical torque and the machine mechanical torque. Hence the machine speed will change and the governor will respond accordingly.

The steam control valve housing is called the steam chest [24 p425]. A substantial amount of steam can be accommodated in the steam chest and the inlet piping to the high pressure section of the steam turbine [24 p 425]. The response of the steam flow to a change in the control valve opening exhibits a time constant T_{CH} due to the charging time of the steam chest and the inlet piping [24 p 425]. For AGC studies, a steam turbine can be represented by first order transfer function with a time constant T_{CH} [24 p 598].

The steam turbine governing system can be Mechanical-hydraulic, Electrohydraulic or Digital Electro-hydraulic [24 pp 434-443]. The governing system response exhibits a time constant T_G due to the response time of the overall governor. For dynamic studies, a steam turbine governing system can be represented by first order transfer function with a time constant T_G [24 p 589].

For AGC studies the steam turbine and its governing system can be represented by two first order transfer functions as shown in Figure 1 [5,25,24 pp 589-598].

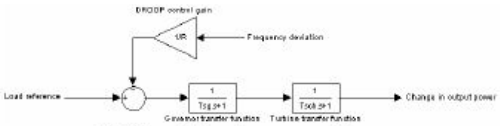

Fig. 1 Steam turbine and governor model.

In Figure 1 Tg (in seconds) is the governor time constant, Tch (in seconds) is the charging time constant of the turbine and R (Hz/pu MW) is the static speed droop of the turbine generator. To a very good approximation, the typical values of these constants are 0.3 s for Tch and 0.2 s for Tg [24 p 598]. In PDO and OETC, the droop control is set to 4% of the nominal frequency of 50Hz and hence:

$$R = 0.04 \times 50Hz = 2Hz / puMW$$

2) *Modelling of gas turbines*

Studies of gas turbines system revealed that the gas turbine and its governing system can be represented by three first order transfer functions [23 p121-122, p221]. One transfer function is to represent the governor lag time, the second transfer to represent the control valve lag time and the third transfer function is to represent the fuel charging characteristics. Figure 2 shows the dynamic model of gas turbine generators which will be used for this study. The same model is used by PDO for dynamic studies [27]. The governor time constant (Tg) is 0.05 s, the control valve time constant (Tc) is 0.05 s and the fuel system time constant (Tf) is 0.4s. The droop control is set to 4% of the nominal frequency of 50Hz and hence:

$$R = 0.04 \times 50 = 2Hz / puMW$$

Fig. 2 Governor/turbine model of gas turbine generator [27].

B. PDO-OETC interconnected model

1) Modelling of control areas

The following analysis is based on the assumption that the electrical interconnection within each individual control area (PDO & OETC) (Figure 3) is so strong, at least in relation to the ties between them, so that the whole area can be characterized by a single frequency only [25].

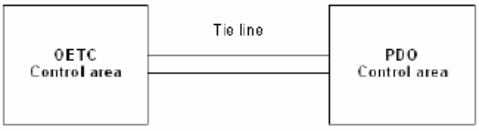

Fig. 3 Interconnection of individual control areas.

Practically, when the system deviates from the constant nominal frequency, every bus voltage will experience its own angular velocity or frequency. Assuming electrical interconnection within a control area is so strong, this will result in all generators belonging to that area swing in unison. Should this assumption not be permissible, then one must subdivide the area into sub-areas. Having said this assumption is valid for PDO and OETC grids, only two control areas will be considered; PDO and OETC.

To start with, exactly the same standard modelling process for AGC studies was followed as outlined by KUNDUR [24 p 601]. A general two areas with one turbine each AGC model is shown in Figure 4 [24 p 603]. There is no necessity to go through the whole modelling process in this paper. The paper will address how the standard model is customised to PDO and OETC systems.

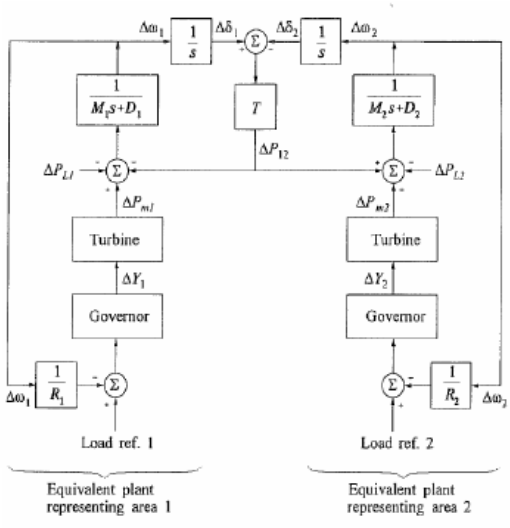

Fig. 4 Two-area system with only primary control [24 p603].

2) Overall PDO system model

PDO power system consists of thirteen power stations. Each of them will be represented as subsystem in PDO model where each subsystem will contain its turbines models in parallel. For example, a power station consisting of two gas turbine generators running in parallel is shown in Figure 5. The output of each turbine is multiplied by a factor to counter for its rating in per unit.

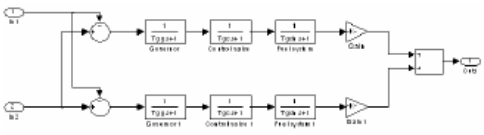

Fig. 5 Example of a power station model.

Upon combining the block diagrams of all Power Stations Subsystems as one equivalent area, we obtain the overall PDO perturbation model shown in Figure 6.

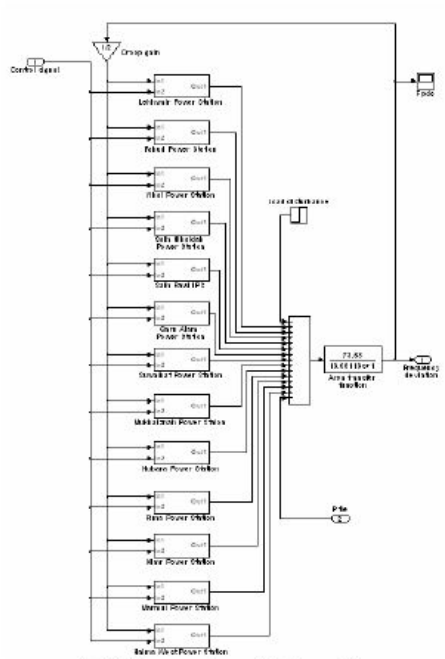

Fig. 6 PDO power system perturbation model.

3) Overall OETC system model

OETC power system was modeled in the same manner as PDO power system. Since there are steam and gas turbines installed at OETC, each subsystem in the model will contain its steam and gas turbines models accordingly. For example, a power station consisting of two gas turbine generators and one steam turbine generator running in parallel is shown in Figure 7. The output of each turbine is multiplied by a factor to counter for its rating in per unit.

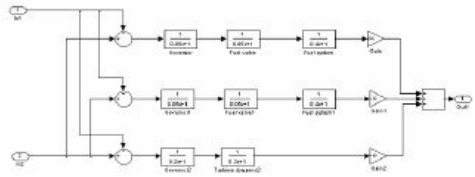

Fig. 7 Example of a power station model consisting of two gas turbines and one steam turbine generators.

C. Overall perturbation model of PDO and OETC systems

By masking PDO power system model and OETC power system model into subsystems and combining those as traditionally done as in Figure 4, the overall perturbation model of PDO-OETC systems is achieved and is shown in Figure 8. This model will serve as the basis for further analysis.

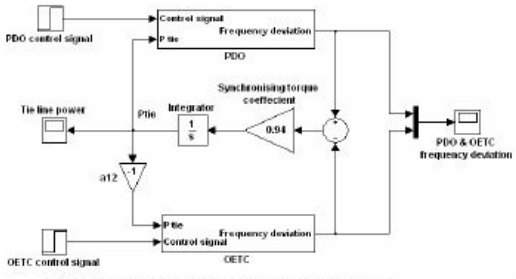

Fig. 8 Block diagram of PDO-OETC perturbation model.

Table 1 summarizes the parameters values of the complete perturbation model of PDO and OETC system.

	Control area		Overall perturbation model	
	D (p.u.MW/Hz)	H (s)	Tiv	a_{12}
PDO	13.6×10^{-3}	4.450985	0.94	-1
OETC	29.76×10^{-3}	14.03546		

Table 1 Overall perturbation model parameters.

Tiv is the sysnchronising torque coefficient between PDO and OETC power systems. The control area parameters D and H are the load damping factor and the area overall inertia respectively.

III. Novel Approaches

In order to make the developed model to behave as close as possible to the real system, some novel approaches were developed in this research. The following two phenomenons have been modelled as a novel approach in the modelling process of AGC:

A. Base load and Pre-select load effect

This is the effect of generators being at maximum load or fixed load. When the generator is at base load, it won't be able to supply any more power because it is already at its thermal limits. Moreover, when the generator is at fixed load, then it is not participating during load disturbances. All this will have an impact on the frequency response characteristics and need to be modelled.

Both of the above phenomenons have been modelled by introducing zero gain in series of the droop control signal to the particular generation unit.

B. Generators damper windings effect

None of the literature attempt to incorporate this effect in the AGC modelling process. As a novel approach in this

research, the generators damper windings effect was incorporated in the AGC modelling process. This was achieved by calculating the damping torque coefficient of all generators and incorporating it in the overall area model. This process showed great improvement in the frequency response characteristics.

Generators damper windings are usually in the form of copper or brass rods embedded in pole face of the generator rotor. These rods are connected to end rings to form short-circuited windings similar to squirrel cage induction motors [24 p 47]. As long as there is a slip between the system frequency and the generator rotor speed, induction motor action will take place between the rotating magnetic filed of the stator and the damper windings. Accordingly a damping torque will be established on the rotor trying to minimise the slip between the angular velocity of the rotor and the system frequency [26 p 473]. The damping power is approximately proportional to the speed deviation and is represented as follows [26 p 473]:

$$Pd = K_D \frac{d\delta}{dt} \quad (1)$$

Where K_D is the damping coefficient which can be determined either from the design data or by test. K_D is given in p.u. torque/p.u. speed [24 p 131). Since base torque is given as [24 p 130]:

$$T_{base} = \frac{MVA_{base}}{\omega_0} \quad (2)$$

Where ω_0 is the rated angular speed in rad/s.

Therefore,

$$T_{p.u.} = \frac{T}{T_{base}} = \frac{MVA}{\omega_0} \times \frac{\omega_0}{MVA_{base}} = \frac{MVA}{MVA_{base}} = P_{p.u.} \quad (3)$$

Hence, K_D can be considered as in p.u. Power/p.u. speed.

The rate of change of torque angle represents a change in the angular frequency as follows:

$$\Delta\omega = \frac{d\delta}{dt} \quad (4)$$

The damping power is then given as:

$$Pd = K_D \Delta\omega \quad (5)$$

Where $\Delta\omega$ is in p.u.

In order to integrate the damping power to the overall model swing equation, speed deviation must be in Hz. Since,

$$\Delta\omega_{p.u.} = \Delta f_{p.u.} = \frac{\Delta\omega}{\omega_0} = \frac{\Delta f}{f_0} \quad (6)$$

Therefore,

$$Pd = \frac{K_D}{f_0} \Delta f \quad (7)$$

Introducing:

$$K = \frac{K_D}{f_0} \quad (8)$$

Where K is in p.u. Power/Hz

The damping power is then given by the simple expression:

$$Pd = K\Delta f \quad (.9)$$

Where,

Pd = p.u. power

K= p.u. power/Hz

Δf = Hz

Back to the assumption that all power stations in one area are strongly interconnected and hence are assumed to be connected to one bus, the same assumption will be applied to the damper windings power. Based on this assumption, all generators will swing in unison and the damping power produced by all generators damper windings will be in phase and acting in the same direction. Hence all damper windings power of all generators in one area will be summated together and included in the swing equation as one element. Furthermore, during transients and for PDO generators, PDO frequency will be considered as the generators speed and OETC frequency will be considered as the grid speed. Therefore as long as there is a difference between PDO frequency and OETC frequency, PDO generators damper windings will try to minimise the slip between the two frequencies by producing a damping power. Similarly, for OETC generators, OETC frequency will be considered as OETC generators speed and PDO frequency will be considered as the grid speed. The term Δf will be the difference between the PDO and OETC frequencies deviation which effectively equals to the difference between the two frequencies. The Δf value will be used to calculate the PDO generators damper windings power and the same value but with a negative sign will be used to calculate the OETC generators damper windings.

From above discussion, the change in PDO generators damper windings power is given as:

$$\Delta Pd_i = K_i(\Delta f_i - \Delta f_v) \quad (10)$$

Where i denotes PDO and v denotes OETC

And by Laplace transform:

$$\Delta Pd_i(s) = K_i(\Delta F_i(s) - \Delta F_v(s)) \quad (11)$$

The generators damper windings power can be integrated to the overall model swing equation as below [24 p 131, 26 p 473]:

$$\Delta P_{Gi} - \Delta P_{Di} = 2\frac{W^*_{kin}}{f^*}\frac{d}{dt}(\Delta f_i) + D_i\Delta f_i + \Delta P_{di} + \Delta P_{tiei} \quad (12)$$

And in the overall transfer function:

$$\left[\Delta P_{Gi}(s) - \Delta P_{Di}(s) - \Delta P_{tiei}(s) - \Delta P_{di}(s)\right]\frac{K_{pi}}{1+sT_{pi}} = \Delta Fi(s) \quad (13)$$

The overall perturbation model will look as shown in Figure 9. PDO and OETC subsystems are shown in Figures 10 and 11 respectively where Kdwpdo is PDO generators damper

windings torque coefficient and Kdwoetc is OETC generators damper windings torque coefficient.

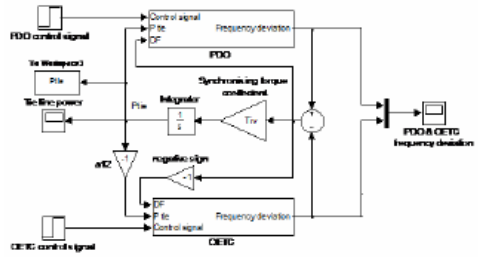

Fig. 9 PDO-OETC perturbation model including generators damper windings torque

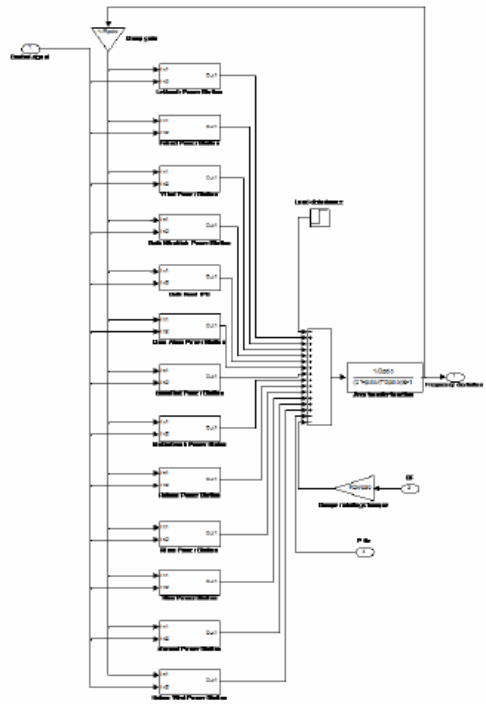

Fig. 10 PDO perturbation model including generators damper windings torque

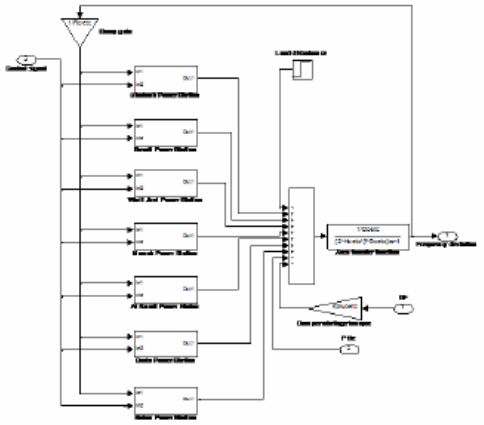

Fig. 11 OETC perturbation model including generators damper windings torque

IV. Simulation Results & Model Validation

Extensive work has been done in testing and validating the model. It was the field data that constrained the validation of the model. The model was validated based on the available field data. Figure 9 shows a real system response graph and simulated ones. The real scenario graph was captured at PDO side when a 140MW generator tripped at OETC grid. The real scenario then has been simulated twice, one time using the traditional AGC model and the other time using the refined AGC model with the novel approaches. From Figure 12, it is clear that the novel approaches have improved the accuracy of the model. To a practical extent, the model response is close enough to the real system response. Considering the complexity of the real system a certain error is expected and should be acceptable. From these results, the model is considered valid for further analysis.

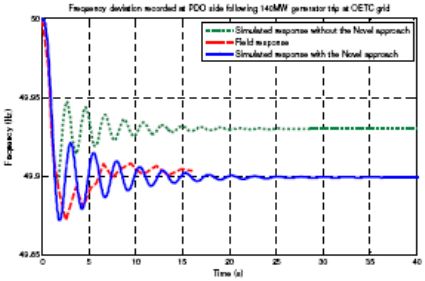

Fig. 12 Real and simulated frequency response to 140MW generator trip at OETC grid measured at PDO side.

V. AGC OF PDO-OETC INTERCONNETCTED POWER SYSTEM

A. AGC controller structure using the Area Control Error (ACE)

The concept of ACE is introduced to satisfy the following two objectives of AGC following load disturbance at any control area [24 p. 606]:

Maintain the grid frequency at the nominal value

Maintain the power exchange between the control areas at scheduled value.

The ACE is a feedback signal to the AGC controller made up of the tie line power deviation added up to the frequency deviation weighted by a bias factor. The concept of ACE is proved to satisfy the above two objectives of AGC [24 p. 606]. The frequency-response characteristic factor β is used for calculating the ACE [24 p. 606]. Thus the ACE for PDO is calculated as:

$$ACE_{pdo} = \Delta P_{tie} + \beta_{pdo}\Delta f_{pdo} \quad \text{.....(14)}$$

Where

$$\beta = \frac{1}{R} + D$$

.....(15)

R is the droop setting in Hz/p.u.MW and D is the load damping factor in p.u.MW/Hz. The term $\frac{1}{R}$ must be scaled to reflect the p.u. capacity of each area. This is achieved by multiplying the term $\frac{1}{R}$ by the area MW capacity and dividing by the base MVA. For PDO and OETC, β is calculated to be 0.24215 Hz/p.u.MW and 0.76151 hz/p.u.MW respectively.

Using ACE as a feedback signal to the AGC controller for both PDO and OETC control areas, the overall perturbation model will look as in Figure 13.

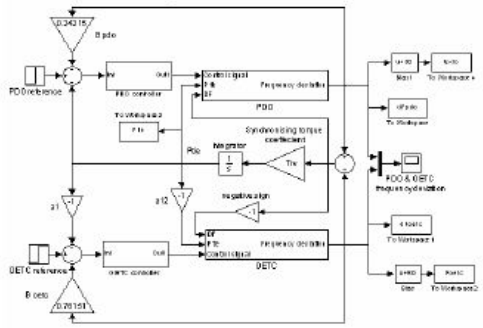

Fig. 13 PDO-OETC perturbation model using ACE as a feedback signal to AGC controllers

B. Design of LQR AGC of PDO-OETC interconnected power system

Linear Quadratic Regulators are considered as one branch of modern optimal control theory which has enabled control engineers to handle large multivariable control problems with ease. Here, LQR is used to design an AGC controller for PDO-OETC power system. The PDO-OETC power system has to be in the state variable form. The desired performance has to be mathematically represented in terms of a cost function to be minimised. Linear Quadratic Regulator (LQR) is known of its robustness to dynamic systems non-linearity and parameters variations.

The Linear Quadratic Regulator is an optimal controller which can have different parameters for the same control topology depending on the design requirements. LQR can take the very basic format whereby all the system parameters are equally important. On the other hand, the designer can be selective and modify the basic LQR design so that he cares mostly of a selected number of system parameters.

Given PDO-OETC power system represented by the state variable differential equation [28 p. 897]:

$$\dot{x} = Ax + Bu$$

.....(16)

Where:

x : n x 1 state vector

u : m x 1 control vector

A : n x n state distribution matrix

B : n x m control distribution matrix

And the dot indicates the time derivative d/dt.

The main job of LQR is to find the matrix K of the optimal control vector [28 p 897]:

$$u(t) = -Kx(t) \quad \text{.....(17)}$$

which minimises the cost function [28 p 897]:

$$C = \int_0^\infty (x'Qx + u'Ru)dt \quad \text{.....(18)}$$

where:

Q: n x n positive semidefinite symmetric state cost weighting matrix.

R: m x m positive definite symmetric control cost weighting matrix.

' : transpose.

For state space representation there are certain equations can be summated together and represented by one equation giving the same output as the whole set. For example PDO has 25 gas turbines running in parallel in different power stations and are represented by one gas turbine with a capacity equaling to the 25 gas turbines. OETC has two types of turbines, gas and steam turbines; therefore it will be represented by one steam turbine and one gas turbine. Their capacity will equal to the accumulated capacity of all turbines of the same type. The above assumption has resulted in great reduction in the number of the state variables of the states

space representation. Hence, the complete PDO-OETC perturbation model shown in Figure 13 is represented in state space matrices form as show below:

$$A=\begin{bmatrix}
0 & T_{s} & 0 & 0 & 0 & -T_{s} & 0 & 0 & 0 & 0 & 0 & 0 & 0\\
-\frac{f}{2W_{pdo}} & -\frac{f}{2W_{pdo}}(D_{pdo}+Kde_{pdo}) & \frac{f}{2W_{pdo}}Kgg_{pdo} & 0 & 0 & \frac{f}{2W_{pdo}}Kde_{pdo} & 0 & 0 & 0 & 0 & 0 & 0 & 0\\
0 & 0 & \frac{-1}{Tgch} & \frac{1}{Tgch} & 0 & 0 & 0 & 0 & 0 & 0 & 0 & 0 & 0\\
0 & 0 & 0 & \frac{-1}{Tgc} & \frac{1}{Tgc} & 0 & 0 & 0 & 0 & 0 & 0 & 0 & 0\\
0 & \frac{-1}{TggR_{pdo}} & 0 & 0 & \frac{-1}{Tgg} & 0 & 0 & 0 & 0 & 0 & 0 & 0 & 0\\
-\frac{fa_{12}}{2W_{oetc}} & -\frac{fa_{12}}{2W_{oetc}}Kde_{oetc} & 0 & 0 & 0 & \frac{f}{2W_{oetc}}(a_{12}Kde_{oetc}-D_{oetc}) & \frac{f}{2W_{oetc}}Kgg_{oetc} & 0 & 0 & \frac{f}{2W_{oetc}}Ksg_{oetc} & 0 & 0 & 0\\
0 & 0 & 0 & 0 & 0 & 0 & \frac{-1}{Tgch} & \frac{1}{Tgch} & 0 & 0 & 0 & 0 & 0\\
0 & 0 & 0 & 0 & 0 & 0 & 0 & \frac{-1}{Tgc} & \frac{1}{Tgc} & 0 & 0 & 0 & 0\\
0 & 0 & 0 & 0 & 0 & \frac{-1}{TggR_{oetc}} & 0 & 0 & \frac{-1}{Tgg} & 0 & 0 & 0 & 0\\
0 & 0 & 0 & 0 & 0 & 0 & 0 & 0 & 0 & \frac{-1}{Tsch} & \frac{1}{Tsch} & 0 & 0\\
0 & 0 & 0 & 0 & 0 & \frac{-1}{TsgR_{oetc}} & 0 & 0 & 0 & 0 & \frac{-1}{Tsg} & 0 & 0\\
-1 & -B_{pdo} & 0 & 0 & 0 & 0 & 0 & 0 & 0 & 0 & 0 & 0 & 0\\
-a_{12} & 0 & 0 & 0 & 0 & -B_{oetc} & 0 & 0 & 0 & 0 & 0 & 0 & 0
\end{bmatrix}$$

......................................(19)

$$B=\begin{bmatrix}
0 & 0\\
0 & 0\\
0 & 0\\
0 & 0\\
\frac{1}{Tgg} & 0\\
0 & 0\\
0 & 0\\
0 & 0\\
0 & \frac{1}{Tgg}\\
0 & 0\\
0 & \frac{1}{Tsg}\\
0 & 0\\
0 & 0
\end{bmatrix}$$

.............(20)

Equally penalising the individual states in the state space and equally penalising the control effort and the states, the matrices Q and R are as shown below:

$$Q=\begin{bmatrix}
1&0&0&0&0&0&0&0&0&0&0&0&0\\
0&1&0&0&0&0&0&0&0&0&0&0&0\\
0&0&1&0&0&0&0&0&0&0&0&0&0\\
0&0&0&1&0&0&0&0&0&0&0&0&0\\
0&0&0&0&1&0&0&0&0&0&0&0&0\\
0&0&0&0&0&1&0&0&0&0&0&0&0\\
0&0&0&0&0&0&1&0&0&0&0&0&0\\
0&0&0&0&0&0&0&1&0&0&0&0&0\\
0&0&0&0&0&0&0&0&1&0&0&0&0\\
0&0&0&0&0&0&0&0&0&1&0&0&0\\
0&0&0&0&0&0&0&0&0&0&1&0&0\\
0&0&0&0&0&0&0&0&0&0&0&1&0\\
0&0&0&0&0&0&0&0&0&0&0&0&1
\end{bmatrix}$$

....(21)

$$R=\begin{bmatrix}1 & 0\\ 0 & 1\end{bmatrix}$$

....(22)

Using MATLAB, the command "lqr(A,B,Q,R)" will return the matrix K for the described system:

$$K=\begin{bmatrix}
-1.0993 & 0.4092 & 0.7827 & 0.2776 & 0.5985 & 0.1557 & 0.0171 & 0.0010 & 0.0005 & 0.0018 & -0.0028 & -1.0000 & 0.0065\\
0.1256 & -0.0715 & -0.0169 & -0.0010 & -0.0002 & 1.5061 & 1.2598 & 0.3187 & 0.5995 & 0.3366 & 0.3781 & -0.0065 & -1.0000
\end{bmatrix}$$

..........(23)

The reduced PDO-OETC power system model with the PDO and OETC LQR AGC controller is shown in Figure 14.

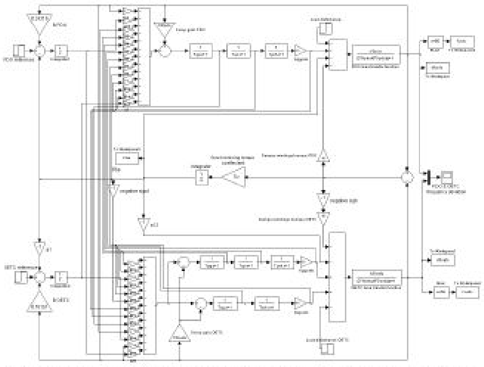

Fig. 14 Reduced PDO-OETC power system with LQR AGC applied to both PDO and OETC

C. Design of Fuzzy Logic PID AGC of PDO-OETC interconnected power system

Fuzzy Logic theory is known of its flexibility and ability to deal with non linear systems. Nowadays, fuzzy logic has been used in almost all sectors of industries including power systems control. The fuzzy logic fundamental structure for all controller design is summarised in Figure 15 [11].

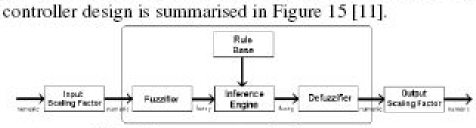

Fig. 15 components of a fuzzy system

The fuzzy logic theory is very well established and is available for readers in almost all recent control engineering text books [29, 30]. There are four main parts in a Fuzzy Logic system [11]:

1. The Fuzzifier: this structure is meant to transform the numeric values into fuzzy sets. It measures the values of input variables then performs a scale transformation which maps the physical values of the process state variables into a normalised universe of discourse [29 p. 790]. The measured crisp value will eventually be converted to a fuzzy set. The so called Membership Functions (MF) are spread over the universe of discourse where any input crisp

value will have a membership in one or more of MFs. There are many shapes for the MFs but the most popular one is the triangular one. The MFs can overlap in the universe of discourse depending on the design requirements.

2. The Inference Engine: it is the engine that performs all logic manipulations in a fuzzy system. The result of the inference process is an output represented by a fuzzy set.
3. The Rule Base: the Rule Base basic function is representing the control policy of an experienced process operator and/or control engineer in a structured way as a set of production rules e.g. If (process state)-Then (control output).
4. The Defuzzifier: transforms the output fuzzy set into a numeric value suitable to be fed to the process.

In addition, input and out scaling factors are used to tune the fuzzy controller to obtain the desired dynamic properties of the process controller closed loop [11].

In general, conventional Fuzzy Logic controllers are not suitable for controlling dynamic systems because they do not produce a reliable transient response and are unable to eliminate steady state error [10, 14, 16]. However combining Fuzzy logic technique with other techniques underwent an extensive research and has produced wonderful results [7, 8, 10, 11, 12, 13, 17].

In this part, the Fuzzy Logic PID AGC will be designed for PDO-OETC interconnected power system. In the literature, two models of fuzzy PID AGC controller have been considered. Few researchers [11, 12] have introduced the Fuzzy PID AGC controller shown in Figure 16. Shayeghi et al [7] has mentioned another topology of Fuzzy PID AGC controller and is shown in Figure 17. Both Fuzzy PID AGC topologies shown in Figure 16 and Figure 17 will be implemented on PDO-OETC interconnected power system model.

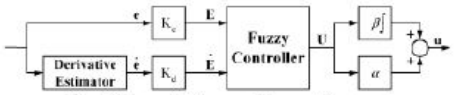

Fig. 16 Fuzzy PID controller architecture 1

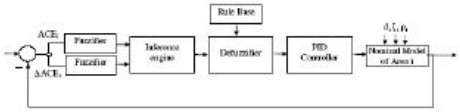

Fig. 16 Fuzzy PID controller architecture 2

From Figure 16 and Figure 17, it is clear that there are two distinctive parts in the controller architecture, the fuzzy and the PI or PID parts. Also it is clear that there are two inputs to the fuzzy controller, the ACE and the derivative of the ACE. This is because human being can actually monitor and feel the errors and the rate of change of errors. This fact is important for the design of a fuzzy controller since it is intended to translate the human being experience into a control system. The error integrator cannot be part of the inputs to the fuzzy controller, simply because the operator or the control engineer cannot realise it. From Figure 16, adding a PI controller after the fuzzy controller actually has implicitly satisfied all the conditions required to form a PID controller. The error and the derivative of the error go into a traditional PI and the total output will contain the proportional, integral and derivative components. Therefore, the architecture shown in Figure 16 is named as Fuzzy PID controller (FPID).

On the other hand the controller shown in Figure 17 has explicit traditional PID controller after the fuzzy logic part. This topology ensures the derivative action is explicitly available after the fuzzy inference.

In the following sections, both FLPID controller architecture shown in Figure 16 (FLPID topology 1) and Figure 17 (FLPID topology 2) will be implemented to design an AGC controller for PDO-OETC interconnected power system. Since it is common for both topologies, the fuzzy logic part will be designed only once.

There are many options and alternatives which can compose a fuzzy logic control system. It must be noted that only one set of options compose the optimum fuzzy logic architecture for a given system. Also, it must be known that even if we managed to setup the optimum fuzzy logic architecture, we may not be successful to optimally tune the parameters to produce the optimum response for a set of control indices. Hence, from its name there is always fuzziness in the design process of a fuzzy logic control system which calls for a wide range of trials and errors to achieve an acceptable performance.

There are many Fuzzy logic design options which are briefly mentioned below but it may not be limited to:

- Mamdani method
- Sugeno method
- Shape of membership functions (MF)
- Number of inputs
- Number of membership functions
- Range of universe of discourse
- Values of input scaling factors
- Value of output scaling factor

There is no rule of thump which tells us which of the above options are most suitable for our case but trial and error method helps deciding some of the options. In our case, many trials and errors proved the below are the most suitable options:

- Mamdani method
- Triangular MF
- Seven MF for each input and output

As in Figures 16 and 17, two inputs to the fuzzy logic system have been used, the ACE and the rate of change of ACE. The input and output scaling factors are assumed to be

unity.

The range of the universe of discourse was calculated empirically using the developed model. The model was subjected to the largest normal load disturbance (200MW) the AGC controller is intended to deal with and then the maximum ACE and rate of change of ACE was recorded. The disturbance was applied once at PDO and another at OETC. From this test, the universe of discourse of both input MFs was decided as in Table 2. Moreover, the output MFs universe of discourse was assumed to be the same as the ACE input MFs because traditionally the control signal is biased by the error; it is also shown in Table 2.

	MFs universe of discourse		
	ACE input	ΔACE input	Output
PDO	-0.21 to +0.21	-0.36 to +0.36	-0.21 to +0.21
OETC	-0.12 to +0.12	-0.15 to +0.15	-0.12 to +0.12

Table 2 universe of discourse ranges of inputs and output membership functions

There are seven MFs evenly distributed in the universe of discourse of the two inputs and the output and are namely summarised as below:

LN: large negative
MN: medium negative
SN: small negative
Z: zero
SP: small positive
MP: medium positive
LP: large positive

The seven MFs ranges for the ACE, ΔACE and the output of PDO are shown in Figure 18, Figure 19 and Figure 20 respectively.

The seven MFs ranges for the ACE, ΔACE and the output of OETC are shown in Figure 21, Figure 22 and Figure 23 respectively.

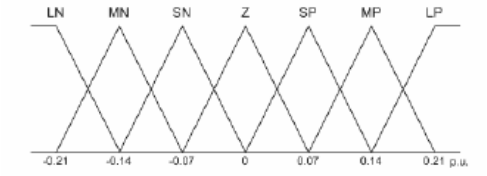

Fig. 18 PDO fuzzy logic controller ACE input MFs

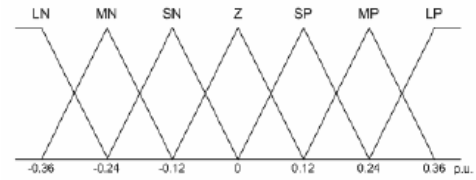

Fig. 19 PDO fuzzy logic controller ΔACE input MFs

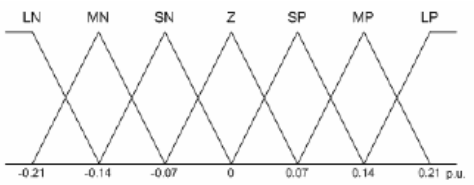

Fig. 20 PDO fuzzy logic controller output MFs

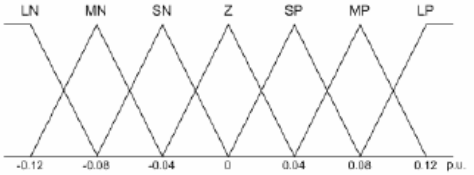

Fig. 21 OETC fuzzy logic controller ACE input MFs

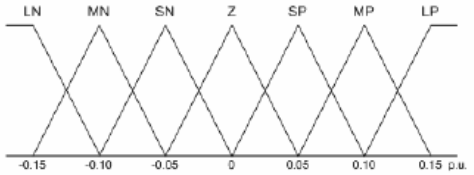

Fig. 22 OETC fuzzy logic controller ΔACE input MFs

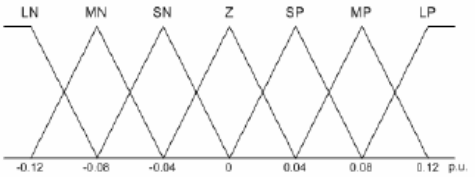

Fig. 23 OETC fuzzy logic controller output MFs

The fuzzy inference rules are set in the form:

If ACE is A_i and ΔACE is B_i THEN u is C_i, where:

i: 1,2,3,…,n

A, B, C: are fuzzy sets

u: is the output

A total number of 49 inference rules are used in both PDO and OETC fuzzy logic controllers which are based on the power system operator experience. They are summarised in Table 3.

Imagine a power system operator monitoring the system frequency and the tie line power. Two main factors will influence his reaction to sudden changes in the system frequency and tie line power, how much deviation is there and the rate of change of deviation. For example following large

sudden load increase at PDO side, the operator will notice the frequency is dropping quickly and the tie line power import is increasing quickly. The operator will then realise that he has to act harshly to balance the generation with the new load, therefore he will harshly increase generators output. In other words, if the ACE is large negative and the rate of change of ACE is large negative, the natural response of the operator is large positive increase of power generation. Another example is when the ACE is large positive and there is a large negative rate of change of ACE, eventually things will be balanced out and the operator doesn't need to do any action i.e. zero action. So on and so forth, from the operator common sense and experience, Table 4 is constructed. The out put states, LP, MP, SP, Z, SN, MN and LN are solely decided by the operator experience and can be always further optimised.

		ACE						
		LN	**MN**	**SN**	**Z**	**SP**	**MP**	**LP**
ΔACE	**LN**	LP	LP	LP	LP	MP	SP	Z
	MN	LP	LP	LP	MP	SP	Z	SN
	SN	LP	LP	MP	SP	Z	SN	MN
	Z	LP	MP	SP	Z	SN	MN	LN
	SP	MP	SP	Z	SN	MN	LN	LN
	MP	SP	Z	SN	MN	LN	LN	LN
	LP	Z	SN	MN	LN	LN	LN	LN

Table 3 Fuzzy inference rules of PDO and OETC fuzzy logic controller

Using MATLAP fuzzy logic toolbox, the PDO and OETC fuzzy logic control systems were designed based on the above details. The generated rules surfaces for both PDO and OETC are shown in Figure 24 and 25 respectively.

Consider the rules surface in Figures 24 and 25 and knowing that the Fuzzy logic part will be followed by the integral action of PID part, it is clear that the overall Fuzzy Logic PID controller will have a mild action around the nominal operating points. It will also have a stiff action for large load disturbances since the rules surface saturates at large positive or large negative depending on the value of the load disturbance.

This is in line with the control engineer requirements. During small disturbances where the frequency and tie line power deviations are within the normal operating envelop, there will be a mild control action from the control engineer. However, during heavy load disturbances, the control engineer will put maximum control effort to restore the frequency and tie line power exchange nominal values in order to stop the system from drifting to unstable condition.

Overall, the controller action is mild around the nominal operating points and stiff off the nominal operating points so that the system will not drift to the uncontrollable conditions.

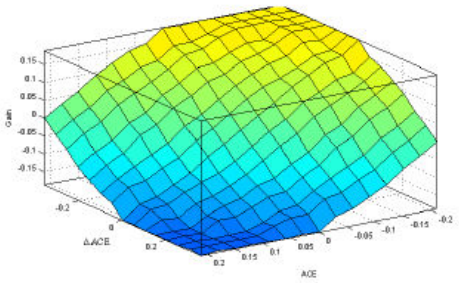

Fig. 24 PDO fuzzy logic controller inference rules surface

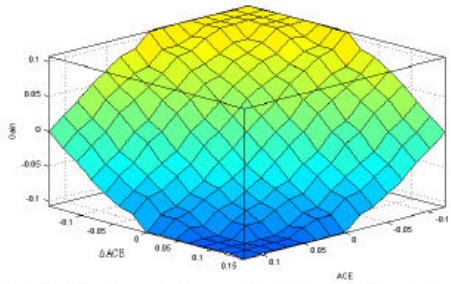

Fig. 25 OETC fuzzy logic controller inference rules surface

The controller structure shown in Figure 16 (FLPID1) is formed by merging the developed Fuzzy logic part with a traditional Proportional Integral (PI) controller. The PI controller is tuned using the Ziegler Nichols closed loop Ultimate Sensitivity Method. During the design and tuning of the PI controller, the uncontrolled complete PDO-OETC model is used without consideration of the fuzzy logic part.

Similarly, the controller structure shown in Figure 17 (FLPID2) is formed by merging the developed Fuzzy logic part with a traditional Proportional Integral Derivative (PID) controller which is tuned using the Ziegler Nichols closed loop Ultimate Sensitivity Method without consideration of the fuzzy logic part.

D. Simulation results

The designed PDO-OETC AGC controllers' using LQR, FLPID1 and FLPID2 structures shown in Figure 14, Figure 16 and Figure 17 respectively are tested by applying a 100MW load disturbances once at PDO side and once at OETC side. The obtained simulation results of both tests for all three controllers' structures are plotted as shown in Figures 26-29. A summary of the performance results in terms for steady state deviations and settling time was attempted and is shown in Table 4. The summary also compares the results of the base case with no controller with the developed AGC controllers' performance.

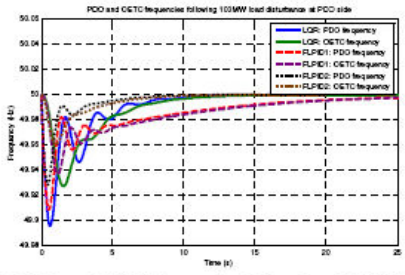

Fig. 26 PDO and OETC frequencies following a 100MW load disturbance at PDO side with the LQR, FLPID1 and FLPID2 AGC applied at both PDO and OETC

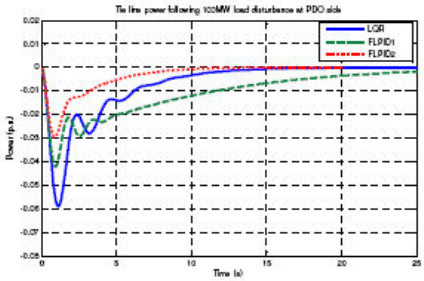

Fig. 27 Tie line power deviation following a 100MW load disturbance at PDO side with the LQR, FLPID1 and FLPID2 AGC applied at both PDO and OETC

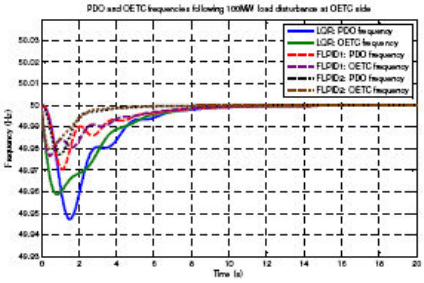

Fig. 28 PDO and OETC frequencies following a 100MW load disturbance at OETC side with the LQR, FLPID1 and FLPID2 AGC applied at both PDO and OETC

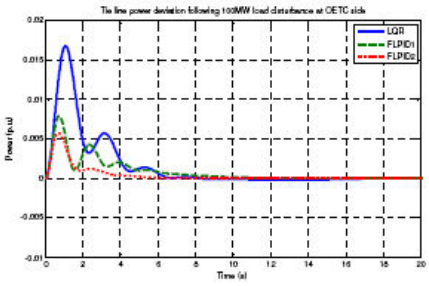

Fig. 29 Tie line power deviation following a 100MW load disturbance at OETC side with the LQR, FLPID1 and FLPID2 AGC applied at both PDO and OETC

		Base case response	LQR controlled response	Fuzzy PID 1 controlled response	Fuzzy PID 2 controlled response
100MW load disturbance at PDO side	Frequency deviation (Hz)	-0.05	0	0	0
	Settling time (s)	10.9	11.3	28.1	8.17
	Tie line power deviation (p.u.)	-0.0379	0	0	0
100MW load disturbance at OETC side	Frequency deviation (Hz)	-0.05	0	0	0
	Settling time (s)	7.74	8.59	8.18	3.92
	Tie line power deviation (p.u.)	0.0121	0	0	0

Table 4 PDO and OETC LQR, FLPID1 and FLPID2 AGC controllers' performance in comparison with the uncontrolled base case.

E. AGC controllers' simulation results discussion

From the simulation results shown in Figures 26-29 and in Table 4, applying AGC to both PDO and OETC leads to the AGC is dealing with all load disturbances in both control areas, PDO and OETC. This has resulted in a zero steady state deviation in the system frequency and tie line following any load disturbance at PDO or OETC which has satisfied the AGC objectives.

Comparing the performance of the LQR, FLPID1 and FLPID2, it clear that FLPID2 has better dynamic performance and shorter settling time.

VI. Conclusion

PDO and OETC interconnected power system has been modeled from first principles. The developed model has been validated using actual response data from the field. The validation process proved the requirement of further improvements. Novel approaches have been followed to refine the developed model which brought the model to an acceptable accuracy. LQR and FL theory have been utilized to design an AGC for PDO-OETC interconnected power system. A combination of FL and traditional PID controllers proved to be superior to LQR in terms of dynamic performance and

settling time. As a further work, the robustness of the LQR and FLPID needs to be assessed in light of model uncertainties and changing system operating points.

ACKNOWLEDGMENT

The authors wish to thank Mr. Saif Al-Sumry (PDO Power System Manager) and Mr. Mohammed Al-Aghbari (PDO Head of Power System Operation and Maintenance) for their endless support.

REFERENCES

[1] H. Shayeghi and H.A. Shayanfar, Application of ANN technique based on μ-synthesis to load frequency control of interconnected power system, *International Journal of Electrical Power & Energy Systems*, Volume 28, Issue 7, September 2006, Pages 503-511.

[2] Y. L. Karnavas and D. P. Papadopoulos, AGC for autonomous power system using combined intelligent techniques, *Electric Power Systems Research*, Volume 62, Issue 3, 28 July 2002, Pages 225-239.

[3] Yusuf Oysal, A comparative study of adaptive load frequency controller designs in a power system with dynamic neural network models, *Energy Conversion and Management*, Volume 46, Issues 15-16, September 2005, Pages 2656-2668.

[4] M. Azzam, Robust automatic generation control, *Energy Conversion and Management*, Volume 40, Issue 13, September 1999, Pages 1413-1421.

[5] Fosha C.E. Jr. and Elgerd O.I., The megawatt-frequency control problem: a new approach via optimal control theory, IEEE Transactions on *Power* Apparatus and *Systems*, vol.Pas-89, no.4, April 1970. p. 563-77.

[6] N. N. Bengiamin and W. C. Chan, Variable Structure Control of Electric Power Generation., IEEE Transactions on *Power Apparatus and Systems*, Vol. PAS-101, No. 2 February 1982.

[7] H. Shayeghi, H.A. Shayanfar and A. Jalili, Multi-stage fuzzy PID power system automatic generation controller in deregulated environments, *Energy Conversion and Management*, Volume 47, Issues 18-19, November 2006, Pages 2829-2845.

[8] H. Shayeghi, A. Jalili and H.A. Shayanfar, Robust modified GA based multi-stage fuzzy LFC, *Energy Conversion and Management*, Volume 48, Issue 5, May 2007, Pages 1656-1670.

[9] S. P. Ghoshal, Application of GA/GA-SA based fuzzy automatic generation control of a multi-area thermal generating system, *Electric Power Systems Research*, Volume 70, Issue 2, July 2004, Pages 115-127.

[10] Ertuğrul Çam and İlhan Kocaarslan, A fuzzy gain scheduling PI controller application for an interconnected electrical power system, *Electric Power Systems Research*, Volume 73, Issue 3, March 2005, Pages 267-274.

[11] A. Demiroren and E. Yesil, Automatic generation control with fuzzy logic controllers in the power system including SMES units, *International Journal of Electrical Power & Energy Systems*, Volume 26, Issue 4, May 2004, Pages 291-305.

[12] E. Yeil, M. Güzelkaya and İ. Eksin, Self tuning fuzzy PID type load and frequency controller, *Energy Conversion and Management*, Volume 45, Issue 3, February 2004, Pages 377-390.

[13] Ertuğrul Çam, Application of fuzzy logic for load frequency control of hydroelectrical power plants, *Energy Conversion and Management*, Volume 48, Issue 4, April 2007, Pages 1281-1288.

[14] Ertuğrul Çam and İlhan Kocaarslan, Load frequency control in two area power systems using fuzzy logic controller, *Energy Conversion and Management*, Volume 46, Issue 2, January 2005, Pages 233-243.

[15] Ali Feliachi and Dulpichet Rerkpreedapong, NERC compliant load frequency control design using fuzzy rules, *Electric Power Systems Research*, Volume 73, Issue 2, February 2005, Pages 101-106.

[16] İlhan Kocaarslan and Ertuğrul Çam, Fuzzy logic controller in interconnected electrical power systems for load-frequency control, *International Journal of Electrical Power & Energy Systems*, Volume 27, Issue 8, October 2005, Pages 542-549.

[17] C.S. Chang and Weihui Fu, Area load frequency control using fuzzy gain scheduling of PI controllers, *Electric Power Systems Research*, Volume 42, Issue 2, August 1997, Pages 145-152.

[18] H. Shayeghi, H.A. Shayanfar and O.P. Malik, Robust decentralized neural networks based LFC in a deregulated power system, *Electric Power Systems Research*, Volume 77, Issues 3-4, March 2007, Pages 241-251.

[19] Ashraf Mohamed Hemeida, Wavelet neural network load frequency controller, *Energy Conversion and Management*, Volume 46, Issues 9-10, June 2005, Pages 1613-1630.

[20] S. P. Ghoshal and S. K. Goswami, Application of GA based optimal integral gains in fuzzy based active power-frequency control of non-reheat and reheat thermal generating systems, *Electric Power Systems Research*, Volume 67, Issue 2, November 2003, Pages 79-88.

[21] M. K. El-Sherbiny, G. El-Saady and Ali M. Yousef, Efficient fuzzy logic load–frequency controller, *Energy Conversion and Management*, Volume 43, Issue 14, September 2002, Pages 1853-1863.

[22] H. Bevrani, Y. Mitani and K. Tsuji, Robust decentralized AGC in a restructured power system, *Energy Conversion and Management*, Volume 45, Issues 15-16, September 2004, Pages 2297-2312.

[23] John R.Smith & Meng-Jen Chen, *Three-Phase Electrical Machines Systems computer simulation*, Research Studies Press LTD, 1993, UK.

[24] PRABHA KUNDUR , *Power system stability and control*, 1st edition, McHill, 1994, USA

[25] Elgerd O.I. and Fosha C.E. Jr., Optimum megawatt-frequency control of multiarea electric energy systems, IEEE Transactions on Power *Apparatus and* Systems, vol.Pas-89, no.4, April 1970. p. 556-63.

[26] Hadi Saadat, *POWER SYSTEM ANALYSIS*, 2nd edition, USA, McGraw-Hill Higher Education, 2002.

[27] Petroleum Development Oman LLC, Fault stability studies, April 2004, Oman.

[28] OGATA, KATSUHIKU (*MODERN CONTROL ENGINEERING.* 4th ed., India: Prentice Hall of India.

[29] Nagrath, I.J. and Gopal, M. (2008) *Control Systems Engineering.* 5th ed., India: New Age International (P) Publishers.

[30] Ghosh, Smarajit (2007) *Control Systems Theory and Applications.* India: Pearson Education.

Appendix 2: MATLAB "Mfile" codes used for fine tuning of PDO-OETC power systems refined model

PdoOetc_Opt

```
 function f = model(k)
global Hoetc Hpdo Tiv treal freal tout Fpdo cost
Hoetc = k(1);
Hpdo = k(2);
Tiv = k(3);
sim('PdoOetcMrunRefinednew',[0 16])
f = cost(160)
plot(tout,Fpdo,treal,freal); %treal and freal are the real life scenario
data, the time and frequency
pause(0.01)
```

Simulator

```
global Hoetc Hpdo Tiv treal freal tout Fpdo cost
load sum2   %loading the real life scenario data
fic = freal(1);
f=50              %system frquency
Tgg=0.05          %gas turbine governor time constant
Tgc=0.05          %gas turbine control valve time constant
Tgch=0.4          %gas turbine fuel charging time constant
Tsg=0.2           %steam turbine governor time constant
Tsch=0.3          %staem turbine steam charging time constant
%Hpdo=4.45098    %PDO power system accumulated inertia
Dpdo=13.6*10^-3 %PDO power system load damping factor
Kdwpdo=23.88*10^-3 %damper windings tourque coeffecient
Rpdo=2            %PDO droop setting
Ldpdo=0      %PDO disturbance
%Hoetc=14.03546  %OETC power system accumulative inertia
Doetc=29.76*10^-3 %OETC power system load damping factor
Kdwoetc=74.09*10^-3 %damper windings tourque coeffecient
Roetc=2           %OETC droop setting
Ldoetc=0.07          %OETC disturbance
%Tiv=0.94         %synchronising torque coeffecient
p=0               %Some units from PDO system are in preselect load control
"p=0"
b=0               %Some units from PDO and OETC systems are at base load
"b=0"
th = fminsearch('PdoOetc_Opt',[14.03546 4.45098 0.94]);
sim('PdoOetcMrunRefinednew',[0 16]) %PDO-OETC refined model
plot(tout,Fpdo,tout,Foetc,treal,freal);grid
```

Appendix 3: MATLAB "Mfile" code used to calculate the state space matrices of PDO-OETC power systems model

```
f=50                %system frequency
Tgg=0.05            %gas turbine governor time constant
Tgc=0.05            %gas turbine control valve time constant
Tgch=0.4            %gas turbine fuel charging time constant
Tsg=0.2             %steam turbine governor time constant
Tsch=0.3            %steam turbine steam charging time constant
Hpdo=4.8417         %PDO power system accumulated inertia
Dpdo=13.6*10^-3     %PDO power system load damping factor
Kdwpdo=23.88*10^-3 %damper windings torque coefficient
Rpdo=2              %PDO droop setting
Hoetc=15.5023       %OETC power system accumulative inertia
Doetc=29.76*10^-3 %OETC power system load damping factor
Kdwoetc=74.09*10^-3 %damper windings torque coefficient
Roetc=2             %OETC droop setting
Tiv=0.722           %synchronising torque coefficient
a12=-1              %sign reversing coefficient
Kgpdo=914.2/2000    %weighted PDO generation
Kgoetc=2337/2000    %weighted OETC generation from gas turbines
Ksoetc=590/2000     %weighted OETC generation from steam turbines

A=[0 Tiv 0 0 0 -Tiv 0 0 0 0 0
   -(f/(2*Hpdo)) -(f/(2*Hpdo))*(Dpdo+Kdwpdo) (f/(2*Hpdo))*Kgpdo 0 0
(f/(2*Hpdo))*Kdwpdo 0 0 0 0 0
   0 0 -1/Tgch 1/Tgch 0 0 0 0 0 0 0
   0 0 0 -1/Tgc 1/Tgc 0 0 0 0 0 0
   0 -1/(Tgg*Rpdo) 0 0 -1/Tgg 0 0 0 0 0 0
   (-(f/(2*Hoetc))*a12) (-(f/(2*Hoetc))*a12*Kdwoetc) 0 0 0
((f/(2*Hoetc))*(a12*Kdwoetc-Doetc)) ((f/(2*Hoetc))*Kgoetc) 0 0
((f/(2*Hoetc))*Ksoetc) 0
   0 0 0 0 0 0 -1/Tgch 1/Tgch 0 0 0
   0 0 0 0 0 0 0 -1/Tgc 1/Tgc 0 0
   0 0 0 0 0 -1/(Tgg*Roetc) 0 0 -1/Tgg 0 0
   0 0 0 0 0 0 0 0 0 0 -1/Tsch 1/Tsch
   0 0 0 0 0 -1/(Tsg*Roetc) 0 0 0 0 -1/Tsg]

B=[0 0
   0 0
   0 0
   0 0
   1/Tgg 0
   0 0
   0 0
   0 0
   0 1/Tgg
   0 0
   0 1/Tsg]

C=[0 1 0 0 0 0 0 0 0 0 0
   0 0 0 0 0 1 0 0 0 0 0
   1 0 0 0 0 0 0 0 0 0 0]

D=[0 0
   0 0
   0 0]

PDO_OETC=ss(A,B,C,D)
```

Appendix 4: AGC control topologies simulations results

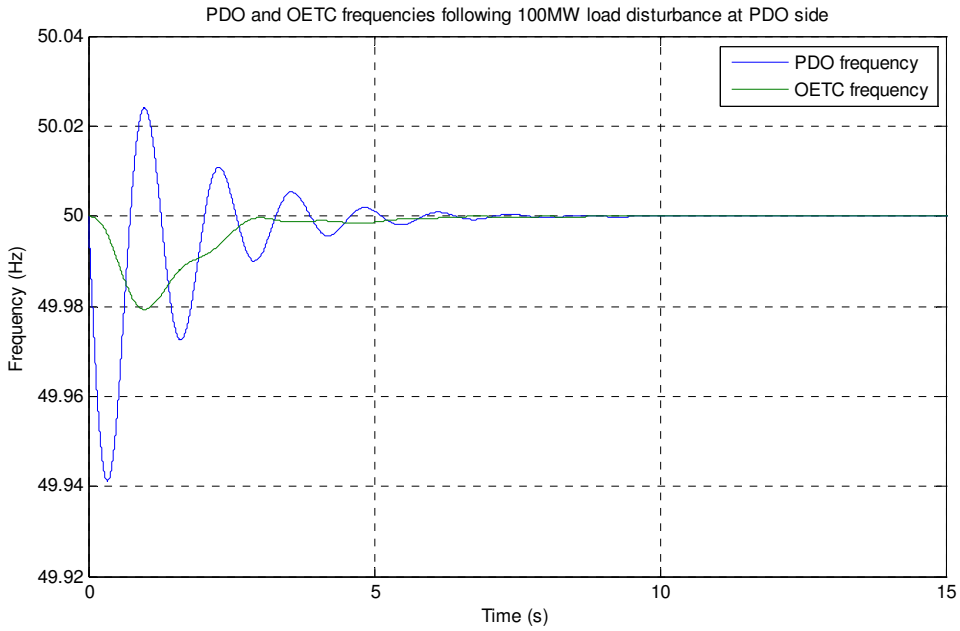

Figure 9.9: Grid frequency following 100MW load disturbance at PDO side with the PDO alone PID frequency controller

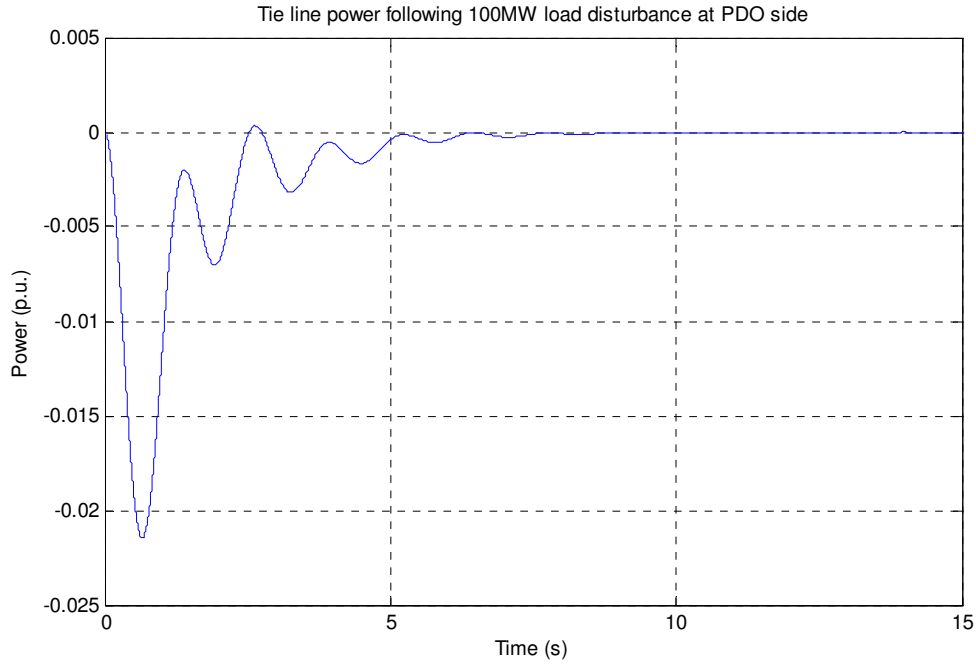

Figure 9.10: Tie line power deviation following 100MW load disturbance at PDO side with the PDO alone PID frequency controller

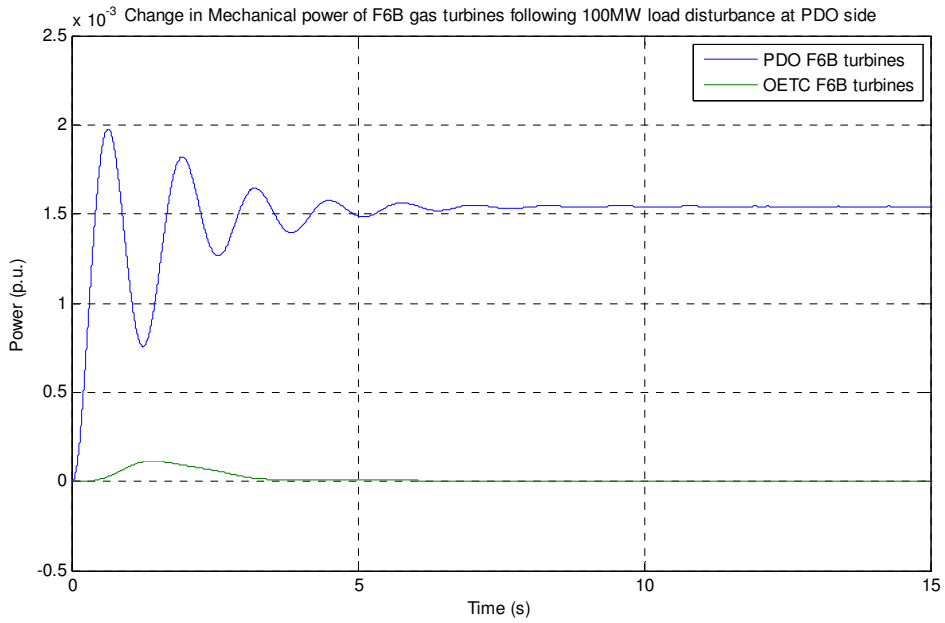

Figure 9.11: Change in Mechanical power of F6B gas turbines following 100MW load disturbance at PDO side with the PDO alone PID frequency controller

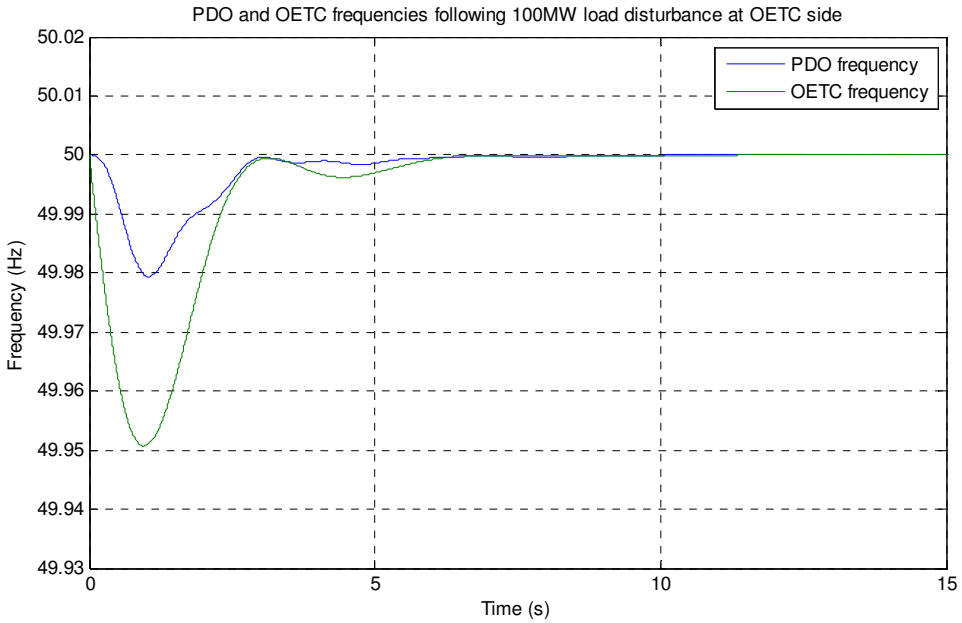

Figure 9.12: Grid frequency following 100MW load disturbance at OETC side with the PDO alone PID frequency controller

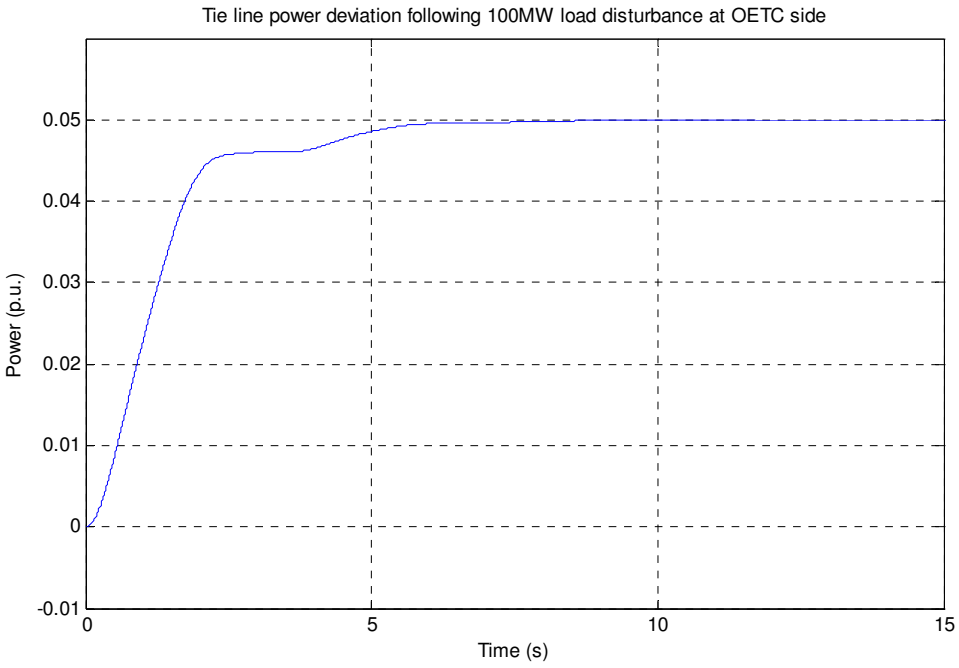

Figure 9.13: Tie line power deviation following 100MW load disturbance at OETC side with the PDO alone PID frequency controller

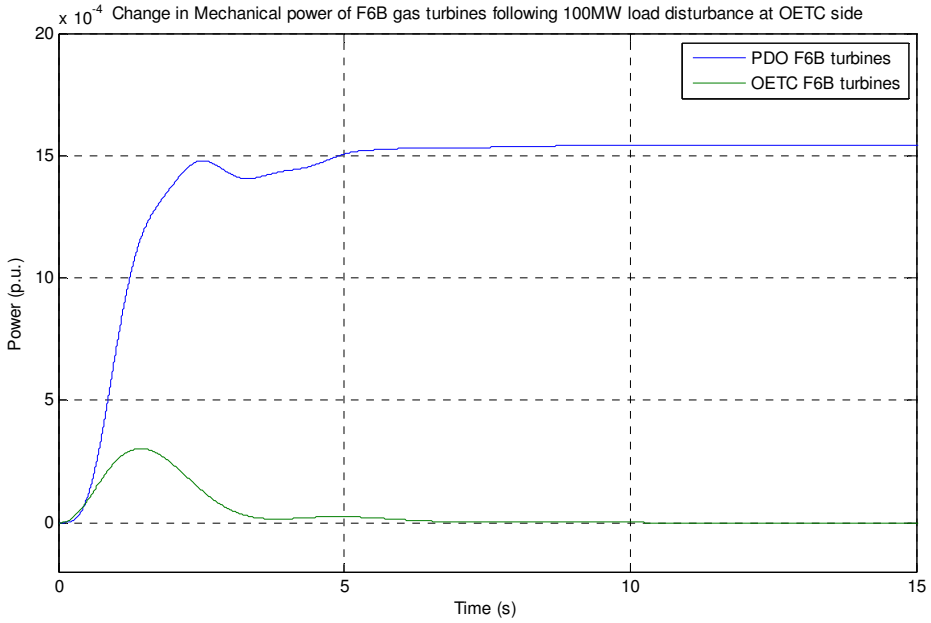

Figure 9.14: Change in Mechanical power of F6B gas turbines following 100MW load disturbance at OETC side with the PDO alone PID frequency controller

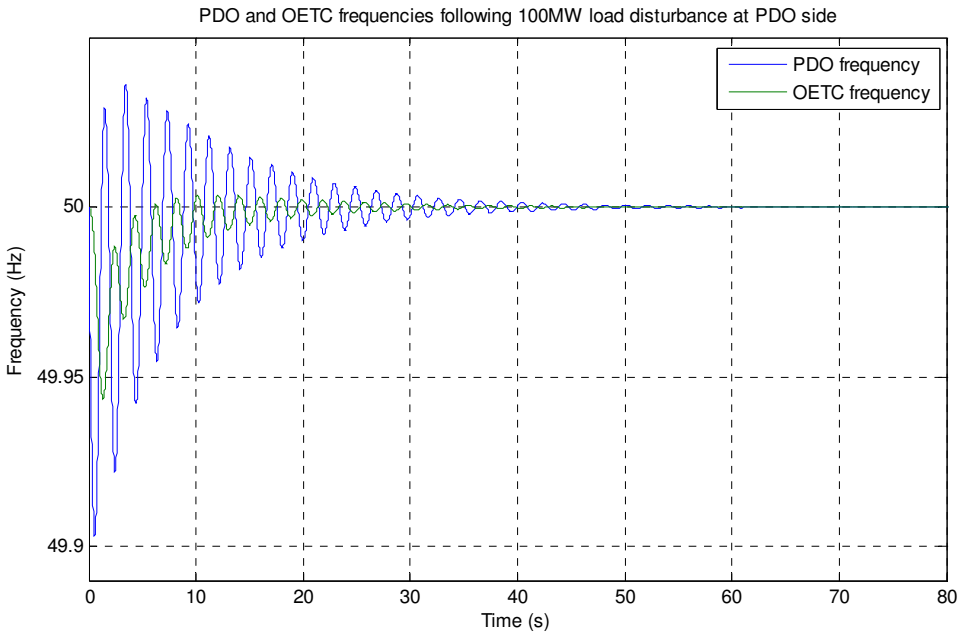

Figure 9.16: Grid frequency following 100MW load disturbance at PDO side with the PDO alone PID tie line power controller

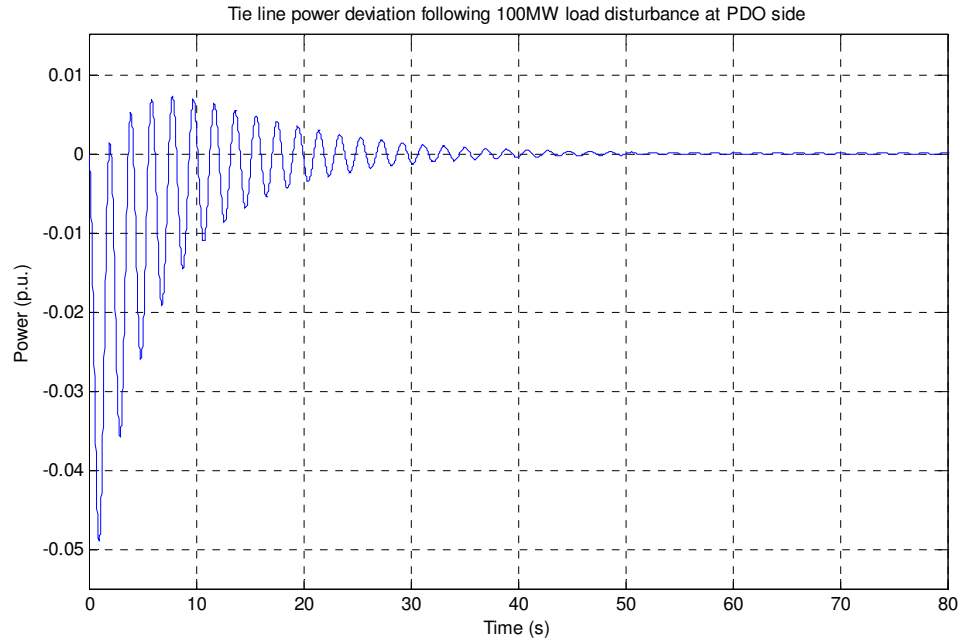

Figure 9.17: Tie line power deviation following 100MW load disturbance at PDO side with the PDO alone PID tie line power controller

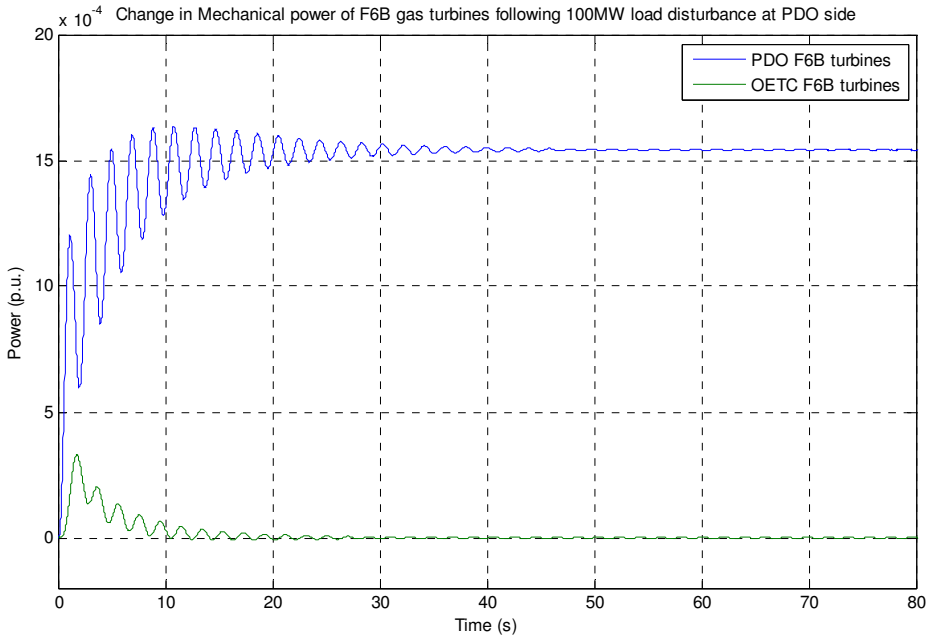

Figure 9.18: Change in Mechanical power of F6B gas turbines following 100MW load disturbance at PDO side with the PDO alone PID tie line power controller

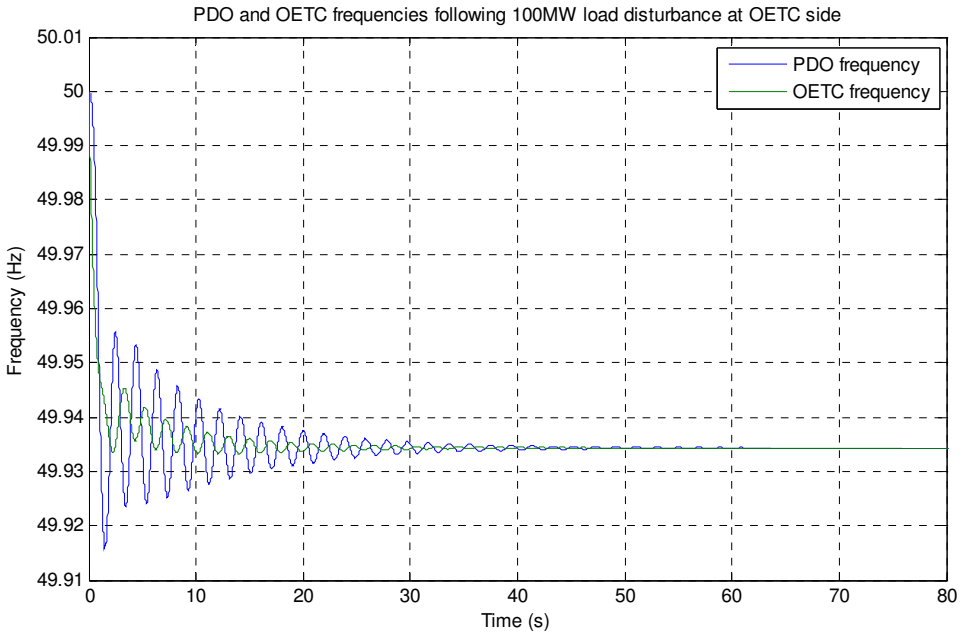

Figure 9.19: Grid frequency following 100MW load disturbance at OETC side with the PDO alone PID tie line power controller

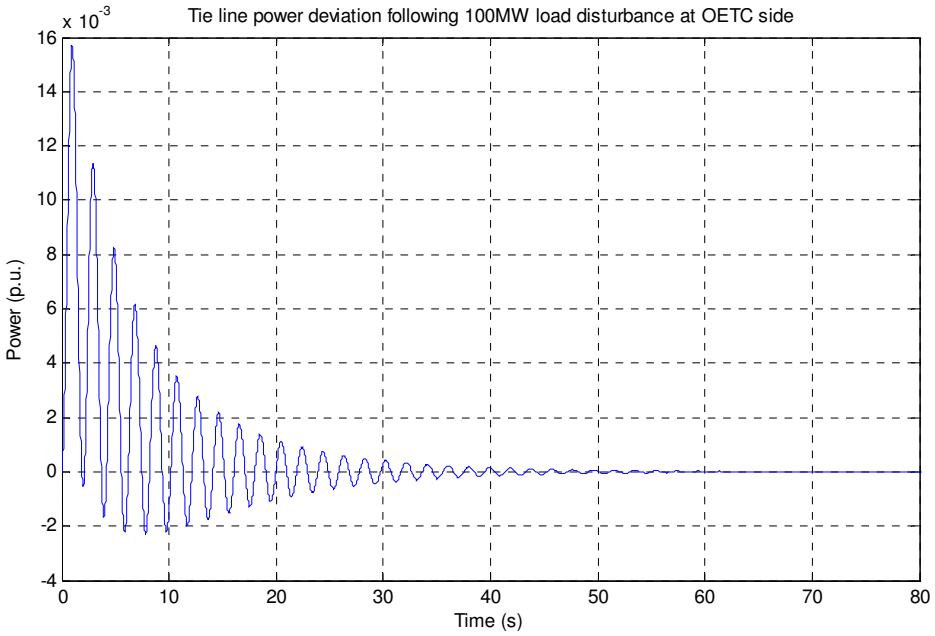

Figure 9.20: Tie line power deviation following 100MW load disturbance at OETC side with the PDO alone PID tie line power controller

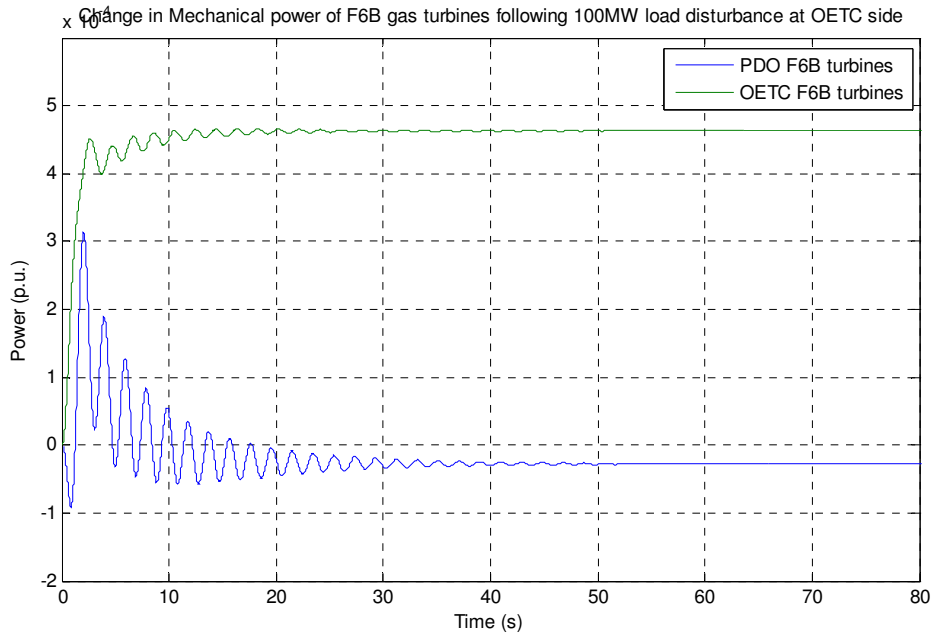

Figure 9.21: Change in Mechanical power of F6B gas turbines following 100MW load disturbance at OETC side with the PDO alone PID tie line power controller

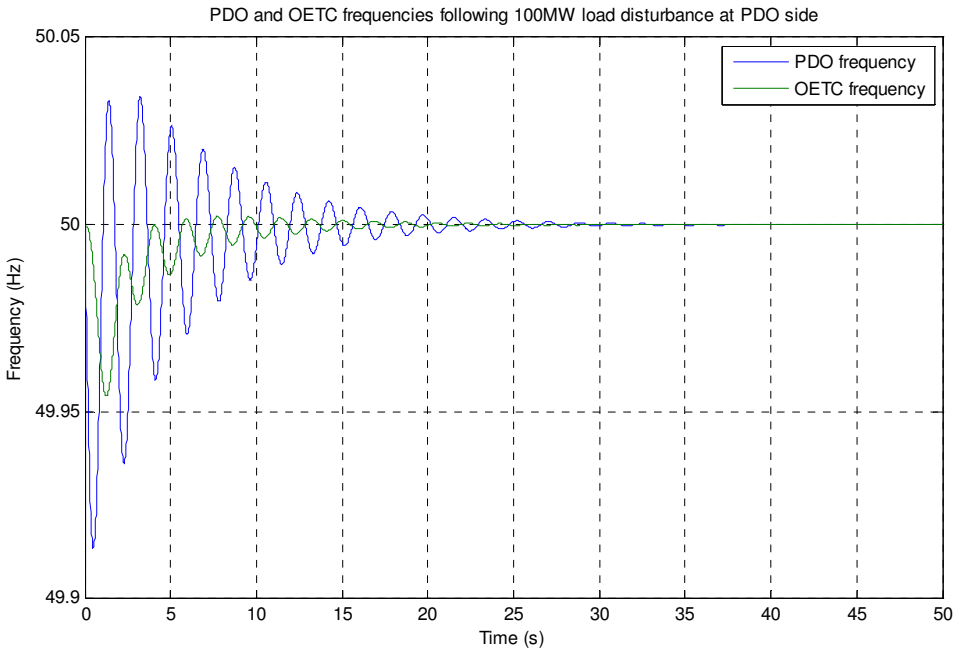

Figure 9.23: Grid frequency following 100MW load disturbance at PDO side with the PDO alone PID frequency and tie line power controller

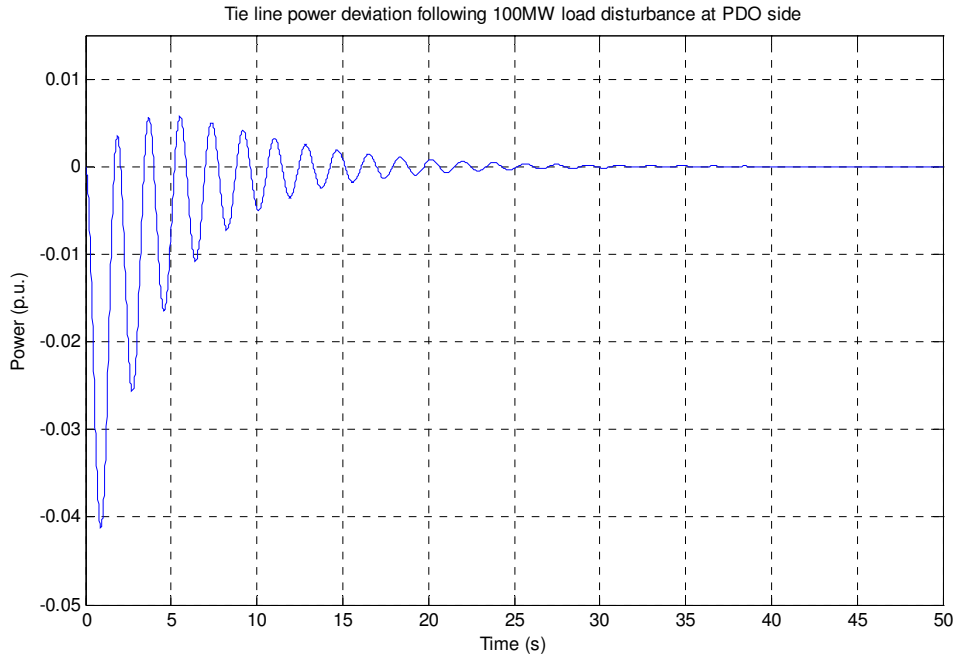

Figure 9.24: Tie line power deviation following 100MW load disturbance at PDO side with the PDO alone PID frequency and tie line power controller

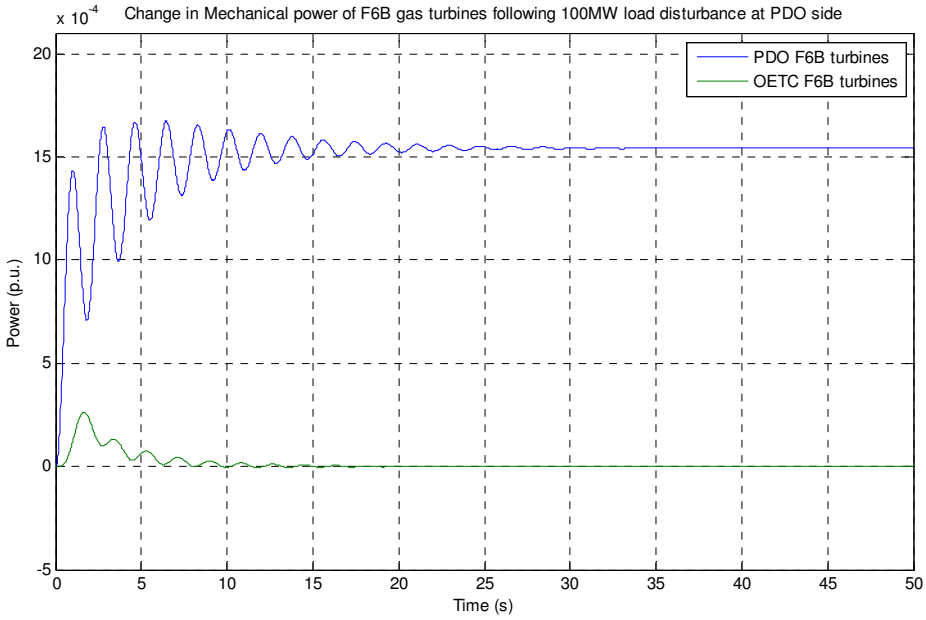

Figure 9.25: Change in Mechanical power of F6B gas turbines following 100MW load disturbance at PDO side with the PDO alone PID frequency and tie line power controller

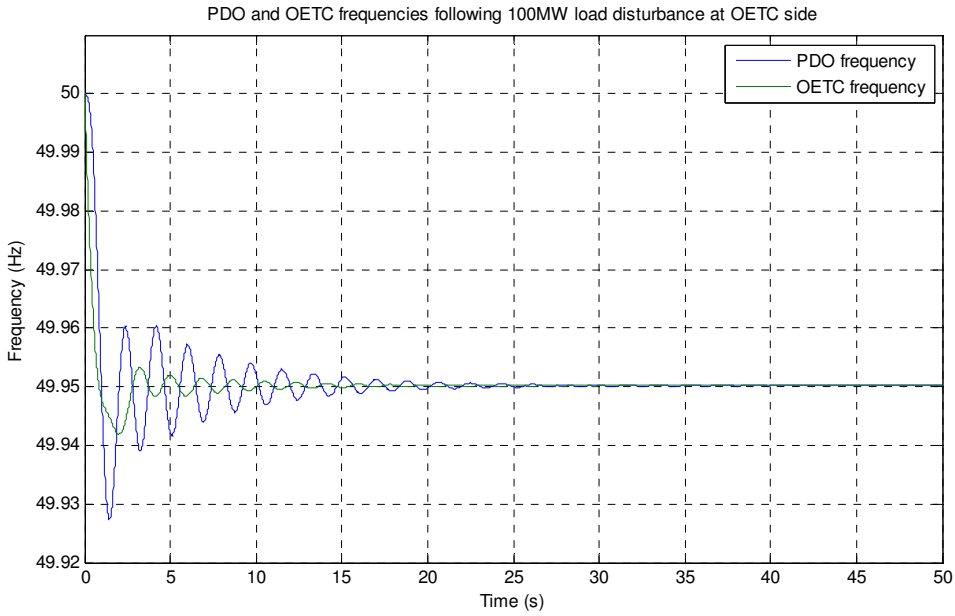

Figure 9.26: Grid frequency following 100MW load disturbance at OETC side with the PDO alone PID frequency and tie line power controller

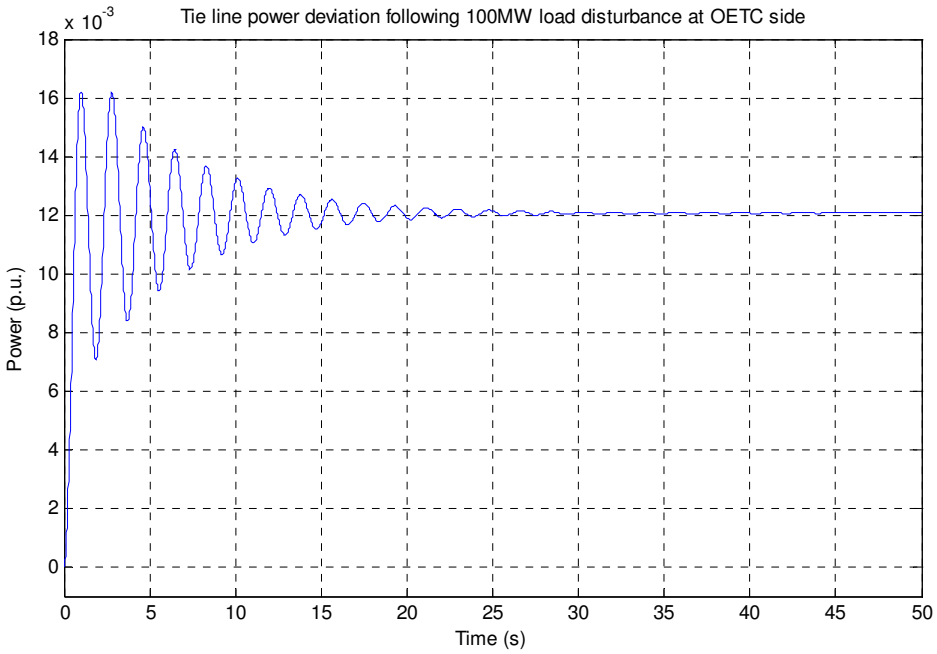

Figure 9.27: Tie line power deviation following 100MW load disturbance at OETC side with the PDO alone PID frequency and tie line power controller

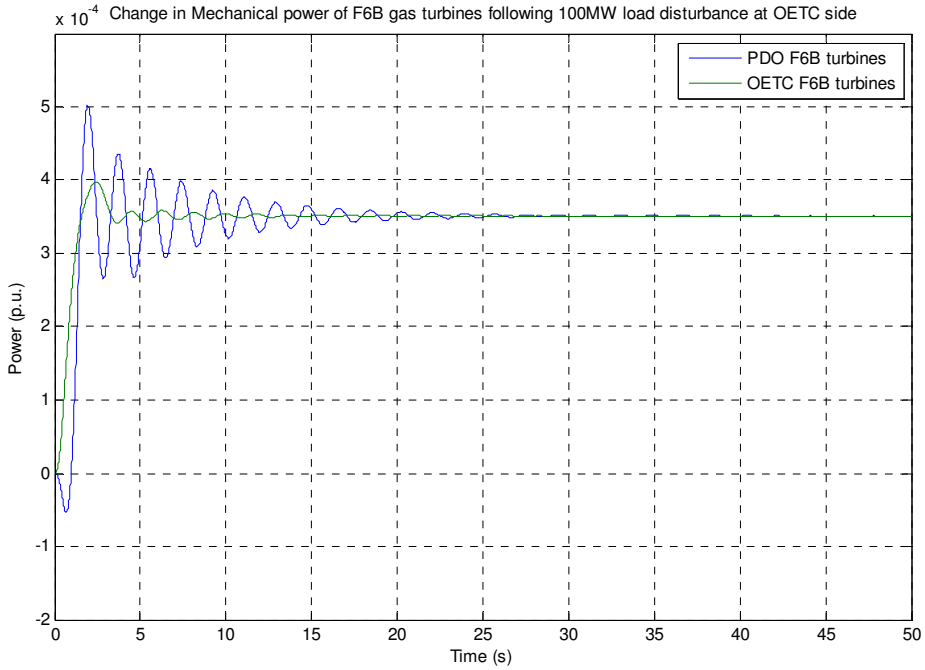

Figure 9.28: Change in Mechanical power of F6B gas turbines following 100MW load disturbance at OETC side with the PDO alone PID frequency and tie line power controller

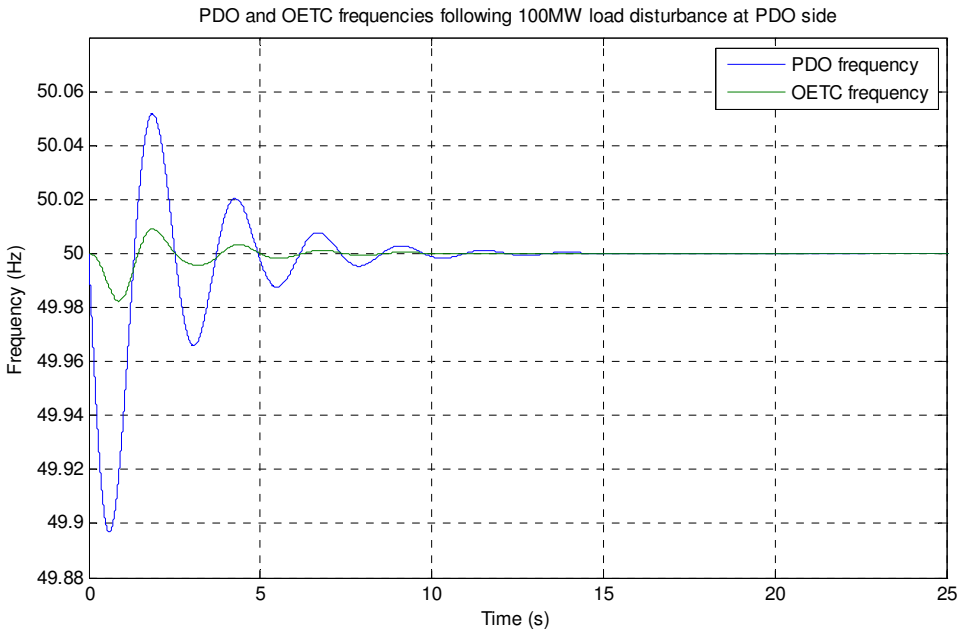

Figure 9.30: Grid frequency following 100MW load disturbance at PDO side with the OETC alone PID frequency controller

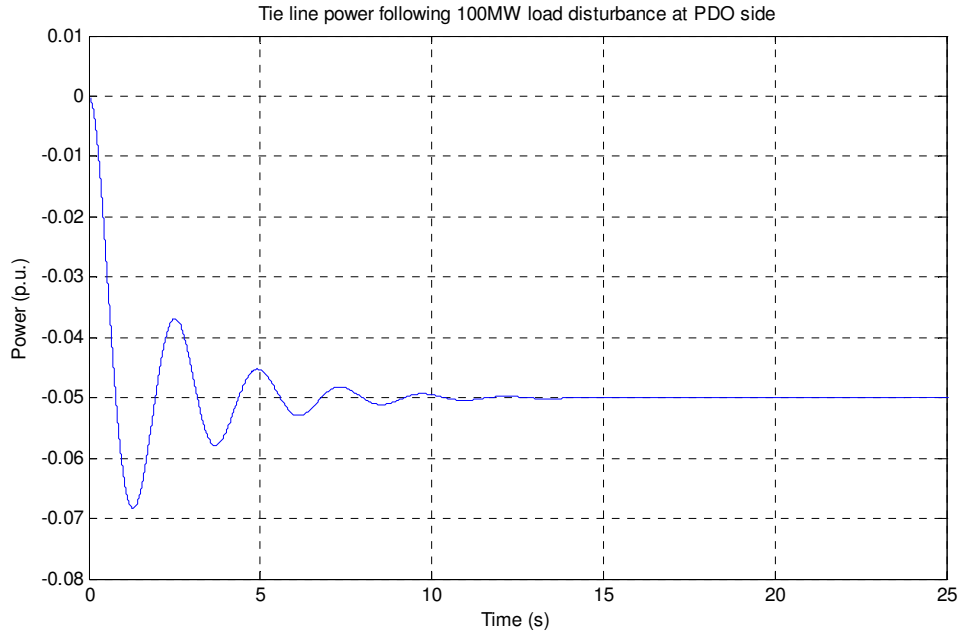

Figure 9.31: Tie line power deviation following 100MW load disturbance at PDO side with the OETC alone PID frequency controller

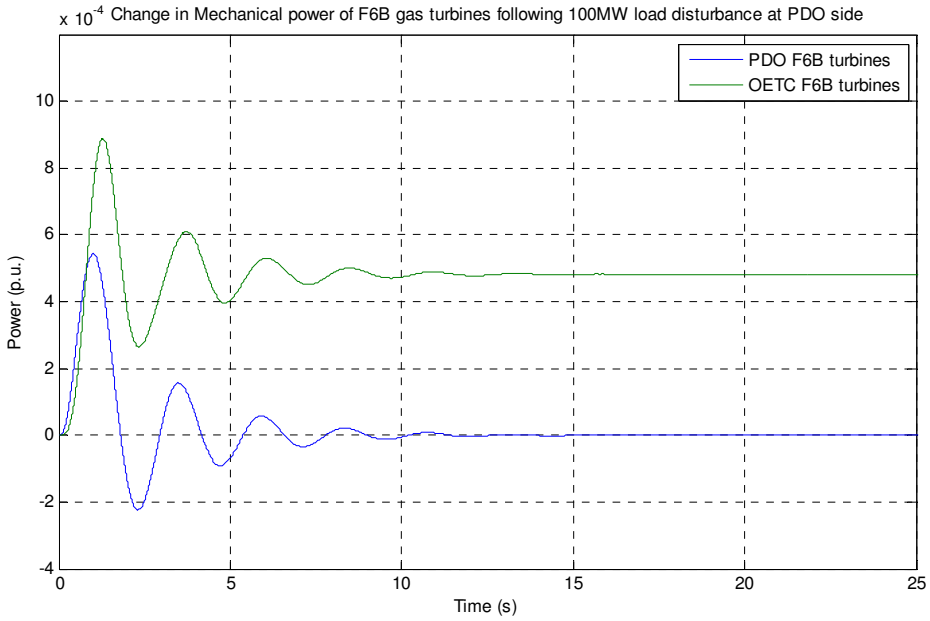

Figure 9.32: Change in Mechanical power of F6B gas turbines following 100MW load disturbance at PDO side with the OETC alone PID frequency controller

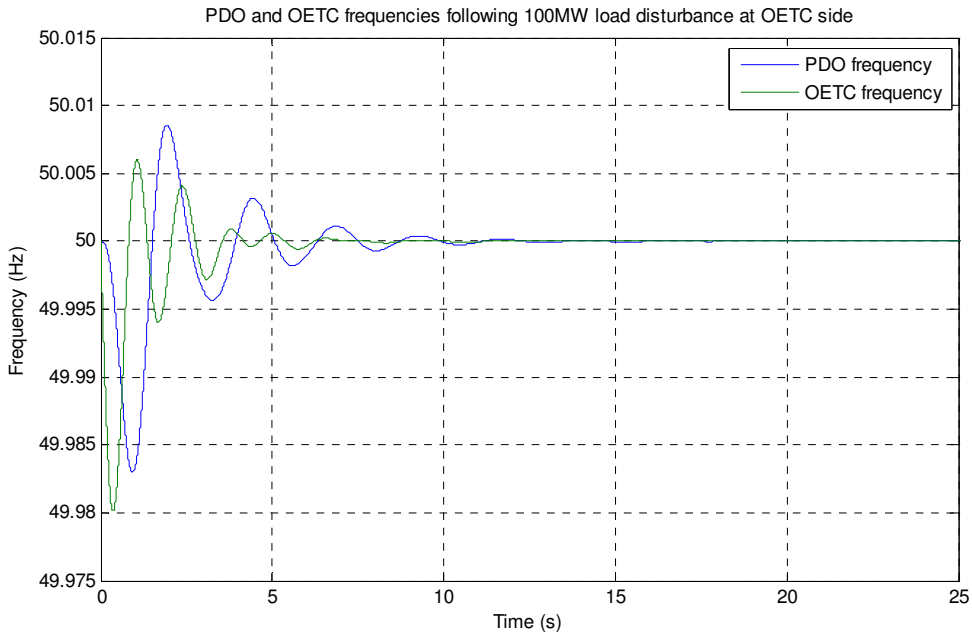

Figure 9.33: Grid frequency following 100MW load disturbance at OETC side with the OETC alone PID frequency controller

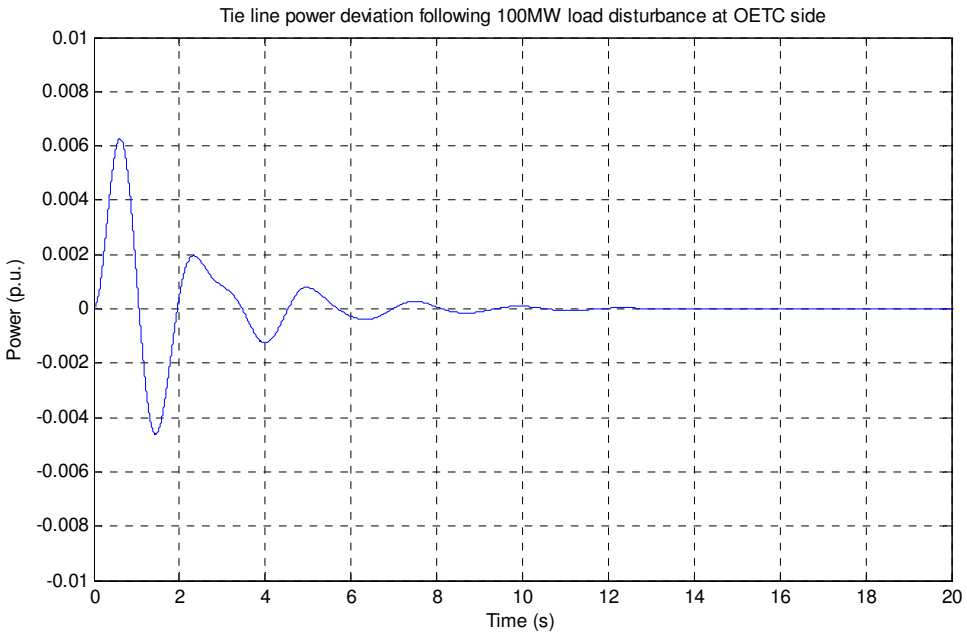

Figure 9.34: Tie line power deviation following 100MW load disturbance at OETC side with the OETC alone PID frequency controller

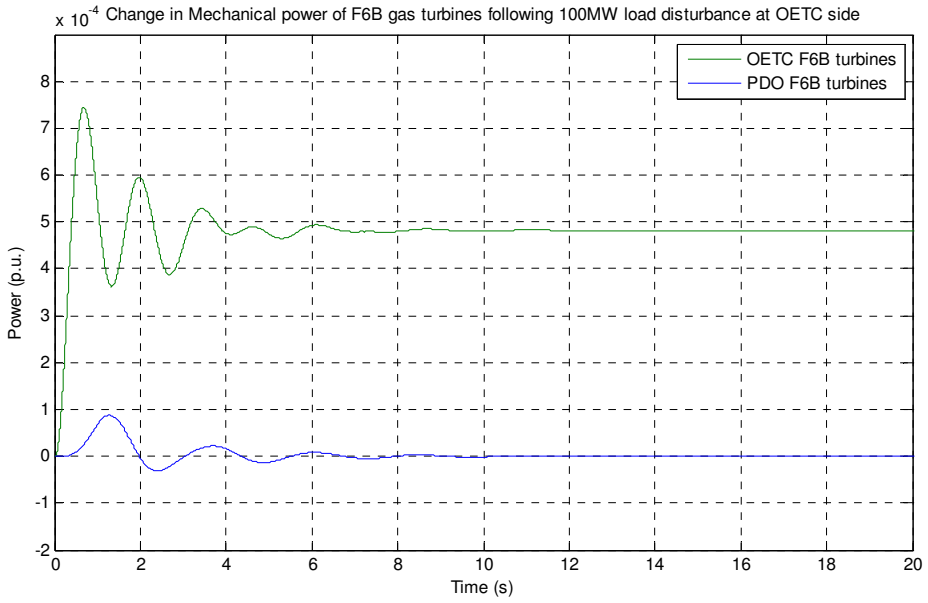

Figure 9.35: Change in Mechanical power of F6B gas turbines following 100MW load disturbance at OETC side with the OETC alone PID frequency controller

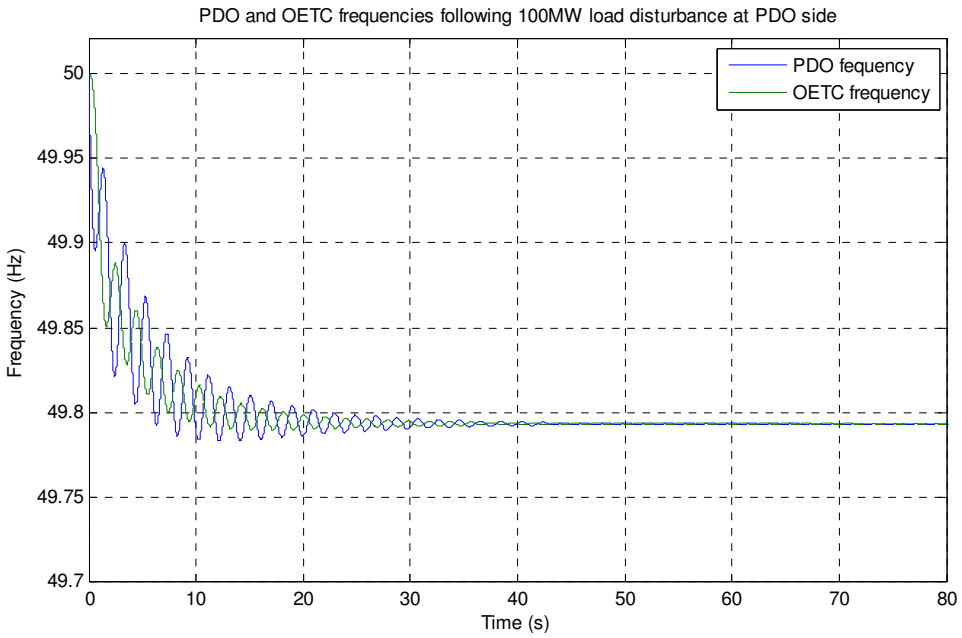

Figure 9.37: Grid frequency following 100MW load disturbance at PDO side with the OETC alone PID tie line power controller

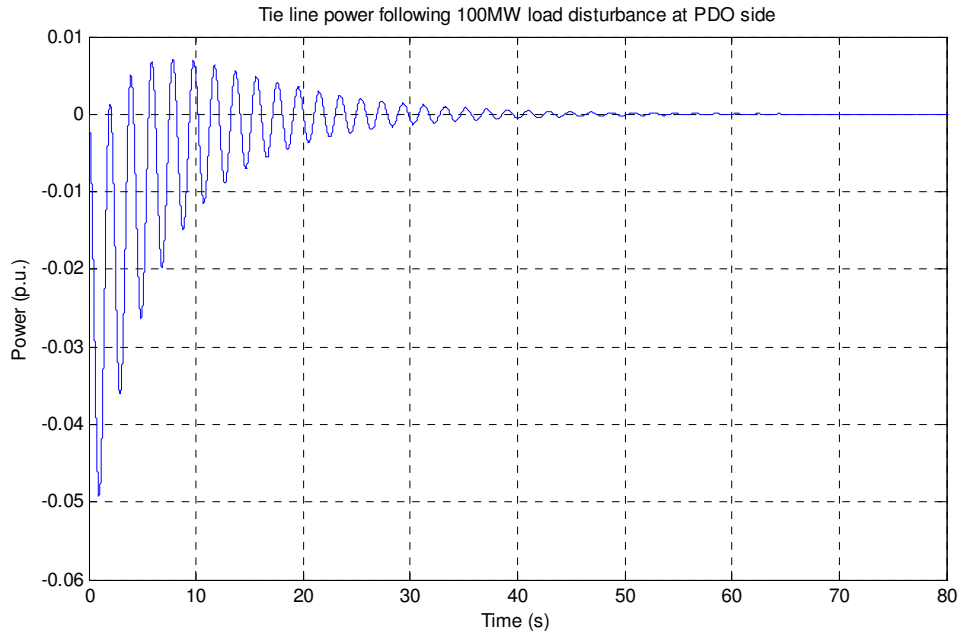

Figure 9.38: Tie line power deviation following 100MW load disturbance at PDO side with the OETC alone PID tie line power controller

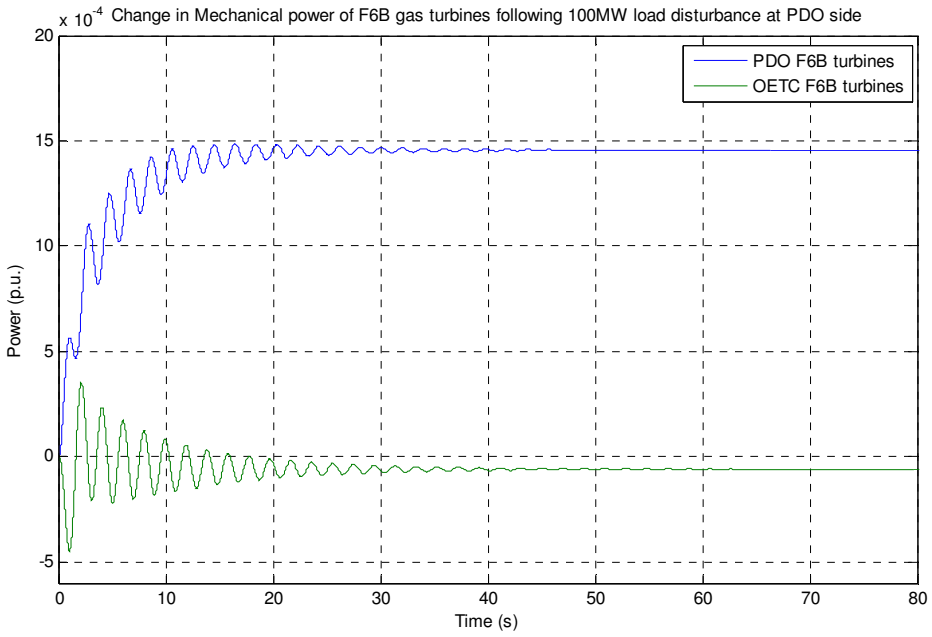

Figure 9.39: Change in Mechanical power of F6B gas turbines following 100MW load disturbance at PDO side with the OETC alone PID tie line power controller

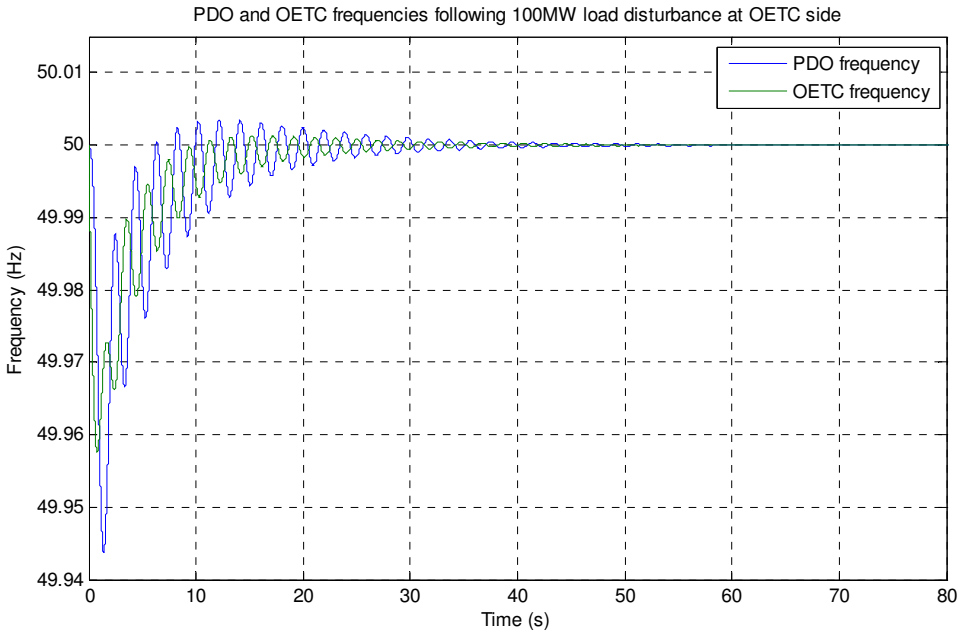

Figure 9.40: Grid frequency following 100MW load disturbance at OETC side with the OETC alone PID tie line power controller

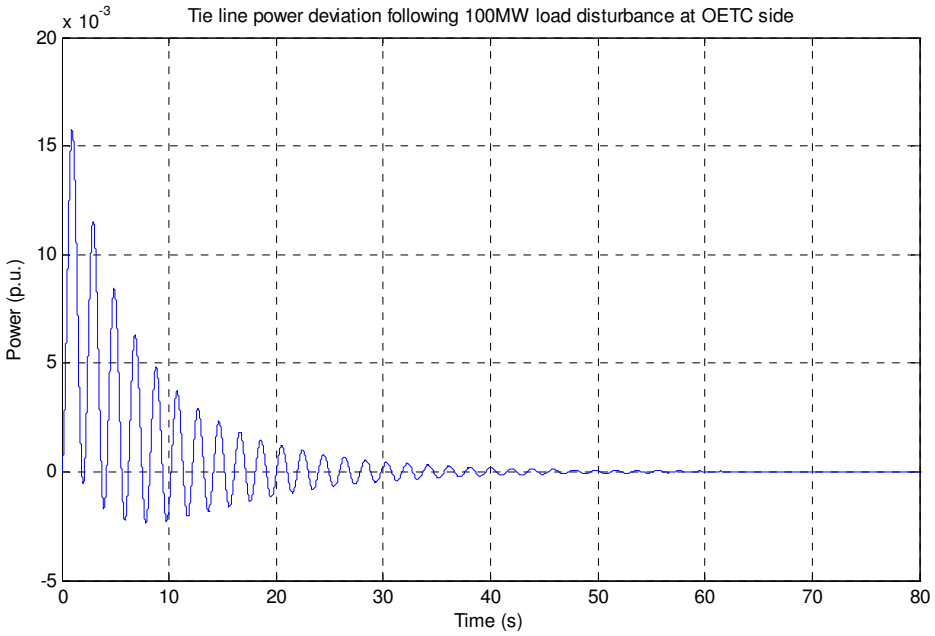

Figure 9.41: Tie line power deviation following 100MW load disturbance at OETC side with the OETC alone PID tie line power controller

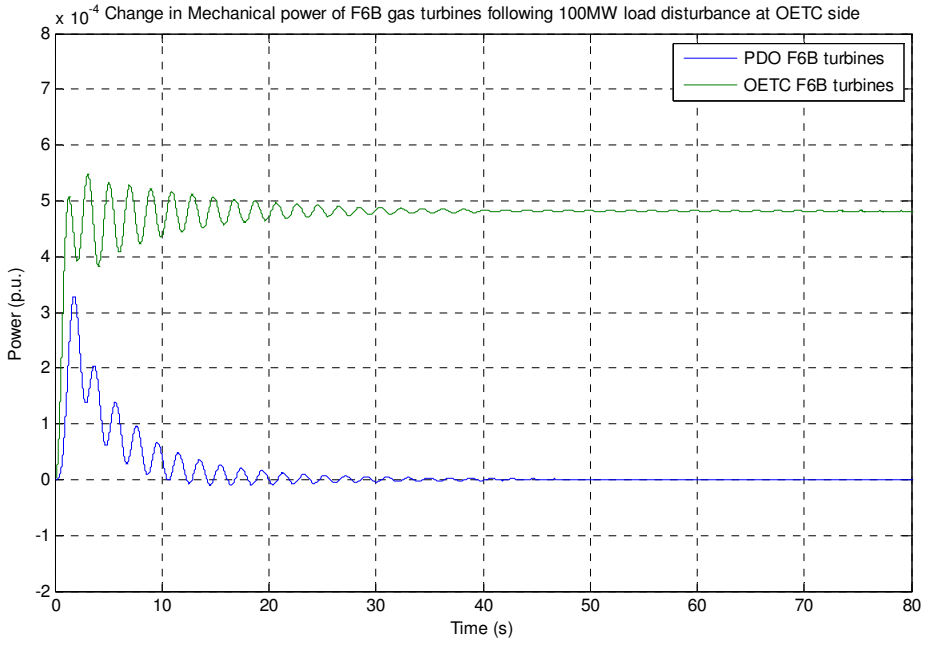

Figure 9.42: Change in Mechanical power of F6B gas turbines following 100MW load disturbance at OETC side with the OETC alone PID tie line power controller

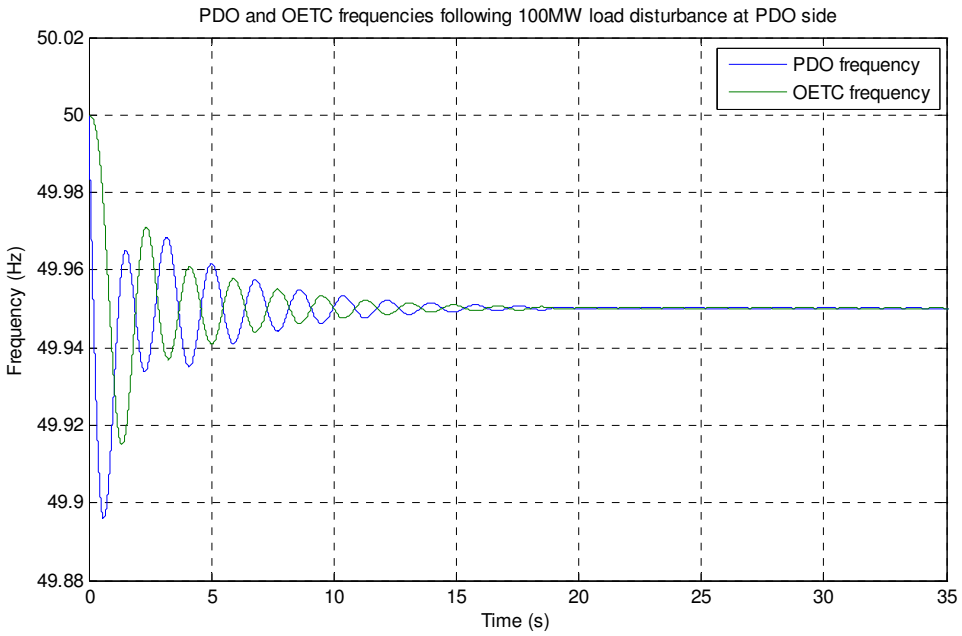

Figure 9.44: Grid frequency following 100MW load disturbance at PDO side with the OETC alone PID frequency and tie line power controller

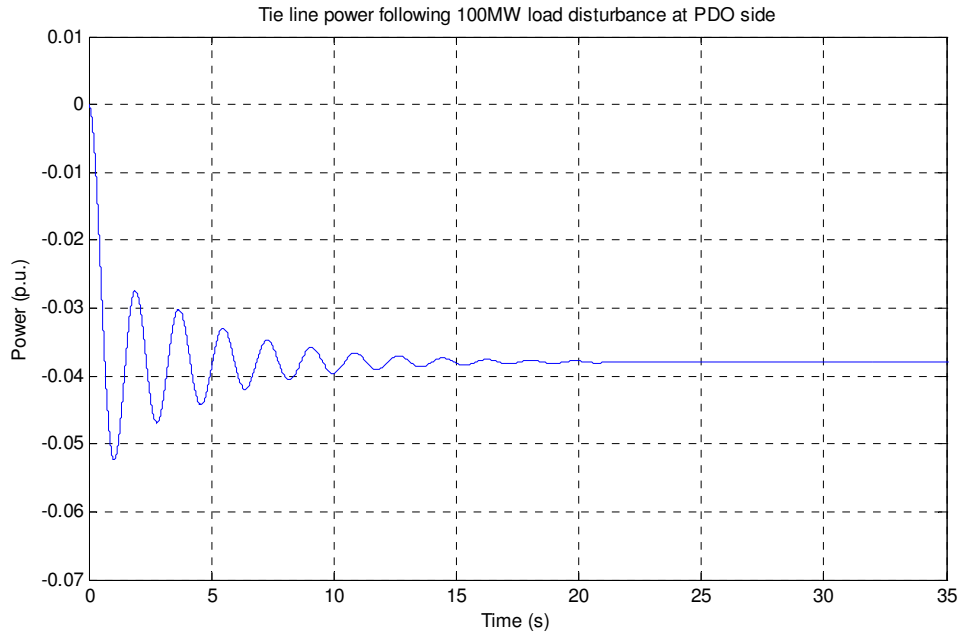

Figure 9.45: Tie line power deviation following 100MW load disturbance at PDO side with the OETC alone PID frequency and tie line power controller

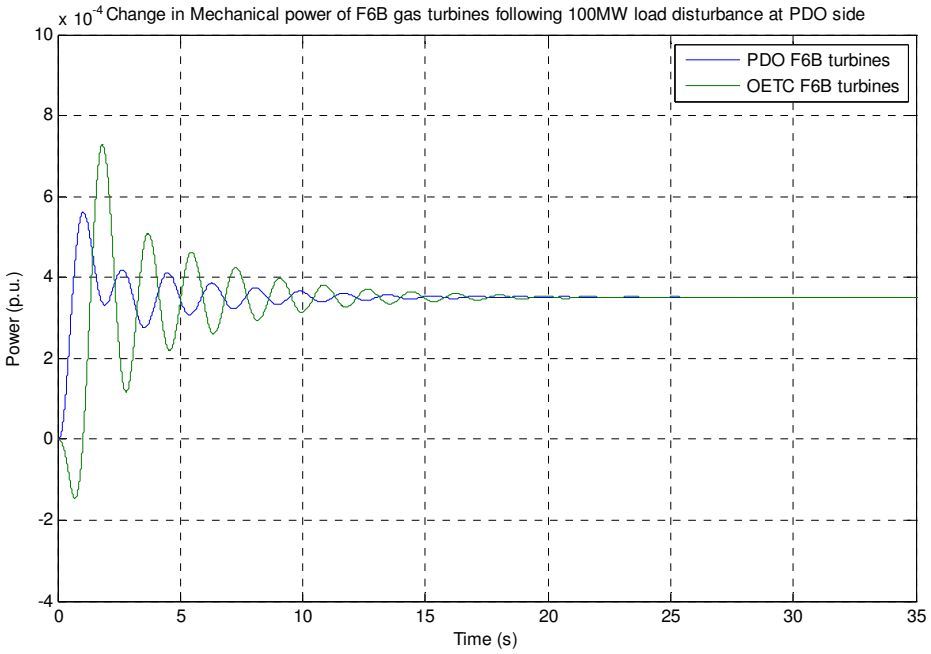

Figure 9.46: Change in Mechanical power of F6B gas turbines following 100MW load disturbance at PDO side with the OETC alone PID frequency and tie line power controller

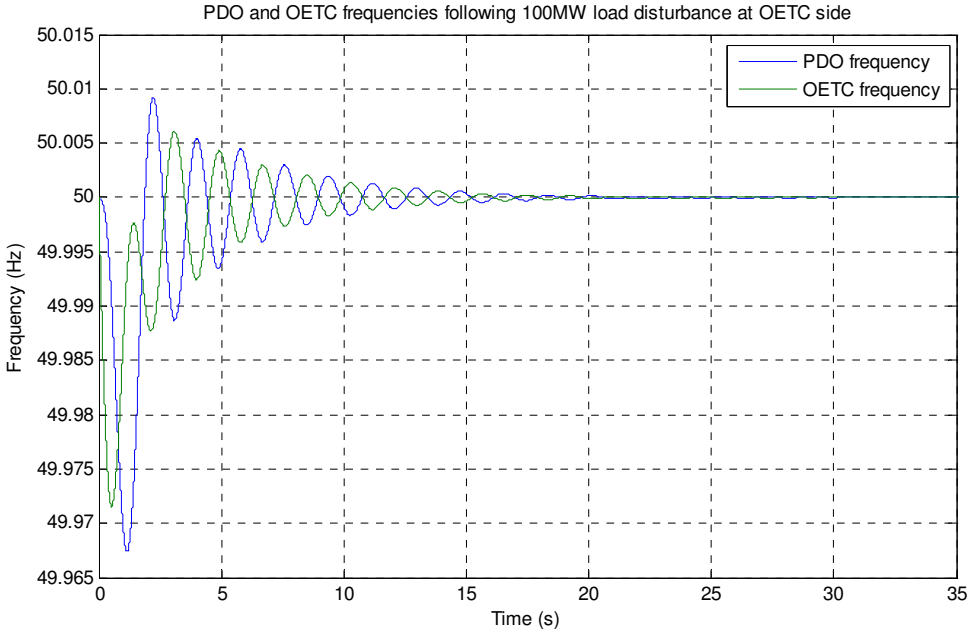

Figure 9.47: Grid frequency following 100MW load disturbance at OETC side with the OETC alone PID frequency and tie line power controller

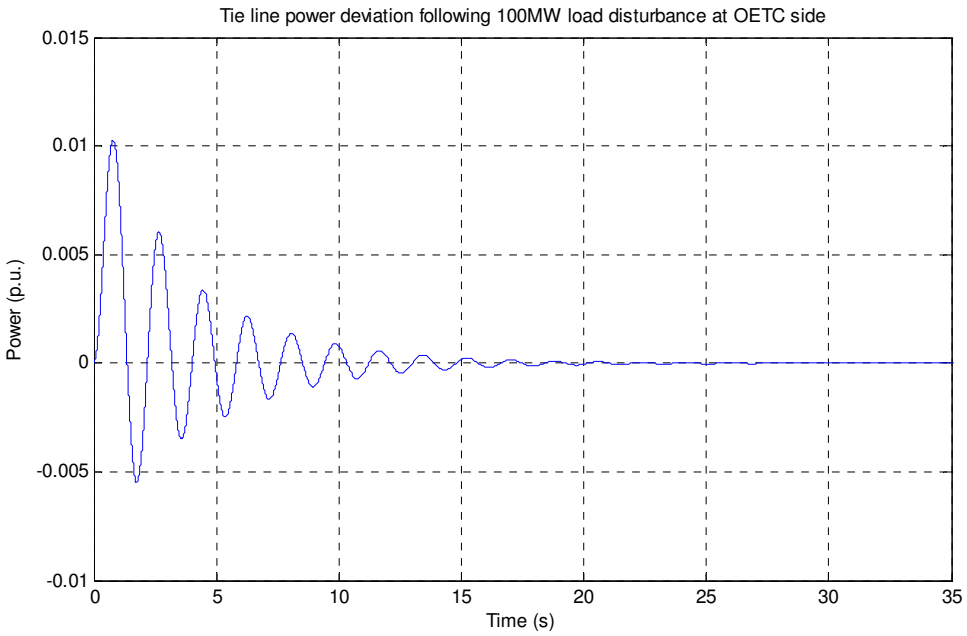

Figure 9.48: Tie line power deviation following 100MW load disturbance at OETC side with the OETC alone PID frequency and tie line power controller

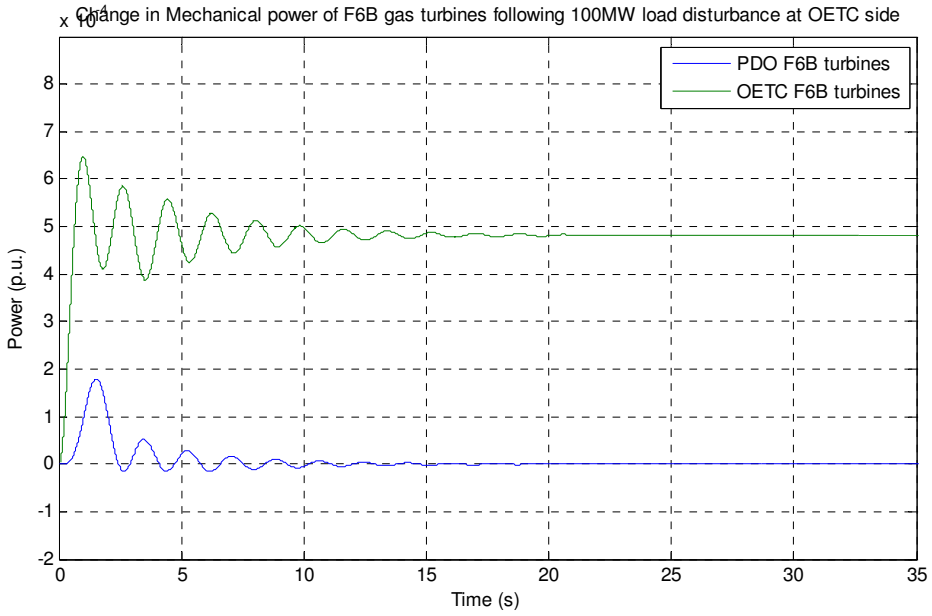

Figure 9.49: Change in Mechanical power of F6B gas turbines following 100MW load disturbance at OETC side with the OETC alone PID frequency and tie line power controller

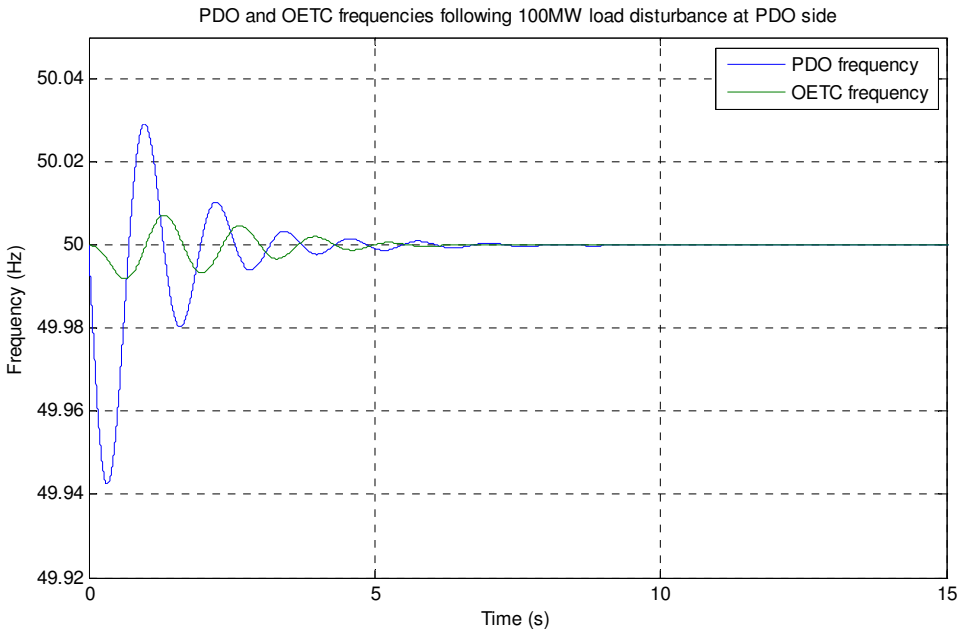

Figure 9.51: Grid frequency following 100MW load disturbance at PDO side with the PDO & OETC PID frequency based AGC controller

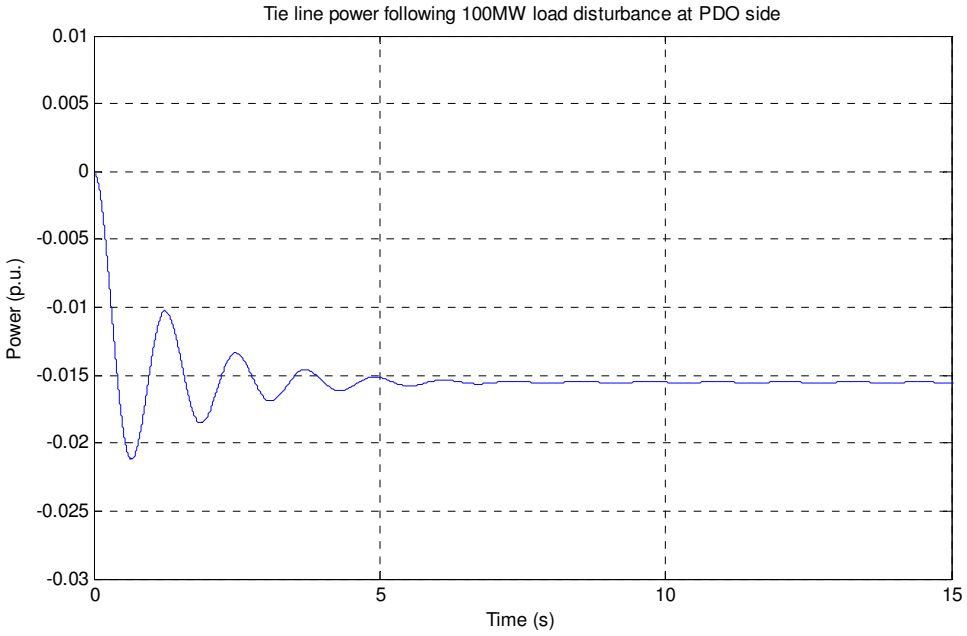

Figure 9.52: Tie line power deviation following 100MW load disturbance at PDO side with the PDO & OETC PID frequency based AGC controller

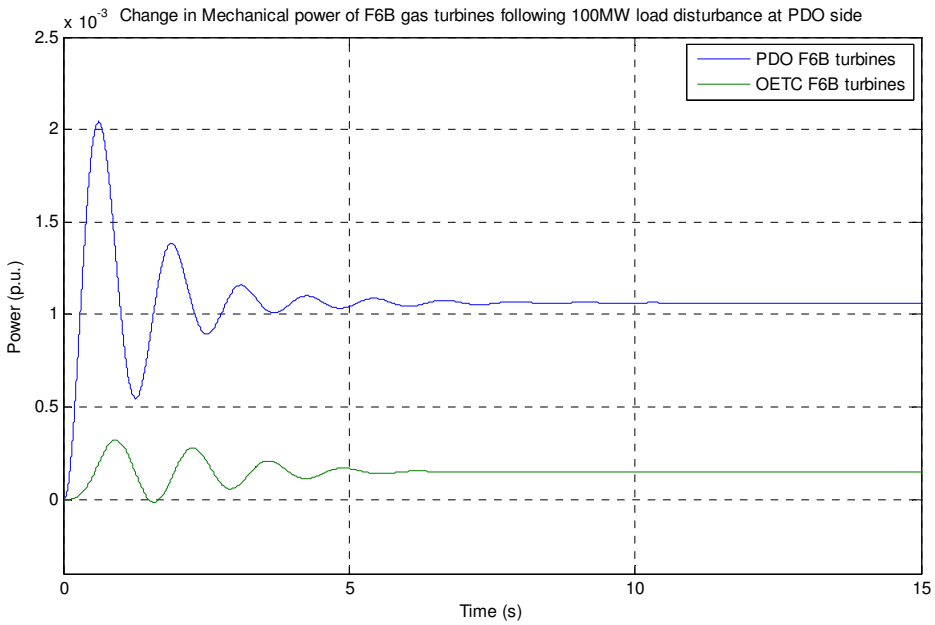

Figure 9.53: Change in Mechanical power of F6B gas turbines following 100MW load disturbance at PDO side with the PDO & OETC PID frequency based AGC controller

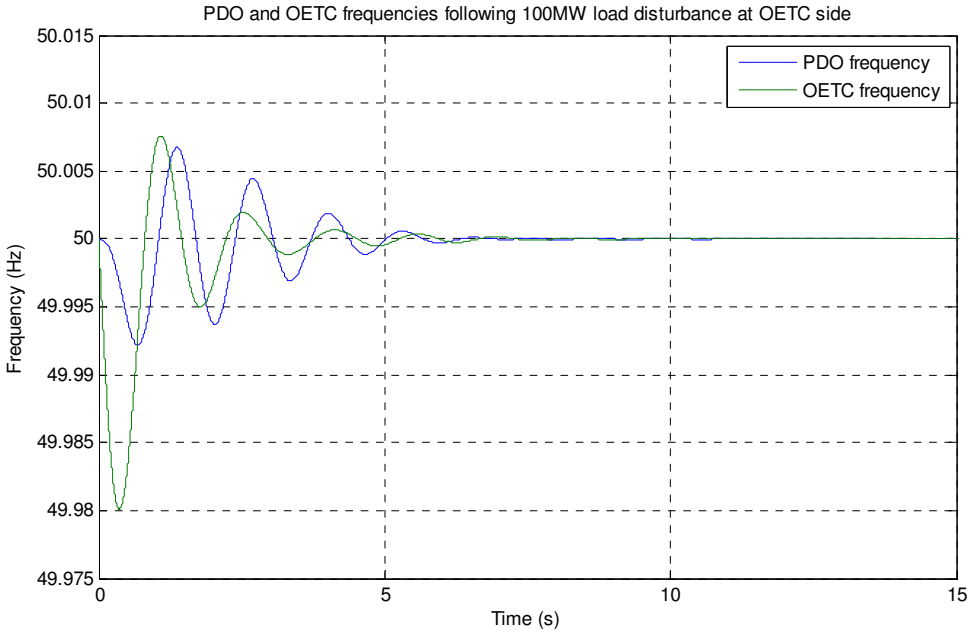

Figure 9.54: Grid frequency following 100MW load disturbance at OETC side with the PDO & OETC PID frequency based AGC controller

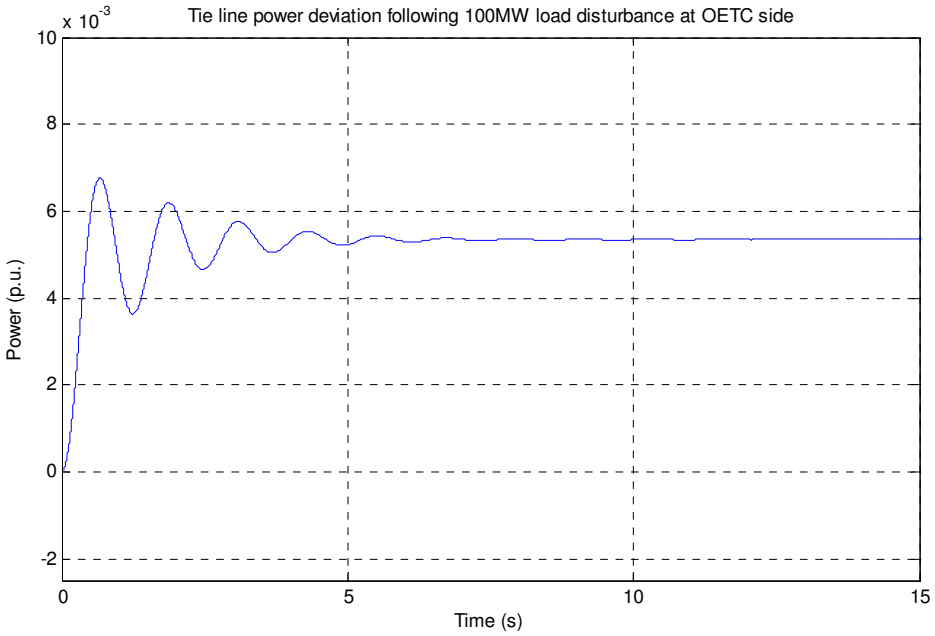

Figure 9.55: Tie line power deviation following 100MW load disturbance at OETC side with the PDO & OETC PID frequency based AGC controller

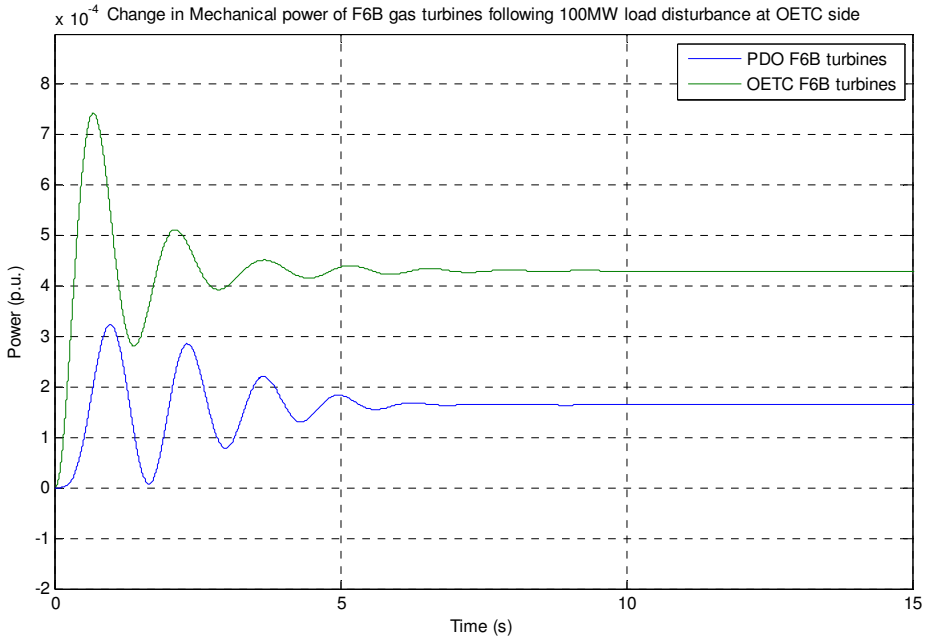

Figure 9.56: Change in Mechanical power of F6B gas turbines following 100MW load disturbance at OETC side with the PDO & OETC PID frequency based AGC controller

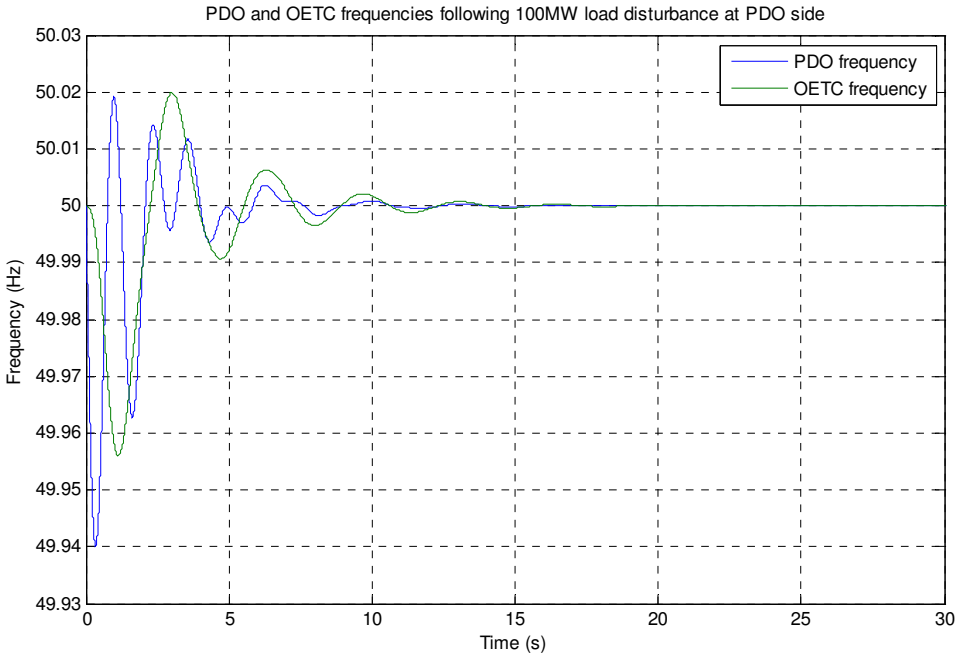

Figure 9.58: Grid frequency following 100MW load disturbance at PDO side with the PDO (using grid frequency) & OETC (using tie line power) PID AGC controller

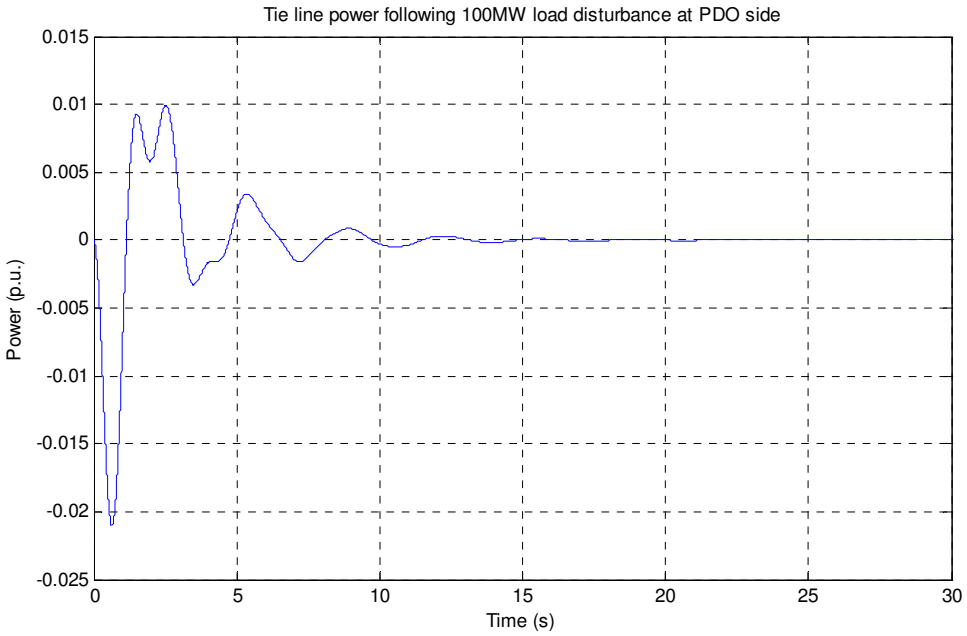

Figure 9.59: Tie line power deviation following 100MW load disturbance at PDO side with the PDO (using grid frequency) & OETC (using tie line power) PID AGC controller

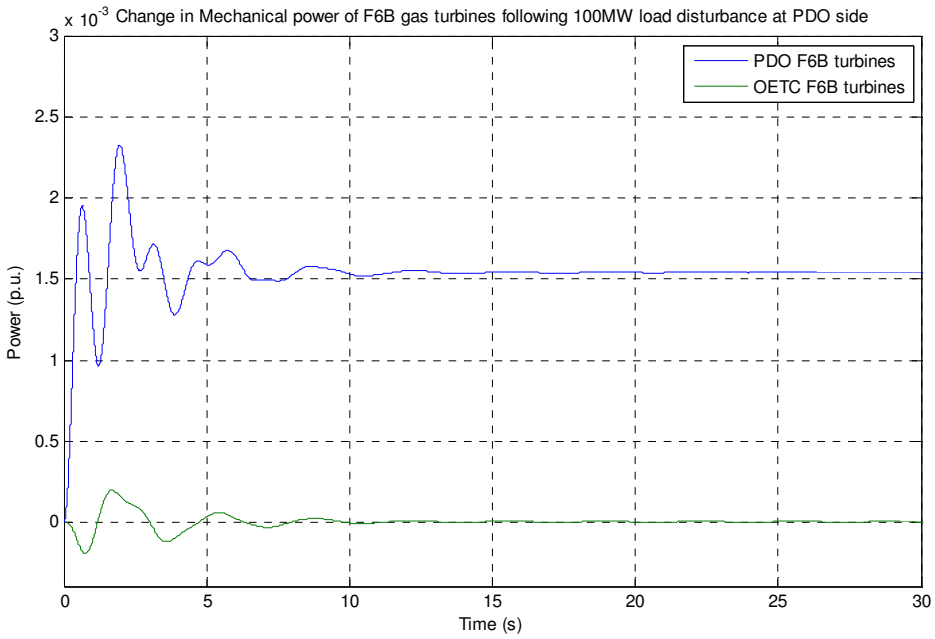

Figure 9.60: Change in Mechanical power of F6B gas turbines following 100MW load disturbance at PDO side with the PDO (using grid frequency) & OETC (using tie line power) PID AGC controller

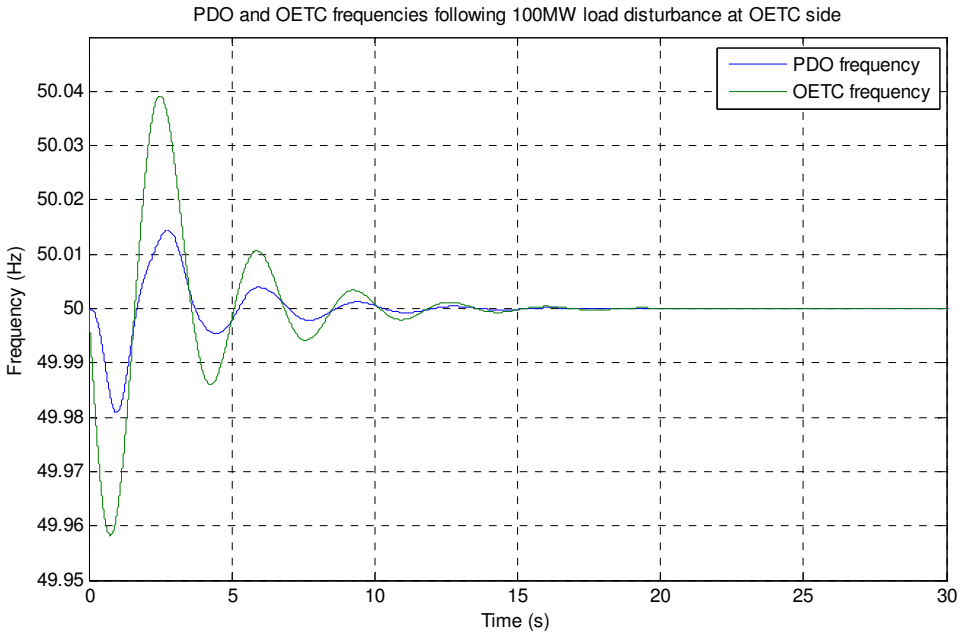

Figure 9.61: Grid frequency following 100MW load disturbance at OETC side with the PDO (using grid frequency) & OETC (using tie line power) PID AGC controller

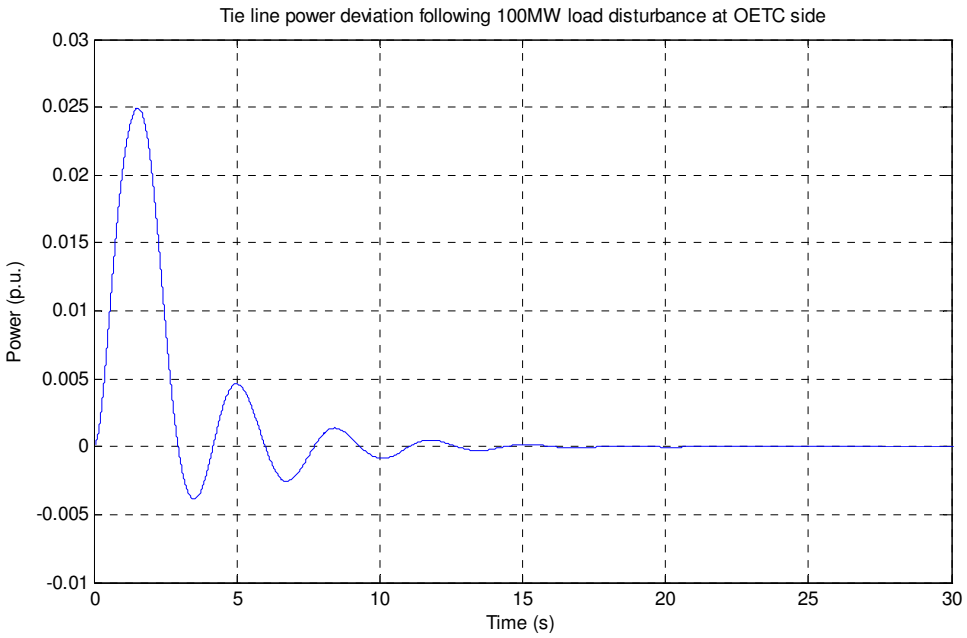

Figure 9.62: Tie line power deviation following 100MW load disturbance at OETC side with the PDO (using grid frequency) & OETC (using tie line power) PID AGC controller

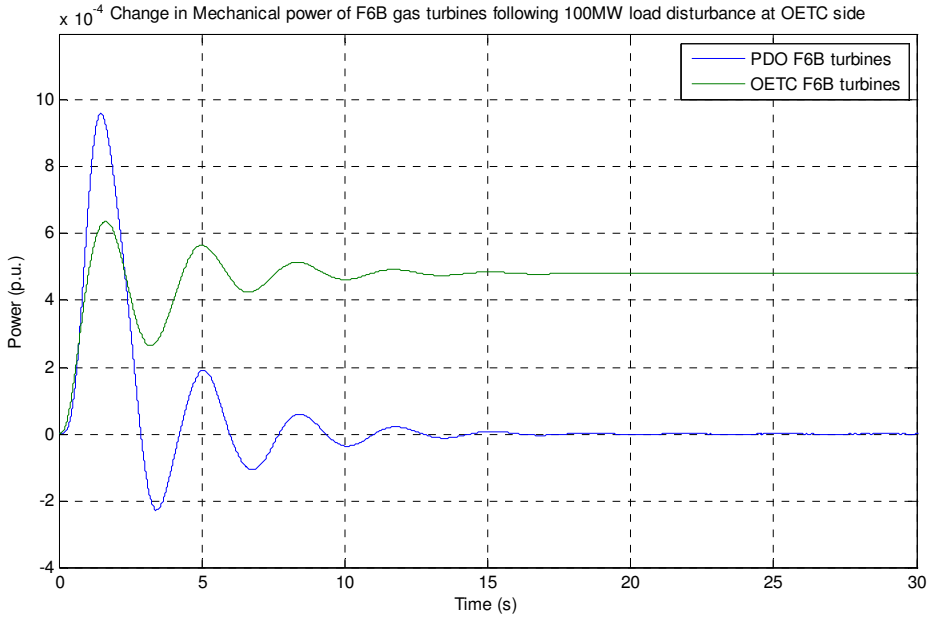

Figure 9.63: Change in Mechanical power of F6B gas turbines following 100MW load disturbance at OETC side with the PDO (using grid frequency) & OETC (using tie line power) PID AGC controller

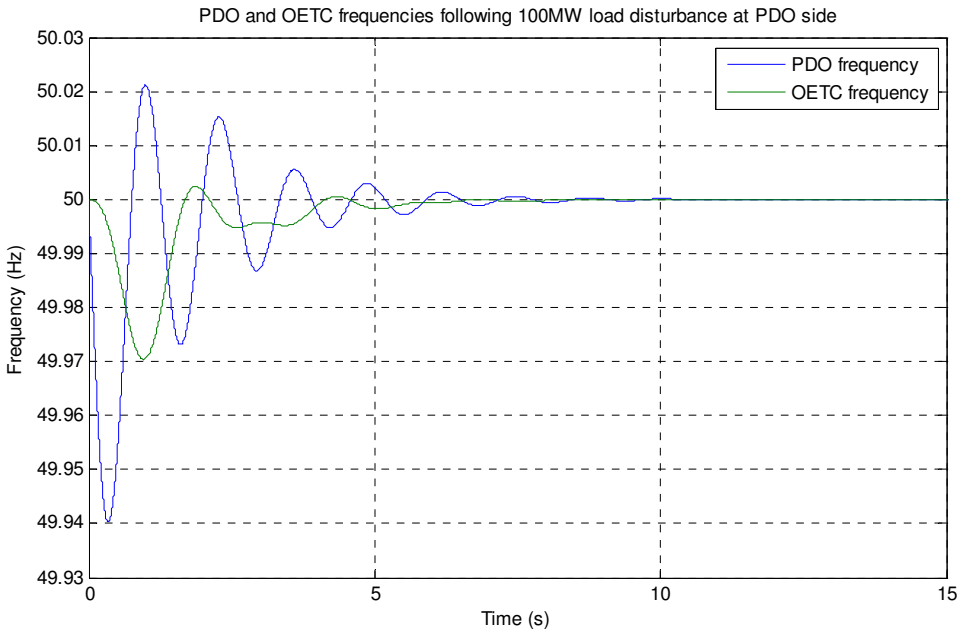

Figure 9.65: Grid frequency following 100MW load disturbance at PDO side with the PDO (using grid frequency) & OETC (using Area Control Error) PID AGC controller

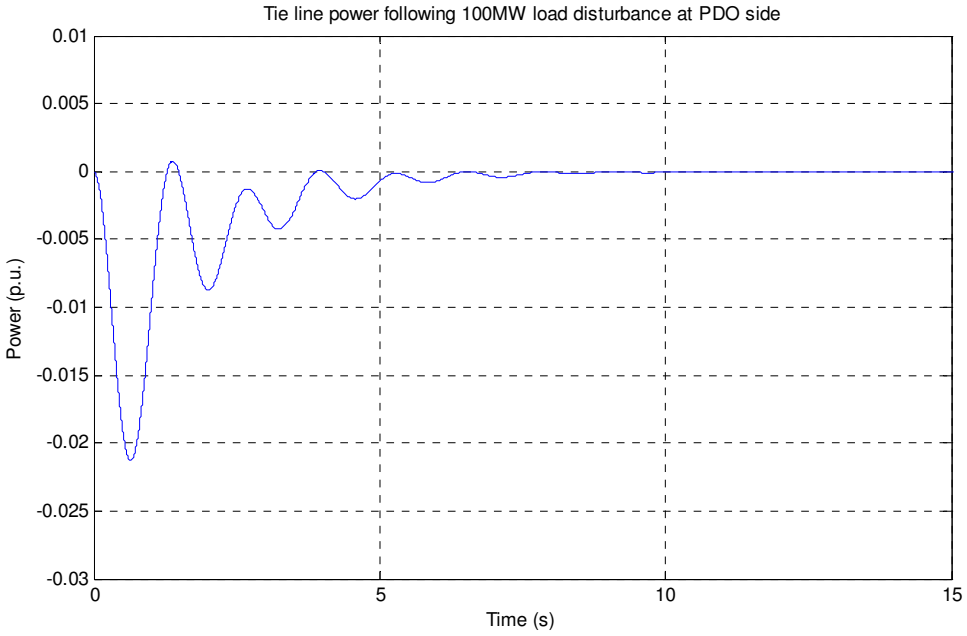

Figure 9.66: Tie line power deviation following 100MW load disturbance at PDO side with the PDO (using grid frequency) & OETC (using Area Control Error) PID AGC controller

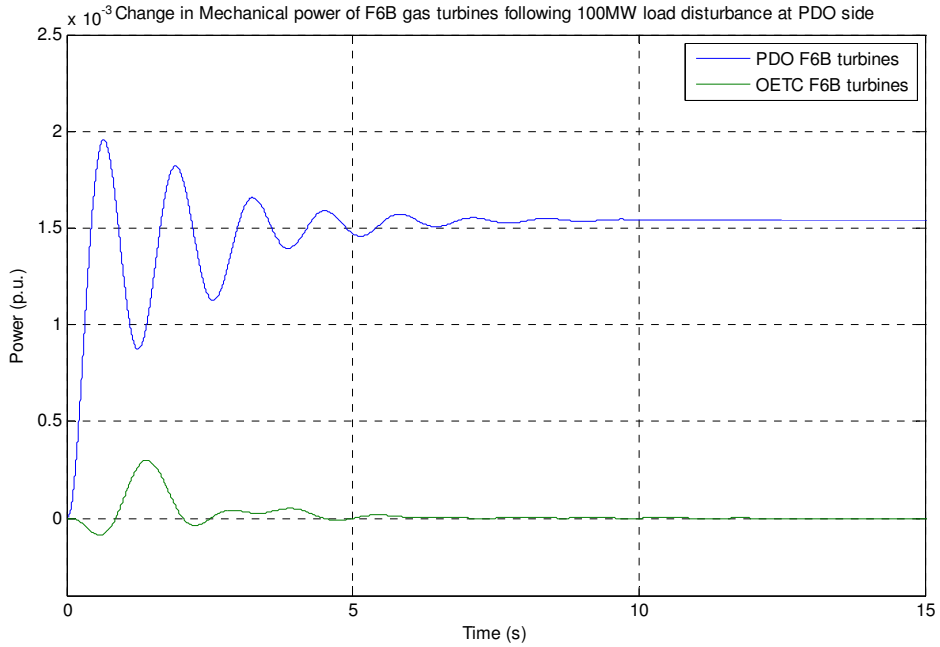

Figure 9.67: Change in Mechanical power of F6B gas turbines following 100MW load disturbance at PDO side with the PDO (using grid frequency) & OETC (using Area Control Error) PID AGC controller

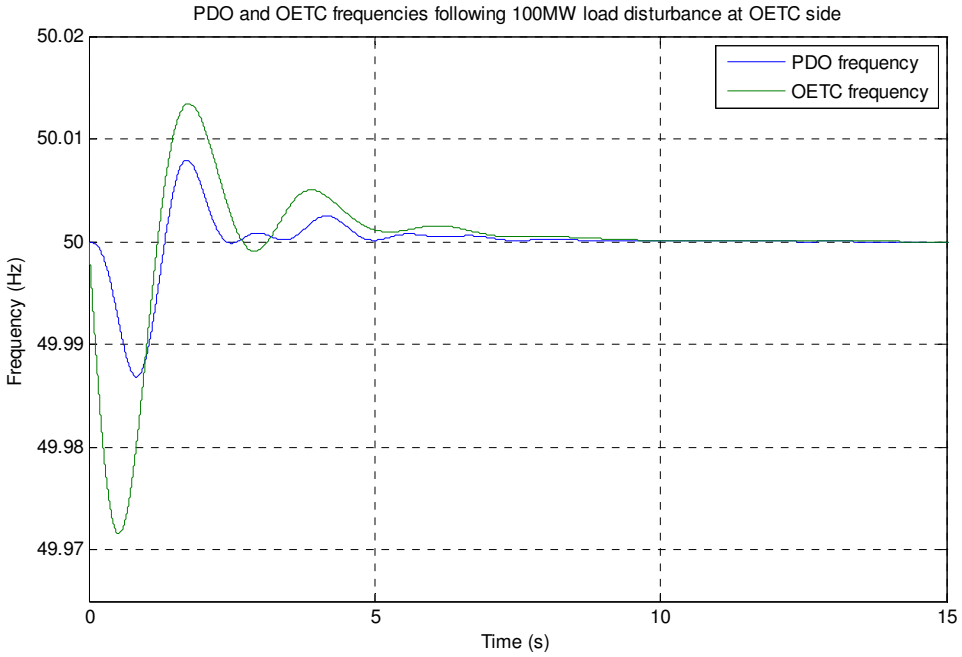

Figure 9.68: Grid frequency following 100MW load disturbance at OETC side with the PDO (using grid frequency) & OETC (using Area Control Error) PID AGC controller

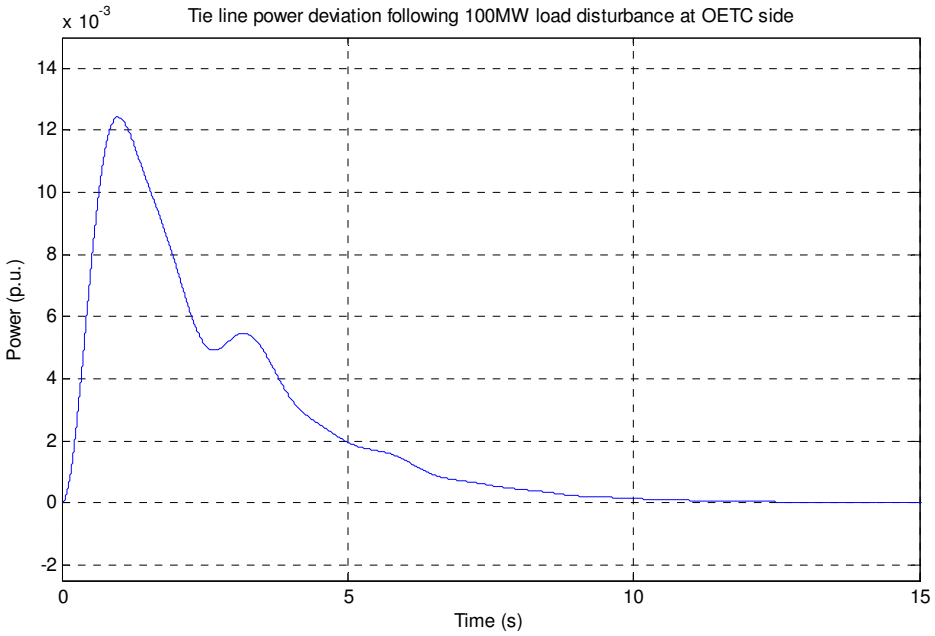

Figure 9.69: Tie line power deviation following 100MW load disturbance at OETC side with the PDO (using grid frequency) & OETC (using Area Control Error) PID AGC controller

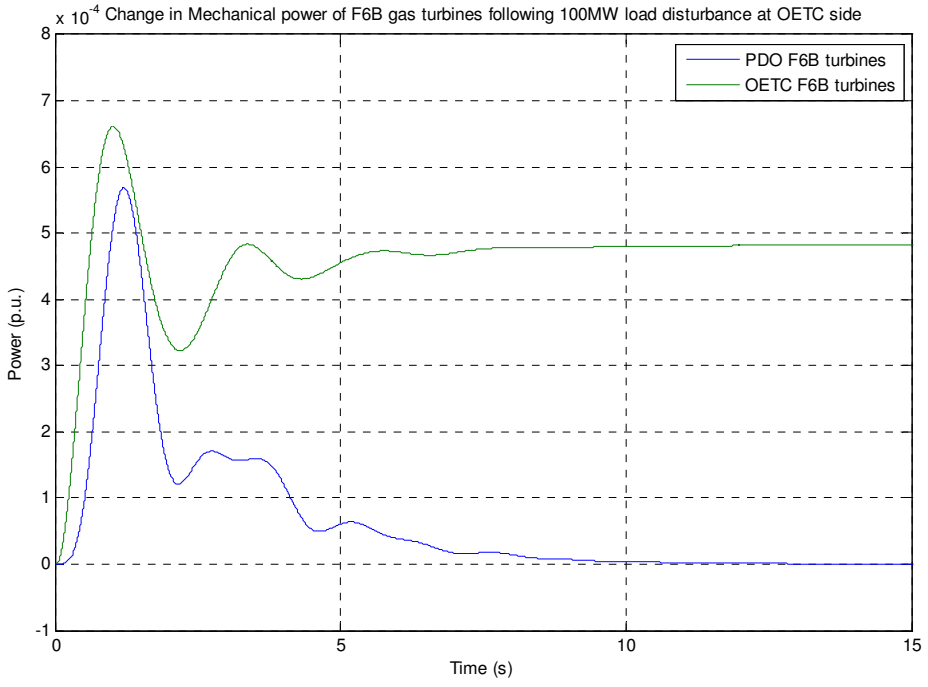

Figure 9.70: Change in Mechanical power of F6B gas turbines following 100MW load disturbance at OETC side with the PDO (using grid frequency) & OETC (using Area Control Error) PID AGC controller

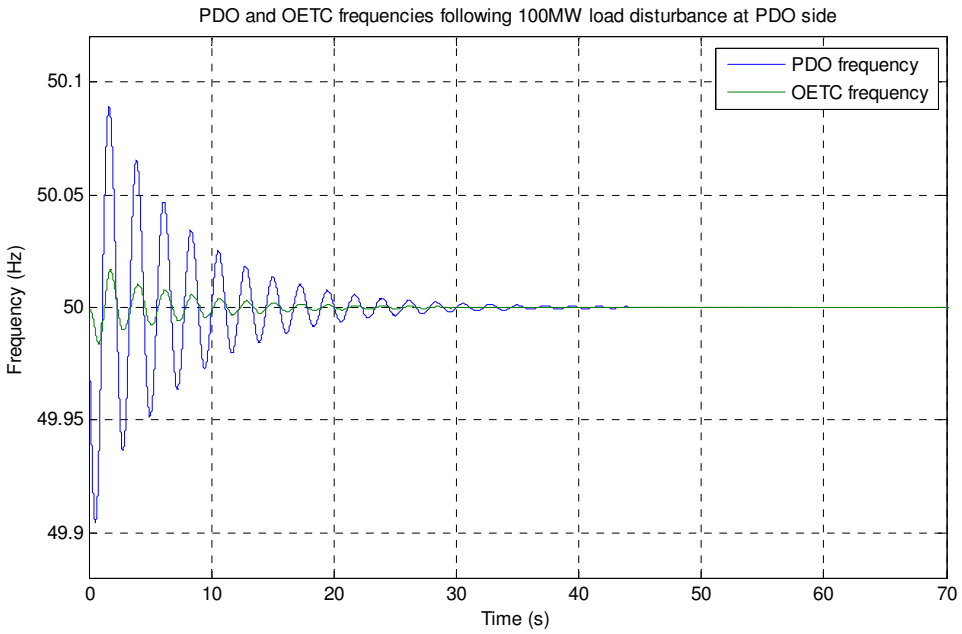

Figure 9.72: Grid frequency following 100MW load disturbance at PDO side with the PDO (using tie line power) & OETC (using grid frequency) PID AGC controller

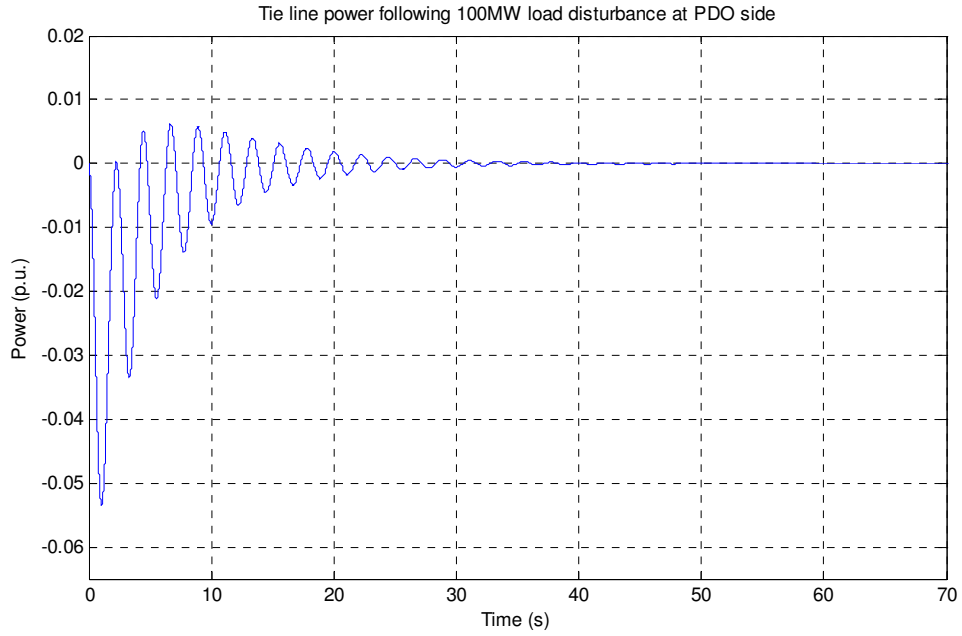

Figure 9.73: Tie line power deviation following 100MW load disturbance at PDO side with the PDO (using tie line power) & OETC (using grid frequency) PID AGC controller

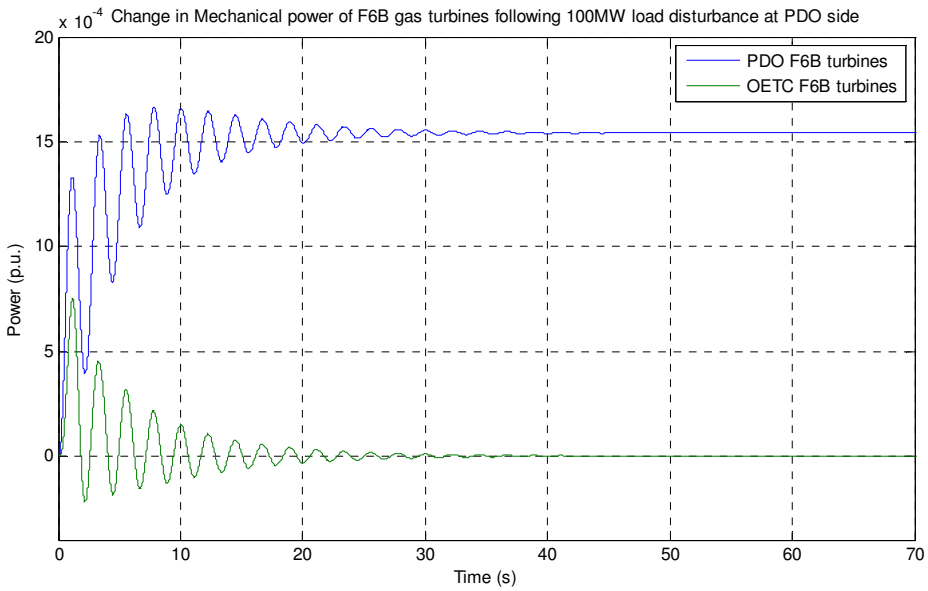

Figure 9.74: Change in Mechanical power of F6B gas turbines following 100MW load disturbance at PDO side with the PDO (using tie line power) & OETC (using grid frequency) PID AGC controller

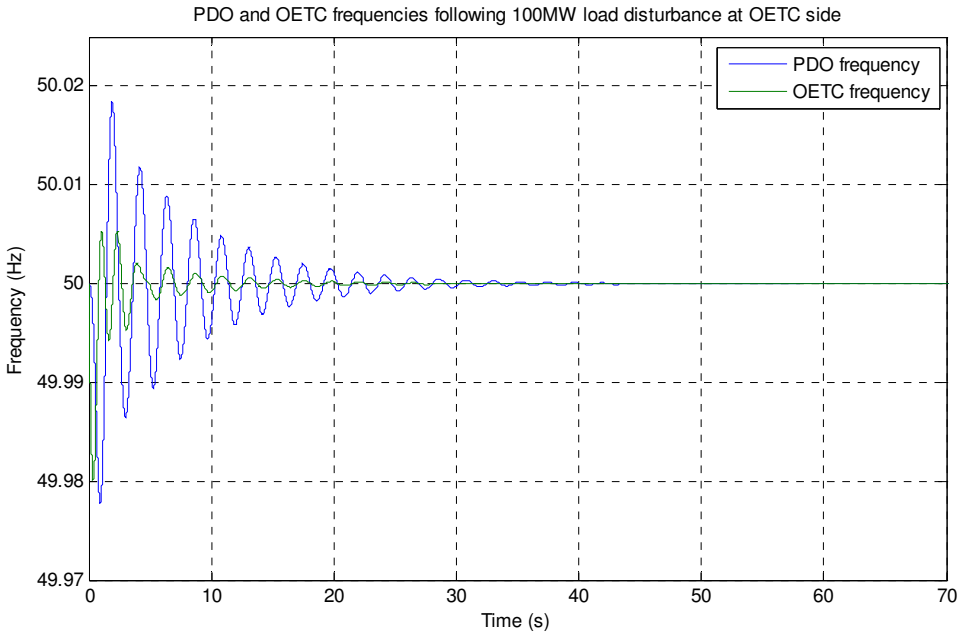

Figure 9.75: Grid frequency following 100MW load disturbance at OETC side with the PDO (using tie line power) & OETC (using grid frequency) PID AGC controller

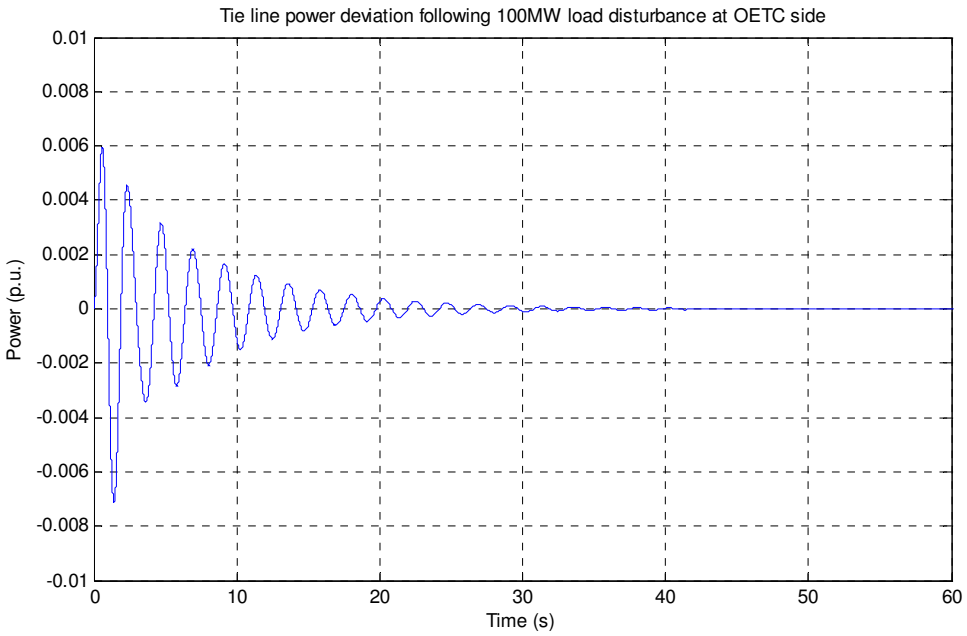

Figure 9.76: Tie line power deviation following 100MW load disturbance at OETC side with the PDO (using tie line power) & OETC (using grid frequency) PID AGC controller

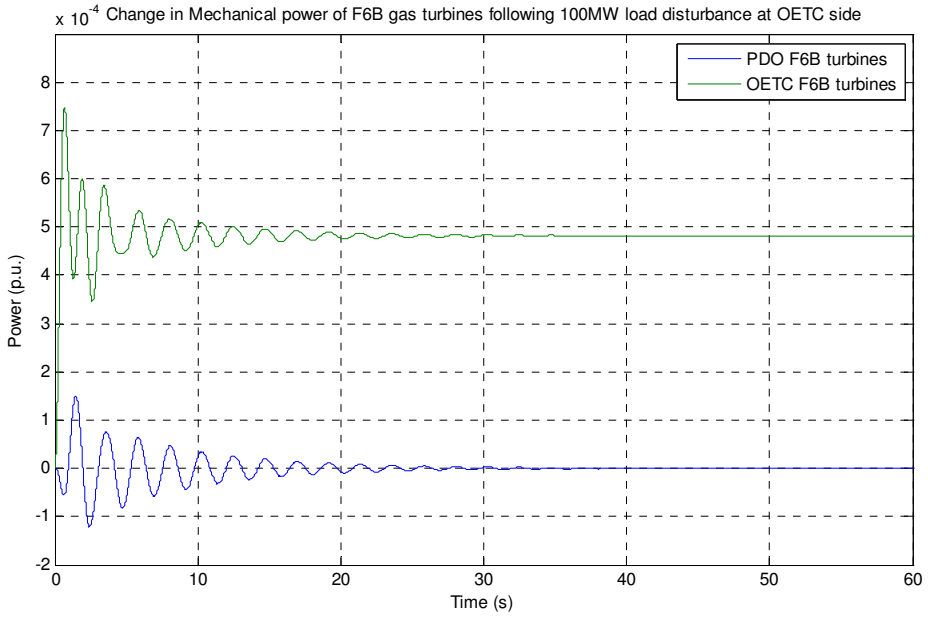

Figure 9.77: Change in Mechanical power of F6B gas turbines following 100MW load disturbance at OETC side with the PDO (using tie line power) & OETC (using grid frequency) PID AGC controller

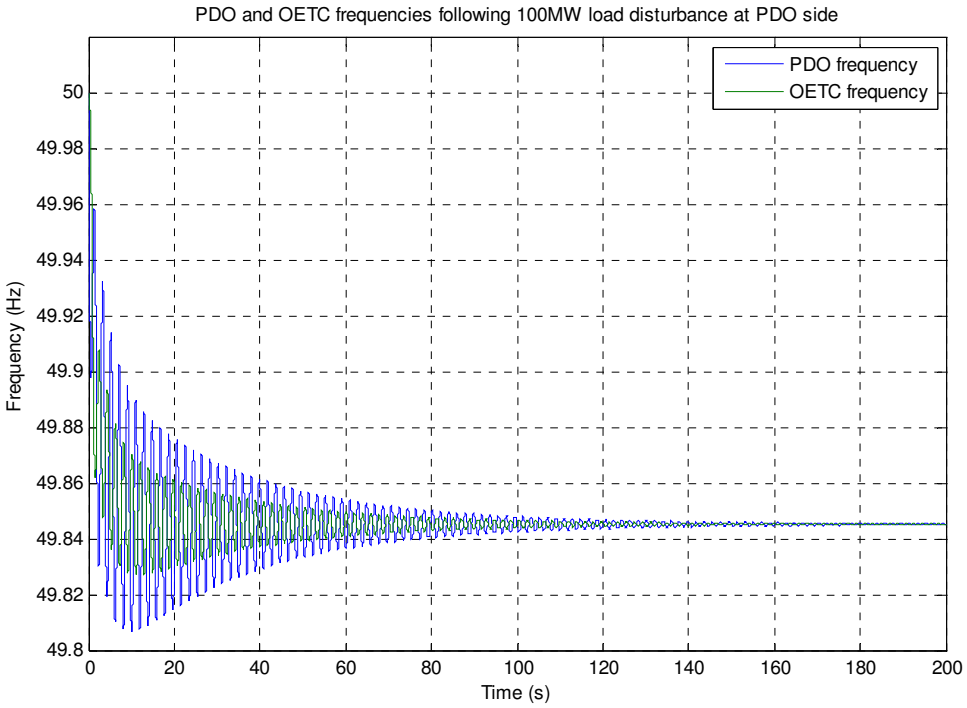

Figure 9.79: Grid frequency following 100MW load disturbance at PDO side with the PDO (using tie line power) & OETC (using tie line power) PID AGC controller

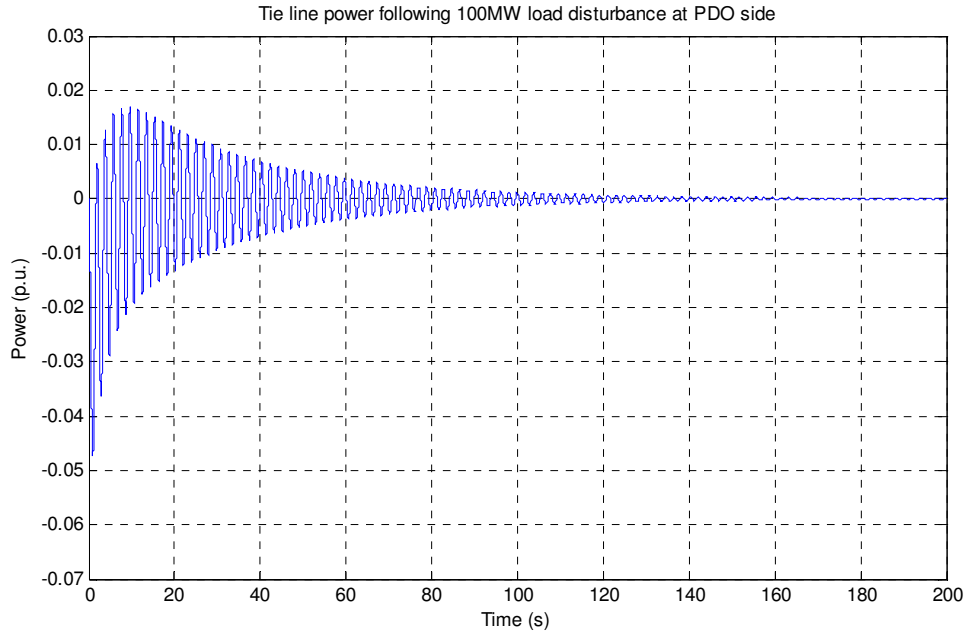

Figure 9.80: Tie line power deviation following 100MW load disturbance at PDO side with the PDO (using tie line power) & OETC (using tie line power) PID AGC controller

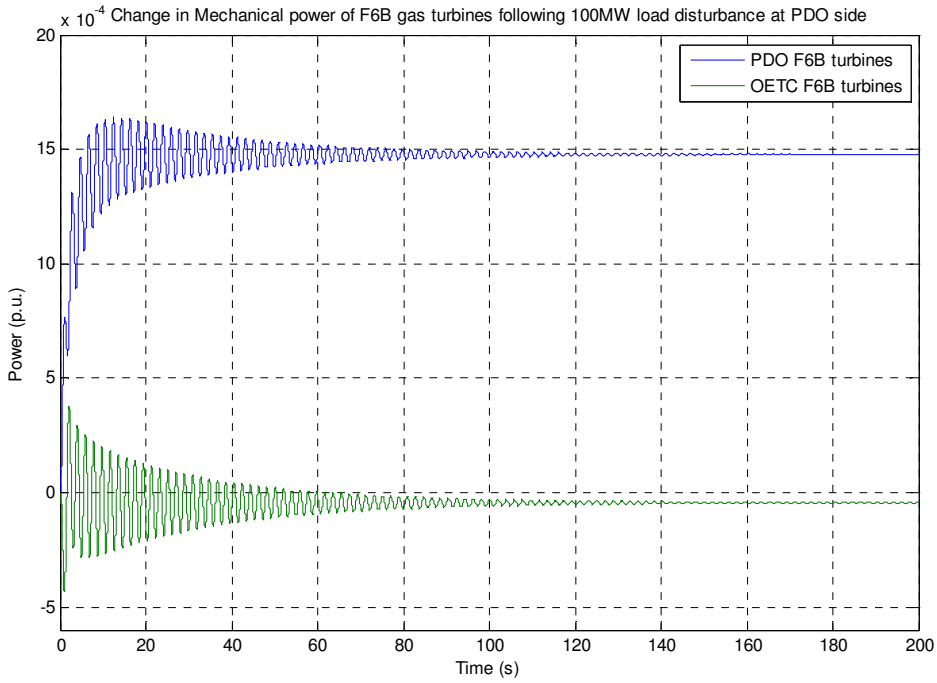

Figure 9.81: Change in Mechanical power of F6B gas turbines following 100MW load disturbance at PDO side with the PDO (using tie line power) & OETC (using tie line power) PID AGC controller

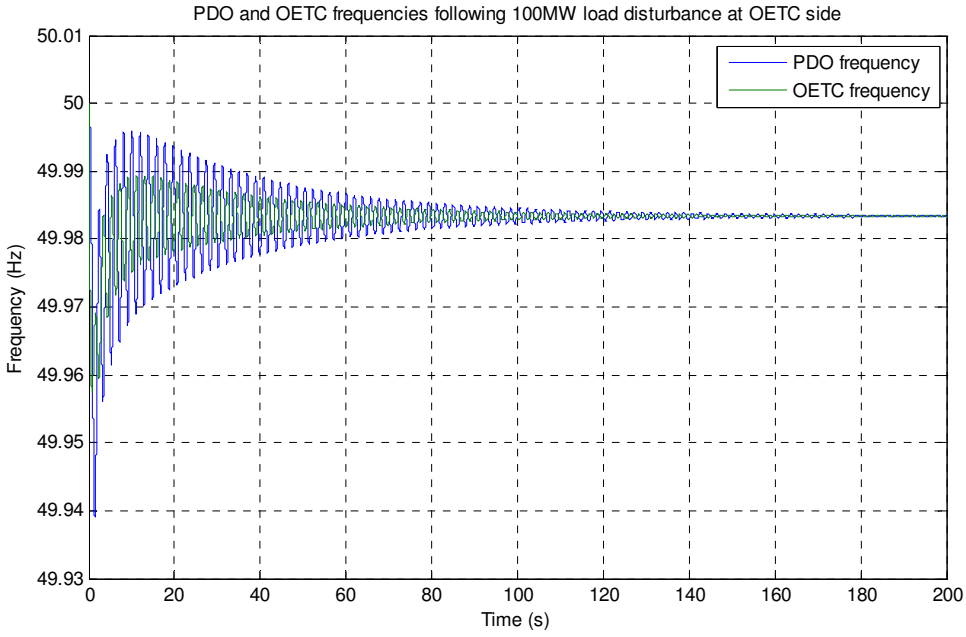

Figure 9.82: Grid frequency following 100MW load disturbance at OETC side with the PDO (using tie line power) & OETC (using tie line power) PID AGC controller

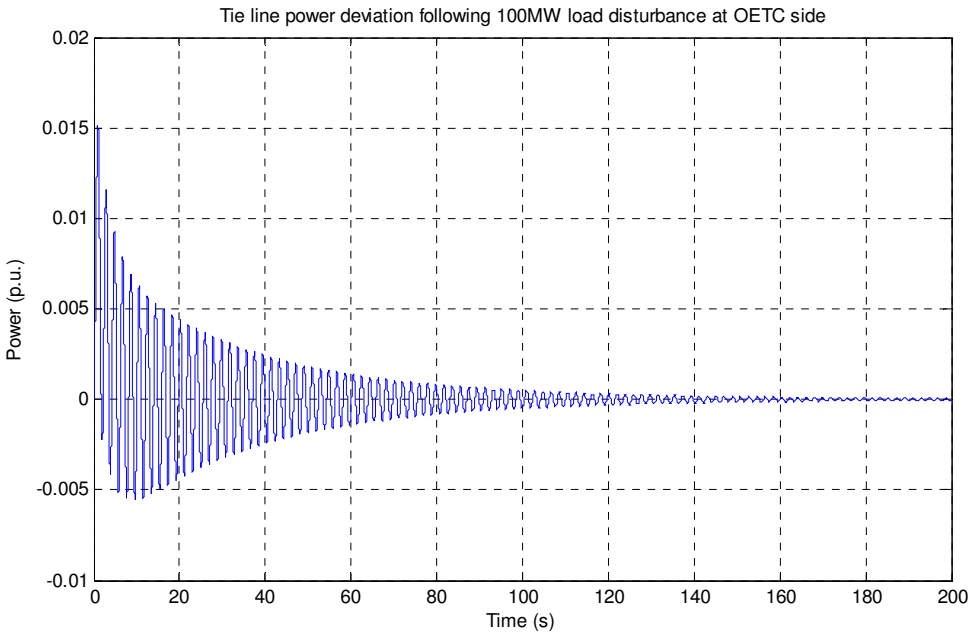

Figure 9.83: Tie line power deviation following 100MW load disturbance at OETC side with the PDO (using tie line power) & OETC (using tie line power) PID AGC controller

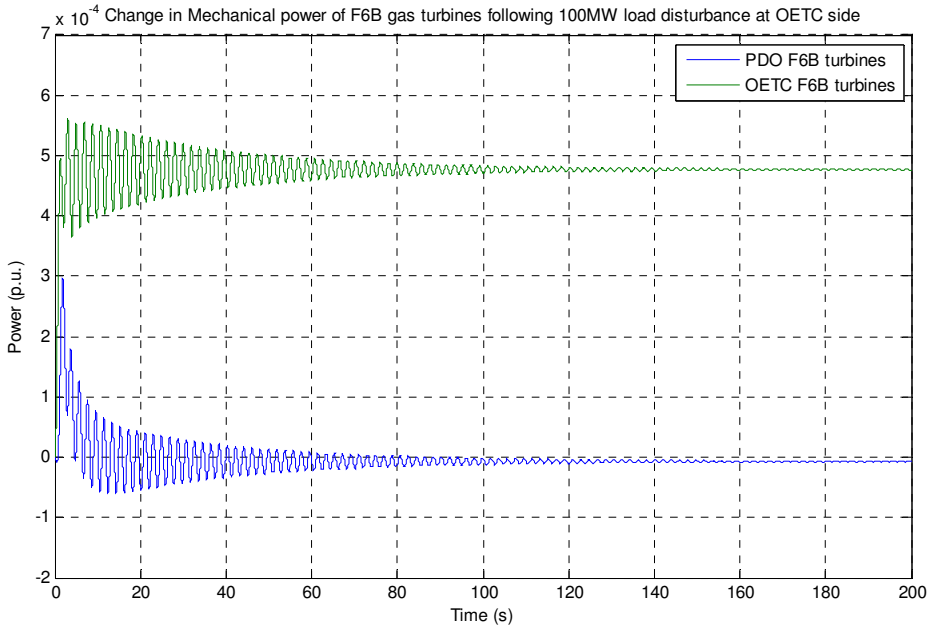

Figure 9.84: Change in Mechanical power of F6B gas turbines following 100MW load disturbance at OETC side with the PDO (using tie line power) & OETC (using tie line power) PID AGC controller

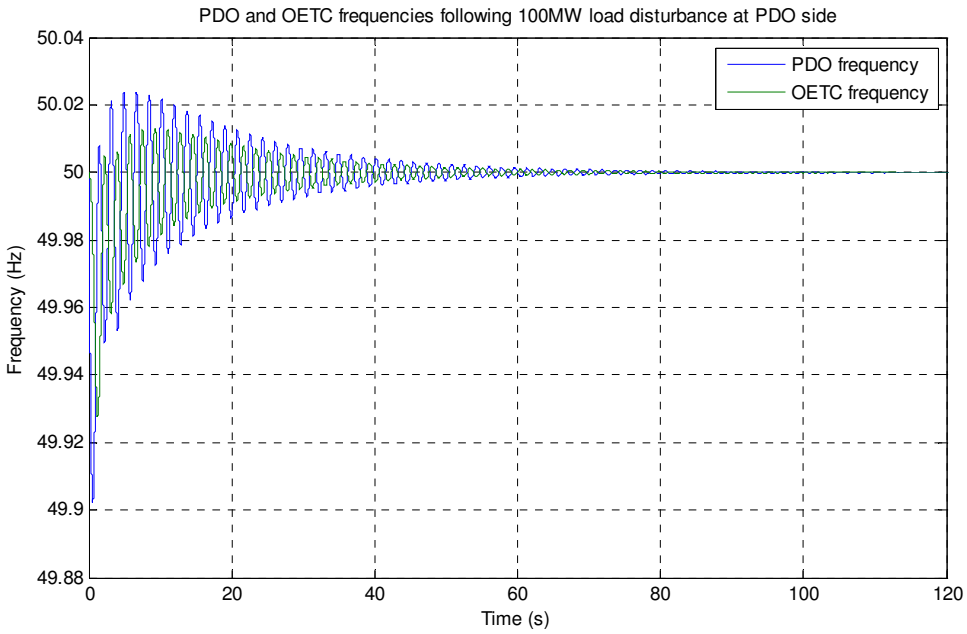

Figure 9.86: Grid frequency following 100MW load disturbance at PDO side with the PDO (using tie line power) & OETC (using Area Control Error) PID AGC controller

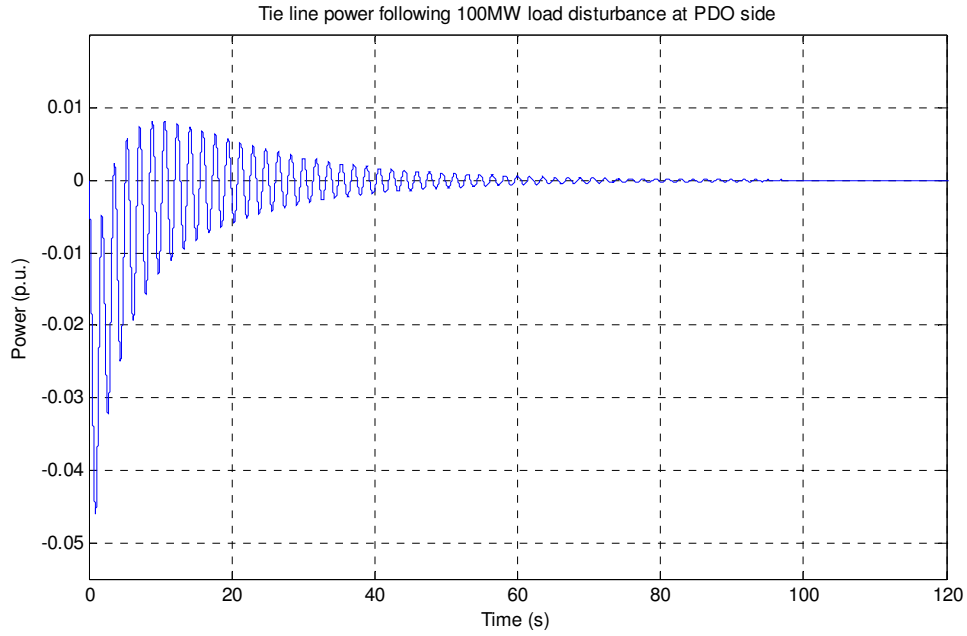

Figure 9.87: Tie line power deviation following 100MW load disturbance at PDO side with the PDO (using tie line power) & OETC (using Area Control Error) PID AGC controller

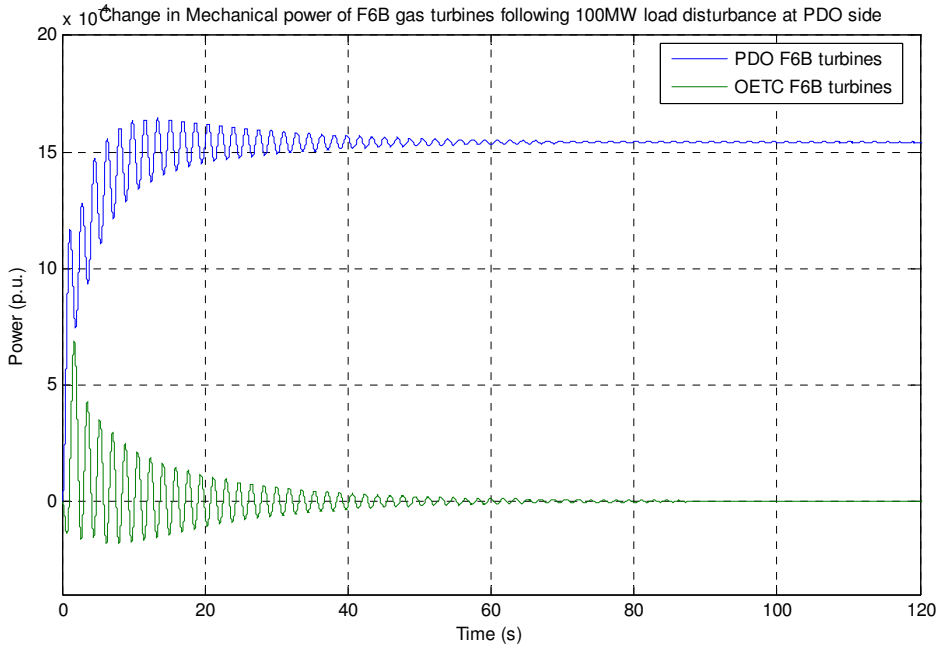

Figure 9.88: Change in Mechanical power of F6B gas turbines following 100MW load disturbance at PDO side with the PDO (using tie line power) & OETC (using Area Control Error) PID AGC controller

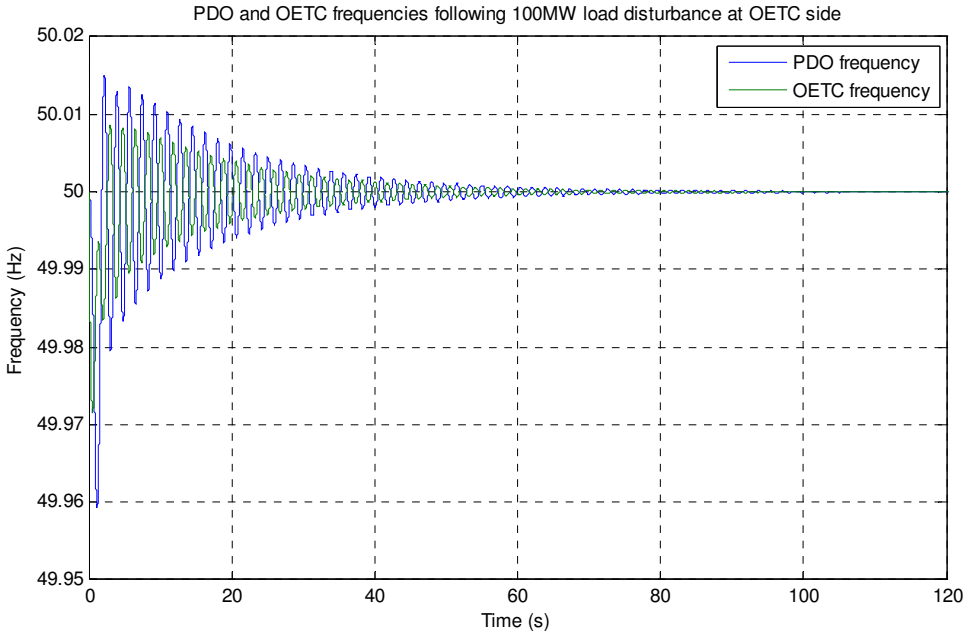

Figure 9.89: Grid frequency following 100MW load disturbance at OETC side with the PDO (using tie line power) & OETC (using Area Control Error) PID AGC controller

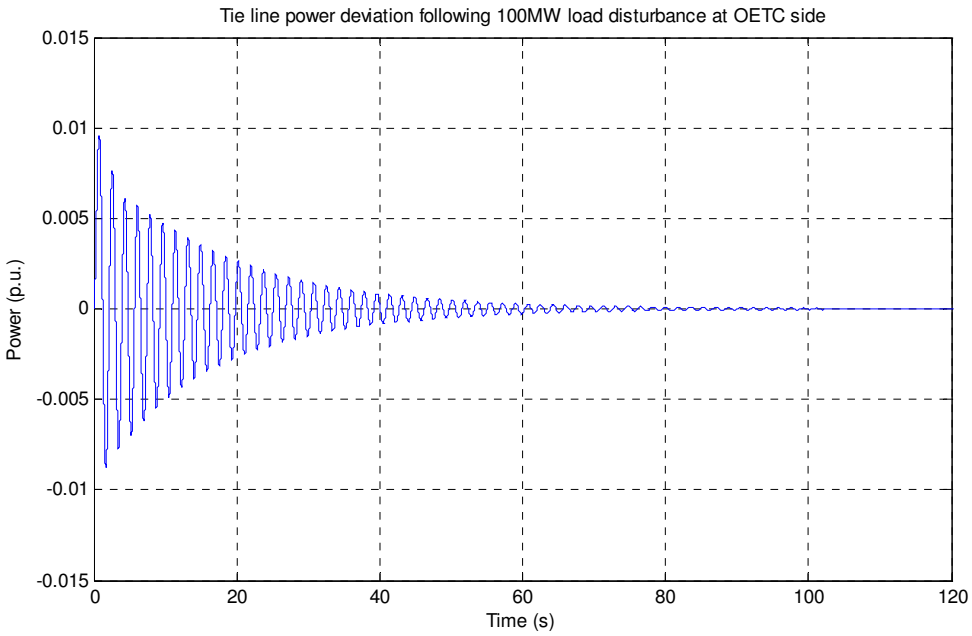

Figure 9.90: Tie line power deviation following 100MW load disturbance at OETC side with the PDO (using tie line power) & OETC (using Area Control Error) PID AGC controller

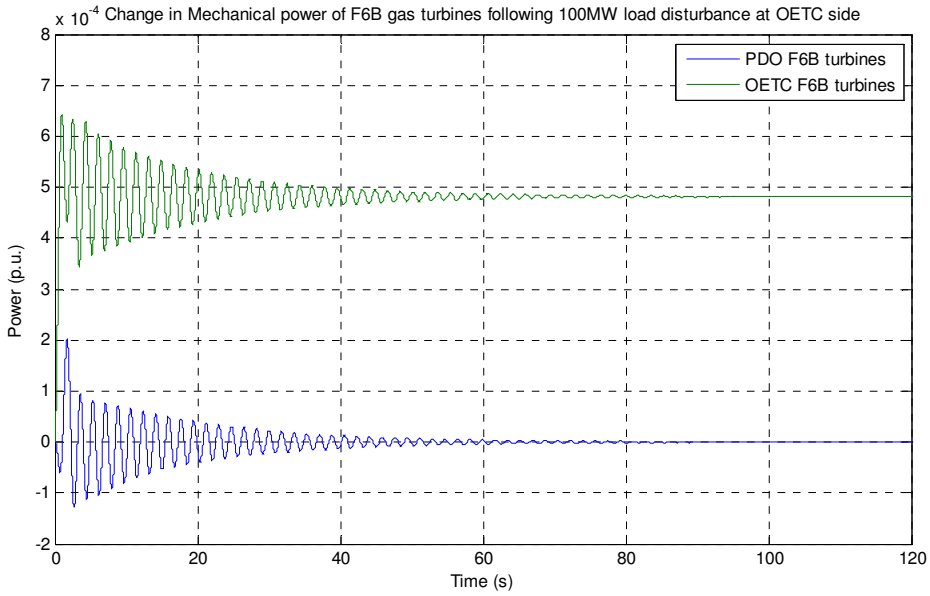

Figure 9.91: Change in Mechanical power of F6B gas turbines following 100MW load disturbance at OETC side with the PDO (using tie line power) & OETC (using Area Control Error) PID AGC controller

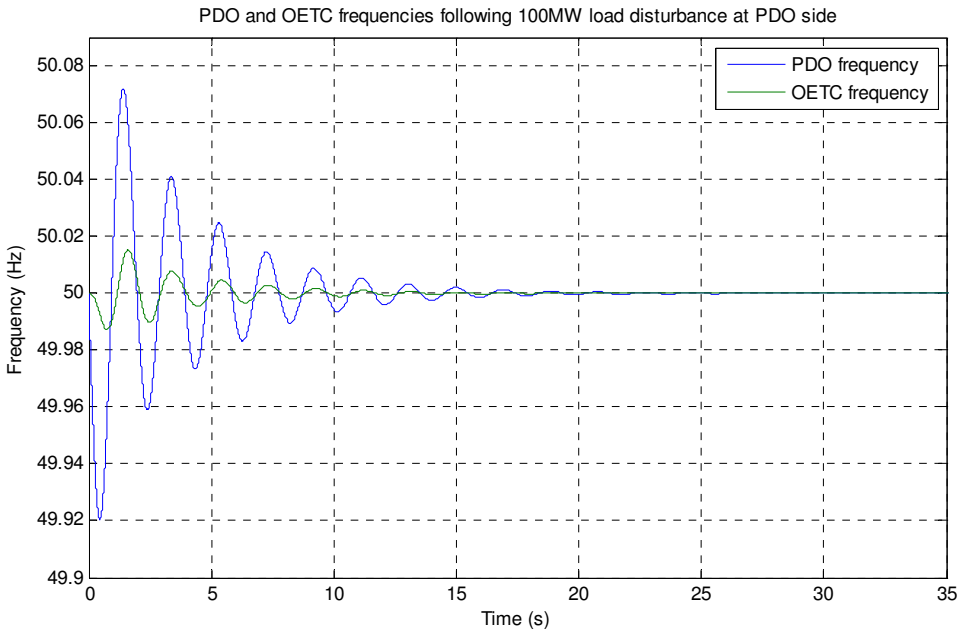

Figure 9.93: Grid frequency following 100MW load disturbance at PDO side with the PDO (using Area Control Error) & OETC (using grid frequency) PID AGC controller

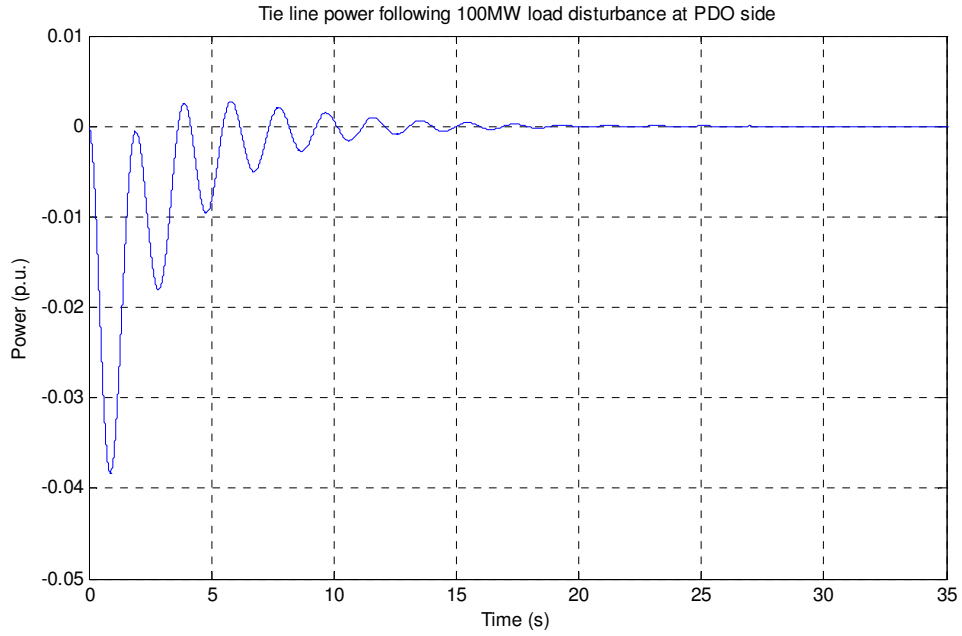

Figure 9.94: Tie line power deviation following 100MW load disturbance at PDO side with the PDO (using Area Control Error) & OETC (using grid frequency) PID AGC controller

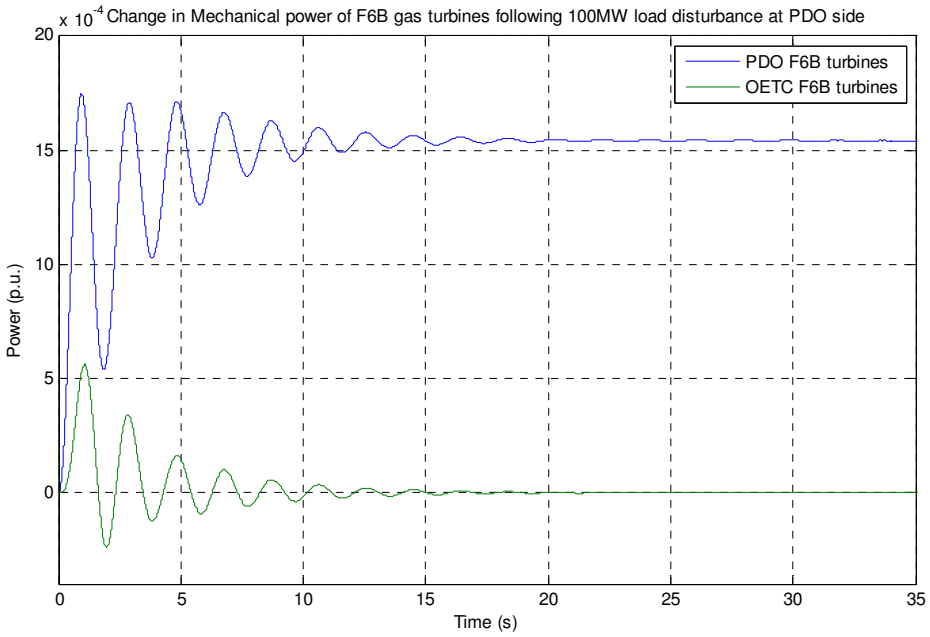

Figure 9.95: Change in Mechanical power of F6B gas turbines following 100MW load disturbance at PDO side with the PDO (using Area Control Error) & OETC (using grid frequency) PID AGC controller

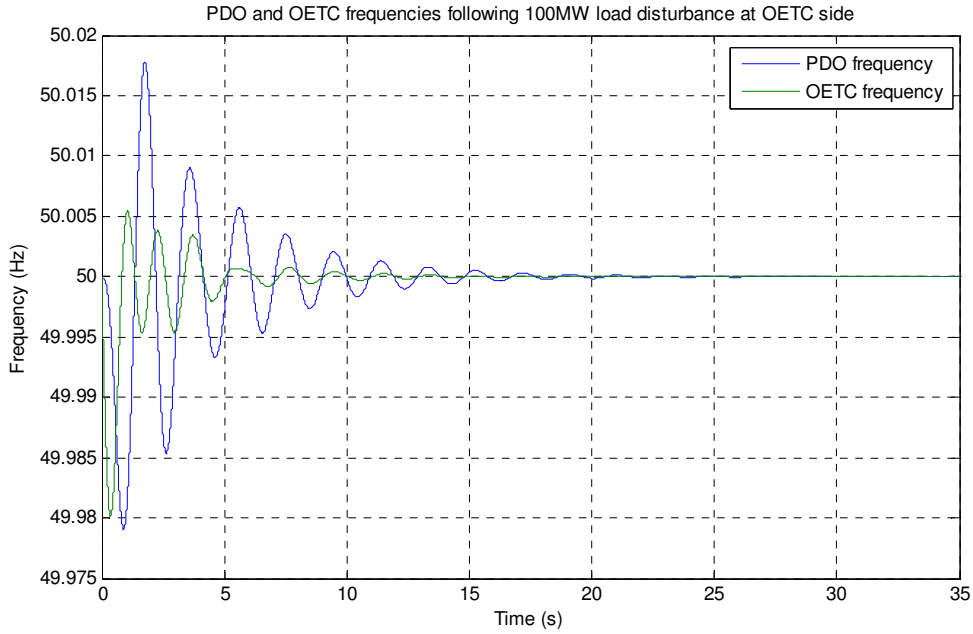

Figure 9.96: Grid frequency following 100MW load disturbance at OETC side with the PDO (using Area Control Error) & OETC (using grid frequency) PID AGC controller

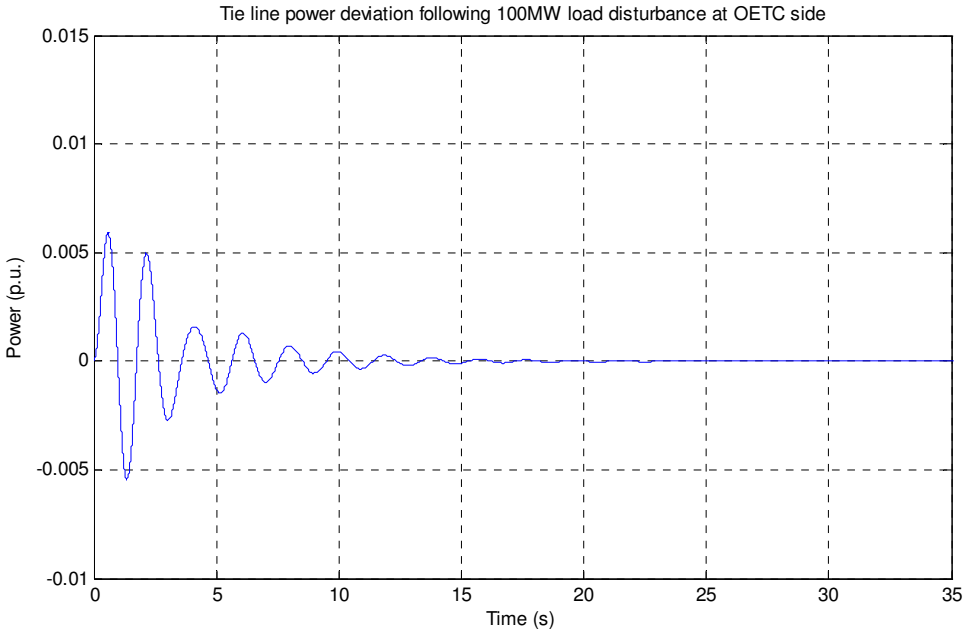

Figure 9.97: Tie line power deviation following 100MW load disturbance at OETC side with the PDO (using Area Control Error) & OETC (using grid frequency) PID AGC controller

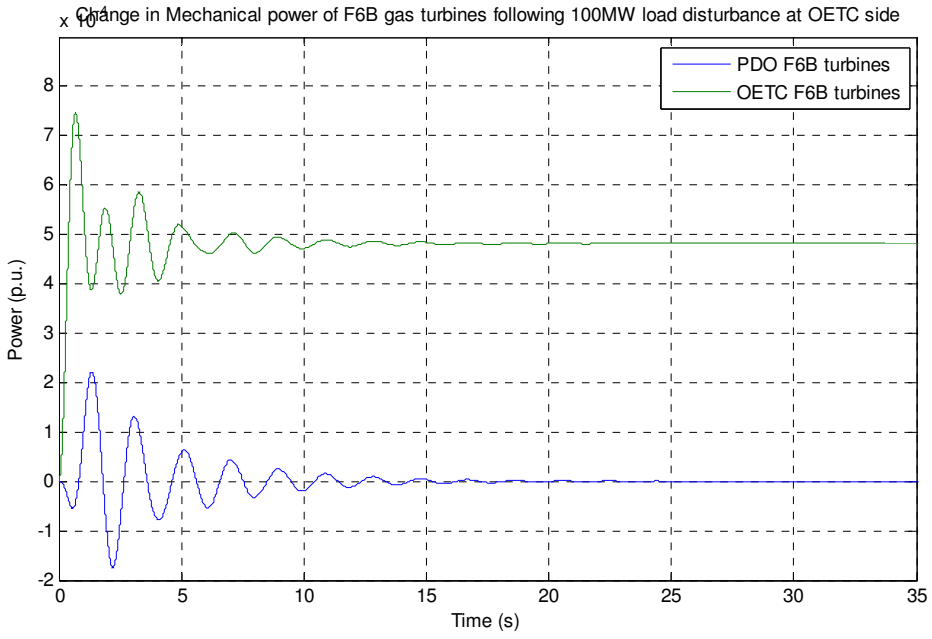

Figure 9.98: Change in Mechanical power of F6B gas turbines following 100MW load disturbance at OETC side with the PDO (using Area Control Error) & OETC (using grid frequency) PID AGC controller

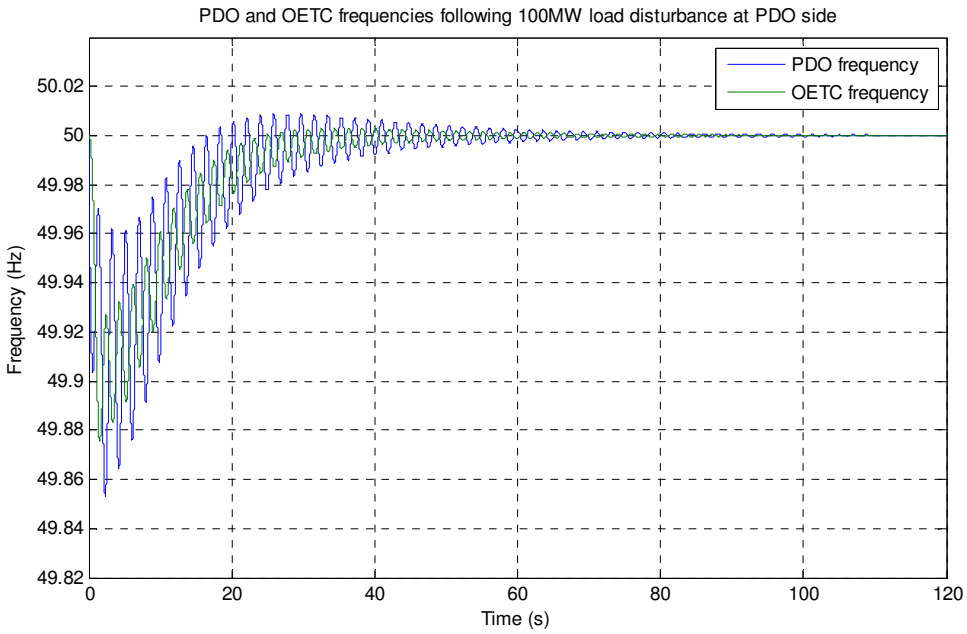

Figure 9.100: Grid frequency following 100MW load disturbance at PDO side with the PDO (using Area Control Error) & OETC (using tie line power) PID AGC controller

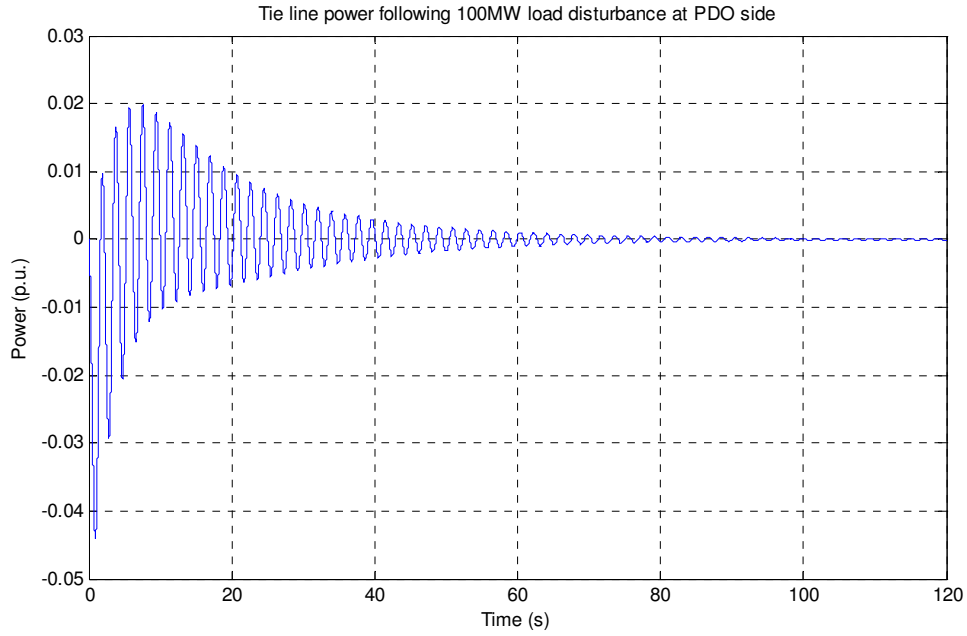

Figure 9.101: Tie line power deviation following 100MW load disturbance at PDO side with the PDO (using Area Control Error) & OETC (using tie line power) PID AGC controller

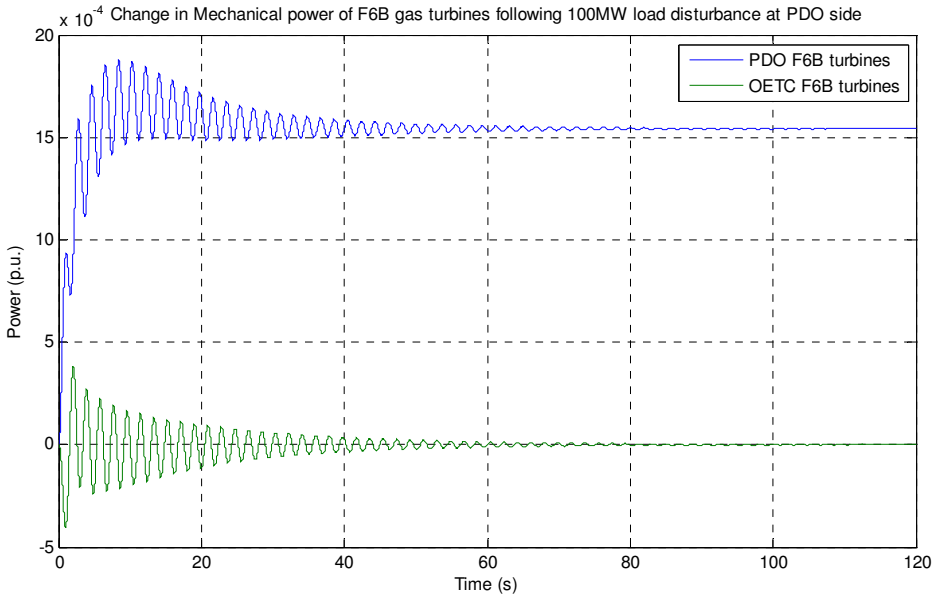

Figure 9.102: Change in Mechanical power of F6B gas turbines following 100MW load disturbance at PDO side with the PDO (using Area Control Error) & OETC (using tie line power) PID AGC controller

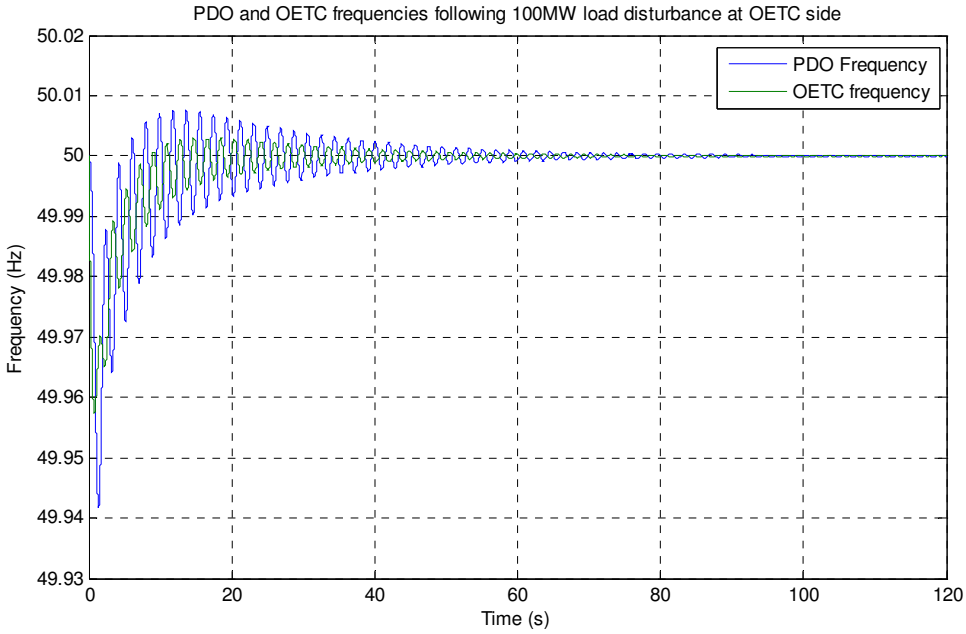

Figure 9.103: Grid frequency following 100MW load disturbance at OETC side with the PDO (using Area Control Error) & OETC (using tie line power) PID AGC controller

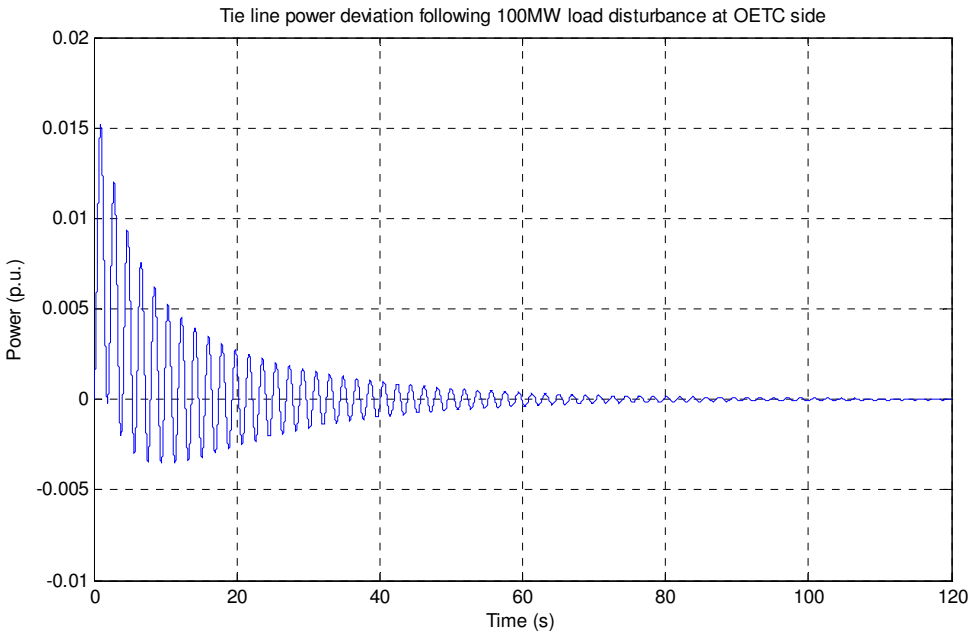

Figure 9.104: Tie line power deviation following 100MW load disturbance at OETC side with the PDO (using Area Control Error) & OETC (using tie line power) PID AGC controller

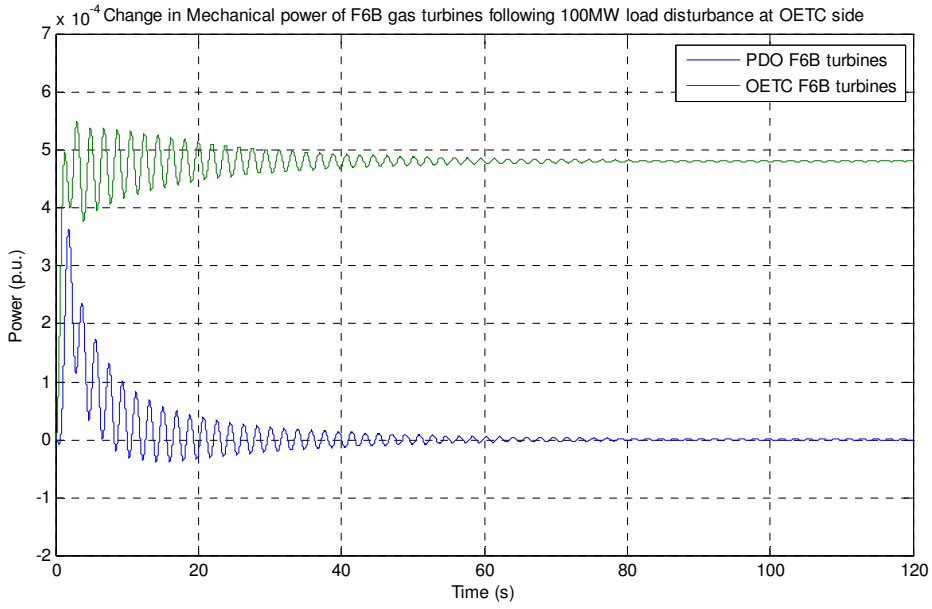

Figure 9.105: Change in Mechanical power of F6B gas turbines following 100MW load disturbance at OETC side with the PDO (using Area Control Error) & OETC (using tie line power) PID AGC controller

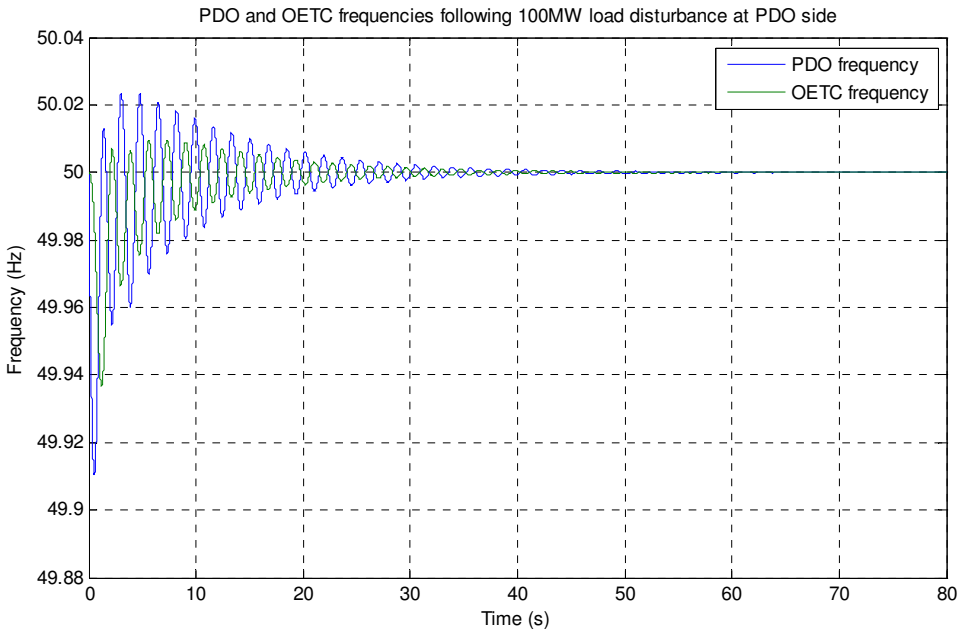

Figure 9.107: Grid frequency following 100MW load disturbance at PDO side with the PDO (using Area Control Error) & OETC (using Area Control Error) PID AGC controller

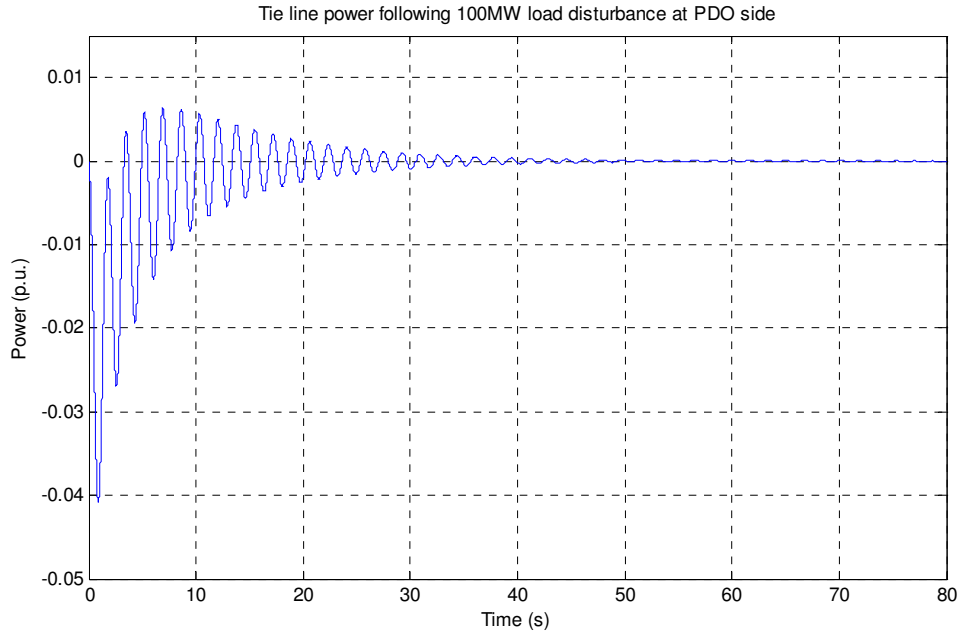

Figure 9.108: Tie line power deviation following 100MW load disturbance at PDO side with the PDO (using Area Control Error) & OETC (using Area Control Error) PID AGC controller

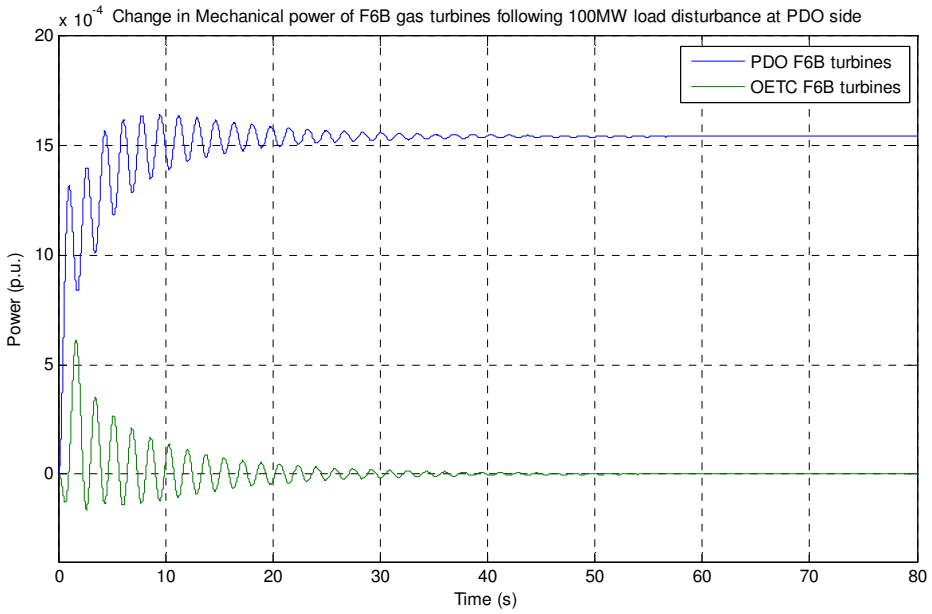

Figure 9.109: Change in Mechanical power of F6B gas turbines following 100MW load disturbance at PDO side with the PDO (using Area Control Error) & OETC (using Area Control Error) PID AGC controller

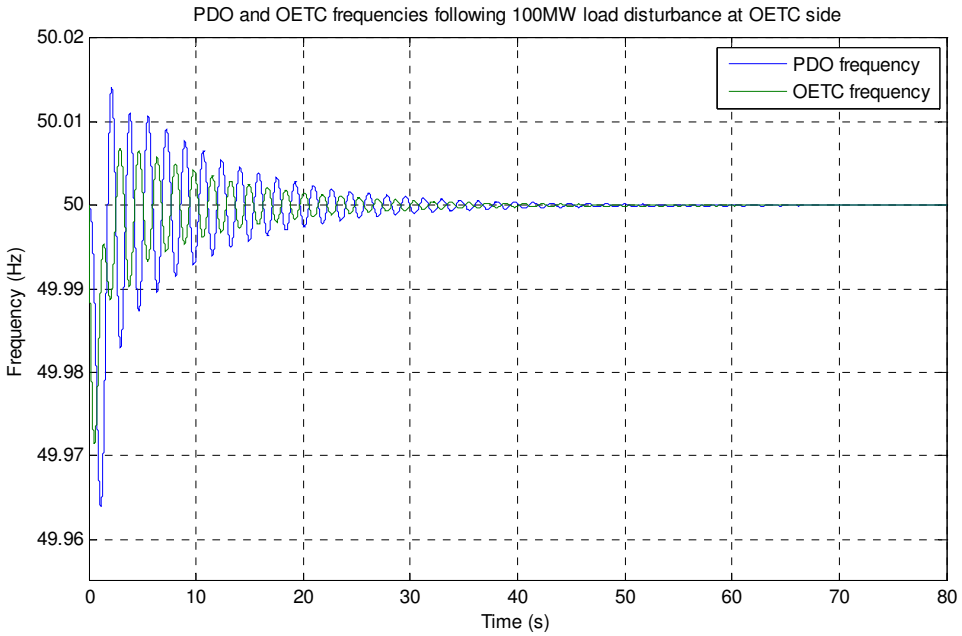

Figure 9.110: Grid frequency following 100MW load disturbance at OETC side with the PDO (using Area Control Error) & OETC (using Area Control Error) PID AGC controller

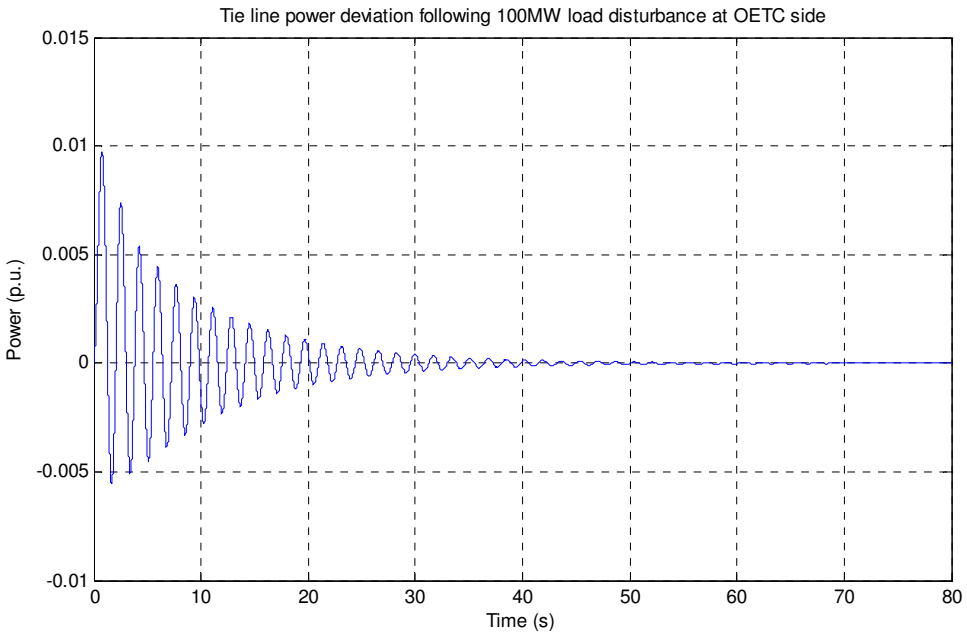

Figure 9.111: Tie line power deviation following 100MW load disturbance at OETC side with the PDO (using Area Control Error) & OETC (using Area Control Error) PID AGC controller

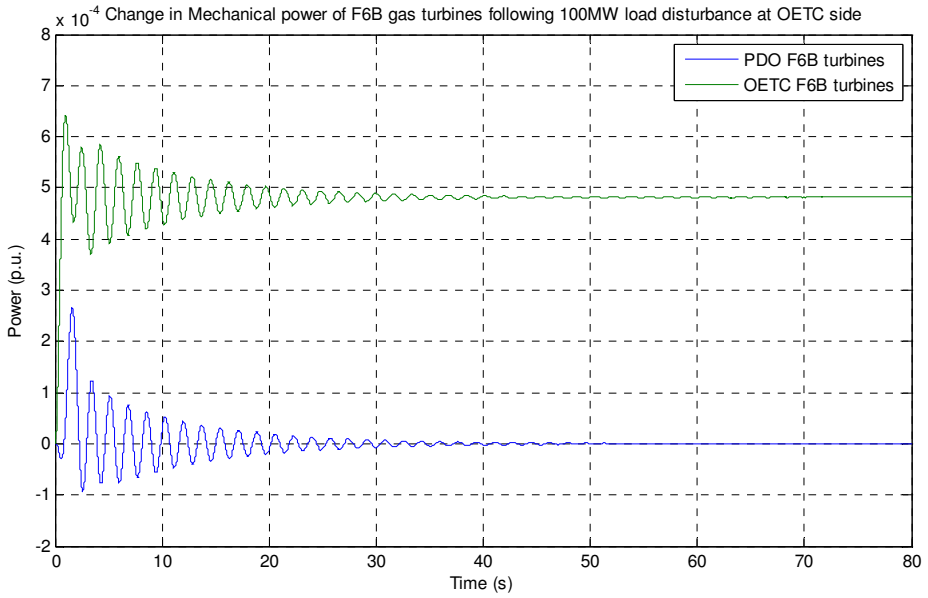

Figure 9.112: Change in Mechanical power of F6B gas turbines following 100MW load disturbance at OETC side with the PDO (using Area Control Error) & OETC (using Area Control Error) PID AGC controller

Appendix 5: MATLAB "Mfile" codes used for calculation of feedback gain matrices of the LQR AGC controllers

Code 1:

```
f=50            %system frequency
Tgg=0.05        %gas turbine governor time constant
Tgc=0.05        %gas turbine control valve time constant
Tgch=0.4        %gas turbine fuel charging time constant
Tsg=0.2         %steam turbine governor time constant
Tsch=0.3        %staem turbine steam charging time constant
Hpdo=4.8417   %PDO power system accumulated inertia
Dpdo=13.6*10^-3 %PDO power system load damping factor
Kdwpdo=23.88*10^-3 %damper windings torque coefficient
Rpdo=2          %PDO droop setting
Hoetc=15.5023  %OETC power system accumulative inertia
Doetc=29.76*10^-3 %OETC power system load damping factor
Kdwoetc=74.09*10^-3 %damper windings torque coefficient
Roetc=2         %OETC droop setting
Tiv=0.722        %synchronising torque coefficient
a12=-1          %sign reversing factor
Bpdo=0.24215    %PDO frequency bias factor
%%%%%%%%%%%%%%%%%%%%%%%%%%%%%%%%%%%%%%%%%%%%%%%%%%
Kgpdo=0.4571    %PDO weighted generation from gas turbines
Kgoetc=1.1685   %OETC weighted generation from gas turbines
Ksoetc=0.295    %OETC weighted generation from steam turbines
%%%%%%%%%%%%%%%%%%%%%%%%%%%%%%%%%%%%%%%%%%%%%%%%%%%%%%%%%%%%%%%%%%%%%%
A=[0 Tiv 0 0 0 -Tiv 0 0 0 0 0 0
   -(f/(2*Hpdo)) -(f/(2*Hpdo))*(Dpdo+Kdwpdo) (f/(2*Hpdo))*Kgpdo 0 0
(f/(2*Hpdo))*Kdwpdo 0 0 0 0 0 0
   0 0 -1/Tgch 1/Tgch 0 0 0 0 0 0 0 0
   0 0 0 -1/Tgc 1/Tgc 0 0 0 0 0 0 0
   0 -1/(Tgg*Rpdo) 0 0 -1/Tgg 0 0 0 0 0 0 0
   (-(f/(2*Hoetc))*a12) (-(f/(2*Hoetc))*a12*Kdwoetc) 0 0 0
((f/(2*Hoetc))*(a12*Kdwoetc-Doetc)) ((f/(2*Hoetc))*Kgoetc) 0 0
((f/(2*Hoetc))*Ksoetc) 0 0
   0 0 0 0 0 0 -1/Tgch 1/Tgch 0 0 0 0
   0 0 0 0 0 0 0 -1/Tgc 1/Tgc 0 0 0
   0 0 0 0 0 -1/(Tgg*Roetc) 0 0 -1/Tgg 0 0 0
   0 0 0 0 0 0 0 0 0 -1/Tsch 1/Tsch 0
   0 0 0 0 0 -1/(Tsg*Roetc) 0 0 0 0 -1/Tsg 0
   -1 -Bpdo 0 0 0 0 0 0 0 0 0 0]
%%%%%%%%%%%%%%%%%%%%%%%%%%%%%%%%%%%%%
B=[0
   0
   0
   0
   1/Tgg
   0
   0
   0
   0
   0
   0
   0]
%%%%%%%%%%%%%%%%%%%%%%%%%%%%%%%
Q=[1 0 0 0 0 0 0 0 0 0 0 0
   0 1 0 0 0 0 0 0 0 0 0 0
   0 0 1 0 0 0 0 0 0 0 0 0
   0 0 0 1 0 0 0 0 0 0 0 0
   0 0 0 0 1 0 0 0 0 0 0 0
```

```
   0 0 0 0 0 1 0 0 0 0 0 0
   0 0 0 0 0 0 1 0 0 0 0 0
   0 0 0 0 0 0 0 1 0 0 0 0
   0 0 0 0 0 0 0 0 1 0 0 0
   0 0 0 0 0 0 0 0 0 1 0 0
   0 0 0 0 0 0 0 0 0 0 1 0
   0 0 0 0 0 0 0 0 0 0 0 1]
%%%%%%%%%%%%%%%%%%%%%%%%%%%%%%%
R=[1]
%%%%%%%%%%%%%%%%%%%%%%%%%%%%%%%
k=LQR(A,B,Q,R)
%%%%%%%%%%%%%%%%%%%%%%%%%%%%%%
k11=k(1,1);
k12=k(1,2);
k13=k(1,3);
k14=k(1,4);
k15=k(1,5);
k16=k(1,6);
k17=k(1,7);
k18=k(1,8);
k19=k(1,9);
k110=k(1,10);
k111=k(1,11);
k112=k(1,12);
%%%%%%%%%%%%%%%%%%%%%%%%%%%%%%%%%%%%%%%%%%%%%%%%%%%%%%%%%%%%%%%%%%%%%%%%%%%%%%%
Ldpdo=0    %PDO disturbance
Ldoetc=0   %OETC disturbance
%%%%%%%%%%%%%%%%%%%%%%%%%%%%%%
sim('PdoOetcMrunReduced',[0 60])
plot(tout,Fpdo,tout,Foetc);grid
```

Code 2:

```
f=50            %system frequency
Tgg=0.05        %gas turbine governor time constant
Tgc=0.05        %gas turbine control valve time constant
Tgch=0.4        %gas turbine fuel charging time constant
Tsg=0.2         %steam turbine governor time constant
Tsch=0.3        %staem turbine steam charging time constant
Hpdo=4.8417   %PDO power system accumulated inertia
Dpdo=13.6*10^-3 %PDO power system load damping factor
Kdwpdo=23.88*10^-3 %damper windings torque coefficient
Rpdo=2          %PDO droop setting
Hoetc=15.5023  %OETC power system accumulative inertia
Doetc=29.76*10^-3 %OETC power system load damping factor
Kdwoetc=74.09*10^-3 %damper windings torque coefficient
Roetc=2         %OETC droop setting
Tiv=0.722        %synchronising torque coefficient
a12=-1          %sign reversing factor
Boetc=0.76151    %PDO frequency bias factor
%%%%%%%%%%%%%%%%%%%%%%%%%%%%%%%%%%%%%%%%%%%%%%%%%%%%%%%%%%%%
Kgpdo=0.4571    %PDO weighted generation from gas turbines
Kgoetc=1.1685   %OETC weighted generation from gas turbines
Ksoetc=0.295    %OETC weighted generation from steam turbines
%%%%%%%%%%%%%%%%%%%%%%%%%%%%%%%%%%%%%%%%%%%%%%%%%%%%%%%%%%%%%%%%%%%%%%%%%%%%%%%
A=[0 Tiv 0 0 0 -Tiv 0 0 0 0 0 0
   -(f/(2*Hpdo)) -(f/(2*Hpdo))*(Dpdo+Kdwpdo) (f/(2*Hpdo))*Kgpdo 0 0
(f/(2*Hpdo))*Kdwpdo 0 0 0 0 0 0
   0 0 -1/Tgch 1/Tgch 0 0 0 0 0 0 0 0
   0 0 0 -1/Tgc 1/Tgc 0 0 0 0 0 0 0
   0 -1/(Tgg*Rpdo) 0 0 -1/Tgg 0 0 0 0 0 0 0
```

```
   (-(f/(2*Hoetc))*a12) (-(f/(2*Hoetc))*a12*Kdwoetc) 0 0 0
((f/(2*Hoetc))*(a12*Kdwoetc-Doetc)) ((f/(2*Hoetc))*Kgoetc) 0 0
((f/(2*Hoetc))*Ksoetc) 0 0
   0 0 0 0 0 0 -1/Tgch 1/Tgch 0 0 0 0
   0 0 0 0 0 0 0 -1/Tgc 1/Tgc 0 0 0
   0 0 0 0 0 -1/(Tgg*Roetc) 0 0 -1/Tgg 0 0 0
   0 0 0 0 0 0 0 0 0 -1/Tsch 1/Tsch 0
   0 0 0 0 0 -1/(Tsg*Roetc) 0 0 0 0 -1/Tsg 0
   -a12 0 0 0 0 -Boetc 0 0 0 0 0 0]
%%%%%%%%%%%%%%%%%%%%%%%%%%%%%%%%%%%%%%
B=[0
   0
   0
   0
   0
   0
   0
   0
   1/Tgg
   0
   1/Tsg
   0]
%%%%%%%%%%%%%%%%%%%%%%%%%%%%%%%%%
Q=[1 0 0 0 0 0 0 0 0 0 0 0
   0 1 0 0 0 0 0 0 0 0 0 0
   0 0 1 0 0 0 0 0 0 0 0 0
   0 0 0 1 0 0 0 0 0 0 0 0
   0 0 0 0 1 0 0 0 0 0 0 0
   0 0 0 0 0 1 0 0 0 0 0 0
   0 0 0 0 0 0 1 0 0 0 0 0
   0 0 0 0 0 0 0 1 0 0 0 0
   0 0 0 0 0 0 0 0 1 0 0 0
   0 0 0 0 0 0 0 0 0 1 0 0
   0 0 0 0 0 0 0 0 0 0 1 0
   0 0 0 0 0 0 0 0 0 0 0 1]
%%%%%%%%%%%%%%%%%%%%%%%%%%%%%%
R=[1]
%%%%%%%%%%%%%%%%%%%%%%%%%%%%%%
k=LQR(A,B,Q,R)
%%%%%%%%%%%%%%%%%%%%%%%%%%%%
k21=k(1,1);
k22=k(1,2);
k23=k(1,3);
k24=k(1,4);
k25=k(1,5);
k26=k(1,6);
k27=k(1,7);
k28=k(1,8);
k29=k(1,9);
k210=k(1,10);
k211=k(1,11);
k212=k(1,12);
%%%%%%%%%%%%%%%%%%%%%%%%%%%%%%%%%%%%%%%%%%%%%%%%%%%%%%%%%%%%%%%%%%%%%%
Ldpdo=0     %PDO disturbance
Ldoetc=0    %OETC disturbance
%%%%%%%%%%%%%%%%%%%%%%%%%%%%%%
sim('PdoOetcMrunReduced',[0 60])
plot(tout,Fpdo,tout,Foetc);grid
```

Code 3:

```
f=50            %system frquency
```

```
Tgg=0.05        %gas turbine governor time constant
Tgc=0.05        %gas turbine control valve time constant
Tgch=0.4        %gas turbine fuel charging time constant
Tsg=0.2         %steam turbine governor time constant
Tsch=0.3        %staem turbine steam charging time constant
Hpdo=4.8417     %PDO power system accumulated inertia
Dpdo=13.6*10^-3 %PDO power system load damping factor
Kdwpdo=23.88*10^-3 %damper windings torque coefficient
Rpdo=2          %PDO droop setting
Hoetc=15.5023   %OETC power system accumulative inertia
Doetc=29.76*10^-3 %OETC power system load damping factor
Kdwoetc=74.09*10^-3 %damper windings torque coefficient
Roetc=2         %OETC droop setting
Tiv=0.94        %synchronising torque coefficient
a12=-1          %sign reversing constant
Bpdo=0.24215    %PDO frequency bias factor
Boetc=0.76151   %OETC frequency bias factor

%%%%%%%%%%%%%%%%%%%%%%%%%%%%%%%%%%%%%%%%%%%%%%%%%%%
Kgpdo=0.4571    %PDO weighted generation from gas turbines
Kgoetc=1.1685   %OETC weighted generation from gas turbines
Ksoetc=0.295    %OETC weighted generation from steam turbines
%%%%%%%%%%%%%%%%%%%%%%%%%%%%%%%%%%%%%%%%%%%%%%%%%%%%%%%%%%%%%%%%%%%%%%%
A=[0 Tiv 0 0 0 -Tiv 0 0 0 0 0 0 0
   -(f/(2*Hpdo)) -(f/(2*Hpdo))*(Dpdo+Kdwpdo) (f/(2*Hpdo))*Kgpdo 0 0
(f/(2*Hpdo))*Kdwpdo 0 0 0 0 0 0 0
   0 0 -1/Tgch 1/Tgch 0 0 0 0 0 0 0 0 0
   0 0 0 -1/Tgc 1/Tgc 0 0 0 0 0 0 0 0
   0 -1/(Tgg*Rpdo) 0 0 -1/Tgg 0 0 0 0 0 0 0 0
   (-(f/(2*Hoetc))*a12) (-(f/(2*Hoetc))*a12*Kdwoetc) 0 0 0
((f/(2*Hoetc))*(a12*Kdwoetc-Doetc)) ((f/(2*Hoetc))*Kgoetc) 0 0
((f/(2*Hoetc))*Ksoetc) 0 0 0
   0 0 0 0 0 0 -1/Tgch 1/Tgch 0 0 0 0 0
   0 0 0 0 0 0 0 -1/Tgc 1/Tgc 0 0 0 0
   0 0 0 0 0 -1/(Tgg*Roetc) 0 0 -1/Tgg 0 0 0 0
   0 0 0 0 0 0 0 0 0 -1/Tsch 1/Tsch 0 0
   0 0 0 0 0 -1/(Tsg*Roetc) 0 0 0 0 -1/Tsg 0 0
   -1 -Bpdo 0 0 0 0 0 0 0 0 0 0 0
   -a12 0 0 0 0 -Boetc 0 0 0 0 0 0 0]
%%%%%%%%%%%%%%%%%%%%%%%%%%%%%%%%%%%%%%
B=[0 0
   0 0
   0 0
   0 0
   1/Tgg 0
   0 0
   0 0
   0 0
   0 1/Tgg
   0 0
   0 1/Tsg
   0 0
   0 0]
%%%%%%%%%%%%%%%%%%%%%%%%%%%%%%%%
Q=[1 0 0 0 0 0 0 0 0 0 0 0 0
   0 1 0 0 0 0 0 0 0 0 0 0 0
   0 0 1 0 0 0 0 0 0 0 0 0 0
   0 0 0 1 0 0 0 0 0 0 0 0 0
   0 0 0 0 1 0 0 0 0 0 0 0 0
   0 0 0 0 0 1 0 0 0 0 0 0 0
   0 0 0 0 0 0 1 0 0 0 0 0 0
   0 0 0 0 0 0 0 1 0 0 0 0 0
   0 0 0 0 0 0 0 0 1 0 0 0 0
```

```
   0 0 0 0 0 0 0 0 1 0 0 0
   0 0 0 0 0 0 0 0 0 1 0 0
   0 0 0 0 0 0 0 0 0 0 1 0
   0 0 0 0 0 0 0 0 0 0 0 1]
%%%%%%%%%%%%%%%%%%%%%%%%%%%%%%
R=[1 0
   0 1]
%%%%%%%%%%%%%%%%%%%%%%%%%%%%%%
k=LQR(A,B,Q,R)
%%%%%%%%%%%%%%%%%%%%%%%%%%%%%%
k11=k(1,1);
k12=k(1,2);
k13=k(1,3);
k14=k(1,4);
k15=k(1,5);
k16=k(1,6);
k17=k(1,7);
k18=k(1,8);
k19=k(1,9);
k110=k(1,10);
k111=k(1,11);
k112=k(1,12);
k113=k(1,13);
k21=k(2,1);
k22=k(2,2);
k23=k(2,3);
k24=k(2,4);
k25=k(2,5);
k26=k(2,6);
k27=k(2,7);
k28=k(2,8);
k29=k(2,9);
k210=k(2,10);
k211=k(2,11);
k212=k(2,12);
k213=k(2,13);
%%%%%%%%%%%%%%%%%%%%%%%%%%%%%%%%%%%%%%%%%%%%%%%%%%%%%%%%%%%%%%%%%%%%%%%%%%%%%%%
Ldpdo=0    %PDO disturbance
Ldoetc=0   %OETC disturbance
%%%%%%%%%%%%%%%%%%%%%%%%%%%%%%
sim('PdoOetcMrunReduced',[0 60])
plot(tout,Fpdo,tout,Foetc);grid
```

Appendix 6: MATLAB "Mfile" codes used for optimization of PDO-OETC AGC controller using Multidimensional unconstrained nonlinear minimization (fminsearch) function

PdoOetcAGC_Opt

```
function f = model(k)
global Kcpdo Tipdo Tdpdo Kcoetc Tioetc Tdoetc k1 k2 k3 k4 tout Fpdo cost
Kcpdo = k(1);
Tipdo = k(2);
Tdpdo = k(3);
Kcoetc = k(4);
Tioetc = k(5);
Tdoetc = k(6);
k1 = k(7);
k2 = k(8);
k3 = k(9);
k4 = k(10);
sim('PdoOetcMrunRefined_FLbPIDD',[0 30])
f = sum(cost)
plot(tout,dFpdo);
%pause(0.01)
```

Simulator

```
global Kcpdo Tipdo Tdpdo Kcoetc Tioetc Tdoetc k1 k2 k3 k4 tout Fpdo cost
f=50              %system frquency
Tgg=0.05          %gas turbine governor time constant
Tgc=0.05          %gas turbine control valve time constant
Tgch=0.4          %gas turbine fuel charging time constant
Tsg=0.2           %steam turbine governor time constant
Tsch=0.3          %staem turbine steam charging time constant
Hpdo=4.8417    %PDO power system accumulated inertia
Dpdo=13.6*10^-3 %PDO power system load damping factor
Kdwpdo=23.88*10^-3 %damper windings tourque coeffecient
Rpdo=2            %PDO droop setting
Ldpdo=0.05      %PDO disturbance
Hoetc=15.5023   %OETC power system accumulative inertia
Doetc=29.76*10^-3 %OETC power system load damping factor
Kdwoetc=74.09*10^-3 %damper windings tourque coeffecient
Roetc=2           %OETC droop setting
Ldoetc=0.05          %OETC disturbance
Tiv=0.722          %synchronising torque coeffecient
p=1               %Some units from PDO system are in preselect load
b=1             %Some units from PDO and OETC systems are at base load
%%%%%%%%%%%%%%%%%%%%%%%%%%%%%%%%%%
th  =  fminsearch('PdoOetcAGC_Opt',[0.825  0.865  0.21625  0.8808  0.8775
0.219375 1 1 1 1]);
sim('PdoOetcMrunRefined_FLbPIDD',[0 16])
plot(tout,Fpdo,tout,Foetc);grid
```

Appendix 7: MATLAB "Mfile" codes used for optimization of PDO-OETC AGC controller using Particle Swarm Optimisation method

corPSO

```
global Kcpdo Tipdo Tdpdo Kcoetc Tioetc Tdoetc K1 K2 K3 K4
c1=2.0;c2=2.01;
n=75;M=5;tmax=100; % n(popullation), M(iterations with constant
solution), tmax(maximum number of iterations)
bounds =[   0.5  1.5;
            0.5  1;
            0.25  0.75;
            0.5  1.5;
            0.5  1;
            0.25  0.75;
            0.5  1.5;
            0.5  1.5;
            0.5  1.5;
            0.5  1.5]; % Parameters max and min intervals
simulator
evalFN = 'objectives';
[Jss,xss,Jsss,t] = psomin(bounds,evalFN,tmax,c1,c2,n,M);
```

simulator

```
f=50              %system frquency
Tgg=0.05          %gas turbine governor time constant
Tgc=0.05          %gas turbine control valve time constant
Tgch=0.4          %gas turbine fuel charging time constant
Tsg=0.2           %steam turbine governor time constant
Tsch=0.3          %staem turbine steam charging time constant
Hpdo=4.8417       %PDO power system accumulated inertia
Dpdo=13.6*10^-3 %PDO power system load damping factor
Kdwpdo=23.88*10^-3 %damper windings tourque coeffecient
Rpdo=2            %PDO droop setting
Ldpdo=0.05        %PDO disturbance
Hoetc=15.5023     %OETC power system accumulative inertia
Doetc=29.76*10^-3 %OETC power system load damping factor
Kdwoetc=74.09*10^-3 %damper windings tourque coeffecient
Roetc=2           %OETC droop setting
Ldoetc=0.05          %OETC disturbance
Tiv=0.94          %synchronising torque coeffecient
p=1               %Some units from PDO system are in preselect load control
"p=0"
b=1               %Some units from PDO and OETC systems are at base load
"b=0"
Sevenpdo=readfis('Sevenpdo'); %loads PDO Fuzzy logic inference system
Sevenoetc=readfis('Sevenoetc');%loads OETC Fuzzy logic inference system
```

Objective

```
function [val] = objectives(sol)
global Kcpdo Tipdo Tdpdo Kcoetc Tioetc Tdoetc K1 K2 K3 K4
Kcpdo=sol(1)
Tipdo=sol(2)
Tdpdo=sol(3)
Kcoetc=sol(4)
Tioetc=sol(5)
Tdoetc=sol(6)
K1=sol(7)
K2=sol(8)
K3=sol(9)
K4=sol(10)
```

```
sim('PdoOetcMrunRefined',[0 15]) %Simulates PDO-OETC model
% FUNCTION TO MINIMISE
   val = sum(cost);
```

PSOmin

```
function [Jss,xss,Jsss,t] = psomin(bounds,evalFN,tmax,c1,c2,n,M)
% PSOmin run a Partical Swarm Optimization to minimize the objective
function.
% function [x,endPop,bPop,traceInfo]=psomin(bounds,evalFN,tmax,c1,c2,n,M)
% Output Arguments:
%   Jss           - the best solution found during the course of the run.
%   xss           - the final population.
%   Jsss          - a trace of the best population.
%   t             - number of iteration.
%
% Input Arguments:
%   bounds        - a matrix of upper and lower bounds on the variables.
%   evalFN        - the name of the evaluation .m function.
%   tmax          - maximum number of iteration.
%   c1            - weighting factor.
%   c2            - weighting factor.
%   n             - number of popualtion.
%   M             - maximum number of iteration of unchanged soltion.
%%%%%%%%%%%%%%%%%%%%%%%%%%
x_int= bounds;
t=1;                        % 1st iteration.
%%%%%%%%%%%%%%%%%%%%%%%%%%
phi=c1+c2;
K=2/(abs(2-phi-sqrt(phi^2-4*phi)));
[row1,col1]=size(x_int);
for i=1:row1
    x(i,:)=x_int(i,1)+(x_int(i,2)-x_int(i,1))*rand(1,n);
end
for i=1:row1
    Vmax(i)=max(x(i,:));Vmin(i)=min(x(i,:));
    vk(i)=(Vmax(i)-Vmin(i))/n;
    V(i,:)=-vk(i)+(vk(i)+vk(i))*rand(1,n);
end
vmax=vk;vmin=-vk;
size_V=size(V);
xs=x;
for i=1:size_V(2)
    xc=x(:,i);
    e1str=['jc=' evalFN '(xc);'];
    eval(e1str);
    J(i)=jc;
end
Js=J;
Jss=min(Js);xss=x(:,find(Jss==Js));
Jsss(t)=Jss;
m=0;
while t<tmax
    if m > M
        break
    end
    t=t+1;
    r1=rand(1);r2=rand(1);
    for i=1:size_V(1)
        for k=1:size_V(2)
            v_cal=K*(V(i,k)+c1*r1*(xs(i,k)-x(i,k))+c2*r2*(xss(i)-
x(i,k)));
            if (v_cal>=vmin(i) & v_cal<=vmax(i))
                V(i,k)=v_cal;
            else
```

```
            end
        end
    end
    for i=1:size_V(1)
        for k=1:size_V(2)
            x_cal=V(i,k)+x(i,k);
            if (x_cal>=x_int(i,1) & x_cal<=x_int(i,2))
                x(i,k)=x_cal;
            else
            end
        end
    end
    for i=1:size_V(2)
        xc=x(:,i);
        e1str=['jc=' evalFN '(xc);'];eval(e1str);
        J(i)=jc;
    end
    for i=1:size_V(2)
        if J(i)<Js(i)
            Js(i)=J(i);
            xs(:,i)=x(:,i);
        else
        end
    end
    Jmin=min(Js);
    if Jmin<Jss
        m=0;
        Jss=Jmin;
        xss=xs(:,find(Jss==Js));xss=xss(:,1);
    else
        m=m+1;
    end
    Jsss(t)=Jss;
end
return
```

Appendix 8: MATLAB "Mfile" code used for PDO-OETC AGC controllers robustness test

```
f=50              %Nominal system frequency
Ldpdo=0.05        %PDO load disturbance
Ldoetc=0          %OETC load disturbance
Tgg=0.05          %gas turbine governor time constant
Tgc=0.05          %gas turbine control valve time constant
Tgch=0.4          %gas turbine fuel charging time constant
Tsg=0.2           %steam turbine governor time constant
Tsch=0.3          %steam turbine steam charging time constant
Dpdo=13.6*10^-3 %PDO power system load damping factor
Kdwpdo=23.88*10^-3 %damper windings torque coefficient
Doetc=29.76*10^-3 %OETC power system load damping factor
Kdwoetc=74.09*10^-3 %damper windings torque coefficient
p=1               %Some units from PDO system are in preselect load control
"p=0"
b=1               %Some units from PDO and OETC systems are at base load
"b=0"
Kdwpdo=23.88*10^-3 %damper windings torque coefficient
Kdwoetc=74.09*10^-3 %damper windings torque coefficient
f1sav=[];
for Hpdo=4:0.25:5
    for Hoetc=14:0.5:16
        for Tiv=0.7:0.1:1
            for Rpdo=1.5:0.5:2.5
                for Roetc=1.5:0.5:2.5
                    for Bpdo=0.21794:0.02421:0.26636
                        for Boetc=0.68536:0.07615:0.83766
                            sim('PdoOetcMrunRefined',[0 15])
                            f1sav = [f1sav Fpdo];
                        end
                    end
                end
            end
        end
    end
end
plot (f1sav);grid
```

Appendix 9: GCC interconnection impact assessment simulations results

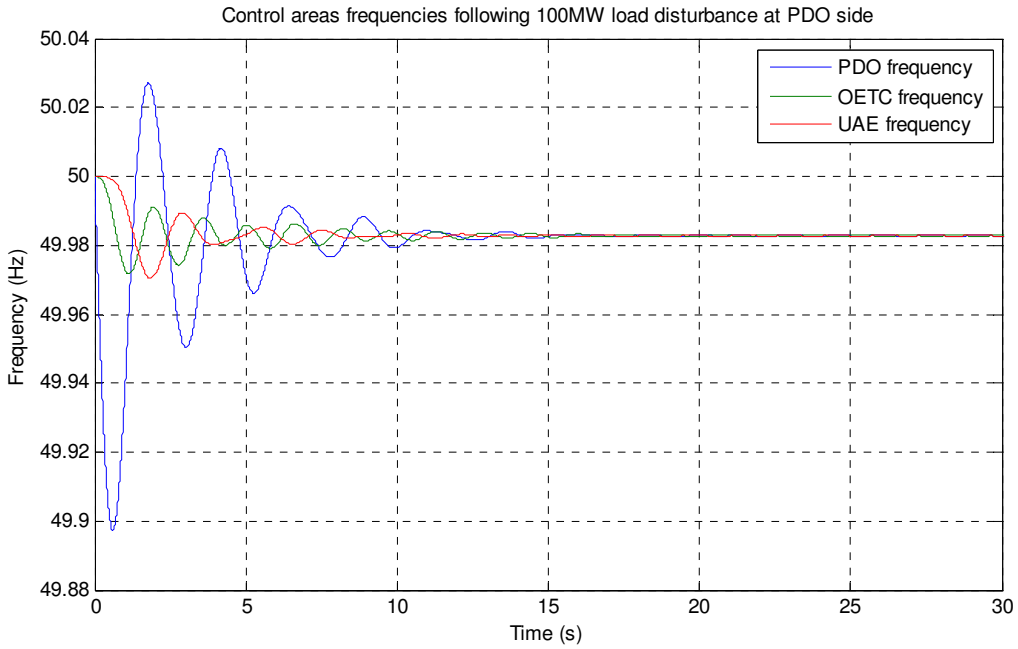

Figure 14.7: PDO, OETC and UAE control areas frequencies following 100MW load disturbance at PDO side with NO AGC

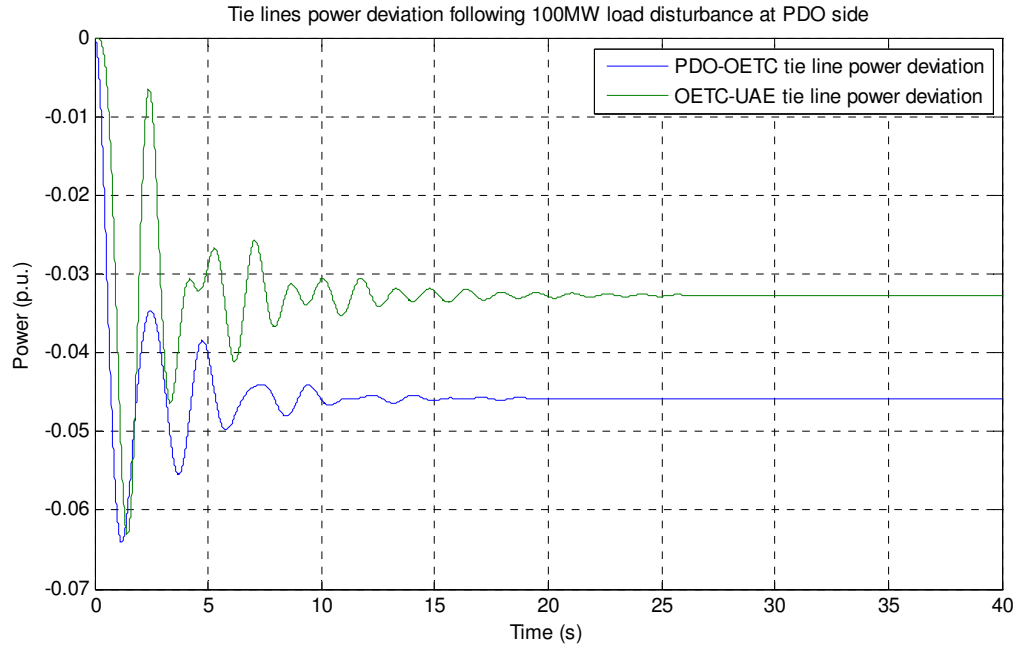

Figure 14.8: PDO-OETC and OETC-UAE tie lines power deviation following 100MW load disturbance at PDO side with NO AGC

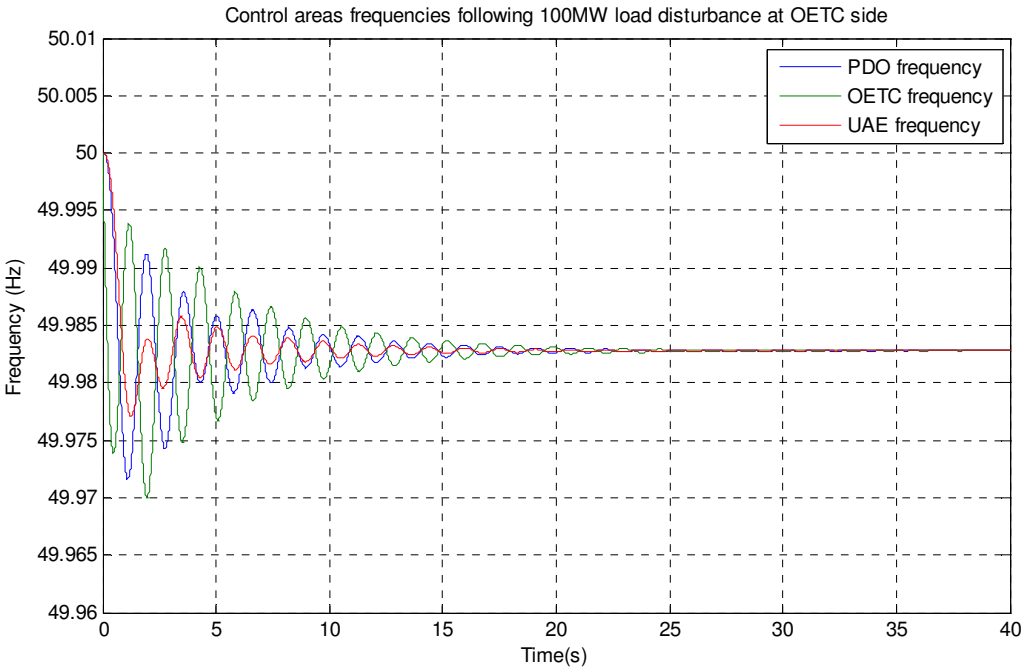

Figure 14.9: PDO, OETC and UAE control areas frequencies following 100MW load disturbance at OETC side with NO AGC

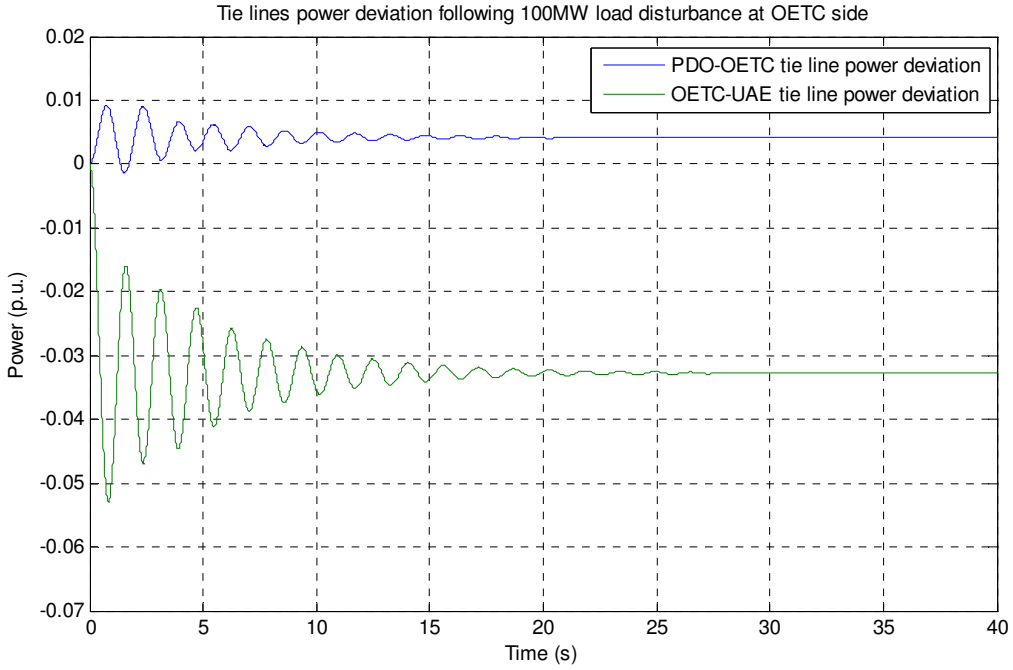

Figure 14.10: PDO-OETC and OETC-UAE tie lines power deviation following 100MW load disturbance at OETC side with NO AGC

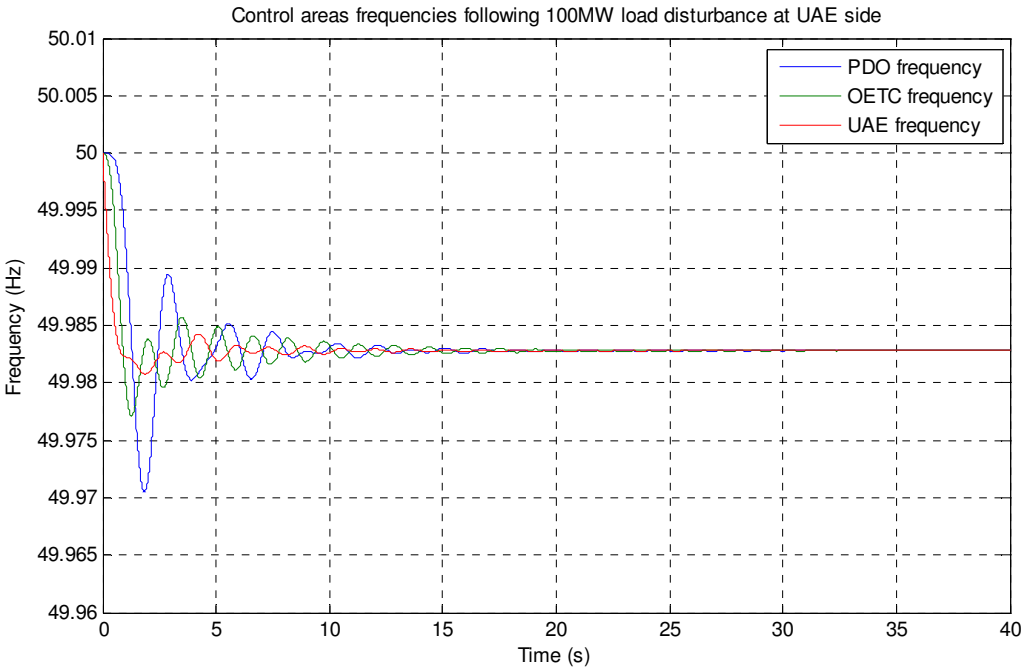

Figure 14.11: PDO, OETC and UAE control areas frequencies following 100MW load disturbance at UAE side with NO AGC

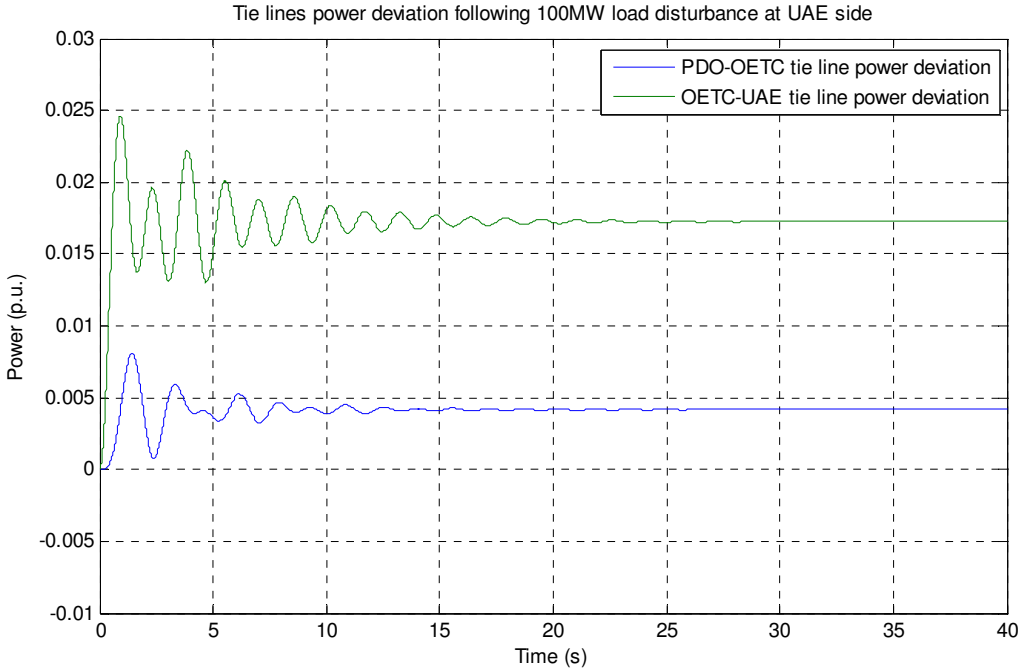

Figure 14.12: PDO-OETC and OETC-UAE tie lines power deviation following 100MW load disturbance at UAE side with NO AGC

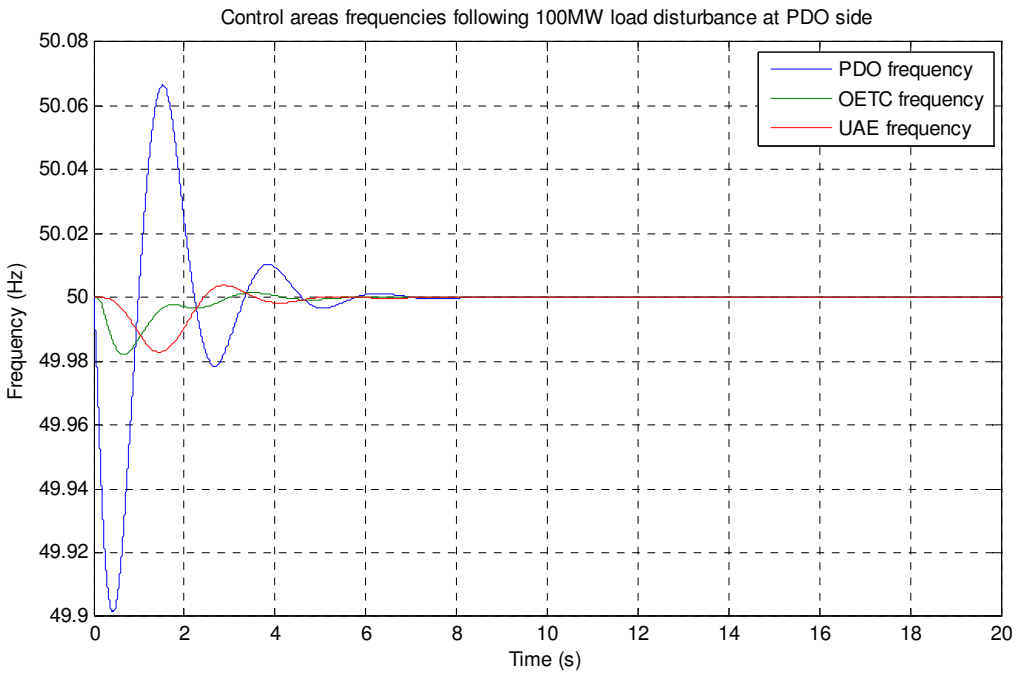

Figure 14.13: PDO, OETC and UAE control areas frequencies following 100MW load disturbance at PDO side with AGC applied at PDO and OETC

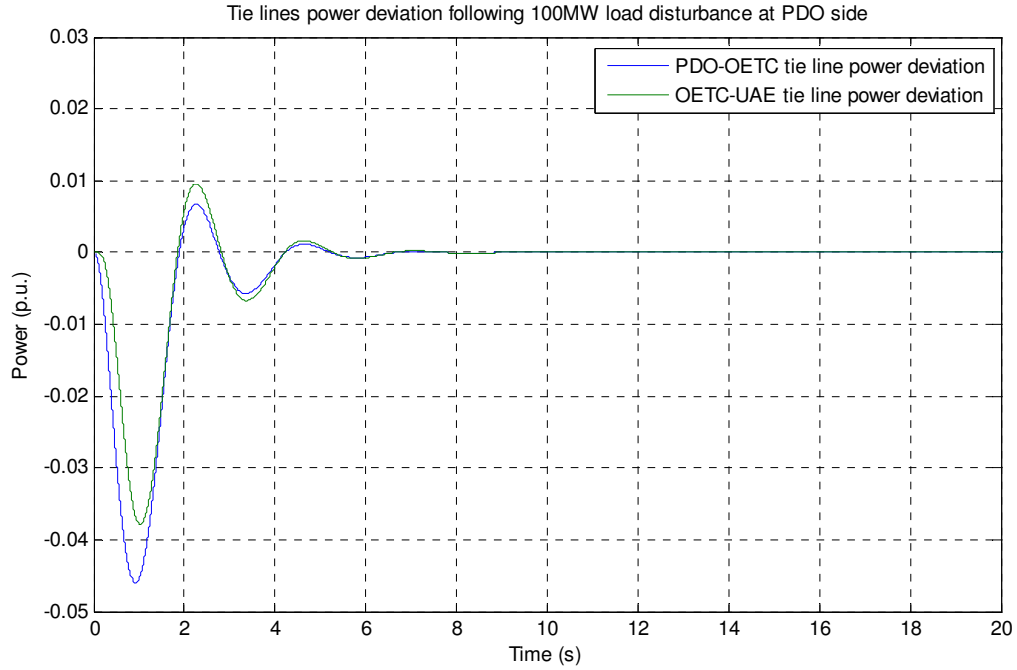

Figure 14.14: PDO-OETC and OETC-UAE tie lines power deviation following 100MW load disturbance at PDO side with AGC applied at PDO and OETC

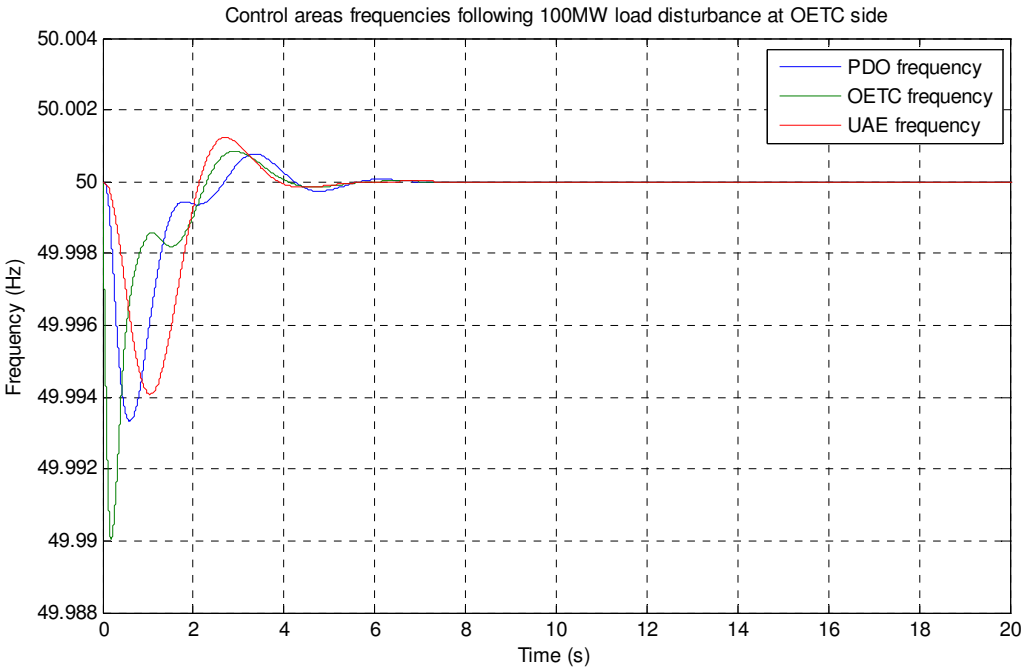

Figure 14.15: PDO, OETC and UAE control areas frequencies following 100MW load disturbance at OETC side with AGC applied at PDO and OETC

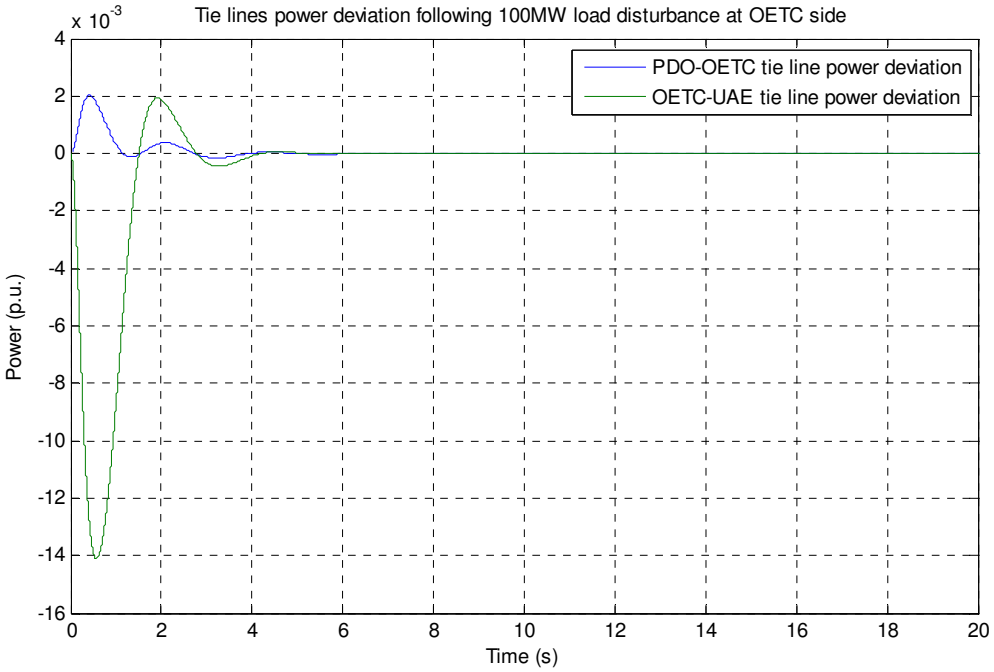

Figure 14.16: PDO-OETC and OETC-UAE tie lines power deviation following 100MW load disturbance at OETC side with AGC applied at PDO and OETC

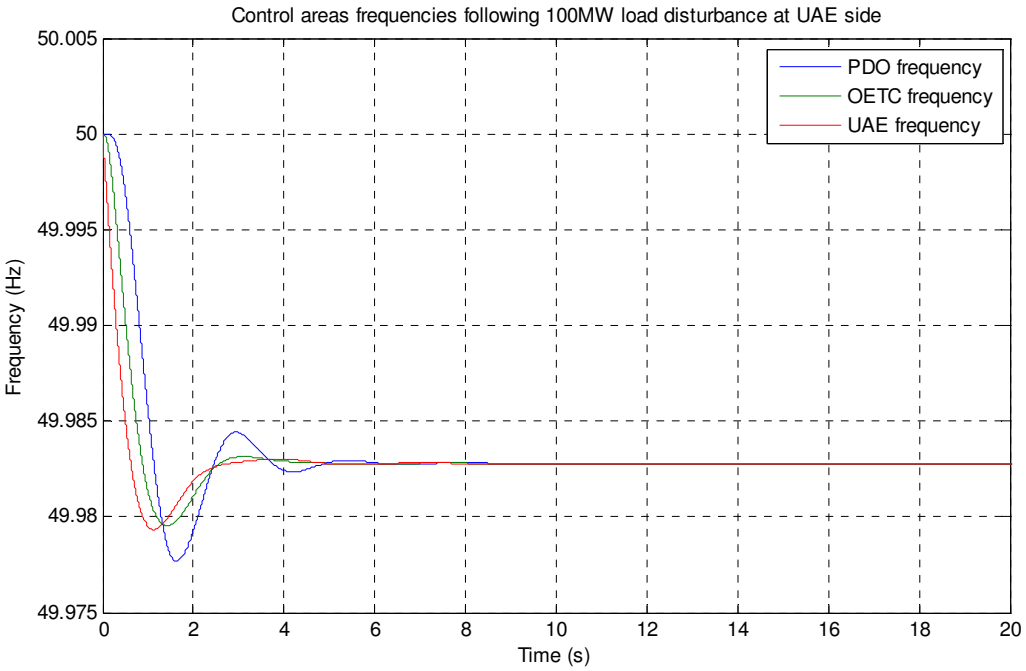

Figure 14.17: PDO, OETC and UAE control areas frequencies following 100MW load disturbance at UAE side with AGC applied at PDO and OETC

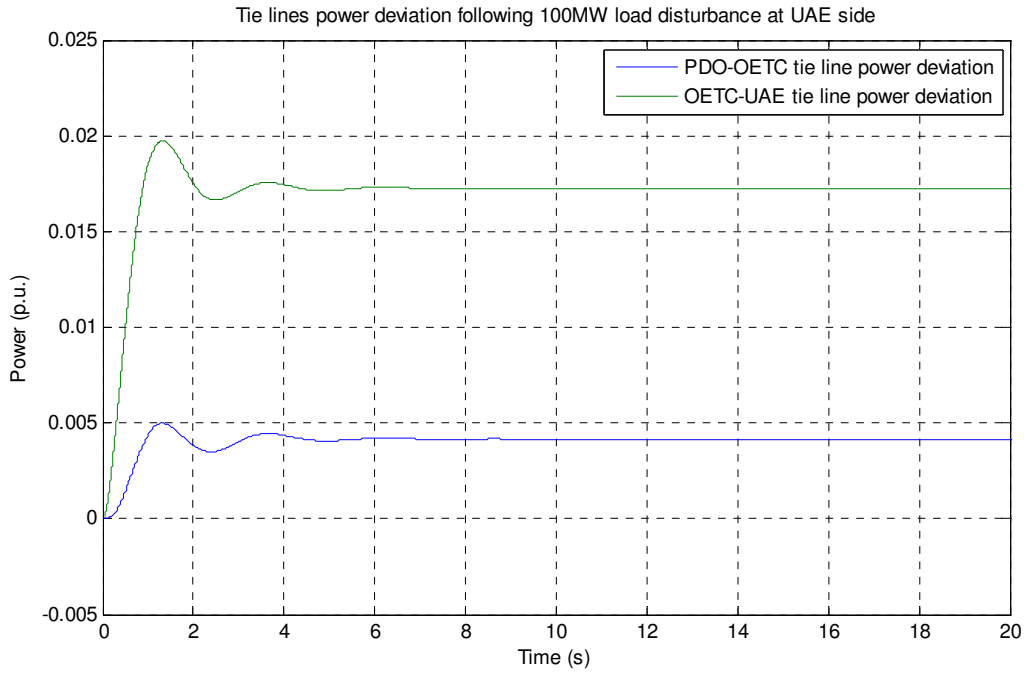

Figure 14.18: PDO-OETC and OETC-UAE tie lines power deviation following 100MW load disturbance at UAE side with AGC applied at PDO and OETC

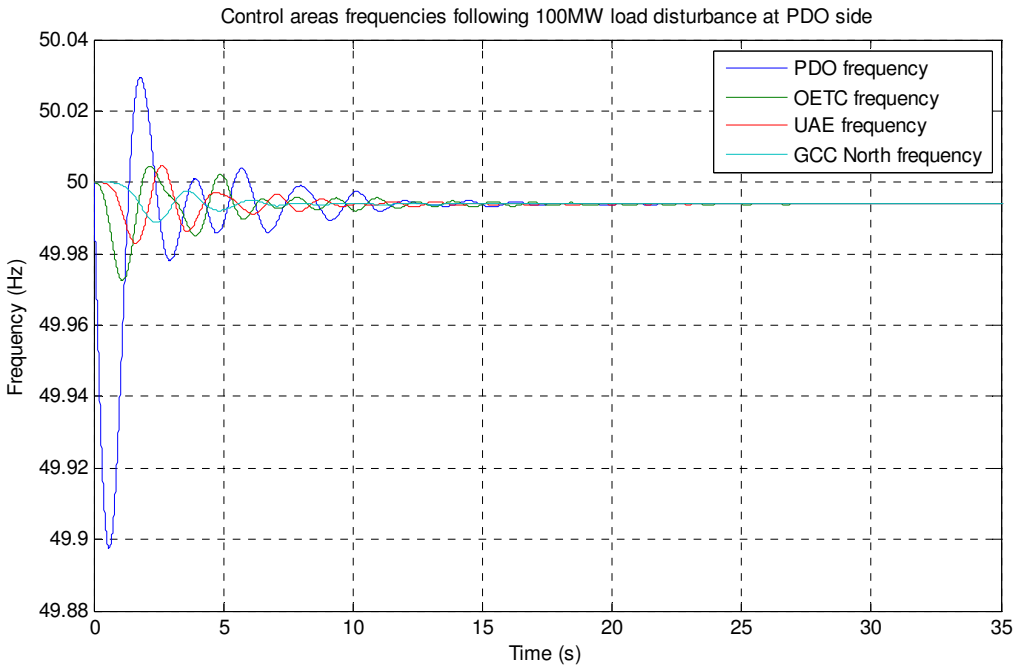

Figure 14.19: PDO, OETC, UAE and GCC North control areas frequencies following 100MW load disturbance at PDO side with NO AGC

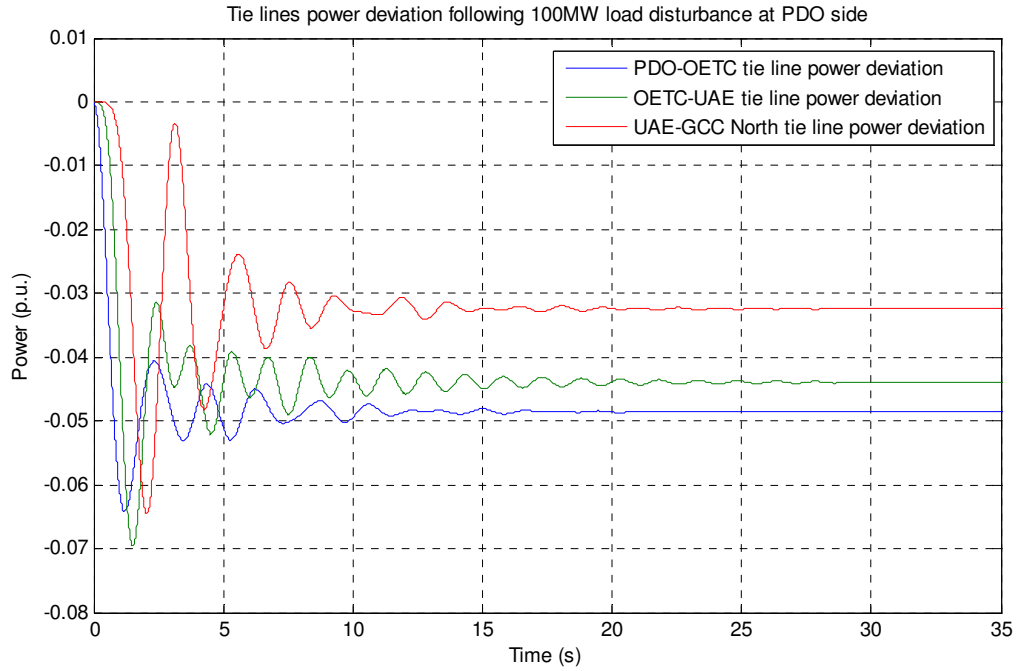

Figure 14.20: PDO-OETC, OETC-UAE and UAE-GCC North tie lines power deviation following 100MW load disturbance at PDO side with NO AGC

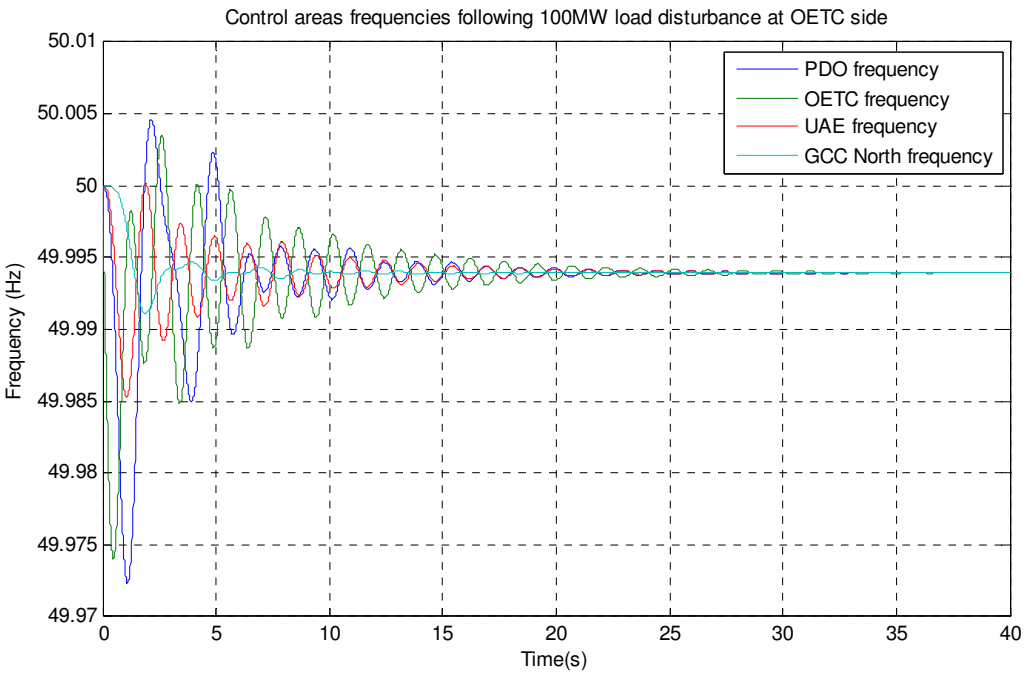

Figure 14.21: PDO, OETC, UAE and GCC North control areas frequencies following 100MW load disturbance at OETC side with NO AGC

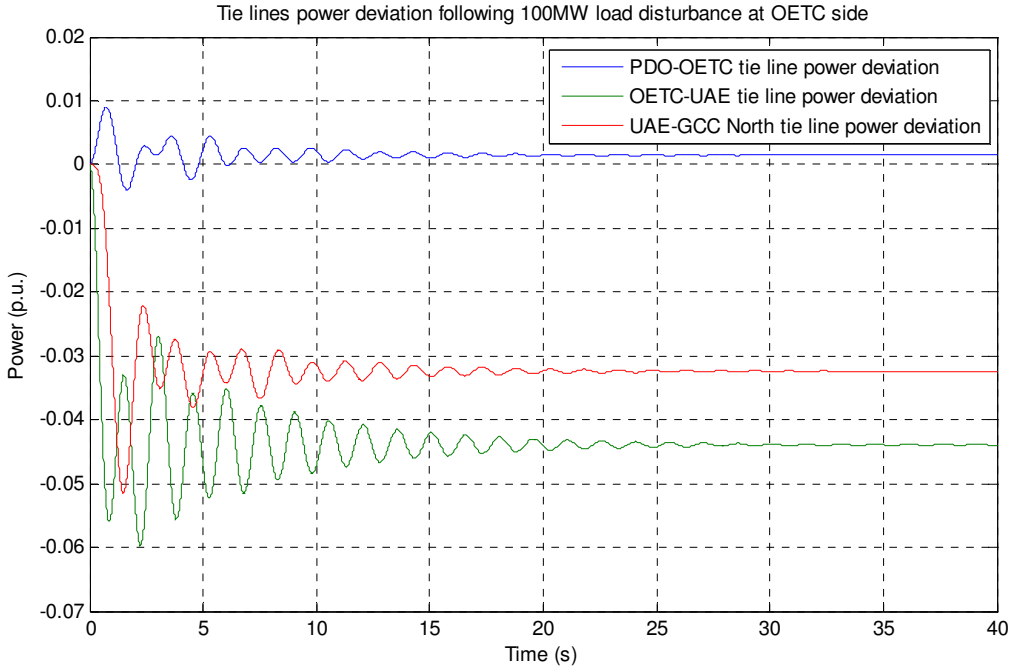

Figure 14.22: PDO-OETC, OETC-UAE and UAE-GCC North tie lines power deviation following 100MW load disturbance at OETC side with NO AGC

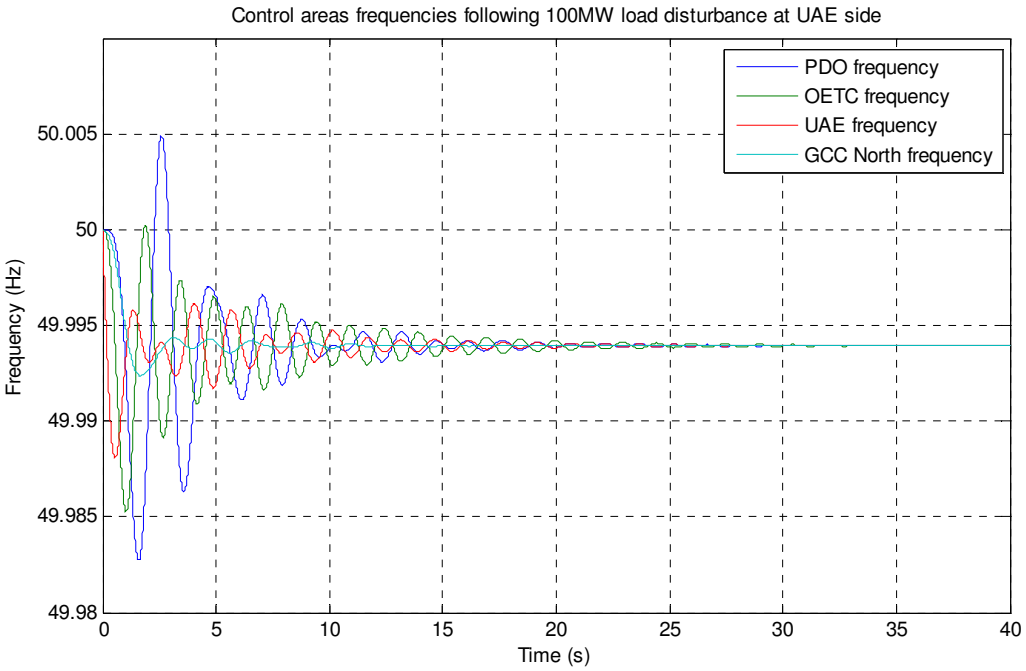

Figure 14.23: PDO, OETC, UAE and GCC North control areas frequencies following 100MW load disturbance at UAE side with NO AGC

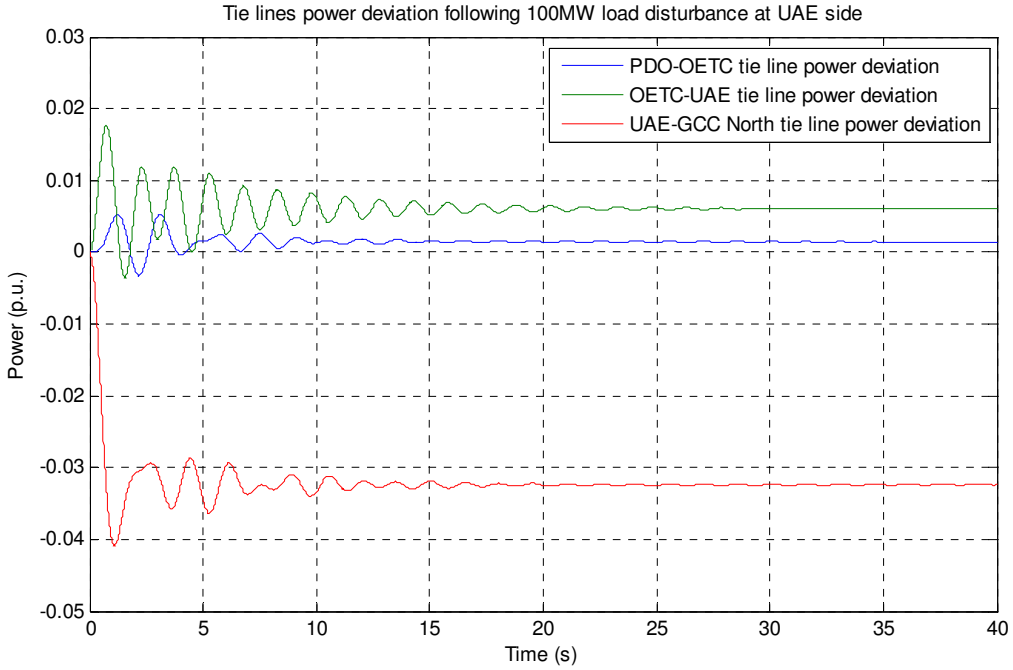

Figure 14.24: PDO-OETC, OETC-UAE and UAE-GCC North tie lines power deviation following 100MW load disturbance at UAE side with NO AGC

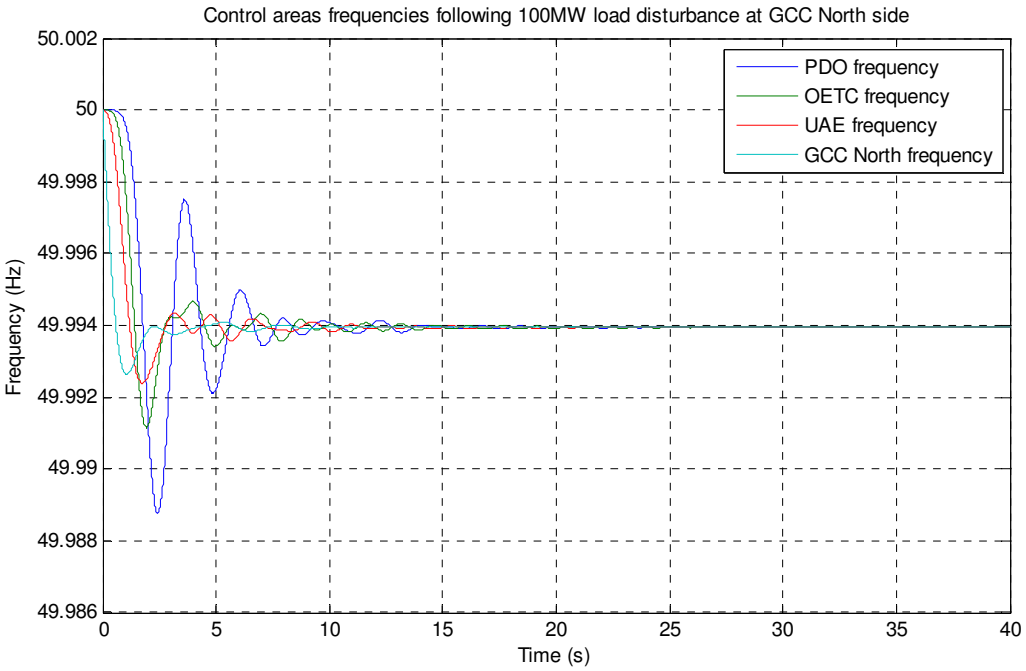

Figure 14.25: PDO, OETC, UAE and GCC North control areas frequencies following 100MW load disturbance at GCC North side with NO AGC

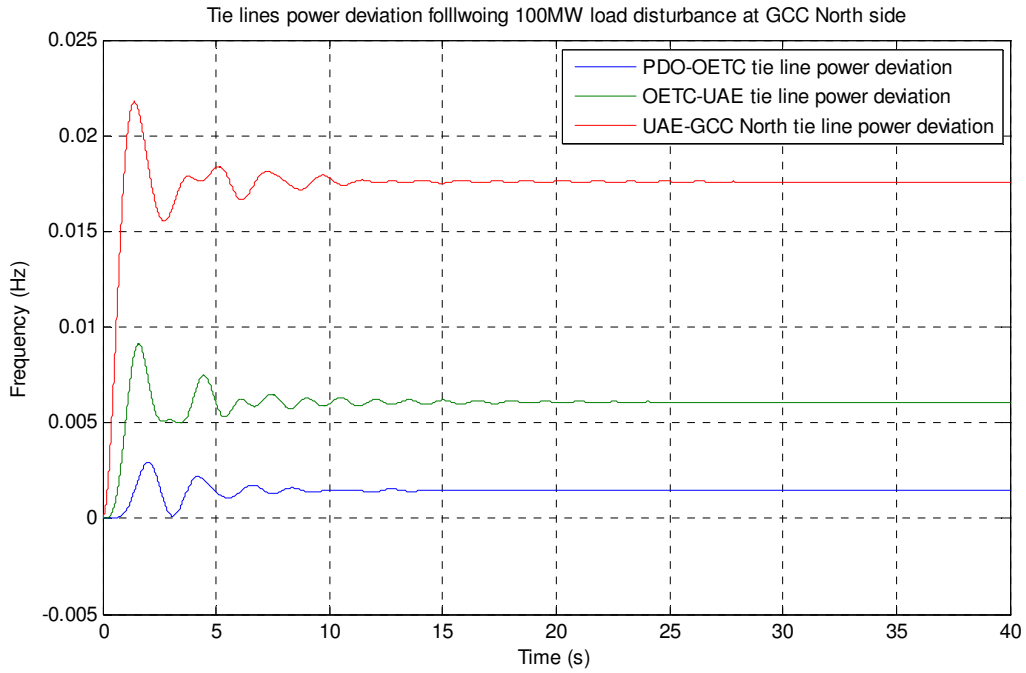

Figure 14.26: PDO-OETC, OETC-UAE and UAE-GCC North tie lines power deviation following 100MW load disturbance at GCC North side with NO AGC

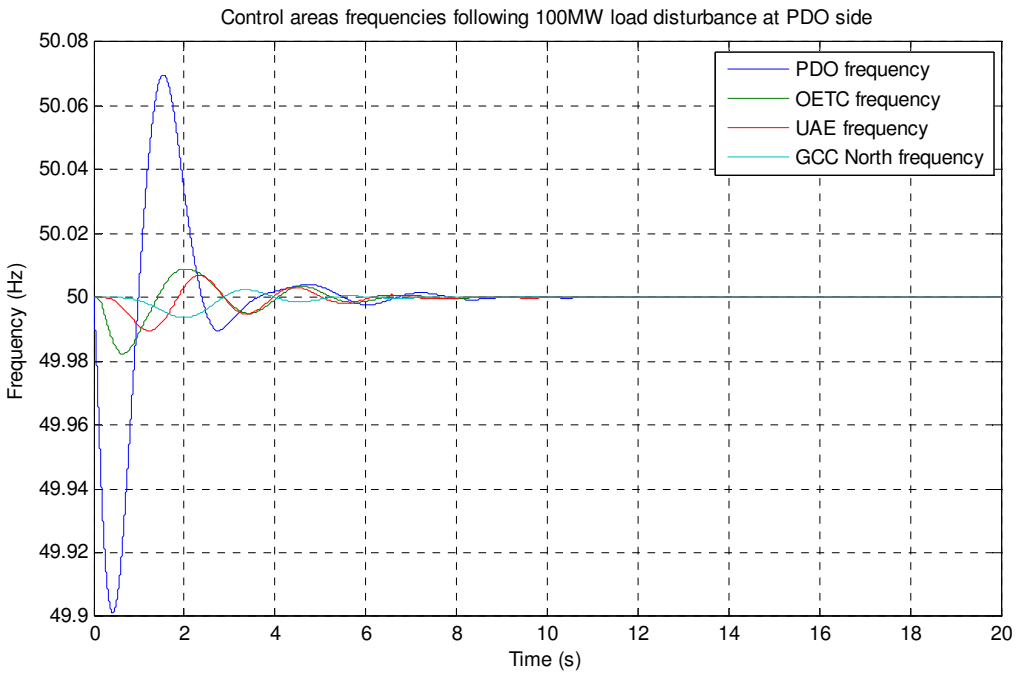

Figure 14.27: PDO, OETC, UAE and GCC North control areas frequencies following 100MW load disturbance at PDO side with AGC applied at PDO and OETC

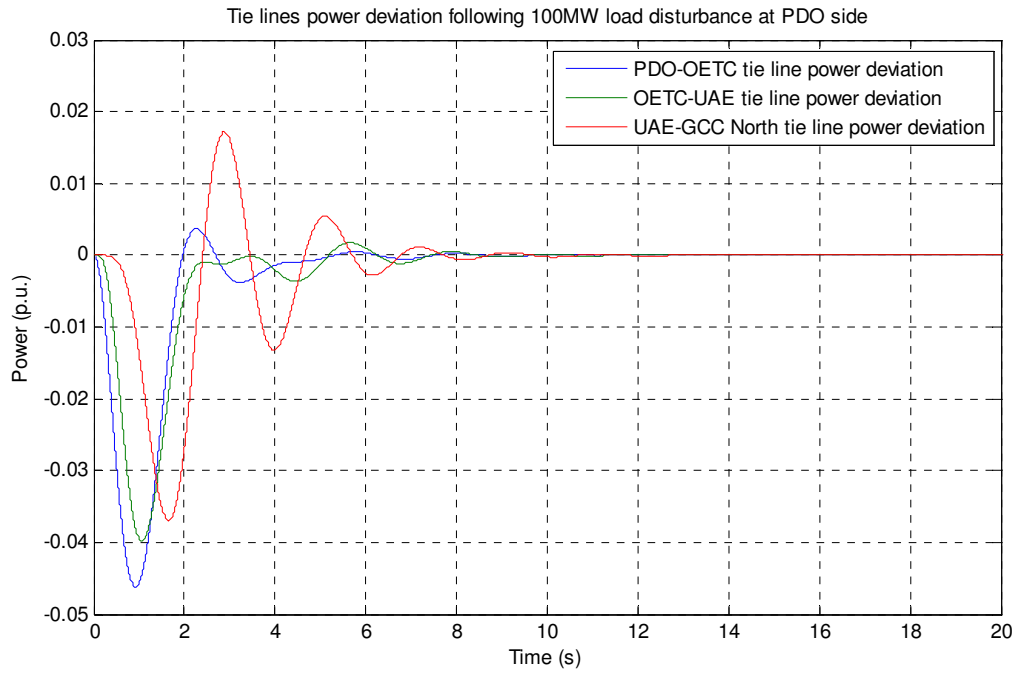

Figure 14.28: PDO-OETC, OETC-UAE and UAE-GCC North tie lines power deviation following 100MW load disturbance at PDO side with AGC applied at PDO and OETC

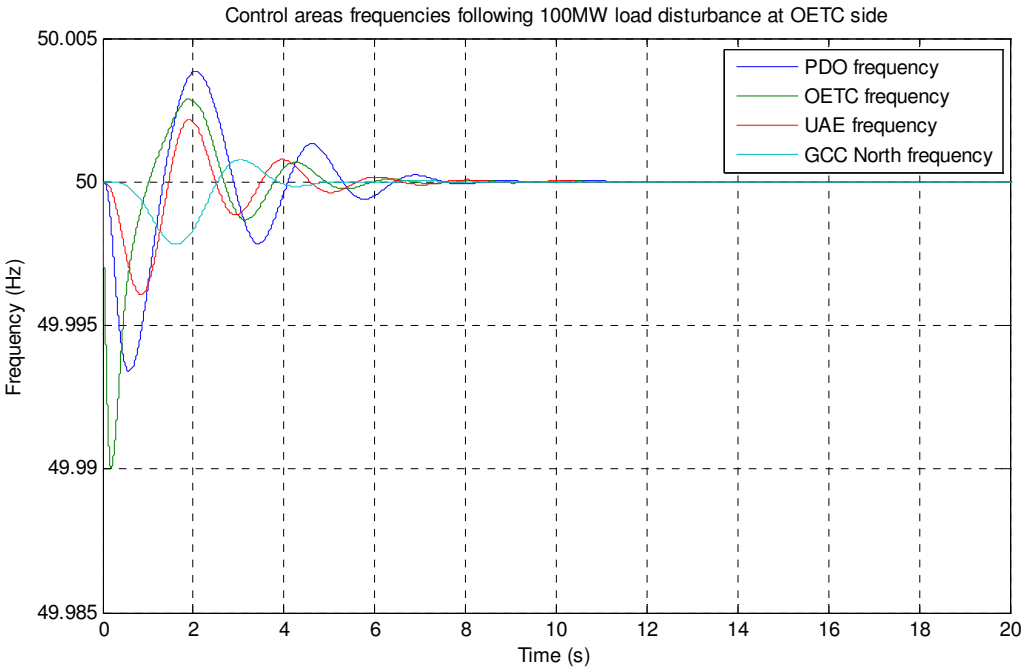

Figure 14.29: PDO, OETC, UAE and GCC North control areas frequencies following 100MW load disturbance at OETC side with AGC applied at PDO and OETC

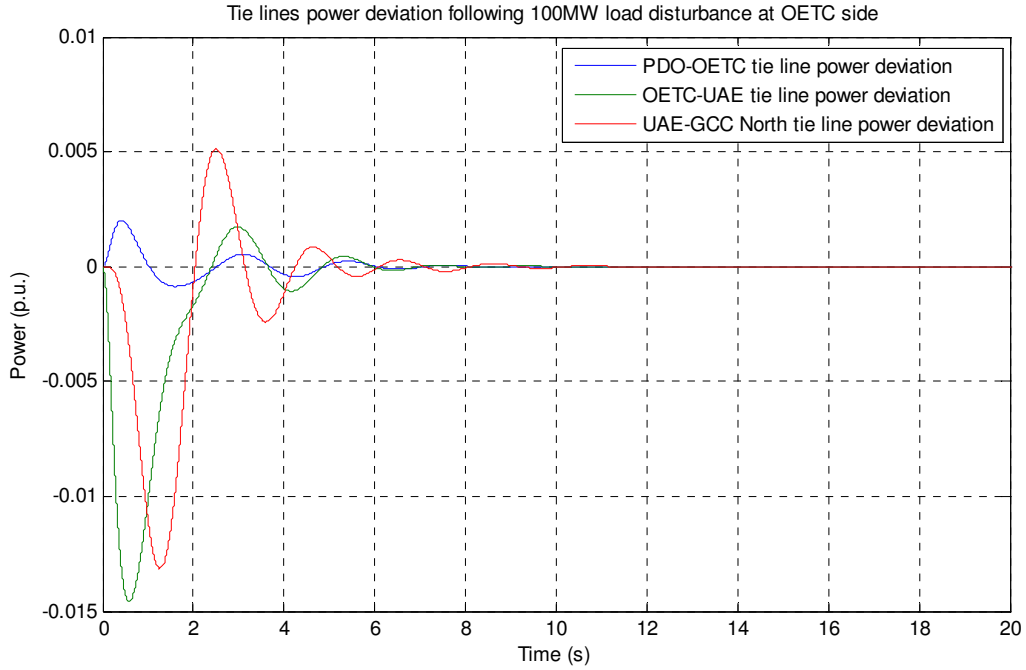

Figure 14.30: PDO-OETC, OETC-UAE and UAE-GCC North tie lines power deviation following 100MW load disturbance at OETC side with AGC applied at PDO and OETC

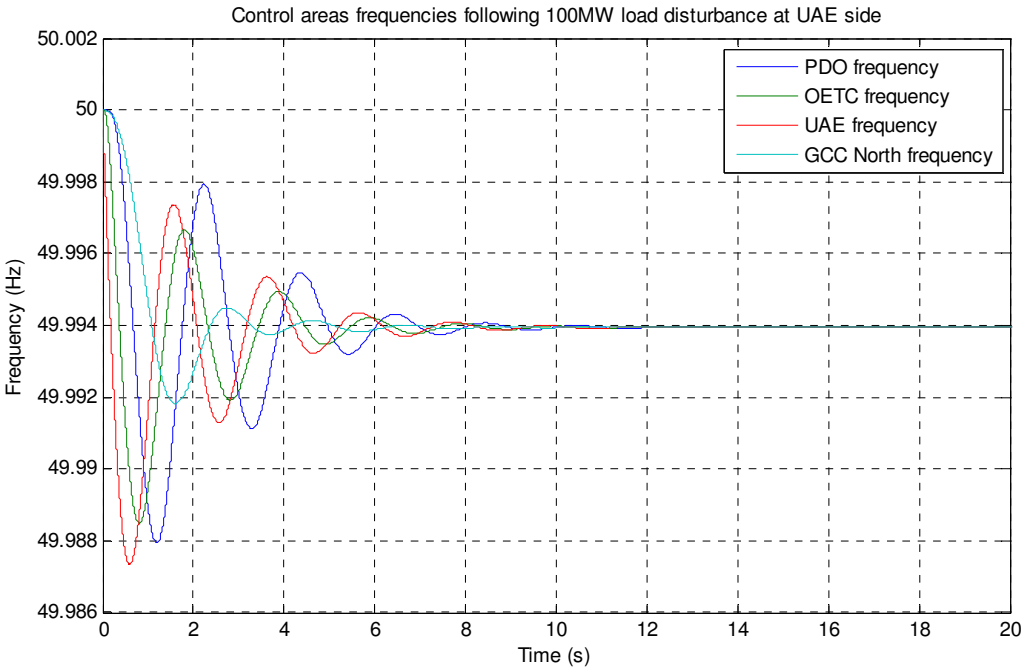

Figure 14.31: PDO, OETC, UAE and GCC North control areas frequencies following 100MW load disturbance at UAE side with AGC applied at PDO and OETC

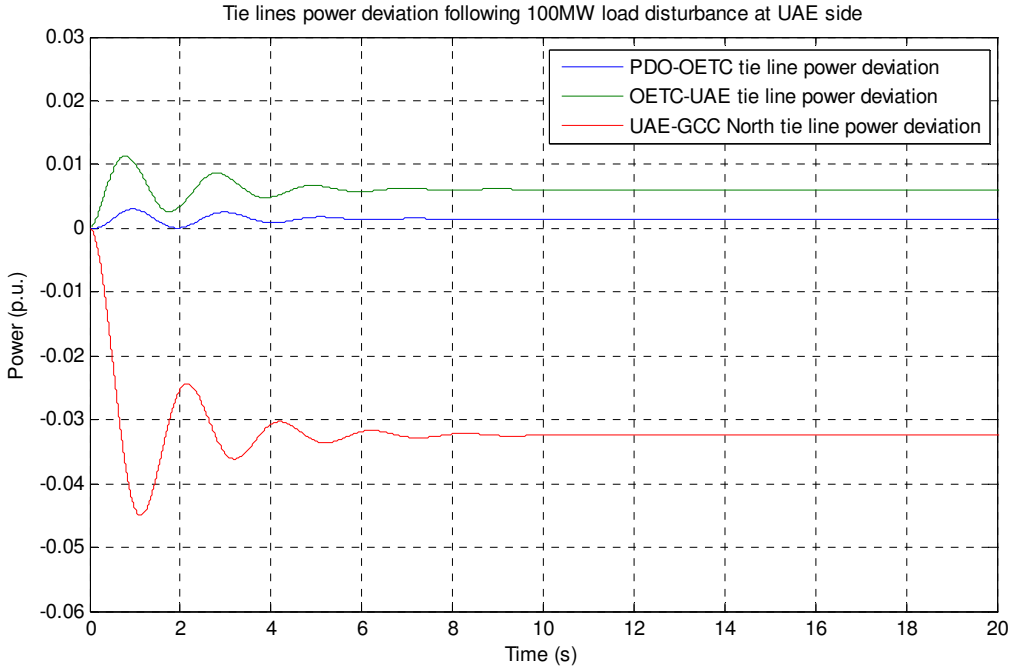

Figure 14.32: PDO-OETC, OETC-UAE and UAE-GCC North tie lines power deviation following 100MW load disturbance at UAE side with AGC applied at PDO and OETC

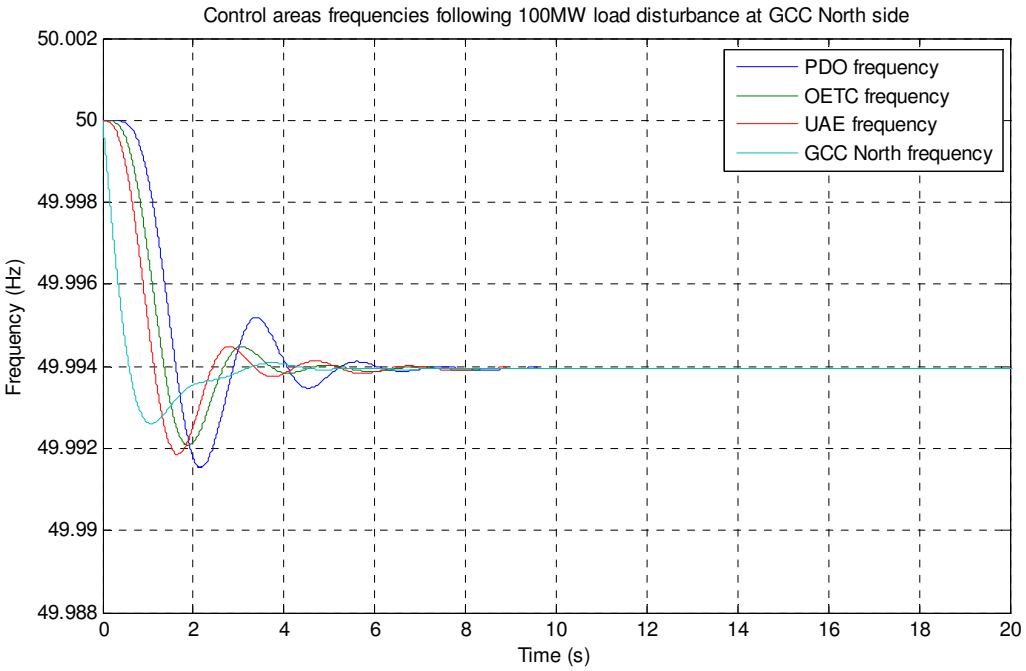

Figure 14.33: PDO, OETC, UAE and GCC North control areas frequencies following 100MW load disturbance at GCC North side with AGC applied at PDO and OETC

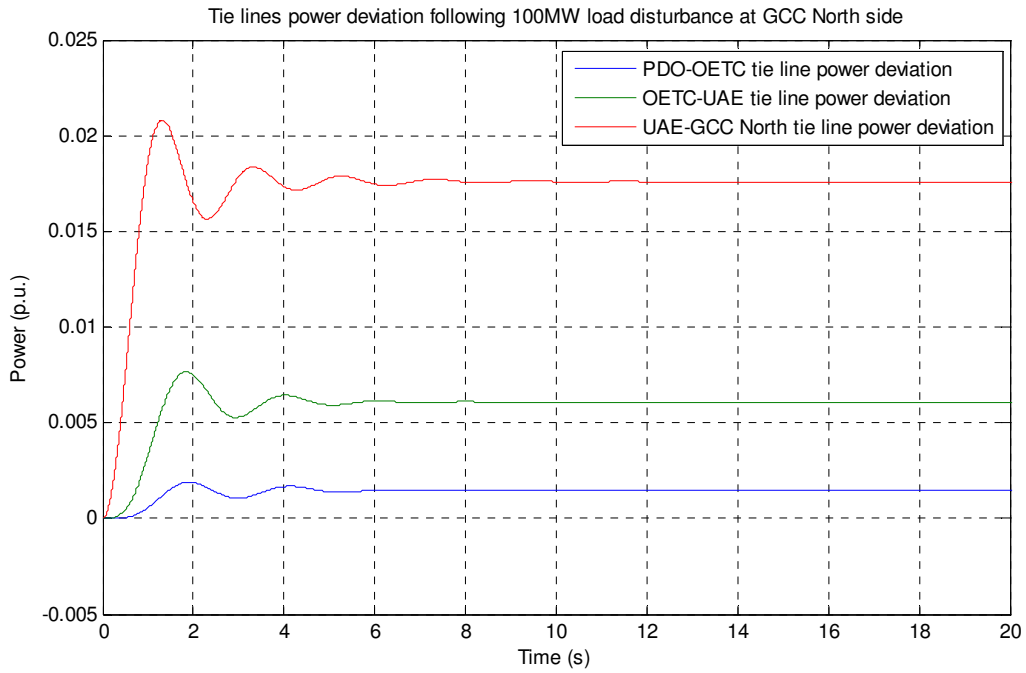

Figure 14.34: PDO-OETC, OETC-UAE and UAE-GCC North tie lines power deviation following 100MW load disturbance at GCC North side with AGC applied at PDO and OETC

List of references

- Al-Alawi, Jamil S. K. (1993) "Towards higher efficiency in water and power utilities", *Desalination*, 123 (2-3), pp. 135-142.
- Al-Asaad, Hassan K. (2009) "Electricity Power Sector Reform in the GCC Region", *The Electricity Journal*, 22 (9), pp. 58-64.
- Ali E.S. and Abd-Elazim S.M. (2011) " Bacteria foraging optimization algorithm based load frequency controller for interconnected power system", *Electrical Power and Energy Systems,* 33, pp.633-638.
- Al-Omairi, Bader (2007) *Design of a Fuzzy-Swarm Load Frequency Controller for Interconnected Power Systems*. MSc thesis, Sultanate of Oman: Department of Electrical and Computer Engineering, Engineering College, Sultan Qaboos University.
- Anderson P. M. and Fouda A. A. (2003) *POWER SYSTEM CONTROL AND STABILITY*. 2nd ed., USA: JOHN WILEY & SONS, INC.
- Azzam, M. (1999) "Robust automatic generation control", *Energy Conversion and Management*, 40 (13), pp. 1413-1421.
- Bengiamin, N. N. and Chan, W. C. (1982) "Variable Structure Control of Electric Power Generation", *IEEE Transactions on Power Apparatus and Systems*, 101 (2).
- Bevrani H., Mitani Y. and Tsuji, K. (2004) "Robust decentralized AGC in a restructured power system", *Energy Conversion and Management*, 45 (15-16), pp. 2297-2312.
- Bhatt P., Roy R. and Ghoshal S.P. (2011) " Comparative performance evaluation of SMES–SMES, TCPS–SMES and SSSC–SMES controllers in automatic generation control for a two-area hydro–hydro system", *Electrical Power and Energy Systems*, 33, pp. 1585-1597.
- Çam, Ertuğrul (2007) "Application of fuzzy logic for load frequency control of hydroelectrical power plants", *Energy Conversion and Management*, 48 (4), pp. 1281-1288.
- Çam, Ertuğrul and Kocaarslan, İlhan (2005) "Load frequency control in two area power systems using fuzzy logic controller", *Energy Conversion and Management*, 46 (2), pp. 233-243.(1)
- Çam, Ertuğrul. and Kocaarslan, İlhan. (2005) "A fuzzy gain scheduling PI controller application for an interconnected electrical power system", *Electric Power Systems Research*, 73 (3), pp. 267-274.(2)
- Chang, C.S. and Fu, Weihui (1997) "Area load frequency control using fuzzy gain scheduling of PI controllers", *Electric Power Systems Research*, 42 (2), pp. 145-152.
- Demiroren, A. and Yesil, E. (2004) "Automatic generation control with fuzzy logic controllers in the power system including SMES units", *International Journal of*

Electrical Power & Energy Systems, 26 (4), pp. 291-305.

- Elgerd, O.I. and Fosha C.E. Jr. (1970) "Optimum megawatt-frequency control of multiarea electric energy systems", *IEEE Transactions on* Power *Apparatus and* Systems, 89 (4), pp. 556-563. (1)
- Elgerd O.I. and Fosha, C.E. Jr. (1970) "The megawatt-frequency control problem: a new approach via optimal control theory", *IEEE Transactions on* Power *Apparatus and* Systems, 89 (4), pp. 563-577. (2)
- El-Sherbiny M. K., El-Saady G. and Yousef Ali M. (2002) "Efficient fuzzy logic load–frequency controller", *Energy Conversion and Management*, 43 (14), pp. 1853-1863.
- Farhangi R., Boroushaki M. and Hosseini S. H. (2012) "Load–frequency control of interconnected power system using emotional learning-based intelligent controller", *Electrical Power and Energy Systems*, 36, pp. 76–83.
- Feliachi, Ali and Rerkpreedapong, Dulpichet (2005) "NERC compliant load frequency control design using fuzzy rules", *Electric Power Systems Research*, 73 (2), pp. 101-106.
- Ghosh, Smarajit (2007) *Control Systems Theory and Applications*. India: Pearson Education.
- Ghoshal, S. P. (2004) "Optimizations of PID gains by particle swarm optimizations in fuzzy based automatic generation control", *Electric Power Systems Research*, 72 (3), pp. 203-212.(1)
- Ghoshal, S. P. (2004) "Application of GA/GA-SA based fuzzy automatic generation control of a multi-area thermal generating system", *Electric Power Systems Research*, 70 (2), pp. 115-127. (2)
- Ghoshal, S. P. and Goswami, S. K. (2003) "Application of GA based optimal integral gains in fuzzy based active power-frequency control of non-reheat and reheat thermal generating systems", *Electric Power Systems Research*, 67 (2), pp. 79-88.
- Hemeida, Ashraf Mohamed (2005) "Wavelet neural network load frequency controller", *Energy Conversion and Management*, 46 (9-10), pp. 1613-1630.
- Hosseini, S.H. and Etemadi, A.H. (2008) "Adaptive neuro-fuzzy inference system based automatic generation control", *Electric Power Systems Research*, 78, pp1230–1239.
- Jadhav, A and Vadirajacharya K. (2012) " Performance Verification of PID Controller in an Interconnected Power System Using Particle Swarm Optimization", *Energy Procedia*, 14, pp. 2075–2080
- Karnavas, Y. L. and Papadopoulos, D. P. (2002) "AGC for autonomous power system using combined intelligent techniques", *Electric Power Systems Research*, 62 (3), pp. 225-239.
- Khodabakhshian, A. and Hooshmand, R. (2010) " A new PID controller design for

automatic generation control of hydro power systems", *Electrical Power and Energy Systems*, 32, pp. 375–382

- Khodabakhshian A., Pour M. E. and Hoshmand R. (2012) " Design of a robust load frequency control using sequential quadratic programming technique", *Electrical Power and Energy Systems*, 40, pp. 1-8.
- Khuntia, R. and Panda, S. (2012) " Simulation study for automatic generation control of a multi-area power system by ANFIS approach", *Applied Soft Computing*, 12, pp. 333–341
- Kocaarslan, İlhan and Çam, Ertuğrul (2005) "Fuzzy logic controller in interconnected electrical power systems for load-frequency control", *International Journal of Electrical Power & Energy Systems*, 27 (8), pp. 542-549.(3)
- Konstantinos D. Patlitzianas, Haris Doukas and Dimitris Th. Askounis (2007) "An assessment of the sustainable energy investments in the framework of the EU–GCC cooperation", *Renewable Energy*, 32 (10), pp. 1689-1704.
- KUNDUR, PRABHA (1994) *Power system stability and control*, 1st ed., USA: McHill.
- Lee Ho. Jae., Park Jin. Bae. and Joo Young. Hoon. (2006) "Robust load-frequency control for uncertain nonlinear power systems: A fuzzy logic approach", *Information Sciences*, 176 (23), pp. 3520-3537.
- Moon Young-Hyun, Ryu Heon-Su, Lee Jong-Gi, Song Kyung-Bin and Shin Myong-Chul (2002) "Extended integral control for load frequency control with the consideration of generation-rate constraints", *Electrical Power and Energy Systems* 24, pp. 263-269
- Nagrath, I.J. and Gopal, M. (2008) *Control Systems Engineering*. 5th ed., India: New Age International (P) Publishers.
- North American Electric Reliability Corporation (NERC) (November 2009) *Reliability Standards for the Bulk Electric Systems of North America*, USA.
- OGATA, KATSUHIKU (2008) *MODERN CONTROL ENGINEERING*. 4th ed., India: Prentice Hall of India.
- Oman Electricity Transmission Company SAOC (May 2005) *The Grid Code*, version 1, Sultanate of Oman.
- Oysal, Yusuf (2005) "A comparative study of adaptive load frequency controller designs in a power system with dynamic neural network models", *Energy Conversion and Management*, 46 (15-16), pp. 2656-2668.
- Petroleum Development Oman LLC (March 2006) *132kV Fault Level Report*, Sultanate of Oman.(1)
- Petroleum Development Oman LLC (April 2004) *Fault stability studies*, Sultanate of Oman.(2)
- Petroleum Development Oman LLC (March 2004) *Data for generators and controls for dynamic studies on PDO system*, Sultanate of Oman.(3)

- Rakhshani, E. and Sadeh, J. (2010) " Practical viewpoints on load frequency control problem in a deregulated power system", *Energy Conversion and Management*, 51, pp. 1148–1156
- Ross, Timothy J. (2007) *Fuzzy Logic with Engineering Applications*. 2nd ed., India: John Wiley & Sons (Asia).
- Saadat, Hadi (2002) *POWER SYSTEM ANALYSIS*. 2nd ed., USA: McGraw-Hill Higher Education.
- Shayeghi H. and Shayanfar H.A. (2006) "Application of ANN technique based on μ-synthesis to load frequency control of interconnected power system", *International Journal of Electrical Power & Energy Systems*, 28 (7), pp. 503-511.
- Shayeghi H., Jalili A. and Shayanfar H.A. (2007) "Robust modified GA based multi-stage fuzzy LFC", *Energy Conversion and Management*, 48 (5), pp.1656-1670.(1)
- Shayeghi H., Shayanfar H.A. and Jalili A. (2006) "Multi-stage fuzzy PID power system automatic generation controller in deregulated environments", *Energy Conversion and Management*, 47 (18-19), pp. 2829-2845.(2)
- Shayeghi H., Shayanfar H.A. and Malik O.P. (2007) "Robust decentralized neural networks based LFC in a deregulated power system", *Electric Power Systems Research*, 77 (3-4), pp. 241-251. (3)
- Shayeghi H., Sheyanfar H.A. and Jalili A. (2009) "Load Frequency Control Strategies: A state-of-the-art survey for the researcher", *Energy Conversion and Management*, 50, pp. 344-353 (4)
- Shell Global Solutions (2007) *Electrical Engineering I course notes*, Netherlands.
- Smith, John R. and Chen, Meng-Jen (1993) *Three-Phase Electrical Machines Systems computer simulation*. UK: Research Studies Press LTD.
- Sudha, R. and Santhi, R. (2011) " Robust decentralized load frequency control of interconnected power system with Generation Rate Constraint using Type-2 fuzzy approach", *Electrical Power and Energy Systems*, 33, pp. 699–707
- Yesil, E., Güzelkaya, M. and Eksin, İ. "Self tuning fuzzy PID type load and frequency controller", *Energy Conversion and Management*, 45 (3), pp. 377-390.